

Université de Montréal

**Synthesis and properties of d^6 metal complexes of
bidentate and tridentate ‘super donor’ ligands**

par

Amlan Kumar Pal

Département de chimie
Faculté des arts et des sciences

**Thèse présentée à la Faculté des études supérieures et postdoctorales
en vue de l’obtention du grade de *Philosophiae Doctor* (Ph.D.)
en chimie**

Mars, 2014

© Amlan Kumar Pal, 2014

Université de Montréal
Faculté des études supérieures et postdoctorales

Cette thèse intitulée :

**Synthesis and properties of d^6 metal complexes of
bidentate and tridentate ‘super donor’ ligands**

présentée par
Amlan Kumar Pal

A été évaluée par un jury composé des personnes suivantes :

Prof. Christian Reber, président-rapporteur
Prof. Garry Hanan, directeur de recherche
Prof. Frank Schaper, membre du jury
Prof. Randolph Thummel, examinateur externe
Prof. Christian Reber, représentant du doyen de la Faculté des arts et des sciences

Abstract

The versatility of C-N cross coupling reactions has been explored for the synthesis of two novel classes of ligands : (i) neutral bidentate N^N ligands and (ii) neutral tridentate N^N^N ligands. Both classes of ligands contain saturated aromatic *N*-heterocycles coupled with the unsaturated hexahydropyrimidopyrimidine (**hpp**) unit. The ligands form six-membered chelate rings upon coordination to a Ru(II) center. This fact is advantageous to improve the photophysical properties of Ru(II)-polypyridyl complexes.

Ru(II) complexes of bidentate ligands can act as red-emitters. The red-emission is dependent on the relative basicity of the *N*-heterocycles. While these complexes are electrochemically and photophysically appealing, the problem of stereopurity can not be avoided. Careful ligand design affords bis-bidentate ligand that is useful to overcome the problem of stereopurity. Due to the speciality of this bis-bidentate ligand, its diruthenium(II,II) complex exhibits high diastereoselectivity without any chiral separation. While the **hpp** unit acts as a nucleophile in the mechanism of C-N cross coupling reaction, it can also act as a leaving group when activated as a monoruthenium complex.

Achiral Ru(II) complexes of the tridentate ligands display improved photophysical properties over the prototype complex [Ru(tpy)₂]²⁺ (tpy = 2,2':6',2''-terpyridine). Introduction of two **hpp** units in the tridentate ligands renders the Ru(II) complex into a 'black absorber' and a 'NIR emitter' (NIR = Near Infra-Red). This fact is a consequence of better octahedral geometry around the Ru(II) ion and strong σ -donation from the **hpp** units. The blue-emitting Re(I) complexes of the tridentate ligands also exhibit interesting redox behavior. The metal-based quasi-reversible oxidation is controlled by the σ -donation from the **hpp** moieties, while the ligand-based reduction is governed by the electronic nature of the central *N*-heterocycle of the same ligand moiety.

This thesis also incorporates self-assembly of metal-chromophores as 'metallo-ligands' to form discrete supramolecular species using neutral metal-complexes. The syntheses and properties of the aforesaid metal-chromophores and the supramolecules are discussed.

Keywords : metal-chromophore, σ -donation, charge transfer, C-N coupling, electrochemistry, photophysics, X-ray crystallography, density functional theory, stereopurity, blue/red/NIR emitter.

Résumé

La polyvalence de la réaction de couplage-croisé C-N a été explorée pour la synthèse de deux nouvelles classes de ligands: (i) des ligands bidentates neutres de type $N^{\wedge}N$ et (ii) des ligands tridentates neutres de type $N^{\wedge}N^{\wedge}N$. Ces classes de ligands contiennent des *N*-hétérocycles aromatiques saturés qui sont couplés avec hexahydropyrimidopyrimidine (**hpp**). Les ligands forment de cycles à six chaînons sur la coordination du centre Ru(II). Ce fait est avantageux pour améliorer les propriétés photophysiques des complexes de polypyridyl de Ru(II).

Les complexes de Ru(II) avec des ligands bidentés ont des émissions qui dépendent de la basicité relative des *N*-hétérocycles. Bien que ces complexes sont électrochimiquement et photophysiquement attrayant, le problème de la stéréopurité ne peut être évité. Une conception soignée du type de ligand nous permet de synthétiser un ligand bis-bidentate qui est utile pour surmonter le problème de stéréopurité. En raison de la spécialité du ligand bis-bidentate, son complexe diruthénium(II,II) présente une grande diastéréosélectivité sans séparation chirale. Alors que l'unité de **hpp** agit comme un nucléophile dans le mécanisme de C-N réaction de couplage croisé, il peut également agir en tant que groupe partant, lorsqu'il est activé avec un complexe de monoruthénium.

Les complexes achiraux de Ru(II) avec les ligands tridentés présentent des meilleures propriétés photophysiques en comparason avec les prototypes $[Ru(tpy)_2]^{2+}$ ($tpy = 2,2': 6', 2''$ -terpyridine). L'introduction de deux unités de **hpp** dans les ligands tridentates rend le complexe de Ru(II) en tant que 'absorbeur noir' et comme 'NIR émetteur' (NIR = de l'anglais, Near Infra-Red). Cet effet est une conséquence d'une meilleure géométrie de coordination octaédrique autour de l'ion Ru(II) et de la forte donation σ des unités **hpp**. Les complexes du Re(I) avec des ligands tridentates présentent un comportement redox intéressant et ils émettent dans le bleu. L'oxydation quasi-réversible du métal est contrôlée par la donation σ des fragments **hpp**, tandis que la réduction du ligand est régie par la nature électronique du motif *N*-hétérocycle central du ligand lui-même.

Cette thèse présente également l'auto-assemblage des métal-chromophores comme 'métallo-ligands' pour former des espèces supramoléculaires discrètes utilisant des complexes neutres. Les synthèses et propriétés des métaux-chromophores précités et les supramolécules sont discutées.

Mots-clés : métal-chromophore, donation σ , transfert de charge, couplage C-N, l'électrochimie, photophysique, cristallographie aux rayons X, théorie de la fonctionnelle de la densité, stéréopureté, émetteur bleu/rouge/NIR.

Table of Contents

Abstract	i
Résumé	iii
Table of Contents	v
List of Tables	ix
List of Figures	xiii
List of Charts and Schemes	xvii
List of abbreviations	xviii
Acknowledgements	xxiii
Chapter 0 : General Introduction	1
0.1. Different sources of emission	2
0.2. Tuning of emission	4
0.3. Luminescent Ru(II)-polypyridyl complexes	8
0.4. Objectives of the Research	10
0.5. References	11
Chapter 1 : Introduction	15
1.1. Introduction	15
1.2. Ruthenium(II) complexes of functionalized 2,2':6',2''-terpyridine (tpy) ligands	18
1.2.1. Direct incorporation of an electron-withdrawing or electron-donating substituent onto tpy	18
1.2.2. Incorporation of extended π -conjugation onto tpy	20
1.2.2. (A) Incorporation of extended π -conjugation onto tpy with acetylene as spacer	20
1.2.2. (B) Direct incorporation of extended π -conjugation onto tpy	21
1.2.3. Co-planarity of aromatic groups on the tpy ligand	22
1.3. π Electron Accepting Ability	23
1.3.1. Introduction of a 2,4(dipyrid-2'-yl)triazine (dpt) unit	23
1.3.2. Introduction of a central diazine unit	24
1.3.3. Introduction of peripheral diazine units	25
1.4. Increasing the energy of the 3MC state	26
1.4.1. σ -Donating ability	26
1.4.1. (A) σ -Donating ability of cyclometallating ligands	26
1.4.1. (B) Alternative <i>N</i> -heterocycles as strong σ donors	28
1.4.1. (B.i) Pyridine ring attached with fused benzimidazolyl ring containing two N	29
1.4.1. (B.ii) Pyridine ring attached with anionic triazole and tetrazole rings containing three N and four N atoms, respectively	30
1.4.1. (B.iii) Incorporation of carbene unit	30
1.4.2. Expanding the chelate ring	31

1.4.2. (A) Single unit expansion to form one six-membered chelate ring.....	31
1.4.2. (B) Double unit expansion to form two six-membered chelate rings with broken π -conjugation.....	32
1.4.2. (C) Double unit expansion to form two six-membered chelate rings with extended π -conjugation	34
1.4.2. (D) Double unit expansion to form two six-membered chelate rings with guanidine backbone	35
1.5. Bichromophoric Systems.....	35
1.6. Summary and outlook.....	37
1.7. References.....	38
Chapter 2: Red Emitting [Ru(bpy)₂(N-N)]²⁺ Photosensitizers: Emission from a Ruthenium(II)-to-2,2'-Bipyridine ³MLCT State in the Presence of Neutral Ancillary 'Super Donor' Ligands	43
2.1. Résumé.....	43
2.2. Table of Content Graphic	46
2.3. Abstract.....	46
2.4. Introduction.....	47
2.5. Experimental Section.....	48
2.5.1 Materials, methods and instrumentations	48
2.6. Results and Discussion	58
2.7. Conclusions.....	71
2.8. Acknowledgements.....	72
2.9. Supporting Information.....	72
2.10. References.....	72
Chapter 3: Stereoselective formation of a meso-diruthenium(II,II) complex and tuning the properties of its monoruthenium analogues	77
3.1. Résumé.....	77
3.2. Table of Content Graphic	78
3.3. Abstract.....	79
3.4. Introduction.....	80
3.5. Experimental section.....	82
3.6. Results and Discussion	88
3.7. Conclusion	102
3.8. Acknowledgment	103
3.9. Supporting Information.....	103
3.10. References.....	103
Chapter 4 : Near Infra-Red emitting Ru(II) complexes: structural, electrochemical and photophysical investigations	109
4.1. Résumé.....	109
4.2. Table of Content Graphic	111
4.3. Abstract.....	113
4.4. Introduction.....	113

4.5. Experimental Section.....	116
4.6. Results and Discussion	124
4.7. Conclusion	136
4.8. Supporting Information.....	137
4.9. References.....	137
Chapter 5: (A) Tuning the structural and electronic properties of rare Re(I)- complexes of κ^3N-tridentate heterocyclic ligands	143
5A.1. Résumé.....	143
5A.2. Table of Content Graphic.....	144
5A.3. Abstract	144
5A.4. Introduction.....	145
5A.5. Experimental section.....	145
5A.6. Results and Discussion	150
5A.7. Conclusion	157
5A.8. Supporting Information.....	158
5A.9. References.....	158
Chapter 5: (B) One- and two-dimensional polymerisation of homoleptic M(II)- complexes of 4'-(3-pyridyl)-2,2';6',2''-terpyridine in the solid state: A combined study by XRD, Cyclic Voltammetry, NMR and UV-vis Spectroscopies	161
5B.1. Résumé.....	161
5B.2. Table of content graphic.....	162
5B.3. Abstract	163
5B.4. Introduction.....	163
5B.5. Experimental section.....	165
5B.6. Results and Discussion.....	170
5B.7. Conclusions.....	183
5B.8. Acknowledgements	184
5B.9. Notes and references	184
Chapter 5: (C) Self-Assembly of supramolecular triangles with neutral directing units	187
5C.1. Résumé.....	187
5C.2. Table of content graphic.....	188
5C.3. Abstract	189
5C.4. Introduction.....	189
5C.5. Experimental section.....	189
5C.6. Results and Discussion.....	192
5C.7. Conclusions.....	201
5C.8. Acknowledgements	201
5C.9. Notes and references	201
Chapter 6: General Conclusion and perspectives	205
6.1. Conclusion and perspectives : Chapter 2.....	205
6.2. Conclusion and perspectives : Chapter 3.....	207

6.3. Conclusion and perspectives : Chapter 4.....	209
6.4. Conclusion and perspectives : Chapter 5.....	210
6.5. References.....	214
Annexes	I
SI – Chapter 2 : Supplementary Information.....	II
SI – Chapter 3 : Supplementary Informations.....	XX
SI – Chapter 4 : Supplementary Informations.....	XXXIX
SI – Chapter 5 : (A) Supplementary Informations.....	LXII
Appendix	LXXI
Appendix 1 : CCDC numbers for Chapters 2, 3, 4, 5A and 5B.....	LXXI
Appendix 2 : Crystal Data for Chapter 2.....	LXXII
Appendix 3 : Crystal Data for Chapter 3.....	LXXXIX
Appendix 4 : Crystal Data for Chapter 4.....	CXV
Appendix 5 : Crystal Data for Chapter 5A.....	CXLII
References.....	CLXIV

List of Tables

Table II-1. Crystal Data and Structure Refinement Information for 2-2a , 2-1b , 2-3b and 2-4b · 5C₂H₆O · 2H₂O	58
Table II-2. Redox data of complexes (2-1b)-(2-5b) in dry, degassed acetonitrile (V).....	65
Table II-3. Absorption data in deaerated CH ₃ CN solutions for (2-1b)-(2-5b).....	67
Table II-4. Photophysical data in deaerated CH ₃ CN solutions for complexes (2-1b)-(2-5b).....	70
Table III-1. Crystal data and details of the structure determination for 3-L1 , 3-(1-meso) ·(2C₂H₃N), 3-2 ·(8C₃H₆O), 3-3 and 3-4 ·(C₃H₆O).....	88
Table III-2. Redox data of 3-L1 and complexes 3-(1-meso) to 3-4 in dry, degassed acetonitrile with some benchmark complexes.	97
Table III-3. Electronic absorption data of 3-L1 and complexes 3-(1-meso) to 3-4 in dry, degassed acetonitrile with some benchmark complexes.	100
Table III-4. Photophysical data in deaerated CH ₃ CN solutions for complexes 3-(1-meso) to 3-4	101
Table IV-1. Crystallographic data for ligand 4-L1 , and complexes 4-1 ·(6(C₃H₆O), 4-2 ·(C₃H₆O), 4-3 ·(C₃H₆O), 4-4 ·(8(C₃H₆O))·(H₂O).....	123
Table IV-2. Electrochemical data of ligand 4-L1 , Ru(II) complexes 4-1 to 4-4 and some benchmark complexes.	130
Table IV-3. Electronic absorption data in dry, deaerated CH ₃ CN solutions of ligands 4-L1 , 4-L2 , complexes 4-1 to 4-4 and some benchmark complexes.....	133
Table IV-4. Photophysical data complexes 4-1 to 4-4 and some benchmark complexes. 135	
Table VA-1. Crystal data and details of the structure determination for 5A-1 , 5A-2	149
Table VA-2. Redox data of 5A-L1 , 5A-L2 and complexes 5A-1 and 5A-2 in dry, degassed acetonitrile with some benchmark complexes.	153
Table VA-3. Electronic absorption and emission data of 5A-L1 , 5A-L2 and complexes 5A-1 and 5A-2 in dry, degassed acetonitrile.....	155
Table VA-4. Infrared Frequencies: Observed vs. Calculated	157
Table VB-1. Crystal data and details of the structure determination for 5B-1b , 5B-3 · 2H₂O , 5B-3 · CH₃CN	170
Table VB-2. Redox data of complexes 5B-1a , 5B-2 to 5B-5 in dry, degassed acetonitrile.	181
Table VB-3. Electronic absorption data of complexes 5B-1a , 5B-2 to 5B-5 in dry, degassed acetonitrile.....	183
Table VC-1. Comparison of chemical shifts (in ppm) of different protons in complexes 5C-1 to 5C-5 and that of their corresponding ligands.....	194
Table VC-2. Redox data of complexes 5C-1 to 5C-4 and some benchmark complexes.	198

Table VC-3. UV-vis absorption data of complexes 5C-1 , 5C-2 and model complex 5C-4 with their respective precursors.....	200
Table II-S1. Comparison of bond distances and angles in 2-1b , 2-3b and 2-4b from X-ray and DFT studies.....	IV
Table II-S2. Electronic absorption data of ligands (2-1a)-(2-5a).....	V
Table II-S3. MO Composition of 2-1b²⁺ in Singlet (<i>S</i> =0) Ground State (b3lyp/LanL2DZ(f)[Ru]6-31G**[C,H,N]).....	V
Table II-S4. Selected Transitions from TD-DFT calculations of 2-1b²⁺ in the Singlet Ground State (b3lyp/LanL2DZ(f)[Ru]6-31G**[C,H,N], CPCM (CH ₃ CN)).....	VII
Table II-S5. MO Composition of 2-3b²⁺ in Singlet (<i>S</i> =0) Ground State (b3lyp/LanL2DZ(f)[Ru]6-31G**[C,H,N]).....	VII
Table II-S6. Selected Transitions from TD-DFT Calculations of 2-3b²⁺ in the Singlet Ground State (b3lyp/LanL2DZ(f)[Ru]6-31G**[C,H,N], CPCM (CH ₃ CN)).....	IX
Table II-S7. MO Composition of 2-4b²⁺ in Singlet (<i>S</i> =0) Ground State (b3lyp/LanL2DZ(f)[Ru]6-31G**[C,H,N]).....	IX
Table II-S8. Selected Transitions from TD-DFT Calculations of 2-4b²⁺ in the Singlet Ground State (b3lyp/LanL2DZ(f)[Ru]6-31G**[C,H,N], CPCM (CH ₃ CN)).....	XI
Table II-S9. Comparison in bond distances and angles of two geometry optimized models of 2-1b²⁺ obtained by DFT calculations with and without the effect of CPCM (acetonitrile).	XII
Table II-S10. TD-DFT calculation of 2-1b²⁺ including CPCM (acetonitrile) starting with geometry optimized model, which was performed excluding CPCM.	XII
Table II-S11. TD-DFT calculation of 2-1b²⁺ including CPCM (acetonitrile) starting with geometry optimized model, which was performed including CPCM (acetonitrile).....	XII
Table II-S12. TD-DFT calculation of 2-1b²⁺ excluding CPCM starting with geometry optimized model, which was performed excluding CPCM.....	XIII
Table II-S13. Optimized Atomic coordinates obtained from DFT for 2-1b²⁺ in singlet ground state (b3lyp/LanL2DZ(f)[Ru]6-31G**[C,H,N]).	XIII
Table II-S14. Optimized Atomic coordinates obtained from DFT for 2-3b²⁺ in singlet ground state (b3lyp/LanL2DZ(f)[Ru]6-31G**[C,H,N]).	XV
Table II-S15. Optimized Atomic coordinates obtained from DFT for 2-4b²⁺ in singlet ground state (b3lyp/LanL2DZ(f)[Ru]6-31G**[C,H,N]).	XVI
Table III-S1. MO Composition of 3-(1-meso)⁴⁺ in singlet (<i>S</i> =0) Ground State (b3lyp/LanL2DZ(f)[Ru]6-31G**[C,H,N]).....	XXIII
Table III-S2. Selected transitions from TD-DFT calculations of 3-(1-meso)⁴⁺ in the singlet ground state (b3lyp/LanL2DZ(f)[Ru]6-31G**[C,H,N], CPCM (CH ₃ CN)).....	XXV
Table III-S3. MO Composition of 2²⁺ in singlet (<i>S</i> =0) ground state (b3lyp/LanL2DZ(f)[Ru]6-31G**[C,H,N,O]).....	XXVI

Table III-S4. Selected transitions from TD-DFT calculations of 3-2²⁺ in the singlet ground state (b3lyp/LanL2DZ(f)[Ru]6-31G**[C,H,N,O], CPCM (CH ₃ CN)).	XXVIII
Table III-S5. MO Composition of 3-3²⁺ in Singlet (<i>S</i> =0) Ground State (b3lyp/LanL2DZ(f)[Ru]6-31G**[C,H,N,O]).	XXVIII
Table III-S6. Selected Transitions from TD-DFT calculations of 3-3²⁺ in the Singlet Ground State (b3lyp/LanL2DZ(f)[Ru]6-31G**[C,H,N,O], CPCM (CH ₃ CN)).	XXX
Table III-S7. MO Composition of 3-4²⁺ in Singlet (<i>S</i> =0) Ground State (b3lyp/LanL2DZ(f)[Ru]6-31G**[C,H,N,O]).	XXXI
Table III-S8. Selected Transitions from TD-DFT calculations of 3-4²⁺ in the Singlet Ground State (b3lyp/LanL2DZ(f)[Ru]6-31G**[C,H,N,O], CPCM (CH ₃ CN)).	XXXIII
Table III-S9. Optimized Atomic coordinates obtained from DFT for 3-(1-<i>meso</i>)⁴⁺ in singlet ground state (b3lyp/LanL2DZ(f)[Ru]6-31G**[C,H,N]).	XXXIII
Table III-S10. Optimized Atomic coordinates obtained from DFT for 3-2²⁺ in singlet ground state (b3lyp/LanL2DZ(f)[Ru]6-31G**[C,H,N,O]).	XXXV
Table III-S11. Optimized Atomic coordinates obtained from DFT for 3-3²⁺ in singlet ground state (b3lyp/LanL2DZ(f)[Ru]6-31G**[C,H,N,O]).	XXXVI
Table III-S12. Optimized Atomic coordinates obtained from DFT for 3-4²⁺ in singlet ground state (b3lyp/LanL2DZ(f)[Ru]6-31G**[C,H,N,O]).	XXXVII
Table IV-S1. Comparison of bond distances and angles in 4-1 to 4-4 from X-ray and DFT studies.	XLI
Table IV-S2. MO composition of 4-1²⁺ in singlet (<i>S</i> =0) ground state (b3lyp/LanL2DZ(f)[Ru]6-31G**[C,H,N]).	XLIII
Table IV-S3. Selected transitions from TD-DFT calculations of 4-1²⁺ in the singlet ground state (b3lyp/LanL2DZ(f)[Ru]6-31G**[C,H,N], CPCM (CH ₃ CN)).	XLV
Table IV-S4. MO composition of 4-2²⁺ in singlet (<i>S</i> =0) ground state (b3lyp/LanL2DZ(f)[Ru]6-31G**[C,H,N]).	XLVI
Table IV-S5. Selected transitions from TD-DFT calculations of 4-2²⁺ in the singlet ground state (b3lyp/LanL2DZ(f)[Ru]6-31G**[C,H,N], CPCM (CH ₃ CN)).	XLVIII
Table IV-S6. MO composition of 4-3²⁺ in singlet (<i>S</i> =0) ground state (b3lyp/LanL2DZ(f)[Ru]6-31G**[C,H,N,Br]).	XLIX
Table IV-S7. Selected transitions from TD-DFT calculations of 4-3²⁺ in the singlet ground state (b3lyp/LanL2DZ(f)[Ru]6-31G**[C,H,N], CPCM (CH ₃ CN)).	LI
Table IV-S8. MO composition of 4-4²⁺ in singlet (<i>S</i> =0) ground state (b3lyp/LanL2DZ(f)[Ru]6-31G**[C,H,N]).	LII
Table IV-S9. Selected transitions from TD-DFT calculations of 4-4²⁺ in the singlet ground state (b3lyp/LanL2DZ(f)[Ru], 6-31G**[C,H,N], CPCM (CH ₃ CN)).	LIV
Table IV-S10. Optimized Atomic coordinates obtained from DFT for 4-1²⁺ in singlet ground state (b3lyp/LanL2DZ(f)[Ru]6-31G**[C,H,N]).	LV

Table IV-S11. Optimized Atomic coordinates obtained from DFT for 4-2²⁺ in singlet ground state (b3lyp/LanL2DZ(f)[Ru]6-31G**[C,H,N]).	LVI
Table IV-S12. Optimized Atomic coordinates obtained from DFT for 4-3²⁺ in singlet ground state (b3lyp/LanL2DZ(f)[Ru]6-31G**[C,H,N]).	LVIII
Table IV-S13. Optimized Atomic coordinates obtained from DFT for 4-4²⁺ in singlet ground state (b3lyp/LanL2DZ(f)[Ru]6-31G**[C,H,N]).	LIX
Table V-S1. Comparison of bond distances and angles in 5A-1 and 5A-2 .	LXIII
Table VA-S2. MO Composition of 5A-1¹⁺ in Singlet (<i>S</i> =0) Ground State (b3lyp/LanL2DZ(f)[Re]6-31G**[C,H,N,O]).	LXIII
Table VA-S3. Selected Transitions from TD-DFT calculations of 5A-1¹⁺ in the Singlet Ground State (b3lyp/LanL2DZ(f)[Re]6-31G**[C,H,N,O], CPCM (CH ₃ CN)).	LXV
Table VA-S4. MO Composition of 5A-2¹⁺ in Singlet (<i>S</i> =0) Ground State (b3lyp/LanL2DZ(f)[Re]6-31G**[C,H,N,O]).	LXV
Table VA-S5. Selected Transitions from TD-DFT calculations of 5A-2¹⁺ in the Singlet Ground State (b3lyp/LanL2DZ(f)[Re]6-31G**[C,H,N,O], CPCM (CH ₃ CN)).	LXVII
Table VA-S6. Optimized Atomic coordinates obtained from DFT calculations of 5A-1¹⁺	LXVII
Table VA-S7. Optimized Atomic coordinates obtained from DFT calculations of 5A-2¹⁺	LXVIII

List of Figures

Figure 0.1. Luminescent Pt complexes when the origin of emission is $^3\text{ILCT}$	2
Figure 0.2. Luminescent complexes when the origin of emission is $^3\text{LMCT}$	3
Figure 0.3. Benchmark high-performance phosphorescence emitters.....	4
Figure 0.4. Color versatility expressed by a series of six cationic Ir(III) complexes.....	5
Figure 0.5. Electronic excitation and emission profile in a luminescent complex.....	5
Figure 0.6. Emission spectra of $[\text{Pt}(\text{X}^{\wedge}\text{N}^{\wedge}\text{N})(\text{C}\equiv\text{CPh})]$ in alcoholic glass.	6
Figure 0.7. Ligand definitions and emission energies of a series of $[\text{Ir}(\text{L})_2(\text{acac})]$ complexes.....	6
Figure 0.8. Molecular orbital interaction in donor (D) and acceptor (A) moieties leading to a D-A monomer	7
Figure 0.9. Emission wavelengths of platinum complexes with DA system in CH_2Cl_2 at 77 K.....	7
Figure 0.10 $\lambda_{\text{max}}^{\text{em}}$, τ and Φ_{p} of some benchmark ruthenium complexes.....	9
Figure 1.1. Qualitative Jablonski diagram illustrating the electronic states of Ru(II) polypyridyl system and transitions among the states..	17
Figure 1.2. Photophysical data for donor-acceptor dyad Ru(II) complexes.....	20
Figure 1.3. Photophysical data for acetylene-substituted $\text{Ru}(\text{tpy})_2^{2+}$ complexes.	21
Figure 1.4. Photophysical data for 4'-tpy-substituted $\text{Ru}(\text{tpy})_2^{2+}$ complexes.....	21
Figure 1.5. Hetero- and homo-leptic Ru(II) complexes of tridentate ligands containing central diazine unit.....	25
Figure 1.6. Ru-polypyridyl complexes with various cyclometallating ligands.	28
Figure 1.7. Ru-polypyridyl complexes with σ -donating ligands.....	29
Figure 1.8. Ru-polypyridyl complexes with σ -donating carbene ligands and their photophysical data in EtOH:MeOH (80:20, v/v) at r.t.	31
Figure 1.9. Increasing ligand field strength by alleviating steric strain in tridentate ligands.....	32
Figure 1.10. Increasing ligand field strength by alleviating steric strain in tridentate ligands.....	33
Figure 1.11. Increasing ligand field strength by alleviating steric strain in tridentate ligands.....	34
Figure 1.12. Bichromophoric Ru(II) complexes of tridentate ligands.....	37
Figure 1.13. Top three complexes with the longest r.t. excited-state lifetimes.	38
Figure 2.1. Crystal structure of ligand 2-2a	60
Figure 2.2. Crystal structure of 2-1b	61
Figure 2.3. Crystal structure of 2-4b	61
Figure 2.4. Crystal structure of 2-3b	61
Figure 2.5. Kohn-Sham orbital sketches for HOMO and LUMO molecular orbitals for 2-1b $^{2+}$, 2-3b $^{2+}$, 2-4b $^{2+}$	65

Figure 2.6. Cyclic voltammogram of 2-1b (at 200 mV/s) in dry, degassed acetonitrile.....	66
Figure 2.7. Electronic absorption spectra of compounds (2-1b)-(2-5b) at room temperature in deareated acetonitrile.....	67
Figure 2.8. Typical figure showing the overlap of experimental electronic absorption spectrum with oscillator strength from TD-DFT calculation of 2-1b ²⁺ ..	68
Figure 2.9. Calculated frontier MO energies of the modeled 2-1b , 2-3b and 2-4b complexes.....	69
Figure 2.10. Emission spectra of compounds 2-1b to 2-5b	70
Figure 3.1. Comparison of ¹ H NMR spectra of 3-(1-meso)	91
Figure 3.2. Perspective view of ligand 3-L1	92
Figure 3.3. Perspective view of 3-(1-meso)	93
Figure 3.4. Perspective view of 3-2	93
Figure 3.5. Perspective view of 3-3	94
Figure 3.6. Perspective view of 3-4	94
Figure 3.7. Cyclic voltammogram (bold) and differential pulse voltammogram (dotted) of 3-(1-meso)	97
Figure 3.8. Calculated frontier MO energies of all the modelled complexes 3-(1-meso) to 3-4	98
Figure 3.9. Electronic absorption spectra of compounds 3-(1-meso) to 3-4	100
Figure 3.10. Uncorrected emission spectra of complexes 3-(1-meso) to 3-4	101
Figure 4.1. Strategies to increase the emissive ³ MLCT lifetime of Ru(II)-polypyridyl complexes.....	116
Figure 4.2. ORTEP views of the X-ray crystal structures of ligand 4-L1 and complexes 4-1 to 4-4	127
Figure 4.3. Cyclic voltammogram of the complexes 4-2 , 4-3 and 4-4 in dry degassed acetonitrile.....	131
Figure 4.4. Calculated frontier MO energies of the modeled 4-1 to 4-4 with [Ru(tpy) ₂] ²⁺	131
Figure 4.5. Overlay of experimental absorption spectra of the complexes 4-1 , 4-2 , 4-3 and 4-4 in acetonitrile with their predicted transitions and oscillator strength, calculated by TD-DFT.....	133
Figure 4.6. Normalized emission spectra of complexes 4-1 , 4-2 and benchmark complex [Ru(Ph-tpy) ₂] ²⁺ in dry, degassed acetonitrile at room temperature.	136
Figure 5A.1. Perspective views of complexes 5A-1 and 5A-2	152
Figure 5A.2. Cyclic voltammogram of complexes 5A-1 and 5A-2	153
Figure 5A.3. Calculated frontier MO energies of the modeled complexes 5A-1 and 5A-2	154
Figure 5A.4. Overlay of experimental absorption spectra and calculated oscillator strengths at different wavelengths of 5A-1 and 5A-2	155
Figure 5A.5. ATR-IR spectra of complexes 5A-1 and 5A-2	157

Figure 5B.1. Comparison in chemical shifts of different protons of 5B-1a and 5B-2 by ^1H NMR spectroscopy	172
Figure 5B.2. Comparison of chemical shifts of different protons of 5B-3 and 5B-4 by ^1H NMR spectroscopy.....	173
Figure 5B.3. Perspective view of $[\mathbf{5B-1b}]^{2+}$	174
Figure 5B.4. Packing diagram of 5B-1a	175
Figure 5B.5. Packing diagram of 5B-1a	175
Figure 5B.6. Part of the infinite 1D-ribbon of 5B-1b	175
Figure 5B.7. Perspective view of complex 5B-3	176
Figure 5B.8. Part of the infinite 2D-sheet of packing of complex 5B-3	177
Figure 5B.9. Perspective view of complex 5B-5	178
Figure 5B.10. Part of the crystal packing of 5B-5	178
Figure 5B.11. Cyclic voltammogram of 5B-2 in dry, degassed acetonitrile	179
Figure 5B.12. Electronic absorption spectra of compounds 5B-1a , 5B-2 to 5B-5 at room temperature in deaerated acetonitrile.....	182
Figure 5C.1. ^1H NMR spectrum of complex 5C-1	193
Figure 5C.2. Overlay of observed high-res LC-TOF MS of $[\text{C}_{120}\text{H}_{84}\text{N}_{24}\text{Fe}_3\text{Pd}_3\text{Cl}_3(\text{PF}_6)_2]^{4+}$	195
Figure 5C.3. Overlay of observed high-res LC-TOF MS of $[\text{C}_{120}\text{H}_{84}\text{N}_{24}\text{Fe}_3\text{Pd}_3\text{Cl}_3(\text{PF}_6)]^{5+}$	196
Figure 5C.4. High-res LC-TOF MS of complex 5C-2 or $\text{C}_{120}\text{H}_{84}\text{N}_{24}\text{Ru}_3\text{Pd}_3\text{Cl}_3(\text{PF}_6)_6$	196
Figure 5C.5. Overlay of observed high-res LC-TOF MS of $(\mathbf{5C-2})^{6+}$ or $[\text{C}_{120}\text{H}_{84}\text{N}_{24}\text{Ru}_3\text{Pd}_3\text{Cl}_3]^{6+}$	196
Figure 5C.6. Overlay of observed high-res LC-TOF MS of $(\mathbf{5C-2})^{4+}$ or $[\text{C}_{120}\text{H}_{84}\text{N}_{24}\text{Ru}_3\text{Pd}_3\text{Cl}_3(\text{PF}_6)_2]^{4+}$	197
Figure 5C.7. Overlay of observed high-res LC-TOF MS of $(\mathbf{5C-2})^{5+}$ or $[\text{C}_{120}\text{H}_{84}\text{N}_{24}\text{Ru}_3\text{Pd}_3\text{Cl}_3(\text{PF}_6)]^{5+}$	197
Figure 5C.8. Cyclic voltammograms of complex 5C-1 and Fe-metallo-ligand.....	198
Figure 5C.9. Cyclic voltammograms of complex 5C-2	199
Figure 5C.10. Electronic absorption spectra of complexes 5C-1 , 5C-2 and their respective metallo-ligands.....	200
Figure 6.1. Mixture of possible diastereomers in a dinuclear complex.....	206
Figure 6.2. ^1H NMR spectrum of complex 6-3 in CD_3CN	208
Figure 6.3. Comparison of ^1H NMR spectra of complex 6-3 in presence of 1 equivalent of ethylene glycol in CD_3CN	209
Figure 6.4. Proposed structure of self-assembly of complex 5B-2 , using neutral, <i>trans</i> - PtR_2Cl_2 (R = 1-pyrynylacetylde) as binder.....	213
Figure 2.S1. Packing diagram of ligand 2-2a along normal to 100 plane.....	III
Figure 2.S2. Kohn-Sham orbital sketches in different MOs for $\mathbf{2-1b}^{2+}$	VI
Figure 2.S3. Kohn-Sham orbital sketches in different MOs for $\mathbf{2-3b}^{2+}$	IX
Figure 2.S4. Kohn-Sham orbital sketches in different MOs for $\mathbf{2-4b}^{2+}$	XI

Figure 3.S1. LC-MS of reaction ii using an achiral support.....	XXI
Figure 3.S2. View of capped stick model of <i>rac</i> - $\Lambda\Lambda$ or $\Delta\Delta$ -diastereomer, as the initial coordinates for DFT calculation.....	XXII
Figure 3.S3. View of capped stick model of 3-L1	XXII
Figure 3.S4. Cyclic voltammogram of 3-3 and 3-4 in dry, degassed CH ₃ CN.....	XXIII
Figure 3.S5. Kohn-Sham molecular orbital sketches for 3-(1-meso) ⁴⁺	XXIV
Figure 3.S6. Overlap of experimental electronic absorption spectra with oscillator strength from TD-DFT calculation of 3-(1-meso) ⁴⁺	XXV
Figure 3.S7. Kohn-Sham molecular orbital sketches for 3-2 ²⁺	XXVII
Figure 3.S8. Overlap of experimental electronic absorption spectrum with oscillator strength from TD-DFT calculation of 3-2 ²⁺	XXVII
Figure 3.S9. Kohn-Sham molecular orbital sketches for 3-3 ²⁺	XXIX
Figure 3.S10. Overlap of experimental electronic absorption spectrum with oscillator strength from TD-DFT calculation of 3-3 ²⁺	XXX
Figure 3.S11. Kohn-Sham Electron density sketches for 3-4 ²⁺	XXXII
Figure 3.S12. Overlap of experimental electronic absorption spectra with oscillator strength from TD-DFT calculation of 3-4 ²⁺	XXXII
Figure 4.S1. Packing diagram of ligand 4-L1 along crystallographic <i>a</i> -axis.	XL
Figure 4.S2. Perspective views of complexes 4-1 to 4-4 , as cations only, with complete labeling.....	XL
Figure 4.S3. Kohn-Sham Electron density sketches for different MOs for 4-1 ²⁺	XLIV
Figure 4.S4. Kohn-Sham electron density sketches for different MOs for 4-2 ²⁺	XLVII
Figure 4.S5. Kohn-Sham electron density sketches for different M.O.s for 4-3 ²⁺	L
Figure 4.S6. Kohn-Sham electron density sketches for different M.O.s for 4-4 ²⁺	LIII
Figure 5.S1. Kohn-Sham molecular orbital diagrams of 5A-1 ¹⁺	LXIV
Figure 5.S2. Kohn-Sham molecular orbital diagrams of 5A-2 ¹⁺	LXVI

List of Charts and Schemes

Scheme 1.1. General syntheses of substituted 2,2':6',2''-terpyridines (tpy-X/Y) and their homo- and hetero-leptic Ru(II) complexes.	19
Scheme 1.2. Syntheses of a variety of substituted pyrimidyl terpyridine heteroleptic Ru(II) complexes and their r.t. excited-state lifetimes.	23
Scheme 1.3. Syntheses of tridentate dpt-based ligands and its homo- and hetero-leptic Ru(II) complexes with photophysical data.	24
Scheme 1.4. Strong σ -donor ligand dgpy and its heteroleptic Ru(II) complex.	35
Chart 2.1. 1,3,4,6,7,8-Hexahydro-2 <i>H</i> -pyrimido[1,2- <i>a</i>]pyrimidine (H-hpp) attached to various <i>N</i> -heterocycles.	48
Scheme 2.1. Syntheses of the complexes 2-1b to 2-5b	59
Chart 3.1. 1,3,4,6,7,8-Hexahydro-2 <i>H</i> -pyrimido[1,2- α]pyrimidine (H-hpp) attached to pyrimidine (3-L1 , dgpm) and some benchmark ligands.	81
Scheme 3.1. Syntheses of ligand 3-L1 and complexes 3-(1-meso) , 3-2 , 3-3 , 3-4	89
Scheme 4.1. Syntheses of the ligands 4-L1 and 4-L2	124
Scheme 4.2. Syntheses of the terpyridine (tpy, 4-1 and 4-2) and 2,4-dipyrid-2'-yl-triazine (dpt, 4-3 and 4-4) containing complexes.	125
Scheme 5A.1. Syntheses of ligands 5A-L1 , 5A-L2 and complexes 5A-1 and 5A-2	150
Scheme 5B.1. Syntheses of ligand 5B-L and complexes 5B-1a , 5B-1b , 5B-2 , 5B-3 , 5B-4	171
Scheme 5C.1. Syntheses of complexes 5C-1 and 5C-2	192
Chart 5C.1. Model complexes 5C-3 to 5C-5 with proton labelling scheme.	194
Scheme 6.1. Homocoupling of mononuclear complexes 2-2b and 2-4b	206
Scheme 6.2. Proposed mechanism of solvolysis of the complex 6-3	207
Scheme 6.3. Synthesis of complex 6-7 to improve photophysical properties of complex 5A-1	211
Scheme 6.4. Proposed scheme of supramolecular cube formation using vacant coordination sites of a trans-PtR ₂ unit.	212

List of abbreviations

ACN	Acetonitrile
ATR	Attenuated total reflectance
ATR-IR	Attenuated total reflectance infrared
BINAP	2,2'-bis(diphenylphosphino)-1,1'-binaphthyl
B3LYP	Becke, three-parameter, Lee-Yang-Parr exchange-correlation functional
bpy	2,2'-Bipyridine
br	Broad
ⁿ Bu	ⁿ Butyl
CCD	Charged-Coupled Device
CIF	Crystallographic information file
CV	Cyclic voltamperometry
d	Doublet
dd	Doublet of doublet
ddd	Doublet of doublet of doublet
deg	Degree
DFT	Density functional theory
DCM	Dichloromethane
dgpy	2,6-Diguanidylpyridine
dgpm	4,6-Diguanidylpyrimidine
dgpz	2,6-Diguanidylpyrazine
DMF	<i>N,N'</i> -Dimethylformamide
DMSO	Dimethylsulfoxide
dpt	2,4-Dipyrid-2-yl-triazine
DPV	Differential pulse voltammetry
dt	Doublet of triplet
ED	Electron donor
EDG	Electron-donating group
ESI-MS	Electrospray ionization mass spectrometry
EWG	Electron-withdrawing group

equiv.	Equivalent
eq.	<i>cf.</i> Equiv.
Et	Ethyl
fwhm	Full-width at half-maximum
GOF	Goodness of fit
GS	Ground state
H-hpp	1,3,4,6,7,8-Hexahydro-2 <i>H</i> -pyrimido[1,2- <i>a</i>]pyrimidine
HOMO	Highest occupied molecular orbital
<i>I</i>	Luminescence intensity
IR	Infrared
ISC	Intersystem crossing
LANL2DZ	<i>Los Alamos National Laboratory 2 double ζ</i>
LMCT	Ligand-to-metal charge transfer
LUMO	Lowest occupied molecular orbital
m	Multiplet
Me	Methyl
MC	Metal-centered
MLCT	Metal-to-ligand charge transfer
(ML)LCT	Metal-ligand-to-ligand charge transfer
m/z	Ratio of mass to charge
NIR	Near Infra-Red
NMR	Nuclear magnetic resonance
OAc	Acetate
ORTEP	Oak Ridge thermal ellipsoid program
PCET	Proton coupled electron transfer
PCM	Polarized continuum model
Ph	Phenyl
phen	1,10-Phenanthroline
pm	Pyrimidine
ppm	Parts per million
PS	Photosensitizer

py	Pyridine or pyridyl
pz	Pyrazine
quint	Quintuplet
SCE	Standard calomel electrode
sh	Shoulder
SOMO	Singly occupied molecular orbital
SUMO	Singly unoccupied molecular orbital
SWV	Square-wave voltamperometry
t	Triplet
TBAP	Tetrabutylammonium hexafluorophosphate
td	Triplet of doublet
TD-DFT	Time-dependent Density Functional theory
THF	Tetrahydrofuran
TLC	Thin layer chromatography
tpy	2,2':6',2''-terpyridine
v:v	Volume:volume
UV	Ultraviolet
vis	Visible
XRD	X-ray diffraction

*In the loving memory of my parents, who always taught me how to fight in
hard times.*

Acknowledgements

I would like to begin by thanking my supervisor, Professor Garry Hanan for giving me the opportunity to carry out this research towards my PhD. His experience, advice and motivation have been fundamental to the completion of this thesis and as inspiration for the future.

This research would not have been possible without the financial assistance from the Natural Sciences and Engineering Research Council of Canada (NSERC), the Centre for Self-Assembled Chemical Structure (CSACS) and the Université de Montréal.

I want to thank all the supporting teams and services of Université de Montréal:

-Group XRD : Pr Frank Schaper, Dr Michel Simard, Françoise Bélanger-Gariépy and Dr Thierry Maris.

-Mass spectrometry service : Dr Alexandra Furtos, Marie-christine Tang and Karine Venne.

-NMR spectroscopy service : Dr Minh Tan Phan Viet, Dr Cédric Malveau, Sylvie Bilodeau and Antoine Hamel.

-Elemental analysis service : Elena Nadezhina and Françoise Bélanger-Gariépy.

I would like to thank the many graduate students and post doctoral fellows I have had the pleasure to work with Garry's group. A big thanks to the senior students who guided me in my early days in Canada, Dr Marie-Pierre Santoni, Dr Samik Nag, Daniel Chartrand and Mihaela Cibian. I wish to thank Daniel in particular for his patience, advice and insights, which have been in-valuable over the years. Thanks also go to the students who were part of the group, that I've worked during these years Baptiste Laramée-Milette, Carlos A. Ruiz Castro, Sophia Derossi, Janaina Ferreira, André Bessette, Nicholas Randell, Matthias Geist, Élodie Rousset, Brodie Reid and Mathieu Leblanc.

I would like to thank again Daniel and Mihaela who helped me in the revision of an article.

I would also like to thank the students from other research groups of Professor Schaper, Professor Zargarian, Professor Reber, Professor Lafleur and Professor Skene for

their friendly behaviour. I would like to thank Dr Andréanne Bolduc for taking the time to show me how to use the instruments in the Skene laboratory.

Additional thanks go to the groups of Prof. Sebastiano Campagna at the University of Messina, Italy and Dr. Nelsi Zaccheroni, University of Bologna, Italy for their collaboration with photophysical measurements.

I thank my parents, Late Smt Sandhya Paul and Sri Amal Kumar Paul for always believing in me, their motivation and encouragement in difficult times, my sisters Sayanti and Ananya for their friendship and responsibilities. I would also like to thank my cousin brothers Pradip and Arun and my friends for their help and co-operation during the difficult time of my PhD.

Finally, I thank heartfully my fiancée *Sneha* for her continuous support, encouragement and belief in me and her family for encouragement.

Chapter 0 : General Introduction

Room temperature phosphorescent transition metal complexes, containing Ru(II), Re(I), Ir(III), Au(III), Cu(I) and other metal ions emitting in the visible (red, green and blue) region, have been a major focus of research due to their wide and useful applications in organic light-emitting diodes (OLEDs),^{1,2} photovoltaic cells (PVCs),³ light-emitting electrochemical cells (LHCs),^{4,5} chemosensors,^{6,7} triplet-triplet annihilation based upconversion (TTAU),⁸ and molecular therapy.⁹ In recent years, near-infrared (NIR) phosphorescence beyond the visible region (700-2500 nm, 120 to 430 THz) has emerged as a promising research field with potential applications toward NIR-OLEDs,¹⁰ fiber optic telecommunication,¹¹ night-vision readable displays and real time *in vivo* cell-imaging systems, as biological tissues have minimal absorption and auto-fluorescence in the NIR region, allowing for deeper penetration of light compared to visible light.¹²

The origin of the research based on NIR absorbers and emitters stems from the fact that the maximum photon density of the incident radiation from the sun is in the NIR, which could allow commercialization of the harvested energy in the form of chemical energy. Nearly 50% of the energy from the sun reaching the Earth is in the form of NIR radiation.¹³ At present, one of the key limiting factors for organic solar cells or photovoltaic cells (PVCs) is the mismatch between the absorption spectrum of organic dyes and the solar emission spectrum, thus it is important to extend the absorption of organic dyes from the ultraviolet (UV)/visible into the NIR region.

Light-harvesting, luminescent transition metal complexes that absorb in the visible region and emit in the red-NIR region are more suitably applicable for device fabrication compared to the conventional organic emitters or fluorescent complexes based on lanthanides. The former class of compounds exhibit phosphorescence, which involves an inter-system crossing (ISC) from triplet excited-state to singlet ground-state ($T_1 \rightarrow S_0$), while the latter class of compounds display electronic transition between states of similar spin-multiplicity ($S_1 \rightarrow S_0$). Phosphorescent emitters possess several advantages over fluorescence emitters, e.g., (i) the $T_1 \rightarrow S_0$ electronic transition enables the harvest of both singlet and triplet excitons to achieve a maximum internal quantum efficiency of 100% in OLEDs,^{10,14} (ii) phosphorescence from transition metal complexes provides a longer excited-state lifetime, up to milliseconds,^{15,16} (iii) phosphorescence exhibits larger Stokes'

shifts compared to fluorescence due to the energy loss in intersystem crossing between S_1 and T_1 , thus decreasing spectral interference between the excitation light and the phosphorescent emission, (iv) they can serve as oxygen sensors,¹⁷ as the triplet ground state of oxygen quenches the triplet emissive state of the luminophore by through-space energy transfer.

0.1. Different sources of emission

Based on the presence of different metal centers, chemical structures and triplet state energy levels of the ligands, local environment, and intermolecular interaction the emission may originate from different sources, as discussed below.

(A) Metal-centered (MC) d-d excited state. Low-energy MC states originate from hopping of electrons between bonding (d_π) and antibonding (d_σ^*) orbital in a partially filled d-shell of a metal-center. The features of this emission are (i) they have especially low-transition probability as these transitions are Laporte forbidden, (ii) the MC-based absorption interferes with the emission, (iii) broad and structureless emission bands, (iv) relatively matrix-independent but temperature dependent. Typical example includes weak emission from $\text{Pt}(\text{bpy})(\text{Cl})_2$ (bpy = 2,2'-bipyridine) at ~ 620 nm at 77 K.¹⁸

(B) Intra-ligand (IL) or ligand-centered (LC) charge transfer. The emission originates from the transfer of an electron between two π -orbitals based on ligand chromophores. The features of this kind of emission are (i) relatively independent on the perturbation of different metal-coordination to the ligand, (ii) generally solvent-independent. Typical examples include emission from $\text{Pt}(\text{TPP})$ (TPP = *meso*-tetraphenylporphyrin)¹⁹ and $[\text{Pt}(\text{bpy})(\text{en})]^{2+}$ (en = ethylenediamine).²⁰ The emission from the former appears at 668 nm and 734 nm in CH_2Cl_2 at room temperature, while the emission from TPP occurs at 658 nm and 726 nm under similar experimental condition.¹⁹

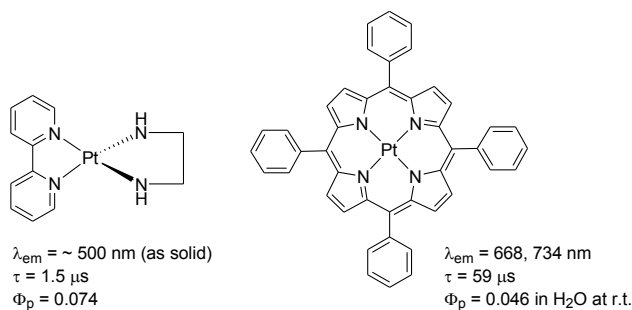


Figure 0.1. Luminescent Pt complexes when the origin of emission is $^3\text{ILCT}$.^{19,20}

(C) Ligand-to-metal charge transfer (LMCT). Transition metal complexes with redox active metal and ligand moieties and a high oxidation state of the metal center exhibit this kind of emission profile. Transition metal complexes with metal center with full d-shell but electronically unsaturated valence shell can also exhibit this kind of emission. The features of this emissions are (i) red-shifted emission due to a low energy-gap between the ligand-centered highest occupied molecular orbital (HOMO) and metal-centered lowest unoccupied molecular orbital (LUMO), (ii) associated with low phosphorescence quantum efficiency (Φ_p) compared to ILCT. Typical examples include emission from Ta(V) complexes²¹ or polynuclear d^{10} complexes consisting Au(I) or Cu(I).²²

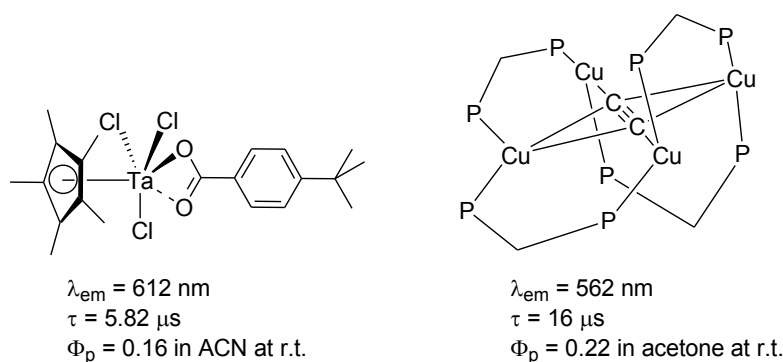


Figure 0.2. Luminescent complexes when the origin of emission is ³LMCT.^{21,22}

(D) Metal-to-ligand charge transfer (MLCT). Triplet MLCT transitions involve electronic transitions from metal-based d orbitals to ligand-based π^* antibonding orbitals. These transitions are commonly observed in the middle- and late-transition-metal complexes having relatively low oxidation potentials. Features of this transition are (i) dependent strongly on the reduction potential of the ligand and oxidation potential of the metal, thus can be fine-tuned by controlling the HOMO-LUMO gap, (ii) the transition can have both short and long-lived room temperature, excited-state lifetimes depending on the energy of the electronic-states. Typical examples include $[\text{Ru}(\text{bpy})_3]^{2+}$,²³ $[\text{Pt}(\text{ppy})(\text{acac})]$ (where ppy = 2-phenylpyridyl),²⁴ $[\text{Ir}(\text{ppy})_2(\text{acac})]^{25}$ although for the latter two compounds contribution from ³ILCT can not be avoided. Due to high emission efficiency these complexes often find commercialized applications in high-performance phosphorescent OLED device fabrication.

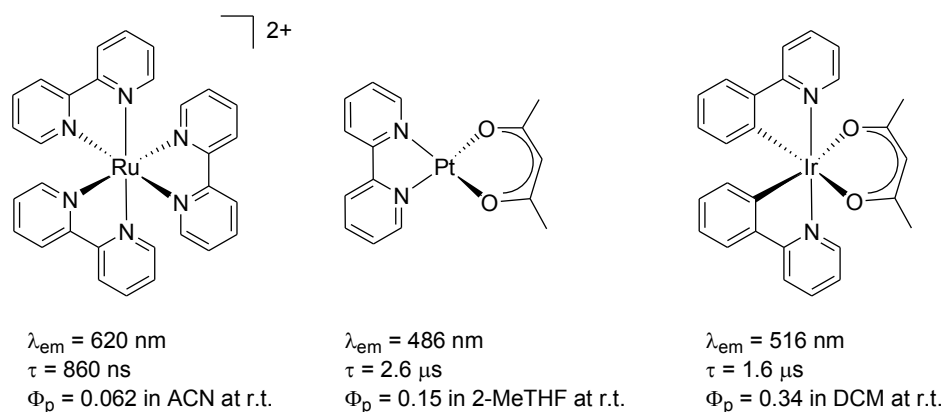


Figure 0.3. Benchmark high-performance phosphorescence emitters.²³⁻²⁵

(E) Metal-metal-to-ligand charge transfer. Based on a series of discrete d^8-d^8 binuclear Pt(II) complexes, namely, $[(Pt(tpy))_2(\mu-L)]^{n+}$ ($tpy = 2,2':6',2''$ -terpyridine, $L =$ bis-monodentate ligand), which exhibit red-to-NIR emission ($\lambda_{em} = 630-730 \text{ nm}$), depending on the Pt–Pt distances ($3.00-3.43 \text{ \AA}$), in the solid state at RT, it has been proposed that the emission originates from a ${}^3[d\sigma^*(d_z^2(Pt)) \rightarrow \pi^*(\text{bridging ligand})]$ transition.²⁶ As the intra-platinum distance increases from 3.00 \AA in $[(Pt(tpy))_2(\mu-L)]^{n+}$ ($L =$ arginine) to 3.43 \AA in $[(Pt(tpy))_2(\mu-L)]^{n+}$ ($L =$ pyrazole) the energy of emission displays a blue-shift from 730 nm to 630 nm .

0.2. Tuning of emission

The electronic and photophysical properties of luminescent transition metal complexes can be fine-tuned by controlling the HOMO-LUMO energy gap. The red shift in the absorption spectra and concomitantly the emission spectra results from the lowering of the energy gap and is the key to the design of NIR emitters. A detailed overview explaining how to red-shift the emission wavelength and to increase the r.t. excited-state lifetimes with mononuclear Ru(II)-tridentate complexes is found in Chapter 1. The factors governing the HOMO-LUMO energy gap are summarized below.

0.2.1. Effect of presence of electron donating groups (EDGs) and/or electron withdrawing groups (EWGs)

The nature and position of electron-donating or -withdrawing substituents can change the electronic and photophysical properties of a complex. Typically, electron-withdrawing substituents tend to stabilize the HOMO by removing electron density from

the metal and result in a blue shift of emission, whereas donating groups have an inverse effect. The cyclometallated and ancilliary ligands can be separately substituted with different EDGs or EWGs, allowing deliberate control of the excited-state from blue-to-red region, as shown in Figure 0.4.²⁷ Other effects, such as vibrational coupling between the emitting $^3\text{MLCT}$ state and the ground state (GS) and the energy-gap law are represented by Figure 0.5.

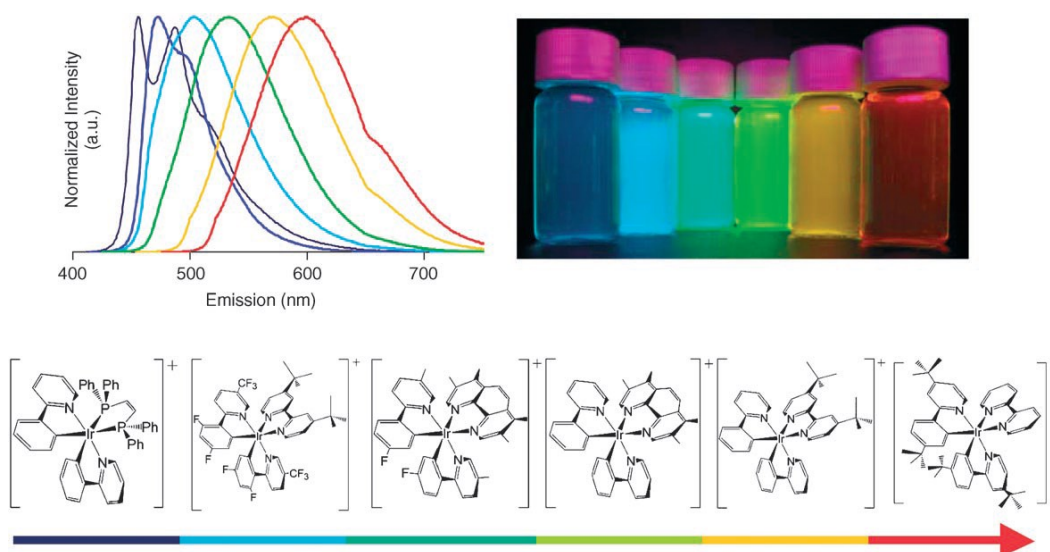


Figure 0.4. Color versatility expressed by a series of six cationic Ir(III) complexes. The evolution of ^3LC (vibrationally structured, high-energy bands) and $^3\text{MLCT}$ character (structureless, low-energy bands) in the luminescence spectra are indicative of a mixed excited state (reproduced with permission from ref 27).

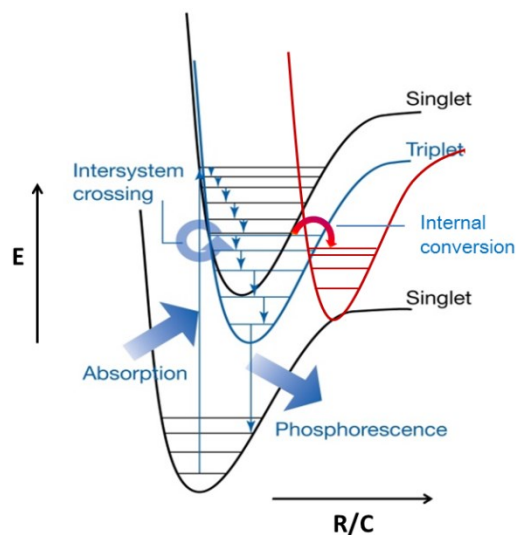


Figure 0.5. Electronic excitation and emission profile in a luminescent complex.

0.2.2. Effect of heteroatoms/heterocycles in the ligand

Complexes containing polarizable heteroatoms such as sulfur and oxygen incorporated in the ligand are much easier to oxidize and display lower transition energies. As shown in Figure 0.6, the complexes containing the thienyl ($X = S$) or furyl ($X = O$) moiety as cyclometalated carbon donors exhibit red-shifted emission compared to that of a $[\text{Pt}(\text{phbpy})(\text{C}\equiv\text{CPh})]$ ($X = \text{CH}=\text{CH}$) complex.²⁸

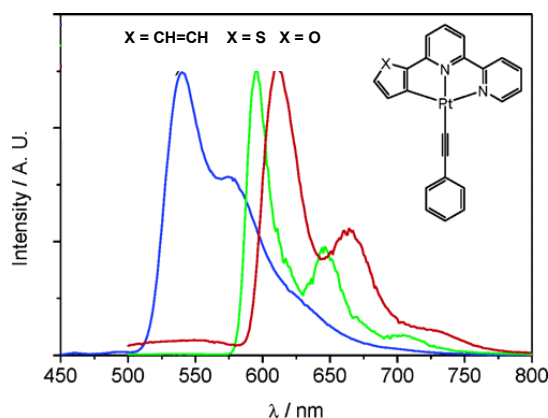


Figure 0.6. Emission spectra of $[\text{Pt}(\text{X}^{\text{N}^{\text{N}}})(\text{C}\equiv\text{CPh})]$ in alcoholic glass at 77 K (reproduced with permission from ref 28).

0.2.3. Effect of π -conjugation in the ligand

For luminescent transition metal complexes, one of the most effective ways to red-shift the emission wavelength and increase the emission efficiency is to increase the length of π -conjugation in the ligand. For example, in comparison to $[\text{Ir}(\text{ppy})_2(\text{acac})]$, other $[\text{Ir}(\text{L})_2(\text{acac})]$ complexes with larger π -conjugated systems of either of an isoquinoline or a naphthyl group, show a red-shift in the emission spectra (Figure 0.7).²⁹

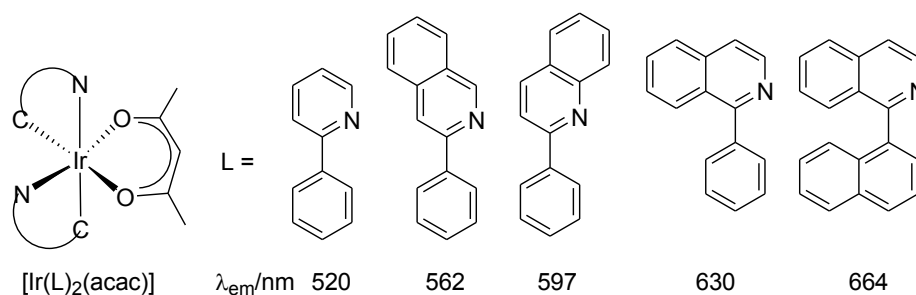


Figure 0.7. Ligand definitions and emission energies of a series of $[\text{Ir}(\text{L})_2(\text{acac})]$ complexes.²⁹

0.2.4. Effect of donor-acceptor (DA) system in the ligand

The DA system is a strategy for phosphorescent transition metal complexes to achieve the purpose of lowering the HOMO-LUMO energy-gap (Figure 0.8).^{30a}

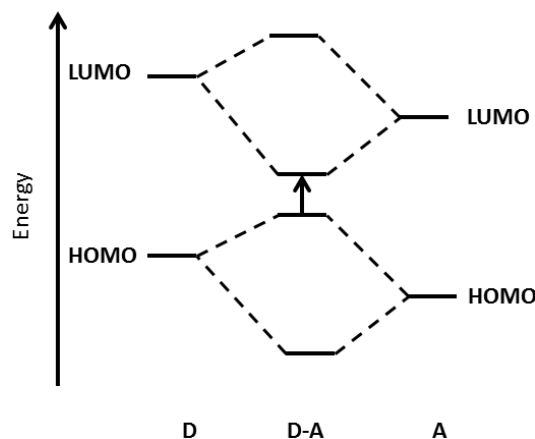


Figure 0.8. Molecular orbital interaction in donor (D) and acceptor (A) moieties leading to a D-A monomer with low HOMO-LUMO energy separation.^{30a}

Examples of this kind include platinum complexes incorporating donor DA-system in the backbone of bpy (Figure 0.9). The $[\text{Pt}(\text{DAbpy})(\text{Ph})_2]$ complex shows a red-shifted emission when compared to $[\text{Pt}(\text{D}_2\text{bpy})(\text{Ph})_2]$ and $[\text{Pt}(\text{A}_2\text{bpy})(\text{Ph})_2]$ complexes, with only donors or acceptors, respectively.^{30b}

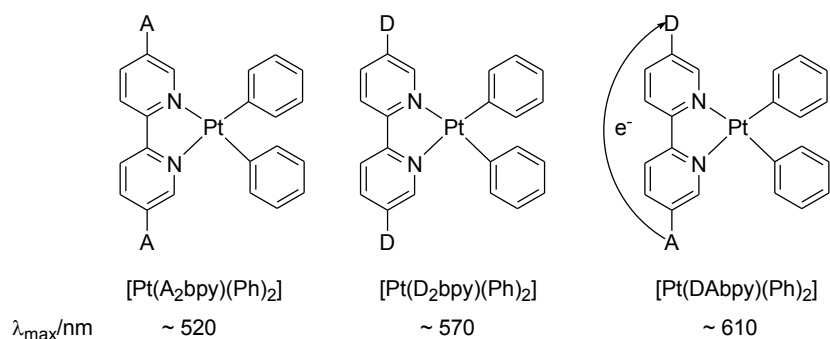


Figure 0.9. Emission wavelengths of platinum complexes with DA system in CH_2Cl_2 at 77 K.^{30b}

Apart from these principal factors, other effects can tune the HOMO-LUMO gap, such as (a) intermolecular metal-metal interactions,³¹ (b) intermolecular hydrogen bonding, molecular π - π stacking and aggregation. These effects should also be taken into account in order to change the photophysical properties of luminescent transition metal complexes.³²

0.3. Luminescent Ru(II)-polypyridyl complexes

The rich photophysics and photochemistry of Ru(II)-polypyridyl complexes have gathered an intense amount of research over the last few decades. The widespread research on Ru(II) complexes stems from their use in light-harvesting devices (LHDs),¹³ as water oxidation catalysts (WOCs) in artificial photosynthesis,¹² red-emitting bio-sensors³³ and recently in dye-sensitized solar cells (DSSCs).³⁴ The prototype complex, $[\text{Ru}(\text{bpy})_3]^{2+}$ containing the bidentate 2,2'-bipyridine ligand has an excited-state lifetime of 860 ns at 620 nm, with an associated Φ_p of 0.062 in deaerated acetonitrile solution.²³ This emission has been attributed to ³MLCT-based emission, as discussed in Section 0.1(D). The ligand-field splitting of the Ru(II) complexes has an intermediate value between the Fe(II) (non-emissive) and Os(II)/Ir(III) (highly emissive) complexes.¹³ Thus the triplet metal-centered (³MC) states are thermally more accessible compared to the similar case for Os(II)/Ir(III) complexes, restricting the Ru(II) complexes to exhibit $\Phi_p < 0.1$.

To improve the photophysical properties, i.e., to increase the room temperature excited-state lifetime (τ), to obtain $\Phi_p > 0.1$ and to red-shift the luminescence maxima of Ru(II) complexes based on bidentate ligands, several modifications with EDGs and EWGs have been performed on the ligand moiety.³⁵ Introduction of a π -delocalized system is also helpful to improve the photophysical properties of Ru(II) complexes containing bidentate ligands in comparison to $[\text{Ru}(\text{bpy})_3]^{2+}$.^{36,37} In general, while EWGs help to increase τ and Φ_p , the presence of EDGs tend to red-shift the emission maxima. A noteworthy example from Zhao's group takes advantage of an auxiliary chromophore to dramatically increase the value of τ up to 58.4 μs .¹⁵ The effect of an auxiliary chromophore has been discussed in detail in Chapter 1, section 1.5. A few other recent examples along these lines are shown below (Figure 0.10).

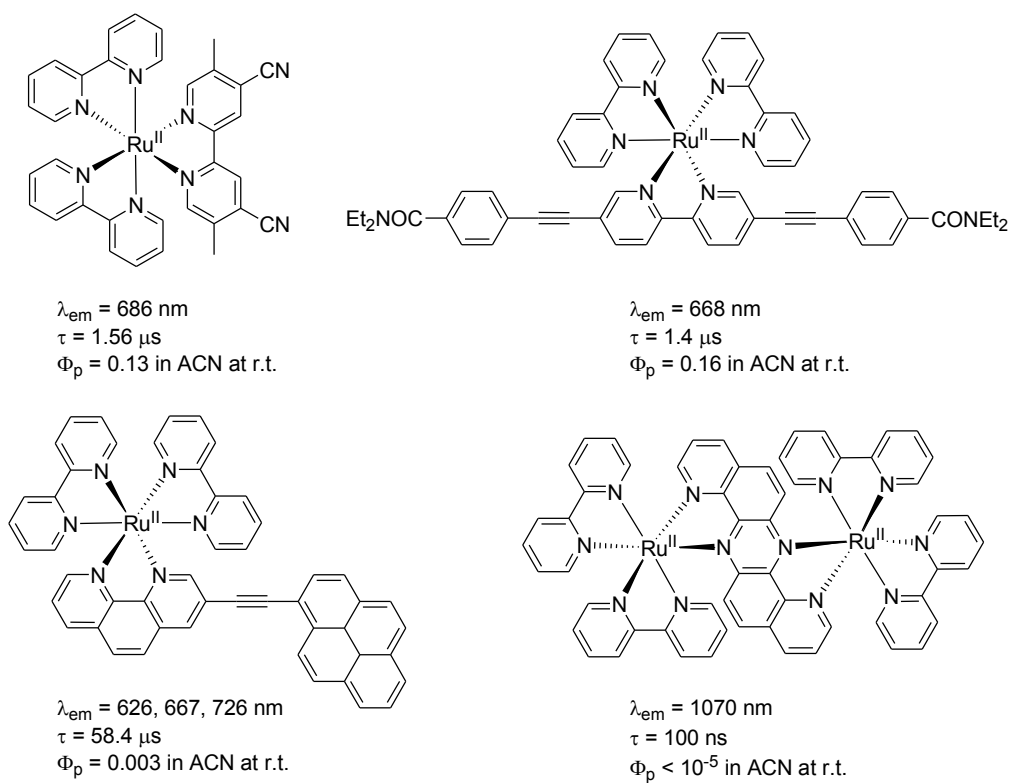


Figure 0.10. λ_{max}^{em} , τ and Φ_p of some benchmark ruthenium complexes.^{15,35-37}

Despite the interesting photophysical properties obtained for the Ru(II) complexes containing bidentate ligands, due to the inherent stereogenicity of the metal centre (Δ and Λ -enantiomers), rapid synthesis of polymetallic systems can be problematic. Many attempts have been made to separate enantiomers and diastereomers of Ru-polypyridyl complexes. Although the pioneering work of chromatographic separation based on cation exchange and ion pairing using non-chiral anionic additives, such as toluene-4-sulfonate, developed by Keene and co-workers, does work, the major drawback of this method is that relatively long separation times are sometimes required.³⁸ Chiral resolution using capillary electrophoresis³⁹ and capillary zone electrophoresis with enantiopure tartrate salts⁴⁰ and chiral-DNA³⁹ have also been proven to be useful. Chiral discrimination of Ru-complexes on silica column using Δ or Λ -P(V)catecholato complexes could also be achieved, as shown by Lacour⁴¹ and Gruselle.⁴² Recently, Vos and MacDonnell *et al.* have developed enantiomeric separations of Ru(II)-polypyridyl complexes using HPLC with teicoplanin⁴³ and cyclodextrin⁴⁴ chiral stationary phases.

To overcome the problem of stereopurity, interest has turned to complexes based on tridentate ligands, for e.g., 2,2':6',2''-terpyridine (tpy), due to the achiral nature and higher

symmetry of the complex. Mononuclear complexes based on tpy also allows one to construct rod-like linear arrays upon suitable substitution at the 4'-position of tpy. Although achiral complexes based on tpy are synthetically appealing, $[\text{Ru}(\text{tpy})_2]^{2+}$ has poor excited-state properties; the r.t. excited-state lifetime is only 0.25 ns with a quantum yield (Φ_p) of $\leq 5 \times 10^{-6}$. A detailed discussion about improving the photophysical properties of mononuclear Ru(II) complexes based on tridentate ligands has been provided in Chapter 1.

0.4. Objectives of the Research

The principal objective of this research is the design and synthesis of strong σ -donating 'super donor' bidentate and tridentate ligands, which can fine tune the HOMO-LUMO gap and, thus, the electrochemical and photophysical properties of their Ru(II) complexes. While the Ru(II) complexes act as red or NIR emitters, the Re(I) analogues act as blue emitters. Self-assembly using metal chromophores as 'metallo-ligands' to form discrete triangular assemblies has also been carried out. The complexes have been characterized by various analytical techniques including structural analysis using X-ray diffraction in many cases.

Chapter 0: This chapter consists of a brief introduction into the application and photophysical properties of different metal complexes in various areas of coordination chemistry. This introduction is complementary and serves as a platform to the short introductions given in each chapter.

Chapter 1: This chapter will introduce synthetic strategies employed in the synthesis of Ru(II) complexes of tridentate ligands with desirable photophysical properties, such as long-lived $^3\text{MLCT}$ excited-states at r.t.

Chapter 2: This chapter will discuss the synthesis of a novel family of bidentate 'super donor' ligands and their complexation with $\text{Ru}(\text{bpy})_2^{2+}$ core. The complexes emit in the far-red region due to a decreased HOMO-LUMO gap as supported by DFT and TD-DFT calculations. This observation is a consequence of strong σ -donation from the neutral 'super donor' ligands.

Chapter 3: The problem of stereopurity of Ru(II) complexes of bidentate ligands has been successfully overcome in this chapter by careful design of a bis-bidentate ligand, that offers parallel coordination vectors. Due to the unique design of the ligand, a dinuclear

Ru(II,II) complex can be isolated in diastereomerically pure *meso*-form, without using any chiral [Ru] precursor or chiral column chromatography. Several other mononuclear complexes have also been isolated as solvolysis by-products. The latter compounds exhibit interesting electrochemical and photophysical properties based on the relative basicity of the ligands.

Chapter 4: This chapter will discuss the synthesis of achiral heteroleptic Ru(II) complexes based on a novel tridentate ‘super donor’ ligand and other substituted tpy- or triazine-based ligands. The resulting complexes exhibit fascinating electrochemical and photophysical properties, which are well supported by DFT and TD-DFT analyses. These observations are due to strong σ -donation from the neutral ‘super donor’ ligands and increased octahedral geometry around the ruthenium centers.

Chapter 5: This chapter is divided into three sub-chapters. The first part (chapter 5A) will present the synthesis, electrochemical and photophysical properties of Re(I) complexes based on two structurally similar but electronically different ‘super donor’ ligands. The second part (chapter 5B) will include the synthesis and characterization of homoleptic d^6 - d^9 metal complexes of tpy, substituted at 4'-position by a pendant 3-pyridyl group. An interesting phenomenon in crystal packing upon changing the counter anion is also mentioned here. The third sub-chapter (chapter 5C) will focus on the self-assembly of metal chromophores, synthesized in the previous chapter, using neutral PdCl₂ as binding motif. The self-assembly has been performed by taking advantage of 60° coordination vector exhibited by the metallo-ligands to give discrete triangular hexametallic assemblies.

Chapter 6: This chapter will review the results, highlight the most important points, as well as discuss future perspectives of the projects reported.

0.5. References

- (1) Chi, Y.; Chou, P. T. *Chem. Soc. Rev.* **2010**, *39*, 638.
- (2) Xiao, L. X.; Chen, Z. J.; Qu, B.; Luo, J. X.; Kong, S.; Gong, Q. H.; Kido, J. *Adv. Mater.* **2011**, *23*, 926.
- (3) Hagfeldt, A.; Boschloo, G.; Sun, L. C.; Kloo, L.; Pettersson, H. *Chem. Rev.* **2010**, *110*, 6595.
- (4) Holder, E.; Langeveld B. M. W.; Schubert, U. S. *Adv. Mater.* **2005**, *17*, 1109.
- (5) Campagna, S.; Puntoriero, F.; Nastasi, F. *Top. Curr. Chem.* **2007**, *280*, 117.
- (6) Zhao, Q.; Huang, C. H.; Li, F. Y. *Chem. Soc. Rev.* **2011**, *40*, 2508.
- (7) Yam, V. W. W.; Wong, K. M. C. *Chem. Commun.* **2011**, *47*, 11579.

Chapter 0

- (8) Singh-Rachford, T. N.; Castellano, F. N. *Coord. Chem. Rev.* **2010**, *254*, 2560.
- (9) Sun, R. W. Y.; Che, C. M. *Coord. Chem. Rev.* **2009**, *253*, 1682.
- (10) Baldo, M. A.; O'Brien, D. F.; You, Y.; Shoustikov, A.; Sibley, S.; Thompson M. E.; Forrest, S. R. *Nature* **1998**, *395*, 151.
- (11) Qian, G.; Wang, Z. Y. *Chem. Asian J.* **2010**, *5*, 1006.
- (12) Eisenberg, R. *Science* **2009**, *324*, 44.
- (13) Xiang, H.; Cheng, J.; Ma, X.; Zhou, X.; Chruma, J. J. *Chem. Soc. Rev.* **2013**, *42*, 6128.
- (14) Adachi, C.; Baldo, M. A.; Thompson, M. E.; Forrest, S. R. *J. Appl. Phys.*, **2001**, *90*, 5048.
- (15) Ji, S.; Wu, W. H.; Wu, W. T.; Song, P.; Han, K. L.; Wang, Z. G.; Liu, S. S.; Guo, H. M.; Zhao, J. Z. *J. Mater. Chem.* **2010**, *20*, 1953.
- (16) Ragazzon, G.; Verwilt, P.; Denisov, S. A.; Credi, A.; Jonusauskas, G.; McClenaghan, N. D. *Chem. Commun.* **2013**, *49*, 9110.
- (17) Grist, S. M.; Chrostowski, L.; Cheung, K. C. *Sensors* **2010**, *10*, 9286.
- (18) Houlding, V. H.; Miskowski, V. M. *Coord. Chem. Rev.* **1991**, *111*, 145.
- (19) Drouet, S.; Paul-Roth, C. O.; Fattori, V.; Cocchic, M.; Williams, J. A. G. *New J. Chem* **2011**, *35*, 438.
- (20) Miskowski, V. M.; Houlding, V. H. *Inorg. Chem.* **1989**, *28*, 1529.
- (21) Paulson, S.; Sullivan, B. P.; Caspar, J. V. *J. Am. Chem. Soc.*, **1992**, *114*, 6905.
- (22) Yam, V. W. W.; Lo, K. K. W. *Chem. Soc. Rev.* **1999**, *28*, 323.
- (23) Calvert, J. M.; Caspar, J. V.; Binstead, R. A.; Westmoreland, T. D. and Meyer, T. J. *J. Am. Chem. Soc.* **1982**, *104*, 6620.
- (24) Brooks, J.; Babayan, Y.; Lamansky, S.; Djurovich, P. I.; Tsyba, I.; Bau, R.; Thompson, M. E. *Inorg. Chem.* **2002**, *41*, 3055.
- (25) Kim, T.; Kim, H.; Lee, K. M.; Lee, Y. S.; Lee, M. H. *Inorg. Chem.* **2013**, *52*, 160.
- (26) Bailey, J. A.; Miskowski, V. M.; Gray, H. B. *Inorg. Chem.* **1993**, *32*, 369.
- (27) Lowry, M. S.; Bernhard, S. *Chem. Eur. J.* **2006**, *12*, 7970.
- (28) Lu, W.; Mi, B.-X.; Chan, M. C. W.; Hui, Z.; Che, C.-M.; Zhu, N.; Lee, S.-T. *J. Am. Chem. Soc.* **2004**, *126*, 4958.
- (29) *Highly efficient OLEDs with phosphorescent materials*, ed. H. Yersin, Wiley, 2007.
- (30) (a) Ajayaghosh, A. *Chem Soc. Rev.* **2003**, *32*, 181. (b) Sun, Y.; Wang, S. N. *Inorg. Chem.* **2009**, *48*, 3755.
- (31) Lai, S. W.; Chan, M. C. W.; Cheung, T. C.; Peng, S. M.; Che, C. M. *Inorg. Chem.* **1999**, *38*, 4046.
- (32) Mishra, A.; Behera, R. K.; Behera, P. K.; Mishra, B. K.; Behera, G. B. *Chem. Rev.* **2000**, *100*, 1973.
- (33) Gill, M. R.; Garcia-Lara, J.; Foster, S. J.; Smythe, C.; Battaglia, G.; Thomas, J. A. *Nat. Chem.* **2009**, *1*, 662.
- (34) Gratzel, M. *Nature* **2001**, *414*, 338.
- (35) McCusker, C. E.; McCusker, J. K. *Inorg. Chem.*, **2011**, *50*, 1656.
- (36) Wang, Y. S.; Liu, S.; Pinto, M. R.; Dattelbaum, D. M.; Schoonover, J. R. Schanze, K. S. *J. Phys. Chem. A* **2001**, *105*, 11118.
- (37) Treadway, J. A.; Strouse, G. F.; Ruminski, R. R.; Meyer, T. J. *Inorg. Chem.* **2001**, *40*, 4508.

Chapter 0

- (38) (a) Rutherford, T. J.; Quagliotto, M. G.; Keene, F. R. *Inorg. Chem.* **1995**, *34*, 3857. (b) Keene, F. R. *Chem. Soc. Rev.* **1998**, *27*, 185 and references cited therein.
- (39) Kane-Maguire, N. P.; Wheeler, J. F. *Coord. Chem. Rev.* **2001**, *211*, 145.
- (40) Harris, J. E.; Desai, N.; Seaver, K. E.; Watson, R. T.; Kane-Maguire, N. A. P.; Wheeler, J. F. *J. Chromatogr. A* **2001**, *919*, 427.
- (41) Lacour, J.; Torche-Haldimann, S.; Jodry, J. J.; Ginglinger, C.; Favarger, F. *Chem. Commun.* **1998**, *16*, 1733.
- (42) Gruselle, M.; Thouvenot, R.; Caspar, R.; Boubekour, K.; Amouri, H.; Ivanov, M.; Tonsuaadu, K. *Mendeleev Commun.* **2004**, *6*, 282.
- (43) Browne, W. R.; O'Connor, C. M.; Villani, C.; Vos, J. G. *Inorg. Chem.* **2001**, *40*, 5461.
- (44) Janaratne, T. K.; Yadav, A.; Ongeri, F.; MacDonnell, F. M. *Inorg. Chem.* **2007**, *46*, 3420.

Chapter 1 : Introduction

Design, synthesis and excited-state properties of Ru(II) complexes of tridentate heterocyclic ligands

1.1. Introduction

Studying the fundamental process of electron and energy transfer as found in natural photosynthetic biosystems continues to be a vital area of research.¹ Due to their capacity to absorb visible light, metal-polypyridyl complexes are analogous to natural chromophores, such as chlorophyll-*b* and β -carotenoid in photosystem II (PSII). Among the d^6 metal complexes (where M = Re(I), Ir(III), Rh(III), Os(II), Ru(II)), Ru(II) complexes are of particular interest as photosensitizers in light-harvesting devices (LHDs)² and red-emitting bio-sensors³ due to their chemical robustness, ease of synthesis and relatively inexpensive Ru-starting material. Thus, Ru(II) complexes that mimic PSII are highly sought after. In PSII, upon absorption of solar energy the secondary chromophores transfer the generated excited-state energy efficiently to the “special pair” of chlorophylls, which transfer an electron, through a series of electron-transfer steps, to plastoquinone, which ultimately leads to the production of ATP.⁴ The Ru-polypyridyl chromophores give rise to a singlet metal-to-ligand charge-transfer (¹MLCT) excited state upon photoexcitation, which produces a potentially emitting triplet metal-to-ligand charge-transfer excited state (³MLCT) by intersystem crossing (Figure 1.1). To be applied in artificial photosynthetic systems this excited state should possess a sufficiently long lifetime to permit efficient vectorial electron or energy transfer. Careful ligand design is necessary in this context as the ligands can play a direct role in governing the energies of the related states which determine the excited-state lifetime.⁵

Considerable attention has been focused on the development of LHDs with the photophysically appealing tris(2,2'-bipyridine)ruthenium(II) ($[\text{Ru}(\text{bpy})_3]^{2+}$) motif due to its long-lived room temperature (r.t.) excited-state lifetime (~ 860 ns).⁶ However, due to the inherent stereogenicity of the metal centre (Λ and Δ -enantiomers), the purity of polynuclear systems based on these chiral units becomes questionable due to the increasing number of diastereomers for larger polymers. Furthermore, when the complexity of *meridional* and *facial* isomerization is considered, the number of species present becomes daunting.⁷ Much interest has focused on complexes based on tridentate ligands, for e.g.,

2,2':6',2''-terpyridine (tpy), due to its achiral nature and higher symmetry of the complex (D_{2d} instead of D_3 in $[\text{Ru}(\text{bpy})_3]^{2+}$), which allows rod-like linear arrays to be constructed upon suitable substitution at the 4'-position of tpy.^{8a} Although achiral complexes are synthetically accessible, $[\text{Ru}(\text{tpy})_2]^{2+}$ has poor excited-state properties; the r.t. excited-state lifetime is only 0.25 ns with a quantum yield (Φ) of $\leq 5 \times 10^{-6}$,^{8b} a consequence of the deviation from ideal octahedral geometry around ruthenium in $[\text{Ru}(\text{tpy})_2]^{2+}$ as compared to that in $[\text{Ru}(\text{bpy})_3]^{2+}$. Moreover, due to the rigidity of the tpy ligand, which forms two five-membered chelate rings upon coordination to Ru(II), the N-Ru-N *trans* angle is only 158.6° . On the other hand the N-Ru-N *trans* angle in $[\text{Ru}(\text{bpy})_3]^{2+}$ is 173.0° .⁹ Due to this distorted octahedral geometry of the N atoms around the ruthenium center, the overall tpy ligand-field strength is weak, so that the non-emissive dd metal-centered triplet state (^3MC) is in close equilibrium with the emissive $^3\text{MLCT}$ state. Hence a non-radiative decay *via* ^3MC state to the ground state (GS or S_0) is facilitated upon its thermal population from $^3\text{MLCT}$ state (Figure 1.1).¹⁰

To enhance the excited-state properties of these complexes the process of thermally induced non-radiative deactivation through the ^3MC state has to be reduced. The two primary pathways to reduce the non-radiative decay constant are (i) stabilization of the $^3\text{MLCT}$ state and (ii) destabilization of the ^3MC state, both of which increase the $^3\text{MLCT}$ - ^3MC energy-gap. However, if the energy of the $^3\text{MLCT}$ state is very low, a direct radiative decay from $^3\text{MLCT}$ to GS comes into play according to energy-gap law,¹¹ thus shortening the excited-state lifetime (Figure 1.1).

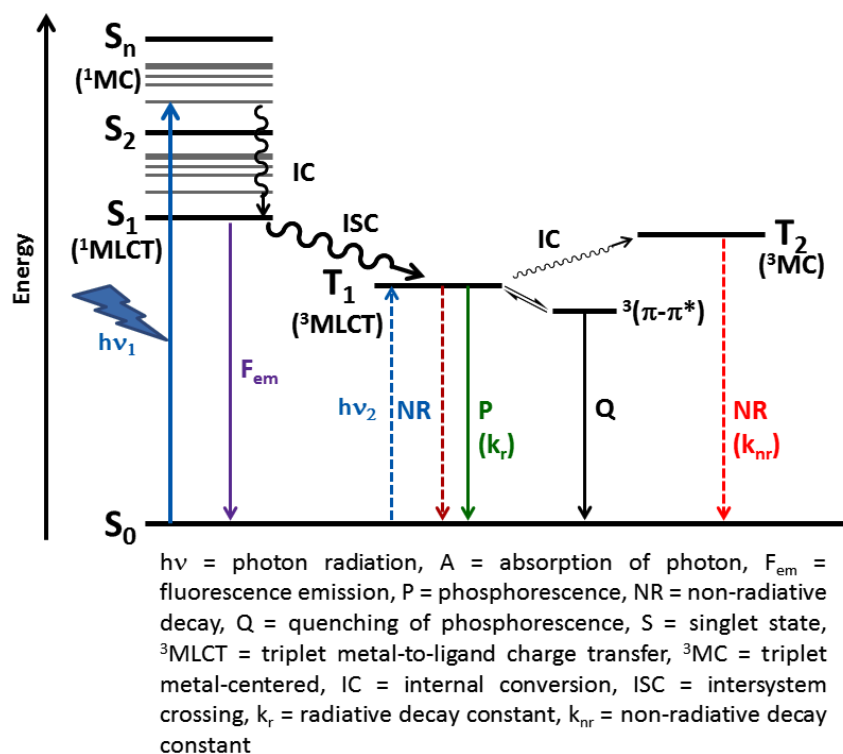


Figure 1.1. Qualitative Jablonski diagram illustrating the electronic states of Ru(II) polypyridyl system and transitions among the states. The ${}^3(\pi-\pi^*)$ state of a secondary chromophore (if present) in this system is in equilibrium with the ${}^3\text{MLCT}$ state.

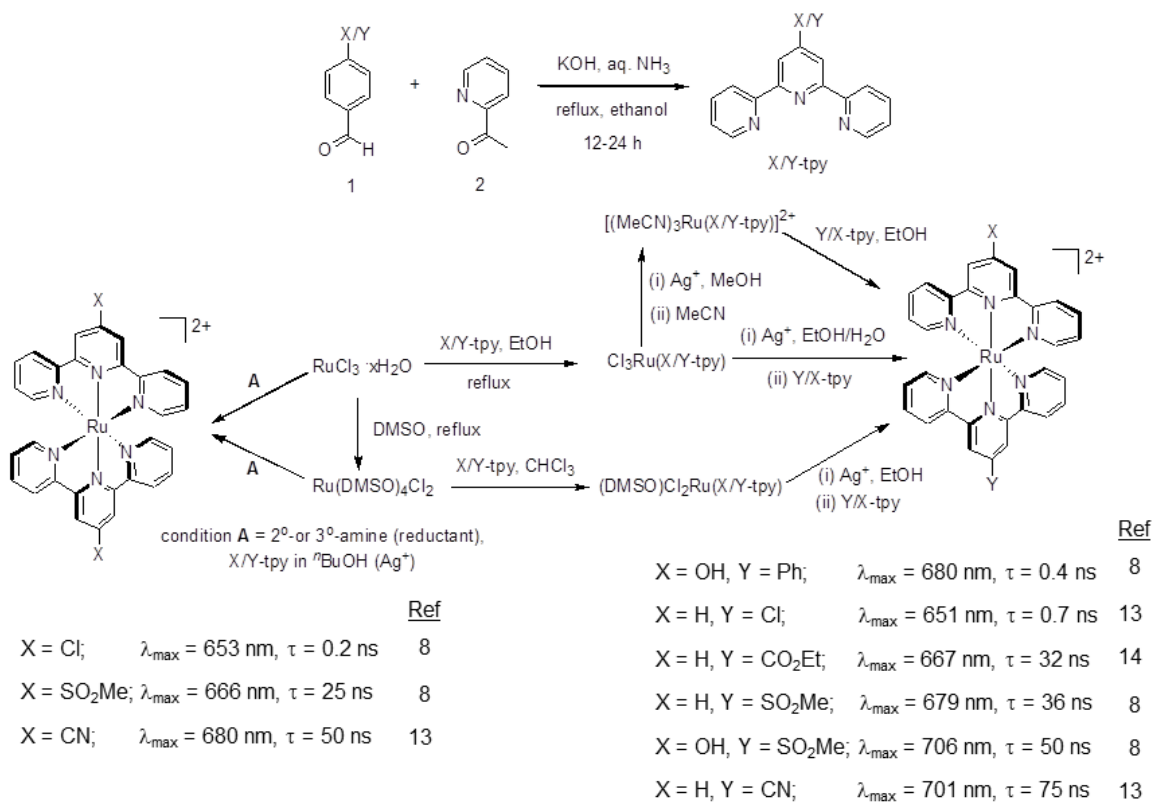
In this Chapter the strategies used to synthesize different tridentate ligands, which govern the photophysical properties of their Ru(II) complexes, will be reported. In addition to the various strategies adopted to increase the ${}^3\text{MLCT}$ - ${}^3\text{MC}$ energy-gap, an alternate pathway is to introduce auxiliary chromophore(s), whose triplet ($\pi-\pi^*$) is quasi-isoenergetic to the ${}^3\text{MLCT}$ state, and thus the ${}^3(\pi-\pi^*)$ repopulates the ${}^3\text{MLCT}$ state through a ${}^3\text{MLCT}$ - ${}^3\text{MC}$ oscillating equilibrium, effectively acting as an energy reservoir (Figure 1.1). In the following four sections, we will review the strategies developed to date and highlight the most efficient. For the sake of numerous derivatives of Ru(II) polypyridyl complexes containing tridentate ligands, this Chapter is strictly confined to mononuclear homo- or hetero-leptic Ru(II) tridentate complexes with RuN_6 - and RuN_5C -cores.¹²

1.2. Ruthenium(II) complexes of functionalized 2,2':6',2''-terpyridine ligands

1.2.1. Direct incorporation of an electron-withdrawing or electron-donating substituent onto tpy

Direct substitution by electron-withdrawing groups (EWGs) or electron-donating groups (EDGs) on the 4'-position of the central pyridyl ring have pronounced effects on the photophysical properties of Ru(II) complexes of type $[\text{Ru}(\text{tpy-X})(\text{tpy-Y})]^{2+}$ (where X or Y = EWG or EDG). The EWGs operate by stabilizing the ligand-based lowest-unoccupied molecular orbital (LUMO) with a minimal effect onto the metal-based highest occupied molecular orbital (HOMO), while the EDGs destabilize the HOMO without much affecting the LUMO in heteroleptic complexes. In both the cases, a concomitant red-shift in $^1\text{MLCT}$ and $^3\text{MLCT}$ maxima has been observed compared to the prototypical $\text{Ru}(\text{tpy})_2^{2+}$ ($^1\text{MLCT}$ and $^3\text{MLCT}$ maxima of $\text{Ru}(\text{tpy})_2^{2+}$ are 475 nm and 629 nm, respectively). Substitution by EWGs shows the additional advantage of an increased $^3\text{MLCT}$ - ^3MC energy gap due to stabilization of the LUMO, and subsequently lower thermal population of ^3MC states. The luminescence lifetimes of these complexes were increased and dramatic improvements were observed for complexes with strong EWGs and also in complexes with both EWG and EDG.^{8,13,14} The ligands for these complexes could be synthesized using recently developed single-step one pot condensation of (X/Y)-substituted arylaldehyde with two equivalents of 2-acetylpyridine in presence of aqueous ammonia (as a source of NH_3), to form the central pyridine ring.¹⁵ The homo- or heteroleptic complexation could be performed by heating 2:1 molar ratio of tpy-X/Y with RuCl_3 or $\text{Ru}(\text{DMSO})_4\text{Cl}_2$ and heating a suspension of equimolar amount of $\text{Cl}_3\text{Ru}(\text{tpy-X/Y})$ or its solvent adduct with opposite tpy-Y/X, generally in high boiling alcoholic solvents and in the presence of a reductant (Scheme 1.1).

Chapter 1



Scheme 1.1. General syntheses of substituted 2,2':6',2''-terpyridines (tpy-X/Y) and their homo- and hetero-leptic Ru(II) complexes with their photophysical data.^{8,13-14}

The incorporation of a positively-charged pyridinium moiety at the 4'-position of a tpy unit has the pronounced effect of stabilizing the ligand-based LUMO in its heteroleptic Ru-complex, as evidenced by a red-shifted ³MLCT emission maximum (775 nm) and long lifetime (125 ns) in [Ru(tpy)(MePy-tpy)]³⁺ (MePy-tpy = 4'-methylpyridinium-2,2':6',2''-terpyridine).¹⁶ Heteroleptic Ru(II) complexes of metal-organic rotaxane frameworks (MORFs) containing interlocked alkylpyridinium-tpy and crown ethers also exhibit red-shifted ³MLCT maxima (788-850 nm) with improved excited-state lifetimes (9-24 ns).¹⁶ Molecular dyads of Ru(II)-chromophores and expanded pyridinium acceptors (Figure 1.2) have a low-energy emission (670 nm) and extended r.t. luminescence lifetime of 55 ns,¹⁷ although, the first generation pyridinium acceptor with a phenyl spacer and second generation pyridinium acceptor exhibit reduced lifetimes of 15 ns and 8 ns, respectively, nonetheless two orders of magnitude higher than that of [Ru(tpy)₂]²⁺.

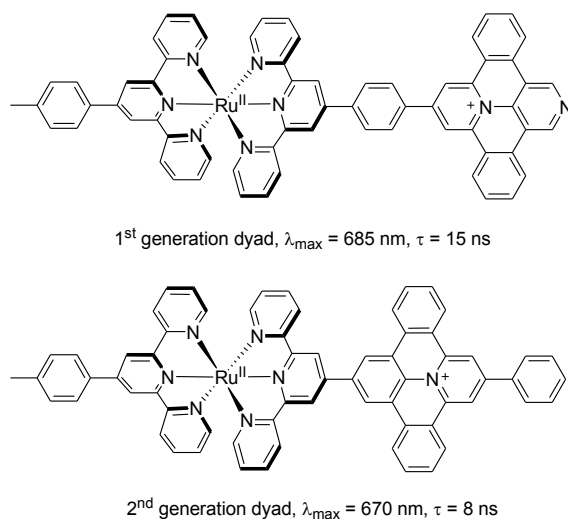


Figure 1.2. Photophysical data for donor-acceptor dyad Ru(II) complexes.¹⁸

1.2.2. Incorporation of extended π -conjugation onto tpy

1.2.2. (A) Incorporation of extended π -conjugation onto tpy with acetylene as spacer

The enhanced electronic delocalization between a tpy unit and an aryl group, that are connected together by alkynyl linkers, grafted directly at the 4'-position of the tpy unit or at the 4,4''-position(s) of the peripheral pyridyl groups of tpy unit,¹⁹ greatly stabilizes the ligand-based LUMO of Ru(II) polypyridyl complexes and thus results in a higher ³MLCT-³MC energy gap. The subsequent effect is a decrease in emission energy and an increase in the lifetime of the excited state. These effects are proportional with the number (n) of alkynyl unit(s) when two tpy units are connected in a back-to-back fashion (n = 1; $\lambda_{\text{max}} = 690 \text{ nm}$, $\tau = 55 \text{ ns}$; n = 2; $\lambda_{\text{max}} = 710 \text{ nm}$, $\tau = 170 \text{ ns}$). The longest r.t. lifetime for acetylene-based complexes corresponds to the acetylene-pyrene complex (580 ns), which is due to thermal population of the alkyne-pyrene's triplet state (³Alk-Pyr) from the ³MLCT state of the tpy, thus delaying the emission. A similar effect may be responsible for the extended lifetime of the ferrocene- and terthiophene-based acetylene complexes (Figure 1.3).^{20,21}

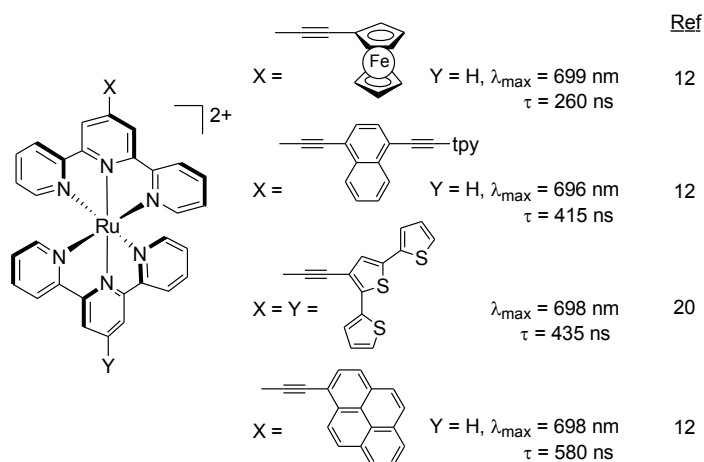


Figure 1.3. Photophysical data for acetylene-substituted $[\text{Ru}(\text{tpy})_2]^{2+}$ complexes.^{12,20}

1.2.2. (B) Direct incorporation of extended π -conjugation onto tpy

The recent fruitful approach of attaching substituted imidazole unit at the 4'-position of tpy to increase the r.t. lifetime of the excited state takes advantage of extended π -delocalization.²² Attachment of a ferrocenyl group to tpy lowers the energy of ligand-based LUMO and establishes an equilibrium between the ferrocene's triplet state and ³MLCT state of Ru-tpy, which results in a dramatic enhancement in r.t. lifetime of the corresponding complex (Figure 1.4).²³

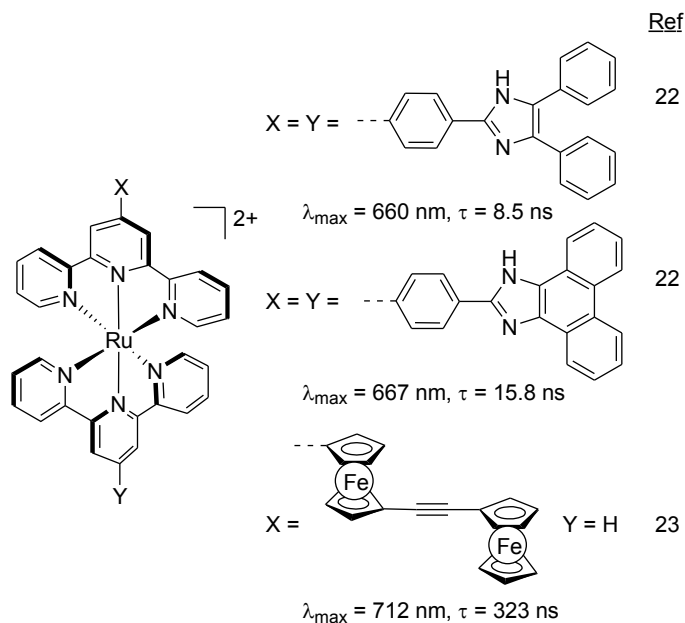
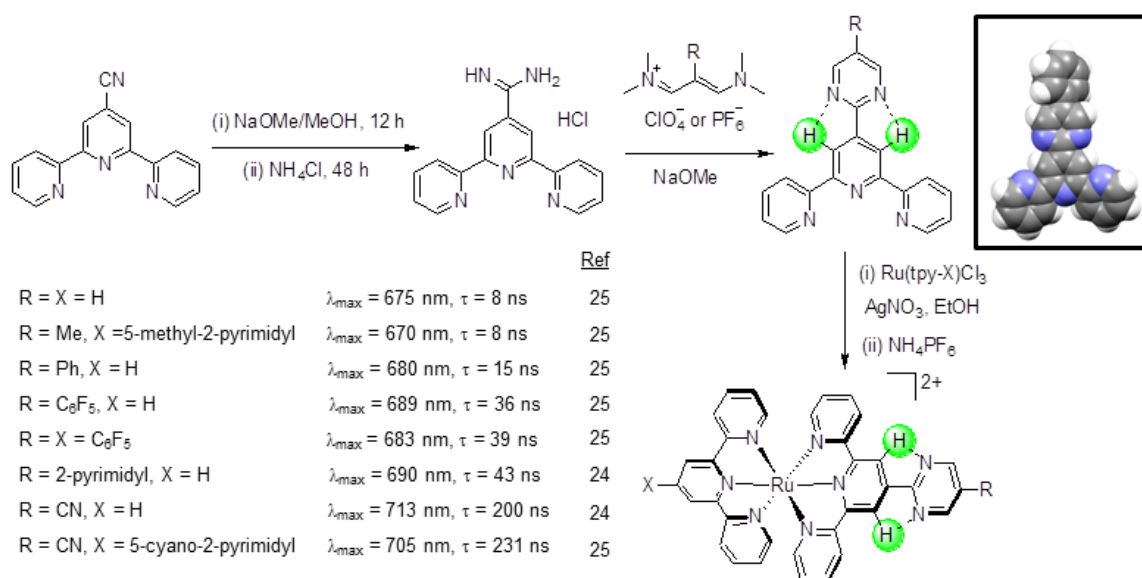


Figure 1.4. Photophysical data for 4'-tpy-substituted $\text{Ru}(\text{tpy})_2^{2+}$ complexes.^{22,23}

1.2.3. Co-planarity of aromatic groups on the tpy ligand

A direct and relatively unexplored approach of introducing co-planar aromatic rings to improve the π -delocalization at GS employs a pyrimidyl spacer attached to the 4'-position of the tpy unit. The collective effect of electrostatic interactions between the N atoms of the 2-pyrimidyl substituent and the H atoms of the central pyridine ring renders the 2-pyrimidyl substituent coplanar to the central terpyridine ring (inset crystal structure of similar ligand in Scheme 1.2). Further stabilization of the $^3\text{MLCT}$ state can be achieved through substitution of electron-withdrawing groups in the 5-pyrimidyl position.²⁴ The syntheses of these types of ligands include transformation of a cyano group to amidinate to obtain 4'-amidinate-2,2':6',2''-terpyridine, which is subsequently reacted with R-substituted vinamidium cations (Scheme 1.2) to form the R-substituted pyrimidyl ring at the 5'-position. The homo- and hetero-leptic Ru(II) complexes were synthesized following Scheme 1.1.²⁵ All of the complexes exhibit red-shifted $^3\text{MLCT}$ maxima and improved r.t. lifetime of excited-state compared to those of $[\text{Ru}(\text{tpy})_2]^{2+}$. A relative comparison among the photophysical properties of homoleptic complexes, when R = X = Me and R = X = CN suggests that the EDG do not destabilize the ^3MC state to a great extent and non-radiative decay back to the GS was facilitated, while the stabilization of $^3\text{MLCT}$ state is more pronounced with EWG(s), thus leading to higher $^3\text{MLCT}$ - ^3MC energy-gap and much improved r.t. excited-state lifetimes.



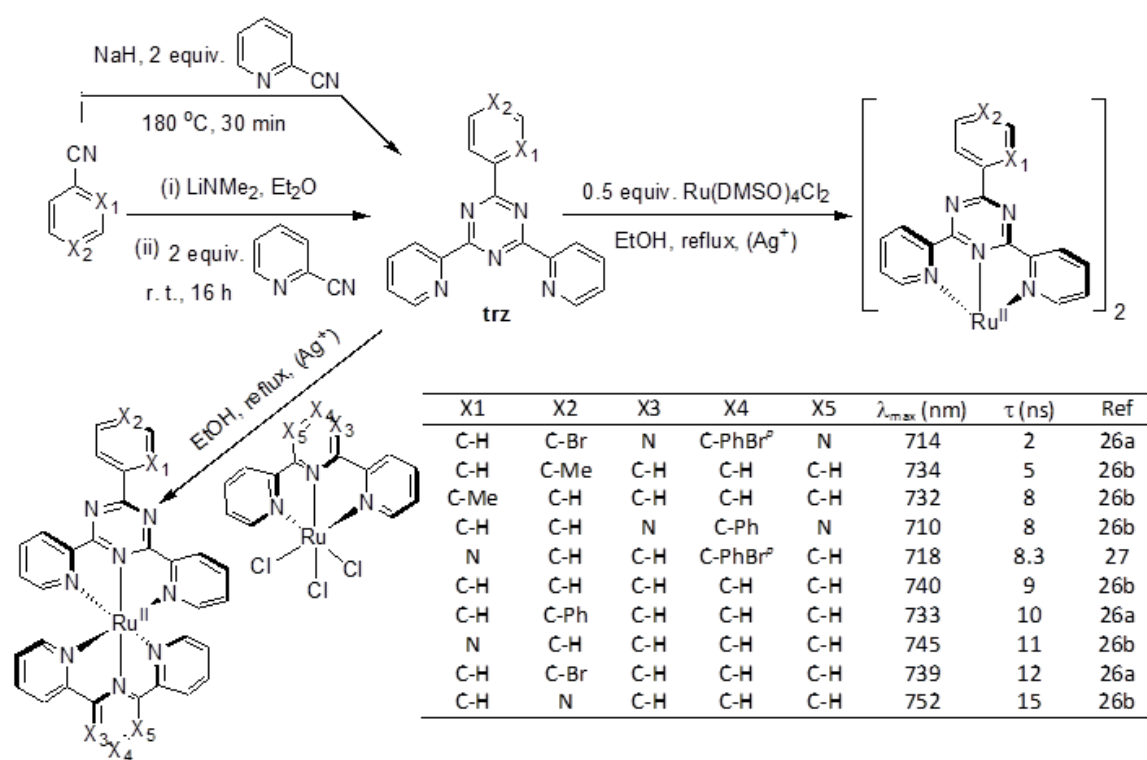
Scheme 1.2. Syntheses of a variety of substituted pyrimidyl terpyridine heteroleptic Ru(II) complexes and their r.t. excited-state lifetimes (solid-state structure of the ligand (R = Ph) in inset shows the planar arrangement of the central pyridine and the 2-pyrimidyl units).^{24,25}

1.3. π Electron Accepting Ability

1.3.1. Introduction of a 2,4(dipyrid-2'-yl)triazine (dpt) unit

The stabilization of ¹MLCT and consequently ³MLCT state can be achieved by introduction of a better π -accepting triazine core in place of the central pyridine ring in a tpy unit. The operating coulombic C-H ^{δ^+} -N ^{δ^-} interactions, as discussed in Section 1.2.3, are also responsible for overall ligand planarity and subsequently further stabilization of emissive ³MLCT state. A series of dpt ligands containing EDGs and EWGs were synthesized by cyclotrimerization of nitrile groups either (a) in the presence of catalytic amount of NaH at high temperature or (b) *via.* organolithium intermediate under milder conditions (Scheme 1.3). The homoleptic complexes [Ru(dpt)₂]²⁺ and the heteroleptic complexes [Ru(dpt)(tpy)]²⁺ were synthesized by standard procedures (Scheme 1.1). Concomitant with the bathochromic shift of the ¹MLCT maxima in [Ru(dpt)₂]²⁺ and [Ru(dpt)(tpy)]²⁺ complexes as compared to that in [Ru(tpy)₂]²⁺, the ³MLCT emission maxima of these homo- or hetero-leptic complexes are also considerably red-shifted compared to that in [Ru(tpy)₂]²⁺.^{26,27} The heteroleptic complex [Ru(dpt)(tpy)]²⁺, with a 4-pyridyl group as a substituent in dpt unit, emits at 752 nm, with an associated r.t. excited-

state lifetime of 15 ns. The homoleptic complexes have shorter excited-state lifetimes as compared to that of heteroleptic complexes, presumably due to facilitated non-radiative decay due to solvent interaction with the non-coordinated nitrogen atoms on the triazine ring. Although the homoleptic Ru(II) complex of 4'-phenyl substituted dpt units exhibit a longer r.t. excited-state lifetime of 8 ns, and a longer wavelength emission ($\lambda_{\text{max}} = 710$ nm) compared to $\text{Ru}(\text{tpy})_2^{2+}$, homoleptic Ru(II) complexes with other substituents, such as, 1-naphthyl, 9-phenanthryl, 1-pyrenyl are non-emissive due to the weaker ligand-field strength of dpt unit compared to the tpy unit, which results in non-radiative deactivation *via* the ^3MC state.²⁸



Scheme 1.3. Syntheses of tridentate dpt-based ligands and its homo- and hetero-leptic Ru(II) complexes with photophysical data.^{26,27}

1.3.2. Introduction of a central diazine unit

Ligands containing differently substituted pyrazine or pyrimidine rings in place of a central pyridine ring in tpy have been synthesized (2,3,5,6-tetrakis(2-pyridyl)pyrazine (**tpy**)), 4-chloro-2,6-bis(2-pyridyl)pyrimidine (**cyy**)) and their homo- and heteroleptic complexes with the Ru(II)(tpy)-core were also prepared (Figure 1.5-top).²⁹ All

the complexes show better photophysical properties than that of $[\text{Ru}(\text{tpy})_2]^{2+}$, although the sharp decrease in excited-state lifetime of the **cpp** analogue is presumably due to the overly stabilized $^3\text{MLCT}$ state, which deactivates to the ground state as described by the energy-gap law.

1.3.3. Introduction of peripheral diazine units

Attaching two pyrazine heterocycles in the 2,6-positions of a 4-substituted pyridine ring to furnish different types of tridentate ligands should also improve the π accepting ability of these ligands. Indeed, the corresponding homoleptic Ru(II) complex of 4-*p*-tolyl-2,6-bis(2-pyrazinyl)pyridine exhibits a red-shifted $^3\text{MLCT}$ maximum (667 nm) with a longer r.t. excited-state lifetime (18 ns in the solid state).³⁰ The deactivation of its r.t. emission is presumably due to strong interaction of the lone pair of the pyrazine N atoms with the solvent.

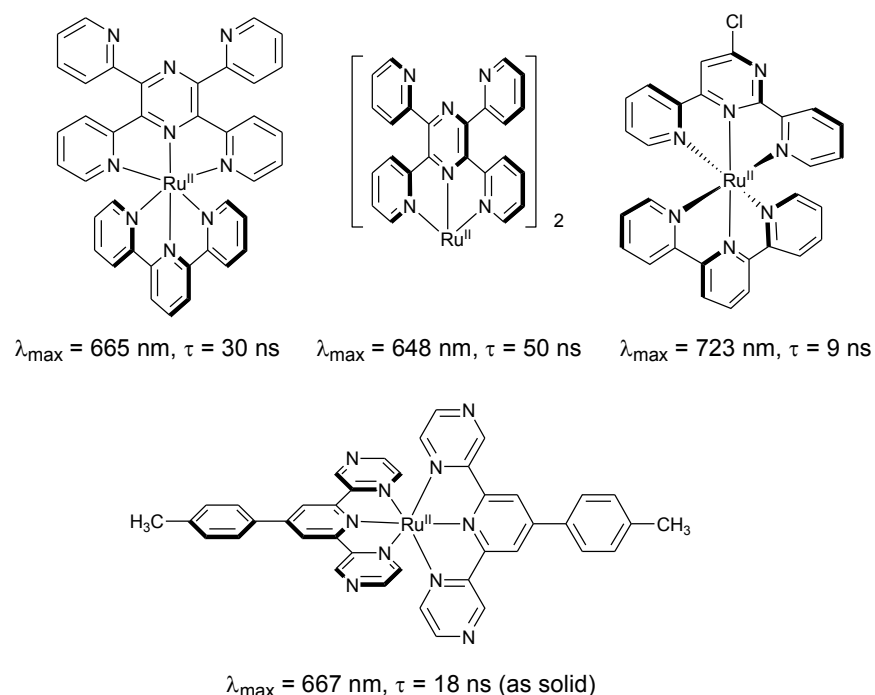


Figure 1.5. Hetero- and homo-leptic Ru(II) complexes of tridentate ligands containing central diazine units (top). Homoleptic Ru(II) complex of 2,6-dipyrazinylpyridine (bottom).^{12,30}

1.4. Increasing the energy of the ^3MC state

1.4.1. σ -Donating ability

Sigma-donor ligands operate by interacting with the metal-based d orbitals, with a minimal effect on the π^* orbitals of the ancillary ligand attached to the metal in a heteroleptic complex; thus giving fine control over the HOMO-LUMO gap. Since the interaction destabilizes the HOMO, the overall effect of incorporating σ -donor ligands in Ru(II)-polypyridyl complexes is the lowering of $^1\text{MLCT}$ energy, and consequently, the $^3\text{MLCT}$ energy as well. Thus, the effective surface crossing from $^3\text{MLCT}$ state to ^3MC state is reduced, which in turn, results in a longer excited-state r.t. luminescence lifetime. However, if the $^3\text{MLCT}$ state is too low in energy, non-radiative decay directly to the GS may occur according to the energy gap law. A few major ways of increasing the σ -donor strength of the tridentate ligand are described in the following sections.

1.4.1. (A) σ -Donating ability of cyclometallating ligands

The anionic nature of cyclometallating ligands makes them appealing as they are strong σ -donors, which significantly increase the $^3\text{MLCT}$ - ^3MC energy gap in their heteroleptic Ru(II) complexes with tpy. Although the excited state is typically quite short lived due to the energy gap law, it is still possible for rapid photoinjection into the conduction band of TiO_2 semi-conductors with efficient photoelectric current conversion (efficiency up to 12% in test cells). Thus, the visible light absorbing Ru(II) cyclometallated complexes have been incorporated into ‘next generation’ dye-sensitized solar cells (DSSCs).³¹ These cyclometallating ligands bind in either $\text{N}^{\wedge}\text{C}^{\wedge}\text{N}$ or $\text{N}^{\wedge}\text{N}^{\wedge}\text{C}$ coordination modes, thus replacing a Ru-N bond with a Ru-C bond. Several strategies have been adopted to develop various types of cyclometallating ligands, for e.g., (a) quaternization of a tpy-N (or 4'-methylthiotpy-N) atom by trimethyloxonium tetrafluoroborate so that the quaternized N atom is no longer available for coordination, thereby giving a $[(\text{N}^{\wedge}\text{N}^{\wedge}\text{C})\text{Ru}(\text{tpy})]^+$ complex,³² (b) coupling of a 3-bromo-2,2'-bipyridine with 4-trimethylstannylpyridine to furnish 2,2':6',4''-terpyridine, which exhibits a $\text{N}^{\wedge}\text{N}^{\wedge}\text{C}$ tridentate binding mode,³³ (c) attachment of 2,2'-bipyridine with thiophene to afford 6-(2-thienyl)-2,2'-bipyridine which can bind by either $\text{N}^{\wedge}\text{N}^{\wedge}\text{S}$ or $\text{N}^{\wedge}\text{N}^{\wedge}\text{C}$ coordination mode, depending on the pH of the reaction media,³⁴ (d) incorporation of a phenyl ring into tpy instead of the peripheral or central pyridyl ring to force $\text{N}^{\wedge}\text{N}^{\wedge}\text{C}$ or $\text{N}^{\wedge}\text{C}^{\wedge}\text{N}$ coordination, respectively.³⁵ Although

several homo- and hetero-leptic Ru(tpy) complexes with these kinds of ligands have been synthesized, their luminescence properties have rarely been reported.

The strongly-donating cyclometallating ligands interact with the metal-based $T_2[d(Ru)]$ orbitals, thereby increasing the energy of the HOMO. As the 3MLCT state lies on the non-cyclometallated ligand, a significant amount of red-shift (743-807 nm) is observed in the r.t. emission energy of a series of weakly emissive $[(N^{\wedge}N^{\wedge}C)Ru(tpy)]^+$ or $[(N^{\wedge}C^{\wedge}N)Ru(tpy)]^+$ type of complexes compared to that of $[Ru(tpy)_2]^{2+}$.³⁵ The poor emission properties, as revealed by the relatively low r.t. excited-state lifetime of $[Ru(p\text{-tolyl-tpy})(\mathbf{dpb})]^+$ (where \mathbf{dpb} = 2,6-dipyridylbenzene) of 4.5 ns at 784 nm, is possibly due to the small 3MLCT -GS energy gap, which facilitates non-radiative decay from 3MLCT state to GS.

The effect of enhanced π -delocalization in cyclometallated Ru-polypyridyl complexes greatly stabilizes the 3MLCT state, dramatically increasing the r.t. excited-state lifetime. Complexes with cyclometallating ligands, substitution by aromatic groups in the position ortho to the coordinating N atom, for e.g., $[Ru(\mathbf{mappy})(\mathbf{dtp})]^+$ (where \mathbf{mappy} = 2-*p*-anisyl-9-(4-methyl-2-pyridyl)-1,10-phenanthroline and \mathbf{dtpH} = 2,9-bis(*p*-tolyl)-1,10-phenanthroline), and several of their derivatives exhibit r.t. low-energy 3MLCT emission maxima (778-816 nm) with longer excited-state lifetimes (70.5-106 ns) at r.t. compared to that of $[Ru(tpy)_2]^{2+}$.³⁶

Cyclometallated $[(N^{\wedge}C^{\wedge}N)Ru(tpy)]^+$ -complexes containing fused benzimidazolyl (\mathbf{Mebib})³⁷ or substituted triazole units³⁸ also exhibit improved r.t. excited-state lifetimes due to a combination of favourable effects of σ -donation (Figure 1.6), which counteracts the unfavourable effects of steric strain in these complexes and increases π -delocalization.

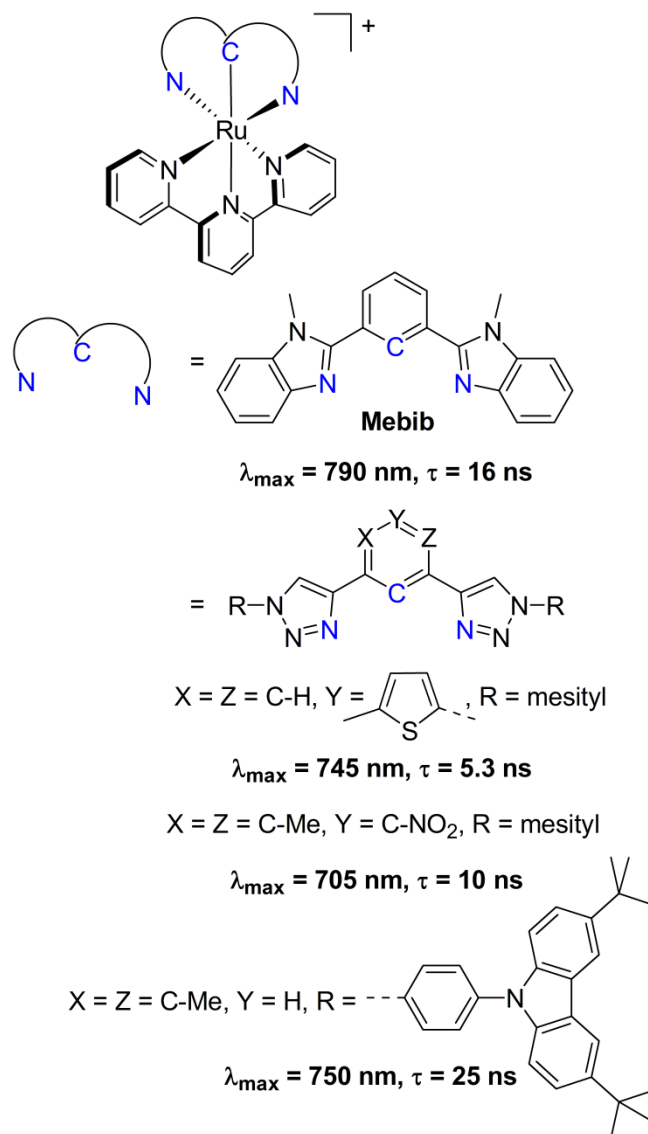


Figure 1.6. Ru-polypyridyl complexes with various cyclometallating ligands.^{37,38}

1.4.1. (B) Alternative *N*-heterocycles as strong σ donors

Attaching different *N*-heterocycles in the 2,6-positions of a pyridine ring affords tridentate heterocyclic ligands that fine-tune the $^3\text{MLCT}$ - ^3MC energy gap in their homo- or hetero-leptic Ru(II) complexes. The increased N content in these ligands enhances σ -donation onto the metal (due to resonance effects) and thus destabilizes the metal-based ^3MC state. Three different approaches have been adopted to develop σ -donating neutral tridentate ligands with increased N content.

1.4.1. (B.i) Pyridine ring attached with fused benzimidazolyl ring containing two N

In a typical approach, the bis(benzimidazolyl)pyridine (**bip**) and bis(*N,N'*-dimethylbenzimidazolyl)pyridine (**Mebip**)³⁷ can be synthesized by condensation of 1,2-phenylenediamine and *N*-methyl-1,2-phenylenediamine, respectively, with pyridine-2,6-dicarboxylic acid in polyphosphoric acid at elevated temperature (~ 200 °C). The heteroleptic complexes can be synthesized as shown in Scheme 1.1. The complexes exhibit r.t. luminescence at lower energy associated with a longer excited-state lifetime (Figure 1.7). The unfavorable consequences of increased steric strain due to the fused benzene rings in **bip** are countered by the favorable σ -donation due to increased N content. A linear relationship with positive slope of $\ln(k_{nr})$ vs. E_{em}^{max} clearly indicates that the predominant pathway of non-radiative decay via ³MLCT-to-³MC surface crossing has been efficiently reduced with increasing electron withdrawing influence of the substituent at 4'-position of tpy.³⁹

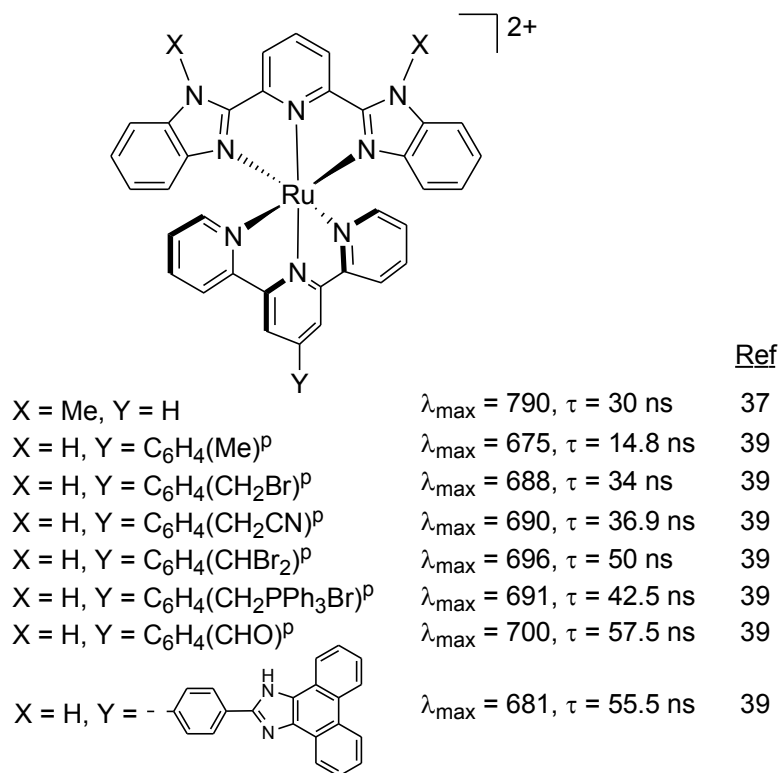


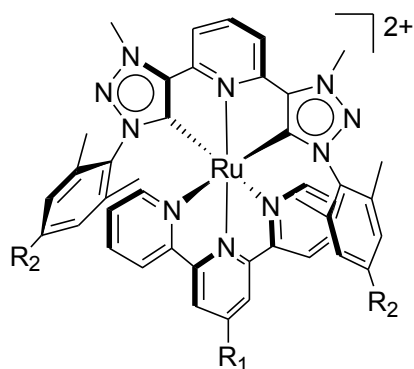
Figure 1.7. Ru-polypyridyl complexes with σ -donating bis(benzimidazolyl)pyridine (**bip**) ligands.^{37,39}

1.4.1. (B.ii) Pyridine ring attached with anionic triazole and tetrazole rings containing three N and four N atoms, respectively

The deprotonation of triazole or tetrazole rings in the tridentate core of 2,6-bis([1,2,4]triazol-3-yl)pyridine and 2,6-bis([1,2,3,4]tetrazol-5-yl)pyridine, respectively, leads to neutral heteroleptic Ru(tpy)-complexes that have improved photophysical properties. Anionic ligands donate more electron density towards the metal compared to neutral ligands. The use of triazole units is relatively unexplored due to the complications in the purification of Ru-complexes that give rise to mixture of different substitutional isomers. Nonetheless, by increasing the σ -electron density a red-shift is observed in the r.t. $^3\text{MLCT}$ emission maxima (in an average of ~ 70 nm compared to that of $[\text{Ru}(\text{tpy})_2]^{2+}$ with a much improved excited-state lifetime (24-77 ns).⁴⁰

1.4.1. (B.iii) Incorporation of carbene unit

The most recent and powerful way to destabilize the ^3MC state and thus separate the $^3\text{MLCT}$ from the ^3MC state is the incorporation of strong σ -donating and π -accepting mesoionic carbene into the tridentate ligand. The multistep synthesis of these carbene ligands includes synthesis of neutral 2,6-bis(substituted-triazolyl)pyridine precursors with $\text{C}^{\wedge}\text{N}^{\wedge}\text{C}$ cores formed by reacting 2,6-diethynylpyridine and substituted-arylazides in presence of Cu(I)-salt. These precursors were then dimethylated in presence of Me_3OBF_4 , followed by the addition of fresh Ag_2O to form the respective carbene ligands as their Ag(I)-salt. The transmetallation reaction of these Ag(I)-activated $\text{C}^{\wedge}\text{N}^{\wedge}\text{C}$ carbenes and cis- $[\text{Ru}(\text{tpy-R}_1)(\text{DMSO})\text{Cl}_2]$ (where $\text{R}_1 = \text{H}, \text{CO}_2\text{Me}, 2\text{-furyl}$ positioned at the 4'-position of tpy) under mild condition provided the heteroleptic complexes as BF_4 salts. The long τ values of these complexes are governed by the increased separation between the emissive $^3\text{MLCT}$ and deactivating ^3MC state at r.t. due to high σ -donation by the neutral-carbene moieties (Figure 1.8). This fact is also supported by the 77 K emission data, where the compounds exhibit excited-state lifetime of 13-18 μs , which is comparable to that of $[\text{Ru}(\text{tpy})_2][(\text{PF}_6)_2]$ ($\tau = 11 \mu\text{s}$) at this temperature. The unexceptionally long lifetime of the complex substituted by Br at ambient temperature is believed to be due to inductive effect operating on the carbene ligand.⁴¹



$R_1 = \text{H}, R_2 = \text{Me} \quad \lambda_{\text{max}} = 643 \text{ nm}, \tau = 385 \text{ ns}$

$R_1 = \text{CO}_2\text{Me}, R_2 = \text{Me} \quad \lambda_{\text{max}} = 688 \text{ nm}, \tau = 1720 \text{ ns}$

$R_1 = \text{furan ring}, R_2 = \text{Me} \quad \lambda_{\text{max}} = 691 \text{ nm}, \tau = 6980 \text{ ns}$

$R_1 = \text{furan ring}, R_2 = \text{Br} \quad \lambda_{\text{max}} = 694 \text{ nm}, \tau = 7900 \text{ ns}$

Figure 1.8. Ru-polypyridyl complexes with σ -donating carbene ligands and their photophysical data in EtOH:MeOH (80:20, v/v) at r.t.⁴¹

1.4.2. Expanding the chelate ring

Ligand-field splitting is amplified with a hexacoordinated metal ion in octahedral (or near octahedral) geometry as opposed to a distorted octahedral geometry. Following this argument, approaches have been made to reduce the angular strain formed between the Ru(II) ion and the tridentate ligands, which raises the energy of the ^3MC state. This section can be sub-categorized into four other sections, and has seen the greatest interest by researchers in the last decade.

1.4.2. (A) Single unit expansion to form one six-membered chelate ring

Flexible ligands were synthesized by introducing a sp^3 hybridised carbon-spacer between the *N*-heterocyclic rings and the 2,2'-bipyridine unit (Figure 1.9) and their complexation reactions with $[\text{RuCl}_3]$ or $[(p\text{-tolyl-tpy})\text{RuCl}_3]$ have been performed. In a general approach these flexible ligands can be synthesized by coupling 2-*N*-heterocyclic arylbromide with 6-cyano-2,2'-bipyridine in presence of $n\text{BuLi}$ to furnish a bipyridyl-*N*-heterocyclic-ketone, which can be subsequently reduced to form the sp^3 -C. Although the heteroleptic $[(p\text{-tolyl-tpy})\text{Ru}(\text{bpy-CMe}_2\text{-py})]$ was found to be very weakly emissive, other

complexes exhibit slightly improved r.t. luminescence excited-state lifetime with red-shifted emission maxima.^{42,43}

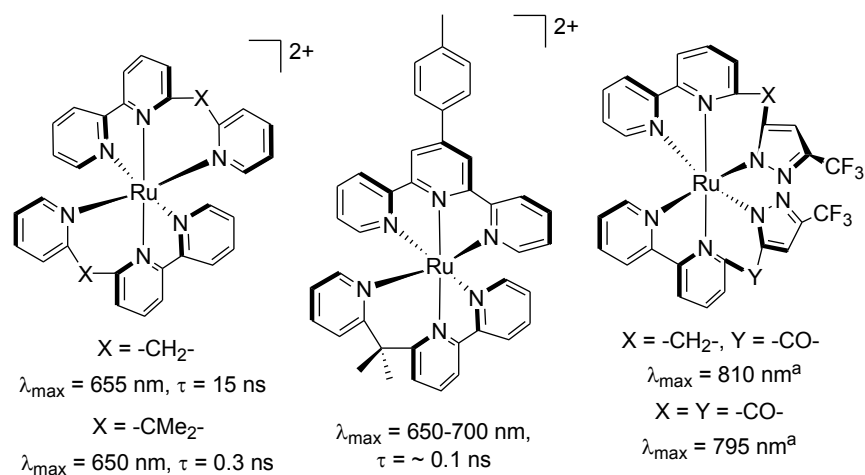


Figure 1.9. Increasing ligand field strength by alleviating steric strain in tridentate ligands.^{42,43} ^aAs solid, no τ is reported.⁴³

1.4.2. (B) Double unit expansion to form two six-membered chelate rings with broken π -conjugation

The coordination geometry around ruthenium can be made more octahedral by incorporating two $-\text{NMe}-$ units between the pyridine rings.⁴⁴ The resulting tridentate ligand furnishes two six-membered chelate rings upon complexation. The *N,N'*-dimethyl-*N,N'*-dipyridin-2-yl-pyridine-2,6-diamine (**ddpd**) ligand can be synthesized by base-catalyzed nucleophilic substitution of 2,6-dibromopyridine by *N*-methylpyridin-2-yl-amine or by taking advantage of C-N bond forming reaction between 2,6-dibromopyridine and *N*-methylpyridin-2-yl-amine. The corresponding heteroleptic complexes were synthesized following complexation reaction in Scheme 1.1 by microwave-assisted heating. The **ddpd** $\text{N}_{\text{cis}}\text{-Ru-N}_{\text{cis}}$ bite angles expands upto $87\text{-}88^\circ$, which is very close to ideal 90° octahedral bite angle, resulting in effective σ -overlap of metal d orbitals (“ e_g ”) with the lone pairs of the **ddpd** nitrogen donor atoms. Due to this optimal overlap, the energy of the metal-based ^3MC state increases, thus prolonging the excited-state lifetime at r.t. for these complexes. The added ‘push-pull’ effect by N donors in **ddpd** moiety and EWGs in tpy moiety, respectively, also decreases the HOMO-LUMO gap, resulting in the low-energy $^3\text{MLCT}$ emission (Figure 1.10).

Another photophysically appealing Ru(II) complex containing two tridentate ligands is the homoleptic Ru(II) complex of 2,6-bis(2-pyridylmethylketone)pyridine, which exhibits r.t. excited-state lifetime up to 3.3 μs in deaerated acetonitrile solution, albeit the $^3\text{MLCT}$ maxima shift to a higher-energy region (608 nm) compared to that of $[\text{Ru}(\text{tpy})_2]^{2+}$. The homoleptic Ru(II) complex of the ligand 2,6-bis(2-pyridylmethylketone)pyridine could be obtained by reaction of 2,6-bis(2-pyridylmethyl)pyridine (**bpmp**) and $\text{Ru}(\text{DMSO})_4\text{Cl}_2$ (DMSO = dimethylsulfoxide) at 100 $^\circ\text{C}$ in *N,N'*-dimethylformamide (DMF). This reaction leads to coordination of the two **bpmp** ligands with one Ru(II) ion, accompanied by simultaneous oxidation of the methylene groups of the **bpmp** ligand to the corresponding diketone ligand. Any attempt to react 2,6-bis(2-pyridylmethylketone)pyridine directly with $\text{Ru}(\text{DMSO})_4\text{Cl}_2$ failed to yield the homoleptic complex. Nonetheless, the almost perfect octahedral geometry around Ru, where $\text{N}_{\text{cis}}\text{-Ru-N}_{\text{cis}}$ and average $\text{N}_{\text{trans}}\text{-Ru-N}_{\text{trans}}$ bite angles are $89.58(12)^\circ$ and $178.48(12)^\circ$, increases the $^3\text{MLCT}$ - ^3MC energy gap in such a way that the complex also exhibit r.t. excited-state lifetime upto 1.36 μs in air-equilibrated acetonitrile solution.⁴⁵

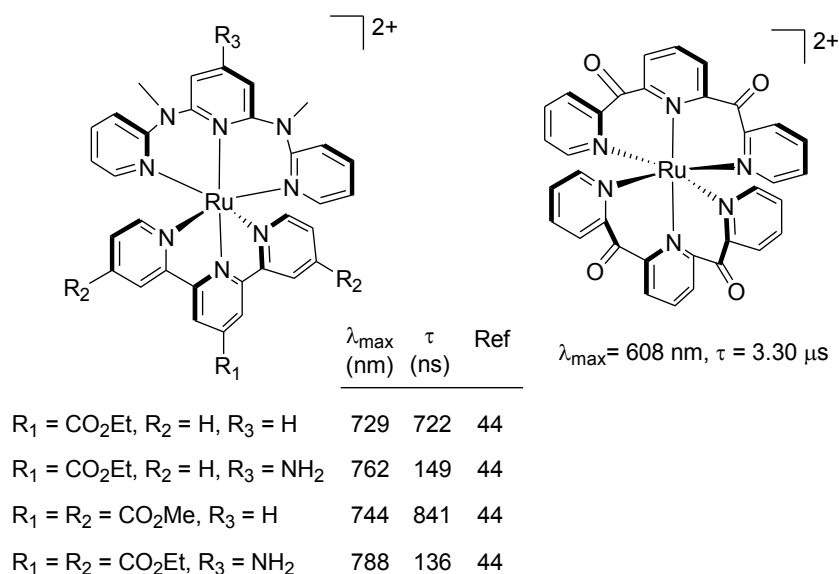


Figure 1.10. Increasing ligand field strength by alleviating steric strain in tridentate ligands.^{44,45}

1.4.2. (C) Double unit expansion to form two six-membered chelate rings with extended π -conjugation

Considerable attention has focused on attaching quinoline, quinoxaline or 7-azaindole groups on to suitably substituted 2,6-dibromopyridine to give tridentate ligands that are able to form two six-membered chelate rings with extended π -conjugation and almost linear $N_{\text{trans}}\text{-Ru-}N_{\text{trans}}$ bite angle upon coordination (Figure 1.11).⁴⁶ Several homo- and hetero-leptic Ru-complexes with these ligands have been synthesized. The complexes containing meridional-2,6-di(quinoline)pyridine (**dqp**) as tridentate ligands, and the ester-substituted versions exhibit exceedingly long r.t. excited-state lifetime in MeOH-EtOH mixtures. The relatively short r.t. excited-state lifetime of homoleptic Ru(II) complex of 2,6-di-(quinoxalin-5-yl)pyridine (**dqxp**) is presumably due to the higher stabilization of the ³MLCT state compared to that of the homoleptic Ru(**dqp**)²⁺ complex, so that the direct deactivation to the ground state is viable, although the ³MC state remains high in energy due to near-octahedral geometry and consequently larger ligand-field splitting.^{47,48}

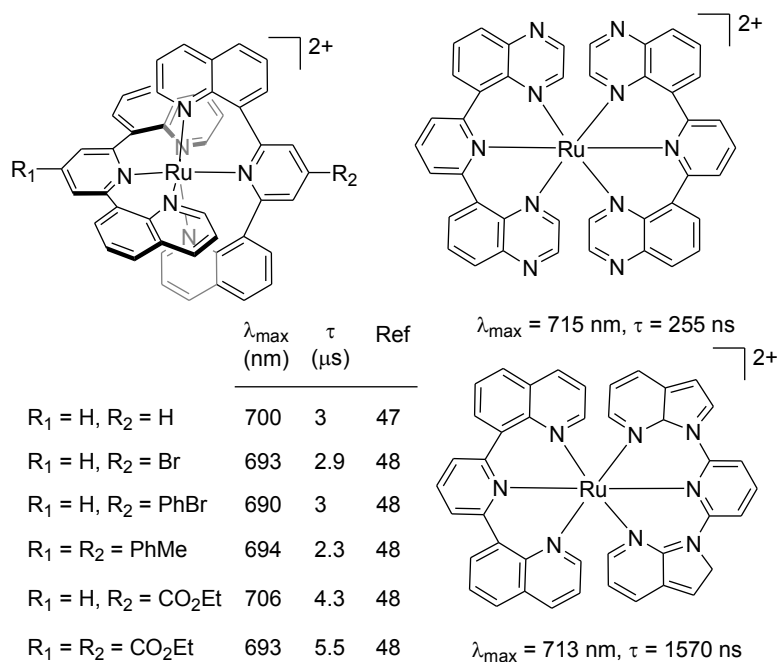
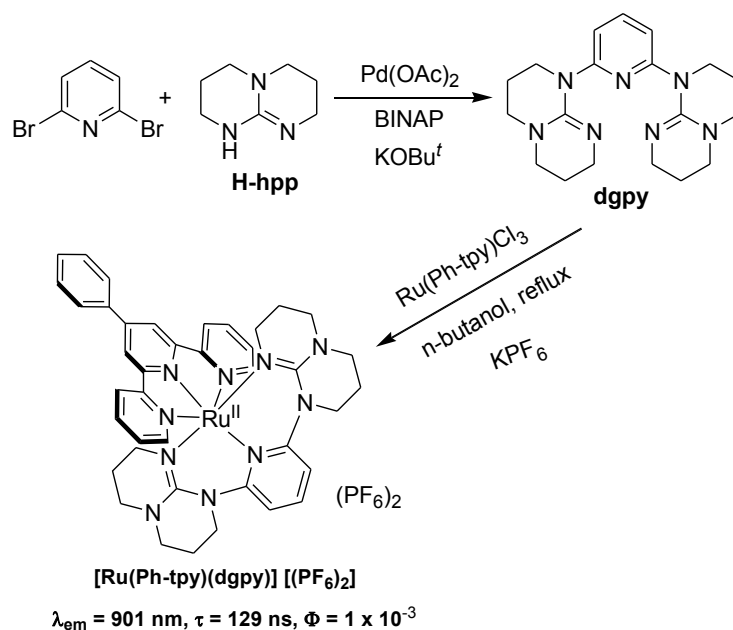


Figure 1.11. Increasing ligand field strength by alleviating steric strain in tridentate ligands.^{47,48}

1.4.2. (D) Double unit expansion to form two six-membered chelate rings with guanidine backbone

We recently adopted a mixed strategy in which both the effects, for e.g., (i) destabilization of metal-based 3MC states due to increased σ -donor ability and (ii) improved ligand-field strength with decrease in angular strain around ruthenium by forming two six-membered chelate rings. Incorporation of 1,3,4,6,7,8-hexahydro-2H-pyrimido[1,2- α]pyrimidine (**H-hpp**) in the 2,6-positions of a pyridine ring gives 2,6-di(**hpp**)pyridine (diguanidylpyridine or **dgpy**) and subsequent complexation with Ru(Ph-tpy)Cl₃ in 1:1 molar ratio affords the heteroleptic complex (Scheme 1.4). The [Ru(Ph-tpy)(**dgpy**)]²⁺ complex is a NIR-emitter with long r.t. excited-state lifetime and high quantum yield (Φ). These properties are fruitful for vectorial electron and energy transfer processes in solution or at semiconductor interfaces and also in biological applications as luminescent sensors in cell-imaging systems.⁴⁹



Scheme 1.4. Strong σ -donor ligand **dgpy** and its heteroleptic Ru(II) complex.⁴⁹

1.5. Bichromophoric Systems

The most successful method that has been adopted so far is the incorporation of an organic chromophore onto the tpy unit. The necessary criterion in this bichromophoric approach is that the newly-introduced auxiliary chromophore should have a triplet state that is quasi-isoenergetic with the emissive 3MLCT state. This will permit reversible inter-

component excited-state energy transfer between the equilibrating $^3\text{MLCT}$ and $^3(\pi-\pi^*)$ state of the chromophore, so that the organic chromophore basically acts as an energy reservoir to repopulate the emissive $^3\text{MLCT}$ state, with an overall effect of ‘delaying’ the emission giving longer excited-state lifetimes. The successful incorporation of aromatic hydrocarbons, such as pyrene, naphthalene and anthracene, onto the tpy backbone supports this fact (Figure 1.12). The most widely-used auxiliary chromophore is the anthracene (or its substituted derivatives) as its triplet state (^3An) is lower in energy ($E^{00} = 1.85$ eV, 671 nm) compared to $^3\text{MLCT}$ energy of tpy-based Ru(II) complexes, whereas pyrene’s triplet state (^3Pyr) is higher in energy ($E^{00} = 2.10$ eV, 590 nm).^{50,51} Despite this mismatch in energy, incorporation of pyrene and naphthalene moieties onto tpy do indeed prolong the r.t. excited-state lifetimes of their corresponding homo- or hetero-leptic complexes (top-left and top-middle complexes in Figure 1.12). A dual emission feature is presumably due to the fact that the first component of emission with associated excited-state lifetime of 1.5-2.1 ns is attributed to the $^3\text{MLCT}$ state based on the tpy or phenyl-terpyridine units, respectively, and the second component arises from the equilibrium with ^3Pyr or ^3Np (triplet naphthalene) which repopulate the $^3\text{MLCT}$ state after the initial emission.⁵²

The parent homoleptic Ru(II) complex, $[\text{Ru}(\text{tpy-An})_2]^{2+}$, which consists of an anthracene moiety directly connected to the 4’-position of terpyridine, is not luminescent at room temperature. This is due to the fact that the energy of the $^3\text{MLCT}$ state is significantly higher in energy than the non-emissive ^3An state and irreversible energy transfer occurs thereby quenching the $^3\text{MLCT}$ excited state. The complexes with ligands containing a phenyl or 2-pyrimidyl spacer between the 4’-position of a dpt or tpy unit, respectively, and the (substituted)anthracene exhibit prolonged r.t. excited state lifetimes. This is due to the fact that the incorporation of phenyl-dpt or 2-pyrimidyl-tpy spacers render the ^3An state nearly isoenergetic to the emissive $^3\text{MLCT}$ state and hence the $^3\text{MLCT}$ - ^3An equilibrium is now more facile. The mono-exponential decay in the r.t. excited state lifetime of the Ru(II) complexes containing dpt core (top-right complexes in Figure 1.12) may be explained as an emission from a triplet intraligand state, resulting from the mixing of triplet $^3\text{MLCT}$ and ^3An state.^{26a} Homo- or hetero-leptic Ru(II) complexes of 4’-[5-(9-anthryl)-pyrimid-2-yl]tpy and tpy or 5-chloro-pyrimid-2-yl-tpy (bottom-left and bottom-middle complexes in Figure 1.12) exhibit a first relatively short-lived r.t. excited-state lifetime associated with $^3\text{MLCT}$

state of pyrimidyl-tpy and a second fairly long-lived, particularly for the homoleptic complex, ‘delayed’ excited-state lifetime resulting from its repopulation from the ^3An state.

The longest r.t. excited-state lifetime from a Ru(II)-bis(tridentate) complex (bottom-right complex in Figure 1.12), reported to date gains mixed advantage of (i) relieved angular strain by forming two π -delocalized six-membered rings around Ru and (ii) the bichromophoric effect, rendering it to be luminescent with a secondary excited-state lifetime of 42 μs at r.t. in degassed acetonitrile. This extremely long lifetime is due to near quantitative reversible electronic energy transfer between the $^3\text{MLCT}$ and ^3An states. The excited-state equilibration is essentially complete in less than 400 picoseconds with an average of 94% of energy being stocked on the organic energy reservoir, as revealed by ultrafast time-resolved spectroscopies.⁵³

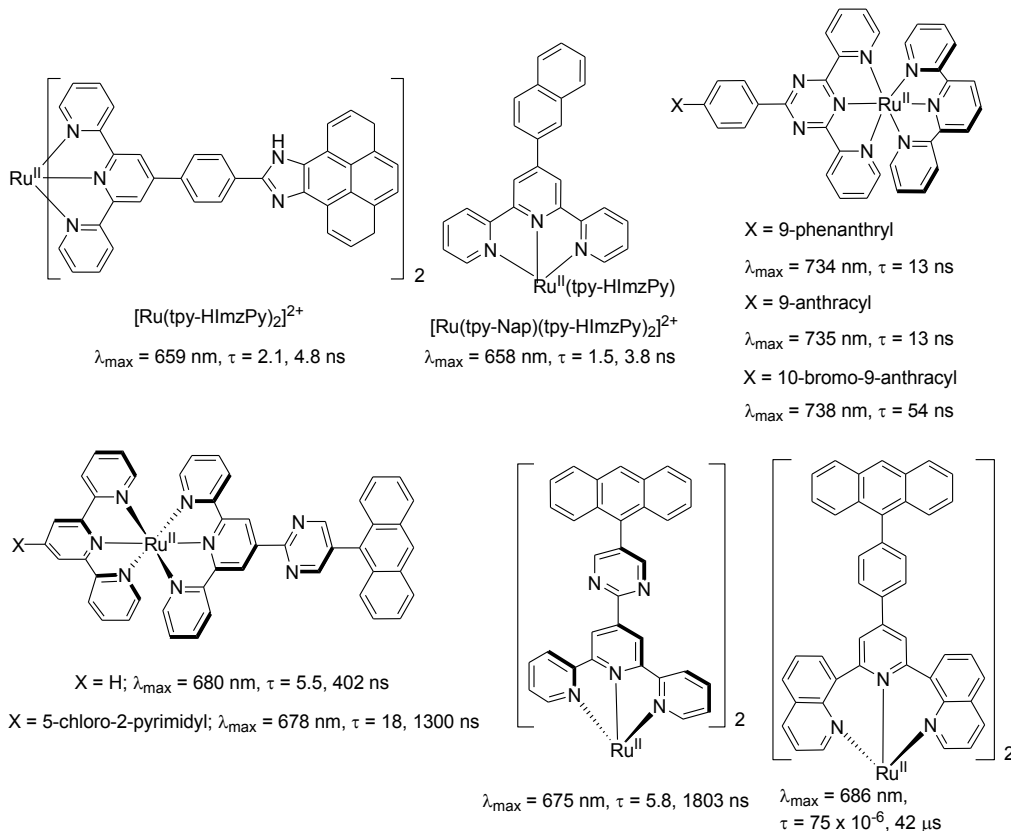


Figure 1.12. Bichromophoric Ru(II) complexes of tridentate ligands.

1.6. Summary and outlook

In this Chapter, different strategies to synthesize new tridentate ligands with different electronic and substitutional properties and their mononuclear homo- or heteroleptic Ru(II) complexes have been presented. Various approaches to enhance the r.t.

excited-state lifetime of these complexes, based on judicious design of ligands, are also discussed. To date, the most efficient means of prolonging r.t. luminescence lifetimes is through a combination of the bichromophoric approach and the effect of reducing the angular strain around the metal ion. The incorporation of strong σ -donor tridentate ligands in the form of **dgpy** or NHC is also reasonably promising. Figure 1.13 gives a summary of the mononuclear tridentate complexes with the longest reported r.t. excited-state lifetimes. Although the optimization of the photophysical properties of Ru(II) complexes of tridentate ligands is still a developing area of polypyridine chemistry, it is clearly apparent from the survey of recent literature that considerable potential exists to increase the luminescence lifetimes of Ru(II) complexes of tridentate ligands using a combination of the strategies outlined herein. Considering recent interest in polyruthenium dendrimers and polymers containing tridentate ligands, the ability to make them r.t. luminescent bodes well for future applications.

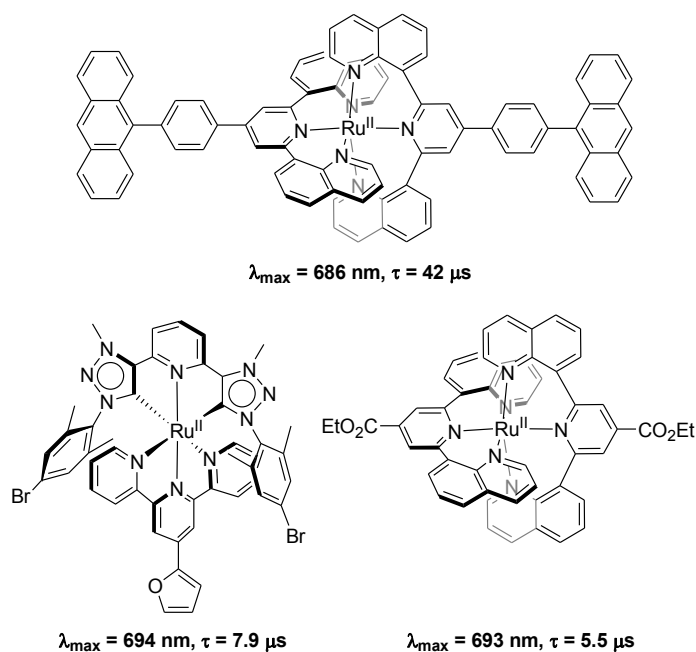


Figure 1.13. Top three complexes with the longest r.t. excited-state lifetimes.

1.7. References

- (1) E. Baranoff, J.-P. Collin, L. Flamigni and J.-P. Sauvage, *Chem. Soc. Rev.*, 2004, **33**, 147.
- (2) H. Xiang, J. Cheng, X. Ma, X. Zhou, J. J. Chruma, *Chem. Soc. Rev.*, 2013, **42**, 6128.
- (3) M. R. Gill, J. Garcia-Lara, S. J. Foster, C. Smythe, G. Battaglia, J. A. Thomas, *Nat. Chem.*, 2009, **1**, 662.

Chapter 1

- (4) J. Barber, B. Anderson, *Nature*, 1994, **370**, 31.
- (5) E. A. Medlycott, G. S. Hanan, *Coord. Chem. Rev.*, 2006, **250**, 1763.
- (6) J. K. McCusker, *Acc. Chem. Res.*, 2003, **36**, 876 and references cited therein.
- (7) J. P. Sauvage, J. P. Collin, J. C. Chambron, S. Guillerez, C. Coudret, V. Balzani, F. Barigelletti, L. De Cola and L. Flamigni, *Chem. Rev.*, 1994, **94**, 993.
- (8) (a) F. S. Han, M. Higuchi, D. G. Kurth, *J. Am. Chem. Soc.*, 2008, **130**, 2073, (b) M. Maestri, N. Armaroli, V. Balzani, E. C. Constable, A. M. W. C. Thompson, *Inorg. Chem.*, 1995, **34**, 2759 and references cited therein.
- (9) S. Pyo, E. Perez-Cordero, S. G. Bott and L. Echegoyen, *Inorg. Chem.*, 1999, **38**, 3337.
- (10) J. M. Calvert, J. V. Caspar, R. A. Binstead, T. D. Westmoreland and T. J. Meyer, *J. Am. Chem. Soc.*, 1982, **104**, 6620.
- (11) A. Juris, V. Balzani, F. Barigelletti, S. Campagna, P. Belser and A. Von Zelewsky, *Coord. Chem. Rev.*, 1988, **84**, 85.
- (12) E. A. Medlycott, G. S. Hanan, *Chem. Soc. Rev.*, 2005, **34**, 133.
- (13) J. Wang, Y.-Q. Fang, G. S. Hanan, F. Loiseau and S. Campagna, *Inorg. Chem.*, 2005, **44**, 5.
- (14) H. J. Bolink, L. Cappelli, E. Coronado and P. Gaviña, *Inorg. Chem.*, 2005, **44**, 5966.
- (15) J. Wang, G. S. Hanan, *Synlett*, 2005, 1251.
- (16) G. J. E. Davidson, S. J. Loeb, P. Passaniti, S. Silvi and A. Credi, *Chem. Eur. J.* 2006, **12**, 3233.
- (17) E. C. Constable, C. E. Housecroft, E. R. Schofield, S. Encinas, N. Armaroli, F. Barigelletti, L. Flamigni, E. Figgemeier and J. G. Vos, *Chem. Commun.*, 1999, 869.
- (18) J. Fortage, G. Dupeyre, F. Tuyèras, V. Marvaud, P. Ochsenbein, I. Ciofini, M. Hromadová, L. Pospíšil, A. Arrigo, E. Trovato, F. Puntoriero, P. P. Lainé and S. Campagna, *Inorg. Chem.*, 2013, **52**, 11944 and references cited therein.
- (19) (a) C. Goze, C. Sabatini, A. Barbieri, F. Barigelletti, R. Ziessel, *Inorg. Chem.*, 2007, **46**, 7341; (b) A. Barbieri, B. Ventura, R. Ziessel, *Coord. Chem. Rev.*, 2012, **256**, 1732 and references cited therein.
- (20) P. Manca, M. I. Pilo, G. Sanna, A. Zucca, Gi. Bergamini and P. Ceroni, *Chem. Commun.*, 2011, **47**, 3413.
- (21) P. J. Vallett, N. H. Damrauer, *J. Phys. Chem. A*, 2013, **117**, 6489.
- (22) C. Bhaumik, S. Das, D. Maity and S. Baitalik, *Dalton Trans.*, 2012, **41**, 2427.
- (23) K.-Q. Wu, J. Guo, J.-F. Yan, L.-L. Xie, F.-B. Xu, S. Bai, P. Nockemann and Y.-F. Yuan, *Organometallics*, 2011, **30**, 3504.
- (24) Y.-Q. Fang, N. J. Taylor, G. S. Hanan, F. Loiseau, R. Passalacqua, S. Campagna, H. Nierengarten and A. Van Dorsselaer, *J. Am. Chem. Soc.*, 2002, **124**, 7912.
- (25) Y.-Q. Fang, N. J. Taylor, F. Laverdière, G. S. Hanan, F. Loiseau, F. Nastasi, S. Campagna, H. Nierengarten, E. Leize-Wagner and A. V. Dorsselaer, *Inorg. Chem.*, 2007, **46**, 2854.

Chapter 1

- (26) (a) E. A. Medlycott, G. S. Hanan, F. Loiseau, S. Campagna, *Chem. Eur. J.*, 2007, **13**, 2837; (b) M. I. J. Polson, E. A. Medlycott, G. S. Hanan, L. Mikelsons, N. J. Taylor, M. Watanabe, Y. Tanaka, F. Loiseau, R. Passalacqua, S. Campagna, *Chem. Eur. J.*, 2004, **10**, 3640.
- (27) M. Schwalbe, M. Karnahl, H. Görls, D. Chartrand, F. Laverdiere, G. S. Hanan, S. Tschierlei, B. Dietzek, M. Schmitt, J. Popp, J. G. Vos, S. Rau, *Dalton Trans.*, 2009, **20**, 4012 and references cited therein.
- (28) F. Nastasi, F. Loiseau, S. Campagna, E. A. Medlycott, M.-P. Santoni, G. S. Hanan, *Can. J. Chem.*, 2009, **87**, 254.
- (29) M. I. J. Polson, F. Loiseau, S. Campagna and G. S. Hanan, *Chem. Commun.*, 2006, **12**, 1301 and references cited therein.
- (30) R. Liegghio, P. G. Potvin, A. B. P. Lever, *Inorg. Chem.*, 2001, **40**, 5485.
- (31) P. G. Bomben, K. C. D. Robson, B. D. Koivisto, C. P. Berlinguette, *Coord. Chem. Rev.*, 2012, **256**, 1438 and references cited therein.
- (32) T. Koizumi, T. Tomon and K. Tanaka, *Organometallics*, 2003, **22**, 970.
- (33) D. A. Beauchamp, S. J. Loeb, *Supramol. Chem.*, 2005, **17**, 617.
- (34) B. Bozic-Weber, E. C. Constable, C. E. Housecroft, P. Kopecky, M. Neuburger, J. A. Zampese, *Dalton Trans.*, 2011, **40**, 12584.
- (35) S. H. Wadman, M. Lutz, D. M. Tooke, A. L. Spek, F. Hartl, R. W. A. Havenith, G. P. M. van Klink, G. van Koten, *Inorg. Chem.*, 2009, **48**, 1887.
- (36) F. Barigelletti, B. Ventura, J.-P. Collin, R. Kayhanian, P. Gavina, J.-P. Sauvage, *Eur. J. Inorg. Chem.*, 2000, 113.
- (37) W.-W. Yang, Y.-W. Zhong, S. Yoshikawa, J.-Y. Shao, S. Masaoka, K. Sakai, J. Yao, M. Haga, *Inorg. Chem.*, 2011, **50**, 3959.
- (38) B. Schulze, D. Escudero, C. Friebe, R. Siebert, H. Görls, S. Sinn, M. Thomas, S. Mai, J. Popp, B. Dietzek, L. González, U. S. Schubert, *Chem. Eur. J.*, 2012, **18**, 4010.
- (39) (a) C. Bhaumik, S. Das, D. Saha, S. Dutta, S. Baitalik, *Inorg. Chem.*, 2010, **49**, 5049 and references cited therein, (b) C. Bhaumik, D. Saha, S. Das, S. Baitalik, *Inorg. Chem.*, 2011, **50**, 12586.
- (40) M. Duati, S. Tasca, F. C. Lynch, H. Bohlen, J. G. Vos, *Inorg. Chem.*, 2003, **42**, 8377.
- (41) D. G. Brown, N. Sangantrakun, B. Schulze, U. S. Schubert, C. P. Berlinguette, *J. Am. Chem. Soc.*, 2012, **134**, 12354.
- (42) M. Abrahamsson, M. J. Lundqvist, H. Wolpher, O. Johansson, L. Eriksson, J. Bergquist, T. Rasmussen, H.-C. Becker, L. Hammarström, P.-O. Norrby, B. Åkermark, P. Persson, *Inorg. Chem.*, 2008, **47**, 3540.
- (43) J.-L. Chen, Y. Chi, K. Chen, *Inorg. Chem.*, 2010, **49**, 823.
- (44) A. Breivogel, M. Meister, C. Förster, F. Laquai, K. Heinze, *Chem. Eur. J.*, 2013, **19**, 13745 and references cited therein.
- (45) F. Schramm, V. Meded, H. Fliegl, K. Fink, O. Fuhr, Z. Qu, W. Klopffer, S. Finn, T. E. Keyes, M. Ruben, *Inorg. Chem.*, 2009, **48**, 5677.

Chapter 1

- (46) L. Hammarström, O. Johansson, *Coord. Chem. Rev.*, 2010, **254**, 2546 and references cited therein.
- (47) G. A. Parada, L. A. Fredin, M.-P. Santoni, M. Jäger, R. Lomoth, L. Hammarström, O. Johansson, P. Persson, S. Ott, *Inorg. Chem.*, 2013, **52**, 5128 and references cited therein.
- (48) M. Jäger, R. J. Kumar, H. Görls, J. Bergquist, O. Johansson, *Inorg. Chem.*, 2009, **48**, 3228.
- (49) A. K. Pal, N. Zaccheroni, S. Campagna, G. S. Hanan, *Chem. Commun.*, 2014, accepted for publication.
- (50) S. Murov, I. Carmichael, G. L. Hugin, *Handbook of Photochemistry*, 2nd edn, Marcel Dekker, New York, 1993.
- (51) J. P. Prieto, L. P. Pérez, M. González-Béjar, M. A. Miranda, S.-E. Stiriba, *Chem. Commun.*, 2005, **44**, 5569.
- (52) D. Maity, C. Bhaumik, D. Mondal, S. Baitalik, *Inorg. Chem.*, 2013, **52**, 13941.
- (53) G. Ragazzon, P. Verwilst, S. A. Denisov, A. Credi, G. Jonusauskas, N. D. McClenaghan, *Chem. Commun.*, 2013, **49**, 9110.

Chapter 2: *Red Emitting [Ru(bpy)₂(N-N)]²⁺*

Photosensitizers: Emission from a Ruthenium(II)-to-2,2'-Bipyridine ³MLCT State in the Presence of Neutral Ancillary 'Super Donor' Ligands

2.1. Résumé

La synthèse et la caractérisation d'une nouvelle famille de complexes [Ru^{II}(bpy)₂(N-N)] (PF₆)₂ (bpy = 2,2'-bipyridine) sont rapportés, où N-N = pyridine/pyrimidine/pyrazine fonctionnalisé dans des positions différentes de l'unité hexahydropyrimidopyrimidine bicyclique donneur d'électrons (**HPP**). Une série de ligands bidentate **1a-5a** ont été synthétisés avec des rendements élevés (55-96 %). Les complexes correspondants **1b**, **2b** et **5b** ont été préparés dans du n-butanol, tandis que les complexes **3b** et **4b** ont été préparés dans un mélange de n-butanol et d'eau (1:1, v/v) dans de bons rendements modestes (23 à 76%). Les deux structures complexes ligand et ont été entièrement caractérisés par une variété de techniques, y compris la cristallographie aux rayons-X. Dans les études de voltampérométrie cyclique, tous les complexes présentent un couple Ru^{III}/II, qui est de ~500 mV moins positive que le couple Ru^{III}/II en Ru(bpy)₃²⁺. Les ¹MLCT et ³MLCT états de tous les complexes (530-560 nm) sont décalés les 732-745 nm bathochrome par rapport au Ru(bpy)₃²⁺ (450 nm/620 nm). Ces valeurs sont en bon accord avec les calculs DFT et TD-DFT.

Chapter 2

Contribution :

Amlan K. Pal : Optimised syntheses and characterisation of ligands and complexes, crystal structure determination of the ligand and complexes, photophysical studies, computational modeling of complexes by DFT and TD-DFT calculations, writing the full-paper.

Samik Nag : Preliminary syntheses and characterisations of some ligands and complexes.

Janaina G. Ferreira : Crystal structure determination of one of the complexes.

Victor Brochery : Preliminary synthesis of a ligand.

Giuseppina La Ganga : Photophysical (luminescence) measurements of the complexes.

Antonio Santoro : Photophysical (luminescence) measurements of the complexes.

Scolastica Serroni : Photophysical (luminescence) measurements of the complexes.

Sebastiano Campagna : Photophysical (luminescence) measurements of the complexes.

Garry S. Hanan : Supervision, revision of the article.

Red Emitting $[\text{Ru}(\text{bpy})_2(\text{N-N})]^{2+}$
Photosensitizers: Emission from a Ruthenium(II)-
to-2,2'-Bipyridine $^3\text{MLCT}$ State in the Presence
of Neutral Ancillary ‘Super Donor’ Ligands

*Amlan K. Pal,[†] Samik Nag,[‡] Janaina G. Ferreira,[†] Victor Brochery,[†] Giuseppina La
Ganga,[§] Antonio Santoro,[§] Scolastica Serroni,[§] Sebastiano Campagna,^{*§} and Garry S.
Hanan^{*†}*

[†]Département of Chemistry, Université de Montréal, Montréal, Québec, H3T-1J4, Canada,
[‡]Department of Chemical Sciences, Sikkim University, Sixth Mile, Tadong, Gangtok,
Sikkim, India 737102, and [§]Dipartimento di Scienze Chimiche, Università di Messina, Via
Sperone 31, I-98166 Messina, Italy.

Received: November 12, 2013; Published: January 13, 2014

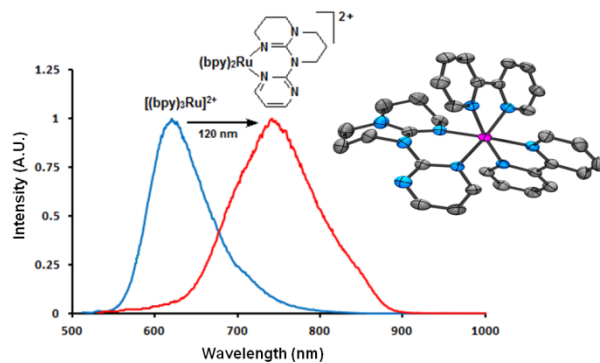
[dx.doi.org/10.1021/ic4028332](https://doi.org/10.1021/ic4028332)

Reproduced with permission from *Inorg. Chem.* **2014**, 53, 1679–1689.

Copyright 2014 American Chemical Society.

KEYWORDS: neutral bidentate ligands, low-energy MLCT, redox mediators, red emitters.

2.2. Table of Content Graphic



A series of complexes containing bis(2,2'-bipyridine)ruthenium(II) and neutral ancillary “super donor” ligands were synthesized and characterized. Their structural, electrochemical, and photophysical properties were studied and compared to those of tris(2,2'-bipyridine)ruthenium(II) and some reference compounds. Their properties were also modeled by density functional theory calculations, and trends were found *vs.* the nature of the basicity of the heterocycle attached to the saturated aliphatic guanidyl moiety.

2.3. Abstract

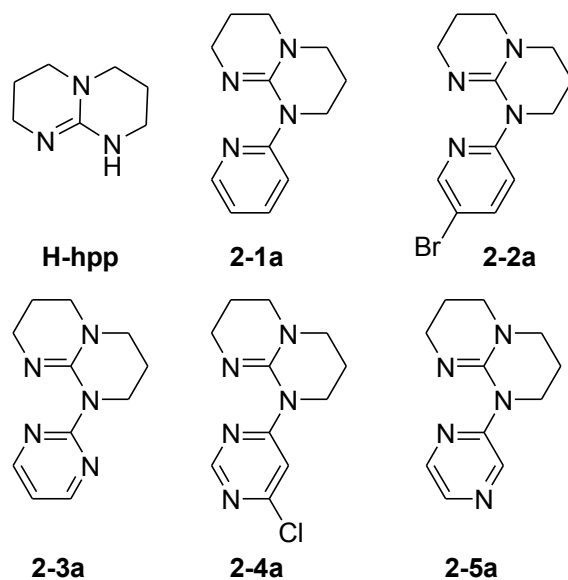
The synthesis and characterization of a novel family of $[\text{Ru}^{\text{II}}(\text{bpy})_2(\text{N-N})](\text{PF}_6)_2$ (bpy = 2,2'-bipyridine) complexes are reported, where N-N = pyridine/pyrimidine/pyrazine functionalized in different positions with the electron-donating bicyclic hexahydropyrimidopyrimidine (**hpp**) unit. A series of bidentate ligands **1a-5a** were synthesized in good to high yields (55-96%). The corresponding complexes **1b**, **2b** and **5b** were prepared in *n*-butanol, while complexes **3b** and **4b** were prepared in a mixture of *n*-butanol and water (1:1, v/v) in modest to good yields (23-76%). Both ligand and complex structures were fully characterized by a variety of techniques including X-ray crystallography. In cyclic voltammetric studies, all the complexes exhibit a $\text{Ru}^{\text{III/II}}$ couple, which is ~ 500 mV less positive than the $\text{Ru}^{\text{III/II}}$ couple in $[\text{Ru}(\text{bpy})_3]^{2+}$. The $^1\text{MLCT}$ and $^3\text{MLCT}$ states of all the complexes (530-560 nm/732-745 nm) are shifted bathochromically as compared to $[\text{Ru}(\text{bpy})_3]^{2+}$ (450 nm/620 nm). These values are in good agreement with DFT and TD-DFT calculations.

2.4. Introduction

For decades Ru(II)(bpy)₃ (bpy = 2,2'-bipyridine) type complexes have attracted considerable interest because of their tunable photophysical properties^{1a-e} as well as their potential for applications in water oxidation,² artificial photosynthesis,³ and more generally in solar energy conversion.^{3a,4} More recently, Ru(II)-based red-emitting photosensitizers with relatively long excited-state lifetimes have drawn attention as they exhibit potential application in biological systems⁵ and as low-lying energy traps in multichromophore arrays.⁶ Judicious choice of the ligands bonded to Ru(II) can tune the energy of the excited state,^{7a-c} the excited-state lifetime^{1c,7,8} and the absorption energy of the complex,⁷⁻⁹ while overcoming the limitation imposed by the energy gap law^{7b-c} on the excited-state lifetime at the same time. Several strategies have been adopted by various groups to red-shift the absorption and emission of Ru(II)-heteroleptic complexes and to prolong their excited-state lifetimes; for e.g., (a) introduction of coplanar electron-withdrawing aromatic moiety containing bidiazine ligands bearing two-ring *N*-heteroatoms,¹⁰⁻¹⁴ thereby stabilizing the ³MLCT state, (b) functionalization of bpy with various substituents in order to lower the LUMO,^{15,16} (c) introduction of an organic chromophore to establish an equilibrium between the ³MLCT and the organic chromophore triplet ³LC states, (d) introduction of fused polyaromatic systems (benzoeilatin: 952 nm,¹⁷ isoeilatin: 994 nm,¹⁸ dipyridophenazine: 790 nm¹⁹), (e) the formation of oligonuclear complexes with additional electron-withdrawing metal ions.^{1,20} In general, the two principle approaches towards red-emitting Ru(II) complexes are (i) the incorporation of either a better acceptor ligand,^{15,16} in place of one bpy in [Ru(bpy)₃]²⁺, thereby decreasing the energy of the LUMO of the new [Ru(bpy)₂(acceptor)]²⁺ species or (ii) introduction of a better donor ligand that functions by raising the energy of the HOMO in the new [Ru(bpy)₂(donor)]²⁺ species.²¹

In a recent communication²¹ we demonstrated that the presence of a strongly donating **hpp** unit attached to pyridine or pyrimidine units helps to red-shift the lowest energy ³MLCT maxima of complexes **2-1b** and **2-3b** by about 100 nm compared to that of Ru(bpy)₃²⁺. Herein, we report the complete synthesis and characterization of new, neutral bidentate ligands (**2-1a** to **2-5a**; Chart 2.1) and their Ru(bpy)₂(L-L)²⁺ type (where L-L = ligands **2-1a** to **2-5a**) compounds (**2-1b** to **2-5b**). The observed redox and photophysical properties are in good agreement with the density functional theory (DFT) and time-dependent density functional theory (TD-DFT) studies of the compounds.

Chart 2.1. 1,3,4,6,7,8-Hexahydro-2*H*-pyrimido[1,2-*a*]pyrimidine (**H-hpp**) attached to various *N*-heterocycles: 2-pyridyl (**2-1a**), 5-bromo-2-pyridyl (**2-2a**), 2-pyrimidyl (**2-3a**), 6-chloro-4-pyrimidyl (**2-4a**) and 2-pyrazyl (**2-5a**).



2.5. Experimental Section

2.5.1 Materials, methods and instrumentations

Nuclear magnetic resonance (NMR) spectra were recorded in CD₃CN and CDCl₃ at room temperature (r.t.) on Bruker AV300, AV400, AV700 spectrometers and at 300, 400 and 700 MHz, respectively for ¹H NMR and at 75, 100 and 175 MHz, respectively for ¹³C NMR. Chemical shifts are reported in part per million (ppm) relative to residual solvent protons (1.94 ppm for CD₃CN, 7.26 ppm for CDCl₃) and the carbon resonance (118.69 ppm for CD₃CN, 77.00 ppm for CDCl₃) of the solvent.

Absorption spectra were measured in deaerated acetonitrile at r.t. on a Cary 500i UV-Vis-NIR Spectrophotometer. For luminescence spectra a Jobin Yvon-Spex Fluoromax 2 spectrofluorimeter was used, equipped with a Hamamatsu R3896 photomultiplier, and the spectra were corrected for photomultiplier response using a program purchased with the fluorimeter. Luminescence lifetimes were determined by time-correlated single-photon-counting (TCSPC) with an Edinburgh OB900 spectrometer (light pulse: Hamamatsu PL2 laser diode, pulse width 59 ps at 408 nm; or nitrogen discharge, pulse width at 337 nm: 2 ns). Luminescence quantum yields have been performed by the optical dilution method.²²

As quantum yield reference, $[\text{Ru}(\text{bpy})_3]^{2+}$ in aqueous deaerated solution was used ($\Phi = 0.028$).²³

Accurate mass measurements were performed on a 6210 TOF mass spectrometer from Agilent technologies, coupled to a 1100 series LC system in positive electrospray mode. Appropriate $[\text{M}]^{n+}$, $[\text{M}-\text{PF}_6]^{n+}$ or $[\text{M}+\text{H}]^{n+}$ species were used for empirical formula determination, and exact masses were calculated using Analyst® QS Software from Applied Biosystems. Electrochemical measurements were carried out in argon-purged purified acetonitrile at room temperature with a BAS CV50W multipurpose equipment interfaced to a PC. The working electrode was a glassy carbon electrode. The counter electrode was a Pt wire, and the pseudo-reference electrode was a silver wire. The reference was set using an internal 1 mM ferrocene/ferrocinium sample at 395 mV vs SCE in acetonitrile. The concentration of the compounds was about 1 mM. Tetrabutylammonium hexafluorophosphate (TBAPF_6) was used as supporting electrolyte and its concentration was 0.10 M. Cyclic voltammograms were obtained at scan rates as mentioned in the main text. The criteria for reversibility were the separation of 60 mV between cathodic and anodic peaks, the close to unity ratio of the intensities of the cathodic and anodic currents, and the constancy of the peak potential on changing scan rate. Experimental uncertainties are as follows: absorption maxima, ± 2 nm; molar absorption coefficient, 10%; redox potentials, ± 10 mV, emission maxima, ± 2 nm, emission lifetimes, $\pm 10\%$, luminescence quantum yields, $\pm 20\%$.

1,3,4,6,7,8-Hexahydro-2*H*-pyrimido[1,2-*a*]pyrimidine (**H-hpp**), 2-bromopyridine, 2-bromopyrimidine, 2,2'-bipyridine, 2,5-dibromopyridine, 4,6-dichloropyrimidine, 2-chloropyrazine, (\pm)2,2'-bis(diphenylphosphino)-1,1'-binaphthyl (BINAP) and ammonium hexafluorophosphate were purchased from Aldrich Chemicals and used as received. $\text{Pd}(\text{OAc})_2$ was purchased from Pressure Chemicals and used as received. The $\text{Ru}(\text{bpy})_2\text{Cl}_2 \cdot 2\text{H}_2\text{O}$ starting material was synthesized following a literature procedure.²⁴

2.5.2. Synthetic Methods

*1-(pyridin-2-yl)-2,3,4,6,7,8-hexahydro-1*H*-pyrimido[1,2-*a*]pyrimidine* : **2-1a**

(\pm) BINAP (0.06 mmol, 38 mg) was taken in a oven-dried round bottomed flask, which was purged with argon and sealed with a septum. Dry toluene (3 mL) was injected inside. The resulting suspension was heated at 90 °C for 2 min to dissolve the BINAP. This

mixture was cooled to room temperature and Pd(OAc)₂ (0.04 mmol, 9 mg) was added and stirred for 3 min. To the resulting bright yellow solution was added 2-bromopyridine (4 mmol, 0.38 mL) and 1,3,4,6,7,8-hexahydro-2*H*-pyrimido[1,2-*a*]pyrimidine (4.3 mmol, 600 mg). Stirring for 5 min at ambient temperature resulted in a pale orange slurry to which was added *t*-BuOK (5.6 mmol, 640 mg). The flask was again purged with argon and the reaction mixture was then stirred at 90 °C for 3h after which time it was cooled to r.t. and diethyl ether (60 mL) was added and the solution was filtered. Evaporation of the filtrate gave the ligand as yellow oil. Yield = 780 mg (90%). ¹H NMR (CDCl₃, 300 MHz); 8.24 (dd, J^d = 6.0 Hz, J^d = 2.0 Hz, 1 H), 7.65 (d, J^d = 8.0 Hz, 1 H), 7.47 (td, J^t = 6.0 Hz, J^d = 2.0 Hz, 1 H), 6.77 (td, J^t = 6.0 Hz, J^d = 2.0 Hz, 1 H), 3.87 (t, J^t = 6.0 Hz, 2 H), 3.41 (t, J^t = 6.0 Hz, 2 H), 3.21 (m, 4 H), 2.02 (quint., J^{qt} = 6.0 Hz, 2 H), 1.88 (quint., J^{qt} = 6.0 Hz, 2 H) ppm. ¹³C NMR (CDCl₃, 75 MHz); 156.6, 149.9, 147.1, 135.9, 118.7, 116.9, 48.8, 48.6, 43.8, 43.7, 23.7, 22.7 ppm. HRMS (ESI), m/z: 217.14452 [M+H⁺]⁺ (C₁₂H₁₇N₄ requires 217.14477).

*1-(5-bromopyridin-2-yl)-2,3,4,6,7,8-hexahydro-1*H*-pyrimido[1,2-*a*]pyrimidine* : **2-2a**

A 30 mL pressure tube with a stirring bar was charged with 2,5-dibromopyridine (474 mg, 2 mmol) and 1,3,4,6,7,8-hexahydro-2*H*-pyrimido[1,2-*a*]pyrimidine (557 mg, 4 mmol). The tube was sealed and heated to 90 °C in an oil bath for 3 h, after which time it was cooled to room temperature. Toluene (5 ml) was added to the resulting yellow mixture, followed by the addition of diethyl ether (40 mL). After filtration and evaporation of the solvents, a light yellow crystalline solid was obtained which was dried under vacuum overnight. The product was purified by sublimation as white crystalline solid. Yield = 568 mg (96%). ¹H NMR (400 MHz, CDCl₃); 8.27 (dd, J^{dd} = 0.5, 2.5 Hz, 1 H), 7.67 (dd, J^{dd} = 0.5, 9.0 Hz, 1 H), 7.55 (dd, J^{dd} = 2.5, 9.0 Hz, 1 H), 3.89 - 3.83 (m, 2 H), 3.42 (t, J^t = 6.0 Hz, 2 H), 3.32 - 3.27 (m, 4 H), 2.04 (quint., J^{qt} = 6.0 Hz, 2 H), 1.90 (quint., J^{qt} = 6.0 Hz, 2 H) ppm. ¹³C NMR (100 MHz, CDCl₃); 154.9, 149.3, 147.3, 137.9, 119.7, 111.4, 48.5, 48.3, 43.6, 43.3, 23.3, 22.4 ppm. HRMS (ESI), m/z: 295.05554 [M+H⁺]⁺ (C₁₂H₁₆BrN₄ requires 295.05529). Anal. Calc. for C₁₂H₁₅N₄Br: C, 48.83; N, 18.98; H, 5.12; found: C, 48.83; N, 18.79; H, 5.14.

*1-(pyrimidin-2-yl)-2,3,4,6,7,8-hexahydro-1*H*-pyrimido[1,2-*a*]pyrimidine* : **2-3a**

1,3,4,6,7,8-Hexahydro-2*H*-pyrimido[1,2-*a*]pyrimidine (150 mg, 1.1 mmol) and 2-bromopyrimidine (160 mg, 1 mmol) were taken in a pressure tube and slowly heated to 130 °C, wherein a brown sticky-solid was obtained. Heating was maintained at 130 °C for an

hour, after which time the tube was cooled to room temperature and the solid was purified by column-chromatography on Al_2O_3 with 10% MeOH in CHCl_3 as eluent. The product was obtained by evaporation of the solvent and overnight drying under vacuum as white solid powder. Yield = 60 mg (55 %). ^1H NMR (CDCl_3 , 400 MHz); 8.72 (d, Hz, $J^d = 5.0$ Hz, 2 H), 7.17 (t, $J^t = 5.0$ Hz, 1 H), 4.34 (t, $J^t = 6.0$ Hz, 2 H), 3.75 (m, 4 H), 3.69 (t, $J^t = 6.0$ Hz, 2 H), 2.27 (quint., $J^{\text{qt}} = 6.0$ Hz, 2 H), 2.18 (quint., $J^{\text{qt}} = 6.0$ Hz, 2 H) ppm. ^{13}C NMR (CDCl_3 , 75 MHz); 158.3, 157.7, 151.2, 117.1, 48.7, 48.6, 43.7, 39.1, 20.8, 19.5 ppm. HRMS (ESI), m/z : 218.13925 $[\text{M}+\text{H}^+]^+$ ($\text{C}_{11}\text{H}_{16}\text{N}_5$ requires 218.14002).

1-(6-chloropyrimidin-4-yl)-2,3,4,6,7,8-hexahydro-1H-pyrimido[1,2-a]pyrimidine : **2-4a**

A 25 mL microwave tube was charged with 4,6-dichloropyrimidine (152 mg, 1 mmol) and 1,3,4,6,7,8-hexahydro-2H-pyrimido[1,2-a]pyrimidine (282 mg, 2 mmol). To this mixture was added toluene (15 mL). The tube was placed in a 400 MW microwave reactor and heated at 160 °C for 2 h. After the completion of the reaction, the solvent was decanted out and evaporated to dryness under reduced pressure. The product was purified by overnight sublimation at 1.8 mbar and 100 °C followed by recrystallisation by slow diffusion of hexane in chloroform. The product was obtained as pale yellow micro-crystalline solid. Yield = 652 mg (92%). ^1H NMR (CDCl_3 , 400 MHz); 8.51 (d, $J^d = 0.9$ Hz, 1 H), 7.93 (d, $J^d = 0.9$ Hz, 1 H), 4.02 (t, $J^t = 6.0$ Hz, 2 H), 3.51 (t, $J^t = 6.0$ Hz, 2 H), 3.27 (t, $J^t = 6.0$ Hz, 2 H), 3.18 (t, $J^t = 6.0$ Hz, 2 H), 2.01 (quint., $J^{\text{qt}} = 6.0$ Hz, 2 H), 1.92 (quint., $J^{\text{qt}} = 6.0$ Hz, 2 H) ppm. ^{13}C NMR (CDCl_3 , 100 MHz) 161.5, 159.3, 157.7, 147.9, 110.3, 48.64, 48.61, 43.8, 42.6, 23.6, 22.3 ppm. HRMS (ESI), m/z : 252.10105 $[\text{M}+\text{H}^+]^+$ ($\text{C}_{11}\text{H}_{15}\text{N}_5\text{Cl}^{35}$ requires 252.10158); m/z : 254.09860 $[\text{M}+\text{H}^+]^+$ ($\text{C}_{11}\text{H}_{15}\text{N}_5\text{Cl}^{37}$ requires 254.10158).

1-(pyrazin-2-yl)-2,3,4,6,7,8-hexahydro-1H-pyrimido[1,2-a]pyrimidine : **2-5a**

A 30 mL pressure tube with a stirring bar was charged with 1,3,4,6,7,8-hexahydro-2H-pyrimido[1,2-a]pyrimidine (292 mg, 2.1 mmol) and 2-chloropyrazine (115 mg, 1 mmol) was added dropwise. The tube was sealed and heated at 95 °C in an oil bath for 3 h, after which time it was cooled down to room temperature. Toluene (6 ml) was added to the resulting yellow viscous-oil followed by diethyl ether (40 mL). After filtration and evaporation of the solvents, the product was obtained as colourless oil, which could be solidified by keeping the oil at -20 °C for a week to give pale yellow solid. The solid was dissolved into minimal volume of dichloromethane and filtered through a plug of celite to give a clear colourless solution. Upon evaporation of the solvent under reduced pressure colourless oil was obtained. The oil was solidified at -20 °C and then dried under vacuum

to furnish the product as colourless solid. Yield = 189 mg (87%). ^1H NMR (400 MHz, CDCl_3); 9.06 (d, $J^d = 1.2$ Hz, 1 H), 8.12 (dd, $J^{dd} = 1.2, 4.0$ Hz, 1 H), 7.94 (d, $J^d = 2.4$ Hz, 1 H), 3.83 (t, $J^t = 6.0$ Hz, 2 H), 3.42 (t, $J^t = 6.0$ Hz, 2 H), 3.25 (t, $J^t = 6.0$ Hz, 2 H), 3.21 (t, $J^t = 6.0$ Hz, 2 H), 2.05 (quint., $J^q = 6.0$ Hz, 2 H), 1.90 (quint., $J^{qt} = 6.0$ Hz, 2 H) ppm. ^{13}C NMR (100 MHz, CDCl_3); 152.9, 148.7, 141.9, 140.6, 135.2, 48.6, 48.4, 43.6, 42.8, 23.4, 22.5 ppm. HRMS (ESI), m/z : 218.13975 $[\text{M}+\text{H}^+]^+$ ($\text{C}_{11}\text{H}_{16}\text{N}_5$ requires 218.14002).

[Ru(bpy)₂(2-1a)](PF₆)₂: 2-1b

A 100 mL round-bottomed flask was charged with **2-1a** (0.22 mmol, 50 mg), *cis*- $\text{Ru}(\text{bpy})_2\text{Cl}_2\cdot 2\text{H}_2\text{O}$ (0.2 mmol, 104 mg) and 1-butanol (10 mL) and the resulting dark purple solution was heated at reflux for 30 min. After cooling to ambient temperature, the dark solution was added dropwise to 50 mL of diethyl ether with vigorous stirring. A dark purple gum formed. The supernatant liquid was decanted and the gum was dissolved in 10 mL methanol. To this solution was added dropwise an aqueous solution of NH_4PF_6 (200 mg in 5 mL water) with constant stirring. A dark red precipitate appeared immediately. This was allowed to stand for 1 h and filtered and then washed with water (20 mL) and diethyl ether (20 mL) and air dried. Red crystals suitable for X-ray crystallography were grown by diffusion of isopropyl ether into a moderately concentrated solution of the complex in acetonitrile. Yield = 110 mg (60%). ^1H NMR (CDCl_3 , 700 MHz); 8.74 (d, $J^d = 5.0$ Hz, 1 H), 8.53 (d, $J^d = 8.0$ Hz, 1 H), 8.50 (d, $J^d = 8.0$ Hz, 1 H), 8.42 (m, 2 H), 8.37 (d, $J^d = 8.0$ Hz, 1 H), 8.13 (m, 2 H), 7.88 (m, 2 H), 7.80 (td, $J^t = 8.0$ Hz, $J^d = 2.0$ Hz, 1 H), 7.65 (m, 2 H), 7.59 (m, 2 H), 7.35 (d, $J^d = 8.0$ Hz, 1 H), 7.22 (t, $J^t = 7.0$ Hz, 1 H), 7.19 (t, $J^t = 7.0$ Hz, 1 H), 7.09 (d, $J^d = 5.0$ Hz, 1 H), 6.80 (td, $J^t = 7.0$ Hz, $J^d = 1.0$ Hz, 1 H), 3.79 (m, 1 H), 3.36 (m, 1 H), 3.18 (m, 3 H), 3.04 (m, 1 H), 2.91 (m, 1 H), 2.34 (m, 1 H), 2.25 (m, 1 H), 2.12 (m, 1 H), 1.63 (m, 1 H), 1.08 (m, 1 H) ppm. ^{13}C NMR (CDCl_3 , 175 MHz); 158.8, 158.6, 158.5, 158.4, 157.7, 153.85, 153.81, 153.4, 152.7, 152.6, 151.2, 139.9, 137.9, 137.6, 137.3, 137.1, 127.6, 127.5, 127.1, 125.2, 125.1, 124.6, 124.2, 121.8, 117.3, 49.2, 49.1, 48.5, 47.9, 23.5, 23.3 ppm. HRMS (ESI), m/z : 775.14399 $[\text{M}-\text{PF}_6]^+$ ($\text{C}_{32}\text{H}_{32}\text{N}_8\text{PF}_6\text{Ru}$ requires 775.14297), 315.09062 $[\text{M}-2\text{PF}_6]^{2+}$ ($\text{C}_{32}\text{H}_{32}\text{N}_8\text{Ru}$ requires 315.08912). Anal. Calc. for $\text{C}_{32}\text{H}_{32}\text{N}_8\text{RuP}_2\text{F}_{12}$: C, 41.79; H, 3.51; N, 12.18; found: C, 41.70; H, 3.31; N, 11.95.

[Ru(bpy)₂(2-2a)](PF₆)₂: 2-2b

Ligand **2-2a** (65 mg, 0.22 mmol) and *cis*- $\text{Ru}(\text{bpy})_2\text{Cl}_2\cdot 2\text{H}_2\text{O}$ (104 mg, 0.2 mmol) were dissolved in 1-butanol (15 ml) in a 50 ml round-bottomed flask and the resulting dark purple solution was heated to reflux. The reaction was followed by TLC. After 3 h, the

brown-red solution was cooled to room temperature. The solvent was evaporated under reduced pressure and the residue was dissolved in the minimum volume of methanol and to it was added a saturated aqueous solution of ammonium hexafluorophosphate to give a brown-red precipitate, which was filtered. The product was purified by flash column-chromatography on silica using 10% saturated aqueous KNO₃ in acetonitrile. The nitrate salt was metathesized to the PF₆ salt by addition of excess of solid NH₄PF₆ to the aqueous solution of the product. The precipitate was then filtered and dried under vacuum to give the product as a red solid. Yield = 141 mg (71%). ¹H NMR (400 MHz, CD₃CN); 8.79 (d, J^d = 5.8 Hz, 1 H), 8.54 (t, J^t = 8.9 Hz, 2 H), 8.42 (m, 3 H), 8.16 (m, 2 H), 7.92 (m, 3H), 7.71 (ddd, J^{ddd} = 1.4, 5.8, 7.5 Hz, 1 H), 7.64 (m, 3 H), 7.25 (m, 3 H), 7.12 (d, J^d = 2.0 Hz, 1 H), 3.75 (m, 1 H), 3.37 (m, 2 H), 3.21 (m, 3 H), 3.07 (td, J^{td} = 6.0, 12.0 Hz, 1 H), 2.84 (m, 1 H), 2.23 (m, 1 H), 2.12 (m, 1 H), 1.65 (m, 1 H), 1.14 (dd, J^{dd} = 3.5, 7.5 Hz, 1 H) ppm. ¹³C NMR (100 MHz, CD₃CN); 158.6, 158.5, 158.4, 158.2, 157.2, 153.7, 153.6, 153.5, 152.8, 152.7, 150.9, 142.2, 138.3, 137.9, 137.5, 137.4, 127.7, 127.65, 127.63, 127.3, 125.2, 125.1, 124.7, 124.4, 124.2, 115.8, 49.2, 49.1, 48.5, 47.8, 23.3, 23.1 ppm. HRMS (ESI), m/z: 853.05265 [M-PF₆]⁺ (C₃₂H₃₁BrN₈PF₆Ru requires 853.05349), 354.04497 [M-2PF₆]²⁺ (C₃₂H₃₁BrN₈Ru requires 354.04438). Anal. Calc. for C₃₂H₃₁BrN₈BrRuP₂F₁₂ : C, 38.49; N, 11.22; H, 3.13; found : C, 38.35; N, 11.25; H, 2.92.

[Ru(bpy)₂(2-3a)](PF₆)₂ : 2-3b

A 100 mL round-bottomed flask was charged with **2-3a** (22 mg, 0.1 mmol) and *cis*-Ru(bpy)₂Cl₂·2H₂O (50 mg, 0.1 mmol) and to it was added an aliquot of 1:1 (v/v) mixture of 1-butanol-water (10 mL). The resulting clear dark-purple solution was refluxed for 16 h. After cooling to ambient temperature, the solvent was evaporated. The residue was taken in 1:1 (v/v) methanol-water mixture and filtered. To the filtrate was added, dropwise, an aqueous solution of NH₄PF₆ (200 mg in 5 mL water) with constant stirring, while no precipitate appeared immediately. Precipitate, which was observed after overnight standing, was filtered, washed with water (5 mL) and diethyl ether (20 mL) and air dried. The crude product was dissolved in acetonitrile and purified by column chromatography (SiO₂, acetonitrile: saturated aq. KNO₃, 7:2, v/v). The third reddish purple band contained the product. The nitrate salt was metathesized to the PF₆ salt by addition of solid NH₄PF₆ to the aqueous solution of the product. The precipitate was then filtered and dried under vacuum to give the product as a red solid. Yield = 21 mg (23%). ¹H NMR (CDCl₃, 700 MHz); 8.88 (d, J^d = 6.0 Hz, 1 H), 8.56 (dd, J^d = 5.0 Hz, J^d = 2.0 Hz, 1 H), 8.52 (m, 2 H), 8.46 (d, J^d =

8.0 Hz, 1 H), 8.39 (d, $J^d = 8.0$ Hz, 1 H), 8.35 (d, $J^d = 8.0$ Hz, 1 H), 8.14 (m, 2 H), 7.88 (td, $J^t = 8.0$ Hz, $J^d = 2.0$ Hz, 1 H), 7.85 (td, $J^t = 8.0$ Hz, $J^d = 2.0$ Hz, 1 H), 7.67 (td, $J^t = 8.0$ Hz, $J^d = 2.0$ Hz, 1 H), 7.62 (m, 2 H), 7.58 (d, $J^d = 6.0$ Hz, 1 H), 7.50 (dd, $J^d = 6.0$ Hz, $J^d = 2.0$ Hz, 1 H), 7.20 (m, 2 H), 6.82 (dd, $J^d = 6.0$ Hz, $J^d = 1.0$ Hz, 1 H), 3.89 (m, 1 H), 3.52 (m, 1 H), 3.32 (m, 2 H), 3.22 (m, 2 H), 3.09 (m, 1 H), 2.72 (m, 1 H), 2.29 (m, 1 H), 2.17 (m, 1 H), 1.68 (m, 1 H), 1.25 (m, 1 H) ppm. ^{13}C NMR (CDCl_3 , 175 MHz): 161.2, 160.8, 158.8, 158.6, 158.44, 158.41, 158.3, 153.9, 153.5, 152.6, 152.5, 152.4, 138.1, 137.9, 137.4, 137.2, 127.7, 127.4, 127.2, 124.9, 124.8, 124.7, 124.4, 118.1, 49.5, 49.2, 47.9, 46.1, 23.1, 22.6. HRMS (ESI), m/z : 776.1382 $[\text{M-PF}_6]^+$ ($\text{C}_{31}\text{H}_{31}\text{N}_9\text{PF}_6\text{Ru}$ requires 776.13822), 315.58803 $[\text{M-2PF}_6]^{2+}$ ($\text{C}_{31}\text{H}_{31}\text{N}_9\text{Ru}$ requires 315.58675).

[Ru(bpy)₂(2-4a)](PF₆)₂: 2-4b

Ligand **2-4a** (72 mg, 0.3 mmol) and *cis*-Ru(bpy)₂Cl₂·2H₂O (160 mg, 0.3 mmol) were taken in 1:1 (v/v) 1-butanol-water mixture (15 mL) in a round-bottomed flask and the solution was refluxed for 8 h. After cooling down to ambient temperature, the solvent was evaporated to dryness under reduced pressure. The residue was dissolved in minimum volume of methanol, and then to it was added a saturated aqueous solution of NH₄PF₆ (200 mg in 5 mL of water) to give a precipitate which was filtered off. The product was purified by column chromatography (silica, saturated aq. KNO₃:acetonitrile = 1:3 v/v). The reddish brown band contained the desired product. The nitrate salt was metathesized to the PF₆ salt by addition of solid NH₄PF₆ to the aqueous solution of the product. The precipitate was then filtered and dried under vacuum to give the product as a red solid. Crystals suitable for X-ray crystallography were grown by diffusion of diethyl ether into a moderately concentrated solution of the complex in acetone. Yield = 179 mg (62%). ^1H NMR (400 MHz, CD₃CN); 8.79 (d, $J^d = 5.6$ Hz, 1 H), 8.50 (m, 3 H), 8.38 (dd, $J^{\text{dd}} = 8.0, 3.6$ Hz, 2 H), 8.16 (t, $J^t = 8.0$ Hz, 2 H), 7.88 (m, 2 H), 7.60 (m, 5 H), 7.32 (s, 1 H), 7.13 - 7.27 (m, 2 H), 3.75 (dt, $J^{\text{dt}} = 14.0, 4.0$ Hz, 1 H), 3.33 (m, 6 H), 3.08 (m, 1 H), 2.77 (d, $J^d = 4.0$ Hz, 1 H), 2.28 (m, 1 H), 1.67 (m, 1 H), 1.25 (m, 1 H) ppm. ^{13}C NMR (100 MHz, CD₃CN); 171.8, 162.9, 160.1, 158.9, 158.8, 158.7, 158.6, 158.5, 153.9, 153.8, 152.9, 152.8, 152.7, 138.2, 137.9, 137.4, 137.3, 127.8, 127.7, 127.6, 127.4, 125.3, 124.9, 124.6, 97.1, 68.7, 48.3, 47.9, 31.4, 23.2, 23.0 ppm. HRMS (ESI), m/z : 810.10117 $[\text{M-PF}_6]^+$ ($\text{C}_{31}\text{H}_{30}\text{N}_9\text{ClPF}_6\text{Ru}$ requires 810.09925), 332.56806 $[\text{M-2PF}_6]^{2+}$ ($\text{C}_{31}\text{H}_{30}\text{ClN}_9\text{Ru}$ requires 332.56726). Anal. Calc. for $\text{C}_{31}\text{H}_{30}\text{N}_9\text{F}_{12}\text{P}_2\text{ClRu}$: C, 38.98; N, 13.20; H, 3.17; found: C, 38.90; N, 13.06; H, 3.22.

[Ru(bpy)₂(2-5a)](PF₆)₂: 2-5b

Ligand **2-5a** (48 mg, 0.22 mmol) and *cis*-Ru(bpy)₂Cl₂·2H₂O (104 mg, 0.2 mmol) were taken in 1-butanol (15 mL) in a round-bottomed flask and the solution was refluxed for 4 h. After evaporation of the solvent, the residue was dissolved in minimum volume of methanol, and then to it was added a saturated aqueous solution of NH₄PF₆ (200 mg in 5 mL of water) to give a precipitate which was filtered. The product was purified by column chromatography (silica, saturated aq. KNO₃:acetonitrile = 1:3 v/v). The brownish-red band contained the desired product. The nitrate salt was metathesized to the PF₆ salt by addition of solid NH₄PF₆ to the aqueous solution of the product. The precipitate was then filtered and dried under vacuum to give the product as a red solid. Yield = 138 mg (76%). ¹H NMR (400 MHz, CD₃CN); 8.72 (d, J^d = 5.0 Hz, 1 H), 8.58 (m, 2 H), 8.51 (m, 3 H), 8.41 (d, J^d = 8.0 Hz, 1 H), 8.18 (m, 2 H), 7.91 (m, 2 H), 7.86 (d, J^d = 3.5 Hz, 1 H), 7.70 (ddd, J^{ddd} = 1.3, 5.8, 7.4 Hz, 1 H), 7.61 (m, 3 H), 7.27 (ddd, J^{ddd} = 1.4, 5.8, 7.4 Hz, 1 H), 7.23 (ddd, J^{ddd} = 1.3, 5.8, 7.4 Hz, 1 H), 7.09 (d, J^d = 2.6 Hz, 1 H), 3.94 (m, 1 H), 3.37 (m, 2 H), 3.21 (m, 2 H), 3.07 (td, J^{td} = 6.0, 12.0 Hz, 1 H), 2.92 (m, 1 H), 2.16 (m, 1 H), 1.65 (ddd, J^{ddd} = 3.4, 6.7, 9.9 Hz, 1 H), 1.11 (m, 2 H), 0.87 (m, 1 H) ppm. ¹³C NMR (100 MHz, CD₃CN); 158.6, 158.33, 158.30, 158.2, 154.4, 153.7, 153.4, 153.3, 152.7, 152.6, 144.7, 140.5, 139.4, 138.5, 138.1, 137.9, 137.5, 127.9, 127.7, 127.2, 125.4, 125.3, 124.8, 124.3, 106.9, 49.3, 49.2, 48.3, 48.1, 23.4, 23.3 ppm. HRMS (ESI), m/z: 776.13732 [M-PF₆]⁺ (C₃₁H₃₁N₉PF₆Ru requires 776.13822), 315.58713 [M-2PF₆]²⁺ (C₃₁H₃₁N₉Ru requires 315.58675). Anal. Calc. for C₃₁H₃₁F₁₂N₉P₂Ru₁: C, 40.44; N, 13.69; H, 3.39; found: C, 40.57; N, 13.31; H, 3.50.

2.5.3. Computational Methods

All calculations were performed with the Gaussian03²⁵ employing the DFT method, the Becke three-parameter hybrid functional,²⁶ and Lee-Yang-Parr's gradient-corrected correlation functional (B3LYP).²⁷ Singlet ground state geometry optimizations for (**2-1b**)²⁺, (**2-3b**)²⁺ and (**2-4b**)²⁺ were carried out at the (R)B3LYP level in the gas phase, using their respective crystallographic structures as starting points. All elements except ruthenium were assigned the 6-31G(d,f) basis set.²⁸ The double- ζ quality LANL2DZ ECP basis set²⁹ with an effective core potential and one additional f-type polarization was employed for the Ru atom. Vertical electronic excitations based on (R)B3LYP-optimized geometries were computed for (**2-1b**)²⁺, (**2-3b**)²⁺ and (**2-4b**)²⁺ using the TD-DFT formalism³⁰ in acetonitrile using conductor-like polarizable continuum model (CPCM).³¹ CPCM model for geometry

optimization was not used as for closed-shell geometry optimization calculations, the effect of solvent has a very little influence on computed geometries and this fact has well been established in a recent literature report³² and also to prove this fact additional DFT and TD-DFT calculations were performed with one of the complexes (**2-1b**)²⁺ in the following way: (i) a DFT geometry optimization calculation taking into account the possible effect of solvent (through a polarized continuum model using acetonitrile as solvent) and the bond distances and angles of this model were compared (Table II-S9) to that of the DFT geometry optimized model, which does not incorporate the effect of solvent (i.e., without CPCM). The result shows little variation with respect to bond distances and angles, which is not a critical aspect in this work. (ii) A TD-DFT calculation of (**2-1b**)²⁺ including CPCM (acetonitrile) starting with a geometry optimized model, which was performed including CPCM (acetonitrile) and the principle transitions with their respective oscillator strengths and major transitions with relative contributions are tabulated in Table II-S11. (iii) A TD-DFT calculation of (**2-1b**)²⁺ excluding CPCM (i.e., in vacuum) starting with a geometry optimized model, which was performed excluding CPCM and the principle transitions with respective oscillator strengths and major transitions with relative contributions are tabulated in Table II-S12. A direct comparison among the wavelengths of principal transitions with oscillator strengths and nature of the transitions in Table II-S10, II-S11 and II-S12 clearly indicate that for the closed-shell geometry optimization, the effect of solvent (through a polarized continuum model) has little influence on computed geometries, as the wavelengths of a particular transition, calculated by these three different types of TD-DFT calculations, fall in the experimental error range (± 2 nm as mentioned in the experimental section in ESI) except for the transition at 279 nm, for which the maximum variation is ± 4 nm. Although the relative contributions and oscillator strengths vary little, the nature of the particular transition remains unchanged. Vibrational frequency calculations were performed to ensure that the optimized geometries represent the local minima and there are only positive eigenvalues. The electronic distribution and localization of the singlet excited states were visualized using the electron density difference maps (ED-DMs).³³ *Gausssum* 2.2 was employed to visualize the absorption spectra (simulated with Gaussian distribution with a full-width at half maximum (fwhm) set to 3000 cm^{-1}) and to calculate the fractional contributions of various groups to each molecular orbital. All calculated structures were visualized with ChemCraft.³⁴

2.5.4. Crystal structure determination

Diffraction data were collected on a Bruker SMART 6000 with Montel 200 monochromator, equipped with a rotating anode source for Cu K α radiation. The diffraction quality of the crystals were checked, revealing in some cases poor diffraction with a large amount of diffuse scattering, signaling extensive crystal disorder. Cell refinement and data reduction were done using APEX2.³⁵ Absorption corrections were applied using SADABS.³⁶ Structures were solved by direct methods using SHELXS97 and refined on F^2 by full-matrix least squares using SHELXL97.³⁷ All non-hydrogen atoms were refined anisotropically. Hydrogen atoms were refined isotropic on calculated positions using a riding model. For compound **2-4b** during the refinement of the structure, electron density peaks were located and were believed to be two highly disordered water molecules and four severely disordered solvated acetone molecules (by counting the number of electrons suppressed). All the attempts made to model the solvent molecules were not successful and they were removed using the SQUEEZE routine from PLATON,³⁸ which resulted in a significant improvement of R1 factor by $\sim 4\%$. For compound **2-1b**, the highest difference peak is located 1.08 Å from atom Ru and the deepest hole is 0.84 Å from the metal center, whereas for compound **2-4b** the highest difference peak is 1.08 Å far from Ru atom and the deepest hole is 0.51 Å from atom O1. In addition, in **2-1b** two more peaks with density around $1 \text{ e}/\text{Å}^3$ were present essentially due to the quality of the crystal employed, which was the best available. The structure of **2-1b** also showed that the guanidine moiety is positionally disordered over two positions. The disorder was modelled as two components [0.52(2):0.48(2)] and refined anisotropically. In both complexes **2-1b** and **2-3b**, one anion PF₆⁻ was found on a general position and another one with a significant degree of rotational disorder about the central P atom over three positions, with their occupancies constrained to sum to unity and refined anisotropically. Some similarity restraints were applied between the disorder components to modeled the anion positions but not applicable for the cation structure. Specific parameters of each measurement are located in Table II-1.

Table II-1. Crystal Data and Structure Refinement Information for **2-2a**, **2-1b**, **2-3b** and **2-4b·5C₂H₆O·2H₂O**

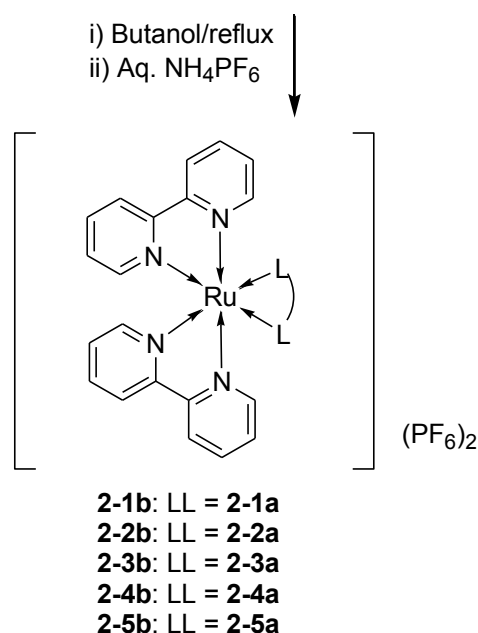
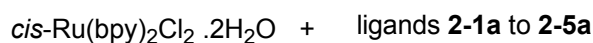
	2-2a	2-1b	2-3b	2-4b·5C₂H₆O·2H₂O
Formula	C ₁₂ H ₁₅ N ₄ Br	[C ₃₂ H ₃₂ N ₈ Ru][PF ₆] ₂	[C ₃₁ H ₃₁ N ₉ Ru][PF ₆] ₂	[C ₃₁ H ₃₀ N ₉ ClRu][PF ₆] ₂ [5C ₂ H ₆ O][2H ₂ O]
Crystal System	monoclinic	monoclinic	monoclinic	Triclinic
Space Group	P2 ₁ /n	C2/c	P2 ₁ /c	P-1
<i>a</i> (Å)	5.0181(2)	35.6514(10)	20.4021(8)	12.0837(5)
<i>b</i> (Å)	18.1139(6)	10.1520(3)	10.5565(4)	12.3164(4)
<i>c</i> (Å)	13.0979(4)	26.1512(12)	16.4117(7)	14.5069(5)
<i>α</i> (deg)	90	90	90	88.110(2)
<i>β</i> (deg)	92.255(2)	130.121(1)	95.787(2)	81.464(2)
<i>γ</i> (deg)	90	90	90	82.341(2)
<i>V</i> (Å ³)	1189.64(7)	7273.7(4)	3516.7(2)	2115.87(13)
<i>Z</i>	4	8	4	2
R1;wR2(<i>I</i> > 2σ(<i>I</i>))	0.0366; 0.0899	0.0640; 0.1766	0.0362; 0.0971	0.0611; 0.1853
R1;wR2 (all data)	0.0442; 0.0950	0.0813; 0.1889	0.0415; 0.0999	0.0623; 0.1867
R _σ ; R(int)	0.0487; 0.0689	0.0453; 0.070	0.0286; 0.0570	0.0341; 0.0451
GoF(<i>F</i> ²)	1.028	0.980	1.038	1.089

2.6. Results and Discussion

A series of substituted neutral bidentate *N*-heterocyclic ligands **2-1a** to **2-5a** (Chart 2.1) were synthesized by reaction of 1,3,4,6,7,8-hexahydro-2*H*-pyrimido[1,2-*a*]pyrimidine (**H-hpp**) with various heterocycles (halo-pyridine/pyrimidine/pyrazine) by C-N bond forming reactions. Ligand **2-1a** was synthesized by Pd-catalysed Buchwald C-N cross-coupling reaction,³⁹ whereas the other ligands were synthesized by neat reaction of the reactants at 90-130 °C or assisted by microwave heating at 160 °C. The ligands were synthesized in neat reaction procedures, which provide a green route of using **H-hpp** as its own base and recuperating the relatively costly starting material by simple acid-base work up. Attaching a heterocycle to the guanidine *NH* position of **H-hpp** renders the six annular methylene units non-equivalent by both ¹H and ¹³C NMR spectroscopy in contrast to free **H-hpp**, in which the tautomerization of the guanidine proton leads to only three proton resonances in its ¹H NMR at 400 MHz. Similar observations were reported by Coles and co-workers for a methylene-linked bis(guanidine) compound, H₂C{hpp}₂.⁴⁰

Ligands **2-1a** to **2-5a** were characterized by high-resolution mass spectrometry, where the most abundant peaks were found to be $[M+H]^+$, with the $[M+2H]^{2+}$ species (see experimental section for details).

The stoichiometric reaction of **2-1a** to **2-5a** with *cis*-Ru(bpy)₂Cl₂·2H₂O in refluxing 1-butanol or 1:1 (v/v) 1-butanol-H₂O mixture followed by the addition of aqueous NH₄PF₆ affords [Ru(bpy)₂{(2-1a)-(2-5a)}](PF₆)₂ (**2-1b** to **2-5b**) as dark red powders (Scheme 2.1). While compound **2-1b** could be isolated as a pure product without further purification, compounds **2-2b** to **2-5b** needed additional purification by column chromatography.



Scheme 2.1. Syntheses of the complexes **2-1b** to **2-5b**

Complexes **2-1b** to **2-5b** were characterized by high-resolution mass spectrometry, where the most abundant peaks were found to be $[M-2PF_6]^{2+}$ in all the cases. The $[M-PF_6]^+$ species could also be identified (see experimental section for details).

2.6.1. Crystallography

X-Ray quality single crystals were obtained for compounds **2-1b**, **2-2a**, **2-3b** and **2-4b**·5C₂H₆O·2H₂O (Table II-1, Figures 2.1 to 2.4). Slow diffusion of diisopropyl ether into an acetonitrile solution of **2-1b** and **2-3b** afforded the best single crystals, whereas crystals of **2-2a** and **2-4b** could be grown by sublimation of **2-2a** and slow diffusion of diethyl ether

into an acetone solution of **2-4b**, respectively. Ligand **2-2a** and complexes **2-1b** and **2-3b** crystallize in monoclinic crystal system, while complex **2-4b** crystallizes in triclinic crystal system. The crystallographic data are summarized in Table II-1 (see Figure 2.S1 for packing of ligand **2-2a** and Table II-S1 for selected bond angles and distances in comparison to the same by DFT calculations). In ligand **2-2a**, the guanidine moiety adopts a more redundant twisted chair conformation instead of the boat conformation (Figure 2.1). To minimize the lone pair-lone pair repulsion, atoms N1 and N4 adopt a *trans* geometry around C8-N3 bond. The N3-C1 [1.413(4) Å] and N2-C1 [1.391(3) Å] bond distances clearly suggest that there is delocalization around N3-C1-N2 core, whereas, N1-C1 seems to be a localized C-N double bond with a distance of 1.283(4) Å. Extensive π - π interactions between the aromatic rings, non-covalent solid state Br-Br interactions, aromatic C-H—Br interactions along with aromatic C-H—N interactions all play a role in the solid-state packing of molecule **2-2a**.

Complexes **2-1b**, **2-3b** and **2-4b** exhibit coordinatively saturated ruthenium atoms in a distorted octahedral geometry, with four nitrogen atoms of two bpy ligands, one nitrogen from guanidine and another one either of the pyridine, pyrimidine²¹ or chloropyrimidine moiety, respectively.

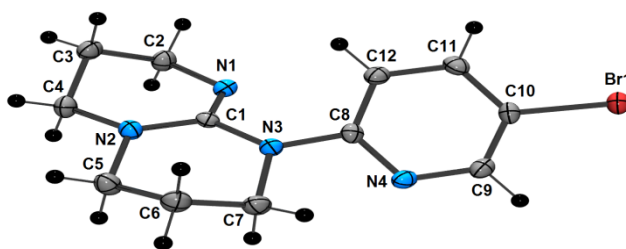


Figure 2.1. Crystal structure of ligand **2-2a**. Thermal ellipsoids are shown at a 50% probability level.

Chapter 2

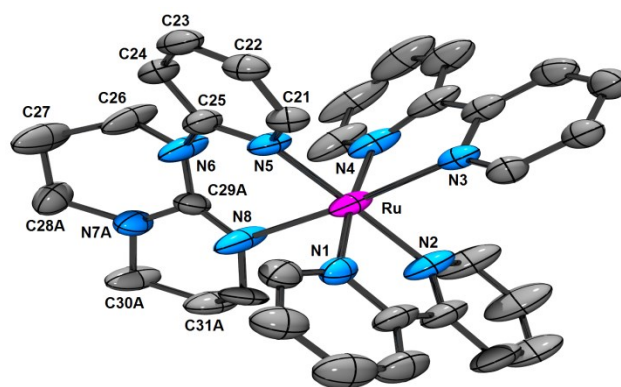


Figure 2.2. Crystal structure of **2-1b**. Hydrogen atoms, PF_6 anions and a disordered part of the guanidine moiety were omitted for clarity. Thermal ellipsoids are shown at a 50% probability level.

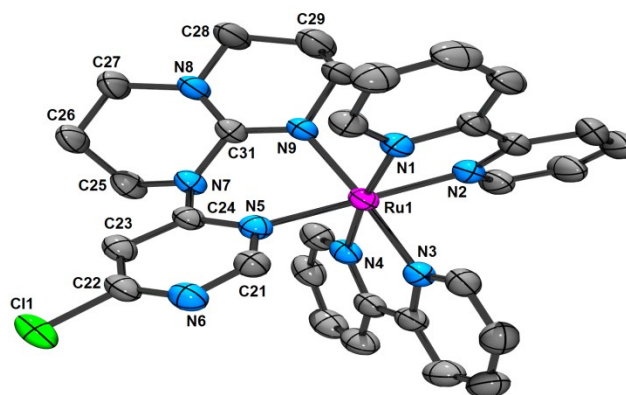


Figure 2.3. Crystal structure of **2-4b**. Hydrogen atoms, solvated acetone and PF_6 anions were omitted for clarity. Thermal ellipsoids are shown at a 50% probability level.

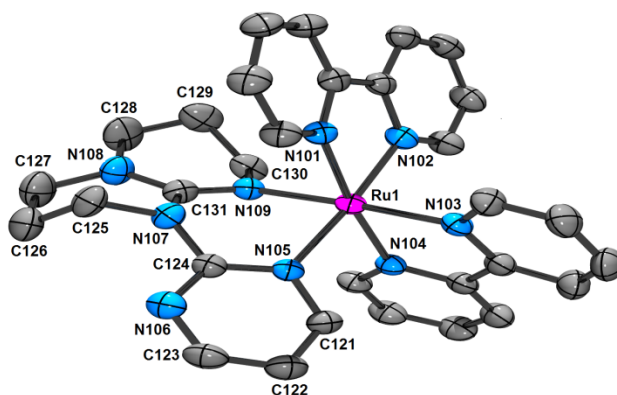


Figure 2.4. Crystal structure of **2-3b**. Hydrogen atoms, solvated acetone and PF_6 anions were omitted for clarity. Thermal ellipsoids are shown at a 50% probability level. Structure is redrawn using crystal data in ref 21.

The distortion from a regular octahedron is due to the smaller ligand bite angles at the metal center formed by the two 2,2'-bipyridine ligands. Selected bond distances and angles are tabulated for compounds **2-1b**, **2-3b**²¹ and **2-4b** in observance with the values obtained from DFT calculation (see Table II-S1 in ESI). The average bite angles for the bпыs are 80.45°, 78.82° and 78.85° for compound **2-1b**, **2-3b** and **2-4b**, respectively. In general, the average of the aforesaid bite angles N-Ru-N (average = 79.37°) is lower by five degrees to the average value observed in other Ru complexes containing two bpy as ligands (average = 84.8(5)°).⁴¹ In the complexes, the bicyclic ligands **2-1a**, **2-3a** and **2-4a** adopt six-membered twisted-chair chelate ring conformations, having bite angles of 82.8(3)°, 84.9(8)° and 85.2(1)°, respectively. Although not significant, this gradual increase in bite angle with decreasing nucleophilicity of the ligands, from **2-1a** to **2-3a** to **2-4a**, which suggests that the angle opens up due to less strong bonding of the heterocyclic ligands. The six Ru-N distances range between 1.992(6) Å to 2.187(7) Å, from 2.051(2) Å to 2.090(2) Å and from 2.054(4) Å to 2.090(4) Å for compounds **2-1b**, **2-3b** and **2-4b**, respectively. The Ru-N distances for the coordinated bpy ligands are mainly the same for compound **2-1b** and to some extent different for compound **2-3b** and **2-4b**, whereas the average for Ru-N was found to be almost the similar for compounds **2-1b**, **2-3b** and **2-4b** (2.056 Å, 2.060 Å and 2.059 Å, respectively). These values are at the intermediate of the distances observed in Ru-bpy complexes in general (1.96 Å – 2.16 Å, average = 2.06(5) Å).⁴¹ The Ru-N_{pyrimidine} and Ru-N_{chloropyrimidine} bond distances only differ slightly in the complexes, whereas the bond distance for Ru-N_{pyridine} was found to be somewhat different (Ru-N_{pyridine} [2.011(6) Å], Ru1-N_{pyrimidine} [2.090(2) Å] and Ru1-N_{chloropyrimidine} [2.089(4) Å] for **2-1b**, **2-3b** and **2-4b** respectively). the Ru-N_{pyridine} bond is shorter than the other two by a noticeable amount of ~0.08 Å. This fact in turn supports for higher nucleophilicity of ligand **2-1a** with respect to **2-3a**, but similar nucleophilicity between ligands **2-3a** and **2-4a**. The Ru-N_{guanidine} distances, for e.g., Ru-N109 [2.087(2) Å] and Ru1-N9 [2.090(4) Å] in **2-3b** and **2-4b**, respectively, are found to be closer to the distance Ru-N_{bpy} when compared to **2-1b** (Ru-N8 [2.187(7) Å]). Steric factors due the disordered guanidine rings might also play a role in these bond lengths since it displays a distortion over two positions. This fact is also supported by the higher dihedral angle subtended by N5-C25-N6-C29 (56.42±1°) in compound **2-1b** with respect to the same by N105-C124-N107-C131 (41.38±1°) and N5-

C24-N7-C31 ($40.45 \pm 1^\circ$) in compounds **2-3b** and **2-4b**, respectively, indicating the fact that ligand **2-1a** in compound **2-1b** is more sterically hindered with respect to the ligand moieties in compound **2-3b** and **2-4b**.

In compound **2-3b**, the N107-C124 [1.392(3) Å] and N107-C131 [1.408(3) Å] bond distances may suggest that there is delocalization between the pyrimidine ring and guanidine to some extent, whereas N109-C131 appears to be a localized C-N double bond with a distance of 1.314(4) Å. Delocalization between the pyridine ring and guanidine moiety is also observed in compound **2-1b** as revealed by N6-C25 [1.418(10) Å] and N6-C29* [1.40(3) Å] (the asterisk denotes the bond average of N6-C29A and N6-C29B; for clarity C29B is not shown in Figure 2.2) bond distances. Double bond character is observed in N8-C29** [1.32(2) Å] (the double asterisk denotes the bond average of N6-C29A and N6-C29B) bond in compound **2-1b**. The delocalization is limited for compound **2-4b** as revealed by the C-N bond distances in **2-4b** [N7-C24 1.377(6) Å and N7-C31 1.421(6) Å]. The bond distances suggest that N9-C31 [1.301(6) Å] is of more localized C-N double bond character in compound **2-4b**. The alkyl chains are directed away from the Ru(II) centre, and thus the conformation of the saturated ring does not appear to have any noticeable influence on the structure, as opposed to other coordination complexes incorporating (CH₂)-bridged donor atoms.⁴²

2.6.2. Electrochemistry

The redox behaviour of complexes (**2-1b**)-(**2-5b**) has been examined by cyclic voltammetry using a glassy carbon electrode in purified acetonitrile containing [*n*-Bu₄N]PF₆ as the supporting electrolyte versus Fc⁺/Fc as the internal standard, under a dry argon atmosphere and data are gathered in Table II-2. B3LYP density functional theory (DFT) calculations (see Figure 2.5 and ESI for computational details) predict that ligand (**2-1a**)-(**2-5a**) cause a significant destabilization of the HOMO, which is located principally on the ruthenium ion and partially on the ligand environment (see Figures 2.S2-2.S4 in ESI). The oxidation process is therefore assigned to the removal of one electron from the metal-centered orbitals. The higher energies calculated for the HOMO of [**2-1b**]²⁺ (-5.51 eV), [**2-3b**]²⁺ (-5.64 eV) and [**2-4b**]²⁺ (-5.72 eV) compared with that of [Ru(bpy)₃]²⁺ (-6.11 eV)⁴⁷ are in good agreement with the lower anodic potentials measured for **2-1b**, **2-3b** and **2-4b** (Table II-2) in comparison with [Ru(bpy)₃]²⁺ as they may suggest strong σ-donation from

the saturated ligand backbone to the metal based orbitals, thereby increasing the energy of HOMO. This trend is in accordance to the conclusions of Bolink *et al.*⁴⁸ At positive potentials, complexes **2-1b** (Figure 2.6) and **2-2b** show quasi-reversible Ru(II) to Ru(III) oxidations at 0.73 V *vs.* SCE with a peak-to-peak separation (ΔE_p) of 100 mV at 200 mV/s. This value is 0.54 V less positive than that observed for the same Ru(III/II) couple in $[\text{Ru}(\text{bpy})_3]^{2+}$ which appears at 1.27 V *vs.* SCE,⁴³⁻⁴⁵ i.e., **2-1b** is much easier to oxidize than $[\text{Ru}(\text{bpy})_3]^{2+}$, confirming that **2-1a** is a stronger donor than bpy, although the effect of introducing an electron withdrawing bromine atom does not seem to be so well pronounced for **2-2b**. Complex **2-3b** also shows a quasi-reversible Ru(III/II) couple at 0.75 V *vs.* SCE ($\Delta E_p = 90$ mV). This marginal increase in the Ru(III/II) couple in **2-3b** in comparison to **2-1b** may be attributed to the substitution of the pyridine donor in **2-1a** with a pyrimidine in **2-3a**. As pyrimidine is a weaker donor ligand, the Ru centre in **2-3b** is more difficult to oxidize.^{12,49} Complex **2-4b** presents a well-defined reversible peak at 0.78 V, with respect to SCE, with a peak-to-peak separation of 69 mV. The oxidation peak of **2-4b** is more positively shifted by 50 mV and 30 mV in comparison to **2-1b** (so also **2-2b**) and **2-3b**, respectively, indicating the electron-withdrawing nature of the chlorine atom. Complex **2-5b** exhibits a one-electron quasi-reversible Ru(III/II) couple at 0.79 V ($\Delta E_p = 92$ mV) *vs.* SCE. This value is 60 mV, 40 mV and 10 mV more positive with respect to **2-1b** (see also **2-2b**), **2-3b** and **2-4b**, respectively. Since pyrazine is a weaker donor ligand in comparison to both pyrimidine and pyridine, the Ru(II) centre in **2-5b** is more difficult to oxidise and indeed it is the most difficult compound to oxidise in the series. It is worthwhile noting that the new (**2-1a**)-(**2-5a**) ligands reported in this work are even more electron donating than 2-(2'-aminoethyl)-pyridine (AETPy) or ethylenediamine (en), as revealed by the Ru(III/II) couples of the complexes $[\text{Ru}(\text{bpy})_2(\text{AETPy})]^{2+}$ (1.12 V *vs.* SCE) and $[\text{Ru}(\text{bpy})_2(\text{en})]^{2+}$ (0.96 V *vs.* SCE) reported in Table II-2.

Table II-2. Redox data of complexes (**2-1b**)-(**2-5b**) in dry, degassed acetonitrile.^a

Compound	$E_{1/2}(\text{ox})$	$E_{1/2}(\text{red})$	$\Delta E_{1/2}$
2-1b	0.73 (100)	-1.41(82), -1.66(86), -2.30 (irr) ^b	2.14
2-2b	0.73 (105)	-1.40 (82), -1.67 (210)	2.13
2-3b	0.75 (90)	-1.42 (62), -1.63 (133), -1.96 (145)	2.17
2-4b	0.78 (69)	-1.37 (71), -1.63 (90), 1.86 (irr) ^b	2.15
2-5b	0.79 (92)	-1.24 (85), -1.69 (130), -1.97 (160)	2.03
Ru(bpy) ₃ ²⁺	1.27 ^c	-1.35 ^c , -1.55 ^c , -1.76 ^c	2.62
Ru(bpy)(en) ²⁺	0.96 ^d	-1.46 ^d , -1.71 ^d	2.42
Ru(bpy)(AETPy) ²⁺	1.12 ^e	-1.41 ^e , -1.63 ^e	2.53

^aPotentials are in volts vs. SCE for acetonitrile solutions, 0.1 M in [*n*-Bu₄N]PF₆, recorded at 25 ± 1 °C at a sweep rate as mentioned in text. The difference between cathodic and anodic peak potentials (millivolts) is given in parentheses. $\Delta E_{1/2}$ (in volts) for each compound is the difference between the first oxidation potential and first reduction potential. ^bIrreversible; potential is given for the anodic wave. ^cFrom refs 43-45. ^dFrom ref 43 (en is ethylenediamine). ^eFrom ref 46 (AETPy is aminoethylpyridine).

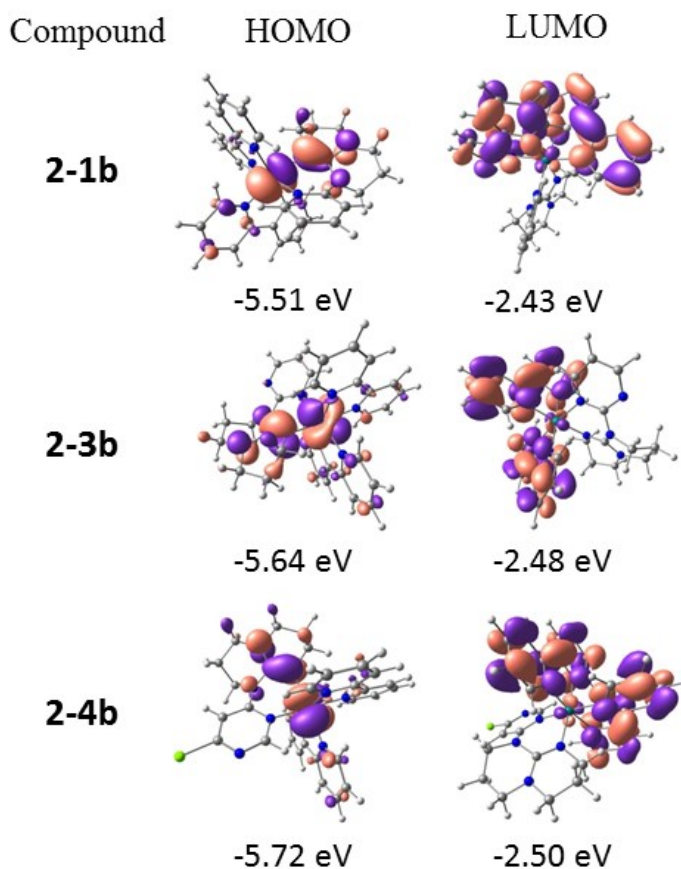


Figure 2.5. Kohn-Sham orbital sketches for HOMO and LUMO molecular orbitals for **2-1b**²⁺, **2-3b**²⁺, **2-4b**²⁺ in (*S*=0) ground state.

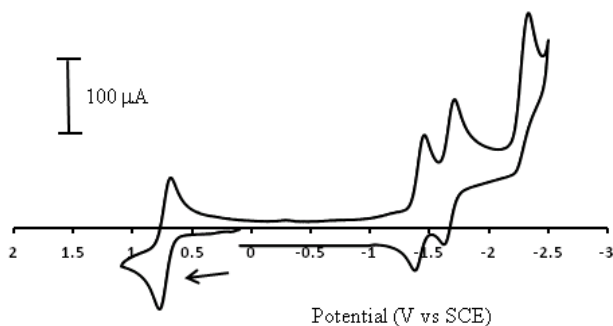


Figure 2.6. Cyclic voltammogram of **2-1b** (at 200 mV/s) in dry, degassed acetonitrile with 0.1 M TBAPF₆.

All the complexes display ligand-based reduction peaks. The first two reduction peaks are assigned to bpy-based processes, by comparing their potential values to those of [Ru(bpy)₃]²⁺ (-1.35 V, -1.55 V and -1.76 V vs. SCE).^{1b,44,45} DFT calculations confirm that the lowest unoccupied molecular orbital (LUMO) is fully localized on the bpy ligand for **2-1b** (-2.43 eV), **2-3b** (-2.48 eV) and **2-4b** (-2.50 eV) (Figures 2.S2-2.S4 in ESI) and is calculated at ~ 0.04-0.11 eV higher than the LUMO of [Ru(bpy)₃]²⁺ (-2.54 eV).⁴⁷ The destabilization of the LUMO explains the shifts of 60 mV, 70 mV and 20 mV to more negative values measured for the first reduction potential of **2-1b** (-1.41 V), **2-3b** (-1.42 V) and **2-4b** (-1.37 V) compared with that of [Ru(bpy)₃]²⁺ (-1.35 V),⁴³ respectively. The sharp decrease of the first reduction potential of compound **2-5b** with respect to compound **2-4b** may be attributed to the poor nucleophilicity of **2-5a** compared to **2-4a**. As **2-5a** is less basic the extent of back bonding from the metal centre to bpy will also be decreased, hence the blys are poor in electron density, thus rendering them easier to reduce. The third reduction peak for **2-1b** had an anodic peak potential of -2.30 V vs. SCE whereas that for **2-3b** is more well-defined and is centred at -1.96 V vs. SCE. These peaks can be designated as reductions occurring at **2-1a** and **2-3a**, respectively. These peaks for **2-4b** and **2-5b** appear at -1.86 V and -1.97 V vs. SCE, respectively. As pyrimidine is a better π -acceptor than pyridine, it is easier to reduce ligand **2-3a** in complex **2-3b** than ligand **2-1a** in complex **2-1b**. Similarly, the chloro-substituted pyrimidine moiety in ligand **2-4a** is better π -acceptor than pyrimidine in **2-3a** and thus, the third reduction for complex **2-4b** appears at more positive potential with respect to complex **2-3b**.

2.6.3. Photophysical Investigation and Comparison with Theoretical Models

The absorption spectra of the ligands as well as of the complexes were measured in acetonitrile solutions and are compared to the TD-DFT calculations, with a solvent dielectric potential to simulate solvation. The data for the electronic transitions for the complexes are gathered in Table II-3 and those of ligands are collected in Table II-S2. It is noteworthy that these calculations only take into account the singlet-state transitions.

The electronic absorption spectra of ligands (**2-1a**)-(**2-5a**) are rather featureless and display conventional spin-allowed $\pi \rightarrow \pi^*$ transition(s) centered around 230-290 nm.

Table II-3. Absorption data in deaerated CH₃CN solutions for (**2-1b**)-(**2-5b**).

Compound	λ_{\max} , nm ($\epsilon \times 10^{-3}$, M ⁻¹ cm ⁻¹)
2-1b	242 (34.6), 293 (53.2), 357 (9.5), 487 (7.1), 560 (3.9)
2-2b	246 (23.3), 292 (31.8), 355 (4.8), 474 (4.4), 546 (2.3)
2-3b	241 (30.5), 293 (41.4), 350 (6.7), 474 (6.4), 550 (2.9)
2-4b	246 (16.4), 292 (26.6), 356 (4.1), 463 (4.1), 532 (2.1)
2-5b	244 (24.5), 291 (42.9), 357 (5.1), 468 (7.5), 531 (5.2)
Ru(bpy) ₃ ²⁺	450 (14) ^a

^afrom ref 50a.

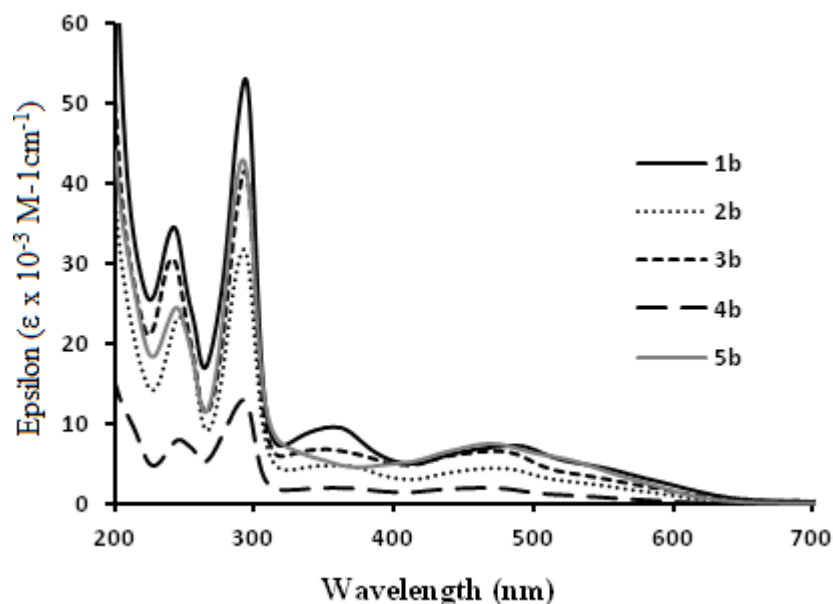


Figure 2.7. Electronic absorption spectra of compounds (**2-1b**)-(**2-5b**) at room temperature in deaerated acetonitrile at a concentration of 1.2×10^{-5} M.

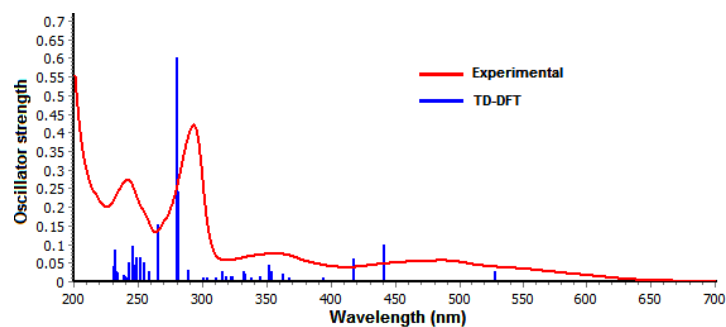


Figure 2.8. Typical figure showing the overlap of experimental electronic absorption spectrum with oscillator strength from TD-DFT calculation of **2-1b**²⁺ in ($S=0$) ground state.

The UV-vis absorption spectra of compounds (**2-1b**)-(**2-5b**) in acetonitrile solution (Table II-3 and Figure 2.7) display spin allowed ¹MLCT (Metal-Ligand to Ligand Charge Transfer) bands in the 400-600 nm region. These bands correspond to electronic transitions from the HOMO to virtual unoccupied molecular orbitals. As suggested by TD-DFT calculation of **2-1b**²⁺, **2-3b**²⁺ and **2-4b**²⁺, the HOMOs of these compounds possess significant **hpp** character (27-29%) (Figure 2.9), however, assigning these transitions as Metal-Ligand to Ligand Charge-Transfer {¹(ML)-LCT} states instead of ¹MLCT states may not be appropriate either. The UV region is dominated by the $\pi \rightarrow \pi^*$ transition in the ligand (bpy) moieties centered around 290 nm for all the compounds.^{1b,7b,7c} The most noticeable feature in the visible region of the electronic absorption spectra of the complexes is that the lowest-energy ¹MLCT maxima are red-shifted with respect to the ¹MLCT of Ru(bpy)₃²⁺, and the amount of shift depends on the electronic properties of the heterocycle coupled with the guanidine moiety.⁵⁰ Ligands (**2-1a**)-(**2-5a**) being stronger donors than bpy, they are expected to interact with the *d* orbitals of ruthenium more strongly than bpy, raising the metal-based HOMO energy. This is perfectly in line with the DFT calculation reported above. On the other hand, the LUMO is still bpy-based, as also indicated by the first reduction potentials of (**2-1b**)-(**2-5b**). This results in a lowering of the energy of the $d\pi \rightarrow \pi^*$ ¹MLCT transition and, hence, a red shift in the absorption spectra. As ligand **2-1a** being the strongest donor in the series (**2-1a**)-(**2-5a**), complex **2-1b** displays a more pronounced red-shift in its ¹MLCT as compared to the other complexes (see last column in Table II.3). Ligand **2-2a** appears to have equal donor capacity as **2-3a**, but more than ligands **2-4a** and **2-5a**, containing electron withdrawing chloropyrimidine and pyrazine moieties, respectively. Moreover, the complexes show additional bands at approximately

350 nm, which receive contributions from a $^1\text{MLCT}$ transition involving the higher-energy orbital of bipyridine.⁵¹ It may be noted that such a band is usually observed for $\text{Ru}(\text{bpy})_2(\text{diamine})^{2+}$ chromophores.⁴³

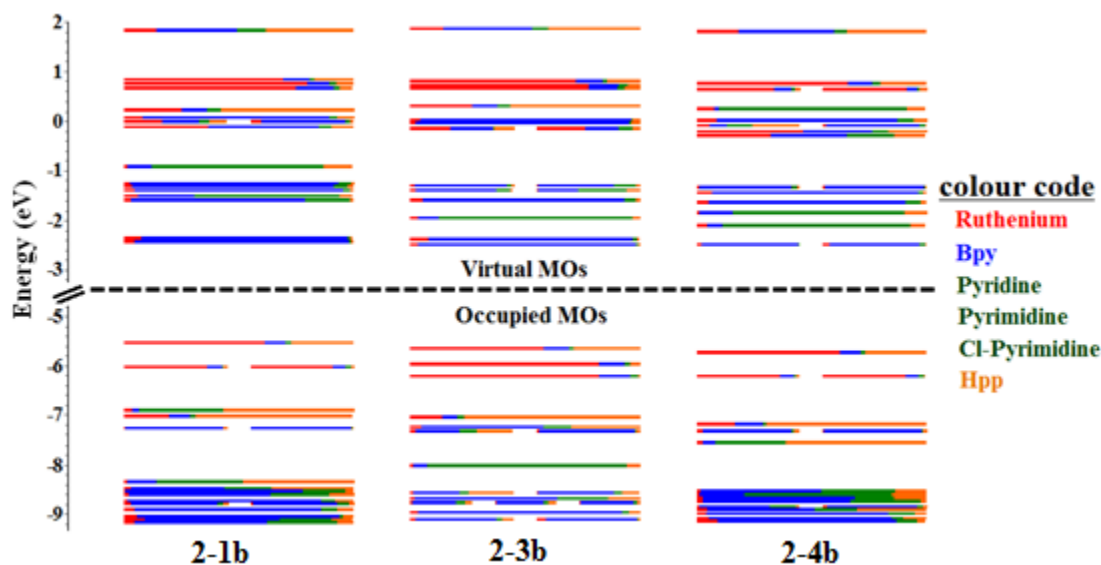


Figure 2.9. Calculated frontier MO energies of all the modeled **2-1b**, **2-3b** and **2-4b** complexes obtained from DFT($\text{rb3lyp}/\text{LanL2DZ}(\text{f})[\text{Ru}]/6\text{-}31\text{G}^{**}[\text{NCN}]$ with CPCM(CH_3CN) and 0.05 eV of threshold of degeneracy.

The luminescence properties of all the complexes were studied in dry, degassed acetonitrile at room temperature. The corrected emission spectra maxima (λ_{max}) along with lifetime (τ), quantum yield (Φ), excited-state radiative (k_r) and non-radiative (k_{nr}) decay values are reported in Table II-4, whereas the corrected spectra are shown in Figure 2.10. In all cases, the emission is attributed to a triplet Ru-to-bpy CT excited state. Interestingly, to the best of our knowledge, these are the lowest-energy Ru-to-bpy CT emissions for $[\text{Ru}(\text{bpy})_2(\text{N-N})]^{2+}$ compounds where N-N is a neutral ligand, and demonstrate that anionic ligands are not strictly required to obtain a large red-shift of $^3\text{MLCT}$ emissive states involving bpy. Concomitant with the bathochromic shift of the $^1\text{MLCT}$ absorption bands in the absorption spectra compared to that of $[\text{Ru}(\text{bpy})_3]^{2+}$, there is a red shift in $^3\text{MLCT}$ emission bands in comparison to the emission of $[\text{Ru}(\text{bpy})_3]^{2+}$. To note the emission maxima are red-shifted with an increase in basicity of the moiety containing the **hpp** subunit. The emission energy (λ_{max} , nm) and the energy gap as expressed by $\Delta E_{1/2}$ are correlated, albeit without solvation effects being taken into account. Indeed the red shift of

the Ru-to-bpy CT-emission for all the studied complexes compared to $[\text{Ru}(\text{bpy})_3]^{2+}$ is due to the narrower HOMO-LUMO energy gap calculated for $[\mathbf{2-1b}]^{2+}$ (3.08 eV), $[\mathbf{2-3b}]^{2+}$ (3.16 eV) and $[\mathbf{2-4b}]^{2+}$ (3.22 eV) compared to that of $[\text{Ru}(\text{bpy})_3]^{2+}$ (3.57 eV),⁴⁸ thereby confirming the agreement between redox, TD-DFT and emission data.

Table II-4. Photophysical data in deaerated CH_3CN solutions for complexes (**2-1b**)-(**2-5b**).

Compound	Luminescence ^a @ 298 K				
	λ_{max} , nm	τ , ns	$10^{-4}\phi$	10^3k_r (s ⁻¹)	10^3k_{nr} (s ⁻¹)
2-1b	745	54	3.4	6.3	18.5
2-2b	745	51	5.0	9.8	19.6
2-3b	740	73	3.6	4.9	13.7
2-4b	732	78	6.8	8.7	12.8
2-5b	736	67	5.5	8.2	14.9
$\text{Ru}(\text{bpy})_3^{2+}$	620 ^{b,c}	860 ^b	620 ^b	72.1	1.1

^acorrected for the photomultiplier response. ^bfrom ref 50, ^cfrom ref 51.

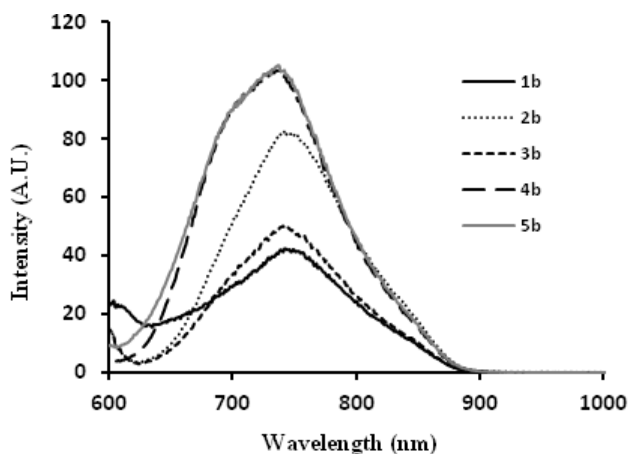


Figure 2.10. Emission spectra of compounds (**2-1b**)-(**2-5b**), corrected for photomultiplier response.

The red shift in emission energy is accompanied by a sharp decrease in emission quantum yield and lifetime compared to $[\text{Ru}(\text{bpy})_3]^{2+}$ and similar species,^{1b} as expected on the basis of the energy gap law.^{7b,7c,52,53} In heteroleptic Ru(II)-polypyridyl complexes, substituents with extended p systems permit greater delocalization of the excited MLCT state, with smaller bond displacement changes, and, a concomitant decrease in nonradiative decay, eventually allowing for relatively long lifetimes.^{54,55} However, this is valid only when the acceptor ligand of the emissive ³MLCT state is a large aromatic ligand, which is

not occurring here, where the emitting $^3\text{MLCT}$ state is a bpy ligand in all the complexes. Due to the presence of thermally accessible low lying triplet metal-centered (^3MC) states close to the radiative $^3\text{MLCT}$ states, the energy gap law, predicting a roughly inversed linear dependence of $\ln k_{\text{nr}}$ on the emission energy, is sometimes not followed by luminescence properties of Ru(II) complexes at room temperature.^{1b,7} However, in the present series of compounds, the inversed linear relationship between $\ln k_{\text{nr}}$ and the emission energy (in cm^{-1}) is roughly kept - also considering the experimental uncertainties in lifetime and quantum yield determination - suggesting that the energy gap law plays a significant role in determining the excited-state lifetime.

Finally, a cursory look at the data in Table II-4 also indicates that the radiative decay constants of **(2-1b)**-**(2-5b)** are one order of magnitude smaller than that of $\text{Ru}(\text{bpy})_3^{2+}$. Of course, this negatively affects the luminescence performance of the compounds, in particular quantum yield data. Lower values are also found (see data in Table II-3) for the molar absorption coefficient of the lowest-energy $^1\text{MLCT}$ bands of the new compounds (around $5000 \text{ M}^{-1} \text{ cm}^{-1}$) compared to MLCT of $[\text{Ru}(\text{bpy})_3]^{2+}$ (about $15000 \text{ M}^{-1} \text{ cm}^{-1}$). Although the emission process refers to a triplet $^3\text{MLCT}$ state, and the absorption to the corresponding singlet state, the combination of molar absorption coefficient and radiative decay data suggests that the oscillator strength(s) of MLCT transitions in **(2-1b)**-**(2-5b)** are smaller than in $[\text{Ru}(\text{bpy})_3]^{2+}$. A possible explanation lies in the distortion from the octahedral arrangement around the metal center, which is larger in **(2-1b)**-**(2-5b)** than in the prototype $[\text{Ru}(\text{bpy})_3]^{2+}$ compound, as indicated by the crystal structure data of **2-2b**, **2-3b**, and **2-4b**, reported above. Such an increased octahedral distortion would negatively affect metal and bpy orbital overlaps, so decreasing oscillator strength and therefore probability of $^1\text{MLCT}$ transitions.

2.7. Conclusions

In conclusion, five novel N_{amine} -substituted guanidine-pyridine/pyrimidine/pyrazine ligands were synthesized and their coordination to ruthenium(II) formed stable six-membered chelate rings. From the Ru(III/II) potentials of the new complexes, it is found that all the new ligands possess strong donating ability as compared to common polypyridyls, e.g., bpy or phenanthroline. In fact the ligands reported in this work are even more electron donating than 2-(2'-aminoethyl)-pyridine (AETPy) or ethylenediamine (en)

as revealed by the Ru(III/II)-couples of the complexes $[\text{Ru}(\text{bpy})_2(\text{AETPy})]^{2+}$ (1.12 V vs. SCE) and $[\text{Ru}(\text{bpy})_2(\text{en})]^{2+}$ (0.96 V vs. SCE).^{43,46,56} As a result of strong σ donation from the ligands, complexes (2-1b)-(2-5b) have low energy $^1\text{MLCT}$ absorptions in the visible region in comparison to $[\text{Ru}(\text{bpy})_3]^{2+}$. The 298 K fluid solution emission maxima for the complexes are also red-shifted by ~ 100 nm with respect to that for $[\text{Ru}(\text{bpy})_3]^{2+}$, and they arise due to Ru^{II}-to-bpy $^3\text{MLCT}$ states, since the π^* orbitals are predominantly bpy based, as evidenced by DFT calculations. Thus, the complexes, having interesting photophysical and unique redox properties, can serve as excellent red-absorbing and light-harvesting materials.

2.8. Acknowledgements

AKP and GSH thank the Natural Sciences and Engineering Research Council of Canada (NSERC) and Centre for Self-Assembled Chemical Structure (CSACS) for financial support. SC thanks MIUR (PRIN: 2010-11 and FIRB: Nanosolar projects) for financial support. We also thank Johnson Matthey PLC for a generous loan of ruthenium trichloride.

2.9. Supporting Information

CIF files, text, tables, and figures giving crystallographic data for CCDC files 954083–954086 and further details as noted in the text along with the computational data. This material is available free of charge via the Internet at <http://pubs.acs.org>.

2.10. References

- (1) (a) Balzani, V.; Scandola, F. *Supramolecular Photochemistry*; Horwood: Chichester, U.K., 1991. (b) Juris, A.; Balzani, V.; Barigelletti, F.; Campagna, S.; Belser, P.; von Zelewsky, A. *Coord. Chem. Rev.* **1988**, *84*, 85. (c) Balzani, V.; Juris, A.; Venturi, M.; Campagna, S.; Serroni, S. *Chem. Rev.* **1996**, *96*, 759. (d) Medlycott, E. A.; Hanan, G. S. *Chem. Soc. Rev.* **2005**, *34*, 133. (e) Medlycott, E. A.; Hanan, G. S. *Coord. Chem. Rev.* **2006**, *250*, 1763.
- (2) (a) Concepcion, J. J.; Jurss, J. W.; Templeton, J. L.; Meyer, T. J. *J. Am. Chem. Soc.* **2008**, *130*, 16462. (b) Zong, R.; Thummel, R. P. *J. Am. Chem. Soc.* **2005**, *127*, 12802.
- (3) (a) Balzani, V.; Barigelletti, F.; De Cola, L. *Top. Curr. Chem.* **1990**, *158*, 31. (b) Alstrum-Acevedo, J. H.; Brennaman, M. K.; Meyer, T. J. *Inorg. Chem.* **2005**, *44*, 6802.

- (4) Nazeeruddin, M. K.; Kay, A.; Rodicio, I.; Humphrybaker, R.; Muller, E.; Liska, P.; Vlachopoulos, N.; Gratzel, M. *J. Am. Chem. Soc.* **1993**, *115*, 6382.
- (5) Yam, V. W.-W.; Lo, K. K.-W. *Coord. Chem. Rev.* **1998**, *184*, 157 and references cited therein.
- (6) MacDermott, G.; Prince, S. M.; Freer, A. A.; Hawthornthwaite-Lawless, A. M.; Papiz, M. Z.; Cogdell, R. J.; Isaacs, N. W. *Nature* **1995**, *374*, 517.
- (7) (a) Kalyanasundaram, K.; Grätzel, M.; Nazeeruddin, M. K. *J. Chem. Soc., Dalton Trans.* **1991**, *23*, 343. (b) Sauvage, J. P.; Collin, J. P.; Chambron, J. C.; Guillerez, S.; Coudret, C.; Balzani, V.; Barigelletti, F.; DeCola, L.; Flamigni, L. *Chem. Rev.* **1994**, *94*, 993. (c) Meyer, T. J. *Pure Appl. Chem.* **1986**, *58*, 1193.
- (8) Balzani, V.; Juris, A. *Coord. Chem. Rev.* **2001**, *211*, 97.
- (9) Anderson, P. A.; Keene, F. R.; Meyer, T. J.; Moss, J. A.; Strouse, G. F.; Treadway, J. A.; *J. Chem. Soc., Dalton Trans.* **2002**, *20*, 3820 and refs. therein.
- (10) Kitamura, N.; Kawanishi, Y.; Tazuke, S. *Chem. Phys. Lett.* **1983**, *97*, 103.
- (11) Rillema, D. P.; Allen, G.; Meyer, T. J.; Conrad, D. *Inorg. Chem.* **1983**, *22*, 1617.
- (12) Ernst, S.; Kaim, W. *Inorg. Chem.* **1989**, *28*, 1520.
- (13) Ioachim, E.; Medlycott, E. A.; Hanan, G. S.; Loiseau, F.; Campagna, S. *Inorg. Chim. Acta* **2006**, *359*, 766.
- (14) Ioachim, E.; Medlycott, E. A.; Hanan, G. S.; Loiseau, F.; Ricevuto, V.; Campagna, S. *Inorg. Chem. Commun.* **2005**, *8*, 559.
- (15) Cook, M. J.; Lewis, A. P.; McAuliffe, G. S. G.; Skarda, V.; Thompson, A. J.; Glasper, J. L.; Robbins, D. J. *J. Chem. Soc., Perkin Trans.* **1984**, *2*, 1303.
- (16) de Carvalho, I. M. M.; de Sousa Moreira, I.; Gehlen, M. H. *Inorg. Chem.* **2003**, *42*, 1525.
- (17) Bergman, S. D.; Goldberg, I.; Barbieri, A.; Barigelletti, F.; Kol, M. *Inorg. Chem.* **2004**, *43*, 2355.
- (18) Bergman, S. D.; Goldberg, I.; Barbieri, A.; Kol, M. *Inorg. Chem.* **2005**, *44*, 2513.
- (19) Ruminski, R. R.; Deere, P. T.; Olive, M.; Serveiss, D. *Inorg. Chim. Acta.* **1998**, *281*, 1.
- (20) (a) Johansson, K. O.; Lotoski, J. A.; Tong, C. C.; Hanan, G. S. *Chem. Commun.* **2000**, *10*, 819. (b) Denti, G.; Campagna, S.; Sabatino, L.; Serroni, S.; Ciano, M.; Balzani, V. *Inorg. Chem.* **1990**, *29*, 4750.
- (21) Nag, S.; Ferreira, J. G.; Chenneberg, L.; Ducharme, P. D.; Hanan, G. S.; Ganga, G. L.; Serroni, S.; and Campagna, S. *Inorg. Chem.* **2011**, *50*, 7.
- (22) Crosby, G. A.; Demas, J. N. *J. Phys. Chem.* **1971**, *75*, 991.
- (23) Nakamaru, N. *Bull. Chem. Soc. Jpn.* **1982**, *55*, 2697.
- (24) Sprintschnik, G.; Sprintschnik, H. W.; Kirsch, P. P.; Whitten, D. G. *J. Am. Chem. Soc.* **1977**, *99*, 4947.
- (25) Frisch, M. J.; Trucks, G. W.; Schlegel, H. B.; Scuseria, G. E.; Robb, M. A.; Cheeseman, J. R.; Montgomery, J. A.; Vreven, T. J.; Kudin, K. N.; Burant, J. C.; Millam, J. M.; S., I. S.; Tomasi, J.; Barone, V.; Mennucci, B.; Cossi, M.; Scalmani, G.; Rega, N.; Petersson, G. A.; Nakatsuji, H.; Hada, M.; Ehara, M.; Toyota, K.;

Chapter 2

- Fukuda, R.; Hasegawa, J.; Ishida, M.; Nakajima, T.; Honda, Y.; Kitao, O.; Nakai, H.; Klene, M.; Li, X.; Knox, J. E.; Hratchian, H. P.; Cross, J. B.; Adamo, C.; Jaramillo, J.; Gomperts, R.; Startmann, R. E.; Yazyev, O.; Austin, A. J.; Cammi, R.; Pomelli, C.; Ochterski, J. W.; Ayala, P. Y.; Morokuma, K.; Voth, G. A.; Salvador, P.; Dannenberg, J. J.; Zakrzewski, V. G.; Dapprich, J. M.; Daniels, A. D.; Strain, M. C.; Farkas, O.; Malick, D. K.; Rabuck, A. D.; Raghavachari, K.; Foresman, J. B.; Ortiz, J. V.; Cui, Q.; Baboul, A. G.; Clifford, S.; Cioslowski, J.; B., S. B.; Liu, G.; Liashenko, A.; Piskorz, I.; Komaromi, I.; L., M. R.; Fox, D. J.; Keith, T.; Al-Laham, M. A.; Peng, C. Y.; Manayakkara, A.; Challacombe, M.; Gill, P. M. W.; Johnson, B. G.; Chen, W.; Wong, M. W.; Gonzalez, C.; Pople, J. A., *Gaussian 2003, Revision C.02; Gaussian Inc.:Pittsburgh PA, 2003.*
- (26) Becke, A. D. *J. Chem. Phys.* **1993**, *98*, 5648.
- (27) Lee, C.; Yang, W.; Parr, R. G. *Phys. Rev. B: Condens. Matter* **1988**, *37*, 785.
- (28) McLean, A. D.; Chandler, G. S. *J. Chem. Phys.* **1980**, *72*, 5639.
- (29) Hay, P. J.; Wadt, W. R. *J. Chem. Phys.* **1985**, *82*, 270.
- (30) (a) Casida, M. E.; Jamorski, C.; Casida, K. C.; Salahub, D. R. *J. Chem. Phys.* **1998**, *108*, 4439. (b) Stratmann, R. E.; Scuseria, G. E.; Frisch, M. J. *J. Chem. Phys.* **1998**, *109*, 8218.
- (31) (a) Cossi, M.; Rega, N.; Scalmani, G.; Barone, V. *J. Comput. Chem.* **2003**, *24*, 669. (b) Cossi, M.; Barone, V. *J. Chem. Phys.* **2001**, *115*, 4708. (c) Barone, V.; Cossi, M. *J. Phys. Chem. A* **1998**, *102*, 1995.
- (32) Dixon, I. M.; Alary, F.; Heully, J.-L. *Dalton Trans.*, **2010**, *39*, 10959.
- (33) Browne, W. R.; O'Boyle, N. M.; McGarvey, J. J.; Vos, J. G. *Chem. Soc. Rev.* **2005**, *34*, 641.
- (34) Zhurko, D. A. and Zhurko, G. A. *ChemCraft 1.5*; Plimus: San Diego, CA. Available at <http://www.chemcraftprog.com>.
- (35) *APEX2 (2007) version 2.4-0; Bruker Molecular Analysis Research Tool*. Bruker AXS Inc., Madison, WI 53719-1173.
- (36) Sheldrick, G. M. (1996). *SADABS*, Bruker Area Detector Absorption Corrections. Bruker AXS Inc., Madison, WI 53719-1173.
- (37) *SHELXTL (2001) version 6.12*; Bruker Analytical X-ray Systems Inc., Madison, WI 53719-1173.
- (38) Platon (A. L. SPEK, 2003).
- (39) Wolfe, J. P.; Buchwald, S. L. *J. Org. Chem.*, **2000**, *65*, 1144.
- (40) Oakley, S. H.; Coles, M. P.; Hitchcock, P. B. *Inorg. Chem.*, **2004**, *43*, 7564.
- (41) Based on 278 ruthenium complexes containing at least two bpy and two more substituent with N atoms coordinated to the metal in the Cambridge Structural Database. Allen, F. H. *Acta Crystallogr. Sect. B: Struct. Sci.* **2002**, *B58*, 380.
- (42) (a) De Groot, B.; Hanan, G. S.; Loeb, S. J. *Inorg. Chem.* **1991**, *30*, 4644. (b) Giesbrecht, G. R.; Hanan, G. S.; Kickham, J. E.; Loeb, S. J. *Inorg. Chem.* **1992**, *31*, 3286.
- (43) Aydin, N.; Schlaepfer, C. W. *Polyhedron* **2001**, *20*, 37.

Chapter 2

- (44) Ji, Z.; Huang, S. D.; Guadalupe, A. R. *Inorg. Chim. Acta* **2000**, 305, 127.
- (45) Tokel-Takvoryan, N. E.; Hemingway, R. E.; Bard, A. J. *J. Am. Chem. Soc.* **1973**, 95, 6582.
- (46) Konno, H.; Ishii, Y.; Sakamoto, K.; Ishitani, O. *Polyhedron* **2002**, 21, 61.
- (47) Gorelsky, S. I.; Lever, A. B. P. *J. Organomet. Chem.* **2001**, 635, 187.
- (48) Bolink, H. J.; Coronado, E.; D. Costa, R.; Gaviña, P.; Ortí, E. and Tatay, S. *Inorg. Chem.* **2009**, 48, 3907.
- (49) Donato, L.; McCusker, C. E.; Castellano, F. N. and Zysman-Colman, E. *Inorg. Chem.*, **2013**, 52, 8495.
- (50) (a) Calvert, J. M.; Caspar, J. V.; Binstead, R. A.; Westmoreland, T. D. and Meyer, T. J. *J. Am. Chem. Soc.* **1982**, 104, 6620. (b) Gorelsky, S. I.; Dodsworth, E. S.; Lever, A. B. P.; Vlcek, A. A. *Coord. Chem. Rev.* **1998**, 174, 469. (c) Gorelsky, S. I. and Lever, A. B. P. *Coord. Chem. Rev.* **2000**, 208, 153.
- (51) Casper, J. V. and Meyer, T. J. *Inorg. Chem.* **1983**, 22, 2444.
- (52) Casper, J. V.; Kober, E. M.; Sullivan, B. P. and Meyer, T. J. *J. Am. Chem. Soc.* **1982**, 104, 630.
- (53) Claude, J. P. and Meyer, T. J. *J. Phys. Chem.* **1995**, 99, 51.
- (54) Fang, Y. -Q.; Taylor, N. J.; Hanan, G. S.; Loiseau, F.; Passalacqua, R.; Campagna, S.; Nierengarten, A.; and Dorselaer, A. V. *J. Am. Chem. Soc.* **2002**, 124, 7912.
- (55) Polson, M. I. J.; Medlycott, E. A.; Hanan, G. S.; Mikelsons, L.; Taylor, N. J.; Watanabe, M.; Tanaka, Y.; Loiseau, F.; Passalacqua, R. and Campagna, S. *Chem. Eur. J.* **2004**, 10, 3640.
- (56) Brown, G. M.; Weaver, T. R.; Keene, F. R. and Meyer, T. J. *Inorg. Chem.* **1976**, 15, 190.

Chapter 3: *Stereoselective formation of a meso-diruthenium(II,II) complex and tuning the properties of its monoruthenium analogues*

3.1. Résumé

Un ligand bis(bidentate), **dgpm** (**dgpm** = 4,6-diguanidylpyrimidine) a été synthétisé par un C-N liaison sans catalyseur réaction de formation avec un rendement élevé (90%) par chauffage par micro-ondes. Le ligand est coordonné à deux $[\text{Ru}(\text{bpy})_2]^{2+}$ noyaux de s'offrir un *méso*-di-Ru(II,II) (**3-(1-meso)**) avec une haute diastéréosélectivité sur sa forme homochiral. Trois de Ru(II) des complexes mononucléaires éther fonctionnalisées (**3-2**: ethoxyether; **3-3**: butoxyether; **3-4**: 2-hydroxy-1-ethoxyether) ont également été isolés. Le ligand et les complexes ont été entièrement caractérisés par une variété de techniques incluant la cristallographie aux rayons-X. Dans les études de voltampérométrie cyclique, les complexes présentent un couple RuIII/II, qui est de ~ 500 mV moins positive que le couple RuIII/II en $[\text{Ru}(\text{bpy})_3]^{2+}$. Les maxima d'absorption $^1\text{MLCT}$ de tous les complexes (510-550 nm) sont nettement décalés vers le rouge par rapport à celle de $[\text{Ru}(\text{bpy})_3]^{2+}$ (450 nm). L'émission maxima $^3\text{MLCT}$ de complexes (**3-(1-meso)**) et **3-3** sont également décalée vers le rouge d'environ 120 nm par rapport à celle de $\text{Ru}(\text{bpy})_3^{2+}$ (620 nm), tandis que les maxima correspondant à des complexes **3-3** et **3-4** sont décalés de 75 nm et 25 nm, respectivement. Ces tendances relatives potentiels redox et $^1\text{MLCT}$ maxima sont en bon accord avec les calculs DFT et TD-DFT, effectués pour tous les complexes. Complexes (**3-(1-meso)**) et **3-3** affichage émission d'un état RuII-à-bpy $^3\text{MLCT}$, ce qui est rarement l'état émettant à $\lambda > 700$ nm dans $[\text{Ru}(\text{bpy})_2(\text{N}-\text{N})]^{2+}$ des complexes lorsque le ligand auxiliaire est neutre.

Contribution :

Amlan K. Pal : All the work presented in this article and its writing.

Garry S. Hanan : Supervision and revision of the article.

Stereoselective formation of a meso-diruthenium(II,II) complex and tuning the properties of its monoruthenium analogues

Amlan K. Pal, Garry S. Hanan*

Department of Chemistry, Université de Montréal, Montréal, QC, H3T 1J4 Canada

Received: January 12, 2014; Published: March 13, 2014

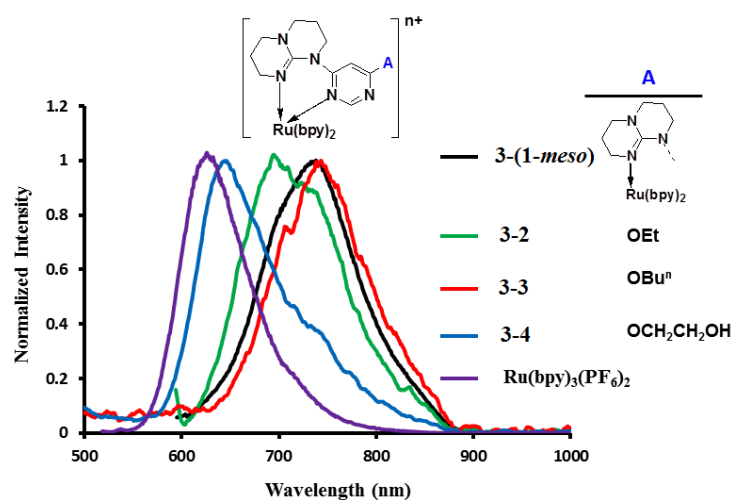
Dalton Trans., 2014, Advance Article. DOI: 10.1039/C4DT00112E

Reproduced with permission from *Dalton Trans.* 2014.

Copyright 2014 Royal Society of Chemistry.

KEYWORDS: Ruthenium complexes, Diastereoselectivity, Ligand design, Electrochemistry, Density functional theory, Photophysical properties

3.2. Table of Content Graphic



Diruthenium(II,II) complex **3-(1-*meso*)** was synthesized with high diastereoselectivity as its *meso*-isomer over the homochiral *rac*-isomers ($\Lambda\Lambda:\Lambda\Delta$ (or $\Delta\Lambda):\Delta\Delta = 1:13:1$) due to unique

design of the bis(bidentate) ligand with parallel coordination vectors. Three mononuclear complexes were also isolated as solvolysis products and their electronic and photophysical properties are found to follow their respective ether adducts based on +I-effect. The experimental observations correlated well with properties predicted by DFT and TD-DFT calculations.

3.3. Abstract

A novel bis(bidentate) ligand **dgpm** (**dgpm** = 4,6-diguanidylpyrimidine) was synthesized by a catalyst-free C–N bond forming reaction in high yield (90%) by microwave-assisted heating. The ligand was coordinated to two $[\text{Ru}(\text{bpy})_2]^{2+}$ cores to afford a *meso*-di-Ru(II,II) complex (**3-(1-*meso*)**) with high diastereoselectivity over its homochiral form. Three mononuclear ether-functionalized Ru(II) complexes (**3-2**: ethoxyether; **3-3**: butoxyether; **3-4**: 2-hydroxy-1-ethoxyether) were also isolated. The ligand and complexes were fully characterized by a variety of techniques including X-ray crystallography. In cyclic voltammetric studies, the complexes exhibit a $\text{Ru}^{\text{III/II}}$ couple, which is ~ 500 mV less positive than the $\text{Ru}^{\text{III/II}}$ couple in $[\text{Ru}(\text{bpy})_3]^{2+}$. The $^1\text{MLCT}$ absorption maxima of all the complexes (510–550 nm) are considerably red-shifted as compared to that of $[\text{Ru}(\text{bpy})_3]^{2+}$ (450 nm). The $^3\text{MLCT}$ emission maxima of complexes **3-(1-*meso*)** and **3-3** are also red-shifted by about 120 nm compared to that of $[\text{Ru}(\text{bpy})_3]^{2+}$ (620 nm), whereas the corresponding maxima for complexes **3-2** and **3-4** are shifted by 75 nm and 25 nm, respectively. These relative trends in redox potentials and $^1\text{MLCT}$ maxima are in good agreement with DFT and TD-DFT calculations, performed for all complexes. Complexes **3-(1-*meso*)** and **3-3** display emission from a Ru^{II} -to-bpy $^3\text{MLCT}$ state, which is rarely the emitting state at $\lambda > 700$ nm in $[\text{Ru}(\text{bpy})_2(\text{N–N})]^{2+}$ complexes when the ancillary ligand is neutral.

3.4. Introduction

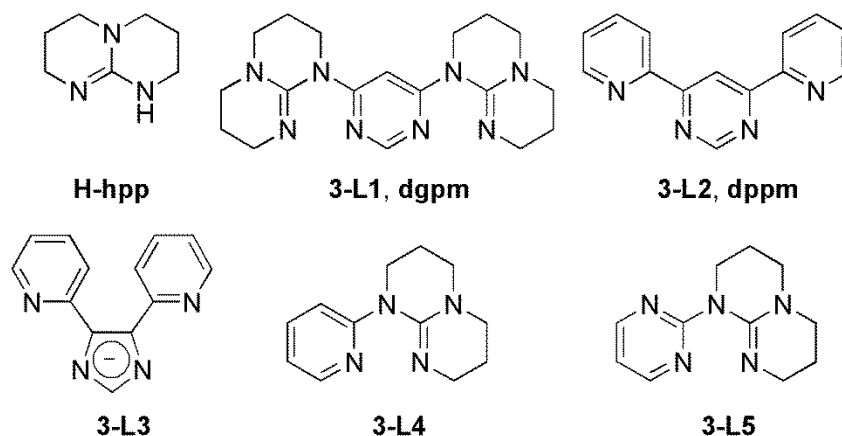
The growing interest in Ru(II)-polypyridyl complexes stems from their unique properties, such as chemical robustness, visible light absorption, tunable and reversible electrochemical processes and relatively long luminescent triplet metal-to-ligand charge transfer ($^3\text{MLCT}$) excited state lifetimes at room temperature (lifetime (τ) of $\text{Ru}(\text{bpy})_3^{2+}$ is $\sim 1 \mu\text{s}$; bpy = 2,2'-bipyridine). This unique combination of tunable electrochemical and photophysical properties^{1a-g} renders these compounds valuable for applications in water oxidation,² artificial photosynthesis,³ and more generally in the conversion of solar energy to chemical energy.^{3a,4} Over the last decade photoinduced electron transfer processes attracted much attention, from dye sensitized solar cell (DSSC) applications to the conversion of light energy into chemical energy.⁵ 'Black absorber' complexes,⁶ which can absorb throughout the visible region, and 'red emitter' complexes,⁷ which can emit at relatively low-energy region while maintaining relatively long excited state lifetime, are of more recent interest. These complexes exhibit potential application in biological systems⁸ and as low-lying energy traps in multichromophore arrays, reminiscent of the protein-embedded natural photosynthetic apparatus.⁹ The convenience in using mononuclear Ru(II)-polypyridyl complexes originates from the judicious choice of ligands, which can tune the energy of the excited state,¹⁰ the excited-state lifetime^{1c,10,11} and the absorption energy of the complexes,^{6b,10,11} while overcoming the limitations imposed by the energy gap law^{10b,c} on the excited-state lifetime of these complexes.

Among the different strategies adopted by various groups to red-shift the absorption and emission of Ru(II)-heteroleptic complexes and to prolong their excited-state lifetimes; the most effective approaches are: (a) (i) to functionalize bpy with various substituents in order to lower the energy of the lowest unoccupied molecular orbital (LUMO),^{12a,b} or (ii) to increase the energy of the highest occupied molecular orbital (HOMO) and consequently the energy of triplet metal-centred (^3MC) states,^{7c-d} thereby increasing the $^3\text{MLCT}$ - ^3MC energy gap, (b) to introduce electron-poor aromatic moieties containing bidiazine ligands,^{7a,b,13-15} thereby stabilizing the $^3\text{MLCT}$ state, (c) to introduce an organic chromophore to establish an equilibrium between the $^3\text{MLCT}$ and the organic chromophore triplet ^3LC states,¹⁶ and (d) to introduce fused polyaromatic systems, albeit with less readily available ligands (for e.g. isoeilatin¹⁷). Ruthenium(II) complexes based on electron donating or withdrawing substituents on 2,2'-bipyridine,^{18,19} 3,3'-bipyridazine,²⁰

2,2'-bipyrazine,¹⁴ 2,2'-bipyrimidine,²¹ and 4,4'-bipyrimidine^{7a,b,22} have been well documented with their potential applications in solar energy conversion devices. However, the complexes bearing diazine ligands with two-ring *N*-heteroatoms are enticing as they exhibit red-shifted absorption and emission maxima compared to that of Ru(bpy)₃²⁺ due to stabilization of the LUMO.

Herein, within a mixed approach of (i) and (ii) we report the synthesis of a bis(bidentate) ligand (**3-L1** or **dgpm** (4,6-diguanidylpyrimidine); Chart 3.1) in which a hexahydropyrimidopyrimidine (**H-hpp**) unit is coupled with pyrimidine to furnish the chelate rings. In a recent communication,²³ we demonstrated that **dgpm** coordinates [Ru(bpy)₂]²⁺ and furnishes a *meso*-diruthenium complex (**3-(1-meso)**), with high diastereoselectivity, and the complex was characterized by solution NMR, LC-MS, XRD, absorption spectroscopy and electrochemistry. In this article, we report the complete characterization of **3-(1-meso)** and its functionalized products **3-2**, **3-3** and **3-4**, which were generated by nucleophilic displacement of the non-coordinated guanidyl portion of the monoruthenium complex of **3-L1**. The redox and photophysical properties are in good agreement with density functional theory (DFT) and time-dependent density functional theory (TD-DFT) studies of the compounds. The complexes described herein have the advantage of being readily synthesized, easily functionalized and they emit at low energy as compared to the Ru-complexes with fused polyaromatic systems.¹⁷

Chart 3.1. 1,3,4,6,7,8-Hexahydro-2*H*-pyrimido[1,2-*a*]pyrimidine (**H-hpp**) attached to pyrimidine (**3-L1**, **dgpm**) and some benchmark ligands.



3.5. Experimental section

3.5.1. Materials, methods and instrumentation

Nuclear magnetic resonance (NMR) spectra were recorded in CD₃CN at room temperature (r.t.) on a Bruker AV400 (400 MHz) and AV700 (700 MHz) spectrometers (as noted in the experimental) for ¹H NMR and at 100 and 175 MHz (as noted in the experimental) for ¹³C NMR, respectively. Chemical shifts are reported in part per million (ppm) relative to residual solvent protons (1.94 ppm for CD₃CN, 7.26 ppm for CDCl₃) and the carbon resonance (1.24 ppm for CD₃CN, 77.00 ppm for CDCl₃) of the solvent.

All the photophysical measurements were carried out in deaerated acetonitrile at r.t. in septa-sealed quartz cells. Absorption spectra were measured on a Cary 500i UV-Vis-NIR Spectrophotometer. For luminescence spectra a Cary Eclipse Fluorescence spectrofluorimeter was used. Luminescence lifetimes were determined by time-correlated single-photon-counting (TCSPC) with an Edinburgh EPL-405 spectrometer (light pulse: picosecond pulse diode laser, pulse width 500 ps at 405 nm). Luminescence quantum yields have been performed by the optical dilute method.²⁴ As quantum yield reference, [Ru(bpy)₃]²⁺ in aqueous deaerated solution was used ($\Phi = 0.095$).²⁵ For each sample, linear least-squares fit of values were obtained from at least three independent solutions at varying concentrations with emission intensity. Electrochemical measurements were carried out in argon-purged purified acetonitrile at room temperature with a BAS CV50W multipurpose equipment interfaced to a PC. The working electrode was a glassy carbon electrode. The counter electrode was a Pt wire, and the pseudo-reference electrode was a silver wire. The reference was set using an internal 1 mM ferrocene/ferrocinium sample at 395 mV vs. SCE in acetonitrile. The concentration of the compounds was about 1 mM. Tetrabutylammonium hexafluorophosphate (TBAP) was used as supporting electrolyte and its concentration was 0.10 M. Cyclic voltammograms of **3-L1**, **3-(1-meso)**, **3-2**, **3-3** and **3-4** were obtained at scan rates of 100, 25 and 50 mV/s, respectively. The criteria for reversibility were the separation of 60 mV between cathodic and anodic peaks, the close to unity ratio of the intensities of the cathodic and anodic currents, and the constancy of the peak potential on changing scan rate. Differential pulse voltammetry was conducted with a sweep rate of 20 mVs⁻¹ and a pulse amplitude, width and period of 50 mV, 50 ms and 200 ms, respectively.

Experimental uncertainties are as follows: absorption maxima, ± 2 nm; molar absorption coefficient, 10%; redox potentials, ± 10 mV, emission maxima, ± 2 nm, emission lifetimes, $\pm 10\%$.

1,3,4,6,7,8-Hexahydro-2*H*-pyrimido[1,2-*a*]pyrimidine (**H-hpp**), 4,6-dichloropyrimidine, AgNO₃, and KPF₆ were purchased from Aldrich as used as received. *Cis*-Ru(bpy)₂Cl₂·2H₂O was synthesized using literature procedure.²⁶

3.5.2. Synthetic Methods

4,6-bis-[1,3,4,6,7,8-Hexahydro-2*H*-pyrimido[1,2-*a*]pyrimidine]pyrimidine (3-L1**) (**dgpm**):** 4,6-Dichloropyrimidine (2 mmol, 0.307 g) and 1,3,4,6,7,8-hexahydro-2*H*-pyrimido[1,2-*a*]pyrimidine (**H-hpp**) (4 eq, 8 mmol, 1.126 g) were combined in toluene (20 mL) in a microwave vial. The tube was sealed and placed in a Biotage 400 MW microwave reactor. The suspension was heated to 160 °C for 2 hours, after which time the solution was slowly decanted out and evaporated to dryness. The crude product could be purified by overnight sublimation at 1.8 mbar and 100 °C, as colourless crystals (**3-L1**). Yield = 638 mg (90%). ¹H NMR: (400 MHz, CDCl₃) δ ppm 8.43 (s, 1 H₁), 8.21 (s, 1 H), 3.96 (t, $J^t = 6$ Hz, 4 H), 3.46 (t, $J^t = 6$ Hz, 4 H), 3.22 (t, $J^t = 6$ Hz, 4 H), 3.14 (t, $J^t = 6$ Hz, 4 H), 1.97 (quint, $J^{qt} = 6$ Hz, 4 H), 1.89 (quint, $J^{qt} = 6$ Hz, 4 H). ¹³C NMR: (100 MHz, CDCl₃) δ ppm 160.9, 156.7, 148.9, 98.9, 48.7, 48.7, 43.9, 42.4, 23.8, 22.6. HRMS (ESI), m/z : 355.23635 [M+H]⁺ (C₁₈H₂₇N₈ requires 355.23532). Anal. Calc. for C₁₈H₂₆N₈: C: 60.99; N: 31.61; H: 7.39. Found: C: 60.75; N: 31.70; H: 7.35. Melting point: 182-185 °C.

Meso-[{Ru(bpy)₂}₂(μ -(3-L1**))](PF₆)₄ (**3-(1-meso)**):**

A 250 mL round-bottomed flask was charged with *cis*-Ru(bpy)₂Cl₂·2H₂O (0.513 g, 0.987 mmol), AgNO₃ (0.344 g, 2.025 mmol, 2.05 eq) in methanol (150 mL). The suspension was heated to reflux for 3 hours to give a dark red solution with a white precipitate of AgCl. The solution was cooled down to room temperature and then filtered through a plug of celite and was washed with methanol (3x30 mL). Filtrate and washings were collected and evaporated to dryness to give a dark red solid. To this solid was added **3-L1** (0.100 g, 0.282 mmol), followed by the addition of *n*-BuOH (150 mL) and the suspension was heated to reflux, under N₂-atmosphere for 16 h. After this time, the solution was cooled down to room temperature and evaporated to dryness. The crude product was purified through a silica column using 7:1 = CH₃CN:saturated aq. KNO₃ solution (v/v) as an eluant and then

increasing the polarity of the eluent to 7:2:1 = CH₃CN:saturated aq. KNO₃ solution:H₂O (v/v/v). The slowest moving and major dark red band was collected, solvent was evaporated to dryness and the NO₃⁻ salt was metathesised to PF₆⁻ salt by addition of saturated aqueous KPF₆ solution. The dark red solid was collected by filtration was dried under vacuum to furnish the product, which could be recrystallised from a concentrated acetonitrile solution by diffusing diethylether into it. Yield = 0.325 g (65%). ¹H NMR (700 MHz, acetonitrile-*d*₃) δ ppm 1.05 (m, 2 H), 1.61 (m, 2 H), 2.04 (m, 2 H), 2.11 (m, 2 H), 2.29 (m, 2 H), 2.89 (m, 2 H), 3.02 (quint, J^{qt} = 6 Hz, 2 H), 3.17 (m, 6 H), 3.37 (m, 2 H), 3.95 (m, 2 H), 6.18 (s, 1 H), 6.87 (s, 1 H), 6.97 (t, J^t = 8 Hz, 2 H), 7.10 (m, 6 H), 7.56 (m, 4 H), 7.81 (dt, J^{dt} = 8, 2.0 Hz, 2 H), 7.89 (dt, J^{dt} = 8, 2 Hz, 2 H), 7.99 (m, 4 H), 8.09 (dt, J^{dt} = 8, 2 Hz, 2 H), 8.17 (d, J^d = 8 Hz, 2 H), 8.20 (d, J^d = 8 Hz, 2 H), 8.29 (d, J^d = 6 Hz, 2 H), 8.37 (d, J^d = 8 Hz, 2 H), 8.65 (d, J^d = 6 Hz, 2 H). ¹³C NMR: (175 MHz, acetonitrile-*d*₃) δ ppm 163.4, 161.1, 158.8, 158.6, 158.2, 157.3, 154.7, 153.9, 152.8, 152.7, 152.3, 139.1, 138.6, 138.4, 138.3, 128.6, 128.3, 128.1, 127.9, 125.9, 125.4, 125.2, 124.4, 103.1, 49.8, 49.7, 48.8, 48.6, 23.3, 23.0. HRMS (ESI), m/z: 1617.20013 [M-PF₆]⁺ (C₅₈H₅₈N₁₆P₃F₁₈Ru₂ requires 1617.20373), 736.11630 [M-2PF₆]²⁺ (C₅₈H₅₈N₁₆P₂F₁₂Ru₂ requires 736.11950), 442.42360 [M-3PF₆]³⁺ (C₅₈H₅₈N₁₆PF₆Ru₂ requires 442.42476), 295.57665 [M-4PF₆]⁴⁺ (C₅₈H₅₈N₁₆Ru₂ requires 295.57738). Anal. Calc. for C₅₈H₅₈N₁₆Ru₂P₄F₂₄ .2H₂O: C: 38.76; N: 12.47; H: 3.48. Found: C: 38.69; N: 12.35; H: 3.26.

Syntheses of the complexes **3-2**, **3-3** and **3-4**: These complexes were obtained during the synthesis of the diruthenium complex of **3-L1**. The syntheses were performed in a large excess of the solvent, for e.g., ethanol, *n*-butanol and ethylene glycol.

In a general procedure, a 100 mL round-bottomed flask was charged with *cis*-Ru(bpy)₂Cl₂·2H₂O (0.513 g, 0.987 mmol), AgNO₃ (0.344 g, 2.025 mmol, 2.05 equiv.) in methanol (150 mL). The suspension was heated to reflux for an hour to give a dark red solution with white precipitate of AgCl. The solution was cooled to room temperature and then filtered through a plug of celite, which was washed with methanol (3 x 10 mL). The solutions were collected and evaporated to dryness to give a dark red solid. To this solid was added **3-L1** (0.100 g, 0.282 mmol), followed by the addition of appropriate alcoholic solvents (150 mL) and the suspension was heated to reflux, under N₂-atmosphere for 3 h. After this time, the solution was cooled down to room temperature and evaporated to dryness. The crude product was purified through a silica column using 7:1 =

CH₃CN:saturated aq. KNO₃ solution (v/v) as an eluant. The fastest moving and major dark red band was collected, the solvent was evaporated to dryness and the NO₃⁻ salt was metathesised to PF₆⁻ salt by addition of a saturated aqueous KPF₆ solution. The dark red solid was collected by filtration and was dried under vacuum to furnish **3-2**, **3-3** and **3-4**.

Ethoxyether adduct (3-2): Crystallized by vapour diffusion of Et₂O into an acetone solution of the title compound. Yield = 0.140 g (28%). ¹H NMR (700 MHz, CD₃CN) δ ppm 1.21 (ddd, J^{ddd} = 12, 6, 4 Hz, 1 H), 1.66 (m, 2 H), 2.17 (m, 2 H), 2.31 (m, 1 H), 2.80 (m, 1 H), 3.08 (dt, J^{dt} = 12, 6 Hz, 1 H), 3.21 (m, 3 H), 3.32 (m, 1H), 3.70 (m, 3 H), 4.30 (m, 2 H), 6.55 (s, 1 H), 7.20 (m, 2 H), 7.35 (s, 1 H), 7.62 (m, 3 H), 7.69 (ddd, J^{ddd} = 8, 6, 2 Hz, 1 H), 7.86 (m, 2 H), 8.13 (t, J^t = 8 Hz, 2 H), 8.36 (d, J^d = 8 Hz, 2 H), 8.50 (m, 3 H), 8.79 (d, J^d = 6 Hz, 1 H). ¹³C NMR: (175 MHz, CD₃CN) δ ppm 171.5, 162.8, 159.9, 158.7, 158.6, 158.5, 158.4, 153.7, 153.6, 152.8, 152.6, 152.5, 138.0, 137.7, 137.3, 137.2, 127.6, 127.5, 127.4, 127.2, 125.1, 125.0, 124.8, 124.4, 97.0, 64.8, 49.4, 49.3, 48.2, 47.8, 23.1, 22.8, 14.4. HRMS (ESI), m/z: 820.16696 [M-PF₆]⁺ (C₃₃H₃₅N₉OPF₆Ru requires 820.16498), 337.60172 [M-2PF₆]²⁺ (C₃₃H₃₅N₉ORu requires 337.60040). Anal. Calc. for C₃₃H₃₅N₉OP₂F₁₂Ru: C: 41.09; N: 13.07; H: 3.66. Found: C: 41.28; N: 13.33; H: 3.92.

Butoxyether adduct (3-3): Crystallized by vapour diffusion of Et₂O into an acetone solution of the title compound. Yield = 0.160 g (32%). ¹H NMR (700 MHz, CD₃CN) δ ppm 0.91 (t, J^t = 8 Hz, 2 H), 1.22 (ddd, J^{ddd} = 12, 6, 4 Hz, 1 H), 1.38 (m, 2 H), 1.66 (m, 2 H), 2.05 (m, 2 H), 2.18 (m, 2 H), 2.31 (ddd, J^{ddd} = 12, 8, 4 Hz, 1 H), 2.79 (m, 1 H), 3.08 (m, 1 H), 3.23 (m, 3 H), 3.33 (ddd, J^{ddd} = 12, 8, 6 Hz, 1 H), 3.70 (ddd, J^{ddd} = 12, 8, 4 Hz, 1 H), 4.23 (m, 2 H), 6.56 (s, 1 H), 7.20 (dddd, J^{dddd} = 8, 6, 4, 2 Hz, 2 H), 7.34 (s, 1 H), 7.61 (dddd, J^{dddd} = 8, 6, 4, 2, 0.75 Hz, 3 H), 7.69 (ddd, J^{ddd} = 8, 6, 2 Hz, 1 H), 7.86 (m, 2 H), 8.14 (m, 2 H), 8.37 (d, J^d = 8 Hz, 2 H), 8.49 (m, 3 H), 8.79 (m, 1 H). ¹³C NMR: (175 MHz, CD₃CN) δ ppm 171.7, 162.8, 159.9, 158.7, 158.6, 158.5, 158.4, 153.7, 153.6, 152.8, 152.6, 152.5, 138.0, 137.7, 137.3, 137.2, 127.6, 127.5, 127.4, 127.2, 125.1, 125.0, 124.8, 124.4, 97.0, 68.6, 49.4, 49.2, 48.1, 47.7, 31.2, 23.1, 22.8, 19.5, 13.8. HRMS (ESI), m/z: 848.19663 [M-PF₆]⁺ (C₃₅H₃₉N₉OPF₆Ru requires 848.19628), 703.23242 [M+e]^{*+} (C₃₅H₃₉N₉OPF₆Ru requires 703.23248), 351.61611 [M-2PF₆]²⁺ (C₃₅H₃₉N₉ORu requires 351.61597). Anal. Calc. for C₃₅H₃₉N₉OP₂F₁₂Ru·H₂O: C: 41.59; N: 12.47; H: 4.09. Found: C: 41.18; N: 12.25; H: 3.77.

2-hydroxy-1-ethoxyether adduct (3-4): Crystallized by vapour diffusion of Et₂O into an acetone solution of the title compound. Yield = 0.125 g (25%). ¹H NMR (700 MHz,

CD₃CN) δ ppm 1.22 (ddd, $J^{\text{ddd}} = 12, 6, 4$ Hz, 1 H), 1.66 (m, 1 H), 2.18 (ddd, $J^{\text{ddd}} = 12, 6, 4$ Hz, 1 H), 2.31 (m, 1 H), 2.80 (m, 1 H), 2.95 (t, $J^{\text{t}} = 6$ Hz, 1 H), 3.08 (dt, $J^{\text{dt}} = 12, 6$ Hz, 1 H), 3.23 (m, 3 H), 3.33 (m, 1H), 3.72 (m, 3 H), 4.28 (m, 2 H), 6.61 (s, 1 H), 7.20 (m, 2 H), 7.36 (s, 1 H), 7.62 (m, 3 H), 7.69 (ddd, $J^{\text{ddd}} = 8, 6, 2$ Hz, 1 H), 7.86 (m, 2 H), 8.13 (t, $J^{\text{t}} = 8$ Hz, 2 H), 8.37 (d, $J^{\text{d}} = 8$ Hz, 2 H), 8.50 (m, 3 H), 8.79 (d, $J^{\text{d}} = 6$ Hz, 1 H). ¹³C NMR: (175 MHz, CD₃CN) δ ppm 171.7, 162.9, 159.9, 158.7, 158.6, 158.5, 158.4, 153.7, 153.6, 152.8, 152.6, 152.5, 138.0, 137.8, 137.3, 137.2, 127.6, 127.6, 127.5, 127.2, 125.1, 125.0, 124.7, 124.4, 97.1, 70.3, 60.5, 49.3, 48.2, 48.1, 47.8, 23.1, 22.8. HRMS (ESI), m/z : 836.15665 [M-PF₆]⁺ (C₃₃H₃₅N₉O₂PF₆Ru requires 836.15935), 345.59731 [M-2PF₆]²⁺ (C₃₃H₃₅N₉ORu requires 345.59731). Anal. Calc. for C₃₃H₃₅N₉O₂P₂F₁₂Ru·C₃H₆O: C: 41.63; N: 12.14; H: 3.98. Found: C: 41.68; N: 12.05; H: 3.87 (presence of acetone was identified in ¹H NMR spectrum and crystal structure).

3.5.3. Computational Methods

All calculations were performed with the Gaussian03²⁷ employing the DFT method, the Becke three-parameter hybrid functional,²⁸ and Lee-Yang-Parr's gradient-corrected correlation functional (B3LYP).²⁹ Singlet ground state geometry optimizations for **3**-(*1-meso*)²⁺, **3-2**²⁺, **3-3**²⁺ and **3-4**²⁺ were carried out at the (R)B3LYP level in the gas phase, using their respective crystallographic structures as starting points. All elements except Ru were assigned the 6-31G(d,f) basis set.³⁰ The double- ζ quality LANL2DZ ECP basis set³¹ with an effective core potential and one additional f-type polarization was employed for the Ru atom. Vertical electronic excitations based on (R)B3LYP-optimized geometries were computed for **3**-(*1-meso*)²⁺, **3-2**²⁺, **3-3**²⁺ and **3-4**²⁺ using the TD-DFT formalism³² in acetonitrile using conductor-like polarizable continuum model (CPCM).³³ CPCM model for geometry optimization was not used as for closed-shell geometry optimization calculations, the effect of solvent has a very little influence on computed geometries and this fact has well been established in a recent literature report.³⁴ Vibrational frequency calculations were performed to ensure that the optimized geometries represent the local minima and there are only positive eigenvalues. The electronic distribution and localization of the singlet excited states were visualized using the electron density difference maps (ED-DMs).³⁵ *Gausssum* 2.2 was employed to visualize the absorption spectra (simulated with Gaussian distribution with a full-width at half maximum (fwhm) set to 3000 cm⁻¹) and to calculate the fractional

contributions of various groups to each molecular orbital. All calculated structures were visualized with ChemCraft.³⁶

3.5.4. Crystal Structure Determination

Diffraction data were collected on Bruker diffractometers, equipped with a rotating anode source for Cu K α radiation. Cell refinement and data reduction were done using APEX2.³⁷ Absorption corrections were applied using SADABS.³⁸ Structures were solved by direct methods using SHELXS97 and refined on F² by full-matrix least squares using SHELXL97.³⁹ All non-hydrogen atoms were refined anisotropically. Hydrogen atoms were refined isotropic on calculated positions using a riding model. For the crystal structure of **3-(1-meso)**, the highest difference peak is located 1.24 Å from atom Ru1. In addition, in **3-(1-meso)** three more peaks with density around 1 e/Å³ were present essentially 1.25 Å from Ru-atoms. The other electron density peak of 0.81 e/Å³ is due to rotational disorder of fluorine atom F12, and this small disorder was not taken into account for modelling. Similarly for complexes **3-3** and **3-4**, these first two and first three high electron density peaks, respectively, are in close proximity to ruthenium atoms (~ 0.91 Å from Ru1 in **3-3** and 0.79-0.90 Å from Ru1 in **3-4**). For complex **3-3**, two other Q peaks of 1.53 e/Å³ and 1.26 e/Å³ were located near to F-atoms. These Q peaks were believed to arise from the positional disorder of F-atoms, which were not taken into consideration for modelling. In complex **3-4**, atom C29 in the cationic moiety was found to be disordered over two positions and the disorder was modelled with occupancy ratios [44:56] and then refined anisotropically. One ‘fixed distance’ (DFIX) restraint was applied to the C28-H28A distance in complex **3-4**. The diffraction quality of the crystal of complex **3-2** was checked, revealing poor diffraction with a large amount of diffuse scattering, signaling extensive crystal disorder. For this compound, during the refinement of its structure, electron density peaks were located and were believed to be eight highly disordered solvated acetone molecules (by counting the number of electrons suppressed). All the attempts made to model the solvent molecules were not successful and they were removed using the SQUEEZE routine from PLATON,⁴⁰ which resulted in a significant improvement of R1 factor by ~ 4%. The two high electron density peaks of 1.22 e/Å³ and 1.06 e/Å³ were essentially due to the positional disorder of F-atoms in freely rotating PF₆ anion, and this disorder was not taken into consideration for modelling. Specific parameters of each measurement are located in Table III-1.

Table III-1. Crystal data and details of the structure determination for **3-L1**, **3-(1-*meso*)·(2C₂H₃N)**, **3-2·(8C₃H₆O)**, **3-3** and **3-4·(C₃H₆O)**

	3-L1^a	3-(1-<i>meso</i>) ·(2C₂H₃N)^{a,b}	3-2·(8C₃H₆O)^a	3-3^c	3-4·(C₃H₆O)^c
Formula	[C ₁₈ H ₂₆ N ₈]	[C ₅₈ H ₅₈ N ₁₆ Ru ₂] [4(PF ₆)] [2(C ₂ H ₃ N)]	[C ₃₆ H ₄₁ N ₉ ORu] [2(PF ₆)] [8(C ₃ H ₆ O)]	[C ₃₅ H ₃₉ N ₉ ORu] [2(PF ₆)]	[C ₃₃ H ₃₅ N ₉ O ₂ Ru] [2(PF ₆)] [C ₃ H ₆ O]
Color/form	colorless needle	red block	red needle	red needle	red needle
<i>T</i> (K); wavelength	150(2); 1.54178	150(2); 1.54178	150(2); 1.54178	100(2); 0.71073	100(2); 1.54178
Crystal System	Orthorhombic	Monoclinic	Monoclinic	Monoclinic	Monoclinic
Space Group	Fdd2	Cc	C2/c	C2/c	P2(1)/c
Unit Cell: <i>a</i> (Å)	16.2300(2)	22.038(2)	42.0995(16)	41.763(2)	19.5419(9)
<i>b</i> (Å)	23.4755(4)	14.0363(13)	9.7518(4)	9.6049(6)	12.9232(6)
<i>c</i> (Å)	8.97820(10)	25.925(3)	25.0993(9)	24.2324(14)	17.6430(9)
α (°)	90	90	90	90	90
β (°)	90	112.384(2)	125.664(2)	122.787(2)	112.899(2)
γ (°)	90	90	90	90	90
<i>V</i> (Å ³); <i>Z</i>	3420.76(8); 8	7415.2(13); 4	8371.8(6); 8	8171.8(8); 8	4104.5(3); 4
R1(F); wR(F ²) [I > 4σ(I)]	0.0330; 0.0846	0.0382; 0.1008	0.0489; 0.1368	0.0617; 0.1716	0.0539; 0.1267
R1(F); wR(F ²) (all)	0.0335; 0.0850	0.0384; 0.1011	0.0505; 0.1392	0.0675; 0.1774	0.0567; 0.1283
R _σ ; R(int)	0.0199; 0.0377	0.0364; 0.0597	0.0241; 0.0438	0.0270; 0.0447	0.0322; 0.0627
GoF(F ²)	1.049	1.052	1.070	1.089	1.101
Flack parameter	n.a.	0.1081 (0.0049)	n.a.	n.a.	n.a.

^aBruker Microstar diffractometer (Platinum 135 CCD Detector, Helios optics and, Kappa goniometer).

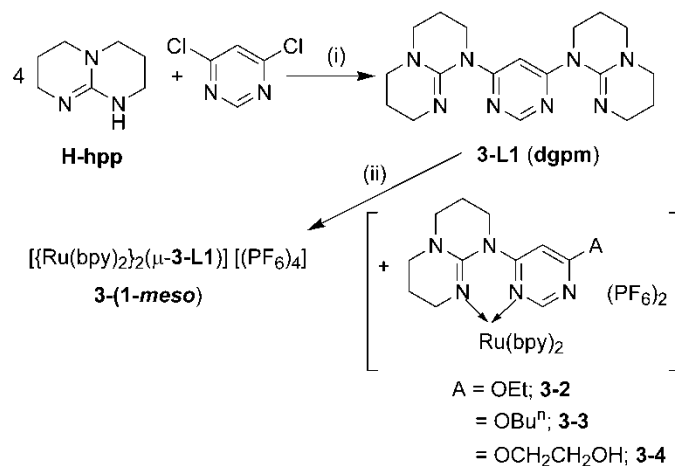
^bFrom reference 23 (CCDC 964842). ^cBruker/AXS Smart 6000 (4K) diffractometer (Mirror Montel 200-monochromated Cu K α radiation, FR591 Rotating Anode), Bruker Smart APEX 2, graphite monochromator.

3.6. Results and Discussion

The bis(bidentate) chelating ligand, **3-L1** (diguanidylpyrimidine; **dgpm**),²³ was synthesized by microwave-assisted heating using 4 equivalents of 1,3,4,6,7,8-hexahydro-2*H*-pyrimido[1,2-*a*]pyrimidine (**H-hpp**) and 4,6-dichloropyrimidine, under catalyst-free conditions in 90% yield (Scheme 3.1).

Complex **3-(1-*meso*)** was synthesized by refluxing an alcoholic mixture of **3-L1** and *cis*-Ru(bpy)₂Cl₂·2H₂O in 1:3.5 molar ratios. Satisfactory yields (65–70%) were obtained after purification by column chromatography, followed by anion metathesis. Addition of an excess of Ru-precursor as [Ru(bpy)₂(solvent)₂]²⁺ was advantageous to minimize the

formation of undesirable by-products, *e.g.*, the scrambling of $[\text{Ru}(\text{bpy})_2(\text{solvent})_2]^{2+}$ to form $[\text{Ru}(\text{bpy})_3]^{2+}$ or formation of homoleptic complex of **3-L1**. At first, complex **3-3** was isolated as dark red mononuclear complex within 3 h of reaction time during the synthesis of **3-(1-meso)** in *n*-butanol. As the uncoordinated **hpp** unit of the mononuclear complex $[(\text{bpy})_2\text{Ru}(\text{hpp}-\text{pm}-(\text{hpp})^*)]^{2+}$, ((**hpp**)^{*} = uncoordinated **hpp**, pm = 4,6-substituted pyrimidine), formed ‘*in situ*’, acts as a leaving group in *n*-butanol to form complex **3-3**, we were interested in verifying its leaving group ability in other alcoholic solvents. Ethanol and ethylene glycol formed complexes **3-2** and **3-4**, respectively, as dark red mononuclear complexes (Scheme 3.1).



Scheme 3.1. Syntheses of ligand **3-L1** and complexes **3-(1-meso)**, **3-2**, **3-3**, **3-4**. (i) toluene, microwave at 160 °C; 90%; (ii) *cis*-Ru(bpy)₂Cl₂ (3.5 eq) in different alcoholic solvents at reflux followed by the addition of KPF₆; 65–70%.

Due to the unique design of **3-L1** with parallel coordination vectors and its ability to form six-membered chelate rings upon coordination, the heterochiral *meso*-diruthenium complex, **3-(1-meso)** can be isolated in 1:13:1 ($\Lambda\Lambda:\Lambda\Delta$ (or $\Delta\Lambda$): $\Delta\Delta$) (Figure 3.S1 in ESI) ratio over its homochiral form. This diastereoselective formation of **3-(1-meso)** is also due to maximization of π - π interactions of the bpy units of each Ru-centre, which in turn results from the special design of **3-L1**. This high diastereoselectivity is supported by DFT calculations, in which a *rac*- $\Lambda\Lambda$ or $\Delta\Delta$ diastereomer leads to rupture of bpy units (Figure 3.S2 in ESI) due to excess unfavourable steric interactions between two mutually colliding bpy units of each Ru-centre in an edge-to-face manner, while the *meso*- $\Lambda\Delta$ form is stabilized. The reactions for the ‘*in situ*’ generation of mononuclear Ru^{II}-complexes **3-2** to

3-4 were relatively straightforward as reactions in their respective solvents; **3-3** in butanol, **3-2** in ethanol, and **3-4** in ethyleneglycol, led to yields of in 32%, 28% and 25%, respectively, due to the higher nucleophilicity of butanol as compared to ethanol or ethylene glycol.⁴¹

3.6.1. NMR spectroscopy and Mass spectrometry

The symmetric nature of ¹H NMR spectrum of **3-L1** suggests a fast equilibrium between the axial and equatorial protons residing on the same carbon atom in the saturated aliphatic backbone of **hpp** unit. Attaching a heterocycle to the guanidine *NH* position of **H-hpp** renders the six annular methylene units nonequivalent by both ¹H and ¹³C NMR spectroscopies in contrast to free **H-hpp**, in which the tautomerization of the guanidyl proton leads to only three proton resonances in its ¹H NMR spectrum at 400 MHz.⁴² The most interesting feature in the ¹H NMR spectra of compounds **3-(1-meso)** to **3-4** in CD₃CN is that multiple methylene signals are found over 0–4 ppm region, some of them integrating for one proton each while the other protons are at the same chemical shift. In the ¹H NMR spectra of the complexes, the farthest upfield singlet peak is at 6.1 ppm, which may be attributed to the 5-pyrimidyl proton due to shielding by adjacent **hpp** moieties. For the dinuclear complex, based on the helicity induced by the bpy units, one would expect a complicated ¹H NMR spectrum, indicative of a mixture of statistically formed $\Lambda\Delta:\Delta\Delta$ (or $\Lambda\Lambda$): $\Delta\Delta$ in 1:2:1 ratio. However, simple ¹H (Figure 3.1) and ¹³C NMR spectra of **3-(1-meso)** with occurrence of one singlet peak at ~ 6.1 ppm region suggest a diastereoselective formation of *meso*-diruthenium(II,II) complex over its homochiral *racemic* counterpart.²³

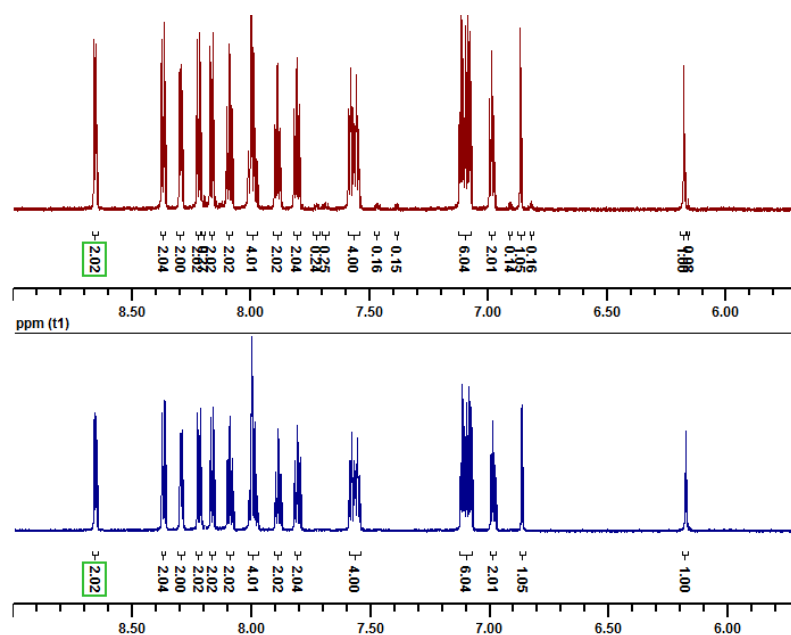


Figure 3.1. Comparison of ¹H NMR spectra of **3-(1-*meso*)** (as its crystalline form) with the product obtained after reaction ii (see Scheme 3.1) at 700 MHz in CD₃CN at room temperature; top - aromatic region of product obtained after reaction ii, bottom - aromatic region of **3-(1-*meso*)**.

Ligand **L1** and complexes **3-(1-*meso*)** to **3-4** were characterized by high-resolution mass spectrometry; where [M+H]⁺ was found to be the most abundant species for **3-L1**, and [M]²⁺ for the complexes. The [M-PF₆]⁺ species could also be identified for the complexes (see experimental section for details).

3.6.2. X-ray Structural Investigation

Slow diffusion of diethyl ether into an acetonitrile and an acetone solution of **3-(1-*meso*)** and **3-2** to **3-4**, respectively, afforded the best single crystals suitable for X-ray crystallography, whereas crystals of **3-L1** could be grown by slow diffusion of diethyl ether into a toluene solution of **3-L1** (Figures 3.1–3.6). Ligand **3-L1** crystallizes in an orthorhombic crystal system, while complexes **3-(1-*meso*)**, **3-2** to **3-4** crystallize in monoclinic crystal system. The crystallographic data are summarized in Table III-1. **3-L1** crystallizes in Fdd2 space group (Figure 3.1), where a two-fold C₂ axis passes through the two C-atoms in the central pyrimidine ring (C1 and C3 atoms). Although the molecule adopts thermodynamically stable chair-conformation (see Figure 3.S3 for capped stick view of **3-L1** in ESI), in which the two **hpp** units are twisted to minimize lone pair-lone

pair repulsions on their respective hetero atoms, the coordination occurs in bis(bidentate) fashion *via.* rotation around the C–N bonds. The N2–C10 [1.4157(16) Å] and N3–C10 [1.3752(15) Å] bond distances clearly suggest that there is delocalization around N3–C10–N2 core, whereas N4–C10 are a localized C–N double bond with a distance of 1.2842(16) Å.

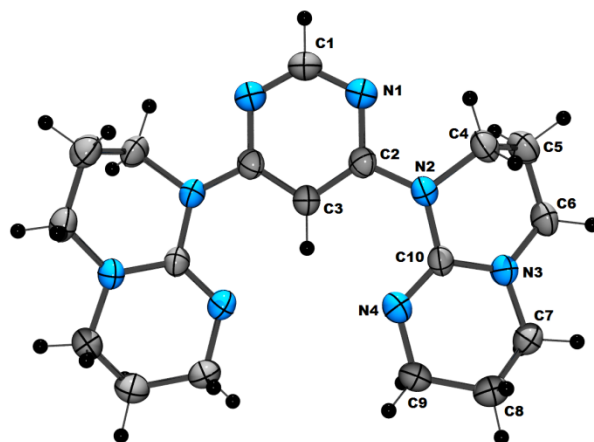


Figure 3.2. Perspective view of ligand **3-L1**. Thermal ellipsoids are shown at a 50% probability level. Selected bond distances and angles: C2–N2 = 1.3507(16) Å, N2–C10 = 1.4157(16) Å, N3–C10 = 1.3752(15) Å, N4–C10 = 1.2842(16) Å; N2–C10–N3 = 113.82(10)°, N3–C10–N4 = 126.89(12)°, N4–C10–N2 = 119.22(11)°, N1–C2–N2–C4 = 8.93(15)°, N1–C2–N2–C10 = 167.07(11)°.

Complexes **3-(1-*meso*)** and **3-2** to **3-4** reveal coordinatively saturated ruthenium atoms in distorted octahedral coordination geometry. The distortion from a regular octahedron is induced by the smaller bite angles at the metal centre subtended by the two 2,2'-bipyridine ligands. The average bite angles for the bpy units are 78.53(10)°, 78.57(15)°, 78.84(13)° and 79.22(14)° for compound **3-2**, **3-3**, **3-4** and **3-(1-*meso*)**, respectively. The dinuclear complex **3-(1-*meso*)** forms with high diastereoselectivity over the formation of its *rac*-counterpart due to the unique design of **3-L1** with parallel coordination vectors and chair-conformation in the solid state structure of **3-L1**.²³ This conformation is retained in the crystal structure of **3-(1-*meso*)**, thereby maximizing the possibility of face-to-face π - π interactions between the bpy units of each stereogenic Ru-centre.

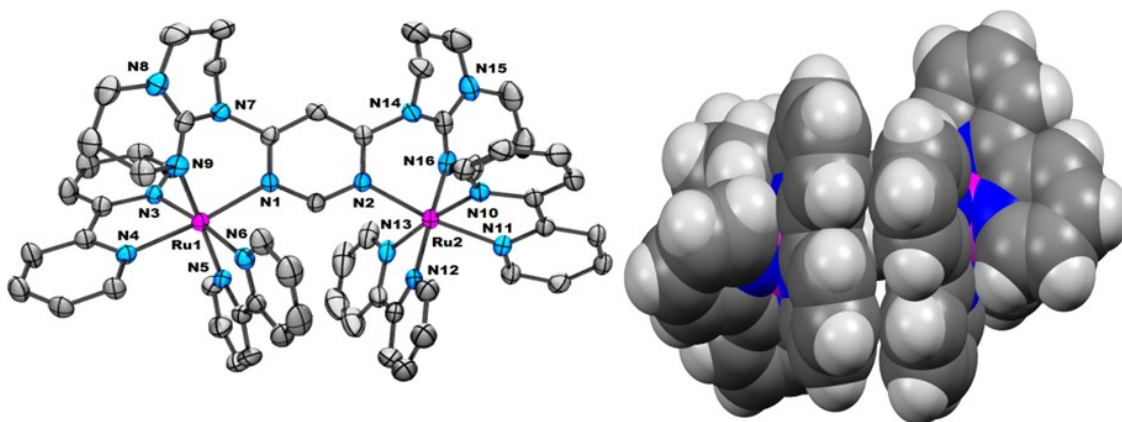


Figure 3.3. Perspective view of **3-(1-*meso*)** (left); spacefilling model of **3-(1-*meso*)** (right), along the plane of central pyrimidine ring, showing the π - π interaction of the bpy units, favoring the diastereoselective formation of $\Lambda\Lambda$ (or $\Delta\Delta$)-isomer over $\Delta\Delta$ or $\Lambda\Lambda$ -isomers. Hydrogen atoms and PF_6 anions are omitted for clarity. Ellipsoids correspond to a 50% probability level. Selected bond distances and angles: $\text{N1-Ru1} = 2.089(3) \text{ \AA}$, $\text{N3-Ru1} = 2.069(3) \text{ \AA}$, $\text{N4-Ru1} = 2.059(3) \text{ \AA}$, $\text{N5-Ru1} = 2.053(3) \text{ \AA}$, $\text{N6-Ru1} = 2.078(3) \text{ \AA}$, $\text{N9-Ru1} = 2.096(3) \text{ \AA}$, $\text{N2-Ru2} = 2.085(3) \text{ \AA}$, $\text{N10-Ru2} = 2.063(3) \text{ \AA}$, $\text{N11-Ru2} = 2.058(3) \text{ \AA}$, $\text{N12-Ru2} = 2.064(4) \text{ \AA}$, $\text{N13-Ru2} = 2.061(3) \text{ \AA}$, $\text{N16-Ru2} = 2.096(4) \text{ \AA}$, $\text{N1-Ru1-N9} = 84.57(12)^\circ$, $\text{N3-Ru1-N4} = 78.87(12)^\circ$, $\text{N5-Ru1-N6} = 79.30(14)^\circ$, $\text{N2-Ru2-N16} = 84.34(12)^\circ$, $\text{N10-Ru2-N11} = 79.23(13)^\circ$, $\text{N12-Ru2-N13} = 79.49(17)^\circ$. Figure is adapted from ref 23.

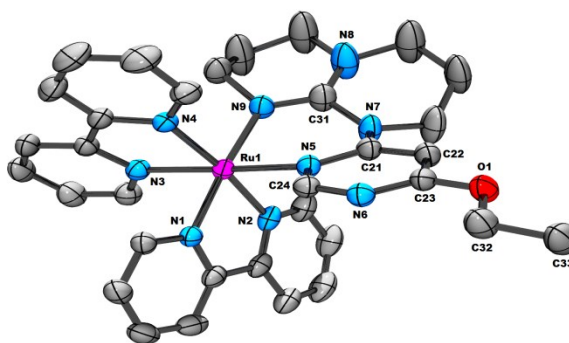


Figure 3.4. Perspective view of **3-2**. Hydrogen atoms and PF_6 anions are omitted for clarity. Thermal ellipsoids are drawn at a 50% probability level. Selected bond distances and angles: $\text{N1-Ru1} = 2.061(3) \text{ \AA}$, $\text{N2-Ru1} = 2.083(3) \text{ \AA}$, $\text{N3-Ru1} = 2.057(3) \text{ \AA}$, $\text{N4-Ru1} = 2.061(3) \text{ \AA}$, $\text{N5-Ru1} = 2.085(3) \text{ \AA}$, $\text{N9-Ru1} = 2.088(3) \text{ \AA}$, $\text{N1-Ru1-N2} = 78.05(10)^\circ$, $\text{N3-Ru1-N4} = 79.01(11)^\circ$, $\text{N5-Ru1-N9} = 84.46(11)^\circ$.

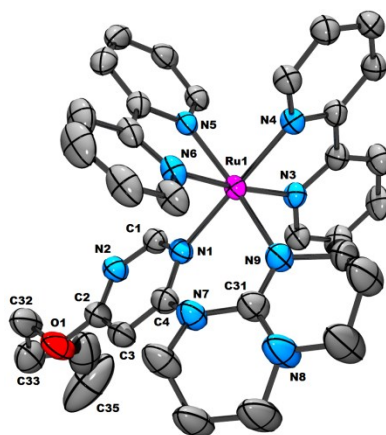


Figure 3.5. Perspective view of **3-3**. Hydrogen atoms and PF_6 anions are omitted for clarity. Ellipsoids correspond to 50% probability level. Selected bond distances and angles: $\text{N1-Ru1} = 2.078(4) \text{ \AA}$, $\text{N3-Ru1} = 2.062(4) \text{ \AA}$, $\text{N4-Ru1} = 2.049(4) \text{ \AA}$, $\text{N5-Ru1} = 2.049(4) \text{ \AA}$, $\text{N6-Ru1} = 2.078(4) \text{ \AA}$, $\text{N9-Ru1} = 2.074(4) \text{ \AA}$, $\text{N1-Ru1-N9} = 84.19(16)^\circ$, $\text{N3-Ru1-N4} = 78.68(15)^\circ$, $\text{N5-Ru1-N6} = 78.45(16)^\circ$.

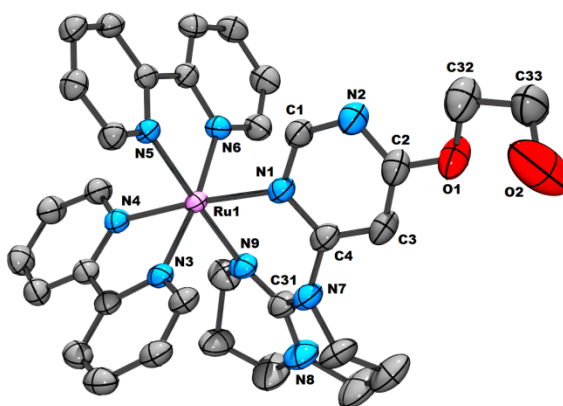


Figure 3.6. Perspective view of **3-4**. Hydrogen atoms, solvated acetone and PF_6 anions and a disordered portion of the **hpp** unit are omitted for clarity. Thermal ellipsoids are drawn at a 50% probability level. Selected bond distances and angles: $\text{N1-Ru1} = 2.083(4) \text{ \AA}$, $\text{N3-Ru1} = 2.063(3) \text{ \AA}$, $\text{N4-Ru1} = 2.053(3) \text{ \AA}$, $\text{N5-Ru1} = 2.063(3) \text{ \AA}$, $\text{N6-Ru1} = 2.059(3) \text{ \AA}$, $\text{N9-Ru1} = 2.098(3) \text{ \AA}$, $\text{N1-Ru1-N9} = 85.20(14)^\circ$, $\text{N3-Ru1-N4} = 78.88(14)^\circ$, $\text{N5-Ru1-N6} = 78.80(13)^\circ$.

In the complexes, the **hpp**-coupled pyrimidyl moieties adopt six-membered twisted-chair chelate ring conformations, having bite angles of $84.19(16)^\circ$, $84.46(11)^\circ$, and $85.20(14)^\circ$ in **3-2**, **3-3** and **3-4**, respectively. This gradual increase in bite angle with decreasing nucleophilicity of the ligands from butoxyether to ethoxyether to

2-hydroxy-1-ethoxyether groups suggests that the angle increases are due to less strong bonding of the **3-L1** ligands.

The three Ru-N_{hpp} distances are 2.088(3) Å, 2.074(3) Å and 2.098(3) Å for **3-2**, **3-3** and **3-4**, respectively, whereas the Ru-N_{pyrimidine} distances are 2.085(3) Å, 2.078(4) Å and 2.083(4) Å. The gradual decrease in Ru-N_{hpp} distances in **3-4**, **3-2** and **3-3**, respectively, are in agreement to the relative donor ability of the different solvent adducts, which are: OCH₂CH₂OH (**3-4**) < OEt (**3-2**) < OBu (**3-3**). The stronger remote +I-effect (positive inductive effect) of butoxyether group onto the **hpp** moiety is also evident in shorter C4–N7 bond distance (1.387(7) Å) in **3-3**, in comparison to the relatively weaker +I-effect of 2-hydroxy-1-ethoxyether group in **3-4** (C4–N7 = 1.401(6) Å). The marginally shorter Ru–N_{pyrimidine} distance in **3-4** compared to that in **3-2** may be due to higher degree of back-donation from the metal centre to the pyrimidine ring in **3-4**, as the 2-hydroxy-1-ethoxyether-substituted pyrimidyl moiety is a better π -acceptor than ethoxyether-substituted pyrimidyl moiety. The Ru–N distances for the coordinated bpy ligands are mainly the same for compounds **3-2** to **3-4** (varies from 2.059(4) Å to 2.065(3) Å). These values are in line to the distances observed in Ru-bpy complexes in general (1.96–2.16 Å, average = 2.06(5) Å).⁴³ The alkyl chains are directed away from the Ru(II) centre, as opposed to other coordination complexes incorporating (CH₂)-bridged donor atoms,⁴⁴ and thus the conformation of the saturated ring does not appear to have any noticeable influence on the structure.

3.6.3. Redox Behaviour

The redox behaviour of **3-L1** and complexes **3-(1-meso)** to **3-4** (Figure 3.7 and Figure 3.S4 in ESI) has been examined and the data are gathered in Table III-2. At positive potential, **3-L1** exhibits two one-electron oxidations, a first irreversible oxidation centred at +0.89 V and a second quasi-reversible peak at +1.18 V. Density functional theory (DFT) calculations using B3LYP functional (see Figure 3.8 and ESI for computational details) predict that **3-L1** results in a significant destabilization of the highest occupied molecular orbital (HOMO) in its Ru(II) complexes, which is located principally on the ruthenium ion and partially on the ligand environment (see Figure 3.8 for population analyses). The oxidation process is therefore assigned to the removal of one electron from the metal-centred orbitals. The higher energies calculated for the HOMO of **3-(1-meso)** (-5.94 eV), **3-**

2 (-5.58 eV), **3-3** (-5.56 eV) and **3-4** (-5.65 eV) compared to that of $[\text{Ru}(\text{bpy})_3]^{2+}$ (-6.11 eV) are in good agreement with the lower anodic potentials measured for **3-(1-meso)** to **3-4** in comparison to $[\text{Ru}(\text{bpy})_3]^{2+}$ (Table III-2). They also clearly indicate strong σ -donation from the saturated ligand backbone to the metal-based orbitals, thus increasing the energy of the HOMO. This trend is in accordance with the conclusions of Bolink *et al.*⁴⁵ At positive potentials, complexes **3-(1-meso)** to **3-4** show quasi-reversible Ru(II) to Ru(III) oxidations at 0.70–0.90 V *vs.* SCE which is 350–550 mV less positive compared to Ru(III/II) couple in $[\text{Ru}(\text{bpy})_3]^{2+}$ and $[\text{Ru}(\text{bpy})_2(\mathbf{3-L2})][(\text{PF}_6)_2]$,^{46,47} thus confirming that **3-L1** is a stronger donor than bpy and **3-L2**. The butoxyether-substituted pyrimidyl moiety in complex **3-3** acts as the strongest σ -donor as suggested by the low oxidation potential of **3-3** as compared to **3-2** and **3-4**. This fact is also supported by the strong positive inductive (+I) effect of butoxyether group as indicated by the higher *Hammett* parameter of butoxyether group (-0.32) compared to ethoxyether (-0.24) and $-\text{OCH}_2\text{CH}_2\text{O}^-$ (-0.12) groups,^{48a} and as observed in other Ru(II) complexes.^{48b} A second quasi-reversible metal-based oxidation from Ru(II)Ru(III) to Ru(III)Ru(III) at +1.0 V is also observed for **3-(1-meso)**. The relatively small comproportionation constant (K_c) value of 506 indicates redox active metal centres that are weakly communicating. Nonetheless, a relative study of the oxidation potentials among dinuclear Ru-complexes, **3-(1-meso)**, *meso*- $[\{\text{Ru}(\text{bpy})_2\}_2(\mu-(\mathbf{3-L2}))][(\text{PF}_6)_4]$ and *meso*- $[\{\text{Ru}(\text{bpy})_2\}_2(\mu-(\mathbf{3-L3}))][(\text{PF}_6)_3]$, suggests that **3-L1** is a stronger donor than **3-L2** and **3-L3** (Table III-2).

Table III-2. Redox data of **3-L1** and complexes **3-(1-meso)** to **3-4** in dry, degassed acetonitrile with some benchmark complexes.

Compound	$E_{1/2}(\text{ox})^a$	$E_{1/2}(\text{red})^a$	$\Delta E_{1/2}^b$
3-L1	1.18 (136), 0.89 (irr) ^c	-----	-----
3-(1-meso)	1.00 (68), 0.84 (84)	-1.36 (68), -1.46 (65), -1.62 (66), -1.78 (68), -1.87 (69)	2.20
3-2	0.89 (139)	-1.43 (71), -1.71 (94), -2.19 (irr), -2.53 (irr)	2.32
3-3	0.70 (80)	-1.48 (60), -1.72 (70), -2.39 (irr), -2.69 (irr)	2.18
3-4	1.05 (70)	-1.15 (65), -1.40 (60), -2.03 (irr), -2.31 (irr)	2.20
[Ru(bpy) ₃] ²⁺ ^d	1.26	-1.33, -1.51, -1.77	2.59
[Ru(bpy) ₂ (μ-(3-L2))] ²⁺ ^e	1.28	-1.03, -1.55, -1.76	2.31
[{Ru(bpy) ₂ } ₂ (μ-(3-L2))] ²⁺ (<i>meso</i>) ^d	1.53, 1.37	-0.57, -1.19, -1.61	1.94
[{Ru(bpy) ₂ } ₂ (μ-(3-L3))] ³⁺ (<i>meso</i>) ^{d,f}	1.15, 0.84	-1.51, -1.74, -2.22	2.35

^aPotentials are in volts vs. SCE for acetonitrile solutions, 0.1 M in [*n*-Bu₄N]PF₆, recorded at 25 ± 1 °C at a sweep rate of 100, 25 and 50 mV/s for **3-L1**, **3-(1-meso)** and **3-2** to **3-4**, respectively (correction factor for ferrocene/ferrocenium couple occurring at +310 mV vs. SCE, applied for last two complexes in first column in this table). The difference between cathodic and anodic peak potentials (millivolts) is given in parentheses. ^b $\Delta E_{1/2}$ is the difference (in V) between first oxidation and first reduction potentials. ^cIrreversible; potential is given for the anodic wave. ^dFrom ref 46. ^eFrom ref 47, ^fPt working electrode.

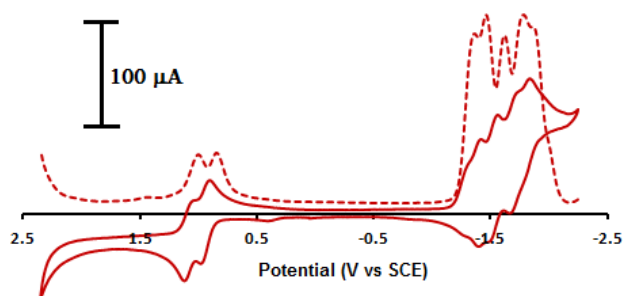


Figure 3.7. Cyclic voltammogram (bold) and differential pulse voltammogram (dotted) of **3-(1-meso)** in dry, degassed CH₃CN, recorded at a scan rate of 25 mV/s. Figure adopted from ref 23.

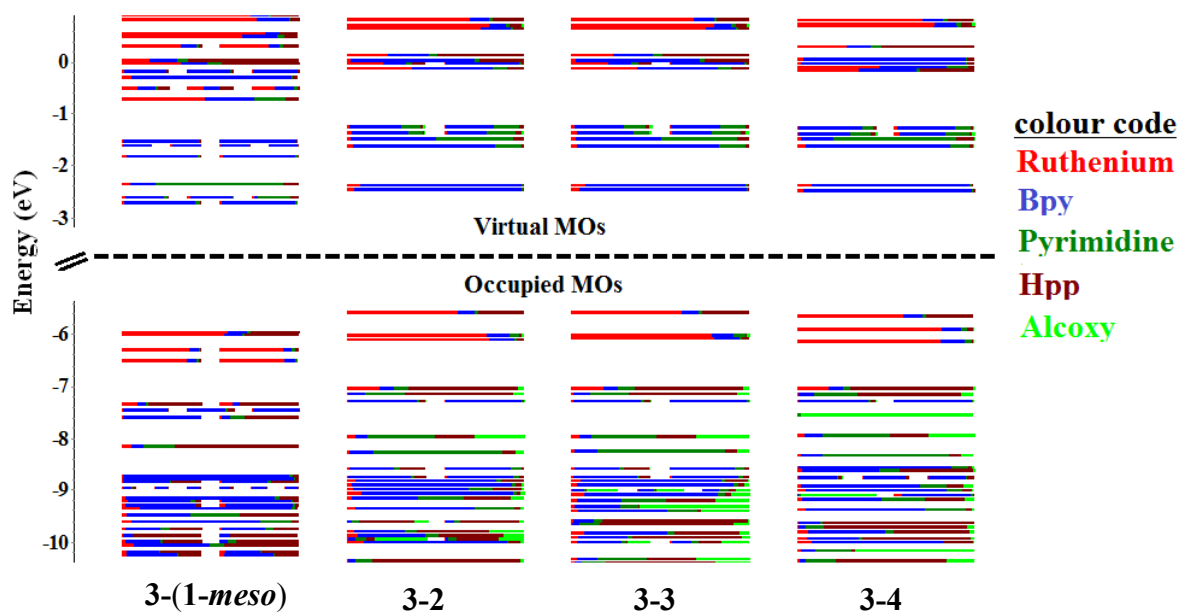


Figure 3.8. Calculated frontier MO energies of all the modelled **3-(1-meso)** to **3-4** complexes obtained from DFT(*rb3lyp/LanL2DZ(f)*)[Ru] 6-31G**[NCN(O)] with CPCM(CH₃CN) and 0.05 eV threshold of degeneracy.

The complexes display monoelectronic ligand-based reduction peaks. Although, the first reduction in Ru(II)-pyrimidyl complexes usually involves electron transfer into electron deficient diazine rings,⁴⁹ due to strong σ -donation from the **hpp** unit(s) and the ether adducts, the diazine ring is now difficult to reduce. This fact is also supported by lower bpy-based reduction potential of structurally similar compounds reported earlier by our group.^{7d} DFT calculations suggest that the lowest unoccupied molecular orbital (LUMO) to LUMO+3 and LUMO to LUMO+2 have predominant bpy character, whereas contribution from the pyrimidyl moiety comes into play only at the LUMO+4 and LUMO+3 levels in **3-(1-meso)** and **3-2** to **3-4**, respectively. Thus, in a very coarse approximation, the first four quasi-reversible reductions in **3-(1-meso)** are bpy-based, while the first three reductions in **3-2** to **3-4** are bpy based, although more detailed calculations would have to be done to confirm this assignment.

The mononuclear complexes, being doubly charged, are significantly more difficult to reduce than the quadruply charged dinuclear complex. As the butoxyether-substituted pyrimidyl ring is the strongest donor compared to the other adducts, complex **3-3** is the hardest to reduce and this trend is evident up to the last reduction, which is pyrimidine based. The sharp decrease of the first reduction potential of compound **3-4** with respect to

that of the other compounds may be attributed to the poor nucleophilicity of 2-hydroxy-1-ethoxyether moiety. As this moiety is less basic, the extent of back-bonding from the metal centre to bpy also decreases, thus rendering them easier to reduce.

3.6.4. Photophysical Investigation

The UV-vis absorption spectra of compounds **3-(1-meso)** to **3-4** in dry, degassed acetonitrile solution (Table III-3 and Figure 3.9) display spin allowed $^1\text{MLCT}$ (Metal-to-Ligand Charge Transfer) bands in the 400–600 nm region. The TD-DFT calculations of **3-(1-meso)** to **3-4** suggest a significant contribution ($\sim 26\%$) from **hpp** units in their HOMOs. The UV region is dominated by the ligand centred (LC) $\pi \rightarrow \pi^*$ transition centred around 240–300 nm for all the compounds (for an overlay of experimental absorption spectrum and TD-DFT calculated oscillator strengths see Figures 3.S6, 3.S8, 3.S10 and 3.S12 in ESI).^{1b,10b,c} The most noticeable feature in the visible region is that the lowest-energy $^1\text{MLCT}$ maxima are red-shifted with respect to the $^1\text{MLCT}$ of $\text{Ru}(\text{bpy})_3^{2+}$ by 60–100 nm, and the amount of shift depends on the electronic properties of the heterocycle or nature of the adduct with the pyrimidyl moiety (for an estimate of different electronic transitions for different complexes see Tables 3.S2, 3.S4, 3.S6 and 3.S8 in ESI).⁵⁰ The stronger the σ -donation, the better is the interaction with the metal d orbitals and hence the HOMO is of higher energy. The **hpp**-substituted pyrimidyl moieties, being stronger donors than bpy, raise the metal-based HOMO energies in **3-(1-meso)** to **3-4** as compared to that of $\text{Ru}(\text{bpy})_3^{2+}$ (-6.11 eV). This is perfectly in line with the DFT calculations reported above. On the other hand, the LUMO is still bpy-based, as also indicated by the first reduction potentials of **3-(1-meso)** to **3-4**, which results in a lowering of the energy of the $d\pi \rightarrow \pi^*$ $^1\text{MLCT}$ transition and, hence, a red shift in the absorption spectra. As the butoxyether-coupled pyrimidyl moiety in complex **3-3** is the strongest donor compared to the other pyrimidyl moieties complex **3-3** displays a more pronounced red-shift in its $^1\text{MLCT}$ as compared to the other complexes. The gradual red-shift in $^1\text{MLCT}$ maxima from **3-4** to **3-2** to **3-3** is also in accordance to the decreasing calculated HOMO-LUMO gap from **3-4** (3.18 eV), to **3-2** (3.13 eV) to **3-3** (3.11 eV). Furthermore, MLCT transitions involving the higher-energy unoccupied orbitals of bpy or pyrimidine may give rise to additional bands at approximately 350 nm, which is usually observed for $\text{Ru}(\text{bpy})_2(\text{diamine})^{2+}$ chromophores.⁵¹

Table III-3. Electronic absorption data of **3-L1** and complexes **3-(1-meso)** to **3-4** in dry, degassed acetonitrile with some benchmark complexes.

Compound	λ_{max} , nm ($\epsilon \times 10^3$, $\text{M}^{-1}\text{cm}^{-1}$)
3-L1	237 (29.9), 285 (9.9)
3-(1-meso)	244 (25.2), 289 (51.5), 345 (7.2), 368 (7.0), 470 (6.8), 511 (5.6)
3-2	246 (33.1), 255 (33.5), 293 (51.6), 353 (9.4), 493 (6.9), 542 (3.9)
3-3	248 (25.2), 255 (25.7), 294 (39.1), 354 (6.9), 494 (5.3), 552 (2.8)
3-4	248 (15.2), 256 (15.9), 293 (25.4), 346 (4.5), 483 (3.5), 538 (1.6)
$[\text{Ru}(\text{bpy})_3]^{2+}$ ^a	450 (14)
$[\text{Ru}(\text{bpy})_2(\mu\text{-}(\mathbf{3-L2}))]^{2+}$ ^b	408, 438, 492

^afrom ref 52. ^bFrom ref 47.

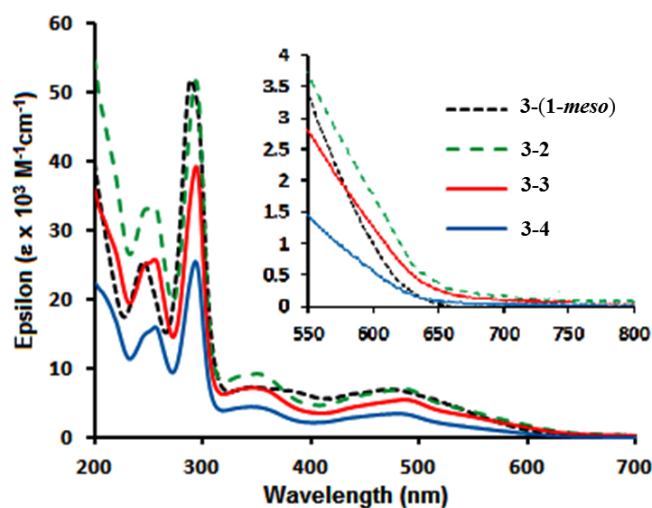


Figure 3.9. Electronic absorption spectra of compounds **3-(1-meso)** to **3-4** at room temperature in deaerated acetonitrile (a zoomed view from 550-800 nm shows visible light absorption by the complexes).

The luminescence properties of complexes **3-(1-meso)** to **3-4**, such as emission data (λ_{max}), lifetime (τ), the quantum yield (ϕ), radiative (k_r) and non-radiative (k_{nr}) constants, are reported in Table III-4. The emission bands are attributed to a triplet excited state of Ru to bpy-CT ($^3\text{MLCT}$) for the complexes (Figure 3.10). In accordance to the red-shift of the $^1\text{MLCT}$ absorption maxima relative to that of $\text{Ru}(\text{bpy})_3^{2+}$, the $^3\text{MLCT}$ emission maxima also shift bathochromically, which is a consequence of strong σ -donation of the **hpp** moiety. The emission maxima are gradually red shifted from **3-4** to **3-2** to **3-3**, which follows the increase in nucleophilicity of the substituted pyrimidyl ethers. The emission energy (λ_{max} , cm^{-1}) and the oxidation potentials of complexes **3-2** to **3-4** are correlated,

indicating that the redox-active orbitals are involved in the excited state properties. The red shift of the ³MLCT maxima of the complexes as compared to that of [Ru(bpy)₃]²⁺ is in accordance with the DFT calculations, and is supported by the smaller HOMO-LUMO energy gap for **3-(1-meso)**⁴⁺ (3.22 eV), **3-2**²⁺ (3.13 eV), **3-3**²⁺ (3.12 eV) and **3-4**²⁺ (3.18 eV) as compared to that of [Ru(bpy)₃]²⁺ (3.57 eV).⁴⁶

Table III-4. Photophysical data in deaerated CH₃CN solutions for complexes **3-(1-meso)** to **3-4**.

Compound	Luminescence ^a @ 298 K				
	λ_{\max} , nm	τ , ns	$10^{-4}\phi$	10^3k_r (s ⁻¹)	10^3k_{nr} (s ⁻¹)
3-(1-meso)	739	100	8.5	8.5	9.1
3-2	695	74	10	14	14
3-3	743	46	3.7	8	22
3-4	646	52	26	50	19
[Ru(bpy) ₂ (μ -(3-L2))][PF ₆] ₂ ^b	745	54	3.4	6.3	18.5
[Ru(bpy) ₂ (μ -(3-L5))][PF ₆] ₂ ^b	740	73	3.6	4.9	13.7
[Ru(bpy) ₃][PF ₆] ₂ ^{c,d}	620	860	950	110	1.0

^auncorrected for photomultiplier response. ^bfrom ref 7d, ^cfrom ref 50, ^dfrom ref 51.

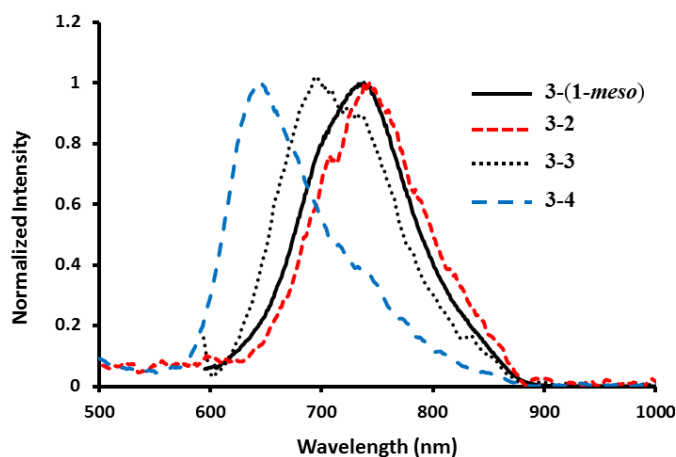


Figure 3.10. Uncorrected emission spectra of complexes **3-(1-meso)** to **3-4**, recorded at ambient temperature in dry, degassed acetonitrile.

It should be noted that the decrease in quantum yield and lifetime compared to that of Ru(bpy)₃²⁺ follows the red-shift of the emission energy. In heteroleptic Ru(II) complexes of polypyridyl ligands, a decrease in non-radiative constants is observed with

systems that allow greater delocalization of the excited MLCT state.^{53,54} However, in complexes **3-(1-meso)** to **3-4**, the ligand involved in the luminescent ³MLCT state is 2,2'-bpy, therefore, these effects should be based on other factors. One contributing factor to the decrease in the lifetime of the excited state may be the low energy emission, which according to the energy gap law,^{10b,c,55,56} leads to non-radiative decay back to the ground state. However, the excited state lifetimes of these complexes are all very similar regardless of the excited state energy of the ³MLCT (*cf.* compounds **3-3** and **3-4** in Table III-4). As the strong σ -donating **hpp** units should increase the energy-gap between the ³MLCT and ³MC state, thus preventing the ³MC states from quenching of the ³MLCT excited states to the ground state, deactivation of the excited state should not be through this mechanism either. The major contributing factor in this case may be due to the presence of saturated **hpp** units, which can contribute to the vibrational decay of the excited state.^{7c,d}

3.7. Conclusion

In conclusion, a new N_{amine}-substituted diguanidylpyrimidine ligand, **dgpm (3-L1)**, was prepared by an efficient, green and catalyst-free synthetic method assisted by microwave heating. The ligand coordinates to ruthenium(II) centres forming six-membered chelate rings to furnish a diruthenium(II,II)- complex, **3-(1-meso)**, which is formed with high diastereoselectivity over its homochiral *rac*-counterpart. This diastereoselectivity is due to the retention of rigid and thermodynamically stable chair conformation of **dgpm**, which offer parallel coordination vectors and maximum π - π interaction between the bpy units of its diruthenium complex. Due to these driving forces, **3-(1-meso)** was isolated using simple silica column chromatography without the need for a chiral support, as opposed to other isolation methods developed by Keene, MacDonnell and Vos *et. al.*⁵⁷⁻⁵⁹ Three other mononuclear Ru(II) complexes were also isolated and the relative formation of these products depends on the comparative nucleophilicities of the different solvents. From the Ru(III/II) potentials of the new complexes, it is found that all the new ligands possess strong donating ability as compared to common polypyridyls, e.g., bpy or phenanthroline. In fact the ligand reported in this work is even more electron donating than 2-(2'-aminoethyl)-pyridine (AETPy) or ethylenediamine (en) as revealed by the Ru(III/II)-couples of the complexes Ru(bpy)₂(AETPy)²⁺ (1.12 V vs. SCE) and Ru(bpy)₂(en)²⁺ (0.96 V vs. SCE).⁶⁰⁻⁶² As the butoxyether group is the strongest σ -donor, complex **3-3** exhibits the lowest Ru(III/II) oxidation potential among complexes **3-(1-meso)** to **3-4**, and this value is

almost 500 mV less positive than that of $\text{Ru}(\text{bpy})_3^{2+}$. As a result of strong σ donation from the ligands, complexes **3-(1-meso)** to **3-4** have low energy $^1\text{MLCT}$ absorptions in the visible region with an average bathochromic shift of ~ 90 nm in comparison to the same absorptions for $\text{Ru}(\text{bpy})_3^{2+}$. Among complexes **3-2** to **3-4**, this red-shift is directly proportional to the σ -donating ability of the ether group. The 298 K fluid solution emission maxima of complexes **3-(1-meso)** and **3-3** are also red-shifted by ~ 100 nm with respect to that for $\text{Ru}(\text{bpy})_3^{2+}$, and they arise from Ru^{II} -to-bpy $^3\text{MLCT}$ states, since the π^* orbitals are predominantly bpy based, as evidenced by DFT calculations. A gradual blue shift in emission maxima from complex **3-3** to **3-2** to **3-4** are in line with the lower nucleophilicity of 2-hydroxy-1-ethoxyether group compared to that of ethoxyether and butoxyether groups, which is also supported by their respective *Hammett* parameters. The interesting photophysical and redox properties of these complexes may serve as excellent redox mediators and light-harvesting materials.

3.8. Acknowledgment

AKP and GSH thank the Natural Sciences and Engineering Research Council of Canada (NSERC) and Centre for Self-Assembled Chemical Structure (CSACS) for financial support. We also thank Johnson Matthey PLC for a generous loan of ruthenium trichloride.

3.9. Supporting Information

X-ray crystallographic data in CIF format, CCDC reference numbers 964842-964843 and 972273-972275, additional figures and tabulated computational data. For ESI and crystallographic data in CIF or other electronic format see DOI: 10.1039/C4DT00112E.

3.10. References

- (1) (a) V. Balzani, F. Scandola, *Supramolecular Photochemistry*, Horwood: Chichester, U.K., 1991; (b) A. Juris, V. Balzani, F. Barigelletti, S. Campagna, P. Belser, A. von Zelewsky, *Coord. Chem. Rev.*, 1988, **84**, 85; (c) V. Balzani, A. Juris, M. Venturi, S. Campagna, S. Serroni, *Chem. Rev.*, 1996, **96**, 759; (d) E. A. Medlycott, G. S. Hanan, *Chem. Soc. Rev.*, 2005, **34**, 133; (e) E. A. Medlycott, G. S. Hanan, *Coord. Chem. Rev.*, 2006, **250**, 1763; (f) M.-P. Santoni, A. K. Pal, G. S. Hanan, A. Proust, B. Hasenknopf, *Inorg. Chem.*, 2011, **50**, 6737; (g) D. G. Brown, N. Sangantrakun, B. Schulze, U. S. Schubert, C. P. Berlinguette, *J. Am. Chem. Soc.*, 2012, **134**, 12354;

- (h) T. J. Meyer, *Acc. Chem. Res.*, 1989, **22**, 163; (i) V. Balzani, G. Bergamini, S. Campagna, F. Puntoriero, *Top. Curr. Chem.*, 2007, **280**, 1.
- (2) (a) J. J. Concepcion, J. W. Jurss, J. L. Templeton, T. J. Meyer, *J. Am. Chem. Soc.*, 2008, **130**, 16462; (b) R. Zong, R. P. Thummel, *J. Am. Chem. Soc.*, 2005, **127**, 12802.
- (3) (a) V. Balzani, F. Barigelletti, L. De Cola, *Top. Curr. Chem.*, 1990, **158**, 31; (b) J. H. Alstrum-Acevedo, M. K. Brennaman, T. J. Meyer, *Inorg. Chem.*, 2005, **44**, 6802.
- (4) M. K. Nazeeruddin, A. Kay, I. Rodicio, R. Humphrybaker, E. Muller, P. Liska, N. Vlachopoulos, M. Grätzel, *J. Am. Chem. Soc.*, 1993, **115**, 6382.
- (5) (a) B. O'Regan, M. Grätzel, *Nature*, 1991, **35**, 737; (b) R. Argazzi, C. A. Bignozzi, T. A. Heimer, F. N. Castellano, T. J. Meyer, *J. Am. Chem. Soc.*, 1995, **117**, 11815.
- (6) S. M. Draper, D. J. Gregg, E. R. Schofield, W. R. Browne, M. Duati, J. G. Vos, P. Passaniti, *J. Am. Chem. Soc.*, 2004, **126**, 8694 and references therein; (b) P. A. Anderson, F. R. Keene, T. J. Meyer, J. A. Moss, G. F. Strouse, J. A. Treadway, *J. Chem. Soc., Dalton Trans.*, 2002, **20**, 3820.
- (7) (a) E. Ioachim, E. A. Medlycott, G. S. Hanan, F. Loiseau, S. Campagna, *Inorg. Chim. Acta*, 2006, **359**, 766; (b) E. Ioachim, E. A. Medlycott, G. S. Hanan, F. Loiseau, V. Ricevuto, S. Campagna, *Inorg. Chem. Commun.*, 2005, **8**, 559; (c) S. Nag, J. G. Ferreira, L. Chenneberg, P. D. Ducharme, G. S. Hanan, G. L. Ganga, S. Serroni, S. Campagna, *Inorg. Chem.*, 2011, **50**, 7; (d) A. K. Pal, S. Nag, J. M. Ferreira, V. Brochery, G. L. Ganga, A. Santoro, S. Serroni, S. Campagna, G. S. Hanan, *Inorg. Chem.*, accepted, 2014, **53**, 1679.
- (8) V. W.-W. Yam, K. K.-W. Lo, *Coord. Chem. Rev.*, 1998, **184**, 157 and references cited therein.
- (9) G. MacDermott, S. M. Prince, A. A. Freer, A. M. Hawthornthwaite-Lawless, M. Z. Papiz, R. J. Cogdell, N. W. Isaacs, *Nature*, 1995, **374**, 517.
- (10) (a) K. Kalyanasundaram, M. Grätzel, M. K. Nazeeruddin, *J. Chem. Soc., Dalton Trans.*, 1991, **2**, 343; (b) J. P. Sauvage, J. P. Collin, J. C. Chambron, S. Guillerez, C. Coudret, V. Balzani, F. Barigelletti, L. DeCola, L. Flamigni, *Chem. Rev.*, 1994, **94**, 993; (c) T. J. Meyer, *Pure Appl. Chem.*, 1986, **58**, 1193.
- (11) V. Balzani, A. Juris, *Coord. Chem. Rev.*, 2001, **211**, 97.
- (12) (a) M. J. Cook, A. P. Lewis, G. S. G. McAuliffe, V. Skarda, A. J. Thompson, J. L. Glasper, D. J. Robbins, *J. Chem. Soc., Perkin Trans.*, 1984, **2**, 1303; (b) I. M. M. de Carvalho, I. de Sousa Moreira, M. H. Gehlen, *Inorg. Chem.*, 2003, **42**, 1525.
- (13) N. Kitamura, Y. Kawanishi, S. Tazuke, *Chem. Phys. Lett.*, 1983, **97**, 103.
- (14) D. P. Rillema, G. Allen, T. J. Meyer, D. Conrad, *Inorg. Chem.*, 1983, **22**, 1617.
- (15) S. Ernst, W. Kaim, *Inorg. Chem.*, 1989, **28**, 1520.
- (16) J. Wang, Y.-Q. Fang, G. S. Hanan, F. Loiseau, S. Campagna, *Inorg. Chem.*, 2005, **44**, 5.
- (17) S. D. Bergman, I. Goldberg, A. Barbieri, M. Kol, *Inorg. Chem.*, 2005, **44**, 2513.
- (18) M. J. Cook, A. P. Lewis, G. S. G. McAuliffe, V. Skarda, A. J. Thompson, J. L. Glasper, D. J. Robbins, *J. Chem. Soc., Perkin Trans.*, 1984, **2**, 1303.

- (19) I. M. M. de Carvalho, I. de Sousa Moreira, M. H. Gehlen, *Inorg. Chem.*, 2003, **42**, 1525.
- (20) N. Kitamura, Y. Kawanishi, S. Tazuke, *Chem. Phys. Lett.*, 1983, **97**, 103.
- (21) H. B. Ross, M. Boldaji, D. P. Rillema, C. B. Blanton, R. P. White, *Inorg. Chem.*, 1989, **28**, 1013.
- (22) D. J. Ma'nuel, D. P. Strommen, A. Bhuiyan, M. Sykora, J. R. Kincaid, *J. Raman Spectrosc.*, 1998, **28**, 933.
- (23) A. K. Pal, P. D. Ducharme, G. S. Hanan, *Chem. Commun.*, 2014, **50**, 3303.
- (24) G. A. Crosby, J. N. Demas, *J. Phys. Chem.*, 1971, **75**, 991.
- (25) V. C. Jonathan, J. M. Thomas, *J. Am. Chem. Soc.* 1983, **105**, 5783.
- (26) G. Sprintschnik, H. W. Sprintschnik, P. P. Kirsch, D. G. Whitten, *J. Am. Chem. Soc.* 1977, **99**, 4947.
- (27) M. J. Frisch, G. W. Trucks, H. B. Schlegel, G. E. Scuseria, M. A. Robb, J. R. Cheeseman, J. A. Montgomery, T. J. Vreven, K. N. Kudin, J. C. Burant, J. M. S. Millam, J. Tomasi, V. Barone, B. Mennucci, M. Cossi, G. Scalmani, N. Rega, G. A. Petersson, H. Nakatsuji, M. Hada, M. Ehara, K. Toyota, R. Fukuda, J. Hasegawa, M. Ishida, T. Nakajima, Y. Honda, O. Kitao, H. Nakai, M. Klene, X. Li, J. E. Knox, H. P. Hratchian, J. B. Cross, C. Adamo, J. Jaramillo, R. Gomperts, R. E. Startmann, O. Yazyev, A. J. Austin, R. Cammi, C. Pomelli, J. W. Ochterski, P. Y. Ayala, K. Morokuma, G. A. Voth, P. Salvador, J. J. Dannenberg, V. G. Zakrzewski, J. M. Dapprich, A. D. Daniels, M. C. Strain, O. Farkas, D. K. Malick, A. D. Rabuck, K. Raghavachari, J. B. Foresman, J. V. Ortiz, Q. Cui, A. G. Baboul, S. Clifford, J. B. Cioslowski, G. Liu, A. Liashenko, I. Piskorz, L. M. R. Komaromi, D. J. Fox, T. Keith, M. A. Al-Laham, C. Y. Peng, A. Manayakkara, M. Challacombe, P. M. W. Gill, B. G. Johnson, W. Chen, M. W. Wong, C. Gonzalez, J. A. Pople, *Gaussian 2003, Revision C.02; Gaussian Inc.:Pittsburgh PA, 2003*.
- (28) A. D. Becke, *J. Chem. Phys.*, 1993, **98**, 5648.
- (29) C. Lee, W. Yang, R. G. Parr, *Phys. Rev. B: Condens. Matter*, 1988, **37**, 785.
- (30) A. D. McLean, G. S. Chandler, *J. Chem. Phys.*, 1980, **72**, 5639.
- (31) P. J. Hay, W. R. Wadt, *J. Chem. Phys.*, 1985, **82**, 270.
- (32) (a) M. E. Casida, C. Jamorski, K. C. Casida, D. R. Salahub, *J. Chem. Phys.*, 1998, **108**, 4439; (b) R. E. Stratmann, G. E. Scuseria, M. J. J. Frisch, *Chem. Phys.*, 1998, **109**, 8218.
- (33) (a) M. Cossi, N. Rega, G. Scalmani, V. Barone, *J. Comput. Chem.*, 2003, **24**, 669; (b) M. Cossi, V. Barone, *J. Chem. Phys.*, 2001, **115**, 4708; (c) V. Barone, M. Cossi, *J. Phys. Chem. A*, 1998, **102**, 1995.
- (34) I. M. Dixon, F. Alary, J.-L. Heully, *Dalton Trans.*, 2010, **39**, 10959.
- (35) W. R. Browne, N. M. O'Boyle, J. J. McGarvey, J. G. Vos, *Chem. Soc. Rev.*, 2005, **34**, 641.
- (36) D. A. Zhurko, G. A. Zhurko, *ChemCraft 1.5*; Plimus: San Diego, CA. Available at <http://www.chemcraftprog.com>.

- (37) *APEX2 (2007) version 2.4-0; Bruker Molecular Analysis Research Tool*. Bruker AXS Inc., Madison, WI 53719-1173.
- (38) Sheldrick, G. M. (1996). *SADABS*, Bruker Area Detector Absorption Corrections. Bruker AXS Inc., Madison, WI 53719-1173.
- (39) *SHELXTL (2001) version 6.12*; Bruker Analytical X-ray Systems Inc., Madison, WI 53719-1173.
- (40) *Platon (A. L. Spek, 2003)*.
- (41) C. C. Weber, A. F. Masters, T. Maschmeyer, *Org. Biomol. Chem.*, 2013, **11**, 2534.
- (42) S. H. Oakley, M. P. Coles, P. B. Hitchcock, *Inorg. Chem.*, 2004, **43**, 7564.
- (43) Based on 278 ruthenium complexes containing at least two bpy and two more substituent with N atoms coordinated to the metal in the Cambridge Structural Database. F. H. Allen, *Acta Cryst.*, 2002, **B58**, 380.
- (44) (a) B. De Groot, G. S. Hanan, S. J. Loeb, *Inorg. Chem.*, 1991, **30**, 4644; (b) G. R. Giesbrecht, G. S. Hanan, J. E. Kickham, S. J. Loeb, *Inorg. Chem.*, 1992, **31**, 3286.
- (45) H. J. Bolink, E. Coronado, R. D. Costa, P. Gavina, E. Ortí, S. Tatay, *Inorg. Chem.*, 2009, **48**, 3907.
- (46) J. W. Slater, D. M. D'Alessandro, F. R. Keene, P. J. Steel, *Dalton Trans.*, 2006, **16**, 1954.
- (47) I. G. Phillips, P. J. Steel, *Aust. J. Chem.*, 1998, **51**, 371.
- (48) (a) C. Hansch, A. Leo, W. Taft, *Chem. Rev.*, 1991, **91**, 165; (b) Y.-Q. Fang, N. J. Taylor, F. Laverdière, G. S. Hanan, F. Loiseau, F. Nastasi, S. Campagna, H. Nierengarten, E. Leize-Wagner, Al. V. Dorsselaer, *Inorg. Chem.*, 2007, **46**, 2854.
- (49) P. J. Steel, *Coord. Chem. Rev.*, 1990, **106**, 227.
- (50) (a) S. I. Gorelsky, E. S. Dodsworth, A. B. P. Lever, A. A. Vlcek; *Coord. Chem. Rev.*, 1998, **174**, 469; (b) S. I. Gorelsky, A. B. P. Lever, *Coord. Chem. Rev.*, 2000, **208**, 153.
- (51) J. V. Casper, T. J. Meyer, *Inorg. Chem.*, 1983, **22**, 2444.
- (52) (a) J. M. Calvert, J. V. Caspar, R. A. Binstead, T. D. Westmoreland, T. J. Meyer, *J. Am. Chem. Soc.*, 1982, **104**, 6620; (b) V. C. Jonathan, J. M. Thomas, *J. Am. Chem. Soc.*, 1983, **105**, 5783.
- (53) Y.-Q. Fang, N. J. Taylor, G. S. Hanan, F. Loiseau, R. Passalacqua, S. Campagna, H. Nierengarten, A. van Dorsselaer, *J. Am. Chem. Soc.*, 2002, **124**, 7912.
- (54) (a) M. I. J. Polson, E. A. Medlycott, G. S. Hanan, L. Mikelsons, N. J. Taylor, M. Watanabe, Y. Tanaka, F. Loiseau, R. Passalacqua, S. Campagna, *Chem. Eur. J.*, 2004, **10**, 3640; (b) E. A. Medlycott, G. S. Hanan, F. Loiseau, S. Campagna, *Chem. Eur. J.*, 2007, **13**, 3837; (c) M. Schwalbe, M. Karnahl, H. Gorgs, D. Chartrand, F. Laverdiere, G. S. Hanan, S. Tschierlei, B. Dietzek, M. Schmitt, J. Popp, *Dalton Trans.* 2009, **20**, 4012; (d) M.-P. Santoni, E. A. Medlycott, G. S. Hanan, B. Hasenknopf, A. Proust, F. Nastasi, S. Campagna, C. Chiorboli, R. Argazzi, F. Scandola *Dalton Trans.* 2009, **20**, 3964; (e) M.-P. Santoni, G. S. Hanan, B. Hasenknopf, A. Proust, F. Nastasi, S. Serroni, S. Campagna *Chem. Commun.* 2011,

Chapter 3

- 47, 3586; (f) M.-P. Santoni, F. Nastasi, S. Campagna, G. S. Hanan, B. Hasenknopf, I. Ciofini *Dalton Trans.* 2013, **42**, 5281.
- (55) J. V. Casper, E. M. Kober, B. P. Sullivan, T. J. Meyer, *J. Am. Chem. Soc.*, 1982, **104**, 630.
- (56) J. P. Claude, T. J. Meyer, *J. Phys. Chem.*, 1995, **99**, 51.
- (57) (a) T. J. Rutherford, M. G. Quagliotto, F. R. Keene, *Inorg. Chem.*, 1995, **34**, 3857;
(b) F. R. Keene, *Chem. Soc. Rev.*, 1998, **27**, 185 and references cited therein.
- (58) T. K. Janaratne, A. Yadav, F. Onger, F. M. MacDonnell, *Inorg. Chem.*, 2007, **46**, 3420.
- (59) W. R. Browne, C. M. O'Connor, C. Villani, J. G. Vos, *Inorg. Chem.*, 2001, **40**, 5461.
- (60) N. Aydin, C. W. Schlaepfer, *Polyhedron*, 2001, **20**, 37.
- (61) H. Konno, Y. Ishii, K. Sakamoto, O. Ishitani, *Polyhedron*, 2002, **21**, 61.
- (62) G. M. Brown, T. R. Weaver, F. R. Keene, T. J. Meyer, *Inorg. Chem.*, 1976, **15**, 190.

Chapter 4 : Near Infra-Red emitting Ru(II) complexes: structural, electrochemical and photophysical investigations

4.1. Résumé

Un ligand tridenté N^NN **dgpy** (**dgpy** = diguanidylpyridine) a été synthétisé par couplage de Buchwald. Une nouvelle famille de complexes [Ru^{II}(tpy')(**dgpy**)] (PF₆)₂ (**4-1** et **4-2**) ou [Ru^{II}(dpt')(**dgpy**)] (PF₆)₂ (**4-3** et **4-4**) (tpy' = substitué -2,2':6',2"-terpyridine, dpt' = substitué-2,4-di-(2'-pyridyl)-1,3,5-triazine) sont rapportés. Le ligand **dgpy** (80%) et les complexes hétéroleptiques **4-1** à **4-4** (37-60%) ont été obtenus sous modeste à de bons rendements. Le ligand **dgpy** et ses complexes ont été entièrement caractérisés par une variété de techniques incluant la cristallographie aux rayons-X et de la théorie fonctionnelle de densité (DFT). Dans les études de voltampérométrie cyclique, les complexes présentent un couple Ru(III/II), qui est de 600-800 mV moins positive que le couple Ru(III/II) dans Ru(tpy)₂²⁺. Les maxima d'absorption ¹MLCT de tous les complexes (620-740 nm) sont nettement décalées vers le rouge par rapport à celle de Ru(tpy)₂²⁺ (474 nm). L'absorption ³MLCT de complexes **4-1** et **4-2** sont également décalées vers le rouge d'environ 270 nm par rapport à celle de Ru(tpy)₂²⁺ (629 nm) à température ambiante (298 K), tandis que les maxima correspondant à des complexes **4-3** et **4-4** sont décalées d'environ 330 nm à 77 K. Ces tendances relatives à des potentiels redox et ¹MLCT maxima sont en bon accord avec les calculs DFT et TD-DFT, réalisés pour les complexes. Complexes **4-1** à **4-4** ont une émission d'un état Ru(II)-à-tpy ³MLCT, ce qui est rarement l'état émettant à λ > 850 nm dans [Ru(tpy)(N^NN)]²⁺ complexes lorsque le ligand auxiliaire est neutre. Complexes **4-1** et **4-2** présentent également la température ambiante à l'état excité vie (τ) avec des rendements quantiques associés (Φ) de 0.001. La signalé τ et Φ valeurs sont environ 400-500 fois et 1000 fois plus élevés par rapport à ceux de Ru(tpy)₂²⁺ (τ = 0.25 ns, Φ ≤ 5x10⁻⁶), respectivement. Ces propriétés photophysiques amélioration des complexes sont des conséquences de la séparation élargie de l'état ³MLCT-³MC, en raison du fort σ-donation du ligand **dgpy** et la diminution de l'encassement angulaire autour du ruthenium.

Chapter 4

Contribution :

Amlan K. Pal : All the work presented in this article and its writing.

Nelsi Zaccheroni : Photophysical (luminescence) measurements of the complexes.

Sebastiano Campagna : Photophysical (luminescence) measurements of the complexes.

Garry S. Hanan : Supervision and revision of the article.

Near Infra-Red emitting Ru(II) complexes: structural, electrochemical and photophysical investigations

*Amlan K. Pal,^a Nelsi Zaccheroni,^{*b} Sebastiano Campagna,^{*c} and Garry S. Hanan^{*a}*

^aDépartement de Chimie, Université de Montréal, Montréal, Québec, H3T 1J4, Canada

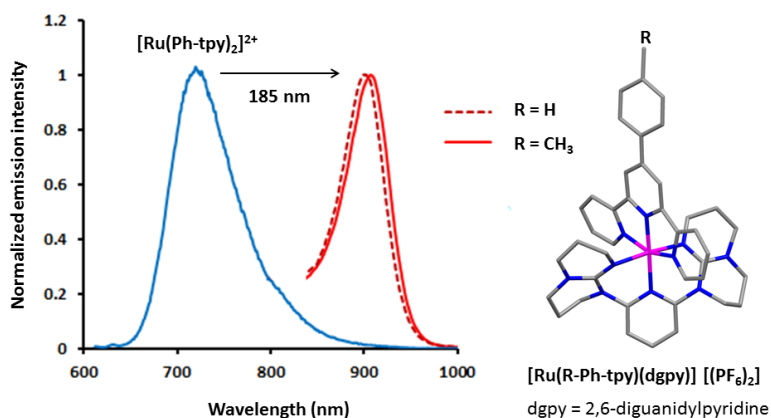
^bDipartimento di Chimica «G. Ciamician», Università di Bologna, 40126 Bologna, Italia

^cDipartimento di Scienze Chimiche, Università di Messina, 98166 Messina, Italia

Manuscript in preparation

KEYWORDS: Ligand design, Ruthenium chromophores, Photophysics, Electrochemistry, Density functional theory.

4.2. Table of Content Graphic



A series of heteroleptic Ru(II) complexes containing substituted 2,2':6',2''-terpyridine (tpy) or 2,4-dipyridin-2'-yl-1,3,5-triazine (dpt) unit and neutral 'super donor' **dgpy** (**dgpy** = 2,6-diguanyldipyridine) ligands were synthesized and characterized. Their structural, electrochemical and photophysical properties were studied and compared to bis-(tpy)ruthenium(II) and some reference compounds. Their properties were also modeled by

Chapter 4

density functional theory calculation and trends were found vs. the electronic nature of the tpy or dpt core attached to the ruthenium center.

4.3. Abstract

A novel N[^]N[^]N tridentate ligand **dgpy** (**dgpy** = 2,6-diguanidylpyridine) was synthesized by a Pd-catalyzed C-N bond-forming reaction. A novel family of [Ru^{II}(tpy')(**dgpy**)](PF₆)₂ (**4-1** and **4-2**) or [Ru^{II}(dpt')(**dgpy**)](PF₆)₂ (**4-3** and **4-4**) (tpy' = substituted-2,2':6',2'-terpyridine, dpt' = substituted-2,4-dipyrid-2'-yl-1,3,5-triazine) complexes are reported. The **dgpy** ligand (80%) and the heteroleptic complexes **4-1** to **4-4** (37-60%) were obtained in modest-to-good yields. The **dgpy** ligand and its complexes were fully characterized by a variety of techniques including X-ray crystallography and density functional theory (DFT). In cyclic voltammetric studies, the complexes exhibit a Ru^{III/II} couple, which is 600-800 mV less positive than the Ru^{III/II} couple in Ru(tpy)₂²⁺. The ¹MLCT absorption maxima of all the complexes (620–740 nm) are considerably red-shifted as compared to that of [Ru(tpy)₂]²⁺ (474 nm). The ³MLCT emission maxima of complexes **4-1** and **4-2** are also red-shifted by about 270 nm compared to that of [Ru(tpy)₂]²⁺ (629 nm) at room temperature (298 K), whereas the corresponding maxima for complexes **4-3** and **4-4** are shifted by about 330 nm at 77 K. The relative trends in redox potentials and ¹MLCT maxima are in good agreement with DFT and TD-DFT calculations. Complexes **4-1** and **4-2** emit from a Ru^{II}-to-tpy ³MLCT state, which is rarely the emitting state at λ > 850 nm in [Ru(tpy)(N[^]N[^]N)]²⁺ complexes when the ancillary ligand is neutral. Complexes **4-1** and **4-2** also exhibit long excited-state lifetimes (τ) at room temperature with associated quantum yield (Φ) of 0.001. The reported τ and Φ values are approximately 400-500 times and 1000 times higher compared to those of [Ru(tpy)₂]²⁺ (τ = 0.25 ns, Φ ≤ 5x10⁻⁶), respectively. Complexes **4-3** and **4-4** emit from a Ru^{II}-to-dpt ³MLCT state at 935 nm and 965 nm, respectively, albeit only at 77 K (τ = 0.25 ns) due to rapid deactivation of their ³MLCT state according to the energy-gap law. The improved photophysical properties of the complexes are consequences of enlarged separation of the ³MLCT-³MC states, due to the strong σ-donation of the **dgpy** ligand.

4.4. Introduction

Ru(II)-polypyridine complexes continue to draw considerable interest in the context of molecular electronics, photochemical conversion solar energy,¹ photoluminescence biosensors,² or electroluminescent dyes in organic light-emitting devices³ due to their remarkable redox and photophysical properties.⁴⁻⁸ As effective light-harvesting materials,

these compounds should exhibit (i) low energy metal-to-ligand charge transfer (MLCT) transitions, (ii) long room-temperature (r.t.) lifetime of the excited $^3\text{MLCT}$ states, (iii) high emission quantum yields and (iv) a structural arrangement suitable to yield, upon synthetic elaboration, vectorial electron or energy transfer along a predesigned direction.⁹ Tris-bidentate Ru(II) complexes, for example, $[\text{Ru}(\text{bpy})_3]^{2+}$ (bpy = 2,2'-bipyridine) or its derivatives, are of particular interest in this context.¹⁰ However, complexes of these types are often limited to tiresome stereoisomeric purification procedures, when they are incorporated into larger polynuclear assemblies and the desired vectorial transfer of electron or energy along a specific direction is not easily achieved.

In contrast to tris(bidentate)-Ru^{II} complexes, achiral $[\text{Ru}(\text{tpy})_2]^{2+}$ (tpy = 2,2':6',2'-terpyridine) type complexes are structurally more appealing due to their higher symmetry (D_{2d} instead of D_3 for $[\text{Ru}(\text{bpy})_3]^{2+}$) and their inherent linearity and generation of isomerically pure rod-like multiunit assemblies when substituted along the C_2 axis.^{6,11-16} Although the ground-state properties of $[\text{Ru}(\text{tpy})_2]^{2+}$ type complexes are similar to those of $[\text{Ru}(\text{bpy})_3]^{2+}$ type complexes, the r.t. $^3\text{MLCT}$ excited-state lifetime of the former is limited to only 0.25 ns, consequently limiting its use in photosensitizer applications.¹⁷ This is due to rapid population and deactivation via short-lived and non-emissive triplet metal-centered (^3MC) state, which remains in close equilibrium with the emissive $^3\text{MLCT}$ state.^{4,5a} The equilibrium has been attributed to the unfavourable bite angles of the *mer*-coordinated tridentate ligands, thereby generating a weak ligand field, leading to a low-lying thermally accessible ^3MC state, quasi iso-energetic to the $^3\text{MLCT}$ state.¹⁸

Much attention has been devoted to design and synthesis of new tpy based Ru(II)-complexes with extended excited-state lifetimes. The typical approach is to increase the energy gap between the $^3\text{MLCT}$ and ^3MC states (Figure 1), which could be performed either by stabilizing the $^3\text{MLCT}$ state or destabilizing the ^3MC state or doing both at a time. Stabilization of $^3\text{MLCT}$ state can be achieved by substitution of the tpy ligand by electron-withdrawing substituents.^{13,16,19} An alternative approach introduces coplanar aromatic moieties with extended π -conjugated systems to take advantage of increased delocalization in the acceptor ligand of the MLCT emitting state, thereby reducing the Franck-Condon factors for radiationless decay.²⁰⁻²⁴ Another approach introduces an organic chromophore to establish an equilibrium between the $^3\text{MLCT}$ and the usually long-lived, organic chromophore triplet ^3LC (LC = ligand-centered) states, where the ^3LC state serves as an

excited state storage element, leading to repopulation of the emissive $^3\text{MLCT}$ state.^{15,25-28} All these strategies have led to an increase in the r.t. lifetime of the excited $^3\text{MLCT}$ state, ($\tau = 1\text{--}200$ ns, leaving aside the lifetimes attributed to the equilibrated state in the presence of organic chromophores, which can be significantly longer). However, in most cases, the 4'-position of the tpy ligand is already functionalized, which limits its use for further derivatization or nucleation in supramolecular assemblies.

Another strategy to increase the $^3\text{MLCT}$ and ^3MC energy-gap is to increase the energy of the MC state by increasing the ligand field strength by widening the ligand bite angle, bringing them closer to ideal 90° and 180° angles, thereby affording octahedral coordination geometry by the N atoms around the metal ion. The MC state is similarly destabilized by cyclometallating tridentate ligands (as $\text{N}^{\wedge}\text{C}^{\wedge}\text{N}$ or $\text{N}^{\wedge}\text{N}^{\wedge}\text{C}$), which also red-shift the $^3\text{MLCT}$ excited state compared to N_6 analogues. Emission lifetimes in the range 4.5–20 ns has been reported with $\text{N}^{\wedge}\text{C}^{\wedge}\text{N}$ type ligands.^{10,29-35} Other types of strong σ -donor ligands, e.g., *N*-heterocyclic carbenes (NHC), also give rise to relatively long r.t. excited-state lifetimes, for example ~ 8 μs in a heteroleptic Ru(II)-complex containing a substituted tpy.^{35b} A close-to-ideal octahedral geometry also improves the $^3\text{MLCT}$ excited-state lifetime; for example, introduction of alkyl (-CRR'-, where R = Me, R' = OH, OMe) spacers in BPy-Py ligands or -CO- spacer in polypyridyl systems, increases the lifetime to 1.4 ns to 3.3 μs (in deaerated solutions), respectively,³⁶⁻³⁹ whereas Ru(II)-homoleptic complexes containing **dqp** (**dqp** = 2,6-di(quinoline)pyridine) ligand, exhibit long excited-state lifetimes ($\tau = 5.5$ μs) and high quantum yields ($\Phi = 0.07$).⁴⁰ The combination of ideal octahedral geometry using **dqp** ligand and an equilibrated ^3LC state with phenylanthracene, has also led to a homoleptic Ru(II) complex that exhibits the longest r.t. excited-state lifetime ($\tau = 42$ μs) reported so far considering Ru(II) complexes of tridentate ligands.^{28b}

We recently reported a series of tris-bidentate Ru(II) complexes, where a bpy unit had been substituted by a guanidyl-*N*-heterocyclic moiety. The introduction of an electron-rich guanidine unit significantly red-shifted the $^1\text{MLCT}$ and $^3\text{MLCT}$ states for these complexes as compared to $[\text{Ru}(\text{bpy})_3]^{2+}$ (440 nm/620 nm).⁴¹ To this end, following the similar arguments with decreased chelate-ring strain and strong σ -donation, we prepared a novel symmetrical tridentate ligand (**4-L1**) by coupling two of **H-hpp** units (**H-hpp** = 1,3,4,6,7,8-hexahydro-2*H*-pyrimido[1,2-*a*]pyrimidine) with 2,6-dibromopyridine. The **H-**

hpp as the coupling agent can be introduced by cross coupling in good yield.^{42,43} The aliphatic backbones on **hpp** increases the strong σ -donor character of **4-L1** as compared to tpy. The chelating N atoms in the ligand form two 6-membered chelate rings with the central pyridine ring, thereby offering larger bite angles upon coordination to Ru(II), with near-octahedral geometry.^{37,44,45} The last two modifications destabilize the ^3MC state, as discussed earlier.

Herein, we present the synthesis and characterization of novel heteroleptic Ru(II) complexes containing substituted tpy (**4-1** and **4-2**) ligands and substituted 2,4-dipyrid-2'-yl-triazine (dpt) ligands (**4-3** and **4-4**) together with **dgpy** (**4-L1**). Furthermore, the choice tpy and dpt was to examine the effect of planarity in triazine-related complexes compared to that of tpy-based compounds.^{21,22} The redox and photophysical consequences due the strong donor **hpp** units are also reported.

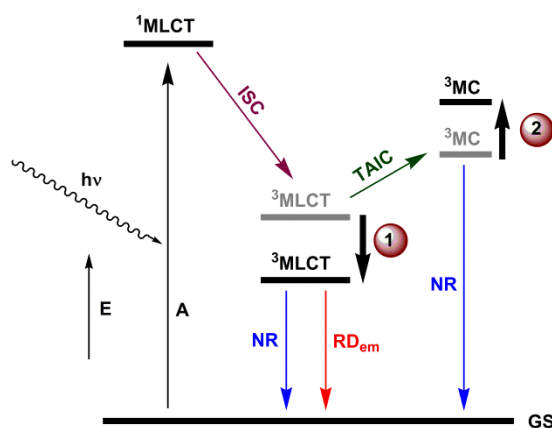


Figure 4.1. Strategies to increase the emissive $^3\text{MLCT}$ lifetime of Ru(II)-polypyridyl complexes; (1) stabilizing the $^3\text{MLCT}$ state, (2) destabilizing the ^3MC state. (E = energy, A = absorption of photon, ISC = intersystem crossing, TAIC = thermally-activated internal conversion, NR = non-radiative decay, RD_{em} = radiative decay)

4.5. Experimental Section

4.5.1. Materials and Instrumentation

Nuclear magnetic resonance (NMR) spectra were recorded in CD_3CN at room temperature (r.t.) on Bruker AV400 (400 MHz) and Bruker AV700 (700 MHz) spectrometers for ^1H NMR and at 100 and 175 MHz for ^{13}C NMR respectively, as mentioned in the experimental. Chemical shifts are reported in part per million (ppm)

relative to residual solvent protons (1.94 ppm for CD₃CN, 7.26 ppm for CDCl₃) and the carbon resonance (118.69 ppm for CD₃CN, 77.00 ppm for CDCl₃) of the solvent.

Absorption spectra were measured in deaerated acetonitrile at r.t. on a Cary 500i UV-Vis-NIR Spectrophotometer. Corrected fluorescence emission spectra (450 W Xe lamp) in the IR range were obtained with a modular UV-VIS-NIR spectrofluorimeter Edinburgh Instrument, equipped with an Edinburgh Instruments Ge detector (for the 800–1600 nm spectral range). Corrections for instrumental response, inner filter effects and phototube sensitivity were performed. The luminescence quantum yield of **4-1** and **4-2** were calculated⁴⁶ by optical dilution method recording the emission spectra of the degassed solution in acetonitrile and of a solution of cyanine IR-125 in dimethylsulfoxide ($\Phi = 0.23$)⁴⁷ as the reference. Luminescence lifetimes were determined by time-correlated single-photon-counting (TCSPC) with an Edinburgh EPL-405 spectrometer (light pulse: picosecond pulse diode laser, pulse width 500 ns at 405 nm).

Electrochemical measurements were carried out in argon-purged purified acetonitrile at room temperature with a BAS CV50W multipurpose potentiostat. The working electrode was a glassy carbon electrode. The counter electrode was a Pt wire, and the pseudo-reference electrode was a silver wire. The reference was set using an internal 1 mM ferrocene/ferrocinium sample at 395 mV vs. SCE in acetonitrile. The concentration of the compounds was about 1 mM. Tetrabutylammonium hexafluorophosphate (TBAP) was used as supporting electrolyte and its concentration was 0.10 M. Cyclic voltammograms were obtained at scan rates of 100 mV/s. The criteria for reversibility were the separation of 60 mV between cathodic and anodic peaks, the close to unity ratio of the intensities of the cathodic and anodic currents, and the constancy of the peak potential on changing scan rate. Estimated experimental uncertainties are as follows: absorption maxima, ± 2 nm; molar absorption coefficient, 10%; redox potentials, ± 10 mV.

Hydrated ruthenium trichloride, 1,3,4,6,7,8-hexahydro-2*H*-pyrimido[1,2-*a*]pyrimidine, (\pm) BINAP, *t*-BuOK, 2-acetylpyridine, benzaldehyde, 4-methylbenzaldehyde, 4-bromobenzonitrile, 4-*tert*-butylbenzonitrile, 2-cyanopyridine, 2,6-dibromopyridine and potassium hexafluorophosphate were purchased from Aldrich Chemicals and used as received. Pd(OAc)₂ was purchased from Pressure Chemicals. The ligands 4-phenyl-2,2':6',2''-terpyridine (Ph-tpy), 4-*para*-tolyl-2,2':6',2''-terpyridine (Tolyl-tpy), 2,4-di(2'-pyridyl)-6-(*p*-bromophenyl)-1,3,5-triazine (Br-Ph-dpt) and the complexes

[Ru(Ph-tpy)Cl₃], [Ru(*p*-Tolyl-tpy)Cl₃], [Ru(Br-Ph-dpt)Cl₃], [Ru(^tBu-Ph-dpt)Cl₃] starting materials were synthesized following literature procedures.^{48,49}

4.5.2. Synthetic Methods

2,6-bis-(1,3,4,6,7,8-hexahydropyrimido[1,2-*a*]pyrimidyl)pyridine (**4-L1** or **dgpy**)^{41e} :

(±) BINAP (0.06 mmol, 38 mg) was taken in an oven-dried round-bottomed flask purged with argon and sealed with a septum. Dry toluene (3 mL) was injected inside. The resulting suspension was heated at 90 °C for 2 min to dissolve the BINAP. This was cooled to room temperature and Pd(OAc)₂ (0.04 mmol, 9 mg) was added and stirred for 3 min. To the resulting bright yellow solution, 2,6-dibromopyridine (2 mmol, 474 mg) and 1,3,4,6,7,8-hexahydro-2*H*-pyrimido[1,2-*a*]pyrimidine (4.3 mmol, 600 mg) were added respectively. Stirring for 5 min at ambient temperature resulted in a pale orange slurry to which was added *t*-BuOK (5.6 mmol, 640 mg). The flask was again purged with argon and 2 mL more dry toluene was injected in to rinse the walls of the flask. The reaction mixture was then stirred at 90 °C for 3.5 h, after which time the reaction mixture was cooled at room temperature and diethyl ether (60 mL) was added and filtered. Evaporation of the filtrate afforded the ligand (**4-L1**) as crystalline pale yellow solid. Single crystals suitable for X-ray crystallography were grown by slow evaporation of a diethyl ether solution of the compound. Yield = 563 mg (80 %). ¹H NMR (CDCl₃, 300 MHz); 7.34 (t, *J*^t = 8 Hz, 2H), 7.11 (d, *J*^d = 8 Hz, 2H), 3.83 (t, *J*^t = 6 Hz, 4H), 3.40 (t, *J*^t = 6 Hz, 4H), 3.21 (t, *J*^t = 6 Hz, 4H), 3.14 (t, *J*^t = 6 Hz, 4H), 1.95 (quint., *J*^{qt} = 6 Hz, 4H), 1.86 (quint., *J*^{qt} = 6 Hz, 4H). ¹³C NMR (CDCl₃, 75 MHz); 154.5, 150.2, 136.6, 110.4, 48.8, 48.6, 43.9, 43.6, 23.7, 22.8. HRMS (ESI), *m/z*: 117.62399 [M+2H⁺]²⁺ (C₁₉H₂₉N₇ requires 117.62367), 354.24006 [M+H⁺]⁺ (C₁₉H₂₈N₇ requires 354.24007), 376.22216 [M+Na⁺]⁺ (C₁₉H₂₇N₇Na requires 376.22201). Anal. Calc for C₁₉H₂₇N₇·H₂O : C, 61.43; H, 7.87; N, 26.39. Found: C, 61.57; H, 7.95; N, 26.53.

2,4-di(2'-pyridyl)-6-(*p*-*tert*-butylphenyl)-1,3,5-triazine (**4-L2**) (^tBu-Ph-dpt) :

The ligand 2,4-di(2'-pyridyl)-6-(*p*-*tert*-butylphenyl)-1,3,5-triazine was synthesized using a modified literature procedure.^{41,42} To a stirred solution of HNMe₂ (2 M in THF, 8.37 mL, 16.59 mmol) in anhydrous Et₂O (150 mL) was added *n*-BuLi (1.6 M in hexanes, 10.41 mL, 16.59 mmol), dropwise, under an inert atmosphere. The mixture was stirred for 30 min until a white suspension formed and *p*-*tert*-butylbenzotrile (2.4 g, 15.08 mmol) was added. Stirring was continued for 1 h at room temperature followed by the addition of 2-

cyanopyridine (3.14 g, 30.16 mmol). Stirring was continued for 16 h after which time the reaction was diluted with a 5 : 1 mixture of water–EtOH (250 mL : 50 mL, v/v) and the solution was heated to remove the Et₂O. The white precipitate thus formed was collected by filtration and washed with EtOH (10 mL) and Et₂O (2x25 mL) and dried under vacuum to afford **4-L2** as a white powder. The compound could be crystallized from EtOH-H₂O. Yield = 3.6 g (65%). ¹H NMR (DMSO-*d*₆, 400 MHz); 1.37 (s, 9H), 7.64-7.76 (m, 4H), 8.13 (td, *J*^{td} = 8, 2 Hz, 2H), 8.65 (d, *J*^d = 8 Hz, 2H), 8.74 (d, *J*^d = 8 Hz, 2H), 8.91 (d, *J*^d = 4 Hz, 2H). ¹³C NMR (DMSO-*d*₆, 100 MHz); 171.7, 171.1, 156.3, 152.9, 150.1, 137.4, 132.4, 128.7, 126.7, 125.8, 124.7, 34.8, 30.8. HRMS (ESI), *m/z*: 184.59777 [M+2H⁺]²⁺ (C₂₃H₂₃N₅ requires 184.59712), 368.18809 [M+H⁺]⁺ (C₂₃H₂₂N₅ requires 368.18697), 390.16982 [M+Na⁺]⁺ (C₂₃H₂₁N₅Na requires 390.16892). Anal. Calc for C₂₃H₂₁N₅ : C, 75.18; H, 5.76; N, 19.06. Found: C, 74.96; H, 5.81; N, 18.94.

[Ru(*Ph-tpy*)(**4-L1**)](PF₆)₂ (**4-1**)^{41e} :

A mixture of [Ru(*Ph-tpy*)Cl₃] (100 mg, 0.193 mmol) and 4-ethylmorpholine (10 drops) in nitrogen-degassed *n*-butanol (60 mL) was heated at 80 °C for half an hour to give a dark brown-red suspension. After cooling of the mixture to ambient temperature, to the suspension was added **4-L1** (72 mg, 0.203 mmol) and the resulting mixture was refluxed for 12 h under nitrogen atmosphere. After 12 h, the dark purple mixture was cooled down to ambient temperature and solvent was evaporated to dryness. The resulting solid was purified by chromatography on silica using a mixture of 7/1 (v/v) acetonitrile/saturated aq. KNO₃ to afford the pure complex **4-1** as a purple solid. The nitrate salt was metathesized to the PF₆ salt by addition of saturated aqueous KPF₆ solution to the aqueous solution of the compound. Crystals suitable for X-ray crytallography were grown by diffusion of diethyl ether into a moderately concentrated solution of the complex in acetone. Yield = 75 mg (37%). ¹H NMR (CD₃CN, 700 MHz); 8.69 (s, 2H) 8.55 (d, *J*^d = 8.0 Hz, 2H), 8.14 (t, *J*^t = 8 Hz, 1H), 8.09 (dd, *J*^d = 8 Hz, *J*^d = 1.0 Hz, 2H), 8.05 (dd, *J*^d = 6 Hz, *J*^d = 1.0 Hz, 2H), 7.99 (td, *J*^t = 8 Hz, *J*^d = 2.0 Hz, 2H), 7.67 (t, *J*^t = 7 Hz, 2H), 7.59 (t, *J*^t = 7 Hz, 1H), 7.48 (d, *J*^d = 8 Hz, 2H), 7.47 (t, *J*^t = 7 Hz, 2H), 4.05 (m, 2H), 3.58 (m, 2H), 3.20 (m, 2H), 3.05 (m, 2H), 3.00 (m, 2H), 2.77 (m, 2H), 2.32 (m, 2H), 2.11 (m, 2H), 1.67 (m, 2H), 1.45 (m, 2H), 1.21 (m, 2H), 0.85 (m, 2H). ¹³C NMR (CD₃CN, 175 MHz); 159.8, 158.8, 155.9, 154.0, 153.9, 143.7, 140.8, 138.2, 137.1, 130.5, 130.3, 128.2, 126.9, 123.9, 120.9, 112.8, 49.6, 48.8, 48.4, 43.8, 23.3, 23.1. HRMS (ESI), *m/z*: 909.22556 [M-PF₆]⁺ (C₄₀H₄₂N₁₀PF₆Ru requires

909.22737), 382.13215 $[\text{M}-2\text{PF}_6]^{2+}$ ($\text{C}_{40}\text{H}_{42}\text{N}_{10}\text{Ru}$ requires 382.13132). Anal. Calc for $\text{C}_{40}\text{H}_{42}\text{N}_{10}\text{RuP}_2\text{F}_{12}$: C, 45.59; H, 4.02; N, 13.29. Found: C, 45.68; H, 4.08; N, 13.03.

[Ru(p-Toly-tpy)(4-L1)](PF₆)₂ (4-2) :

A mixture of $[\text{Ru}(p\text{-Toly-tpy})\text{Cl}_3]$ (100 mg, 0.188 mmol) and 4-ethylmorpholine (10 drops) in nitrogen-degassed *n*-butanol (60 mL) was heated at 80 °C for half an hour to give a dark brown-red suspension. After cooling of the mixture to ambient temperature, to the suspension was added **4-L1** (70 mg, 0.197 mmol) and the resulting mixture was refluxed for 16 h under nitrogen atmosphere. After 16 h, the dark purple mixture was cooled down to ambient temperature and solvent was evaporated to dryness. The resulting solid was purified by chromatography on silica using a mixture of 7/1 (v/v) acetonitrile/saturated aq. KNO_3 to afford the pure complex **4-2** as a purple solid. The nitrate salt was metathesized to the PF_6 salt by addition of saturated aqueous KPF_6 solution to the aqueous solution of the compound. Crystals suitable for X-ray cryatallography were grown by diffusion of diethyl ether into a moderately concentrated solution of the complex in acetone. Yield = 120 mg (60%). ^1H NMR (CD_3CN , 700 MHz); 8.67 (s, 2H) 8.54 (d, $J^d = 8$ Hz, 2H), 8.14 (t, $J^t = 8$ Hz, 1H), 8.04 (d, $J^d = 6$ Hz, 2H), 7.98 (m, 4H), 7.46 (m, 6H), 4.03 (m, 2H), 3.19 (m, 2H), 3.04 (m, 4H), 2.76 (m, 3H), 2.46 (s, 3H), 2.31 (m, 2H), 2.09 (m, 2H), 1.67 (m, 2H), 1.44 (m, 2H), 1.19 (m, 3H), 0.84 (m, 2H). ^{13}C NMR (CD_3CN , 175 MHz); 159.8, 158.7, 155.9, 154.1, 153.8, 143.7, 140.9, 140.8, 137.1, 135.3, 130.9, 128.0, 126.8, 123.9, 120.5, 112.8, 49.6, 48.8, 48.4, 43.8, 23.3, 23.1, 21.2. HRMS (ESI), *m/z*: 923.24348 $[\text{M}-\text{PF}_6]^+$ ($\text{C}_{41}\text{H}_{44}\text{N}_{10}\text{RuPF}_6$ requires 923.24302), 389.14029 $[\text{M}-2\text{PF}_6]^{2+}$ ($\text{C}_{41}\text{H}_{44}\text{N}_{10}\text{Ru}$ requires 389.13915). Anal. Calc for $\text{C}_{41}\text{H}_{44}\text{N}_{10}\text{RuP}_2\text{F}_{12}$: C, 46.11; H, 4.15; N, 13.12. Found: C, 46.13; H, 4.11; N, 13.01.

[Ru(Br-Ph-dpt)(4-L1)](PF₆)₂ (4-3) :

A mixture of $\text{Ru}(\text{Br-Ph-dpt})\text{Cl}_3$ (100 mg, 0.167 mmol) and 4-ethylmorpholine (10 drops) in nitrogen-degassed *n*-butanol (60 mL) was heated at 80 °C for half an hour to give a dark brown-red suspension. After cooling of the mixture to ambient temperature, to the suspension was added **4-L1** (62 mg, 0.175 mmol) and the resulting mixture was refluxed for 14 h under nitrogen atmosphere. After 14 h, the dark purple mixture was cooled down to ambient temperature and solvent was evaporated to dryness. The resulting solid was purified by chromatography on silica using a mixture of 7/1 (v/v) acetonitrile/saturated aq. KNO_3 to afford the pure complex **4-3** as a purple solid. The nitrate salt was metathesized to the PF_6 salt by addition of saturated aqueous KPF_6 solution to the aqueous solution of the

compound. Crystals suitable for X-ray crytallography were grown by diffusion of diethyl ether into a moderately concentrated solution of the complex in acetone. Yield = 90 mg (47%). ^1H NMR (CD_3CN , 700 MHz); 9.04 (d, $J^d = 7$ Hz, 2H), 8.49 (d, $J^d = 8$ Hz, 2H), 8.23 (m, 3H), 8.20 (t, $J^t = 7$ Hz, 2H), 7.89 (d, $J^d = 8$ Hz, 2H), 7.73 (t, $J^t = 7$ Hz, 2H), 7.58 (d, $J^d = 8$ Hz, 2H), 4.12 (d, $J^d = 14$ Hz, 2H), 3.22 (m, 2H), 3.08 (t, $J^t = 13$ Hz, 2H), 3.01 (m, 2H), 2.73 (m, 4H), 2.34 (m, 2H), 2.12 (m, 2H), 1.47 (m, 2H), 1.18 (m, 4H), 0.78 (m, 2H). ^{13}C NMR (CD_3CN , 175 MHz); 172.9, 162.3, 155.6, 155.4, 155.3, 154.3, 141.7, 137.9, 135.8, 133.4, 131.2, 129.9, 127.9, 127.6, 113.0, 49.4, 48.9, 48.2, 44.0, 23.2, 23.1. HRMS (ESI), m/z : 989.12744 $[\text{M-PF}_6]^+$ ($\text{C}_{38}\text{H}_{39}\text{N}_{12}\text{BrRuPF}_6$ requires 989.12838), 422.08339 $[\text{M-2PF}_6]^{2+}$ ($\text{C}_{38}\text{H}_{39}\text{N}_{12}\text{BrRu}$ requires 422.08183). Anal. Calc for $\text{C}_{38}\text{H}_{39}\text{N}_{12}\text{BrRuP}_2\text{F}_{12}$: C, 40.22; H, 3.46; N, 14.81. Found: C, 40.08; H, 3.45; N, 14.54.

[Ru(^tBu-Ph-dpt)(4-L1)](PF₆)₂ (4-4) :

A mixture of $\text{Ru}(\text{^tBu-Ph-dpt})\text{Cl}_3$ (100 mg, 0.174 mmol) and 4-ethylmorpholine (10 drops) in nitrogen-degassed *n*-butanol (60 mL) was heated at 80 °C for half an hour to give a dark brown-red suspension. After cooling of the mixture to ambient temperature, to the suspension was added **4-L1** (65 mg, 0.184 mmol) and the resulting mixture was refluxed for 16 h under nitrogen atmosphere. After 16 h, the dark purple mixture was cooled down to ambient temperature and solvent was evaporated to dryness. The resulting solid was purified by chromatography on silica using a mixture of 7/1 (v/v) acetonitrile/saturated aq. KNO_3 to afford the pure complex **4-4** as a purple solid. The nitrate salt was metathesized to the PF_6 salt by addition of saturated aqueous KPF_6 solution to the aqueous solution of the compound. Crystals suitable for X-ray crytallography were grown by diffusion of diethyl ether into a moderately concentrated solution of the complex in acetone. Yield = 110 mg (60%). ^1H NMR (CD_3CN , 700 MHz); 9.02 (d, $J^d = 8$ Hz, 2H), 8.85 (d, $J^d = 8$ Hz, 2H), 8.22 (t, $J^t = 8$ Hz, 1H), 8.17 (m, 4H), 7.77 (d, $J^d = 8$ Hz, 2H), 7.72 (t, $J^t = 6$ Hz, 2H), 7.56 (d, $J^d = 8$ Hz, 2H), 4.11 (d, $J^d = 16$ Hz, 2H) 3.13-2.76 (m, 8H), 2.34 (m, 2H), 2.12 (m, 2H), 1.50 (m, 2H), 1.44 (s, 9H), 1.21 (m, 6H), 0.81 (m, 2H). ^{13}C NMR (CD_3CN , 175 MHz); 172.9, 163.8, 157.8, 155.8, 155.6, 155.5, 154.3, 141.6, 137.8, 133.8, 129.8, 129.6, 127.5, 127.2, 118.2, 113.0, 49.5, 48.9, 48.30, 44.0, 35.8, 31.2, 23.2, 23.1. HRMS (ESI), m/z : 967.27643 $[\text{M-PF}_6]^+$ ($\text{C}_{42}\text{H}_{48}\text{N}_{12}\text{Ru PF}_6$ requires 967.28047), 411.15951 $[\text{M-2PF}_6]^{2+}$ ($\text{C}_{42}\text{H}_{48}\text{N}_{12}\text{Ru}$ requires 411.15787). Anal. Calc for $\text{C}_{42}\text{H}_{48}\text{N}_{12}\text{Ru}_1\text{P}_2\text{F}_{12}$: C, 45.37; H, 4.35; N, 15.12. Found: C, 45.38; H, 4.38; N, 15.04.

4.5.3. Crystal Structure Determination

Diffraction data were collected on a Bruker SMART 6000 with Montel 200 monochromator, equipped with a rotating anode source for Cu K α radiation. The diffraction quality of the crystals were checked, revealing in some cases poor diffraction with a large amount of diffuse scattering, signaling extensive crystal disorder. Cell refinement and data reduction were done using APEX2.⁵⁰ Absorption corrections were applied using SADABS.⁵¹ Structures were solved by direct methods using SHELXS97 and refined on F^2 by full-matrix least squares using SHELXL97.⁵² All non-hydrogen atoms were refined anisotropically. Hydrogen atoms were refined isotropic on calculated positions using a riding model. For complexes **4-1** and **4-4**, during the refinement of the structure, electron density peaks were located and were believed to be six severely disordered solvated acetone molecules, and a total of one disordered water and eight disordered acetone molecules, respectively (by counting the number of electrons suppressed). All the attempts made to model the solvent molecules were not successful and they were removed using the SQUEEZE routine from PLATON,⁵³ which resulted in a significant improvement of R1 factor by ~3.5% in all the squeezed structures. For compound **4-1**, the highest difference peak is located 1.09 Å from atom F4 and the deepest hole is 0.51 Å from atom F1A. In addition, three peaks of density ~2 to 1 e/Å³ were present essentially due to the quality of the crystal employed, which was the best available, and is believed due to the frequent discrete positional disorder of the freely rotating anions (see .cif file for more details). The structure of **4-2** and **4-4** also showed that the guanidine moiety is positionally disordered over two positions. The disorder was modelled as two components [~0.58:0.42 for **4-2** and ~0.60:0.40 for **4-4**] and refined anisotropically. In complexes **4-1** and **4-4** positional disorders in anion or solvent molecules were observed, and they were resolved in the aforesaid way. Some atomic displacement restraints were applied among the disorder components to model the anion positions in **4-1** but not applicable for the cation structure. Specific parameters of each measurement are located in Table IV-1.

Table IV-1. Crystallographic data for ligand **4-L1**, and complexes **4-1**·[**6**(C₃H₆O)], **4-2**·[C₃H₆O], **4-3**·[C₃H₆O], **4-4**·[**8**(C₃H₆O)]·[H₂O]

	4-L1 ^a	4-1 ·[6 (C ₃ H ₆ O)] ^{b,c}	4-2 ·[C ₃ H ₆ O] ^a	4-2 ·[C ₃ H ₆ O] ^c	4-4 ·[8 (C ₃ H ₆ O)]·[H ₂ O] ^a
Formula	[C ₁₉ H ₂₇ N ₇]	[C ₄₀ H ₄₂ N ₁₀ Ru] [2(PF ₆)] [6(C ₃ H ₆ O)]	[C ₄₁ H ₄₄ N ₁₀ Ru] [2(PF ₆)] [C ₃ H ₆ O]	[C ₃₈ H ₃₉ N ₁₂ BrRu] [2(PF ₆)] [C ₃ H ₆ O]	[C ₄₂ H ₄₈ N ₁₂ Ru] [2(PF ₆)] [8(C ₃ H ₆ O)] [H ₂ O]
Color/form	colorless needle	purple block	purple needle	purple needle	purple plate
<i>T</i> (K); wavelength	200(2); 1.54178	100(2); 1.54178	150(2); 1.54178	100(2); 0.71073	150(2); 1.54178
Crystal System	Monoclinic	Monoclinic	Triclinic	Monoclinic	Monoclinic
Space Group	C2/c	C2/c	P-1	P2(1)/n	P2(1)/c
Unit Cell: <i>a</i> (Å)	16.6894(3)	40.9186(5)	8.5139(2)	8.5505(3)	9.6046(4)
<i>b</i> (Å)	13.1912(2)	12.9990(2)	13.5117(4)	44.2040(14)	32.8531(14)
<i>c</i> (Å)	17.1396(3)	19.2466(2)	21.1951(6)	12.3222(4)	17.3497(8)
α (°)	90	90	96.6310(10)	90	90
β (°)	107.7520(10)	116.1840(10)	94.8820(10)	96.705(2)	94.903(2)
γ (°)	90	90	106.4660(10)	90	90
<i>V</i> (Å ³); <i>Z</i>	3593.67(11); 8	9186.7(2); 8	2304.75(11); 2	4625.5(3); 4	5454.5(4); 4
R1(F); wR(F ²) [I > 4σ(I)]	0.0727; 0.1959	0.0468; 0.1295	0.0345; 0.0946	0.0457; 0.1142	0.0402; 0.1124
R1(F); wR(F ²) (all)	0.0817; 0.2055	0.0472; 0.1299	0.0347; 0.0950	0.0564; 0.1239	0.0407; 0.1129
R _G ; R(int)	0.0277; 0.039	0.0089; 0.0265	0.0214; 0.0374	0.0479; 0.1031	0.0151; 0.0427
GoF(F ²)	1.046	1.038	1.039	1.036	1.045

^aBruker Microstar diffractometer (Platinum 135 CCD Detector, Helios optics and, Kappa goniometer). ^bFrom reference 41e (CCDC 978431). ^cBruker/AXS Smart 6000 (4K) diffractometer (Mirror Montel 200-monochromated Cu K α radiation, FR591 Rotating Anode), Bruker Smart APEX 2, graphite monochromator.

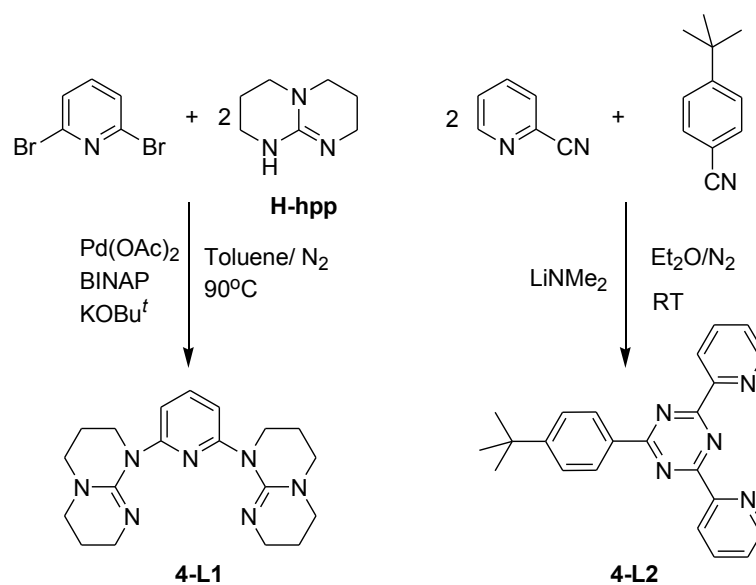
4.5.4. Computational Methods

All calculations were performed with the Gaussian03⁵⁴ employing the DFT method, the Becke three-parameter hybrid functional,⁵⁵ and Lee-Yang-Parr's gradient-corrected correlation functional (B3LYP).⁵⁶ Singlet ground state geometry optimizations for **4-1**²⁺, **4-2**²⁺, **4-3**²⁺ and **4-4**²⁺ were carried out at the (R)B3LYP level in the gas phase, using their respective crystallographic structures as starting points. All elements except Ru were assigned the 6-31G(d,f) basis set.⁵⁷ The LANL2DZ basis set⁵⁸ with an effective core potential and one additional f-type polarization was employed for the Ru atom. Vertical electronic excitations based on (R)B3LYP-optimized geometries were computed for **4-1**²⁺,

4-2²⁺, **4-3²⁺** and **4-4²⁺** using the TD-DFT formalism⁵⁹ in acetonitrile using conductor-like polarizable continuum model (CPCM).⁶⁰ Vibrational frequency calculations were performed to ensure that the optimized geometries represent the local minima and there are only positive eigenvalues. The electronic distribution and localization of the singlet excited states were visualized using the electron density difference maps (ED-DMs).⁶¹ *Gausssum* 2.2 was employed to draw absorption spectra (simulated with Gaussian distribution with a full-width at half maximum (fwhm) set to 3000 cm⁻¹) and to calculate the fractional contributions of various groups to each molecular orbital. All calculated structures were visualized with ChemCraft.⁶²

4.6. Results and Discussion

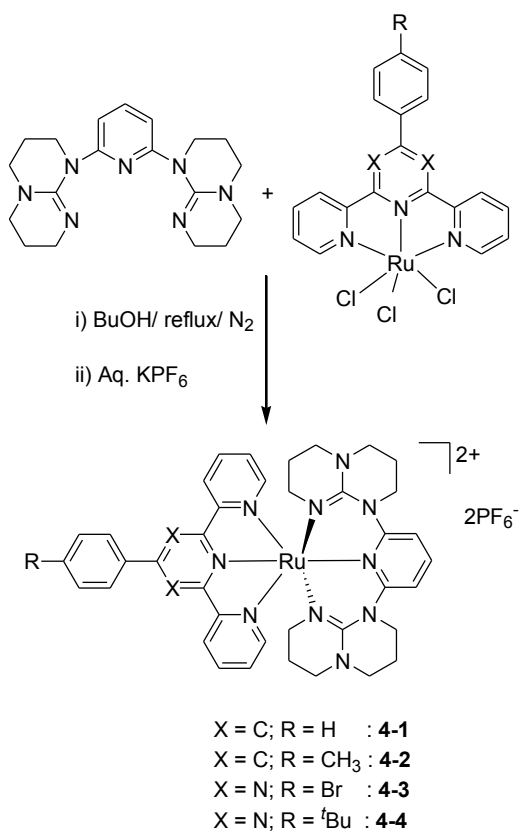
The *N*-heterocyclicguanidyl ligand **4-L1** (2,6-diguanidylpyridine or **dgpy**) (Scheme 4.1) was synthesized by reaction of **H-hpp** with 2,6-dibromopyridine by Pd-catalyzed C–N bond forming reaction following a recently published procedure.^{41d} 1,3,4,6,7,8-Hexahydro-2*H*-pyrimido[1,2- α]pyrimidine (**H-hpp**) and 2,6-dibromopyridine in the molar ratio of 2:1 were reacted in dry toluene under nitrogen atmosphere in presence of Pd(OAc)₂/BINAP (2 mol%) and potassium *tert*-butoxide as a base for 3 h at 90 °C.⁶³ Extraction of the reaction mixture with diethylether:toluene (6:1, v/v) and slow evaporation of the solvent afforded **4-L1** as pale yellow crystalline solid in 80% yield.



Scheme 4.1. Syntheses of the ligands **4-L1** and **4-L2** relevant to the present work.

The ligand 2,4-di(2'-pyridyl)-6-(*p*-*tert*-butylphenyl)-1,3,5-triazine (**4-L2**) was synthesized using modified literature procedure (Scheme 4.1).⁶⁴ The amidinate intermediate generated by the reaction of “*in-situ*” synthesized LiNMe₂ (from HNMe₂ and *n*-BuLi) and *p*-*tert*-butylbenzotrile, could be subsequently cyclized by addition of 2 equivalents of 2-cyanopyridine to afford the tridentate triazine ligand (**4-L2**) as a white solid in good yield.

Ru(II)-heteroleptic complexes were synthesized following the typical procedure available for the synthesis of bis-terpyridyl based Ru(II)-complexes (Scheme 4.2).⁶⁵ The reaction of **4-L1**, with [Ru(Ph-tpy)Cl₃] (Ph-tpy = 4'-phenyl-2,2':6',2''-terpyridine), [Ru(*p*-Tolyl-tpy)Cl₃] (*p*-Tolyl-tpy = 4'-tolyl-2,2':6',2''-terpyridine), [Ru(Br-Ph-dpt)Cl₃] (Br-Ph-dpt = 2,4-di(2'-pyridyl)-6-(*p*-bromo-phenyl)-1,3,5-triazine), [Ru(^tBu-Ph-dpt)Cl₃] (^tBu-Ph-dpt = 2,4-di(2'-pyridyl)-6-(*p*-*tert*-butyl-phenyl)-1,3,5-triazine) in refluxing *n*-butanol, in presence of few drops of 4-ethylmorpholine, provided the complexes **4-1**, **4-2**, **4-3** and **4-4**, respectively, in modest to good yields.



Scheme 4.2. Syntheses of the terpyridine (tpy, **4-1** and **4-2**) and 2,4-dipyrid-2'-yl-triazine (dpt, **4-3** and **4-4**) containing complexes.

The ligands **4-L1**, **4-L2** and complexes **4-1** to **4-4** were characterized by solution NMR spectroscopy, elemental analysis, X-ray crystallography and high-resolution mass spectrometry (HR-MS), UV-vis absorption and emission spectroscopies and electrochemistry. In HR-MS, the most abundant peaks were found to be $[M+H]^+$ and $[M]^{2+}$ for ligands and complexes, respectively.

Multiple unidentified coloured byproducts, as also observed by Hammarström *et al.*,⁴⁴ were always formed, and thus the complexes were purified by column chromatography followed by recrystallization from acetone solutions of **4-1** to **4-4** as purple solids.

4.6.1. NMR Spectroscopy

In solution NMR spectroscopy, incorporation of a heterocycle at the amidine *NH* position of **H-hpp** renders the six annular methylene units in the ligand **4-L1** chemically nonequivalent in contrast to the free **H-hpp** where only three types of methylene groups are perceived. Similar observation was reported by Coles and co-workers for a methylene-linked bis(guanidine) compound, $H_2C\{hpp\}_2$.⁶⁶ The most interesting feature in the 1H NMR spectra of the complexes **4-1** to **4-4** is that the equatorial and axial methylene protons on the saturated aliphatic backbone are different, so that they appear over a wide range of 0–4 ppm integrating to two protons each. They are chemically non-equivalent to the methylene protons of **4-L1**, where only six different methylene proton signals were observed, each integrating for four protons.⁴¹

4.6.2. X-ray Structural Investigation

Slow diffusion of diethyl ether into an acetone solution of **4-1** to **4-4** afforded the best single crystals, whereas crystals of **4-L1** could be grown by slow evaporation of a solution containing **4-L1** in diethyl ether. Ligand **4-L1** and complexes **4-1**, **4-3** and **4-4** crystallize in monoclinic crystal system, whereas complex **4-2** crystallizes in triclinic system. The optimized ground state geometries of **4-1** and **4-2** are in reasonable agreement with the structural data (Table IV-S1 in ESI). The structure of ligand **4-L1** (Figure 4.2) reveals that the guanidine moieties adopt more stable twisted chair conformations instead of higher energy boat conformation. To minimize the lone pair-lone pair repulsions, atoms N1, N4 and N7 adopt *trans* geometry around their respective C-N bonds. The N2-C12 [1.409(3) Å] and N3-C12 [1.383(3) Å] bond distances may suggest that there is

delocalization around N2-C12-N3 core, whereas, N4-C12 seems to be a localized C-N double bond with a distance of 1.278(3) Å. Similar variation in bond lengths were also observed in the other saturated part of **4-L1** [N5-C19 (1.409(3) Å), N6-C19 (1.388(3) Å), N7-C19 (1.260(3) Å)]. Extensive non-aromatic weak C-H hydrogen bonding interactions among the saturated aliphatic backbone play an important role in the solid-state packing of molecule **4-L1** to furnish a 2D- zigzag array (see Figure 4.S1 in ESI).

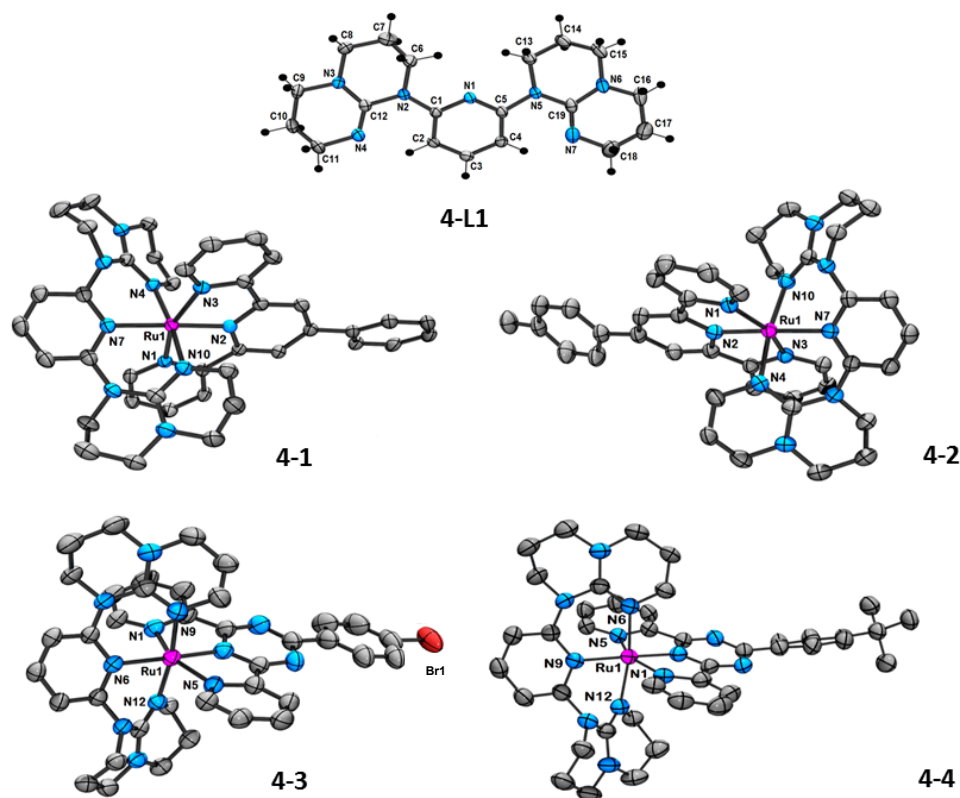


Figure 4.2. ORTEP views of the X-ray crystal structures of (top), (center-left), (center-right), **4-3** (bottom-left) and **4-4** (bottom-right) (50% probability displacement ellipsoids; anion, solvent, any other chemically equivalent molecule and any disordered part(s) in aliphatic backbone of complexes have been removed for clarity).

The structures of **1-4** (Figure 4.2) reveal coordinatively saturated ruthenium ions in a distorted octahedral geometry, where the two tridentate ligands coordinate in a meridional fashion. Selected bond lengths and angles are in good agreement with the values obtained from DFT calculations of respective complexes (Table IV-S1 in ESI). The origin of distortion from regular octahedron in these complexes is due to the smaller bite angles subtended to the metal center by the two tridentate ligands. The N-Ru-N angles generated

by Ph-tpy [$159.28(10)^\circ$] and Toly-tpy [$158.89(8)^\circ$] in complexes **4-1** and **4-2** are similar to the observed average bite angles in homoleptic $\text{Ru}(\text{Ph-tpy})_2^{2+}$ [$158.07(15)^\circ$]⁶⁷ and $\text{Ru}(\text{Toly-tpy})_2^{2+}$ [$157.49(16)^\circ$],⁶⁸ respectively. The ligand **4-L1** exhibits N-Ru-N angles near $\sim 173^\circ$ [$\text{N4-Ru1-N10} = 173.83(10)^\circ$ and $172.68(7)^\circ$ in **4-1** and **4-2**, respectively], which are very close to ideal octahedral angle of 180° . This is a significant improvement over the non-ideal value of 158.2° , exhibited by tpy in prototype⁶⁹ $\text{Ru}(\text{tpy})_2^{2+}$, suggesting a successful design strategy. Both complexes display regular Ru-N bond distances, the shortest Ru-N bonds consisting the N-atom of the central pyridyl unit in tpy core [$\text{Ru1-N2} = 1.946(2) \text{ \AA}$ and $1.931(2) \text{ \AA}$ in **4-1** and **4-2**, respectively], while the longest are the bonds from the **hpp** units [$\text{Ru1-N10} = 2.092(3) \text{ \AA}$ and $\text{Ru1-N4} = 2.095(2) \text{ \AA}$ in **4-1** and **4-2**, respectively]. In both the complexes, a twisted structure of the ligand **4-L1** is observed, where the dihedral angles between the mean plane containing central pyridine ring and that of **hpp** units are in an average 43° (in **4-1**) and 35° (in **4-2**), which render **4-L1** to adopt helical arrangement (Λ or Δ) around the Ru-atom.

Complexes **4-3** and **4-4** are essentially isostructural with **4-1** and **4-2**. The shortest Ru-N bonds consisting the nitrogen of the central triazine unit [$\text{Ru1-N2} = 1.925(3)$ in **4-3** and $1.930(2)$ in **4-4**]. The N1-Ru1-N5 angles of the dpt unit [$= 157.11(11)^\circ$ in **4-3** and $156.29(9)^\circ$ in **4-4**] are similar to what is found in dpt-Ru-dpt homoleptic complexes [$\text{N-Ru-N} = 155.45(19)^\circ$].⁷⁰ Similarly to complexes **4-1** and **4-2**, N-Ru-N angles of **4-L1** in **4-3** and **4-4** expand up to $\sim 172^\circ$ [$\text{N9-Ru1-N12} = 172.14(11)^\circ$ in **4-3** and $\text{N6-Ru1-N12} = 171.02(8)^\circ$ in **4-4**], which should help to increase their ligand field effects and, therefore, the $^3\text{MLCT}-^3\text{MC}$ energy-gap.

4.6.3. Electrochemistry

The electrochemical behavior of the complexes has been examined by cyclic voltammetry using a glassy carbon electrode in purified acetonitrile under a dry argon atmosphere. At positive potentials, vs. saturated calomel electrode (SCE), complex **4-1** shows a quasi-reversible Ru(III/II) couple at 0.50 V with a peak-to-peak separation (ΔE_p) of 95 mV (Figure 4.3, Table IV-2). This is nearly 0.80 V less positive than that observed for the same Ru(III/II) couple in $[\text{Ru}(\text{tpy})_2]^{2+}$ which appears at 1.31 V vs. SCE,⁷¹ indicating that **4-L1** is a much stronger donor than tpy. Complex **4-2** shows a quasi-reversible Ru(III/II) couple at even lower potential, 0.46 V vs. SCE. The lowering by 40 mV in the

corresponding oxidation potentials between complex **4-1** and **4-2** is due to minor destabilization of the metal-based highest-occupied molecular orbital (HOMO) by more electron-donating *p*-Tolyl-tpy in place of Ph-tpy, which is supported by DTF calculations ($E_{\text{HOMO}} = -5.37$ eV and -5.34 eV in **4-1** and **4-2**, respectively) (see Figure 4.4 for population analyses). The Ru(III/II) couples for **4-1** and **4-2** are more similar to the values obtained for the cyclometallated complex $[\text{Ru}(\text{tpy})(1,3\text{-di}(2\text{-pyridyl})\text{benzene})]^+$ and its derivatives.^{72,73} The Ru(III/II) couple for $[\text{Ru}(\text{tpy})(1,3\text{-di}(2\text{-pyridyl})\text{benzene})]^+$ appears at 0.51 V vs. SCE,⁷² which indicates that the donor capacity of **4-L1** is similar to that of a cyclometallating anionic ligands. At negative potentials, complexes **4-1** and **4-2** display two quasi-reversible ligand-based reduction peaks. The more electron-rich metal center in **4-1** and **4-2** compared to that of $[\text{Ru}(\text{tpy})_2]^{2+}$ increases back-donation to both ligands and accordingly shifts the ligand-based reduction to more negative potentials, albeit to a lesser extent than that observed for the oxidation couple. Such observations were previously reported by several groups.^{41,72} The first reduction peak for complex **4-1** is centered at -1.47 V while that for complex **4-2** is at -1.52 V. Both these reduction peaks are tpy-based, which is also suggested by their respective DFT calculations in which a minor destabilization of the tpy-based lowest unoccupied molecular orbital (LUMO) of **4-1** ($E_{\text{LUMO}} = -2.46$ eV) compared to that of **4-2** ($E_{\text{LUMO}} = -2.45$ eV) is found. The second reduction peak for **4-1** had a potential of -2.01 V whereas that for **4-2** is centred at -2.05 V. The LUMO+1 for both the complexes are located principally on the respective tpy units. Thus, in a very coarse approximation, the second quasi-reversible reductions in **4-1** and **4-2** may also be assigned to tpy-based reductions, especially when no ligand-based reduction is observed in free **4-L1** within a potential range of 0 to -2 V, although more detailed calculations are necessary to confirm this assignment.

The electrochemical studies of the 2,4-dipyrid-2'-yl-triazine (dpt) complexes **4-3** and **4-4** also show similar trends. The Ru(III/II) couple appears at 0.71 and 0.67 V vs. SCE for **3** and **4-4**, respectively. These more positive values as compared to **4-1** and **4-2** are due to the replacement of the terpyridines with more π -accepting triazines, which reduces the electron density at the metal center. It is noteworthy that the Ru(III/II) couples for **4-3** and **4-4** are more than 0.7 V less positive than the corresponding couple in tpy-Ru-dpt heteroleptic complexes.⁷⁰ The back π -donation effect is also evident in case of **4-3** and **4-4**. The first reduction, which is triazine based, appears at -0.92 V, while it is observed at -0.97

V vs. SCE for **4-4**. These values are nearly 0.2 V more negative than the corresponding tpy-Ru-dpt heteroleptic complexes.⁷⁰

The above results clearly indicate that **4-L1** is a stronger σ -donor than the classical polypyridine tridentate ligands. The σ -donor ability is also comparable to cyclometallating ligands, a property which is very beneficial to destabilize the ³MC state.

Table IV-2. Electrochemical data of ligand **4-L1**, Ru(II) complexes **4-1** to **4-4** and some benchmark complexes.

Compound	$E_{1/2}(\text{ox})^a$	$E_{1/2}(\text{red})^a$	$\Delta E_{1/2}^b$
4-L1	1.11 (308), 0.77 (irr) ^c	-----	-----
4-1	0.50 (94)	-1.47 (70), -2.01 (84)	1.97
4-2	0.46 (95)	-1.52 (77), -2.05 (83)	1.98
4-3	0.71 (82)	-0.92 (72), -1.72 (irr)	1.63
4-4	0.67 (85)	-0.97 (63), -1.70 (90)	1.64
[Ru(tpy) ₂] ^{2+d}	1.31 (60)	-1.23 (70), -1.47 (69)	2.54
[Ru(<i>p</i> -Tolyl-tpy) ₂] ^{2+e}	1.20 (69)	-1.29 (66), -1.53 (74)	2.49
[Ru(Ph-tpy) ₂] ^{2+f}	1.29	-1.26	2.55
[Ru(tpy)(N [^] C [^] N)] ^{+g}	0.51	-1.55	2.06
[Ru(tpy)(Br-Ph-trz)] ^{2+h}	1.43	-0.75	2.18

^aPotentials are in volts vs. SCE for acetonitrile solutions, 0.1 M in tetrabutylammonium hexafluorophosphate, under a dry argon atmosphere at a glassy carbon electrode, recorded at 25 ± 1 °C at a sweep rate of 100 mV/s with solute concentrations of **4-1** and **4-2**, 1.01 mM; **4-3**, 1.03 mM; **4-4**, 1.02 mM. The difference between cathodic and anodic peak potentials (millivolts) is given in parentheses. ^b $\Delta E_{1/2}$ is the difference (in V) between first oxidation and first reduction potentials. ^cIrreversible; potential is given for the anodic wave. ^dFrom ref 71a, ^efrom ref 71c, ^ffrom ref 16a, ^gfrom ref 72, ^hfrom ref 70.

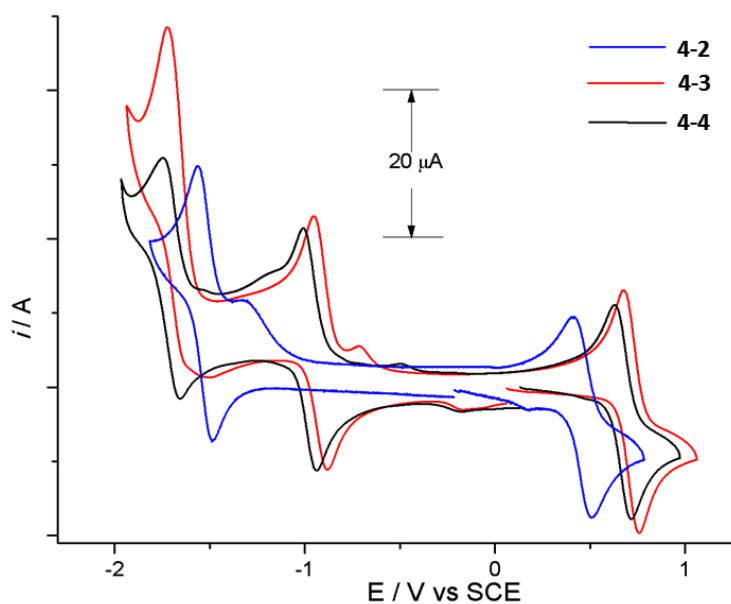


Figure 4.3. Cyclic voltammogram of the complexes **4-2** (blue), **4-3** (red) and **4-4** (black) in dry degassed acetonitrile.

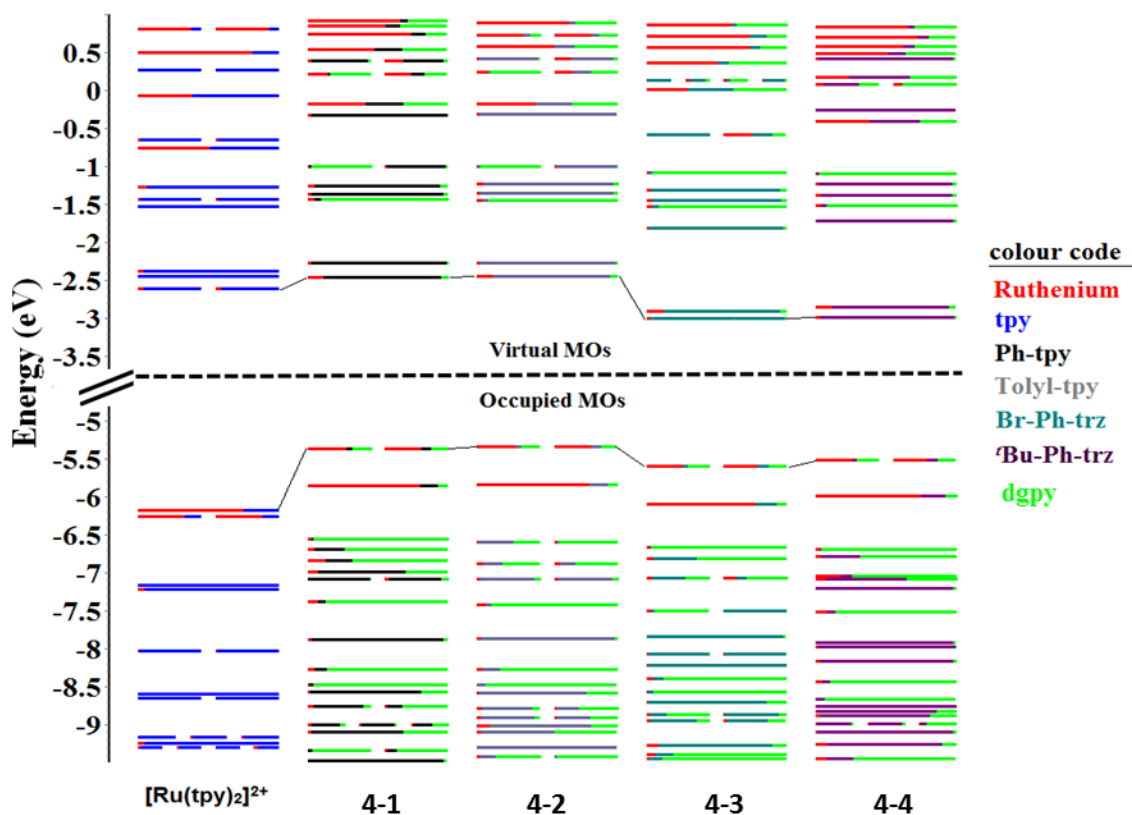


Figure 4.4. Calculated frontier MO energies of the modeled **4-1** to **4-4** with $[\text{Ru}(\text{tpy})_2]^{2+}$ obtained by DFT($\text{rb3lyp}/\text{LanL2DZ}(\text{f})[\text{Ru}]/6\text{-}31\text{G}^{**}[\text{NCN}]$) calculation with CPCM(CH_3CN) and 0.05 eV of threshold of degeneracy.

4.6.4. UV-vis absorption and emission behavior

The UV-vis spectra of **4-1** and **4-2** in acetonitrile solution display $^1\text{MLCT}$ bands in the 500-650 nm regions. The UV part of the spectra is dominated by the $\pi \rightarrow \pi^*$ transitions in the ligand moieties centered around 220-320 nm for both **4-1** and **4-2** (see Table IV-S2 in ESI). The most noticeable feature in the visible region is that the $^1\text{MLCT}$ maxima is red-shifted (148 nm) with respect to that of $\text{Ru}(\text{tpy})_2^{2+}$ for both complexes.⁷⁴ As discussed above, ligand **4-L1** being a stronger donor than tpy, it is expected to interact with the t_2 [d(Ru)] orbitals of ruthenium more strongly than does tpy. Thus the metal based t_2 orbitals will be at higher energy, i.e. the HOMO will be raised. A minor, but noticeable, change due to the change in tpy backbone from phenyl (in **4-1**) to the more electron-donating tolyl group (in **4-2**) can also be observed, as supported by DFT calculations (Figure 4.4 and Tables S3 and S5 in ESI). On the other hand, the LUMO is still tpy-based as revealed by the first reduction potentials of **4-1** and **4-2** and DFT calculations. This fact results in the lowering of the energy of the $d\pi \rightarrow \pi^*$ $^1\text{MLCT}$ transition and hence the observed red shift. Moreover, the complexes exhibit an additional band at approximately 380 nm between the $^1\text{MLCT}$ transition and the first $\pi \rightarrow \pi^*$ transition. Its assignment, though discussed in the literature, is still controversial, and different authors have proposed a metal centered d-d transition,⁷⁵ which borrows intensity from a close-lying allowed transition or to a second $^1\text{MLCT}$ or to $^1\text{LMCT}$ transition.⁷⁶ However, TD-DFT calculations of the complexes suggest that this band is a mixture, predominantly of $^1\text{MLCT}$ origin with minor involvement of a LC transition (see Tables S4, S6, S8 and S10 in ESI).⁴¹ It may be noted that such a band near 345 nm is usually observed for $\text{RuN}_4(\text{diamine})^{2+}$ chromophores.⁷⁷

Complexes **4-3** and **4-4** also exhibit similar ligand $\pi \rightarrow \pi^*$ transitions in the UV region centered on 244 and 290 nm for both the complexes. In the visible region both **4-3** and **4-4** absorb in the 500-800 nm region with maxima around 560 nm and 740 nm. The lowest energy absorption maxima are notably red-shifted by approximately 264 nm and 250 nm, respectively, with respect to those of tpy-Ru-dpt heteroleptic complexes or even homoleptic dpt-Ru-dpt complexes.⁷⁰ Such a red shift is in accordance with the aforesaid destabilization of the metal-based orbitals (HOMO) by the strongly donating **4-L1**. The LUMO being triazine-based is now even lower in energy than in **4-1** or **4-2**, which results in a smaller HOMO-LUMO gap. In addition to these bands, both **4-3** and **4-4** absorb around 415 nm, which may be a transition similar to that found in case of **4-1** and **4-2** at

380 nm. A red-shift in these bands occurs in going from terpyridine to 2,4-dipyrid-2'-yl-triazine complexes, which may be indicative of its nature as a second MLCT transition, suggesting that the ligand-based π^* orbitals are now so low in energy that a transition from HOMO to LUMO+1 is also lowered in energy as compared to tpy-Ru-tpy type complexes.

Table IV-3. Electronic absorption data in dry, deaerated CH_3CN solutions of ligands **4-L1**, **4-L2**, complexes **4-1** to **4-4** and some benchmark complexes.

Compound	λ_{max} , nm ($\epsilon \times 10^3$, $\text{M}^{-1}\text{cm}^{-1}$)
4-L1	228 (29.0), 311 (12.8)
4-L2	245 (9.7), 285 (20.9)
4-1	225 (26.2), 244 (22.6), 289 (26.9), 317 (13.3), 379 (6.1), 541 (5.0), 622 (3.3)
4-2	225 (44.8), 247 (39.7), 288 (45.1), 313 (27.9), 383 (11.3), 538 (9.4), 620 (6.2)
4-3	244 (33.3), 291 (35.3), 380 (7.0), 411 (8.6), 560 (11.8), 740 (3.8)
4-4	243(29.1), 288(27.8), 373(6.7), 405(7.0), 558(9.3), 740(3.0)
$[\text{Ru}(\text{tpy})_2]^{2+a}$	270 (40.9), 307 (66.7), 475 (15.3)
$[\text{Ru}(\text{Br-Ph-Trz})(\text{tpy})]^{2+b}$	282 (53.5), 301 (59.6), 476 (21.7)
$[\text{Ru}(\text{Br-Ph-Trz})_2]^{2+b}$	279 (50.9), 295 (50.6), 491 (27.5)

^aFrom ref 74, ^bfrom ref 70.

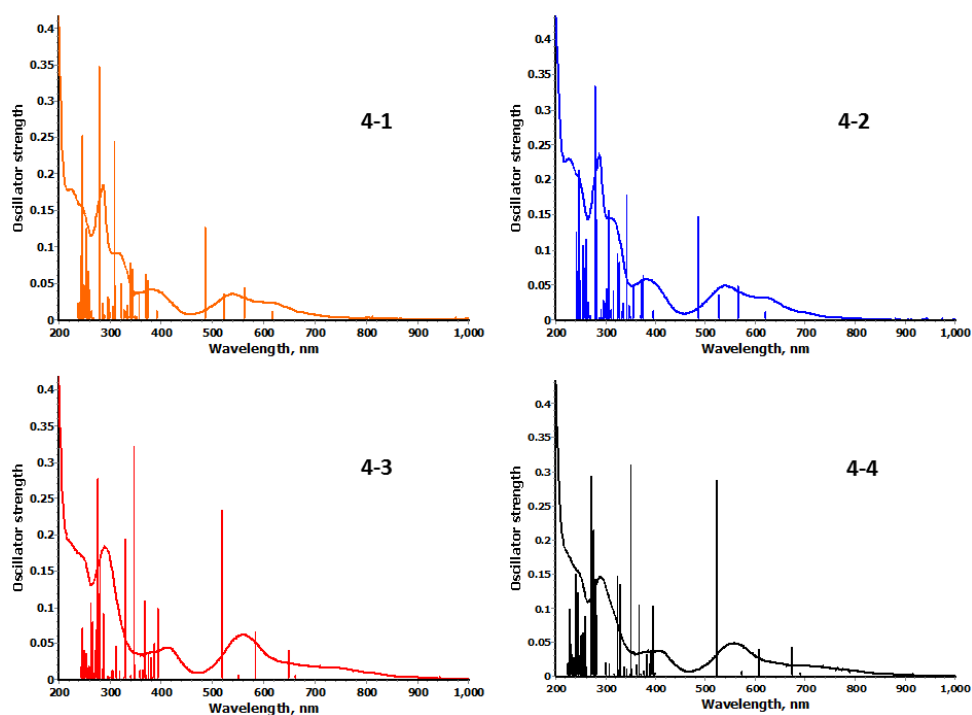


Figure 4.5. Overlay of experimental absorption spectra of the complexes **4-1** (orange), **4-2** (blue), **4-3** (red) and **4-4** (black) in acetonitrile with their predicted transitions and oscillator strength, calculated by TD-DFT.

The luminescence properties of the complexes were studied in dry, degassed acetonitrile at room temperature. The corrected emission spectra maxima (λ_{max}) along with lifetime (τ), quantum yield (Φ), and excited-state radiative (k_r) and non-radiative (k_{nr}) decay values are reported in Table 3, while representative emission spectra are shown in Figure 4.6. Complexes **4-1** and **4-2** exhibit room temperature luminescence in degassed acetonitrile at around 900 nm. As expected, with increased σ -donation the emission wavelength is red-shifted upon introduction of **4-L1** in place of a terpyridine ligand in $[\text{Ru}(\text{Ph-tpy})_2]^{2+}$ and $[\text{Ru}(p\text{-Tolyl-tpy})_2]^{2+}$, whereas the emission maxima for the latter two are observed at 715 and 640 nm, respectively. Complexes **4-3** and **4-4** are non-luminescent at room temperature, while they were found to be very weakly luminescent at 77 K in rigid butyronitrile matrix. For complexes **4-1** and **4-2**, luminescence energy and the blue-shift of the emission on moving from room temperature fluid solution to 77 K rigid matrix, clearly indicate that luminescence originates from the (formally) triplet MLCT state involving substituted tpy ligands, as expected. The red-shift of the Ru-to-substituted-tpy/dpt CT emission for all of the studied complexes in comparison to $[\text{Ru}(\text{ttpy})_2]^{2+}$ is due to the narrower HOMO–LUMO energy gaps calculated for $[\mathbf{4-1}]^{2+}$ (2.91 eV), $[\mathbf{4-2}]^{2+}$ (2.89 eV), $[\mathbf{4-3}]^{2+}$ (2.59 eV) and $[\mathbf{4-4}]^{2+}$ (2.52 eV) in comparison to that of $[\text{Ru}(\text{tpy})_2]^{2+}$ (3.58 eV),⁷⁸ thereby confirming the agreement among redox, TD-DFT, absorption and emission data.

The details of the emission behavior can better be understood by recalling the effect of the nonradiative decay rate constant (k_{nr}), which is an added sum of two contributing factors, k_{nr}^0 and k_{nr}^{\dagger} . The former is related to the direct deactivation from $^3\text{MLCT}$ to the ground-state, whereas the latter is related to the thermally activated process that takes into account a surface crossing from the lowest-lying $^3\text{MLCT}$ state to a closely lying metal-centered (^3MC) level (i.e., the so-called TAIC process in Figure 4.1). In general, for Ru(II)-polypyridyl complexes with tridentate ligands the higher values of k_{nr} (Table 3) at 298 K are predominantly contributed by k_{nr}^{\dagger} . This fact is a consequence with the lower ligand-field strength experienced by the metal center as compared to that in Ru(II)-complexes with bidentate polypyridyl ligands, due to larger deviation from octahedral geometry. The lower values of k_{nr} in complexes **4-1** and **4-2**, compared to that of the benchmark complexes, clearly indicates enhanced $^3\text{MLCT}$ – ^3MC energy gap, thus allowing complexes **4-1** and **4-2** to exhibit much longer r.t. excited-state lifetime. The non-luminescent nature of complexes **4-3** and **4-4** may be explained by enhanced k_{nr}^0 , assuming the energy of the ^3MC state

remaining roughly constant among complexes **4-1** to **4-4**, due to the presence of equal number of σ -donating **hpp** units throughout the series (indeed, the MC level is expected to slightly decrease in energy on passing from **4-1** and **4-2** to **4-3** and **4-4**). The stabilization of the $^1\text{MLCT}$ and consequently the $^3\text{MLCT}$ state is achieved by introduction of a better π -accepting triazine core in dpt unit in place of the central pyridine ring in a tpy unit, thereby lowering the energy of metal-based HOMO (Figure 4.4). This fact is supported by a red-shift of $^1\text{MLCT}$ absorption and $^3\text{MLCT}$ emission maxima of complexes **4-3** and **4-4** compared to that of **4-1** and **4-2** at 77 K, respectively. The increased stabilization of $^3\text{MLCT}$ states of complexes **4-3** and **4-4** in turn facilitates a direct deactivation to the ground-state, thus rendering them non-luminescent at r.t. However at low temperature the rate of this deactivation is decreased. The effect of dipolar interactions of the heteroatom lone-pair of the dpt core in complexes **4-3** and **4-4** with the solvent in quenching the r.t. luminescence may not be excluded either.

Table IV-4. Photophysical data complexes **4-1** to **4-4** and some benchmark complexes.

compound	Absorption	Emission @298 K					Emission @77 K
	λ_{max} , nm ($\epsilon \times 10^3$, $\text{M}^{-1}\text{cm}^{-1}$)	λ_{max} nm	τ ns	$10^{-4}\Phi$	$10^4 k_r$ (s^{-1})	$10^6 k_{\text{nr}}$ (s^{-1})	λ_{max} nm
4-1	541 (5.0) 622 (3.3)	901	129	10	0.77	7.74	840
4-2	538 (9.4) 620 (6.2)	900	89	20	2.25	11.21	840
4-3	560 (11.8) 740 (3.8)	-----	-----	-----	-----	-----	935
4-4	558 (9.3) 740 (3.0)	-----	-----	-----	-----	-----	965
Ru(tpy) $_2^{2+}$	474 (10.4) ^a	629 ^a	0.25 ^b	$\leq 0.05^a$	2.0	3999.9	598
Ru(<i>p</i> -Tolyl-tpy) $_2^{2+}$	490 (28.0) ^c	640	0.95	0.32	3.36	1052.6	628 ^d
Ru(Ph-tpy) $_2^{2+}$	488 (26.2) ^a	715 ^a	1.0 ^a	0.40 ^a	4.0	999.9	629
Ru(tpy)(N [^] C [^] N) ⁺	499 (14.4) ^e	781 ^e	--- ^f	0.09 ^e	--- ^f	--- ^f	--- ^f
Ru(tpy)(Br-Ph-trz) $_2^{2+}$	476 (21.7) ^g	739 ^g	12 ^g	1.2 ^g	1.0	83.3	693

^afrom ref 16a (using Ru(bpy) $_3$ (PF $_6$) $_2$ ($\Phi = 0.028$) as standard); ^bfrom ref 16b; ^cfrom ref 16d; ^dfrom ref 16d, at 90 K; ^efrom ref 72 (using Ru(bpy) $_3$ (PF $_6$) $_2$ ($\Phi = 0.062$) as standard); ^fno data available; ^gfrom ref 70 (using [Ru(μ -2,3-dpp) $_2$] $_3$ Ru $^{8+}$ ($\Phi = 0.005$) (2,3-dpp = 2,3-bis(2'-pyridyl)-pyrazine) as standard).

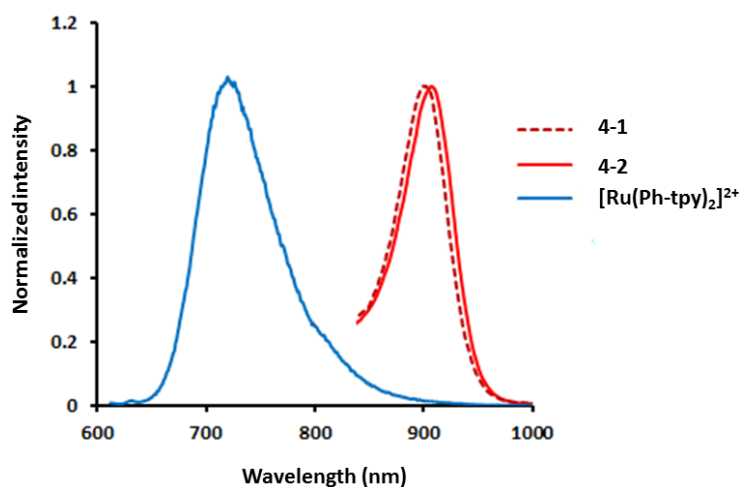


Figure 4.6. Normalized emission spectra of complexes **4-1**, **4-2** and benchmark complex $[\text{Ru}(\text{Ph-tpy})_2]^{2+}$ in dry, degassed acetonitrile at room temperature.

4.7. Conclusion

In conclusion, we synthesized a N_{amine} -substituted 2,6-diguanidyl-pyridine tridentate ligand, **4-L1**, that can coordinate to a ruthenium(II) center forming two six-membered chelate rings, and prepared four heteroleptic Ru(II) complexes (**4-1** to **4-4**) using **4-L1** in connection with four different tridentate ligands. From the Ru(III/II) oxidation potentials of the new complexes, it is found that ligand **4-L1** has strong σ -donating ability as compared to common polypyridyl tridentate ligands. In particular, the redox behavior of **4-1** to **4-4** suggest that **4-L1** has similar electron donating capacity as the cyclometallating ligand 1,3-di(2-pyridyl)benzene ($\text{N}^{\wedge}\text{C}^{\wedge}\text{N}$). As a result of strong σ donation from ligand **4-L1**, complexes **4-1** to **4-4** have $^1\text{MLCT}$ absorption bands in the visible region at significantly lower energy as compared to $[\text{Ru}(\text{tpy})_2]^{2+}$. The $^1\text{MLCT}$ absorption maxima of complexes **4-3** and **4-4** trail to far-red region of the electromagnetic spectrum. Complexes **4-1** to **4-4** emit at 77 K from a Ru^{II} -to-tridentate-ligand $^3\text{MLCT}$ state in the near-infrared region; these emissions are among the lowest energy $^3\text{MLCT}$ luminescence considering mononuclear ruthenium complexes in octahedrally coordinated by six nitrogen atoms. Complexes **4-1** and **4-2** also exhibit room temperature excited-state lifetimes (τ) of 129 ns and 89 ns, with associated quantum yield (Φ) of 0.001. Such emission lifetimes and quantum yields are longer and higher, respectively, in comparison with those reported by other Ru(II) compounds exhibiting emission at similar energies, and are considered to be due to a very large MLCT-MC energy gap. Thus, the excellent electrochemical and photophysical

properties of these complexes, in particular their somewhat unusual long-lived and relatively intense emission in the NIR region, may render them useful for vectorial electron and energy transfer processes in solution or at semiconductor interfaces and also in biological applications as luminescent sensors in cell-imaging systems.

4.8. Supporting Information

Extra figures, tables, computational data, and X-ray data in CIF format. This material is available free of charge via the Internet at <http://pubs.acs.org>. X-ray crystallographic data in CIF format can be obtained from the Cambridge Structural Database (CCDC 988217, 978431, 988218-988220).

4.9. References

- (1) See, for example: (a) Hagfeldt, A.; Graetzel, M. *Chem. Rev.* **1995**, *95*, 49. (b) Sun, L. C.; Hammarström, L.; Åkermark, B.; Styring, S. *Chem. Soc. Rev.* **2001**, *30*, 36. (c) Vos, J. G.; Kelly, J. M. *Dalton Trans.* **2006**, 4869. (d) Arlo, S.; Meyer, G. J. *Chem. Soc. Rev.* **2009**, *38*, 115 and references therein. (e) Concepcion, J. J.; Jurss, J. W.; Brennaman, M. K.; Hoertz, P. G.; Patrocínio, A. O. T.; Iha, N. Y. M.; Templeton, J. L.; Meyer, T. J. *Acc. Chem. Res.* **2009**, *42*, 1954. (f) Chen, Z. F.; Concepcion, J. J.; Hu, X. Q.; Yang, W. T.; Hoertz, P. G.; Meyer, T. J. *Proc. Natl. Acad. Sci. U.S.A.* **2010**, *107*, 7225. (g) Puntoriero, F.; Sartorel, A.; Orlandi, M.; La Ganga, G.; Serroni, S.; Bonchio, M.; Scandola, F.; Campagna, S. *Coord. Chem. Rev.*, **2011**, *255*, 2594 and references therein. (h) P. G. Bomben, K. C. D. Robson, B. D. Koivisto, C. P. Berlinguette, *Coord. Chem. Rev.* **2012**, *256*, 1438 and references cited therein. (i) Swierk, J. R.; Mallouk, T. E. *Chem. Soc. Rev.* **2013**, *42*, 2357.
- (2) Gill, M. R.; Garcia-Lara, J.; Foster, S. J.; Smythe, C.; Battaglia, G.; Thomas, J. A. *Nat. Chem.* **2009**, *1*, 662.
- (3) (a) Bolink, H. J.; Cappelli, L.; Coronado, E.; Gavina, P. *Inorg. Chem.* **2005**, *44*, 5966. (b) Bolink, H. J.; Cappelli, L.; Coronado, E.; Graetzel, M.; Nazeeruddin, M. K. *J. Am. Chem. Soc.* **2006**, *128*, 46.
- (4) Meyer, T. J. *Pure Appl. Chem.* **1986**, *58*, 1193–1206. (b) Thompson, D. W.; Ito, A.; Meyer, T. J. *Pure Appl. Chem.* **2013**, *85*, 1257.
- (5) Juris, A.; Balzani, V.; Barigelletti, F.; Campagna, S.; Belser, P.; von Zelewsky, A. *Coord. Chem. Rev.* **1988**, *84*, 85–277. (b) Balzani, V.; Juris, A.; Venturi, M.; Campagna, S.; Serroni, S. *Chem. Rev.* **1996**, *96*, 759–834.
- (6) Sauvage, J.-P.; Collin, J. P.; Chambron, J. C.; Guillerez, S.; Coudret, C.; Balzani, V.; Barigelletti, F.; De Cola, L.; Flamigni, L. *Chem. Rev.* **1994**, *94*, 993–1019.
- (7) Baranoff, E.; Collin, J. P.; Flamigni, L.; Sauvage, J.-P. *Chem. Soc. Rev.* **2004**, *33*, 147–155.
- (8) Baitalik, S.; Wang, X.; Schmehl, R. H. *J. Am. Chem. Soc.* **2004**, *126*, 16304–16305.

- (9) (a) Bhaumik, C.; Saha, D.; Das, S.; Baitalik, S. *Inorg. Chem.* **2011**, *50*, 12586; (b) Fortage, J.; Dupeyre, G.; Tuyèras, F.; Marvaud, V.; Ochsenbein, P.; Ciofini, I.; Hromadová, M.; Pospíšil, L.; Arrigo, A.; Trovato, E.; Puntoriero, F.; Lainé, P. P. and Campagna, S. *Inorg. Chem.*, **2013**, *52*, 11944.
- (10) Jäger, M.; Smeigh, A.; Lombeck, F.; Görls, H.; Collin, J.-P.; Sauvage, J.-P.; Hammarström, L.; Johansson O. *Inorg. Chem.* **2010**, *49*, 374.
- (11) Constable, E. C. *Chem. Soc. Rev.* **2004**, *33*, 246–253.
- (12) Hofmeier, H.; Schubert, U. S. *Chem. Soc. Rev.* **2004**, *33*, 373–399.
- (13) (a) Medlycott, E. A.; Hanan, G. S. *Coord. Chem. Rev.* **2006**, *250*, 1763–1782. (b) Medlycott, E. A.; Hanan, G. S. *Chem. Soc. Rev.* **2005**, *34*, 133–142.
- (14) Wang, X.-Y.; Del Guerzo, A.; Schmehl, R. H. *J. Photochem. Photobiol. C* **2004**, *5*, 55–77.
- (15) Baba, A. I.; Shaw, J. R.; Simon, J. A.; Thummel, R. P.; Schmehl, R. H. *Coord. Chem. Rev.* **1998**, *171*, 43–59.
- (16) (a) Maestri, M.; Armaroli, N.; Balzani, V.; Constable, E. C.; Thompson, A. *Inorg. Chem.* **1995**, *34*, 2759–2767; (b) Beley, M.; Collin, J. P.; Sauvage, J. P.; Sugihara, H.; Heisel, F.; Mische, A. *J. Chem. Soc., Dalton Trans.*, **1991**, 315. (c) Davidson, G. J. E.; Loeb, S. J.; Passaniti, P.; Silvi, S. and Credi, A. *Chem. Eur. J.* **2006**, *12*, 3233; (d) Collin, J. P.; Guillerez, S.; Sauvage, J. P.; Barigelletti, F.; De Cola, L.; Flamigni, L.; Balzani, V. *Inorg. Chem.* **1991**, *30*, 4230.
- (17) Winkler, J. R.; Netzel, T.; Creutz, C.; Sutin, N. *J. Am. Chem. Soc.* **1987**, *109*, 2381.
- (18) Calvert, J. M.; Caspar, J. V.; Binstead, R. A.; Westmoreland, T. D.; Meyer, T. J. *J. Am. Chem. Soc.* **1982**, *104*, 6620.
- (19) (a) Wang, J. H.; Fang, Y. Q.; Hanan, G. S.; Loiseau, F.; Campagna, S. *Inorg. Chem.* **2005**, *44*, 5–7. (b) Constable, E. C.; Cargill Thompson, A. M. W.; Armaroli, N.; Balzani, V.; Maestri, M. *Polyhedron* **1992**, *11*, 2707–2709.
- (20) Polson, M. I. J.; Loiseau, F.; Campagna, S.; Hanan, G. S. *Chem. Commun.* **2006**, 1301–1303.
- (21) Fang, Y.-Q.; Taylor, N. J.; Laverdiere, F.; Hanan, G. S.; Loiseau, F.; Nastasi, F.; Campagna, S.; Nierengarten, H.; Leize-Wagner, E.; Van Dorsselaer, A. *Inorg. Chem.* **2007**, *46*, 2854.
- (22) Fang, Y.-Q.; Taylor, N. J.; Hanan, G. S.; Loiseau, F.; Passalacqua, R.; Campagna, S.; Nierengarten, H.; Van Dorsselaer, A. *J. Am. Chem. Soc.* **2002**, *124*, 7912.
- (23) Encinas, S.; Flamigni, L.; Barigelletti, F.; Constable, E. C.; Housecroft, C. E.; Schofield, E. R.; Figgemeier, E.; Fenske, D.; Neuburger, M.; Vos, J. G.; Zehnder, M. *Chem. Eur. J.* **2002**, *8*, 137–150.
- (24) (a) Hissler, M.; El-ghayoury, A.; Harriman, A.; Ziessel, R. *Angew. Chem., Int. Ed.* **1998**, *37*, 1717–1720; (b) Barbieri, A.; Ventura, B.; Ziessel, R. *Coord. Chem. Rev.* **2012**, *256*, 1732 and references cited therein; (c) Manca, P.; Pilo, M. I.; Sanna, G.; Zucca, A.; Bergamini, G. and Ceroni, P. *Chem. Commun.* **2011**, *47*, 3413.
- (25) Passalacqua, R.; Loiseau, F.; Campagna, S.; Fang, Y.-Q.; Hanan, G. S. *Angew. Chem., Int. Ed.* **2003**, *42*, 1608.

- (26) Wang, J.; Hanan, G. S.; Loiseau, F.; Campagna, S. *Chem. Commun.* **2004**, 2068.
- (27) Wang, J.; Fang, Y.-Q.; Bourget-Merle, L.; Polson, M. I. J.; Hanan, G. S.; Juris, A.; Loiseau, F.; Campagna, S. *Chem. Eur. J.* **2006**, *12*, 8539.
- (28) (a) McClenaghan, N. D.; Leydet, Y.; Maubert, B.; Indelli, M. T.; Campagna, S. *Coord. Chem. Rev.* **2005**, *249*, 1336–1350; (b) Ragazzon, G.; Verwilt, P.; Denisov, S. A.; Credi, A.; Jonusauskas, G.; McClenaghan, N. D. *Chem. Commun.* **2013**, *49*, 9110.
- (29) Beley, M.; Chodorowski, S.; Collin, J. -P.; Sauvage, J. -P.; Flamigni, L.; Barigelletti, F. *Inorg. Chem.* **1994**, *33*, 2543.
- (30) Indelli, M. T.; Bignozzi, C. A.; Scandola, F.; Collin, J. -P. *Inorg. Chem.* **1998**, *37*, 6084.
- (31) Duati, M.; Fanni, S.; Vos, J. G. *Inorg. Chem. Commun.* **2000**, *3*, 68.
- (32) Duati, M.; Tasca, S.; Lynch, F. C.; Bohlen, H.; Vos, J. G.; Stagni, S.; Ward, M. D. *Inorg. Chem.* **2003**, *42*, 8377.
- (33) Son, S. U.; Park, K. H.; Lee, Y. -S.; Kim, B. Y.; Choi, C. H.; Lah, M. S.; Jang, Y. H.; Jang, D. -J.; Chung, Y. K. *Inorg. Chem.* **2004**, *43*, 6896.
- (34) Collin, J. P.; Beley, M.; Sauvage, J. P.; Barigelletti, F. *Inorg. Chim. Acta* **1991**, *186*, 91.
- (35) (a) Wadman, S. H.; Kroon, J. M.; Bakker, K.; Havenith, R. W. A.; van Klink, G. P. M.; van Koten, G. *Organometallics* **2010**, *29*, 1569; (b) Brown, D. G.; Sangantrakun, N.; Schulze, B.; Schubert, U. S.; Berlinguette, C. P. *J. Am. Chem. Soc.* **2012**, *134*, 12354.
- (36) (a) Abrahamsson, M.; Wolpher, H.; Johansson, O.; Larsson, J.; Kritikos, M.; Eriksson, L.; Norrby, P. -O.; Bergquist, J.; Sun, L.; Åkermark, B.; Hammarström, L. *Inorg. Chem.* **2005**, *44*, 3215. (b) Abrahamsson, M.; Lundqvist, M. J.; Wolpher, H.; Johansson, O.; Eriksson, L.; Bergquist, J. R. T.; Becker, H.-C.; Hammarström, L.; Norrby, P. O.; Åkermark, B.; Persson, P. *Inorg. Chem.* **2008**, *47*, 3540.
- (37) (a) Schramm, F.; Meded, V.; Fliegl, H.; Fink, K.; Fuhr, O.; Qu, Z.; Klopper, W.; Finn, S.; Keyes, T. E.; Ruben, M. *Inorg. Chem.* **2009**, *48*, 5677; (b) Breivogel, A.; Meister, M.; Förster, C.; Laquai, F.; Heinze, K. *Chem. Eur. J.* **2013**, *19*, 13745 and references cited therein.
- (38) (a) Chen, J.-L.; Chi, Y.; Chen, K. *Inorg. Chem.*, **2010**, *49*, 823; (b) Dyker, G.; Muth, O. *Eur. J. Org. Chem.* **2004**, 4319.
- (39) Chen, X.-D.; Mak, T. C. W. *Inorg. Chim. Acta* **2005**, *358*, 1107.
- (40) Abrahamsson, M.; Jäger, M.; Österman, T.; Eriksson, L.; Persson, P.; Becker, H.-C.; Johansson, O.; Hammarström, L. *J. Am. Chem. Soc.* **2006**, *128*, 12616. (b) Jäger, M.; Kumar, R. J.; Görls, H.; Bergquist, J.; Johansson, O. *Inorg. Chem.* **2009**, *48*, 3228.
- (41) (a) Nag, S.; Ferreira, J. G.; Chenneberg, L.; Ducharme, P. D.; Hanan, G. S.; La Ganga, G.; Serroni, S.; Campagna S. *Inorg. Chem.* **2011**, *50*, 7–9. (b) Pal, A. K.; Nag, S.; Ferreira, J. G.; Brochery, V.; La Ganga, G.; Santoro, A.; Serroni, S.; Campagna, S.; Hanan, G. S. *Inorg. Chem.* **2014**, *53*, 1679. (c) Pal, A. K.; Ducharme,

- P. D.; Hanan, G. S. *Chem. Commun.* **2014**, *50*, 3303. (d) Pal, A. K.; Zaccheroni, N.; Campagna, S.; Hanan, G. S. *Chem. Commun.* **2014**, accepted for publication. (d) Pal, A. K.; Hanan, G. S. *Dalton Trans.* **2014**, Advanced article, DOI 10.1039/c4dt00112e.
- (42) Coles, M. P. *Chem. Commun.* **2009**, 3659.
- (43) Wild, U.; Roquette, P.; Kaifer, E.; Mautz, J.; Huebner, O.; Wadepohl, H.; Himmel, H. -J. *Eur. J. Inorg. Chem.* **2008**, 1248.
- (44) Abrahamsson, M.; Jäger, M.; Kumar, R. J.; Österman, T.; Persson, P.; Becker, H.-C.; Johansson, O.; Hammarström, L. *J. Am. Chem. Soc.* **2008**, *130*, 15533.
- (45) Kumar, R. J.; Karlsson, S.; Streich, D.; Rolandini Jensen, A.; Jäger, M.; Becker, H.-C.; Bergquist, J.; Johansson, O.; Hammarström, L. *Chem. Eur. J.* **2010**, *16*, 2830.
- (46) (a) Parker, C. A. and Rees, W. T. *Analyst* **1960**, *85*, 587, (b) Crosby, G. A.; Demas, J. N. *J. Phys. Chem.* **1971**, *75*, 991.
- (47) Würth, C.; Grabolle, M.; Pauli, J.; Spieles, M.; Resch-Genger, U. *Nat. Protocol* **2013**, *8*, 1535.
- (48) Wang, J.; Hanan, G. S. *Synlett* **2005**, *8*, 1251-1254.
- (49) Santoni, M.-P.; Pal, A. K.; Hanan, G. S.; Proust, A.; Hasenknopf, B. *Inorg. Chem. Commun.* **2011**, *14*, 399.
- (50) *APEX2 (2007) version 2.4-0; Bruker Molecular Analysis Research Tool*. Bruker AXS Inc., Madison, WI 53719-1173.
- (51) Sheldrick, G. M. (1996). *SADABS*, Bruker Area Detector Absorption Corrections. Bruker AXS Inc., Madison, WI 53719-1173.
- (52) *SHELXTL (2001) version 6.12*; Bruker Analytical X-ray Systems Inc., Madison, WI 53719-1173.
- (53) Platon (A. L. SPEK, 2003).
- (54) Frisch, M. J.; Trucks, G. W.; Schlegel, H. B.; Scuseria, G. E.; Robb, M. A.; Cheeseman, J. R.; Montgomery, J. A.; Vreven, T. J.; Kudin, K. N.; Burant, J. C.; Millam, J. M.; S., I. S.; Tomasi, J.; Barone, V.; Mennucci, B.; Cossi, M.; Scalmani, G.; Rega, N.; Petersson, G. A.; Nakatsuji, H.; Hada, M.; Ehara, M.; Toyota, K.; Fukuda, R.; Hasegawa, J.; Ishida, M.; Nakajima, T.; Honda, Y.; Kitao, O.; Nakai, H.; Klene, M.; Li, X.; Knox, J. E.; Hratchian, H. P.; Cross, J. B.; Adamo, C.; Jaramillo, J.; Gomperts, R.; Startmann, R. E.; Yazyev, O.; Austin, A. J.; Cammi, R.; Pomelli, C.; Ochterski, J. W.; Ayala, P. Y.; Morokuma, K.; Voth, G. A.; Salvador, P.; Dannenberg, J. J.; Zakrzewski, V. G.; Dapprich, J. M.; Daniels, A. D.; Strain, M. C.; Farkas, O.; Malick, D. K.; Rabuck, A. D.; Raghavachari, K.; Foresman, J. B.; Ortiz, J. V.; Cui, Q.; Baboul, A. G.; Clifford, S.; Cioslowski, J.; B., S. B.; Liu, G.; Liashenko, A.; Piskorz, I.; Komaromi, I.; L., M. R.; Fox, D. J.; Keith, T.; Al-Laham, M. A.; Peng, C. Y.; Manayakkara, A.; Challacombe, M.; Gill, P. M. W.; Johnson, B. G.; Chen, W.; Wong, M. W.; Gonzalez, C.; Pople, J. A., *Gaussian 2003, Revision C.02; Gaussian Inc.:Pittsburgh PA, 2003*.
- (55) Becke, A. D. *J. Chem. Phys.* **1993**, *98*, 5648–5652.
- (56) Lee, C.; Yang, W.; Parr, R. G. *Phys. Rev. B: Condens. Matter* **1988**, *37*, 785–789.

- (57) McLean, A. D.; Chandler, G. S. *J. Chem. Phys.* **1980**, *72*, 5639–5648.
- (58) Hay, P. J.; Wadt, W. R. *J. Chem. Phys.* **1985**, *82*, 270–283.
- (59) (a) Casida, M. E.; Jamorski, C.; Casida, K. C.; Salahub, D. R. *J. Chem. Phys.* **1998**, *108*, 4439–4449. (b) Stratmann, R. E.; Scuseria, G. E.; Frisch, M. J. *J. Chem. Phys.* **1998**, *109*, 8218–8224.
- (60) (a) Cossi, M.; Rega, N.; Scalmani, G.; Barone, V. *J. Comput. Chem.* **2003**, *24*, 669–681. (b) Cossi, M.; Barone, V. *J. Chem. Phys.* **2001**, *115*, 4708–4717. (c) Barone, V.; Cossi, M. *J. Phys. Chem. A* **1998**, *102*, 1995–2001.
- (61) Browne, W. R.; O’Boyle, N. M.; McGarvey, J. J.; Vos, J. G. *Chem. Soc. Rev.* **2005**, *34*, 641–663.
- (62) Zhurko, D. A.; Zhurko, G. A. *ChemCraft 1.5*; Plimus: San Diego, CA. Available at <http://www.chemcraftprog.com>.
- (63) Wolfe, J. P.; Buchwald, S. L. *J. Org. Chem.* **2000**, *65*, 1144.
- (64) Polson, M. I. J.; Medlycott, E. A.; Hanan, G. S.; Mikelsons, L.; Taylor, N. J.; Watanabe, M.; Tanaka, Y.; Loiseau, F.; Passalacqua, R.; Campagna, S. *Chem. Eur. J.* **2004**, *10*, 3640. (b) Medlycott, E. A.; Udachin, K. A.; Hanan, G. S. *Dalton Trans.*, **2007**, 430.
- (65) For a general introduction to the synthesis of bisterpyridyl ruthenium(II) complexes, see: (a) Schubert, U. S.; Hofmeier, H.; Newkome, G. R. *Modern Terpyridine Chemistry*; WILEY-VCH: Weinheim, 2006. (b) Hofmeier, H.; Schubert, U. S. *Chem. Soc. Rev.* **2004**, *33*, 373–399.
- (66) Oakley, S. H.; Coles, M. P.; Hitchcock, P. B. *Inorg. Chem.* **2004**, *43*, 7564.
- (67) McMurtriea, J.; Dance, I. *Cryst. Eng. Comm.*, **2009**, *11*, 1141–1149.
- (68) Beves, J. E.; Chwalisz, P.; Constable, E. C.; Housecroft, C. E.; Neuburger, M.; Schaffner, S.; Zampese, J. A. *Inorg. Chem. Commun.* **2008**, *11*, 1009–1011.
- (69) Pyo, S.; Cordero, E. P.-; Bott, S. G.; Echegoyen, L. *Inorg. Chem.* **1999**, *38*, 3337.
- (70) Medlycott, E. A.; Hanan, G. S.; Loiseau, F.; Campagna, S. *Chem. Eur. J.* **2007**, *13*, 2837.
- (71) (a) Harriman, A.; Mayeux, A.; Nicola, A. D.; Ziessel, R. *Phys. Chem. Chem. Phys.* **2002**, *4*, 2229; (b) Constable, E. C.; Thompson, A. M. W. C.; Tocher, D. A.; Daniels, M. A. M. *New J. Chem.* **1992**, *16*, 855; (c) Hewitt, J. T.; Vallett, P. J.; Damrauer, N. H. *J. Phys. Chem. A*, **2012**, *116*, 11536.
- (72) Wadman, S. H.; Lutz, M.; Tooke, D. M.; Spek, A. L.; Hartl, F.; Havenith, R. W. A.; van Klink, G. P. M.; van Koten, G. *Inorg. Chem.* **2009**, *48*, 1887.
- (73) Bomben, P. G.; Robson, K. C. D.; Sedach, P. A.; Berlinguette, C. P. *Inorg. Chem.* **2009**, *48*, 9631.
- (74) Siemeling, U.; Bruggen, J. V. der; Vorfeld, U.; Neumann, B.; Stammler, A.; Stammler, H.-G.; Brockhinke, A.; Plessow, R.; Zanello, P.; Laschi, F.; Biani, F. F. de; Fontani, M.; Steenken, S.; Stapper, M. and Gurzadyan G. *Chem. Eur. J.*, **2003**, *9*, 2819 – 2833.
- (75) Hanazaki, I.; Nagakura, S. *Inorg. Chem.* **1969**, *8*, 648.
- (76) Bryant, G. M.; Fergusson, J. E.; Powell, H. K. *J. Aust. J. Chem.* **1971**, *24*, 257.

Chapter 4

- (77) Aydin, N.; Schlaepfer, C. W. *Polyhedron* **2001**, *20*, 37.
- (78) Bolink, H. J.; Coronado, E.; D. Costa, R.; Gaviña, P.; Ortí, E.; Tatay, S. *Inorg. Chem.* **2009**, *48*, 3907.

Chapter 5: (A) *Tuning the structural and electronic properties of rare Re(I)-complexes of κ^3 N-tridentate heterocyclic ligands*

5A.1. Résumé

Les complexes *fac, fac*-[Re^I(CO)₃] de nouvelle κ^3 N- tridentate ligands ont été synthétisés et caractérisés par différentes techniques analytiques, y compris XRD. La régulation des propriétés électroniques des complexes sur la modification du ligand est également signalée.

Contribution :

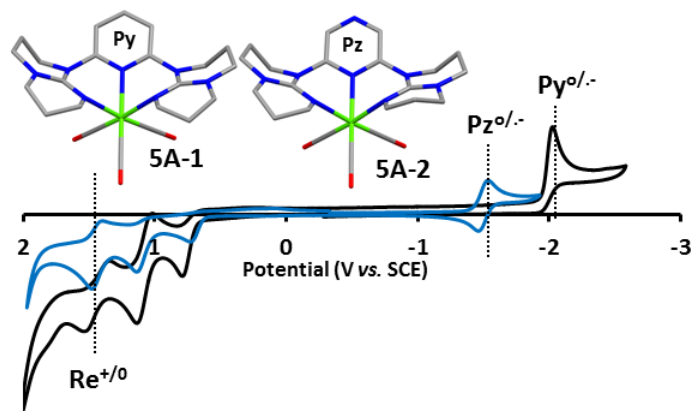
Amlan K. Pal : All the work presented in this chapter and its writing.

Garry S. Hanan : Supervision and revision of the chapter.

Tuning the structural and electronic properties of rare Re(I)-complexes of κ^3N -tridentate heterocyclic ligands

KEYWORDS: Rhenium complexes, Synthesis, Ligand design, Electrochemistry, Density functional theory, Photophysical properties

5A.2. Table of Content Graphic



Convenient one-pot syntheses of *fac, fac*-[Re^I(CO)₃]-complexes of strong σ -donor, κ^3N -tridentate ligands have been reported. Due to broken π -conjugation in the ligand moieties, the metal-based quasi-reversible oxidation and ligand-based reduction can be tuned separately by varying the electronic nature of the ligand moieties. The complexes also act as blue-emitters, which originates from triplet MLCT transitions, owing to high energy π^* -level localized on central aromatic heterocycles.

5A.3. Abstract

Rare *fac, fac*-[Re^I(CO)₃]-complexes of new κ^3N -tridentate ligands were synthesized and characterized by various analytical techniques including XRD. The regulation of the electronic properties of the complexes upon ligand modification is also reported.

5A.4. Introduction

Interest in rhenium(I)-tricarbonyl-polypyridyl complexes has grown considerably as they find use as light-harvesting chromophores in solar energy conversion,¹ fluorescent probes in cell-imaging,² sensor development³ and as supramolecular synthons.⁴ While complexes of type *fac,cis*-[Re(bpy)(CO)₃X]⁵ (X = Cl or Br) (bpy = 2,2'-bipyridine), *fac,cis*-[Re(tpy-κ²N)(CO)₃X]⁶ (tpy = 2,2':6',2''-terpyridine) and *mer,cis*-[Re(tpy-κ³N)(CO)₂X]⁷ are relatively well known, complexes of type *fac, fac*-[Re(L-κ³N)(CO)₃]⁺ (where L = 2,6-disubstituted pyridyl-tridentate ligand) are virtually non-existent.⁸ Although a few reports of macrocyclic⁹ or tripodal face-capping¹⁰ ligands around Re^I(CO)₃-centre exist, their properties are not well explored. The effect of the introduction of electron donating or withdrawing substituents on the ligand would allow the electronic properties to be fine-tuned.

Herein we report the syntheses and characterization of two different *fac, fac*-[Re(dgpy/dgpz-κ³N)(CO)₃]⁺-complexes with **dgpy** (**5A-L1**) (dgpy = 2,6-diguanidylpyridine) and **dgpz** (**5A-L2**) (**dgpz** = 2,6-diguanidylpyrazine), **5A-1** and **5A-2**, respectively, by high-resolution mass spectrometry, solution NMR, UV-vis absorption and emission spectroscopies, elemental analysis, XRD and DFT calculations.

5A.5. Experimental section

5A.5.1. Materials, methods and instrumentation

Nuclear magnetic resonance (NMR) spectra were recorded in CD₃CN, CDCl₃, and DMSO-d₆ at room temperature (r.t.) on a Bruker AV400 (400 MHz) spectrometer for ¹H NMR and at 100 for ¹³C NMR, respectively. Chemical shifts are reported in part per million (ppm) relative to residual solvent protons (1.94 ppm for CD₃CN, 7.26 ppm for CDCl₃, 2.50 ppm for DMSO-d₆) and the carbon resonance (1.24 ppm for CD₃CN, 77.00 ppm for CDCl₃, 39.43 ppm for DMSO-d₆) of the solvent.

All the photophysical measurements were carried out in deaerated acetonitrile at r.t. in septa-sealed quartz cells. Absorption spectra were measured on a Cary 500i UV-Vis-NIR Spectrophotometer. For luminescence spectra a Cary Eclipse Fluorescence spectrofluorimeter was used. Electrochemical measurements were carried out in argon-purged purified acetonitrile at room temperature with a BAS CV50W multipurpose

potentiostat. The working electrode was a glassy carbon electrode. The counter electrode was a Pt wire, and the pseudo-reference electrode was a silver wire. The reference was set using an internal 1 mM ferrocene/ferrocinium sample at 395 mV vs. SCE in acetonitrile. The concentration of the compounds was about 1 mM. Tetrabutylammonium hexafluorophosphate (TBAP) was used as supporting electrolyte and its concentration was 0.10 M. Cyclic voltammograms of **5A-L1**, **5A-L2**, **5A-1** and **5A-2** were obtained at scan rates of 50, 50, 10 and 25 mVs⁻¹, respectively. The criteria for reversibility were the separation of 60 mV between cathodic and anodic peaks, the close to unity ratio of the intensities of the cathodic and anodic currents, and the constancy of the peak potential on changing scan rate. Differential pulse voltammetry was conducted with a sweep rate of 20 mVs⁻¹ and a pulse amplitude, width and period of 50 mV, 50 ms and 200 ms, respectively.

Estimated experimental uncertainties are as follows: absorption maxima, ± 2 nm; molar absorption coefficient, 10%; redox potentials, ± 10 mV, emission maxima, ± 2 nm.

1,3,4,6,7,8-Hexahydro-2H-pyrimido[1,2- α]pyrimidine (**H-hpp**), 2,6-dibromopyridine, 2,6-dichloropyrazine, (\pm) BINAP, *t*-BuOK were purchased from Aldrich and used as received. Re₂(CO)₁₀, Pd(OAc)₂ were purchased from Pressure Chemicals. Ligand **5A-L1** and Re(CO)₅Br were synthesized from Re₂(CO)₁₀ using literature procedures.¹¹

5A.5.2. Synthetic Methods

2,6-Bis-[1,3,4,6,7,8-hexahydro-2H-pyrimido[1,2- α]pyrimido]pyrazine : (**5A-L2**) (**dgpz**) (\pm) BINAP (0.09 mmol, 60 mg) was placed in an oven-dried, nitrogen-purged round-bottomed flask that was sealed with a septum. Dry toluene (3 mL) was added via syringe. The resulting suspension was heated at 90 °C for 2 min to dissolve the BINAP. This was cooled to room temperature and Pd(OAc)₂ (0.06 mmol, 14 mg) was added and stirred for 3 min. To the resulting bright yellow solution, 2,6-dichloropyrazine (3.2 mmol, 479 mg) and 1,3,4,6,7,8-hexahydro-2H-pyrimido[1,2- α]pyrimidine (6.9 mmol, 962 mg) were added. Stirring for 5 min at ambient temperature resulted in a pale orange slurry to which was added *t*-BuOK (9.0 mmol, 1.01 g). The reaction mixture was then stirred at 90 °C for 16 h, was cooled to room temperature and diethyl ether (60 mL) was added and the mixture was filtered. Evaporation of the filtrate followed by purification by column chromatography on deactivated alumina using 3:2 (DCM:MeOH, v/v) afforded the ligand (**5A-L2**) as

crystalline pale yellow solid. Yield = 736 mg (65 %). ^1H NMR (DMSO- d_6 , 400 MHz); 8.38 (s, 2 H), 3.70 (t, $J^t = 6$ Hz, 4 H), 3.25 (t, $J^t = 6$ Hz, 4 H), 3.19 (t, $J^t = 6$ Hz, 4 H), 3.15 (t, $J^t = 6$ Hz, 4 H), 1.94 (quint., $J^q = 6$ Hz, 4 H), 1.77 (quint., $J^q = 6$ Hz, 4 H) ppm. ^{13}C NMR (DMSO- d_6 , 100 MHz); 149.6, 147.9, 130.7, 47.9, 47.6, 43.1, 42.5, 22.8, 22.1 ppm. HRMS (ESI), m/z : 355.23526 $[\text{M}+\text{H}]^+$ ($\text{C}_{18}\text{H}_{27}\text{N}_8$ requires 355.23532; Δppm -0.17), 178.12134 $[\text{M}+2\text{H}]^{2+}$ ($\text{C}_{18}\text{H}_{28}\text{N}_8$ requires 178.12130; Δppm 0.23). Anal. Calc. for $\text{C}_{18}\text{H}_{26}\text{N}_8$: C, 60.99; H, 7.39; N, 31.61. Found: C, 60.99; H, 7.42; N, 31.58.

[Re(5A-L1)(CO)₃][Br] : (**5A-1**)

$\text{Re}(\text{CO})_5\text{Br}$ (50 mg, 0.123 mmol) was dissolved in hot dry toluene (30 mL) under N_2 atmosphere. After cooling to ambient temperature, to the colourless solution, ligand **5A-L1** (48 mg, 0.136 mmol) was added. The resulting suspension was heated to reflux for 3 h under N_2 atmosphere in the dark. A colourless precipitate was observed upon completion of the reaction. The precipitate was isolated by filtration, washed with toluene (3 x 25 mL) and dried under vacuum to afford complex **5A-1** as a colourless solid. Crystals suitable for X-ray crystallography were grown by diffusion of diethyl ether into a concentrated solution of **5A-1** in chloroform:acetone (1:3, v/v). Yield = 80 mg (93%). ^1H NMR (CDCl_3 , 400 MHz); δ 8.12 (t, $J^t = 8$ Hz, 1 H), 7.34 (d, $J^d = 8$ Hz, 2 H), 4.10 (d, $J^d = 12$ Hz, 2 H), 3.64 (m, 4 H), 3.52 (m, 2 H), 3.44 (m, 4 H), 3.37 (m, 2 H), 2.47 (m, 2 H) 2.32 (m, 2 H), 2.01 (m, 4 H), 1.65 (d, $J^d = 12$ Hz, 2 H) ppm. ^{13}C NMR (CDCl_3 , 100 MHz); δ 196.1, 154.2, 153.1, 143.4, 110.7, 51.6, 48.7, 46.5, 22.4, 21.6 ppm (one of the six different methylene carbons could not be seen), ^{13}C NMR (CD_3CN , 100 MHz); δ 197.4, 155.3, 154.3, 143.4, 111.0, 52.3, 49.3, 49.2, 47.1, 22.7, 22.2 ppm (although one of the methylene carbons could not be seen in CDCl_3 solvent, it could be seen when recorded in CD_3CN). HRMS (ESI), m/z : 624.17347 $[\text{M}-\text{Br}]^+$ ($\text{C}_{22}\text{H}_{27}\text{N}_7\text{O}_3$ ^{187}Re requires 624.17274; Δppm 1.17). Anal. Calc. for $\text{C}_{22}\text{H}_{27}\text{N}_7\text{O}_3\text{ReBr}$: C, 37.55; H, 3.87; N, 13.93. Found: C, 37.54; H, 3.78; N, 13.82.

[Re(5A-L2)(CO)₃][Br] : (**5A-2**)

$\text{Re}(\text{CO})_5\text{Br}$ (50 mg, 0.123 mmol) was dissolved in hot dry toluene (30 mL) under N_2 atmosphere. After cooling to ambient temperature, to the colourless solution, ligand **5A-L2** (48 mg, 0.135 mmol) was added. The resulting suspension was heated to reflux for 6 h under N_2 atmosphere in the dark. An olive-green precipitate was observed upon completion of the reaction time. The precipitate was isolated by filtration, washed with toluene (2x10 mL) and Et_2O (2x10 mL) and dried under vacuum to afford complex **5A-2** as a olive-green

solid. Long needle shaped crystals suitable for X-ray crytallography could be grown by diffusion of diethyl ether into a concentrated solution of **5A-2** in dichloromethane. Yield = 78 mg (91%). ^1H NMR (CD_3CN , 400 MHz); δ 8.42 (s, 2 H), 4.13 (dt, $J^{\text{dt}} = 14, 4$ Hz, 2 H), 3.67 (m, 4 H), 3.41 (m, 8 H), 3.28 (ddd, $J^{\text{ddd}} = 12, 10, 6$ Hz, 2 H), 2.25 (m, 4 H), 1.98 (d, $J^{\text{d}} = 6$ Hz, 2 H) 1.90 (m, 2H). ^{13}C NMR (CD_3CN , 100 MHz); δ 197.2, 154.4, 150.4, 132.8, 53.2, 49.9, 49.8, 47.3, 23.4, 22.3 ppm. HRMS (ESI), m/z : 625.16817 [M-Br] $^+$ ($\text{C}_{21}\text{H}_{26}\text{N}_8\text{O}_3$ ^{187}Re requires 625.16799; Δppm 0.29). Anal. Calc. for $\text{C}_{21}\text{H}_{26}\text{N}_8\text{O}_3\text{ReBr}$: C, 35.80; H, 3.72; N, 15.90. Found: C, 35.81; H, 3.69; N, 15.77.

5A.5.3. Computational Methods

All calculations were performed with the Gaussian03¹² suite of programs employing the DFT method, the Becke three-parameter hybrid functional,¹³ and Lee-Yang-Parr's gradient-corrected correlation functional (B3LYP).¹⁴ Singlet ground state geometry optimizations for **5A-1** $^{1+}$ and **5A-2** $^{1+}$ were carried out at the (R)B3LYP level in the gas phase, using their respective crystallographic structures as starting points. All elements except Re were assigned the 6-31G(d,p) basis set.¹⁵ The double- ζ quality LANL2DZ ECP basis set¹⁶ with an effective core potential and one additional f-type polarization was employed for the Re-atom. Vertical electronic excitations based on (R)B3LYP-optimized geometries were computed for **5A-1** $^{1+}$ and **5A-2** $^{1+}$ using the TD-DFT formalism^{17a,b} in acetonitrile using conductor-like polarizable continuum model (CPCM).^{18a-c} Vibrational frequency calculations were performed to ensure that the optimized geometries represent the local minima and there are only positive eigenvalues. The electronic distribution and localization of the singlet excited states were visualized using the electron density difference maps (ED-DMs).¹⁹ *Gausssum* 2.2 and *Chemission* were employed to visualize the absorption spectra (simulated with Gaussian distribution with a full-width at half maximum (fwhm) set to 3000 cm^{-1}) and to calculate the fractional contributions of various groups to each molecular orbital. All calculated structures and Kohn-Sham orbitals were visualized with ChemCraft.²⁰

5A.5.4. Crystal Structure Determination

Diffraction data were collected on a Bruker SMART 6000 with Montel 200 monochromator, equipped with a rotating anode source for Cu $K\alpha$ radiation. The diffraction quality of the crystals were checked, revealing in some cases poor diffraction

with a large amount of diffuse scattering, signaling extensive crystal disorder. Cell refinement and data reduction were done using APEX2.²¹ Absorption corrections were applied using SADABS.²² Structures were solved by direct methods using SHELXS97 and refined on F^2 by full-matrix least squares using SHELXL97.²³ All non-hydrogen atoms were refined anisotropically. Hydrogen atoms were refined isotropic on calculated positions using a riding model. For compound **5A-1** the highest difference peak is 0.93 Å far from Re-atom and the deepest hole is 0.73 Å from Re-atom. In addition, in **5A-1** four more peaks with density around $1 \text{ e}/\text{Å}^3$ were present essentially due to the quality of the crystal employed, which was the best available. For compound **5A-2** the highest difference peak is 1.01 Å far from atom C9 and is believed due to positional disorder of this atom. This disorder was not taken into account for modelling. Except this high electron density peak, four other high electron density peaks of electron density ranging from 2.25-1.16 $\text{e}/\text{Å}^3$ were located and they are in close proximity (1.37-1.05 Å) to the Re-atom. Specific parameters of each measurement are located in Table VA-1.

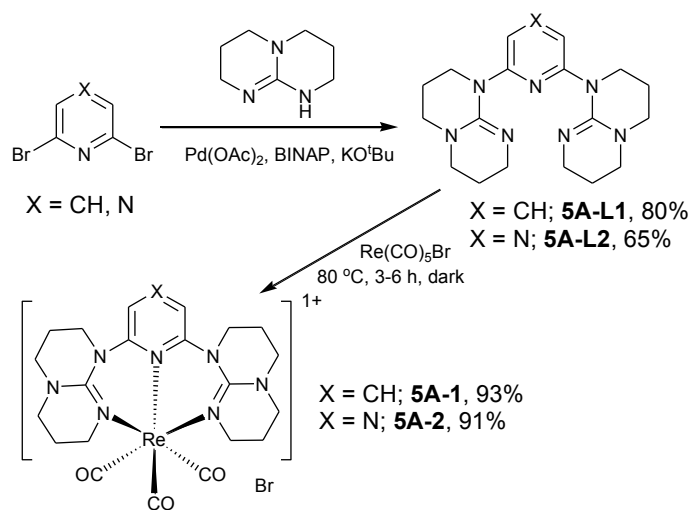
Table VA-1. Crystal data and details of the structure determination for **5A-1**, **5A-2**

	5A-1^a	5A-2^a
Formula	[C ₂₂ H ₂₇ N ₇ O ₃ Re][Br]	[C ₂₁ H ₂₆ N ₈ O ₃ Re][Br]
Color/form	colorless needle	Olive green needle
<i>T</i> (K); wavelength	150(2); 1.54178	150(2); 1.54178
Crystal System	Triclinic	Triclinic
Space Group	P-1	P-1
Unit Cell: <i>a</i> (Å)	8.1289(3)	8.2315(6)
<i>b</i> (Å)	11.6833(5)	11.7681(6)
<i>c</i> (Å)	13.8021(6)	13.3936(8)
α (°)	105.115(2)	104.882(3)
β (°)	105.785(2)	105.407(3)
γ (°)	99.199(1)	99.732(3)
<i>V</i> (Å ³); <i>Z</i>	1179.57(8); 2	1168.99(13); 2
R1(F); wR(F ²)[I>4σ(I)]	0.0271; 0.0709	0.0337; 0.0907
R1(F); wR(F ²) (all)	0.0271; 0.0709	0.0337; 0.0907
GoF(F ²)	1.104	1.082
R _σ ; R(int)	0.0173; 0.0490	0.0229; 0.0536

^aBruker Microstar diffractometer (Platinum 135 CCD Detector, Helios optics and, Kappa goniometer).

5A.6. Results and Discussion

Ligands **5A-L1** and **5A-L2** were synthesized by taking advantage of Pd-catalyzed C-N bond forming reactions.²⁴ Complexes **5A-1** and **5A-2**, were prepared by direct mixing of $\text{Re}(\text{CO})_5\text{Br}$ and ligand in 1:1.2 molar ratio in refluxing toluene media. Although *mer,cis*- $[\text{Re}(\text{tpy}-\kappa^3N)(\text{CO})_2\text{X}]$ (where $\text{X} = \text{Cl}$ or Br)⁷ can be synthesized through a *fac*- $[\text{Re}(\text{tpy}-\kappa^2N)(\text{CO})_3\text{X}]$ intermediate,⁶ the additional thermodynamic stabilization upon κ^3N -coordination by **5A-L1** and **5A-L2** with the formation of sterically relaxed six-membered chelate rings, affords these chemically robust complexes in high yields using much softer reaction conditions.



Scheme 5A.1. Syntheses of ligands **5A-L1**, **5A-L2** and complexes *fac, fac*- $[\text{Re}(\mathbf{5A-L1}-\kappa^3N)(\text{CO})_3][\text{Br}]$ (**5A-1**) and *fac, fac*- $[\text{Re}(\mathbf{5A-L2}-\kappa^3N)(\text{CO})_3][\text{Br}]$ (**5A-2**).

5A.6.1. NMR spectroscopy

The ^1H and ^{13}C NMR spectra of complexes **5A-1** and **5A-2** display C_2 symmetry. The six annular methylene units are nonequivalent by both ^1H and ^{13}C NMR spectroscopy in contrast to free **H-hpp** (**H-hpp** = 1,3,4,6,7,8-hexahydro-2H-pyrimido[1,2-*a*]pyrimidine), in which the tautomerization of the guanidine proton leads to only three proton resonances in its ^1H NMR at 400 MHz.^{11b,25} Similar observations were reported by Coles and co-workers^{25d} for a methylene-linked bis(guanidyl) compound, $\text{H}_2\text{C}\{\mathbf{hpp}\}_2$. The noticeable downfield shift of ~ 22 ppm of the alkene C-atom in the aliphatic backbone of **5A-2** compared to that of **5A-1** suggests a strong electron withdrawing effect of the pyrazine (Pz)

core through the $N_{\text{hpp}}\text{-Re-}N_{\text{pz}}$ unit. This fact is also supported by a shorter $\text{Re-}N_{\text{pz}}$ distance compared to $\text{Re-}N_{\text{py}}$ distance in their respective crystal structures.

5A.6.2. X-ray Structural Investigation

Single crystals were obtained by slow vapour diffusion of diethyl ether into dichloromethane solutions of **5A-1** and **5A-2**. The coordinatively saturated Re(I) in **5A-1** and **5A-2** are in a distorted octahedral geometry, where both ligands **5A-L1**, **5A-L2** and the carbonyl groups adopt *fac*-coordination around Re(I) . This *fac*-coordination is facilitated due to the flexible aliphatic backbone and larger bite angle of **5-L1** and **5-L2**, which form 6-membered chelate rings around the metal ions, while a *mer*-coordination of tpy gives rise to comparatively strained 5-membered chelate rings. Complexes **5A-1** and **5A-2** are virtually isostructural and unlike the symmetrical structure in solution, all of the carbonyl groups in the solid state structures are non-symmetrical. The average N-C-N-C dihedral angle of complexes **5A-1** and **5A-2** are $\sim 130^\circ$ (average of $\langle \text{N1-C1-N5-C19}$ and $\langle \text{N1-C5-N2-C12}$) and 129° (average of $\langle \text{N1-C4-N3-C11}$ and $\langle \text{N1-C1-N6-C18}$), respectively, suggesting broken π -conjugation between the pyridine or pyrazine unit and the **hpp** units. The optimized ground state geometries of **5A-1** and **5A-2** are in reasonable agreement with the X-ray structural data (Table VA-S1 in SI). The Re-C and Re-N distances are in the range expected for similar tricarbonyl complexes.^{8,26,27} The axial Re-C distance (*trans* to pyridine) in **5A-1** is shorter (1.901(5) Å) than that of **5A-2** (1.931(5) Å) due to the lower nucleophilicity and higher π -accepting nature of the pyrazine ring in **5A-2** compared to that of the pyridine ring in **5A-1**. In both the complexes, the central $\text{Re-}N_{\text{py/pz}}$ bond is shorter than the corresponding distances to the outer rings,^{8,28} as found for tridentate terpyridine Re(I) and Ru(II) complexes.

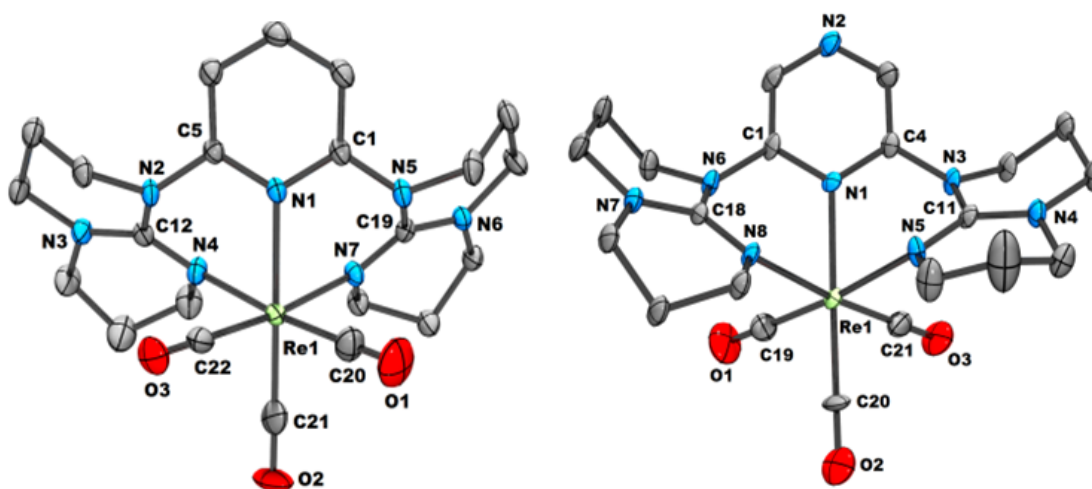


Figure 5A.1. Perspective views of complexes **5A-1** (left) and **5A-2** (right), exhibiting the facial coordination of **5A-L1** and **5A-L2**. Hydrogen atoms and anions are not shown for clarity; ellipsoids correspond to 50% probability.

5A.6.3. Redox Behaviour

The electrochemical behavior of the ligands and complexes was examined by cyclic voltammetry and differential pulse voltammetry (Table VA-II). All of the redox processes were found to be monoelectronic. Complexes **5A-1** and **5A-2** exhibit ligand-based reductions centered on the pyridine and pyrazine units, respectively, as suggested by DFT calculations (Figure 5A.3). The 500 mV anodic shift in reduction potential of complex **5A-2** compared to that of **5A-1** is due to the poorer basicity of pyrazine than pyridine, which is in agreement with the calculated higher energy of the LUMO of **5A-1** (-1.70 eV) than that of **5A-2** (-2.35 eV). This trend has also been reported in structurally similar Ru(II)-polypyridyl complexes.²⁹ In the anodic region, both complexes exhibit two ligand-based oxidations (by comparing to their respective free ligands) at ~ 0.79 V and 1.09 V. In a very coarse approximation these values are also in good agreement with the DFT calculation, as the HOMO and HOMO-1 of both complexes reside predominantly on coordinated **hpp** units, although a detailed DFT calculation is necessary to confirm this fact. The two distinct ligand-based oxidations suggest that a metal-mediated superexchange phenomena exists.³⁰ For both complexes, the third quasi-reversible oxidation at 1.43 V is assigned to metal-based oxidation, which occurs at 320 mV less positive potential than in $[\text{Re}(\text{bpy})(\text{CO})_3(\text{Py})]^+$,³¹ suggesting that ligands **5A-L1** and **5A-L2** are more σ -donating than bpy and Py. The metal-based oxidation is invariant to the changes in electronic

properties of Py or Pz unit, due to broken π -conjugation between the **hpp** and the saturated heterocyclic moieties, and the combined σ -donation from two **hpp** units is the dominating factor in metal-based oxidation. This arrangement should allow the ligand-based reductions to be tuned separately by simply modifying the electronic nature of the central aromatic ring.

Table VA-2. Redox data of **5A-L1**, **5A-L2** and complexes **5A-1** and **5A-2** in dry, degassed acetonitrile with some benchmark complexes.

Compound	$E_{1/2}(\text{ox})^a$	$E_{1/2}(\text{red})^a$	$\Delta E_{1/2}^b$
5A-L1	1.11 (308), 0.77 (irr) ^c	-----	-----
5A-L2	1.14 (189), 0.77 (irr) ^c	-1.99 (irr) ^c	2.76
5A-1	1.43 (100), 1.08 (80), 0.73 (irr) ^c	-1.99 (irr) ^c	2.72
5A-2	1.43 (80), 1.09 (82), 0.72 (irr) ^c	-1.49 (73)	2.22
<i>mer,cis</i> -[Re(tpy- κ^3 N)(CO) ₂ (P(OEt) ₃)](CF ₃ SO ₃) ^d	1.30 (irr) ^c , 0.93 (73)	-1.23, -1.50 (irr) ^c	2.16
<i>mer,cis</i> -[Re(tpy- κ^3 N)(CO) ₂ Cl] ^d	1.22 (irr) ^c , 0.48 (65)	-1.17 (irr) ^c , -1.34 (irr) ^c	1.65
[Re(bpy)(CO) ₃ (Py)](ClO ₄) ^e	1.74	-1.09, -1.39	2.83

^aPotentials are in volts vs. SCE for acetonitrile solutions, 0.1 M in [*n*-Bu₄N]PF₆, recorded at 25 ± 1 °C at a sweep rate of 50, 50, 10 and 25 mV/s for **5A-L1**, **5A-L2**, **5A-1** and **5A-2**, respectively. The difference between cathodic and anodic peak potentials (millivolts) is given in parentheses. ^b $\Delta E_{1/2}$ is the difference (in V) between first oxidation and first reduction potentials. ^cIrreversible; potential is given for the anodic wave. ^dFrom ref 8. ^eFrom ref 31.

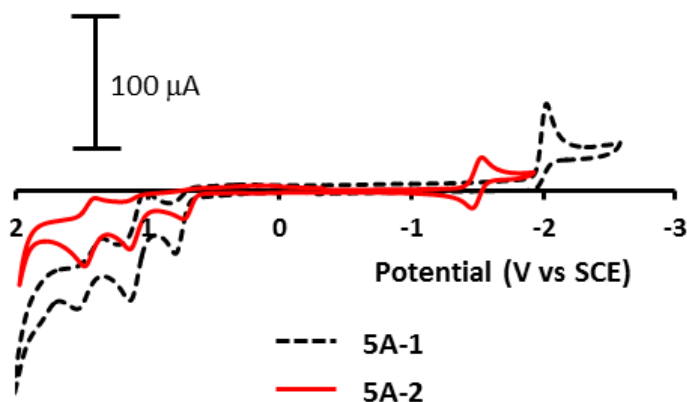


Figure 5A.2. Cyclic voltammogram of complexes **5A-1** and **5A-2** in dry, degassed CH₃CN, recorded at a scan rate of 10 and 25 mV/s, respectively.

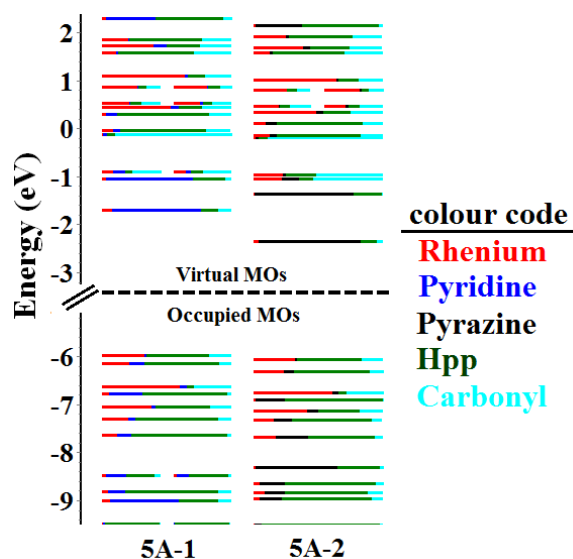


Figure 5A.3. Calculated frontier MO energies of the modeled complexes, **5A-1** and **5A-2** obtained from DFT(b3lyp/LanL2DZ(f)[Re]6-31G**[CHNO] with CPCM(CH₃CN) and 0.05 eV of threshold of degeneracy.

5A.6.4. Photophysical Investigation

The electronic absorption spectra for **5A-L1**, **5A-L2**, **5A-1** and **5A-2** were recorded in dry, degassed acetonitrile at ambient temperature. Both complexes exhibit two ligand-centered (LC) $\pi \rightarrow \pi^*$ transitions below 300 nm.³² A third transition at 318 nm for complex **5A-2** is also LC transition as suggested by TD-DFT calculations (Figure 5A.4 and Table VA-3). A singlet metal-to-ligand charge transfer (¹MLCT) transition is featured by its broad nature with a molar absorptivity of 5000 M⁻¹cm⁻¹ at 350-500 nm.⁸ The observed lowest energy transitions of **5A-1** and **5A-2** at 346 nm and 377 nm, respectively, possess the aforesaid features and they also shift bathochromically upon lowering the polarity of the solvent from acetonitrile to dichloromethane. These facts suggest a ¹MLCT nature for these transitions and indeed the TD-DFT calculations of **5A-1** and **5A-2** support this assignment as HOMO-1 to LUMO for both **5A-1** ($\Delta E_{\text{LUMO-(HOMO-1)}} = 4.44$ eV) and **5A-2** ($\Delta E_{\text{LUMO-(HOMO-1)}} = 3.96$ eV) The transitions have mixed LC (major) and ¹MLCT (minor) components (see Tables VA-S5 and VA-S7 in SI for more details).

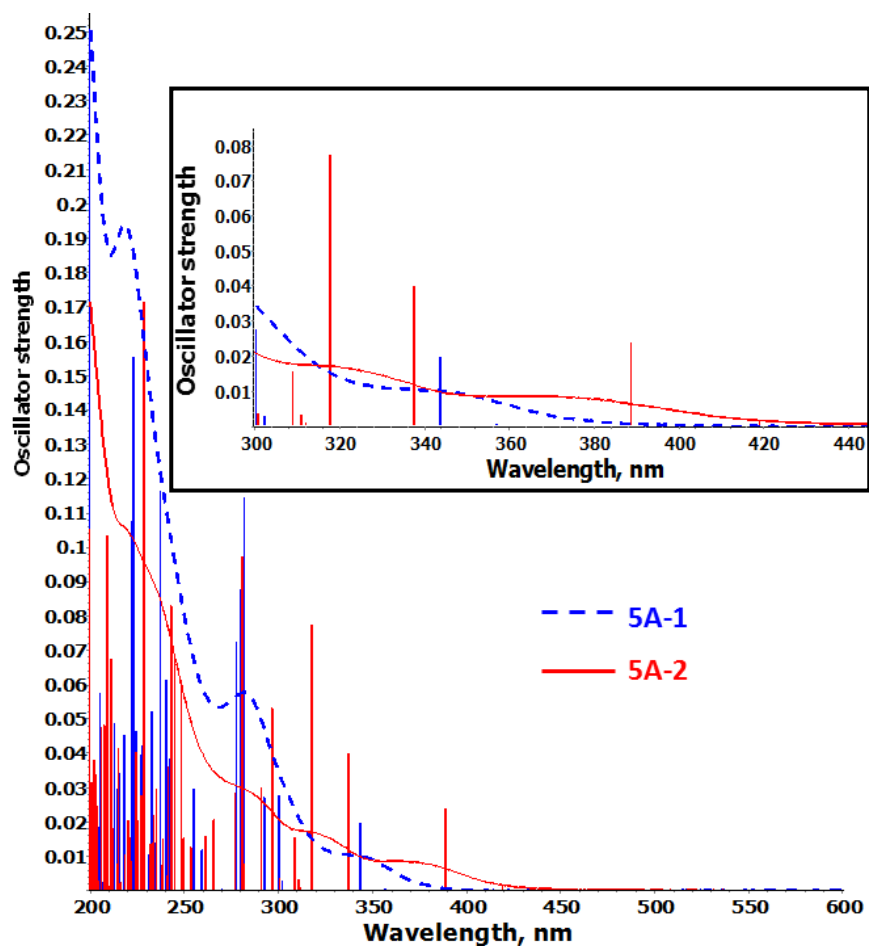


Figure 5A.4. Overlay of experimental (curved lines) absorption spectra and calculated (straight lines) oscillator strengths at different wavelengths of **5A-1** (dashed line) and **5A-2** (solid line), at ambient temperature in dry acetonitrile.

Table VA-3. Electronic absorption and emission data of **5A-L1**, **5A-L2** and complexes **5A-1** and **5A-2** in dry, degassed acetonitrile.

Compound	UV-vis Absorption	Emission	Lifetime
	λ_{\max} , nm ($\epsilon \times 10^3$, $M^{-1}cm^{-1}$)	λ_{\max} , nm	ns
5A-L1	228 (29.0), 311 (12.8)	360	
5A-L2	224 (26.9), 340 (14.1)	382	
5A-1	218 (64.7), 282 (19.2), 346 (3.5)	381	9.3
5A-2	219 (44.5), 283 (12.4), 318 (7.3), 377 (3.4)	418	11.6
$[Re(bpy)(py)(CO)_3]^a$	366 (2.4)	558	658

^afrom ref 31.

The emission spectra of **5A-L1**, **5A-L2** and the complexes were recorded in dry, degassed acetonitrile at ambient temperature and data are gathered in Table VA-3. The

ligands emit in the high energy region (~ 370 nm). A red-shift of 22 nm in the emission maxima from **5A-L1** to **5A-L2** is also observed, which is concomitant with the bathochromic shift of 29 nm in their lowest energy absorptions of **5A-L1** and **5A-L2**, respectively. The red-shift is due to the lower π^* level in **5A-L2** compared to that of **5A-L1**, while the HOMOs for **5A-L1** and **5A-L2** presumably remain at similar energies. Although the average N-Re-N bite angles in **5A-1** and **5A-2** are $81.76(11)^\circ$ and $81.87(15)^\circ$, which are smaller than the ideal 90° bite angle in a facially coordinated compound, due to strong σ -donation from the **hpp** units, the energy of the ^3MC state increases. This increased $^3\text{MLCT}$ - ^3MC band gap allow these complexes to display room temperature $^3\text{MLCT}$ emission albeit at shorter wavelength (~ 400 nm) compared to *fac, fac*-[Re(**dqp**- κ^3N)(CO) $_3$](Cl) (606 nm) (**dqp** = 2,6-di(8'-quinolinyl)pyridine). Associated to the red-shift of 31 nm in the lowest energy $^1\text{MLCT}$ maxima in **5A-2** compared to **5A-1**, the $^3\text{MLCT}$ maxima of complex **5A-2** is also red-shifted by 37 nm to that of complex **5A-1**.

Complex [Re(Py) $_2$ (CO) $_3$ Cl] 33 was found to be non-luminescent as opposed [Re(bpy)(CO) $_3$ X] $^+$ (X = Cl $^-$, CH $_3$ CN) type complexes. 7 Complexes of type *mer, cis*-[Re(tpy- κ^3N)(CO) $_2$ (L)] $^+$ (where L = CH $_3$ CN, PPh $_3$, Py, PEt $_3$) do not exhibit room temperature luminescence due to the lower ligand field strength of tpy, which consequently reduces the energy gap between the triplet metal-to-ligand charge transfer ($^3\text{MLCT}$) states and triplet metal-centered (^3MC) states. 8 In contrast, complexes **5A-1** and **5A-2** exhibit room temperature luminescence due to strong σ -donation from their respective ligands.

The non-equivalency of the carbonyl units is evidenced by IR frequencies (Figure 5A.5), where three different C-O bands are observed. In complex **5A-1**, for example, the strong sharp band at 2003 cm^{-1} may be attributed to C20-O1 stretching, while the strong, broad band at 1867 cm^{-1} , with a shoulder at $\sim 1885\text{ cm}^{-1}$ could be assigned to the C21-O2 and C22-O3 stretching modes, respectively, which are in good agreement with its TD-DFT calculation (Table VA-4).

Table VA-4. Infrared Frequencies: Observed vs. Calculated

Compound	IR stretching		Bond involved
	Obs. stretching (cm ⁻¹)	Calc. stretching (cm ⁻¹)	
5A-1	2003	2093	C20-O1
	1885	2000	C22-O3
	1867	1995	C21-O2
5A-2	2005	2096	C20-O2
	1888	2006	C19-O1
	1868	1999	C21-O3
<i>fac, fac</i> -[Re(dqp - κ^3N)(CO) ₃] ⁺	2028, 1918	-----	-----

dqp = 2,6-di(8'-quinolinyl)pyridine

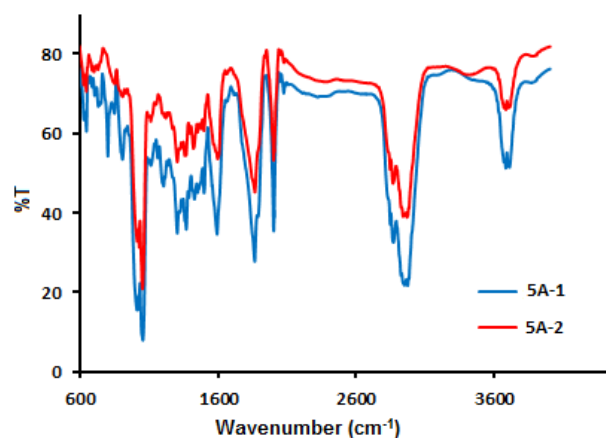


Figure 5A.5. ATR-IR spectra of complexes **5A-1** and **5A-2**, recorded at ambient temperature as solids.

5A.7. Conclusion

In conclusion, the analytical and crystal data provide evidence for the facial coordination of **5A-L1** and **5A-L2** around Re(I)-centres. To the best of our knowledge, these are among the very rare examples of tridentate 2,6-disubstituted pyridyl ligands exhibiting κ^3N -facial coordination around Re(I) in presence of three carbonyls. Due to the strong σ -donation from the ligands, these complexes are electrochemically appealing, as complexes **5A-1** and **5A-2** exhibit quasi-reversible Re-based oxidation at ~ 1.02 V (vs. Fc^+/Fc) which is ~ 320 mV less positive compared to the oxidation of rhenium in [Re(bpy)(CO)₃(Py)][ClO₄] (+1.34 V).^{31,34} The ¹MLCT and ³MLCT maxima can be fine-tuned by modifications in the electronic properties of the unsaturated aromatic backbone. Due to the structural rigidity as face-capped complexes and exciting redox and

photophysical properties, these complexes may be useful as photosensitizers in a range of photochemical reactions.

5A.8. Supporting Information

Synthetic details of all compounds and other figures, tables, DFT, TD-DFT data as indicated in main text. X-ray structural data of **5A-1** (CCDC no. 922649) and **5A-2** (CCDC no. 975057) in CIF format. This material is available free of charge via the internet at <http://pubs.acs.org>.

5A.9. References

- (1) T.J. Meyer, Molecular level artificial photosynthetic materials, in: Progress in inorganic chemistry, 44, John Wiley & Sons, Inc., New York, 1997.
- (2) Amoroso, A. J.; Coogan, M. P.; Dunne, J. E.; Fernandez-Moreira, V.; Hes, J. B.; Hayes, A. J.; Lloyd, D.; Millet, C.; Pope S. J. A.; Williams, C. *Chem. Commun.* **2007**, 29, 3066.
- (3) Bozec, H. L.; Guerchais, V., Molecular organic materials for optics, in: Topics in Organometallic Chemistry, 28, Springer Heidelberg Dordrecht, New York, 2010, Chapter 2.
- (4) (a) Berg-Brennan, C. A.; Yoon, D. I.; Slone, R. V.; Kazala, A. P.; Hupp, J. T. *Inorg. Chem.*, **1996**, 35, 2032. (b) Werrett, M. V.; Chartrand, D.; Gale, J. D.; Hanan, G. S.; MacLellan, J. G.; Massi, M.; Muzzioli, S.; Raiteri, P.; Skelton, B. W.; Silberstein, M.; Stagni, S. *Inorg. Chem.* **2011**, 50, 1229. (c) Chartrand, D.; Ruiz, C. A. C.; Hanan, G. S. *Inorg. Chem.* **2012**, 51, 12738. (d) Bessette, A.; Nag, S.; Pal, A. K.; Derossi, S.; Hanan, G. S. *Supramol. Chem.* **2012**, 24, 595.
- (5) (a) Benson, E. E.; Sampson, M. D.; Grice, K. A.; Smieja, J. M.; Froehlich, J. D.; Friebel, D.; Keith, J. A.; Carter, E. A.; Nilsson, A.; Kubiak, C. P. *Angew. Chem. Int. Ed.* **2013**, 52, 4841. (b) Takeda, H.; Koike, K.; Inoue, H.; Ishitani, O. *J. Am. Chem. Soc.* **2008**, 130, 2023.
- (6) (a) Caspar, J. V.; Meyer, T. J. *J. Phys. Chem.* **1983**, 87, 952. (b) Amoroso, A. J.; Banu, A.; Coogan, M. P.; Edwards, P. G.; Hossain, E. G.; Abdul Malik, K. M. *Dalton Trans.* **2010**, 39, 6993. (c) Black, D. R.; Hightower, S. E. *Inorg. Chem. Commun.* **2012**, 24, 16.
- (7) Juris, A.; Campagna, S.; Bidd, I.; Lehn, J.-M.; Ziessel, R. *Inorg. Chem.* **1988**, 27, 4007.
- (8) Losey, D. J.; Frenzel, B. A.; Smith, W. M.; Hightower, S. E.; Hamaker, C. G. *Inorg. Chem. Commun.* **2013**, 30, 46.
- (9) (a) Casanova, M.; Zangrando, E.; Munini, F.; Iengo, E.; Alessio, E. *Dalton Trans.* **2006**, 42, 5033. (b) De Groot, B.; Hanan, G. S.; Loeb, S. J. *Inorg. Chem.* **1991**, 30, 4644. (c) Giesbrecht, G. R.; Hanan, G. S.; Kickham, J. E.; Loeb, S. J. *Inorg. Chem.* **1992**, 31, 3286.

- (10) (a) Herrick, R. S.; Brunker, T. J.; Maus, C.; Crandall, K.; Cetin A.; Ziegler, C. J. *Chem. Commun.* **2006**, *41*, 4330. (b) Griffiths, D. V.; Cheong, Y.-K.; Duncanson P.; Motevalli, M. *Dalton Trans.* **2011**, *40*, 10215. (c) Wu, K.; Mukherjee, D.; Ellern, A.; Sadow A. D.; Geiger, W. E. *New J. Chem.*, **2011**, *35*, 2169.
- (11) (a) Schmidt, S. P.; Trogler, W. C.; Basolo F. *Inorg. Syn.* **1990**, *28*, 154. (b) Pal, A. K.; Zaccheroni, N.; Campagna, S.; Hanan, G. S. *Chem. Commun.*, **2014**, accepted.
- (12) Frisch, M. J.; Trucks, G. W.; Schlegel, H. B.; Scuseria, G. E.; Robb, M. A.; Cheeseman, J. R.; Montgomery, J. A.; Vreven, T. J.; Kudin, K. N.; Burant, J. C.; Millam, J. M.; S., I. S.; Tomasi, J.; Barone, V.; Mennucci, B.; Cossi, M.; Scalmani, G.; Rega, N.; Petersson, G. A.; Nakatsuji, H.; Hada, M.; Ehara, M.; Toyota, K.; Fukuda, R.; Hasegawa, J.; Ishida, M.; Nakajima, T.; Honda, Y.; Kitao, O.; Nakai, H.; Klene, M.; Li, X.; Knox, J. E.; Hratchian, H. P.; Cross, J. B.; Adamo, C.; Jaramillo, J.; Gomperts, R.; Startmann, R. E.; Yazyev, O.; Austin, A. J.; Cammi, R.; Pomelli, C.; Ochterski, J. W.; Ayala, P. Y.; Morokuma, K.; Voth, G. A.; Salvador, P.; Dannenberg, J. J.; Zakrzewski, V. G.; Dapprich, J. M.; Daniels, A. D.; Strain, M. C.; Farkas, O.; Malick, D. K.; Rabuck, A. D.; Raghavachari, K.; Foresman, J. B.; Ortiz, J. V.; Cui, Q.; Baboul, A. G.; Clifford, S.; Cioslowski, J.; B., S. B.; Liu, G.; Liashenko, A.; Piskorz, I.; Komaromi, I.; L., M. R.; Fox, D. J.; Keith, T.; Al-Laham, M. A.; Peng, C. Y.; Manayakkara, A.; Challacombe, M.; Gill, P. M. W.; Johnson, B. G.; Chen, W.; Wong, M. W.; Gonzalez, C.; Pople, J. A., *Gaussian 2003, Revision C.02; Gaussian Inc.:Pittsburgh PA, 2003*.
- (13) Becke, A. D. *J. Chem. Phys.* **1993**, *98*, 5648.
- (14) Lee, C.; Yang, W.; Parr, R. G. *Phys. Rev. B: Condens. Matter* **1988**, *37*, 785.
- (15) McLean, A. D.; Chandler, G. S. *J. Chem. Phys.* **1980**, *72*, 5639.
- (16) Hay, P. J.; Wadt, W. R. *J. Chem. Phys.* **1985**, *82*, 270.
- (17) (a) Casida, M. E.; Jamorski, C.; Casida, K. C.; Salahub, D. R. *J. Chem. Phys.* **1998**, *108*, 4439. (b) Stratmann, R. E.; Scuseria, G. E.; Frisch, M. J. *J. Chem. Phys.* **1998**, *109*, 8218.
- (18) (a) Cossi, M.; Rega, N.; Scalmani, G.; Barone, V. *J. Comput. Chem.* **2003**, *24*, 669. (b) Cossi, M.; Barone, V. *J. Chem. Phys.* **2001**, *115*, 4708. (c) Barone, V.; Cossi, M. *J. Phys. Chem. A* **1998**, *102*, 1995.
- (19) Browne, W. R.; O'Boyle, N. M.; McGarvey, J. J.; Vos, J. G. *Chem. Soc. Rev.* **2005**, *34*, 641.
- (20) Zhurko, D. A.; Zhurko, G. A. *ChemCraft 1.5*; Plimus: San Diego, CA. Available at <http://www.chemcraftprog.com>.
- (21) *APEX2 (2007) version 2.4-0; Bruker Molecular Analysis Research Tool*. Bruker AXS Inc., Madison, WI 53719-1173.
- (22) Sheldrick, G. M. (1996). *SADABS*, Bruker Area Detector Absorption Corrections. Bruker AXS Inc., Madison, WI 53719-1173.
- (23) *SHELXTL (2001) version 6.12*; Bruker Analytical X-ray Systems Inc., Madison, WI 53719-1173.
- (24) Wolfe, J. P.; Buchwald, S. L. *J. Org. Chem.*, **2000**, *65*, 1144

- (25) (a) Nag, S.; Ferreira, J. G.; Chenneberg, L.; Ducharme, P. D.; Hanan, G. S.; Ganga, G. L.; Serroni, S.; Campagna, S. *Inorg. Chem.* **2011**, *50*, 7. (b) Pal, A. K.; Nag, S.; Ferreira, J. G.; Brochery, V.; Ganga, G. L.; Santoro, A.; Serroni, S.; Campagna, S.; Hanan, G. S. *Inorg. Chem.* **2014**, *53*, 1679. (c) Pal, A. K.; Ducharme, P. D.; Hanan, G. S. *Chem. Commun.* **2013**, 10.1039/C3CC47856D; (d) Oakley, S. H.; Coles, M. P.; Hitchcock, P. B. *Inorg. Chem.* **2004**, *43*, 7564. (e) Pal, A. K.; Hanan, G. S. *Dalton Trans.*, **2014**, DOI: 10.1039/c4dt00112e.
- (26) Hightower, S. E.; Corcoran, R. C.; Sullivan, B. P. *Inorg. Chem.* **2005**, *44*, 9601..
- (27) Hallett, A. J.; Pope, S. J. A. *Inorg. Chem. Commun.* **2011**, *14*, 1606.
- (28) Jäger, M.; Kumar, R. J.; Görls, H.; Bergquist, J.; Johansson, O. *Inorg. Chem.* **2009**, *48*, 3228.
- (29) (a) Johansson, K. O.; Lotoski, J. A.; Tong, C. C.; Hanan, G. S. *Chem. Commun.* **2000**, *10*, 819. (b) Polson, M. I. J.; Lotoski, J. A.; Johansson, K. O.; Taylor, N. J.; Hanan, G. S.; Hasenknopf, B.; Thouvenot, R.; Loiseau, F.; Passalacqua, R.; Campagna, S. *Eur. J. Inorg. Chem.* **2002**, *10*, 2549; (c) Fang, Y.-Q.; Polson M. I. J.; Hanan, G. S. *Inorg. Chem.* **2003**, *42*, 5.
- (30) Dinolfo, P. H.; Williams, M. E.; Stern, C. L.; Hupp, J. T. *J. Am. Chem. Soc.* **2004**, *126*, 12989.
- (31) Sacksteder, L. A.; Zipp, A. P.; Brown, E. A.; Streich, J.; Demas, J. N.; DeGraff, B. A. *Inorg. Chem.* **1990**, *29*, 4335.
- (32) Stufkens, D. J.; Vlček Jr., A. *Coord. Chem. Rev.* **1998**, *177*, 127.
- (33) Wrighton, M.; Morse, D. L. *J. Am. Chem. Soc.* **1974**, *96*, 998.
- (34) A correction factor of 0.395 V corresponding to the oxidation of ferrocene in acetonitrile at ambient temperature using [*n*-Bu₄N]PF₆ (0.1 M) as an electrolyte has been deducted from the reported oxidation value of 1.74 V vs. SCE in ref 18.

Chapter 5: (B) One- and two-dimensional polymerisation of homoleptic M(II)-complexes of 4'-(3-pyridyl)-2,2';6',2''-terpyridine in the solid state: A combined study by XRD, Cyclic Voltammetry, NMR and UV-vis Spectroscopies

5B.1. Résumé

Les complexes homoleptique de Fe(II), Co(II), Ni(II), Cu(II) et Ru(II) fondé sur le ligand tridentate 4'-(3-pyridyl)-2,2':6',2''- tpy (tpy = terpyridine) ont été synthétisés avec de bons rendements et ont été caractérisés par différents techniques. Bien que les complexes de Fe(II) et Ru(II) présentent un comportement diamagnétique dans leur solution de spectres de RMN ^1H , les autres complexes ont également été examinés par RMN ^1H mais les centres métalliques paramagnétiques ont causé des résonances ^1H à être trouvées entre 0 et 100 ppm. Les propriétés électrochimiques et spectroscopiques des complexes ont également été étudiés, et le groupe pyridyle a été de montré à affecter les propriétés des complexes. En outre, un aperçu en profondeur de l'état solide de Co(II)- et Cu(II)-complexes, comme hexafluorophosphate (PF_6) sels, révèle une étreinte de terpyridine à deux dimensions, formée par intermoléculaires face-à-face π - π interactions qui donnent lieu à des feuilles étendues à deux dimensions. La modification des anions PF_6 par des tétraphénylborates volumineux (BPh_4) élimine totalement les interactions intermoléculaires entre les cations dans une dimension et un polymère à une dimension allongée est formée dans l'autre dimension.

Contribution:

Amlan K. Pal: All the work presented in this article and its writing.

Baptiste Laramée-Milette: Preliminary syntheses of the complexes.

Garry S. Hanan: Supervision and revision of the article.

One- and two-dimensional polymerisation of homoleptic M(II)-complexes of 4'-(3-pyridyl)-2,2';6',2''-terpyridine in the solid state: A combined study by XRD, Cyclic Voltammetry, NMR and UV-vis Spectroscopies

Amlan K. Pal,^a Baptiste Laramée-Milette,^a Garry S. Hanan^{a,*}

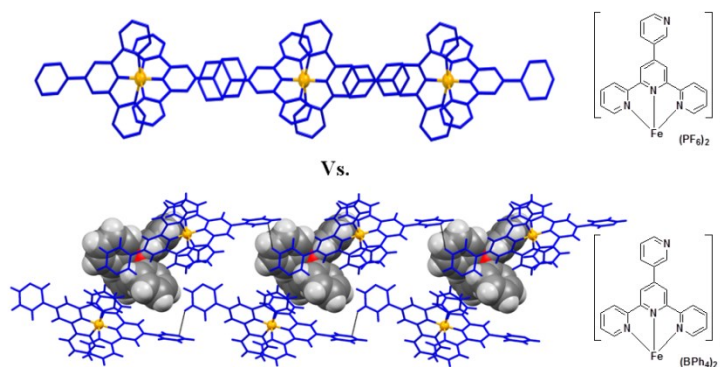
^aDepartment of Chemistry, Université de Montréal, Montréal, QC, H3T 1J4 Canada

Submitted to *Inorganica Chimica Acta* as a full paper

Submission ID: ICA-D-13-00999

KEYWORDS: Homoleptic complexes, Metalloligand, Paramagnetic behaviour, Terpyridine embrace, MLCT vs. *d-d* transition

5B.2. Table of content graphic



5B.3. Abstract

Homoleptic Fe(II), Co(II), Ni(II), Cu(II) and Ru(II) complexes based on tridentate ligand 4'-(3-pyridyl)-2,2':6',2''-tpy (tpy = terpyridine) have been synthesized in good yields and characterized with different techniques. While Fe(II) and Ru(II)-complexes exhibit diamagnetic behaviour in their solution ^1H NMR spectra, the other complexes were also examined by ^1H NMR but the paramagnetic metal centres caused ^1H resonances to be found between 0 to 100 ppm. The electrochemical and spectroscopic properties of the complexes have also been investigated, and the electron-deficient pendant pyridyl group has been shown to affect these properties. Furthermore, a deep insight into the solid state packing of Co(II)- and Cu(II)-complexes, as their hexafluorophosphate (PF_6) salts, reveals a two-dimensional terpyridine embrace, formed by face-to-face intermolecular π - π interactions that give rise to extended sheets in two dimensions. Modification of the PF_6 anions by bulky tetraphenylborate (BPh_4) anions totally eliminates the intermolecular interactions between cations in one dimension and an extended one-dimensional polymer is formed in the other dimension.

5B.4. Introduction

Regulating the structural and electronic properties on transition metal complexes by ligand modification is of interest due to the fine control that can be exerted over their photophysical,¹⁻² redox,³ and spin-state properties.⁴ The incorporation of these complexes into materials for molecular electronics^{2,5} solar energy conversion⁶ and artificial photosynthesis⁷ is thus highly desirable. While bipyridine (bpy) based metal-binding domains are commonly used as scaffolds,⁸ those based on 2,2':6',2''-terpyridine (tpy) are advantageous due to easy one-pot synthesis of structurally and substitutionally versatile motifs. The purification of bpy-based octahedral complexes, that give rise to chiral (Δ - and Λ -enantiomers) [*cis*-M(bpy)₂X₂] and [M(bpy)₃]X₂ species is a lengthy process, which is not found for η_3 -coordinated tpy-complexes. In this context, the prototype 2,2':6',2''-terpyridine and its derivatives are important structural components in metal-directed self-assembly⁸⁻¹⁴ and in the field of homo/heteropolynuclear metal-organic frameworks (MOFs) with unique properties.¹⁵⁻¹⁶

The “metalloligands as building blocks” method has proven to be a very successful pathway to construct large, discrete supramolecular assemblies¹⁷⁻²⁰ with versatile

geometries. This method has been widely accepted by several groups because of stringent control over the products formed by means of suitably oriented and readily available donor sites on the scaffolds.²¹

Reports are well documented using these metallotectons as “extended ligands”, where it has been shown that in homoleptic M(II)-complexes bearing 4'-(4-pyridyl)-2,2':6',2''-terpyridine (4-Pytpy), the N-N distance of the pendant 4-pyridyl donors is 18 Å and can give rise to discrete structures.²² Recently, considerable attention has been focused on crystalline supramolecular motifs that are two-dimensional nets and grids of tpy embraces formed by metal complexes $[M(\text{tpy})_2]^{2+}$. The tpy embrace involves two complexes attracted by offset-face-to-face (off) and edge-to-face (ef) interactions by the outer pyridyl rings of the ligand.²³⁻²⁵

Although complexes of 4-Pytpy have been well studied, those of 4'-(3-pyridyl)-2,2':6',2''-terpyridine (3-Pytpy; **5B-L**) are less explored. The complexes $[M(3\text{-Pytpy})_2]^{n+}$ have received little attention with only $[\text{Ir}(3\text{-Pytpy})_2](\text{PF}_6)_3$,²⁶ $[\text{Ru}(3\text{-Pytpy})_2](\text{PF}_6)_2$,²⁷⁻²⁹ $[\text{Fe}(3\text{-Pytpy})_2](\text{PF}_6)_2$,²⁸⁻²⁹ $[\text{Ni}(3\text{-Pytpy})_2](\text{BF}_4)_2$,²¹ catena- $[\text{Cu}(3\text{-Pytpy})_2]_n$, $n(\text{C}_4\text{Cu}_2\text{N}_4\text{S}_4)$ ³⁰ being reported to date and in most of the cases they have been used for construction of larger assemblies. Homoleptic complexes of 3-Pytpy with first row transition metal ions, such as Co(II), Ni(II) and Cu(II), with characterization by solution NMR, cyclic voltammetry and UV-vis spectroscopy have not been reported.

To this end, we report herein, a series of homoleptic complexes of first row divalent transition metal ions, such as Fe (**5B-1a** and **5B-1b**), Co (**5B-3**), Ni (**5B-4**), Cu (**5B-5**) and second row divalent-Ru (**5B-2**) with 3-Pytpy, with a general molecular formula $[(\text{C}_{40}\text{H}_{28}\text{N}_8)_2\text{M}][(\text{X})_2]$ (where M = Fe^{II}, Co^{II}, Ni^{II}, Cu^{II}, Ru^{II}, X = PF₆, BPh₄), that form either one- or two-dimensional polymers in the solid state. The complete characterization of these complexes by diamagnetic and paramagnetic solution ¹H NMR, HR-MS, EA, cyclic voltammetry, UV-vis spectroscopy, and X-ray diffraction (XRD) is included. We are also interested in the ability to switch between one- and two-dimensional structures by choice of anion, and describe such a case herein.

5B.5. Experimental section

5B.5.1. Materials, methods and instrumentation

Nuclear magnetic resonance (NMR) spectra were recorded in CD₃CN at room temperature (r.t.) on a Bruker AV400 spectrometer at 400 MHz for ¹H NMR and at 100 MHz for ¹³C NMR. Chemical shifts are reported in part per million (ppm). Electrochemical measurements were carried out in argon purged acetonitrile at room temperature with a BAS CV50W multipurpose potentiostat. The working electrode was a glassy carbon electrode. The counter electrode was a Pt wire, and the pseudo-reference electrode was a silver wire. The reference was set using an internal 1 mM ferrocene/ferrocinium sample at 395 mV *vs.* SCE in acetonitrile. The concentration of the compounds was 1 mM. Tetrabutylammonium hexafluorophosphate (TBAP) was used as supporting electrolyte and its concentration was 0.10 M. Cyclic voltammograms were obtained at scan rates of 50, 100, 200 and 500 mVs⁻¹. For irreversible oxidation processes, the cathodic peak was used as E, and the anodic peak was used for irreversible reduction processes. The criteria for reversibility were the separation of 60 mV between cathodic and anodic peaks, the close to unity ratio of the intensities of the cathodic and anodic currents, and the constancy of the peak potential on changing scan rate. The number of exchanged electrons was measured with oscillating square wave voltammetry (OSWV), and by taking advantage of the presence of ferrocene used as the internal reference.

Experimental uncertainties are as follows: absorption maxima, ±2 nm; molar absorption coefficient, 10%; redox potentials, ±10 mV; emission maxima, ±2 nm.

Metal salts and other chemicals (Aldrich) were used as supplied. Ligand **5B-L** was synthesized by a modified literature method, in refluxing ethanolic condition.³¹

5B.5.2. Synthetic methods

Bis-[4'-(3-pyridyl)-(2,2':6',2''-terpyridine)]iron(II) *hexafluorophosphate*,
 $[(C_{40}H_{28}N_8)_2Fe][(PF_6)_2] : (\mathbf{5B-1a})$

Synthesized following previously published procedure²⁹ and recrystallized from a mixture of 1:2 (v/v) acetonitrile:water. Yield 68%. ¹H NMR (400 MHz, acetonitrile-*d*₃) δ: 9.51 (s., 1 H), 9.22 (s., 2 H), 8.91 (d., J = 4 Hz, 1 H), 8.67 (d., J = 8 Hz, 1 H), 8.62 (d., J = 8 Hz, 2 H), 7.93 (t., J = 8 Hz, 2 H), 7.81 (dd., J = 12 Hz, 4 Hz, 1 H), 7.21 (d., J = 4 Hz, 2 H), 7.11

(t., $J = 8$ Hz, 2 H) ppm. $^{13}\text{C}\{^1\text{H}\}$ NMR (100 MHz, acetonitrile- d_3) δ : 161.42, 158.71, 154.02, 151.56, 149.06, 148.09, 139.78, 137.21, 133.97, 128.37, 125.67, 124.88, 122.69 ppm. ESI-MS (in CH_3CN): calculated for $\text{C}_{40}\text{H}_{28}\text{N}_8\text{PF}_6\text{Fe}$: 821.14281; found: 821.14308 (M-PF_6) $^+$, calculated for $\text{C}_{40}\text{H}_{28}\text{N}_8\text{Fe}$: 338.08931; found: 338.08910 (M-2PF_6) $^{2+}$. *Anal.* Calc. for $\text{C}_{40}\text{H}_{28}\text{N}_8\text{P}_2\text{F}_{12}\text{Fe}$: C, 49.71; H, 2.92; N, 11.59. Found: C, 50.12; H, 2.95; N, 11.62.

Bis-[4'-(3-pyridyl)-(2,2':6',2''-terpyridine)]iron(II) *tetraphenylborate,*
 $[(\text{C}_{40}\text{H}_{28}\text{N}_8)_2\text{Fe}][(\text{BPh}_4)_2]$: **(5B-1b)**

Synthesized following previously published procedure,²⁹ and the chloride salt was metathesized to BPh_4 salt by addition of excess aqueous NaBPh_4 and recrystallized from a mixture of 1:2 (v/v) acetonitrile:water. Yield 70%. ^1H NMR (400 MHz, acetonitrile- d_3) δ : 9.49 (s., 1 H), 9.18 (s., 2 H), 8.91 (br. s., 1 H), 8.60 (m., 3 H), 7.89 (br. s., 2 H), 7.78 (br. s., 1 H), 7.25 (m., 8 H), 7.16 (br. s., 2 H), 7.05 (m., 2 H), 6.96 (m., 8 H), 6.82 (m., 4 H) ppm. $^{13}\text{C}\{^1\text{H}\}$ NMR (100 MHz, acetonitrile- d_3) δ : 161.40, 158.70, 153.96, 152.42, 149.76, 148.52, 139.79, 136.61, 136.21, 133.49, 128.33, 126.52, 126.50, 126.47, 126.45, 125.30, 124.85, 122.66 ppm. ESI-MS (in CH_3CN): calculated for $\text{C}_{64}\text{H}_{48}\text{N}_8\text{BFe}$: 995.34444; found: 995.34507 (M-BPh_4) $^+$, calculated for $\text{C}_{40}\text{H}_{28}\text{N}_8\text{Fe}$: 338.08931; found: 338.08880 (M-2BPh_4) $^{2+}$. *Anal.* Calc. for $\text{C}_{88}\text{H}_{68}\text{N}_8\text{B}_2\text{Fe}\cdot\text{H}_2\text{O}$: C, 79.29; H, 5.29; N, 8.41. Found: C, 79.70; H, 5.12; N, 8.47.

Bis-[4'-(3-pyridyl)-(2,2':6',2''-terpyridine)]ruthenium(II) *hexafluorophosphate,*
 $[(\text{C}_{40}\text{H}_{28}\text{N}_8)_2\text{Ru}][(\text{PF}_6)_2]$: **(5B-2)**

Synthesized following previously published procedure²⁷ and recrystallized from a mixture of 1:2 (v/v) acetonitrile:water. Yield 62%. ^1H NMR (400 MHz, acetonitrile- d_3) δ : 9.41 (s., 1 H), 9.05 (s., 2 H), 8.87 (d., $J = 4$ Hz, 1 H), 8.56 (d., $J = 8$ Hz, 2 H), 8.61 (d., $J = 8$ Hz, 1 H), 7.97 (t., $J = 8$ Hz, 2 H), 7.80 (dd., $J = 12$ Hz, 4 Hz, 1 H), 7.45 (d., $J = 4$ Hz, 2 H), 7.21 (t., $J = 8$ Hz, 2 H) ppm. $^{13}\text{C}\{^1\text{H}\}$ NMR (100 MHz, acetonitrile- d_3) δ : 158.88, 156.54, 153.42, 151.33, 148.94, 145.93, 139.09, 137.05, 134.01, 128.52, 125.55, 122.77 (one peak is missing, may be merged with solvent peak at 118) ppm. ESI-MS (in CH_3CN): calculated for $\text{C}_{40}\text{H}_{28}\text{N}_8\text{PF}_6\text{Ru}$: 861.11493; found: 861.11325 (M-PF_6) $^+$, calculated for $\text{C}_{40}\text{H}_{28}\text{N}_8\text{Ru}$: 361.07402; found: 361.07489 (M-2PF_6) $^{2+}$.

Bis-[4'-(3-pyridyl)-(2,2':6',2''-terpyridine)]cobalt(II) *hexafluorophosphate*,
 $[(C_{40}H_{28}N_8)_2Co][(PF_6)_2]$: **(5B-3)**

3-Pytpy (0.478 g, 1.54 mmol) and $CoCl_2 \cdot 6H_2O$ (0.183 g, 0.770 mmol) were dissolved in a mixture of $CHCl_3$ (20 mL) and acetone (20 mL) and the solution was heated to reflux for 2 h. The solvent was evaporated to dryness and the chloride salt was metathesized to the PF_6 salt by addition of saturated aqueous KPF_6 solution to the aqueous solution of the compound. The resulting dark red precipitate was collected by filtration, washed with H_2O (200 mL) and Et_2O (50 mL). The red solid was redissolved in $CH_3CN:H_2O$ (50 mL, 1:1 v/v) and the solution was concentrated by slow evaporation of the solvent, and a red microcrystalline precipitate was obtained. The precipitate was dried under vacuum to afford the product. Yield: 81% (0.60 g). ATR-IR (powder, cm^{-1}): 557, 640, 660, 705, 734, 745, 787, 830, 1024, 1164, 1192, 1248, 1399, 1437, 1473, 1554, 1579, 1604, 1618. 1H NMR (400 MHz, acetonitrile- d_3) δ : 9.04 (br. s., 1 H), 9.36 (br. s., 2 H), 11.51 (br. s., 1 H), 13.76 (br. s., 1 H), 14.66 (br. s., 1 H), 33.12 (br. s., 2 H), 42.59 (br. s., 2 H), 54.74 (br. s., 2 H), 94.15 (br. s., 2 H) ppm. $^{13}C\{^1H\}$ NMR (100 MHz, acetonitrile- d_3) δ : No peak was observed due to paramagnetic nature of the compound. ESI-MS (in CH_3CN): calculated for $C_{40}H_{28}N_8PF_6Co$: 824.14052; found: 824.13968 ($M-PF_6$) $^+$, calculated for $C_{40}H_{28}N_8Co$: 339.58790; found: 339.58910 ($M-2PF_6$) $^{2+}$. *Anal.* Calc. for $C_{40}H_{28}N_8P_2F_{12}Co$: C, 49.55; H, 2.91; N, 11.56. Found: C, 49.55; H, 2.80; N, 11.49.

Bis-[4'-(3-pyridyl)-(2,2':6',2''-terpyridine)]nickel(II) *hexafluorophosphate*,
 $[(C_{40}H_{28}N_8)_2Ni][(PF_6)_2]$: **(5B-4)**

3-Pytpy (0.351 g, 1.131 mmol) and $Ni(OAc)_2 \cdot 4H_2O$ (0.141 g, 0.565 mmol) were dissolved in a mixture of ethanol-chloroform-water (50 mL, 2:2:1, v/v/v) and the solution was heated to reflux for 1 h. The solvent was evaporated to dryness and the acetate salt was metathesized to the PF_6 salt by addition of saturated aqueous KPF_6 solution to the aqueous solution of the compound. The resulting golden yellow precipitate was collected by filtration, washed with H_2O (200 mL) and Et_2O (50 mL). The yellow solid was redissolved in $CH_3CN:H_2O$ (50 mL, 1:1 v/v) and the solution was concentrated by slow evaporation of the solvent, while golden yellow coloured microcrystalline precipitate was obtained. The precipitate was dried under vacuum to afford the product. Yield: 80% (0.44 g). ATR-IR (powder, cm^{-1}): 497, 555, 615, 634, 659, 693, 711, 747, 787, 833, 1019, 1164, 1194, 1248, 1399, 1437, 1473, 1556, 1574, 1605. 1H NMR (400 MHz, acetonitrile- d_3) δ : 8.17 (br. s., 1

H), 11.44 (br. s., 1 H), 13.49 (br. s., 2 H), 43.71 (br. s., 1 H), 66.99 (br. s., 1 H), 74.37 (br. s., 1 H) ppm. $^{13}\text{C}\{^1\text{H}\}$ NMR (100 MHz, acetonitrile- d_3) δ : No peak was observed due to paramagnetic nature of the compound. ESI-MS (in CH_3CN): calculated for $\text{C}_{40}\text{H}_{28}\text{N}_8\text{PF}_6\text{Ni}$: 823.14267; found: 823.14335 (M-PF_6) $^+$, calculated for $\text{C}_{40}\text{H}_{28}\text{N}_8\text{Ni}$: 339.08897; found: 339.08971 (M-2PF_6) $^{2+}$. *Anal. Calc.* for $\text{C}_{40}\text{H}_{28}\text{N}_8\text{P}_2\text{F}_{12}\text{Ni}$: C, 49.56; H, 2.91; N, 11.56. Found: C, 49.27; H, 2.80; N, 11.94.

Bis-[4'-(3-pyridyl)-(2,2':6',2''-terpyridine)]copper(II) *hexafluorophosphate,*
 $[(\text{C}_{40}\text{H}_{28}\text{N}_8)_2\text{Cu}][(\text{PF}_6)_2]$: **(5B-5)**

3-Pytpy (0.231 g, 0.75 mmol) and $\text{CuCl}_2 \cdot 2\text{H}_2\text{O}$ (0.063 g, 0.37 mmol) were dissolved in a mixture of CHCl_3 (20 mL) and acetone (20 mL) and the solution was heated to reflux for 1 h. The solvent was evaporated to dryness and the chloride salt was metathesized to the PF_6 salt by addition of saturated aqueous KPF_6 solution to the aqueous solution of the compound. The resulting green precipitate was collected by filtration, washed with H_2O (200 mL) and Et_2O (50 mL). The green solid was redissolved in $\text{CH}_3\text{CN}:\text{H}_2\text{O}$ (50 mL, 1:1 v/v) and the solution was concentrated by slow evaporation of the solvent, while green microcrystalline precipitate was obtained. The precipitate was dried under vacuum to afford the product. Yield: 61% (0.22 g). ATR-IR (powder, cm^{-1}): 557, 633, 658, 706, 737, 743, 790, 832, 1021, 1054, 1164, 1196, 1248, 1400, 1438, 1475, 1554, 1576, 1594, 1619. ^1H NMR (400 MHz, acetonitrile- d_3) δ : 7.00 (br. s., 1 H), 8.87 (br. s., 1 H), 9.55 (br. s., 2 H), 9.66 (br. s., 2 H), 9.83 (br. s., 2 H) ppm. $^{13}\text{C}\{^1\text{H}\}$ NMR (100 MHz, acetonitrile- d_3) δ : No peak was observed due to paramagnetic nature of the compound. ESI-MS (in CH_3CN): calculated for $\text{C}_{40}\text{H}_{28}\text{N}_8\text{Cu}$: 341.58610; found: 341.58683 (M-2PF_6) $^{2+}$. *Anal. Calc.* for $\text{C}_{40}\text{H}_{28}\text{N}_8\text{P}_2\text{F}_{12}\text{Cu}$: C, 49.32; H, 2.90; N, 11.50. Found: C, 49.40; H, 2.83; N, 11.44.

5B.5.3. Crystal structure determination

X-Ray crystallographic data for **5B-1b**, **5B-3** and **5B-5** were collected from the single crystal samples, which was mounted on a loop fiber. Diffraction data were collected using a Bruker Platform diffractometer, equipped with a Bruker SMART 4 K Charged-Coupled Device (CCD) Area Detector using the program SMART and a rotating anode source $\text{Cu-K}\alpha$ radiation at 150 K. Empirical adsorption corrections were applied using the SADABS program.³² Cell refinement and data reduction were done using APEX2.³³ The structures were solved by direct method and refined using full-matrix least squares on F^2

using the SHELXTL suite of programs.³⁴ All non-H atoms were refined by full-matrix least-squares with anisotropic displacement parameters. The H-atoms were included in calculated positions and treated as riding atoms: aromatic C—H 0.95 Å with $U_{\text{iso}}(\text{H}) = k \times U_{\text{eq}}(\text{parent C-atom})$, where $k = 1.2$ for the aromatic H-atoms. The diffraction quality of the crystals was checked, revealing poor diffraction with a large amount of diffuse scattering, signaling extensive crystal disorder for compound **5B-5**. For this compound, during the refinement of its structure, electron density peaks were located and were believed to be one highly disordered solvated acetonitrile molecule and one severely disordered hexafluorophosphate anion (by counting the number of electrons suppressed). All the attempts made to model the solvent molecules and anion were not successful and they were removed using the SQUEEZE routine from PLATON,³⁵ which resulted in a significant improvement of R1 factor by $\sim 10\%$. Also, for compound **5B-3**, after rigorous refinements small electronic densities due to hydrogen atoms near to O2-atom, with proper geometry, were not found and restraints or constraints were not applied to locate ill-defined hydrogen atoms not to increase data to parameter ratio. Structures have been analysed using MERCURY version 3.3.³⁶ CCDC reference numbers 962834-962836. Specific parameters of each measurement are located in Table VB-1.

Table VB-1. Crystal data and details of the structure determination for **5B-1b**, **5B-3·2H₂O**, **5B-3·CH₃CN**

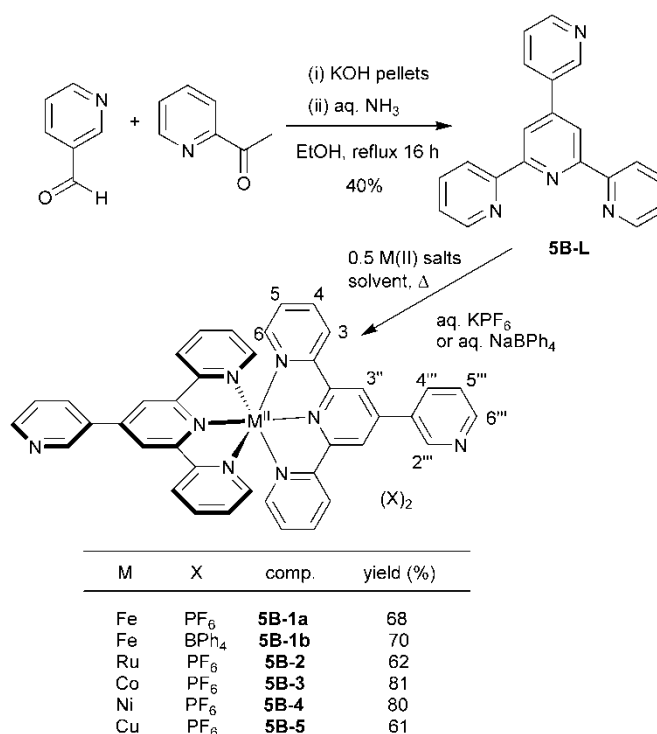
	5B-1b^a	5B-3·2H₂O^a	5B-3·CH₃CN^a
Formula	[C ₄₀ H ₂₈ N ₈ Fe][C ₂₄ H ₂₀ B] ₂	[C ₄₀ H ₂₈ N ₈ Co][PF ₆] ₂ [2H ₂ O]	[C ₄₀ H ₂₈ N ₈ Cu][PF ₆] ₂ [CH ₃ CN]
Color/form	purple needle	red needle	green needle
<i>T</i> (K); wavelength	150(2); 1.54178	150(2); 1.54178	150(2); 1.54178
Crystal System	Monoclinic	Monoclinic	Triclinic
Space Group	P2 ₁ /c	P2 ₁ /c	P-1
Unit Cell: <i>a</i> (Å)	18.0475(12)	16.6279(5)	9.0556(6)
<i>b</i> (Å)	17.6434(11)	14.8960(4)	10.3716(7)
<i>c</i> (Å)	21.3645(14)	16.3103(5)	21.8764(14)
α (°)	90	90	84.796(4)
β (°)	102.510(3)	101.6480(10)	78.733(3)
γ (°)	90	90	73.588(3)
<i>V</i> (Å ³); <i>Z</i>	6641.4(7); 4	3956.7(2); 4	1931.6(2); 2
R1(F); wR(F ²)[I>2 σ (I)]	0.0388; 0.1077	0.0341; 0.0899	0.0566; 0.1381
R1(F); wR(F ²) (all)	0.0403; 0.1102	0.0394; 0.0931	0.0857; 0.1483
GoF(F ²)	1.045	1.052	0.891
R _σ ; R(int)	0.0184; 0.0634	0.0309; 0.0548	0.0772; 0.1041

^aBruker Microstar diffractometer (Platinum 135 CCD Detector, Helios optics and, Kappa goniometer).

5B.6. Results and Discussion

Although the synthesis of the ligand 3-Pytpy has been documented elsewhere,^{27,37,38} it could easily be synthesized in multigram quantities using recently developed single-step one pot condensation procedure, involving condensation of the pyridine-3-carboxaldehyde with two equivalents of 2-acetylpyridine in presence of aqueous ammonia (as a source of NH₃), to form the central pyridine ring.³¹ It has also been reported that refluxing in ethanol helps in improving the yield and shortening the reaction time.²⁸

Chapter 5



Scheme 5B.1. Syntheses of ligand **5B-L** and complexes **5B-1a**, **5B-1b**, **5B-2**, **5B-3**, **5B-4** with atom labelling.

Complexes **5B-1a** and **5B-2** were synthesized using literature procedures.^{27,29} Complex **5B-1b** was synthesized adopting similar synthesis procedure as complex **5B-1a**, the anion was metathesized to BPh₄⁻ by addition of an aliquot of saturated solution of NaBPh₄ in water. Complexes **5B-3** to **5B-5** were synthesized using 2:1 stoichiometric ratio of ligand:metal in a chloroform/ethanol solution at reflux for 1-2 h.[‡] Immediate colour changes were observed depending on the metal ion used. The complexes were methathesized to their respective PF₆⁻ salts by addition of an excess of saturated aqueous KPF₆ solution. Recrystallization of the complexes from hot acetonitrile-water solutions provided the analytically pure complexes in good yields.

5B.6.1. NMR spectroscopy

The ¹H NMR spectra were obtained in CD₃CN for all complexes at 400 MHz, where a free rotation of the pendant 3-pyridyl ring around the C-C bond simplifies the spectra, as also observed by Ollagnier *et. al.*²⁸ While **5B-1a** and **5B-2** are found to be diamagnetic, complexes **5B-3** to **5B-5** reveal themselves to be paramagnetic due to the presence of unpaired electron in their valence shell and the ¹H signals are considerably

shifted and broadened with respect to typical diamagnetic complexes, as similar observation previously reported by Medlycott *et al.* in homoleptic M(II)-triazine (where M = Co, Ni, Cu and triazine = 2,4-di(2-pyridyl)-1,3,5-triazine) complexes.³⁹

The diamagnetic ^1H NMR spectra of **5B-1a** and **5B-2** (Figure 5B.1) resemble to that of low-spin Fe(II)- and Ru(II)- d^6 -ions, thus indicating a high ligand field strength in an approximately octahedral coordination environment of terpyridine ligand.

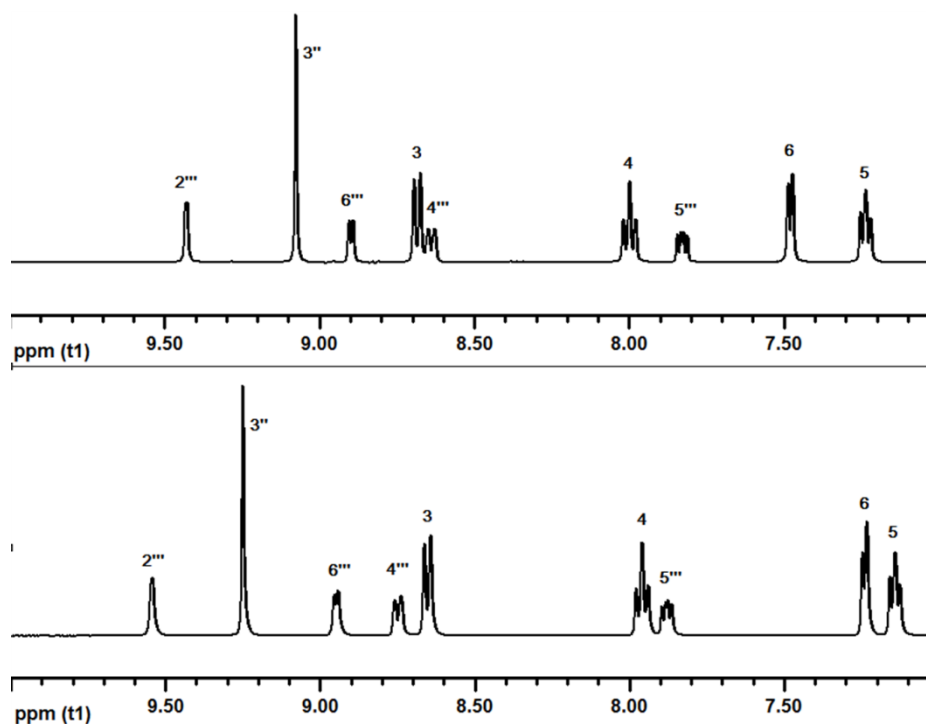


Figure 5B.1. Comparison in chemical shifts of different protons of **5B-1a** (bottom) and **5B-2** (top) by ^1H NMR at 400 MHz in CD_3CN at room temperature. For numbering see Scheme 5B.1.

Although greater downfield shifts (deshielding effect) of protons $2'''$, $3''$, $6'''$, 3 , $5'''$ are observed in Fe(II)-complex compared to its Ru(II) analogue due to the greater electronegativity of Fe(II) with respect to Ru(II), shielding effects are observed for proton numbers 5 and 6, which are closer to the metal centre, as observed by Constable *et al.*²⁹ Broad, paramagnetic signals, integrating for seven chemically distinct protons and expanding up to 100 ppm are observed in the ^1H NMR spectra of **5B-3** and **5B-4**, (Figure 5B.2) albeit, two protons are missing in ^1H NMR spectrum of complex **5B-5** due to the excessive broadening of signals induced by the paramagnetic Cu(II)-ion.

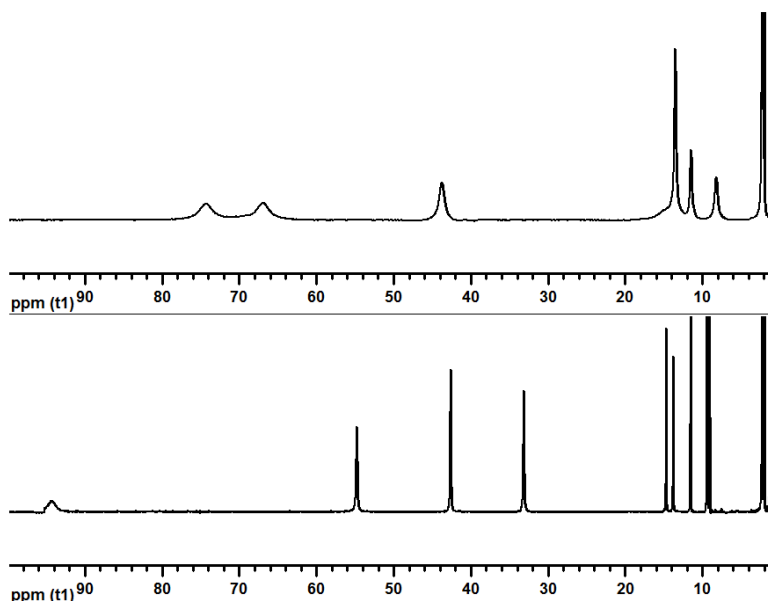


Figure 5B.2. Comparison of chemical shifts of different protons of **5B-3** (bottom) and **5B-4** (top) by ^1H NMR spectroscopy at 400 MHz in CD_3CN at room temperature, showing the paramagnetic shifting of the protons induced by the metal ions.

5B.6.2. X-ray Structural Investigation

Although the solid state structures of cationically similar complexes, for e.g., $[\text{C}_{40}\text{H}_{28}\text{N}_8\text{Fe}] [\text{2PF}_6]$ (**5B-1a**) (CCDC 662662), $[\text{C}_{40}\text{H}_{28}\text{N}_8\text{Ni}] [\text{2BF}_4]$ (CCDC 664985), catena $[\text{C}_{40}\text{H}_{28}\text{N}_8\text{Cu}]_n$, $n[\text{C}_4\text{Cu}_2\text{N}_4\text{S}_4]$ (CCDC 741499) are already reported, the anions are not the same; thereby affecting the packing environment of these structures. So, we proceeded to analyze the crystal structures of complexes **5B-3**, **5B-5** and examined the crystal packing of **5B-1b** more closely with respect to that of **5B-1a**.

X-Ray quality needle shaped crystals of **5B-1b**, **5B-3** and **5B-5** were grown by slow evaporation of a saturated solution of respective complexes in a mixture of water and acetonitrile.

Diffraction analyses reveal that all of the complexes are mononuclear and consist of $[\text{M}(\text{3-Pytpy})_2]^{2+}$ dication and BPh_4^- (for **5B-1b**) and PF_6^- (for **5B-3** and **5B-5**) counter-anions. In all the structures, the metal atom adopts a distorted octahedral geometry in a meridional arrangement of the two tridentate terpyridine units. In the solid state structure of **5B-1b**, (Figure 5B.3) the central Fe-N bonds are shorter (varies from 1.8722(13) Å to 1.8811(12) Å) with respect to the other four Fe-N bonds of the tpy moiety (varies from

1.9664(14) Å to 1.9839(13) Å). The average of bite angles subtended by the N-atoms of the individual tpy units is $162.2(\pm 1)^\circ$. These values are in close agreement to those found for $[\text{C}_{40}\text{H}_{28}\text{N}_8\text{Fe}] [\text{2PF}_6]$. Both the pendant pyridine rings are twisted with respect to the pyridine ring to which they are bonded (angular separation between the least square planes containing N2 and N4, and N6 and N8 are $30.0(\pm 1)^\circ$ and $38.9(\pm 1)^\circ$, respectively). Although in case of complex **5B-1a** with PF_6 as the counter-anions, the two pendant pyridyl rings containing the heteroatoms are spatially separated by an angle of $47.85(\pm 1)^\circ$ in the crystal structure of **5B-1b** where BPh_4 are the counter-anions, the pendant pyridyl rings are approximately perpendicular to each other with an interplanar separation of $88.8(\pm 1)^\circ$, indicating a different type of packing environment in **5B-1b** with respect to that of **5B-1a**.

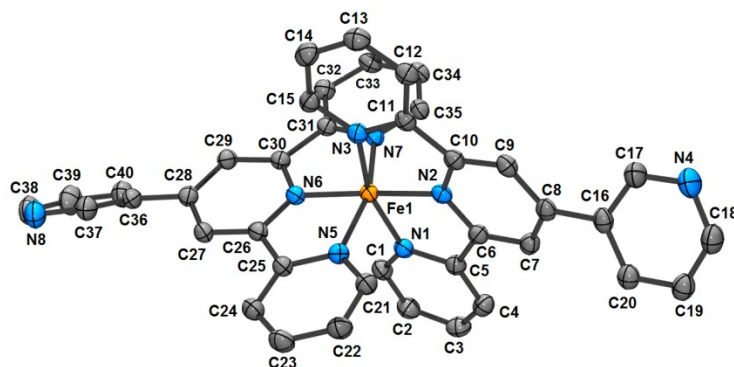


Figure 5B.3. ORTEP view of $[\mathbf{5B-1b}]^{2+}$, showing the labelling scheme. Thermal ellipsoids are drawn at a 50% probability level. Anions and hydrogen atoms are omitted for clarity. Selected bond distances and angles: Fe1-N1 = 1.9664(14) Å, Fe1-N2 = 1.8722(13) Å, Fe1-N3 = 1.9698(12) Å, Fe1-N5 = 1.9839(13) Å, Fe1-N6 = 1.8811(12) Å, Fe1-N7 = 1.9750(12) Å, N1-Fe1-N2 = $80.96(5)^\circ$, N2-Fe1-N3 = $81.33(5)^\circ$, N5-Fe1-N6 = $81.46(5)^\circ$, N6-Fe1-N7 = $80.86(5)^\circ$, N1-Fe1-N3 = $162.13(5)^\circ$, N5-Fe1-N7 = $162.31(5)^\circ$.

In the solid state structure of complex **5B-1a**, the molecules are efficiently packed by two different types of offset face-to-face (OFF) π - π interactions (Figures 5B.4 and 5B.5): (a) interactions between two pendant pyridyl groups of two different molecules and (b) interactions between one pendant pyridyl group of one molecule and the central pyridyl unit of another molecule to form a 2D-layer. Surprisingly, in the packing structure of **5B-1b**, (Figure 5B.6) no intermolecular π - π interactions were observed, rather the molecules are held together by non-classical hydrogen bonding interactions between aromatic hydrogen atoms and N-atom of the pendant pyridyl groups with a distance of 2.71 Å. The

bulky BPh₄ anions are strongly involved in the crystal packing by efficient onset face-to-face π - π interactions with the cationic moieties. These interactions reduce the dimensionality of the cation-cation interactions from two to one.

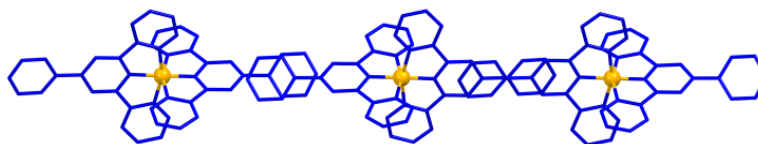


Figure 5B.4. Packing diagram of **5B-1a**, showing the offset face-to-face (OFF) π - π interactions (drawn using the crystal data in ref 29).

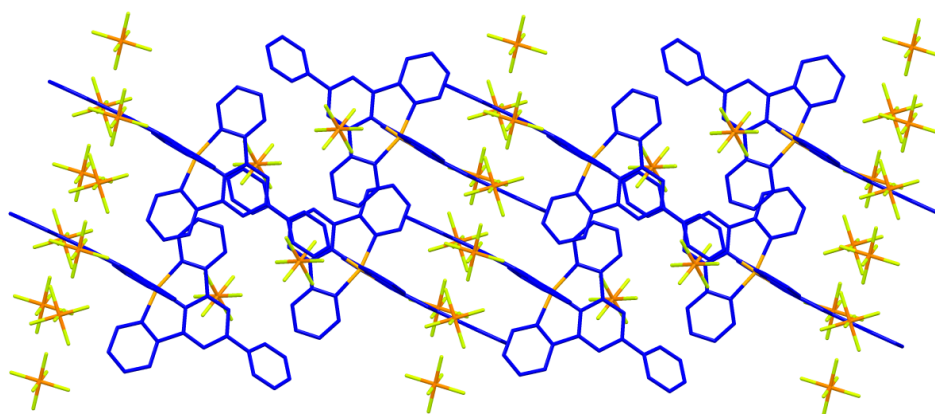


Figure 5B.5. Packing diagram of **5B-1a** in 2D showing the offset face-to-face (OFF) π - π interactions to form a layered structure (drawn using the crystal data in ref 29).

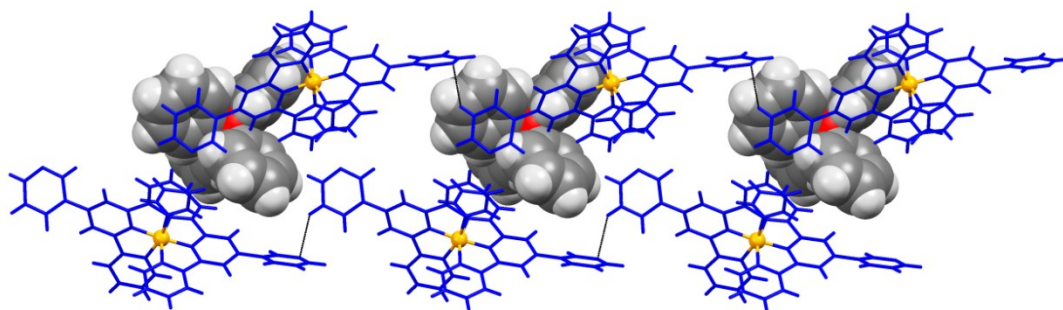


Figure 5B.6. Part of the infinite 1D-ribbon of **5B-1b**, developed by non-classical H-bonding between aromatic hydrogen atoms and N-atom of the pendant pyridyl groups (grey lines). The BPh₄ anions in the channel of two molecular layers are involved in face-to-face onset π - π interactions with the pendant pyridyl groups.

In the solid state structure of **5B-3**, (Figure 5B.7) once again the central Co-N bonds are found to be shorter (varies from 1.9306(16) Å to 1.9728(17) Å) with respect to the other four Co-N bonds of the tpy moiety (varies from 2.0472(17) Å to 2.1761(16) Å). The average of bite angles subtended by the N-atoms of the individual tpy units is 155.8((±1))°, which is ~ 6° narrower to that what is found for **5B-1b**. Unlike the crystal structure of **5B-1b**, based on the intermolecular hydrogen bonding with the co-crystallized water molecules the two pendant pyridyl rings have different angular relationships with the two crystallographically different tpy rings and the angular separation of the least square planes containing the pendant pyridyl rings is only 24.5(±1)°, with the N-atoms facing in the same direction (*cisoid*-fashion). The angle between the least squares planes consisting of the twisted pyridyl group containing N8 and the ring containing N6 atom is 19.5(±1)° and the same between the planes containing N4 and N2 is 45.9(±1)°. The fact that the heteroatoms point in the same direction with a vectorial angular separation of 60°, in turn, opens up a possibility to construct multinuclear discrete supramolecular architect using a *trans*-directing metal-binder, for example, PdCl₂. Thus, the metal complex could be thought as an extended version of 3,3'-bipyridine, where the end-to-end distance (C18-C38) is 17.71 Å.

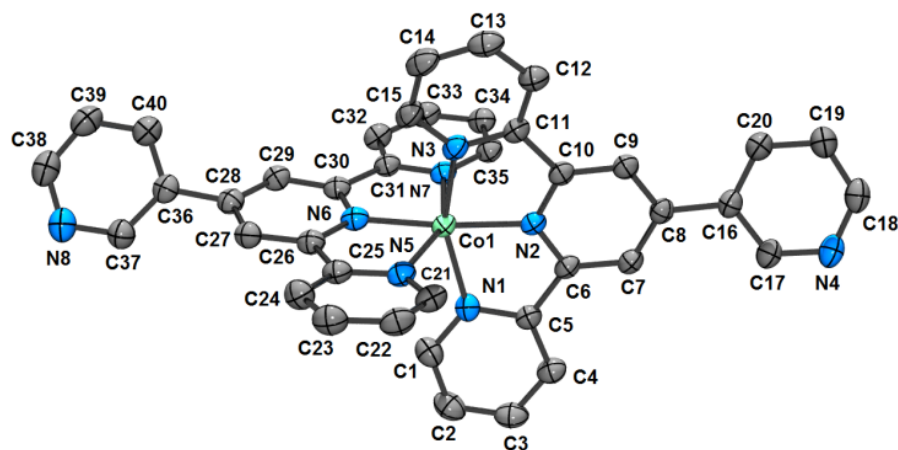


Figure 5B.7. ORTEP view of complex **5B-3**, showing the labelling scheme. Thermal ellipsoids are drawn at 50% probability level. Anions, hydrogen atoms and solvated water molecules are omitted for clarity. Selected bond distances and angles: Co1-N1 = 2.0511(17) Å, Co1-N2 = 1.9306(16) Å, Co1-N3 = 2.0472(17) Å, Co1-N5 = 2.1719(17) Å, Co1-N6 = 1.9728(17) Å, Co1-N7 = 2.1761(16) Å, N1-Co1-N2 = 78.72(6)°, N2-Co1-N3 = 79.26(7)°, N5-Co1-N6 = 77.30(6)°, N6-Co1-N7 = 78.12(7)°, N1-Co1-N3 = 156.27(7)°, N5-Co1-N7 = 155.34(7)°.

The packing of the cations of complex **5B-3** (Figure 5B.8) is supported by intermolecular hydrogen bonding between the H-atom of water with the N-atom of the pendant pyridyl groups as well as between the oxygen atom of water and H-atom of the peripheral pyridine group of the tpy unit.

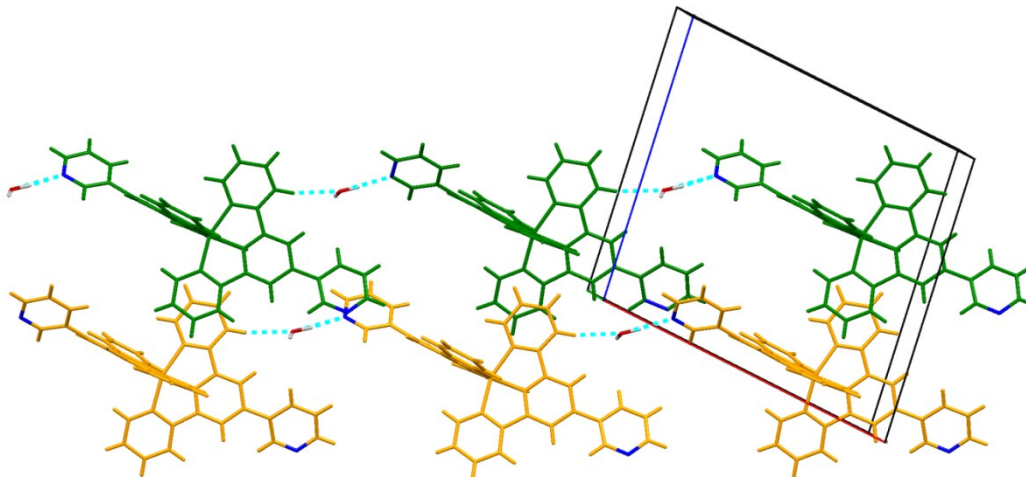


Figure 5B.8. Part of the infinite 2D-sheet of packing of complex **5B-3**, developed by face-to-face offset π - π interaction and hydrogen bonds (dotted lines) by water molecule with nitrogen and aromatic H's.

X-Ray structural analysis of complex **5B-5** (Figure 5B.9) revealed the non-exceptional distorted octahedral geometry around Cu(II)-ion, with similar trends in bond distances as reported earlier for complexes **5B-1b** and **5B-3**. The angle between the least-square's plane containing N8 atom and the same containing N6 atom is $36.9(\pm 1)^\circ$, whereas the least-square's plane containing N4 is twisted by $21.2(\pm 1)^\circ$ from the least square plane containing N2 atom. The least-square's planes containing the two pendant pyridyl substituents are separated from each other by $31.2(\pm 1)^\circ$. In the solid state, the heteroatoms in the pyridyl groups adopt a *transoid*-configuration.

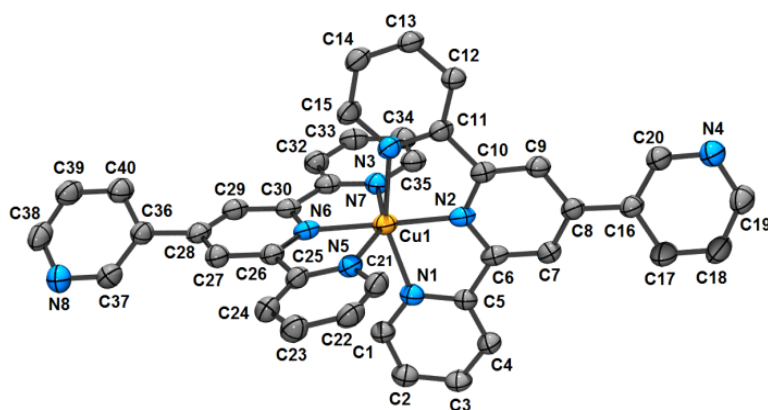


Figure 5B.9. ORTEP view of complex **5B-5**, showing the labelling scheme. Thermal ellipsoids are drawn at 50% probability level. Anions, hydrogen atoms and solvated water molecules are omitted for clarity. Selected bond distances and angles: Cu1-N1 = 2.090(3) Å, Cu1-N2 = 1.947(3) Å, Cu1-N3 = 2.113(3) Å, Cu1-N5 = 2.262(3) Å, Cu1-N6 = 2.012(3) Å, Cu1-N7 = 2.218(3) Å, N1-Cu1-N2 = 78.95(12)°, N2-Cu1-N3 = 78.87(12)°, N5-Cu1-N6 = 75.66(11)°, N6-Cu1-N7 = 77.13(11)°, N1-Cu1-N3 = 157.82(12)°, N5-Cu1-N7 = 152.59(11)°.

In the solid state, the molecules pack over one another efficiently due to aromatic π - π interactions (Figure 5B.10). Two different types of π - π interactions are observed: (i) the pendant pyridyl group of a molecule is involved in π -interactions with the pendant pyridyl group of another molecule with inter-planar distances of 4.14 Å and (ii) the pendant pyridyl group of one molecule is involved in π -interactions with one of the outer pyridyl groups of the tpy core, with interplanar distances of 3.88 Å. Weak, but extensive, electrostatic interactions among the aromatic H-atoms and aromatic π -cloud also contribute significantly to the overall crystal packing of **5B-5**.

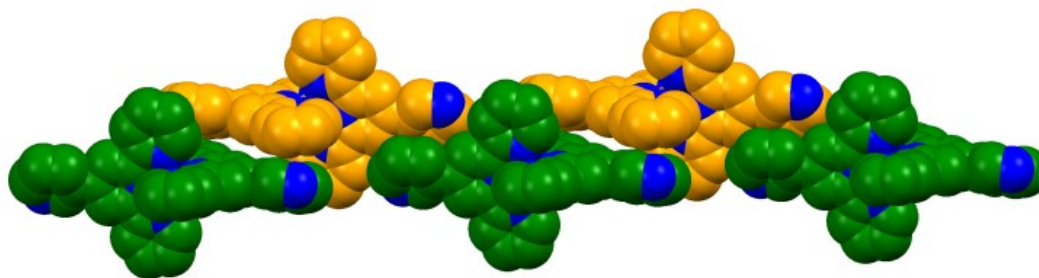


Figure 5B.10. Part of the crystal packing of **5B-5**, showing the onset π - π stacking, leading to a 2D-sheet.

5B.6.3.Redox Behaviour

The electrochemical parameters of complexes **5B-1a**, **5B-2** to **5B-5** were measured in dry, degassed acetonitrile using tetrabutylammonium hexafluorophosphate as the supporting electrolyte and glassy carbon electrode as working electrode and ferrocene as the internal standard. The data (reported vs. SCE) are gathered in Table VB-2. In all the cases the redox processes were found to be monoelectronic. Although the electrochemical behaviour of complexes **5B-1a** and **5B-2** are already documented,²⁹ we report herein the redox potentials of these two complexes calibrated against SCE, as compared to previously reported values against Fc^+/Fc . Quasi-reversible metal-based oxidations are observed within 1.2-1.4 V range, however the Ru(III)/Ru(II) (Figure 5B.11) appears to be ~ 130 mV more positive than the same of Fe(III)/Fe(II) couple, which is also observed in their prototypes $[\text{M}(\text{tpy})_2]^{n+}$.^{40,41} This result supports the red-shifting of the lowest energy ³MLCT maxima of complex **5B-1a** compared to the same of **5B-2**, in their respective electronic absorption spectroscopies.

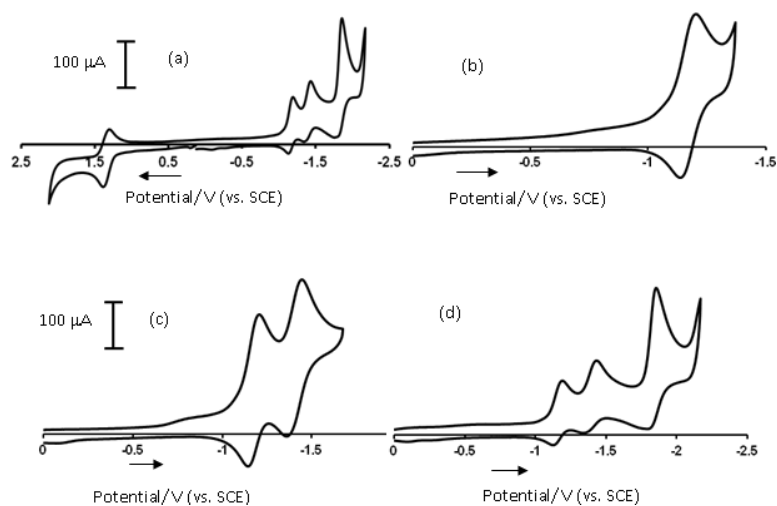


Figure 5B.11. (a) Cyclic voltammogram of **5B-2** at 50 mV/s in dry, degassed acetonitrile with 0.1 (M) TBAPF₆ at ambient temperature with magnified views of (b) first reversible reduction; (c) first and second quasi-reversible reductions; (d) first, second and third quasi-reversible reductions.

In complex **5B-3**, the $\text{Co}^{\text{II/III}}$ couple is quasi-reversibly centered at approximately +0.48 V, which is 210 mV and 240 mV more positive than $\text{Co}(\text{tpy})_2^{3+}/\text{Co}(\text{tpy})_2^{2+}$ and $\text{Co}(\text{tolyl-tpy})_2^{3+}/\text{Co}(\text{tolyl-tpy})_2^{2+}$ couples,^{40,42} respectively, due to the presence of electron-

withdrawing pendant 3-pyridyl moiety. This value is also 100 mV and 60 mV more positive than $\text{Co}(\text{Cl-tpy})_2^{3+}/\text{Co}(\text{Cl-tpy})_2^{2+}$ and $\text{Co}(\text{CH}_3\text{O}_2\text{S-tpy})_2^{3+}/\text{Co}(\text{CH}_3\text{O}_2\text{S-tpy})_2^{2+}$ couples,⁴² respectively, suggesting that the 3-pyridyl group is more electron withdrawing than the chlorine-atom or $\text{CH}_3\text{O}_2\text{S}$ -group. The quasi-reversible nature of this peak may be due to almost equal or slower electron self-exchange rate between Co(II) and Co(III) compared to the electron transfer rate between the cobalt ions and the electrode surface.⁴² The electron self-exchange rate between Co(II) and Co(III) is delayed because of a change in electronic spin states, where Co(III) would favour the low-spin state while Co(II) is a mixture of both spin states, as observed by paramagnetic shifting of peaks in compound **5B-3**. In contrast, the oxidation potential is ~ 280 mV less positive compared to homoleptic $\text{Co}(\text{Ph-dpt})_2^{3+}/\text{Co}(\text{Ph-dpt})_2^{2+}$ (where Ph-dpt = 2,4-di(2'-pyridyl)-6-(phenyl)-1,3,5-triazine),⁴³ due to the electron withdrawing nature of the triazine core.

The cathodic region is rich with several one-electron reduction phenomena, amongst which the first reversible reduction could be assigned to $\text{Co}^{\text{II}}/\text{Co}^{\text{I}}$ couple, which appears at ~ 90 mV more negative compared to $\text{Co}(\text{Ph-dpt})_2^{3+}/\text{Co}(\text{Ph-dpt})_2^{2+}$ system due to the relatively electron rich tpy core instead of an electron deficient triazine moiety. The other reductions, which are also ligand-based, follow the same trend when compared to $\text{Co}(\text{Ph-dpt})_2(\text{PF}_6)_2$.

In the absence of sufficient electrochemical data of Ni(II)-polypyridyl complexes in the literature, in complex **5B-4**, the irreversible peak centered around +1.73 V may be assigned to oxidation of Ni(II) to Ni(III). In the cathodic region the first three quasi-reversible peaks could be assigned to the ligand-based reductions and an irreversible peak at ~ -2.17 V is attributed to the reduction of Ni(II), which is ~ 700 mV more negative than that of Ni(II) in a homoleptic complex with Br-Ph-dpt (where Br-Ph-dpt = 2,4-di(2'-pyridyl)-6-(*p*-bromophenyl)-1,3,5-triazine), due to the significantly higher electron withdrawing effect of a dpt-core compared to a tpy-core.³⁹

No oxidative phenomena were observed for complex **5B-5**, although in the cathodic region a quasi-reversible reduction at -0.23 V is observed followed by a broad reductive signal at -0.83 V. These values are consistent with the metal-based reduction as previously reported by Medlycott *et al.*³⁹ At a sufficiently negative potential a ligand-based reduction can also be observed.

Table VB-2. Redox data of complexes **5B-1a**, **5B-2** to **5B-5** in dry, degassed acetonitrile.

Compound	$E_{1/2}(\text{ox})^a$	$E_{1/2}(\text{red})^a$	$\Delta E_{1/2}^b$
5B-1a	1.22 (60)	-1.13 (85), -1.25 (74), -1.87 (122)	2.35
5B-2	1.35 (86)	-1.16 (61), -1.38 (88), -1.80 (104)	2.51
5B-3	0.48 (100)	-0.51 (64), -1.32 (63), -1.65 (67), -1.96 (93)	0.99
5B-4	1.73 (irr) ^b	-1.18 (71), -1.39 (98), -1.93 (138), -2.17 (150)	2.91
5B-5	-----	-0.23 (65), -0.83 (irr) ^b , -1.94 (110)	-----
Fe(L) ₂	0.78 ^c	-1.30, ^c -1.66, ^c -2.23 ^c	2.08
Fe(tpy) ₂	1.10 (70) ^d	-1.13 (70), ^d -1.27 (60), ^d -1.94 (70) ^d	2.23
Ru(L) ₂	0.96 ^c	-1.25, ^c -1.73 ^c	2.21
Co(tpy) ₂	0.27 (60) ^d	-0.77 (70), ^d -1.66 (60) ^d	1.04
Co(tolyl-tpy) ₂	0.24 ^e	----- ^f	-----
Co(Cl-tpy) ₂	0.38 ^e	----- ^f	-----
Co(CH ₃ O ₂ S-tpy) ₂	0.42 ^e	----- ^f	-----
Co(Ph-trz) ₂	0.76 (irr) ^{b,g}	-0.42 (73), ^g -1.06 (72), ^g -1.47 (85) ^g	1.18
Ni(tpy) ₂	1.65 (60) ^d	-1.20 (80), ^d -1.38 (100) ^d	2.85
Ni(Br-Ph-trz) ₂	----- ^f	-0.76 (72) ^h , -0.88 (76) ^h , -1.46 (irr) ^h , -1.64 (irr) ^{b,h}	-----
Cu(Br-Ph-trz) ₂	----- ^f	-0.11 (irr) ^h , -1.28 (irr) ^h , -1.56 (irr) ^h	-----
Co(tolyl-trz) ₂	----- ^f	-0.50 (irr) ^h , -1.12 (irr) ^h , -1.53 (100) ^h	-----

^aPotentials are in volts vs. SCE for acetonitrile solutions, 0.1 M in TBAPF₆, recorded at 25 ± 1 °C at a sweep rate of 50 mV/s, using ferrocene as internal standard. The difference between cathodic and anodic peak potentials (millivolts) is given in parentheses. All the compounds are recorded as their hexafluorophosphate salts in their divalent states, [b] Irreversible; potential is given for the cathodic wave. ^cfrom ref 29, ^dfrom ref 36, ^efrom ref 38, ^fno data available, ^gfrom ref 39, ^hfrom ref 34.

5B.6.4. UV-vis and Emission Spectroscopy

The electronic absorption spectra of the complexes were recorded in dry, degassed acetonitrile solution at room temperature and the absorption data are gathered in Table VB-3. The UV-region of the electronic spectra are dominated by ligand centered $\pi\text{-}\pi^*$ and $n\text{-}\pi^*$ transitions. While complexes **5B-1a**, **5B-2** and **5B-3** are intensely coloured, complexes **5B-4** and **5B-5** appear to be lightly coloured, due to weak, symmetry forbidden d-d transitions in the visible and near IR regions of their absorption spectra. Complexes **5B-1a** and **5B-2** are intensely coloured due to an allowed metal-to-ligand charge transfer (¹MLCT) band in the visible region, which is characteristic for low-spin, predominantly diamagnetic complexes of d^6 metal ions. The broad ¹MLCT bands in the electronic absorption spectra of both **5B-1a** and **5B-2** can be resolved with higher energy shoulders, which may be a consequence of transitions to a tpy-based LUMO and a second, low-lying tpy based LUMO+1 in the ligand. The 3-pyridyl substituent is more electron withdrawing compared

to a proton at the 4'-position of the parent tpy complex, as indicated by the *Hammett* σ parameter of 0.55 for the pendant 3-pyridyl moiety and hence the bathochromic shift in $^1\text{MLCT}$ maxima of complexes **5B-1a** and **5B-2**, compared to their tpy analogues ($^1\text{MLCT}$ maxima of $(\text{tpy})_2\text{Fe}(\text{II})$ and $(\text{tpy})_2\text{Ru}(\text{II})$ are 548 nm and 475 nm, respectively).⁴¹ The high intensity of the colour of complex **5B-3** (dark red) is due to several modestly absorbing MLCT transitions at a relatively higher energy region compared to complexes **5B-4** (pale yellow) and **5B-5** (pale green).

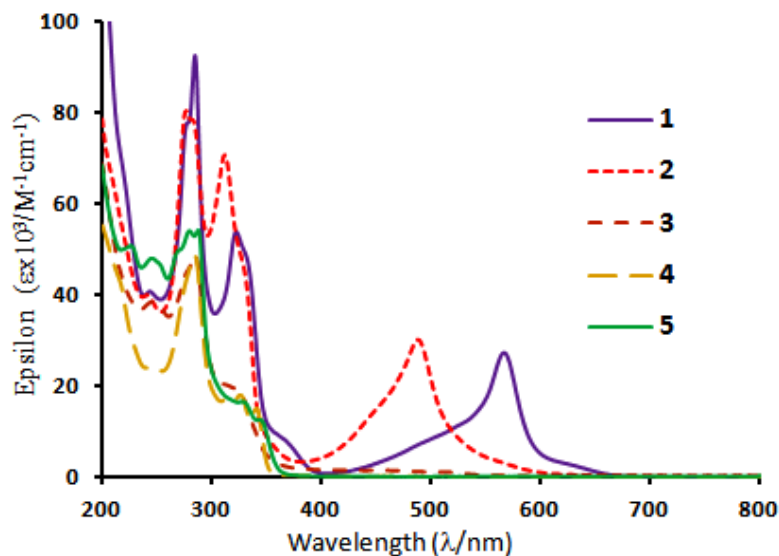


Figure 5B.12. Electronic absorption spectra of compounds **5B-1a**, **5B-2** to **5B-5** at room temperature in deaerated acetonitrile.

The electronic absorption spectra of complexes **5B-3** and **5B-5** are particularly interesting in terms of metal-centered d-d transitions in a tetragonally distorted ligand field, which is deviated from octahedral geometry by means of Jahn-Teller Effect, as found for low-spin Co(II) (d^7) and Cu(II) (d^9)-ions. Considering one unpaired electron in d_z^2 orbital, as evidenced by their paramagnetic ^1H NMR spectra, for complex **5B-3**, the electron occupancy can be $(d_{xz}, d_{yz})^4, (d_{xy})^2, (d_z^2)^1$ and thus, one would expect two different d-d transitions from $(d_{xz}, d_{yz})^4$ to $(d_z^2)^1$ and $(d_{xy})^2$ to $(d_z^2)^1$, with one electron orbital sequence $d_z^2 > d_{xy} > (d_{xz}, d_{yz})$. Indeed, complex **5B-3** exhibits two ligand field transitions centered at 517 nm and 682 nm, which may be assigned to $(d_{xz}, d_{yz})^4$ to $(d_z^2)^1$ and $(d_{xy})^2$ to $(d_z^2)^1$ transitions, respectively.⁴⁴

Following the similar arguments, the electronic configuration in d^9 -Cu(II)-complex, with one electron occupancy would be $(d_{x^2-y^2})^1 > (d_z)^2 > (d_{xy})^2 > (d_{xz}, d_{yz})^4$ and so, the electronic transitions centered at 668 nm and 760 nm could be assigned to transitions from (d_{xz}, d_{yz}) to $d_{x^2-y^2}$ and from d_{xy} to $d_{x^2-y^2}$, respectively, as observed by Nair *et al.*⁴⁴

Emission data were recorded in dry, degassed acetonitrile solution, where only complex **5B-2** was found to be emissive at 695 nm at ambient temperature.

Table VB-3. Electronic absorption data of complexes **5B-1a**, **5B-2** to **5B-5** in dry, degassed acetonitrile.

Compound	UV-vis Absorption
	λ_{\max} , nm ($\epsilon \times 10^3$, $M^{-1}cm^{-1}$)
5B-L^a	245.5, 277
5B-1a	224 (40), 278 (77), 283 (92), 322 (53), 367 (7), 566 (27)
5B-2	241 (38), 277 (80), 283 (78), 312 (70), 488 (28)
5B-3	247 (38), 285 (48), 311 (20), 324 (19), 412 (1.5), 460 (1.4), 517 (1.0), 682 (0.01)
5B-4	249 (23), 284 (48), 315 (17), 327 (17), 341 (15)
5B-5	226 (51), 245 (48), 280 (54), 287 (54), 328 (16), 343 (12), 668 (0.05), 760 (0.04)
[Cu(tolyl-tpy) ₂](ClO ₄) ₂ ^{b,c}	277 (41.4), 360 (3.0), 572 (0.06), 680 (0.09)
[Cu(BrPh-tpy) ₂](ClO ₄) ₂ ^{b,c}	278 (61.9), 360 (6.1), 574 (0.06), 641 (0.07)
[Ni(5B-L) ₂](BF ₄) ₂ ^d	284, 314, 326, 341
[Co(tolyl-tpy) ₂](ClO ₄) ₂ ^e	315 (52), 415 (3.1), 444 (2.7), 480 (2.4), 513 (2.7), 560 (0.6)
[Co(BrPh-trz) ₂](PF ₆) ₂ ^f	295 (54.8), 315 (sh), 421 (0.33), 478 (0.3), 527 (0.26)
[Ni(BrPh-trz) ₂](PF ₆) ₂ ^f	295 (67.2), 328 (sh), 848 (0.07)
[Cu(BrPh-trz) ₂](PF ₆) ₂ ^f	286 (45.8), 325 (sh), 458 (0.05), 713 (0.07)

^afrom ref 28, ^bfrom ref 44, ^cin DMSO, ^dfrom ref 21, ^efrom ref 44, ^ffrom ref 39.

5B.7. Conclusions

Electron-withdrawing 3-pyridyl substituted tpy has been prepared. Homoleptic 1st and 2nd row transition metal complexes in their divalent states were also synthesized. When PF₆ anions were replaced with BPh₄ anions, two-dimensional terpyridine embraces were suppressed in the solid state packing of cation [**5B-1b**]²⁺. UV-vis absorption spectroscopy reveals spin-allowed ¹MLCT transitions for complexes **5B-1a** and **5B-2**, whereas complexes **5B-3** and **5B-5** exhibit d-d transitions at relatively lower energies. The quasi-reversible metal-based oxidation and reduction could be easily achievable for complex **5B-3**, which may allow this complex to behave as a redox mediator.³⁹ In the field of supramolecular chemistry, these complexes with varied intrinsic properties may find

application as “metalloligands as building blocks” which behave similarly as 3,3-bipyridine and 4,7-phenanthroline.⁴⁶

5B.8. Acknowledgements

The authors thank the Natural Sciences and Engineering Research Council of Canada (NSERC) and Centre for Self-Assembled Chemical Structure (CSACS) for financial support.

5B.9. Notes and references

‡Sometimes additional amount of water is needed to dissolve the metal salt.

CCDC reference numbers 962834-962836. For ESI and crystallographic data in CIF or other electronic format see DOI: 10.1039/b000000x.

- (1) A. Juris, V. Balzani, F. Barigelletti, S. Campagna, P. Belser, A. Von Zelewsky, *Coord. Chem. Rev.*, 1988, **84**, 85, and references therein.
- (2) H. Hofmeier, U. S. Schubert, *Chem. Soc. Rev.*, 2004, **33**, 373.
- (3) H.C. Hurrell, H.D. Abruna, *Inorg. Chem.*, 1990, **29**, 736.
- (4) E. Constable, G. Baum, E. Bill, R. Dyson, R. Eldik, D. Fernske, S. Kaderli, D. Morris, A. Neubrand, M. Neuburger, D. Smith, K. Wieghardt, M. Zehnder, A.D. Zuberbuhler, *Chem. Eur. J.*, 1999, **5**, 498.
- (5) P.R. Andres, U.S. Schubert, *Adv. Mater.*, 2004, **16**, 1043.
- (6) J.-P. Sauvage, J. P. Collin, J. C. Chambron, S. Guillerez, C. Coudret, V. Balzani, F. Barigelletti, L. Decola, L. Flamigni, *Chem. Rev.*, 1994, **94**, 993.
- (7) J. H. Alstrum-Acevedo, M. K. Brennaman, T. J. Meyer, *Inorg. Chem.*, 2005, **44**, 6802.
- (8) C. Kaes, A. Katz, M. W. Hosseini, *Chem. Rev.*, 2000, **100**, 3553.
- (9) U. S. Schubert, H. Hofmeier, G. R. Newkome, *Modern Terpyridine Chemistry*; WILEY-VCH: Weinheim, 2006.
- (10) R. Kitaura, G. Onoyama, H. Sakamoto, R. Matsuda, S.-I. Noro, S. Kitagawa, *Angew. Chem., Int. Ed.*, 2004, **116**, 2738.
- (11) J. W. Steed and J. L. Atwood, *Supramolecular Chemistry*, John Wiley and Sons, Ltd, 2nd edn, 2009.
- (12) R. Chakrabarty, P. S. Mukherjee and P. J. Stang, *Chem. Rev.*, 2011, **111**, 6810–6918.
- (13) S. Perera, X. Li, M. Guo, C. Wesdemiotis, C. N. Moorefield and G. R. Newkome, *Chem. Commun.*, 2011, **47**, 4658.
- (14) X. Lu, X. Li, J.-L. Wang, C. N. Moorefield, C. Wesdemiotis and G. R. Newkome, *Chem. Commun.*, 2012, **48**, 9873.
- (15) Y.-B. Dong, M. D. Smith, H.-C. zur Loye, *Inorg. Chem.*, 2000, **39**, 1943.
- (16) S. R. Halper, L. Do, J. R. Stork, S. M. Cohen, *J. Am. Chem. Soc.*, 2006, **128**, 15255.

- (17) P. Wang, C. N. Moorefield, M. Panzer and G. R. Newkome, *Chem. Commun.*, 2005, **35**, 4405.
- (18) S.-S. Sun and A. J. Lees, *Inorg. Chem.*, 2001, **40**, 3154.
- (19) M. Tominaga, S. Tashiro, M. Aoyagi, M. Fujita, *Chem. Commun.*, 2002, **18**, 2038.
- (20) M. Aoyagi, K. Biradha, M. Fujita, *J. Am. Chem. Soc.*, 1999, **121**, 7457.
- (21) L. Gou, L.-F. Xu, H.-M. Hu, B.-C. Wang, Q.-R. Wu, X.-L. Chen, Z.-X. Tang, *Z. Anorg. Allg. Chem.* 2008, **634**, 1215.
- (22) E. C. Constable, *Coord. Chem. Rev.*, 2008, **252**, 842.
- (23) M. L. Scudder, H. A. Goodwin and I. G. Dance, *New J. Chem.*, 1999, **23**, 695.
- (24) J. McMurtrie and I. G. Dance, *Cryst. Eng. Comm.*, 2010, **12**, 2700.
- (25) (a) J. McMurtrie and I. G. Dance, *Cryst. Eng. Comm.*, 2009, **11**, 1141, (b) K. Banerjee, K. Biradha, *Cryst. Growth Des.*, 2012, **12**, 4264.
- (26) K. J. Arm, W. Leslie and J. A. G. Williams, *Inorg. Chim. Acta*, 2006, **359**, 1222.
- (27) E. C. Constable, C. E. Housecroft, M. Neuburger, S. Schaffner and F. Schaper, *Inorg. Chem. Commun.*, 2006, **9**, 433.
- (28) C. M. Ollagnier, D. Nolan, C. M. Fitchett and S. M. Draper, *Inorg. Chem. Commun.*, 2007, **10**, 1045.
- (29) J. E. Beves, E. L. Dunphy, E. C. Constable, C. E. Housecroft, C. J. Kepert, M. Neuburger, D. J. Price and S. Schaffner, *Dalton Trans.*, 2008, 386.
- (30) W.-J. Shi, *Acta Crystallogr., Sect. E*, 2009, **65**, m814.
- (31) J. Wang and G. S. Hanan, *Synlett*, 2005, 1251.
- (32) Sheldrick, G. M. (1996). *SADABS*, Bruker Area Detector Absorption Corrections. Bruker AXS Inc., Madison, WI 53719-1173.
- (33) *APEX2 (2007) version 2.4-0; Bruker Molecular Analysis Research Tool*. Bruker AXS Inc., Madison, WI 53719-1173.
- (34) *SHELXTL (2001) version 6.12*; Bruker Analytical X-ray Systems Inc., Madison, WI 53719-1173.
- (35) Platon (A. L. Spek, 2003).
- (36) I. J. Bruno, J. C. Cole, P. R. Edgington, M. K. Kessler, C. F. Macrae, P. McCabe, J. Pearson, R. Taylor, *Acta Crystallogr., Sect. B*, 2002, **58**, 389.
- (37) C. B. Smith, C. L. Raston and A. N. Sobolev, *Green Chem.*, 2005, **7**, 650.
- (38) L. Persaud and G. Barbiero, *Can. J. Chem.*, 1991, **69**, 315.
- (39) E. A. Medlycott, K. A. Udachin and G. S. Hanan, *Dalton Trans.*, 2007, 430.
- (40) C. Arana, S. Yan, M. Keshavarz-K, K. T. Potts, and H. D. Abruna, *Inorg. Chem.*, 1992, **31**, 3680.
- (41) (a) E. C. Constable and A. M. W. C. Thompson, *J. Chem. Soc., Dalton Trans.*, 1994, 1409, (b) C. Hansch, A. Leo, R. W. Taft, 1991, **91**, 165.
- (42) J. Chambers, B. Eaves, D. Parker, R. Claxton, P. S. Ray, S. J. Slattery, *Inorg. Chim. Acta.*, 2006, **359**, 2400.
- (43) E. A. Medlycott, I. Theobald and G. S. Hanan, *Eur. J. Inorg. Chem.*, 2005, 1223.
- (44) V. Uma, V. G. Vaidyanathan, and B. U. Nair, *Bull. Chem. Soc. Jpn.*, 2005, **78**, 845.

Chapter 5

- (45) J. Lombard, R. Boulaouche, D. A. Jose, J. Chauvin, M. -N. Collomb, A. Deronzier, *Inorg. Chim. Acta.*, 2010, **363**, 234.
- (46) (a) J. R. Hall, S. J. Loeb, G. K. H. Shimizu, G. P. A. Yap, *Angew. Chem., Int. Ed.*, 1998, **37**, 121, (b) M.-P. Santoni, A. K. Pal, G. S. Hanan, M.-C. Tang, K. Venne, A. Furtos, P. Ménard-Tremblay, C. Malveau, B. Hasenknopf, *Chem. Commun.*, 2012, **48**, 200, (c) A. K. Pal, B. Laramée-Milette, G. S. Hanan, *RSC Adv*, 2014, submitted for publication.

Chapter 5: (C) Self-Assembly of supramolecular triangles with neutral directing units

5C.1. Résumé

L' auto-assemblage des complexes métal-polypyridyl homoleptique fonctionnalisés par un groupe 3-pyridyl donne lieu à des métallo-supramoléculaires triangles comme confirmé par une combinaison de techniques analytiques.

Contribution:

Amlan K. Pal: All the work presented in this article and its writing.

Baptiste Laramée-Milette: Preliminary syntheses of the complexes.

Garry S. Hanan: Supervision and revision of the article.

Self-Assembly of supramolecular triangles with neutral directing units

Amlan K. Pal,^a Baptiste Laramée-Milette,^a Garry S. Hanan^{a,*}

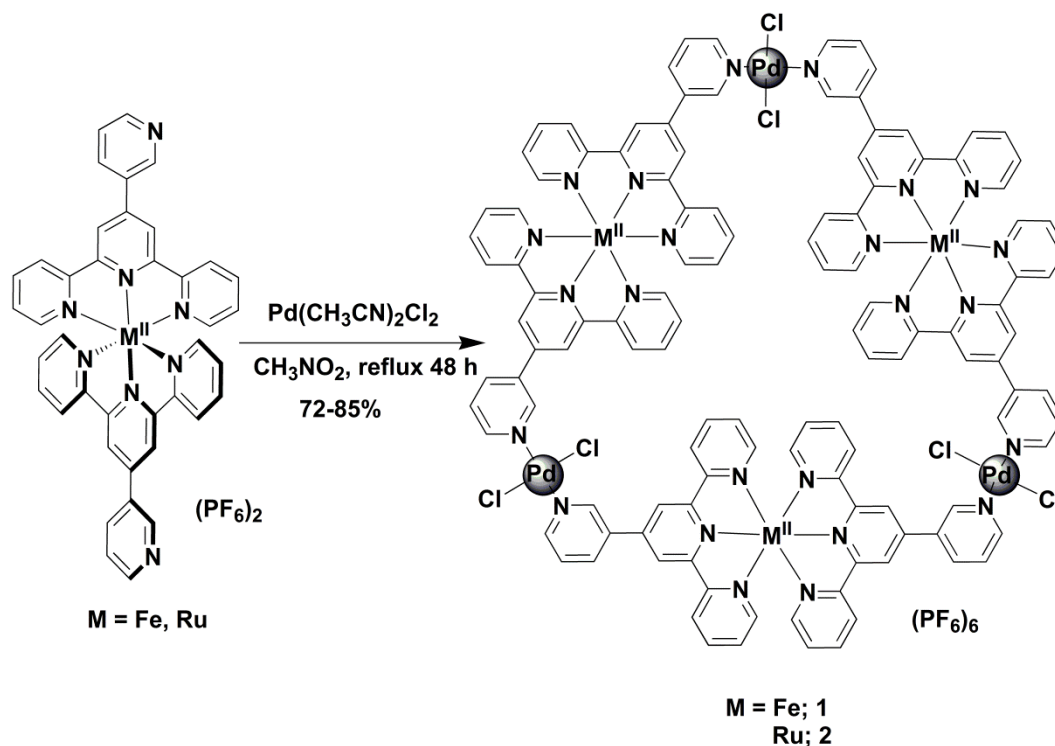
^aDepartment of Chemistry, Université de Montréal, Montréal, QC, H3T 1J4 Canada

Submitted as communication to *RSC Advances*

Submission ID: RA-COM-02-2014-001596

KEYWORDS: Homoletic complexes, Metallo-ligand, Self-assembly, NMR behaviour, Electrochemistry

5C.2. Table of content graphic



5C.3. Abstract

Pd(II)-directed self-assembly of homoleptic metal-polypyridyl complexes functionalized with 3-pyridyl group gives rise to supramolecular metallo-triangles as confirmed by a combination of analytical techniques.

5C.4. Introduction

The self-assembly of building-blocks by carefully designed directing units is of continuing interest due to the growing applications of an ever-increasing number of supramolecular architectures.¹ Since the pioneering work by Lehn² and Sauvage³ these assemblies find diverse applications in encapsulation of guest molecules with unusual chemical activity,⁴ supramolecular catalysis,⁵ *functional* nano-architectures,⁶ and material chemistry⁷ due to their rich redox and photophysical properties.^{8,9} Since the first self-assembled molecular square, prepared by Fujita and co-workers, based on labile and cationic Pd(II)-binder,¹⁰ much attention has been focused on Pd(II), Pt(II) and Re(I) based supramolecular architectures.¹¹ Interestingly, most examples of self-assembly are predominantly based on cationic metal complexes, while reported supramolecules with neutral metal complexes are comparatively few,¹² probably due to the poor solubility of the resulting assemblies. Nonetheless, the latter compounds have an advantage as they can act as both cation and anion-receptors in sensors.

In this context, we present herein the self-assembly of metallo-ligands, i.e., using metal-polypyridyl complexes as bridging ligands with neutral metal complex, trans PdCl₂, to synthesize hexanuclear metallo-triangles. The metallo-ligands used in this study are homoleptic Fe(II) and Ru(II) complexes of 4-(3-pyridyl)-2,2':6',2''-terpyridine, (3-pytpy).

5C.5. Experimental section

5C.5.1. Materials, methods and instrumentation

Nuclear magnetic resonance (NMR) spectra were recorded in CD₃CN at room temperature (r.t.) on a Bruker AV400 (400 MHz) spectrometer for ¹H NMR and at 100 and for ¹³C NMR. Chemical shifts are reported in part per million (ppm) relative to residual

solvent protons (1.94 ppm for CD₃CN) and the carbon resonance (118.69 ppm for CD₃CN) of the solvent.

Absorption spectra were measured in deaerated acetonitrile at room temperature (r.t.) on a Cary 500i UV-Vis-NIR Spectrophotometer. For luminescence spectra a Cary Eclipse Fluorescence spectrofluorimeter was used. Accurate mass measurements were performed on a 6210 TOF mass spectrometer from Agilent technologies, coupled to a 1100 series LC system in positive electrospray mode. Appropriate [M-PF₆]ⁿ⁺ species were used for empirical formula determination, and exact masses were calculated using Analyst® QS Software from Applied Biosystems. Electrochemical measurements were carried out in argon-purged purified acetonitrile at room temperature with a BAS CV50W multipurpose potentiostat. The working electrode was a glassy carbon electrode. The counter electrode was a Pt wire, and the pseudo-reference electrode was a silver wire. The reference was set using an internal 1 mM ferrocene/ferrocinium sample at 395 mV vs. SCE in acetonitrile. The concentration of the compounds was about 1 mM. Tetrabutylammonium hexafluorophosphate (TBAP) was used as supporting electrolyte and its concentration was 0.10 M. Cyclic voltammograms of **5C-1** to **5C-4** were obtained at scan rate of 50 mV/s. The criteria for reversibility were the separation of 60 mV between cathodic and anodic peaks, the close to unity ratio of the intensities of the cathodic and anodic currents, and the constancy of the peak potential on changing scan rate.

Experimental uncertainties are as follows: absorption maxima, ±2 nm; molar absorption coefficient, 10%; redox potentials, ± 10 mV; emission maxima, ±2 nm.

tert-Butylamine, pyridine, 3-picoline and nicotinic acid were purchased from VWR and used as received. 2-Acetylpyridine and pyridine-3-carboxaldehyde were purchased from Aldrich and used as received. Fe and Ru-metal salts were used as supplied from Aldrich. PdCl₂ was received from Pressure Chemicals and used as received. Pd(CH₃CN)₂Cl₂,¹³ 4-(3-Pyridyl)-2,2':6',2''-terpyridine (3-pytpy),¹⁴ Fe(II)- and Ru(II)-metallo-ligands¹⁵ were synthesized using literature procedures.

5C.5.2. Synthetic methods

(PdCl₂[μ-(3-pytpy)₂Fe])₃(PF₆)₆: (**5C-1**)

A 100 mL round-bottomed flask was charged with Fe-metallo-ligand ([*(3-pytpy)*₂Fe] [(PF₆)₂]) (100 mg, 0.103 mmol) and to it Pd(CH₃CN)₂Cl₂ (28 mg, 0.109 mmol) was added,

followed by the addition of nitromethane (50 mL). The resulting purple solution was heated to reflux in the dark for 2 days, after which time the solution was cooled down to r.t. and the solution was concentrated to *ca.* 6-8 mL. Precipitation of the desired metallo-triangle was induced by addition of diethyl ether (~ 20 mL) as purple solid, which was filtered and titrated with acetone (~ 3 mL) and dried under vacuum. Yield = 101 mg (85%). ^1H NMR: (400 MHz, CD_3CN) (see Scheme 5C.1 for numbering) δ ppm 9.59 (s, 2 $\text{H}_2^{\text{---}}$), 9.20 (s, 4 $\text{H}_3^{\text{---}}$), 9.01 (d, $J^{\text{d}} = 8$ Hz, 2 $\text{H}_6^{\text{---}}$), 8.77 (d, $J^{\text{d}} = 8$ Hz, 2 $\text{H}_4^{\text{---}}$), 8.61 (d, $J^{\text{d}} = 8$ Hz, 4 H_3), 7.94 (t, $J^{\text{t}} = 8$ Hz, 4 H_4), 7.88 (t, $J^{\text{t}} = 8$ Hz, 2 $\text{H}_5^{\text{---}}$), 7.19 (d, $J^{\text{d}} = 8$ Hz, 4 H_6), 7.11 (t, $J^{\text{t}} = 8$ Hz, 4 H_5). $^{13}\text{C}\{^1\text{H}\}$ NMR: (100 MHz, CD_3CN) δ ppm 162.47, 159.43, 155.79, 154.79, 153.68, 150.43, 140.62, 136.98, 136.49, 129.19, 127.84, 126.01, 123.65. HRMS (ESI), m/z : calculated for $\text{C}_{40}\text{H}_{28}\text{N}_8\text{PF}_6\text{Fe}$: 821.14281; found: 821.14316 $[(\text{Fe-metallo-ligand})\text{-PF}_6]^+$, calculated for $\text{C}_{40}\text{H}_{28}\text{N}_8\text{Fe}$: 338.08931; found: 338.08955 $[(\text{Fe-metallo-ligand})\text{-}2\text{PF}_6]^{2+}$, calculated for $\text{C}_{120}\text{H}_{84}\text{N}_{24}\text{Fe}_3\text{Pd}_3\text{Cl}_6\text{P}_3\text{F}_{18}$: 998.98427; found: 998.98427, calculated for $\text{C}_{120}\text{H}_{84}\text{N}_{24}\text{Fe}_3\text{Pd}_3\text{Cl}_6\text{P}_2\text{F}_{12}$: 712.99702; found: 712.99702, calculated for $\text{C}_{120}\text{H}_{84}\text{N}_{24}\text{Fe}_3\text{Pd}_3\text{Cl}_6\text{P}_1\text{F}_6$: 541.40467; found: 541.40458. Anal. Calc. for $\text{C}_{120}\text{H}_{84}\text{N}_{24}\text{Fe}_3\text{Pd}_3\text{Cl}_6\text{P}_2\text{F}_{12}\cdot\text{C}_3\text{H}_6\text{O}$: C: 42.34; N: 9.63; H: 2.60. Found: C: 42.58; N: 9.35; H: 2.38 (presence of acetone molecule was also confirmed in the ^1H NMR spectrum of this compound).

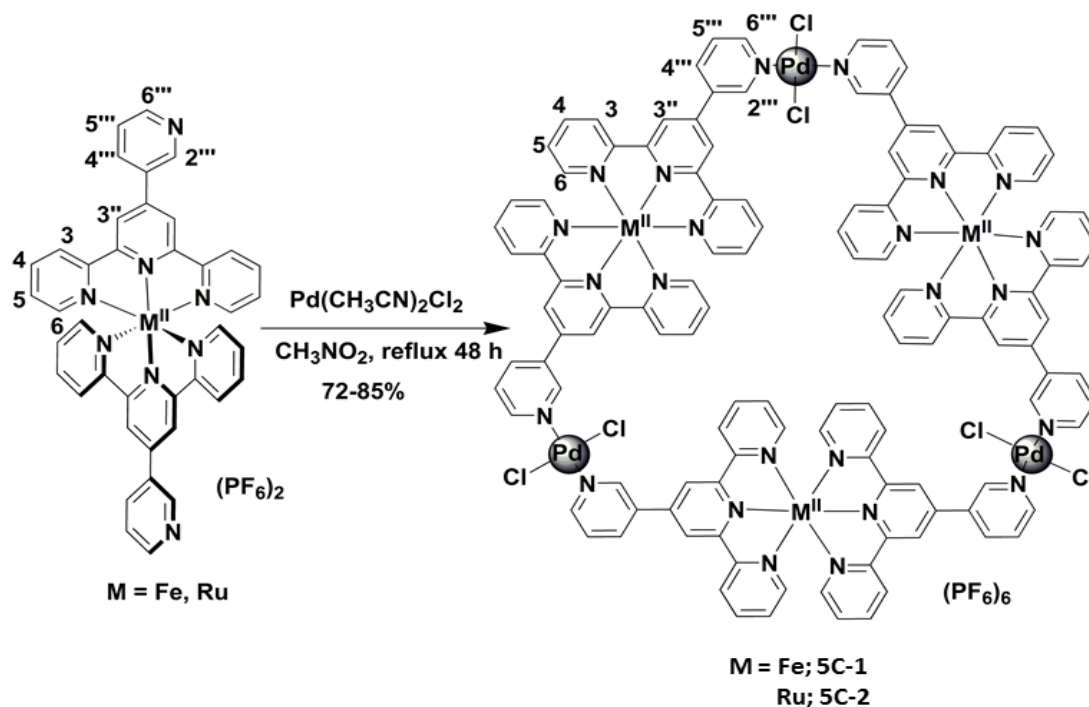
*(PdCl}_2[\mu\text{-}(3\text{-pytpy})_2\text{Ru}])_3(\text{PF}_6)_6 : (**5C-2**)*

A 100 mL round-bottomed flask was charged with Ru-metallo-ligand ($[(3\text{-pytpy})_2\text{Ru}][\text{PF}_6]_2$) (100 mg, 0.098 mmol) and to it $\text{Pd}(\text{CH}_3\text{CN})_2\text{Cl}_2$ (27 mg, 0.103 mmol) was added, followed by the addition of nitromethane (50 mL). The resulting red solution was heated to reflux in the dark for 2 days, after which time the solution was cooled down to r.t. and the solution was concentrated to *ca.* 6-8 mL. Precipitation of the desired metallo-triangle was induced by addition of an aliquot of saturated aqueous KPF_6 solution (3 mL). The resulting red solid was filtered and titrated with acetone (~ 3 mL) and dried under vacuum. Yield = 85 mg (72%). ^1H NMR: (400 MHz, CD_3CN) (see Scheme 5C.1 for numbering) δ ppm 9.48 (s, 2 $\text{H}_2^{\text{---}}$), 9.02 (s, 4 $\text{H}_3^{\text{---}}$), 8.96 (d, $J^{\text{d}} = 8$ Hz, 2 $\text{H}_6^{\text{---}}$), 8.66 (d, $J^{\text{d}} = 8$ Hz, 2 $\text{H}_4^{\text{---}}$), 8.63 (d, $J^{\text{d}} = 8$ Hz, 4 H_3), 7.98 (t, $J^{\text{t}} = 8$ Hz, 4 H_4), 7.82 (t, $J^{\text{t}} = 8$ Hz, 2 $\text{H}_5^{\text{---}}$), 7.43 (d, $J^{\text{d}} = 8$ Hz, 4 H_6), 7.21 (t, $J^{\text{t}} = 8$ Hz, 4 H_5). $^{13}\text{C}\{^1\text{H}\}$ NMR: (100 MHz, CD_3CN) δ ppm 158.74, 158.69, 156.74, 156.68, 154.88, 153.52, 152.92, 139.59, 139.23, 128.62, 126.95, 125.77, 123.12. HRMS (ESI), m/z : calculated for $\text{C}_{40}\text{H}_{28}\text{N}_8\text{Ru}$: 361.07402; found: 361.07234 $[(\text{Ru-metallo-}$

ligand)-2PF₆]²⁺, calculated for C₁₂₀H₈₄N₂₄Ru₃Pd₃Cl₆P₃F₁₈: 1042.95340; found: 1042.95428, calculated for C₁₂₀H₈₄N₂₄Ru₃Pd₃Cl₆P₂F₁₂: 745.97400; found: 745.97521, calculated for C₁₂₀H₈₄N₂₄Ru₃Pd₃Cl₆P₁F₆: 567.78637; found: 567.78785, calculated for C₁₂₀H₈₄N₂₄Ru₃Pd₃Cl₆: 448.99461; found: 448.99572. Anal. Calc. for C₁₂₀H₈₄N₂₄Ru₃Pd₃Cl₆P₂F₁₂·3KPF₆: C: 34.99; N: 8.16; H: 2.06. Found: C: 34.65; N: 7.99; H: 2.27.

5C.6. Results and Discussion

The syntheses of these Fe and Ru-metallo-ligands have been well documented elsewhere.¹⁵ Metallo-triangles **5C-1** and **5C-2** of general formula, (PdCl₂[μ-(3-pytpy)₂M])₃(PF₆)₆, (where M = Fe, **5C-1**; Ru, **5C-2**) were synthesized by refluxing a mixture of the homoleptic Fe(II) and Ru(II)-complexes of 3-pytpy and a slight excess of Pd(CH₃CN)₂Cl₂ in nitromethane (Scheme 5C.1). Subsequent isolation of the precipitate, induced by addition of diethylether to these concentrated reaction mixtures, followed by titration with acetone provided the complexes in analytically pure form.



Scheme 5C.1. Syntheses of complexes **5C-1** and **5C-2** also showing the labeling of different protons adopted for these complexes.

The presence of a polar non-coordinating and non-reducing solvent, e.g., nitromethane, was essential to form the desired assembly compared to the use of other solvents, such as acetonitrile, DMSO and alcohols, which were found to be competitive towards the coordination to $[\text{PdCl}_2]$.

5C.6.1. NMR Spectroscopy

The successful coordination of the heteroatom of the pendant pyridyl group to the neutral $[\text{PdCl}_2]$ was shown by the respective ^1H NMR spectra of **5C-1** and **5C-2**. The formation of metallo-triangles is very well supported by three principal features of these ^1H NMR spectra (Figure 5C.1), for e.g., (i) the symmetric nature suggests formation of a closed-ring discrete species with 1:1 stoichiometry of the metallo-ligand and PdCl_2 , (ii) well-defined integrations exclude the formation of long-chain metallo-polymer, (iii) most importantly, the downfield shift of pyridine (Py)- α ($2'''$ and $6'''$) protons by ~ 0.1 ppm and also similar shifts of β and γ ($5'''$ and $4'''$) protons of the pendant 3-pyridyl unit upon coordination. The terpyridine core-protons, being distant from the coordination site, are barely affected. Unlike the downfield shift of Py- α protons by ~ 1 -2 ppm, as observed by Fujita *et al.* for coordination to cationic $[\text{Pd}]$ -precursor,¹⁶ the lower value of downfield-shifting (0.1-0.8 ppm) is typically indicative of the coordination to neutral-metal centres.^{12c,17}

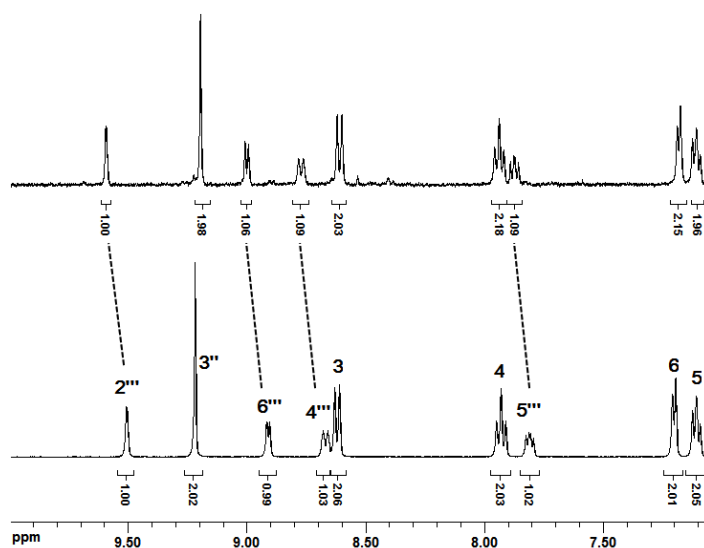


Figure 5C.1. ^1H NMR spectrum of complex **5C-1** (top), recorded at r.t. in CD_3CN , showing the downfield shifting of most affected protons of Fe-metalloligand (bottom) upon coordination.

To verify the downfield-shift of the protons of coordinated pyridyl units, three other model complexes, **5C-3** to **5C-5** (Chart 5C.1), with electron-donating and electron-withdrawing functional groups, were synthesized following literature procedures.^{7d} The chemical shift values of different protons (in ppm) of these complexes are tabulated in comparison to those of their respective free ligands (Table VC-1).

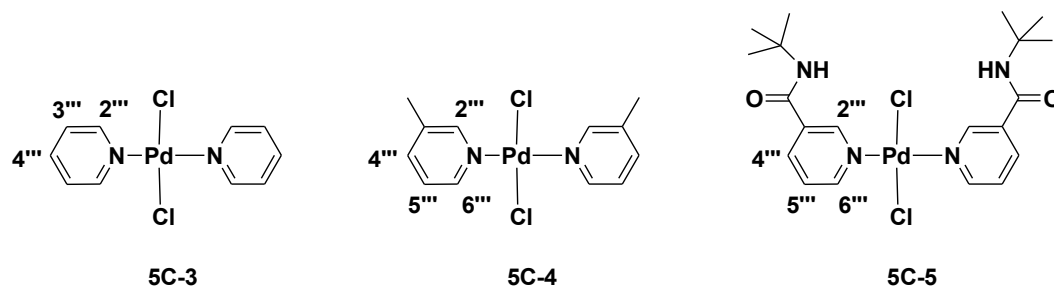
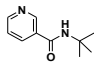


Chart 5C.1. Model complexes **5C-3** to **5C-5** with proton labelling scheme.

Table VC-1. Comparison of chemical shifts (in ppm) of different protons in complexes **5C-1** to **5C-5** and that of their corresponding ligands.

Compounds	Solvent	H2'''	H4'''	H5'''	H6'''
Fe-metallo-ligand	CD ₃ CN	9.51	8.67	7.81	8.91
5C-1	CD ₃ CN	9.59	8.77	7.88	9.01
Ru-metallo-ligand	CD ₃ CN	9.41	8.56	7.80	8.87
5C-2	CD ₃ CN	9.48	8.66	7.98	8.96
Pyridine	DMSO-d ₆	8.58	7.79	---	---
5C-3	DMSO-d ₆	8.75	8.00	---	---
3-Picoline	CD ₃ CN	8.42	7.51	7.19	8.37
5C-4	CD ₃ CN	8.60	7.72	7.32	8.56
	DMSO-d ₆	8.93	8.12	7.46	8.66
5C-5	DMSO-d ₆	9.08	8.23	7.56	8.81

Data in Table VC-1 clearly indicates that the downfield coordination-induced shift (CIS) of the 3-pyridyl protons of **5C-1** and **5C-2** fall in the same range (0.09-0.21 ppm) as observed with the model complexes, which supports for the formation of the cyclic metallo-triangle.

Elemental analyses of complexes **5C-1** and **5C-2** revealed a 1:1 stoichiometry of metallo-ligand and PdCl₂. Together with NMR spectroscopy this data strongly supports the formation of discrete, cyclic trimers.

5C.6.2. Mass Spectrometry

A common and powerful characterization technique of supramolecular species is electrospray mass spectrometry (ESI-MS).^{7c,17} The most abundant species in the LC-TOF HR-ESI-MS for complexes **5C-1** and **5C-2** correspond to $[M]^{2+}$ species of the metallo-ligands. Molecular triangles at different charged states, for e.g., $[(\text{Fe-metallo-ligand})_3(\text{PdCl}_2)_3(\text{PF}_6)_z]^{(6-z)+}$; $z = 3$ ($m/z = 998.98427$), 2 (712.99702), 1 ($m/z = 541.40458$) were observed for complex **5C-1** (Figures 5C.2 and 5C.3). Similar species were also observed for complex **5C-2** (Figures 5C.4-5C.7). More importantly, no signals that would correspond to other oligomers, such as dimers, tetramers, pentamers or higher are present. Therefore, together with NMR spectroscopy and elemental analysis, mass spectrometry provides unambiguous evidence for the existence of the cyclic trimer as the only supramolecular oligomer formed in solid, solution and gas-phase.

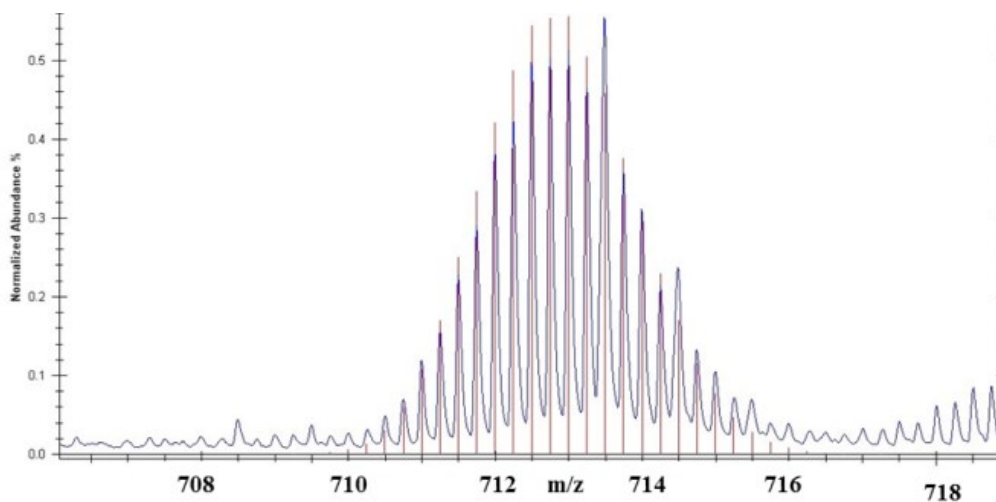


Figure 5C.2. Overlay of observed high-res LC-TOF MS of $[\text{C}_{120}\text{H}_{84}\text{N}_{24}\text{Fe}_3\text{Pd}_3\text{Cl}_3(\text{PF}_6)_2]^{4+}$ (outer trace) with simulated isotope pattern (inner trace).

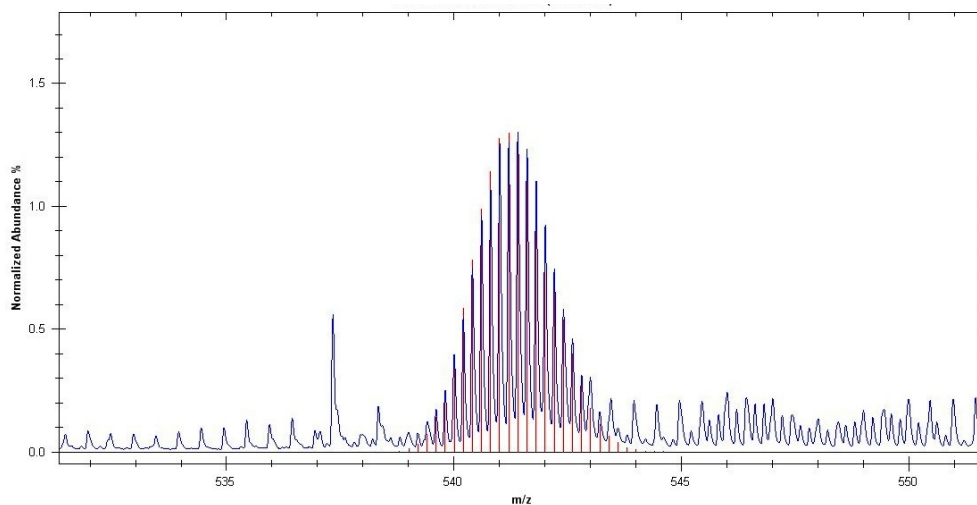


Figure 5C.3. Overlay of observed high-res LC-TOF MS of $[\text{C}_{120}\text{H}_{84}\text{N}_{24}\text{Fe}_3\text{Pd}_3\text{Cl}_3 (\text{PF}_6)]^{5+}$ (outer trace) with simulated isotope pattern (inner trace).

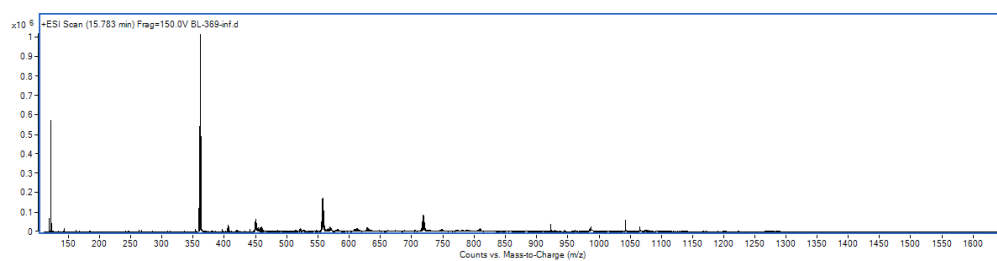


Figure 5C.4. High-res LC-TOF MS of complex **5C-2** or $\text{C}_{120}\text{H}_{84}\text{N}_{24}\text{Ru}_3\text{Pd}_3\text{Cl}_3 (\text{PF}_6)_6$.

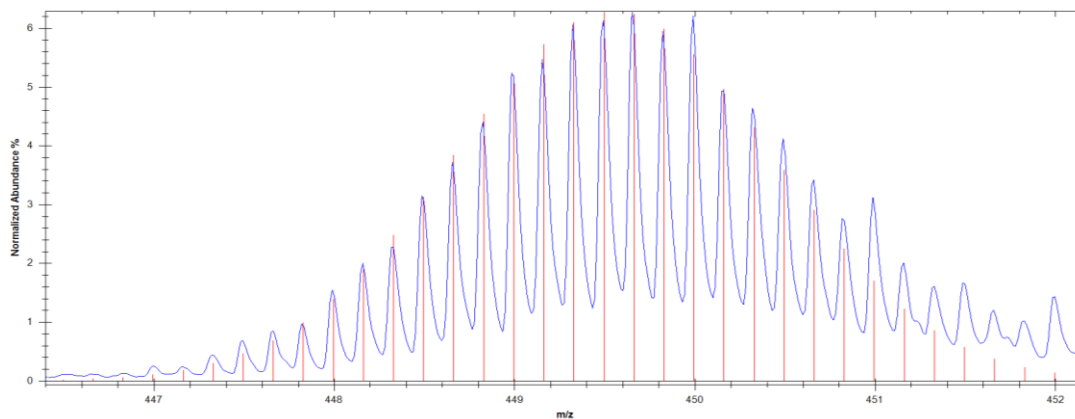


Figure 5C.5. Overlay of observed high-res LC-TOF MS of $(\mathbf{5C-2})^{6+}$ or $[\text{C}_{120}\text{H}_{84}\text{N}_{24}\text{Ru}_3\text{Pd}_3\text{Cl}_3]^{6+}$ (outer trace) with simulated isotope pattern (inner trace).

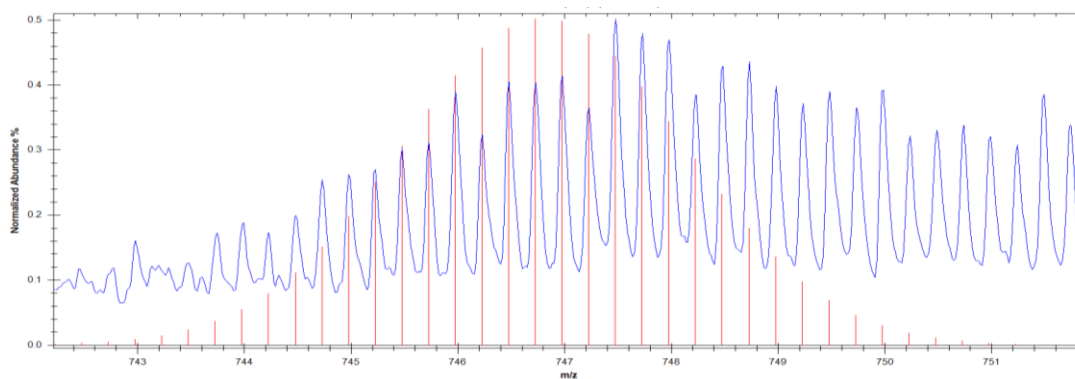


Figure 5C.6. Overlay of observed high-res LC-TOF MS of $(\mathbf{5C-2})^{4+}$ or $[\text{C}_{120}\text{H}_{84}\text{N}_{24}\text{Ru}_3\text{Pd}_3\text{Cl}_3(\text{PF}_6)_2]^{4+}$ (outer trace) with simulated isotope pattern (inner trace).

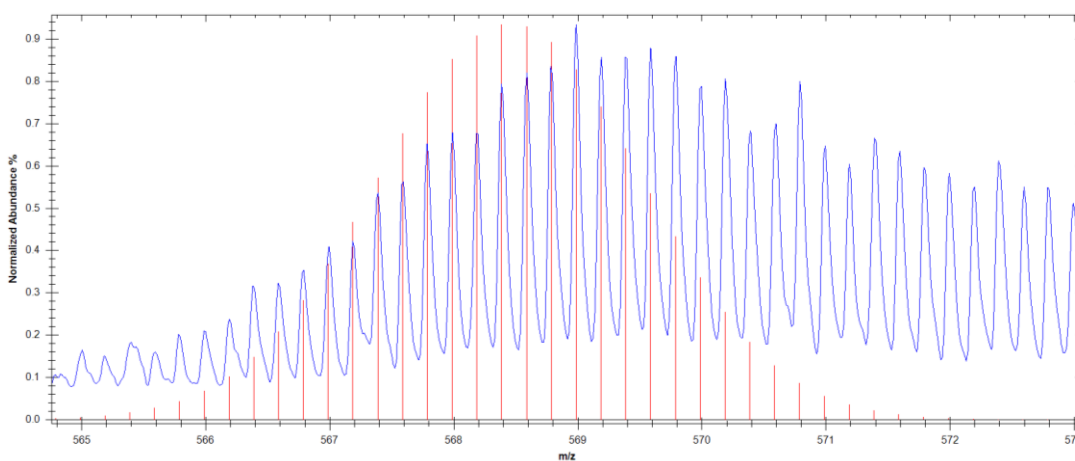


Figure 5C.7. Overlay of observed high-res LC-TOF MS of $(\mathbf{5C-2})^{5+}$ or $[\text{C}_{120}\text{H}_{84}\text{N}_{24}\text{Ru}_3\text{Pd}_3\text{Cl}_3(\text{PF}_6)]^{5+}$ (outer trace) with simulated isotope pattern (inner trace).

5C.6.3. Electrochemistry

The electrochemical behaviour of complexes **5C-1** and **5C-2** were investigated in dry, degassed acetonitrile using tetrabutylammonium hexafluorophosphate as the supporting electrolyte and glassy carbon electrode as the working electrode and ferrocene as the internal standard. The data (reported vs. SCE) are gathered in Table VC-2.

Table VC-2. Redox data of complexes **5C-1** to **5C-4** and some benchmark complexes.

Compound	$E_{1/2}(\text{ox})^a$	$E_{1/2}(\text{red})^a$	$\Delta E_{1/2}^b$
5C-1	1.19 (60)	-0.76 (irr) ^c , -1.14 (70), -1.26 (70), -1.87 (140)	1.95
5C-2	1.37 (70)	-0.77 (irr) ^c , -1.15 (80), -1.40 (70), -1.81 (70)	2.14
Fe-metallo-ligand ^d	1.22 (60)	-1.13 (85), -1.25 (74), -1.87 (122)	2.35
Ru-metallo-ligand ^d	1.35 (86)	-1.16 (61), -1.38 (88), -1.80 (104)	2.51
5C-3	-----	-0.53 (irr) ^c	-----
5C-4	-----	-0.84 (irr) ^c	-----

^aPotentials are in volts vs. SCE for acetonitrile solutions, 0.1 M in TBAPF₆, recorded at 25 ± 1 °C at a sweep rate of 50 mV/s, using ferrocene as internal standard. The difference between cathodic and anodic peak potentials (millivolts) is given in parentheses. All the compounds are recorded as their hexafluorophosphate salts in their divalent states, ^bdifference between the first anodic and first cathodic peaks in volt, ^cIrreversible; potential is given for the cathodic wave, ^dfrom ref 12a.

At positive potentials quasi-reversible metal-based oxidations are observed within 1.18-1.38 V range for complexes **5C-1** and **5C-2**, with the Ru(III)/Ru(II) oxidation in complex **5C-2** being ~180 mV more positive than that of Fe(III)/Fe(II) couple (Figures 5C.8 and 5C.9). This trend is also observed in their corresponding metallo-ligands and their prototypes [M(tpy)₂]ⁿ⁺.¹⁸ This result also supports the observed red-shift of the lowest energy singlet metal-to-ligand charge transfer (¹MLCT) absorption maxima of complex **5C-1** as compared to the same of **5C-2** in their respective electronic absorption spectra. The relative current intensity ratio of the oxidation peaks of either **5C-1** or **5C-2** and that of ferrocene was found to be 3:1, which suggests that the metal centres are redox independent in the final assemblies.¹⁹

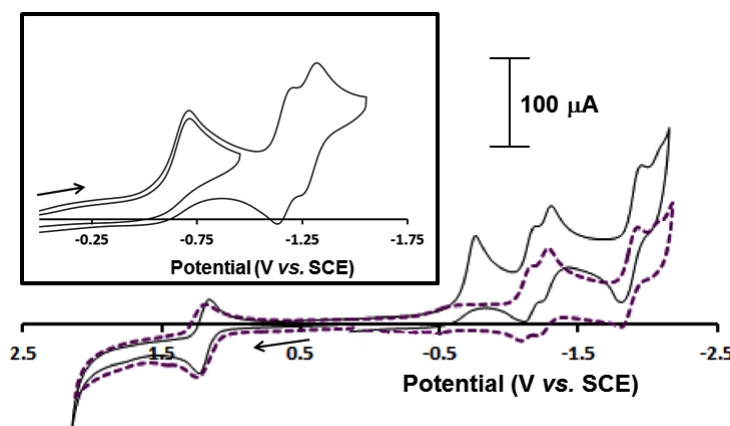


Figure 5C.8. Cyclic voltammograms of complex **5C-1** (bold line) and Fe-metallo-ligand (dashed line). Inset shows the quasi-reversible nature of individual reduction peaks of complex **5C-1**.

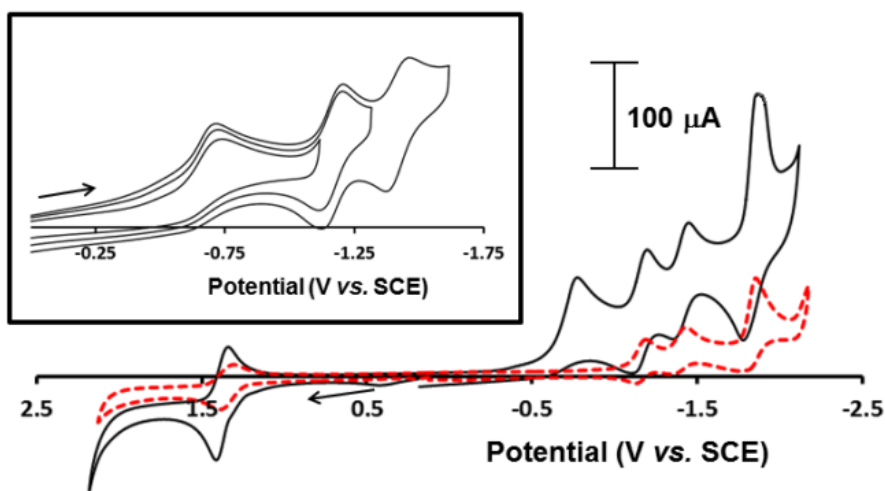


Figure 5C.9. Cyclic voltammograms of complex **5C-2** (bold line) and Ru-metallo-ligand (dashed line). Inset shows the quasi-reversible nature of individual reduction peaks of complex **5C-2**.

The cathodic region is rich with several multi-electron reduction phenomena, with the first irreversible reduction being assigned to reduction of Pd(II) to Pd(0). Comparing this value with the irreversible reduction potentials of Pd(II) to Pd(0) in model complexes **5C-3** and **5C-4** reveals that the *meta*-substituted 3-pyridyl group is more electron donating than a free pyridyl group, but less donating as compared to 3-picoline.²⁰ For complexes **5C-1** and **5C-2**, two quasi-reversible ligand-based reductions are observed between -1.14 V to -1.40 V, whereas other ligand-based quasi-reversible reductions are observed at relatively higher cathodic potentials. The relative current intensity ratio of the different reduction peaks was found to be 2:1:1:2, whereas with respect to equimolar amount of ferrocene, the relative current intensity ratios of the oxidation peak of ferrocene and the reduction peaks of complexes **5C-1** and **5C-2** were found to be 1(Fc⁺/Fc):6:3:3:6. This fact also supports the existence of a trimeric self-assembled oligomer in solution. All the ligand-based reductions in **5C-1** and **5C-2** appear more or less at the same potentials as observed for their respective metallo-ligands, suggesting that coordination of the 3-pyridyl group to the neutral [PdCl₂] has a minimal effect onto the electronic properties of the tpy core.

5C.6.4. Photophysical behavior

The electronic absorption spectra of the complexes were recorded in dry, degassed acetonitrile solution at room temperature and the absorption data are gathered in Table VC-

3. The electronic absorption profile of complexes **5C-1**, **5C-2** and their respective metallo-ligands are shown in Figure 5C.10. The UV-region of the electronic spectra of complexes **5C-1**, **5C-2** and their precursors are dominated by ligand centered (LC) $\pi \rightarrow \pi^*$ and $n \rightarrow \pi^*$ transitions, while the broad absorptions at visible energy region (400-700 nm) are assigned to $^1\text{MLCT}$ transitions. Although coordination induced bathochromic shifts of the absorption maxima are usually expected, the electronic transitions of **5C-1** and **5C-2** appear more or less at the same wavelengths compared to their corresponding metallo-ligands. This observation suggests that coordination of the 3-pyridyl ring to the neutral PdCl_2 does not affect the π^* orbital localized on the pytpy ligand and hence no red-shift is observed. This fact is also supported by the negligible red-shift (3 nm) of LC transition in model complex **5C-4** with respect to that of 3-picoline. For approximately similar molar concentration ($\sim 1.2 \times 10^{-5}$ M) of either of complexes **5C-1** or **5C-2** and their corresponding metallo-ligands, the absorption coefficient of the former was found be roughly 3 times higher than that of the latter, as would be expected.

Table VC-3. UV-vis absorption data of complexes **5C-1**, **5C-2** and model complex **5C-4** with their respective precursors.

Compound	UV-vis Absorption
	λ_{max} , nm ($\epsilon \times 10^3$, $\text{M}^{-1}\text{cm}^{-1}$)
5C-1	244 (126), 278 (243), 286 (289), 323 (167), 267 (25), 568 (85)
5C-2	243 (136), 278 (248), 285 (240), 313 (199), 488 (91)
Fe-metallo-ligand	244 (40), 278 (77), 285 (92), 322 (53), 367 (7), 566 (27)
Ru-metallo-ligand	241 (38), 277 (80), 283 (78), 312 (70), 488 (28)
3-picoline	234
5C-4	237

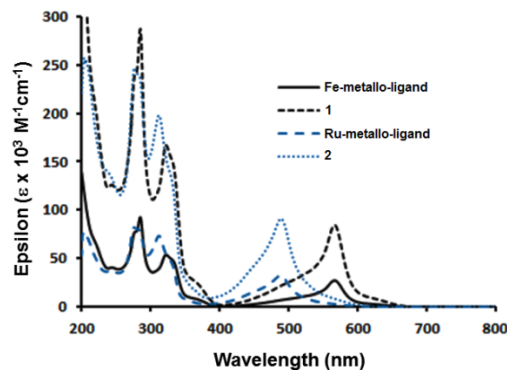


Figure 5C.10. Electronic absorption spectra of complexes **5C-1**, **5C-2** and their respective metallo-ligands.

Complexes **5C-1** and **5C-2** were found to be non-luminescent at r.t. in dry, degassed acetonitrile, although the Ru-metallo-ligand emits at 695 nm at the same experimental conditions. The quenching of luminescence in Fe-metallo-ligand and **5C-1** is attributed to the existence of a non-emitting triplet metal-centered (^3MC) state lower in energy than the triplet metal-to-ligand charge transfer ($^3\text{MLCT}$) state. The $^3\text{MLCT}$ excited state is thermally deactivated through the ^3MC state via an efficient nonradiative decay pathway.¹⁹ In contrast, the Ru-metallo-ligand is emissive due to the higher energy ^3MC state for Ru complexes as compared to Fe complexes. The Ru metallo-ligand $^3\text{MLCT}$ excited state is efficiently quenched in **5C-2** by electron transfer to the easily-reduced [Pd] metal centre.¹⁷

5C.7. Conclusions

In conclusion it has been demonstrated that the judiciously designed metallo-ligand with appropriate coordination vectors gives rise to discrete supramolecular assemblies, such as metallo-triangles, which is unambiguously evidenced by various analytical techniques, especially, ^1H NMR, HR-MS and elemental analysis. The metallo-triangles exhibit multi-electronic redox process with negligible communication among the metal centers. The photophysical properties of the assemblies are dominated by the individual chromophoric components with minimal effect from the neutral binder except the quenching of r.t. luminescence of complex **5C-2**. The properties of these new assemblies, such as anion sensing and host-guest chemistry, will be reported in due course.

5C.8. Acknowledgements

The authors thank the Natural Sciences and Engineering Research Council of Canada (NSERC) and Centre for Self-Assembled Chemical Structure (CSACS) for financial support.

5C.9. Notes and references

- (1) (a) R. Chakrabarty, P. S. Mukherjee, P. J. Stang, *Chem. Rev.*, 2011, **111**, 6810; (b) J. E. Beves, D. A. Leigh, *Nat. Chem.*, 2010, **2**, 708; (c) V. Balzani, A. Credi, M. Venturi, *Chem. Soc. Rev.*, 2009, **38**, 1542; (d) M. Fujita, *Chem. Soc. Rev.*, 1998, **27**, 417; (e) C. G. Oliveri, P. A. Ulmann, M. J. Wiester, C. A. Mirkin, *Acc. Chem. Res.*, 2008, **41**, 1618; (f) F. A. Cotton, C. Lin, C. A. Murillo, *Proc. Natl. Acad. Sci.*, 2002, **99**, 4810.
- (2) (a) J.-M. Lehn, *Supramolecular Chemistry: Concepts and Perspectives*, VCH: Weinheim, Germany, 1995; (b) G. S. Hanan, D. Volkmer, U. S. Schubert, J.-M.

- Lehn, G. Baum, D. Fenske, *Angew. Chem. Int. Ed.*, 1997, **36**, 1842; (c) G. S. Hanan, C. R. Arana, J.-M. Lehn, D. Fenske, *Angew. Chem. Int. Ed.*, 1995, **34**, 1122.
- (3) J.-P. Sauvage, C. Dietrich-Buchecker, Eds. *Molecular Catenanes, Rotaxanes, and Knots: A Journey Through the World of Molecular Topology*, Wiley-VCH: Weinheim, Germany, 1999.
- (4) (a) M. Yoshizawa, J. K. Klosterman, M. Fujita, *Angew. Chem., Int. Ed.*, 2009, **48**, 3418; (b) D. Fiedler, D. H. Leung, R. G. Bergman, K. N. Raymond, *Acc. Chem. Res.*, 2005, **38**, 351; (c) H. Takezawa, T. Murase, G. Resnati, P. Metrangolo, M. Fujita, *J. Am. Chem. Soc.*, 2014, DOI 10.1021/ja412893c; (d) T. Murase, Y. Nishijima, M. Fujita, *J. Am. Chem. Soc.*, 2012, **134**, 162.
- (5) (a) J. Meeuwissen, J. N. H. Reek, *Nat. Chem.*, 2010, **2**, 615; (b) T. S. Koblenz, J. Wassenaar, J. N. H. Reek, *Chem. Soc. Rev.*, 2008, **37**, 247.
- (6) (a) S. T. Nguyen, D. L. Gin, J. T. Hupp, X. Zhang, *Proc. Natl. Acad. Sci.*, 2001, **98**, 11849; (b) S.-S. Li, B. H. Northrop, Q.-H. Yuan, L.-J. Wan, P. J. Stang, *Acc. Chem. Res.*, 2009, **42**, 249; (c) T. Kudernac, S. Lei, J. A. A. W. Elemans, S. De Feyter, *Chem. Soc. Rev.*, 2009, **38**, 402.
- (7) (a) M. W. Cooke, D. Chartrand, G. S. Hanan, *Coord. Chem. Rev.*, 2008, **252**, 903; (b) M. W. Cooke, G. S. Hanan, *Chem. Soc. Rev.*, 2007, **36**, 1466; (c) S. S. Sun, A. Kumar and A. J. Lees, *Coord. Chem. Rev.*, 2008, **252**, 922; (d) M.-P. Santoni, A. K. Pal, G. S. Hanan, M.-C. Tang, K. Venne, A. Furtos, P. Ménard-Tremblay, C. Malveau, B. Hasenknopf, *Chem. Commun.*, 2012, **48**, 200.
- (8) (a) J.-P. Sauvage, J.-C. Collin, S. Chambron, C. Guillerez, V. Coudret, V. Balzani, F. Barigelletti, L. De Cola, L. Flamigni, *Chem. Rev.*, 1994, **94**, 993; (b) V. Balzani, A. Juris, M. Venturi, S. Campagna, S. Serroni, *Chem. Rev.*, 1996, **96**, 759.
- (9) (a) E. Ioachim, E. A. Medlycott, G. S. Hanan, F. Loiseau, S. Campagna, *Inorg. Chim. Acta*, 2006, **359**, 766; (b) A. K. Pal, S. Nag, J. M. Ferreira, V. Brochery, G. L. Ganga, A. Santoro, S. Serroni, S. Campagna, G. S. Hanan, *Inorg. Chem.*, 2014, **53**, 1679; (c) A. K. Pal, P. D. Ducharme, G. S. Hanan, *Chem. Commun.*, 2013, **50**, 3303; (d) E. A. Medlycott, G. S. Hanan, *Chem. Soc. Rev.*, 2005, **34**, 133; (e) Y.-Q. Fang, N. J. Taylor, G. S. Hanan, F. Loiseau, R. Passalacqua, S. Campagna, H. Nierengarten and A. Van Dorsselaer, *J. Am. Chem. Soc.*, 2002, **124**, 7912; (f) M. I. J. Polson, F. Loiseau, S. Campagna and G. S. Hanan, *Chem. Commun.*, 2006, **12**, 1301; (g) E. A. Medlycott, G. S. Hanan, *Coord. Chem. Rev.*, 2006, **250**, 1763.
- (10) M. Fujita, J. Yazaki, K. Ogura, *J. Am. Chem. Soc.*, 1990, **112**, 5645.
- (11) (a) S. Leininger, B. Olenyuk, P. J. Stang, *Chem. Rev.*, 2000, **100**, 853 and references therein; (b) R. V. Slone, D. I. Yoon, R. M. Calhoun, J. T. Hupp, *J. Am. Chem. Soc.*, 1995, **117**, 11813; (c) D. Ghosh, H. Ahmad, J. A. Thomas, *Chem. Commun.*, 2009, **20**, 2947; (d) J. A. Thomas, *Chem., Soc. Rev.*, 2007, **36**, 856; (e) K. Haris, Q.-F. Sun, S. Sato, M. Fujita, *J. Am. Chem. Soc.*, 2013, **135**, 12497.
- (12) (a) A. Granzhan, T. Riis-Johannessen, R. Scopelliti, K. Severin, *Angew. Chem. Int. Ed.*, 2010, **49**, 5515; (b) J. Cookson, P. D. Beer, *Dalton Trans.*, 2011, **40**, 2257; (c)

Chapter 5

- C. M. Hartshorn, P. J. Steel, *Chem. Commun.*, 1997, 541; (d) F. A. cotton, C. Y. Liu, C. A. Murillo, X. Wang, *Inorg. Chem.*, 2006, **45**, 2619.
- (13) C. J. Mathews, P. J. Smith, T. Welton, *J. Mol. Catal. A-Chem.*, 2004, **214**, 27-32.
- (14) J. Wang and G. S. Hanan, *Synlett*, 2005, 1251.
- (15) (a) A. K. Pal, B. Laramée-Milette, G. S. Hanan, *Inorg. Chim. Acta*, submitted for publication; (b) J. E. Beves, E. L. Dunphy, E. C. Constable, C. E. Housecroft, C. J. Kepert, M. Neuburger, D. J. Price and S. Schaffner, *Dalton Trans.*, 2008, 386.
- (16) D. Fujita, A. Takahashi, S. Sato, M. Fujita, *J. Am. Chem. Soc.*, 2011, **133**, 13317 and references cited therein.
- (17) C. M. Drain, F. Nifiatis, A. Vasenko, J. D. Batteas, *Angew. Chem. Int. Ed.*, 1998, **37**, 2344.
- (18) (a) C. Arana, S. Yan, M. Keshavarz-K, K. T. Potts, and H. D. Abruna, *Inorg. Chem.*, 1992, **31**, 3680; (b) E. C. Constable and A. M. W. C. Thompson, *J. Chem. Soc., Dalton Trans.*, 1994, 1409.
- (19) S.-S. Sun, A. J. Lees, *Inorg. Chem.*, 2001, **40**, 3154.
- (20) C. Hansch, A. Leo, R. W. Taft, *Chem. Rev.*, 1991, **91**, 165.

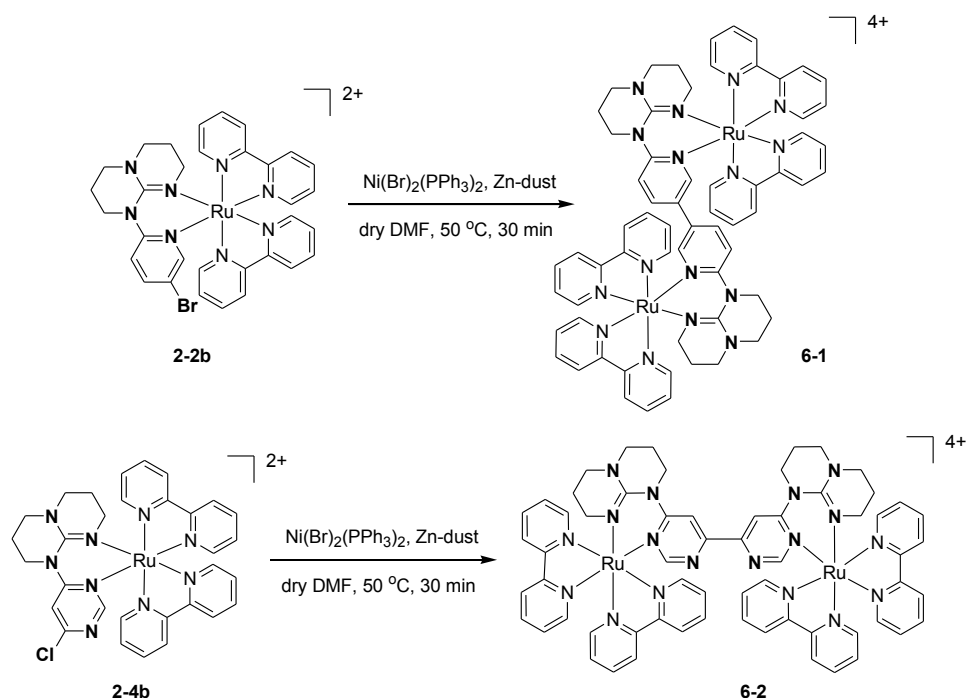
Chapter 6: General Conclusion and perspectives

The initial aim of this thesis was the syntheses of chromophores that can absorb and emit in different regions of the electromagnetic spectrum and to assemble these chromophores in such a way as to have vectorial energy transfer. The former part has been achieved successfully, while the latter part of the goal still requires work. The achievements and further improvements of each Chapter are discussed below and a summary that binds up the different Chapters at the end is provided.

6.1. Conclusion and perspectives : Chapter 2

In Chapter 2, the syntheses, characterization, electrochemical and photophysical properties of a series of Ru(II)-chromophores, comprising a family of judiciously designed polypyridyl ligands, have been reported.¹ The metal-based oxidation and the ³MLCT emission are greatly affected by the σ -donating nature of the different *N*-heterocycles attached to the **hpp** moiety. The higher the basicity of the ligand attached to Ru(bpy)₂²⁺ core, the easier is the metal-based oxidation and higher is the bathochromic shift in the ³MLCT emission maxima of the complexes. In general, chromophores **2-1b** to **2-5b** exhibit red-shifted ¹MLCT and ³MLCT maxima by ~ 95 nm and 120 nm, respectively, in comparison to that of Ru(bpy)₃²⁺ (absorption maxima 450 nm/ emission maxima 620 nm), which is a consequence of strong σ -donation from ancillary ligand and an increased ³MLCT-³MC energy gap.

Complexes **2-2b** and **2-4b** are of particular interest as upon homocoupling they give rise to dinuclear species with extended π -delocalization in the bridging ligand (BL) (Scheme 6.1).^{2,3} It has already been demonstrated that upon homocoupling the lowest energy absorption maxima involve charge transfer from Ru(d π) to BL, which are red-shifted compared to their prototype mononuclear analogues and this red-shift is generally dependent on the relative π -accepting nature of the BL.^{2a} Based on this observation, the homocoupled products **6-1** and **6-2** should also exhibit further red-shifted absorption and emission maxima compared to their prototypes, which may render them useful as luminescence probes in cell-imaging systems.³



Scheme 6.1. Homocoupling of mononuclear complexes **2-2b** and **2-4b**.

However, a stereochemically pure complex is needed for practical application in biological systems. Based on the helicity of the ancillary ligand and the BL, the reactions in Scheme 6.1 lead to mixture of dinuclear complexes with a statistical combination of $\Lambda\Lambda : \Lambda\Delta$ (or $\Delta\Lambda$) : $\Delta\Delta$ in 1 : 2 : 1 ratio as shown in Figure 6.1.

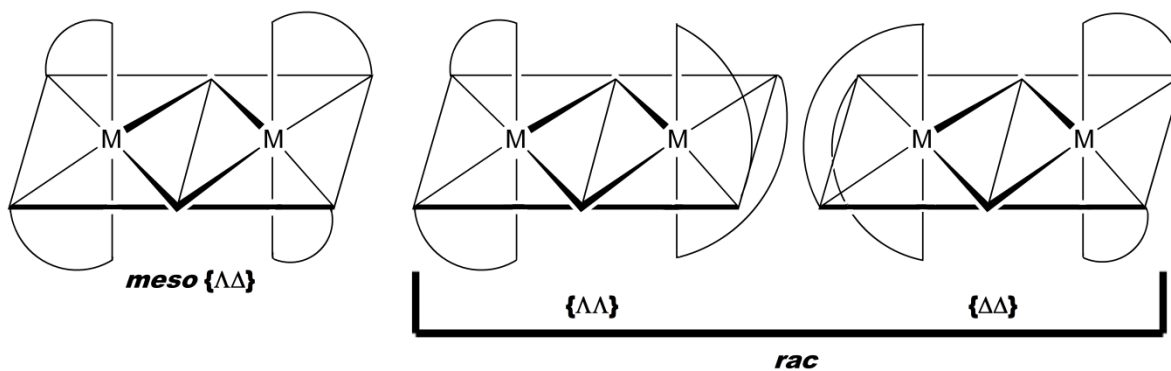


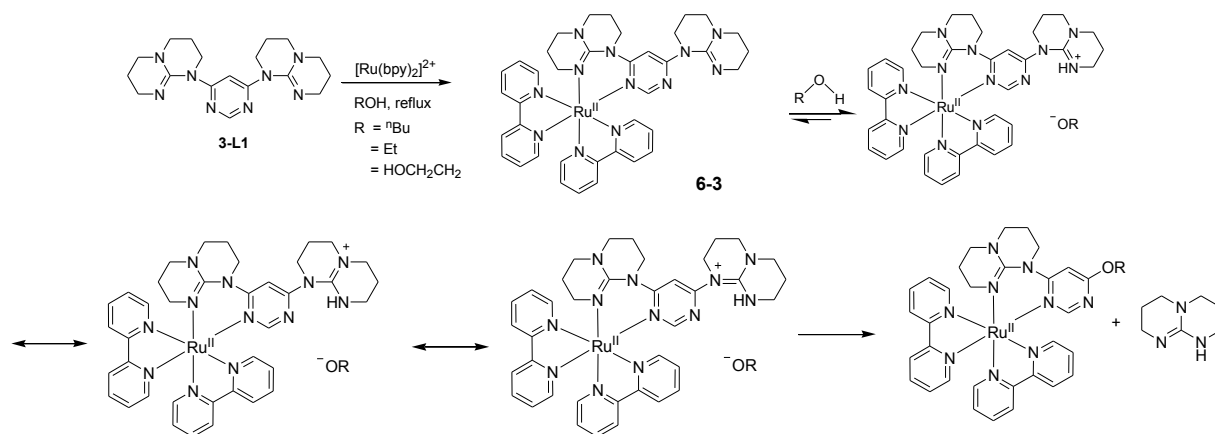
Figure 6.1. Mixture of possible diastereomers in a dinuclear complex.

This stereopurity issue may be easily solved by careful design of a BL, as discussed in Chapter 3 and the next section.

6.2. Conclusion and perspectives : Chapter 3

In Chapter 3, the novel syntheses and characterization of a bis-bidentate ligand (**3-L1**) along with a dinuclear Ru(II,II)-complex have been reported.^{4,5} The aforesaid issue of stereopurity in the previous section and Chapter 2 has been addressed in this Chapter by careful design of **3-L1**, so that the latter (i) retains its thermodynamically stable chair conformation upon complexation due to a flexible aliphatic backbone, (ii) offers parallel coordination vectors towards Ru(II)-centers. These effects in turn lead to maximum possible π - π interactions between the bpy units of two Ru(II)-centers, therefore, affording the *meso*-complex **3-(1-meso)** in 1 : 13 : 1 ratio over its two other homochiral *rac*-isomers. Thus, the enhanced diastereoselectivity may lead to easy synthesis and isolation of stereopure complexes, as compared to the cumbersome and costly techniques developed by Keene, MacDonnell, Vos and co-workers.⁶⁻⁸ In combination with this stereopurity, the added exciting photophysical properties may render the complex **3-(1-meso)** useful as DNA probes⁷ and supramolecular building blocks.⁹ Three other mononuclear complexes were also synthesized as solvolysis products during the synthesis of monoruthenium complex of **3-L1**. As concluded for Chapter 2, the redox and photophysical properties of the ether adducts (**3-2** to **3-4**) were also found to be strongly dependent on the nucleophilicity of the ether adducts.

Syntheses of complexes **3-2** to **3-4** are of added interest as the **hpp** moiety acts as a leaving group in these syntheses. A proposed mechanism of the syntheses of these complexes is depicted below (Scheme 6.2).



Scheme 6.2. Proposed mechanism of solvolysis of the complex **6-3**.

The leaving group capacity of one of the protonated **hpp** moieties is induced by the coordination of **3-L1** with $\text{Ru}(\text{bpy})_2^{2+}$ core. This statement is supported by two experimental facts (i) ligand **3-L1** does not undergo solvolysis in presence of alcohols, (ii) complexes **2-2b** and **2-4b** do not produce any solvolysis products, when the reactions are performed in 1-butanol, although theoretically bromine and chlorine atoms are better leaving groups than an uncoordinated **hpp** unit. Therefore, the nucleophilic substitution at the uncoordinated site of complex **6-3** is facilitated by coordination to $\text{Ru}(\text{bpy})_2^{2+}$ and subsequent capture of a proton by the uncoordinated **hpp** moiety in a protic solvent. The preliminary isolation of complex **6-3** (see Figure 6.2 for its ^1H NMR spectrum) and monitoring of nucleophilic substitution by 1 equivalent of ethylene glycol at the non-coordinated **hpp** site by solution ^1H NMR in CD_3CN after heating at 70-75 °C with different time intervals proves no significant change in the ^1H NMR spectrum of **6-3** proving that large excess of solvent is needed for substitution (Figure 6.3). A kinetic isotope exchange experiment may be useful to fully understand the mechanism of this solvolysis phenomena.

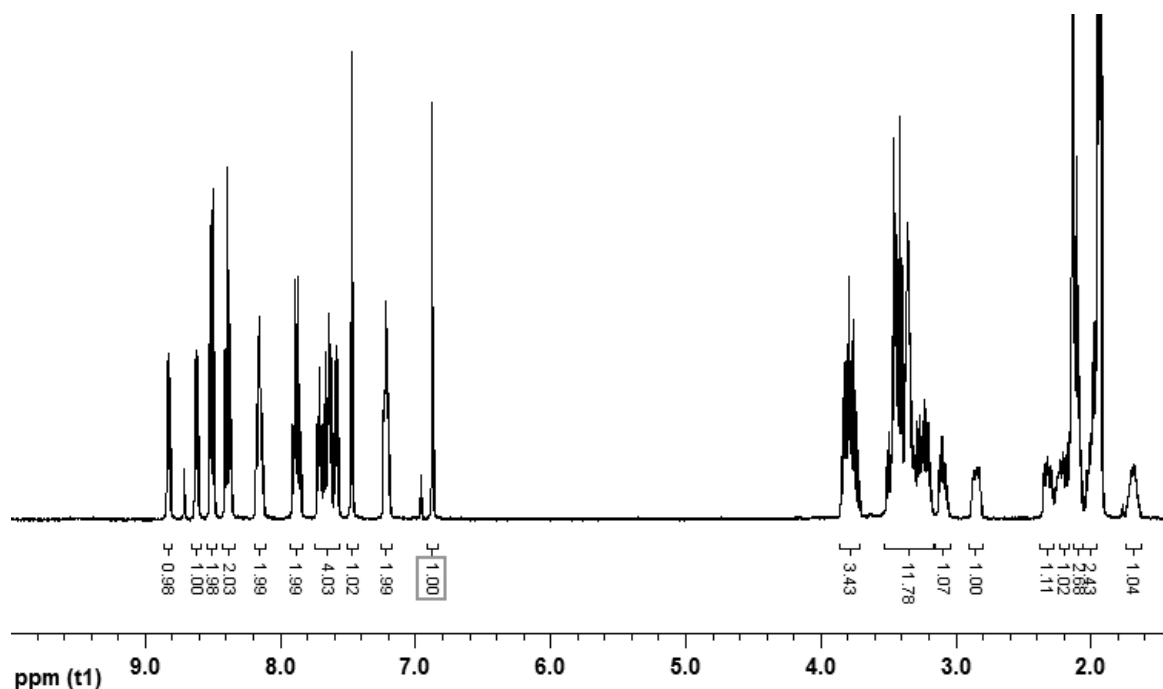


Figure 6.2. ^1H NMR spectrum of complex **6-3** in CD_3CN at room temperature at 400 MHz.

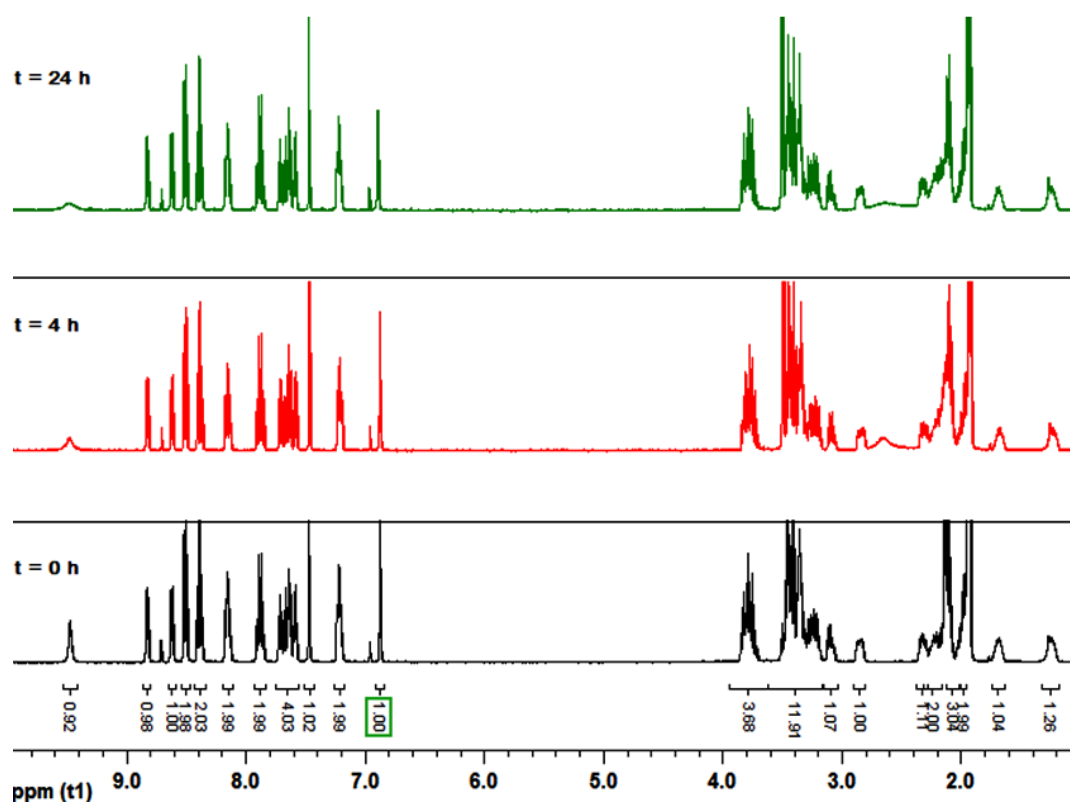


Figure 6.3. Comparison of ^1H NMR spectra of complex **6-3** in presence of 1 equivalent of ethylene glycol in CD_3CN at room temperature at 400 MHz.

Amines being more nucleophilic than alcohols, it is worth trying to substitute the uncoordinated **hpp** moiety stoichiometrically with a long chain alkyl-amine, for e.g., butyl amine.

6.3. Conclusion and perspectives : Chapter 4

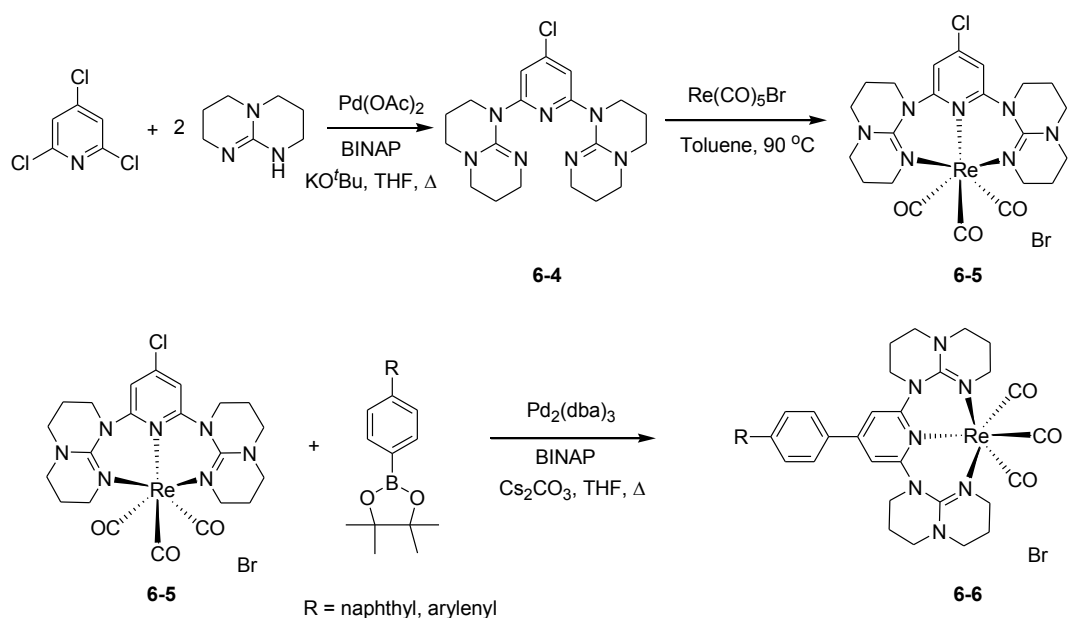
$\text{Ru}(\text{II})$ -polypyridyl complexes based on bidentate ligands often leads to chirally impure Δ and Λ -enantiomers, thus rendering them non-suitable as synthons for building chirally pure supramolecular motifs. The chiral discrimination of the resulting complexes may be overcome with tridentate chelating ligands, for example, 2,2':6':2''-terpyridine (tpy) or 2,4-dipyridyl-1,3,5-triazine (dpt), which leads to achiral complexes upon binding in bis(k^3N) fashion. Chapter 4 contains a strong σ -donating tridentate ligand (**4-L1**) and its $\text{Ru}(\text{II})$ -heteroleptic complexes with different tpy and dpt ligands.^{10,11} Once again the electrochemical properties of the complexes are greatly affected by the σ -donating nature of the ligand **4-L1**. It has been shown that combined donating nature of two **hpp** units are as equivalent as an anionic cyclometallating $\text{N}^-\text{C}^-\text{N}$ ligand. The exciting photophysical

properties of these complexes render them emitting at room temperature in NIR region, which is the farthest red-shifted (~ 900 nm) emission ever recorded for bis(tridentate) ligands in k^3N binding modes around a Ru(II)-center. The NIR emission is also coupled with 90-130 ns of excited-state lifetime at room temperature. Thus, the excited-state lifetime of the heteroleptic tpy analogues, **4-1** and **4-2**, are ~ 500 times higher than that of practically non-emissive Ru(tpy) $_2^{2+}$ (0.25 ns). The calculated DFT and TD-DFT results are in excellent agreement with the experimentally observed values. The excellent electrochemical and photophysical properties and achiral nature of a suitably 4'-substituted homo- or heteroleptic d^6 metal complex of **4-L1** may serve the complex as a promising synthon as a building block in supramolecular array with its inherent NIR room temperature luminescence behavior.

6.4. Conclusion and perspectives : Chapter 5

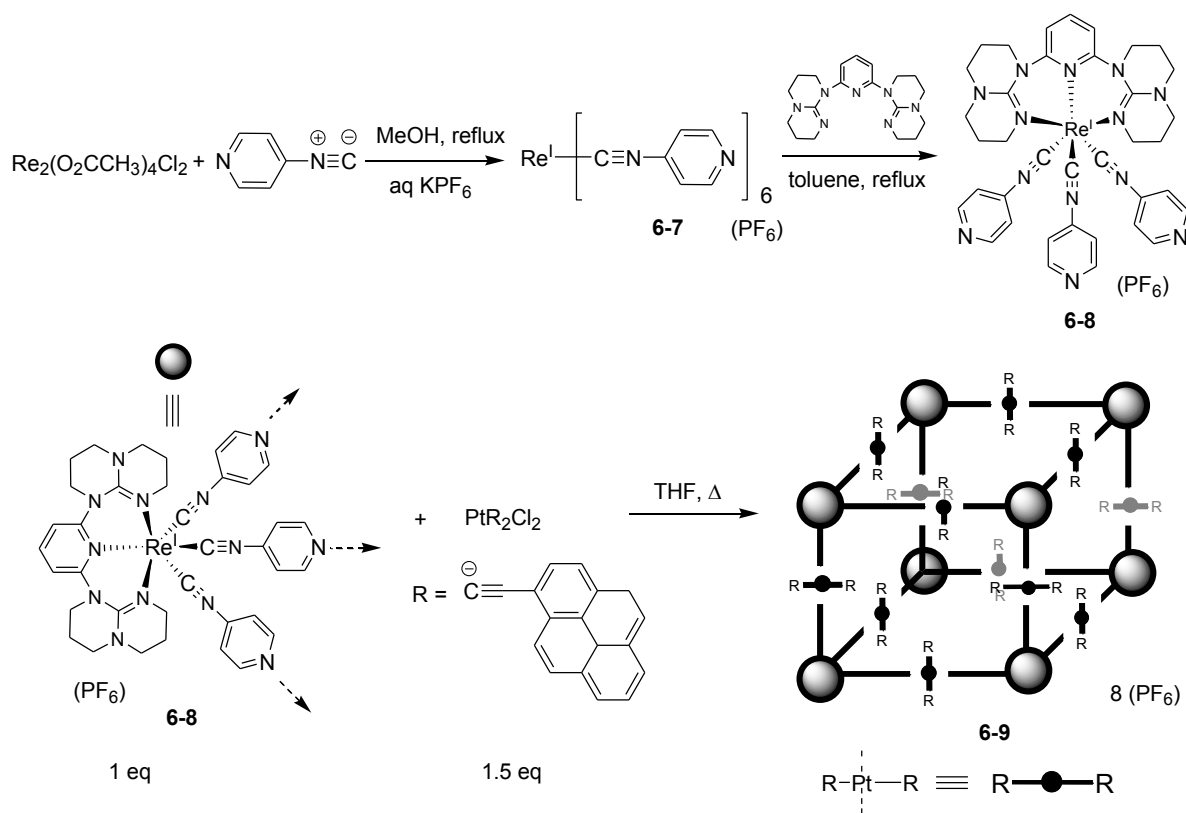
While Chapters 2, 3 and 4 focus mainly on Ru(II)- d^6 metal ion, Chapter 5A focuses on another d^6 ion-Re(I). The complexes in this chapter, **5A-1** and **5A-2**, are based on two structurally similar but electronically different ligands, **5A-L1** and **5A-L2**. Syntheses of these robust complexes do not require decarbonylation at elevated temperature due to the thermodynamic stabilization of two six-membered chelate rings. The broken π -decolization in the ligands plays an important role in the redox chemistry of the complexes, for e.g., the metal-based oxidations are predominantly governed by the electron-donating nature of the hpp units, while the ligand-based reductions are controlled by the central *N*-aromatic heterocycle. The complexes also act as blue-emitter albeit with low excited-state lifetime, which may be due to the vibration of the saturated aliphatic-backbone and low positive charge on the metal-center.

The lifetime of complex **5A-1** may be improved by strategically designing of a new ligand **6-4** (Scheme 6.3). With the help of bichromophoric approach (Section 1.5 in Chapter 1) and using 'Chemistry on the Complex', grafting of arylene-4-phenyl moiety (arylene = arene aromatic hydrocarbon group) at the 4'-position of the central *N*-heterocycle onto complex **6-5** would allow a dynamic equilibrium between the 3MLCT and 3LC states of the auxillary chromophore, such that the arylene moiety acts as an electron-reservoir in the resulting complex **6-6** (see Figure 1.1 in Chapter 1 for bichromophoric approach).¹³



Scheme 6.3. Synthesis of complex **6-6** to improve photophysical properties of complex **5A-1**.

Re(I)(**dgpy**)(PyNC) (PyNC = 4-pyridylisocyanide) complex (**6-8**) analogous to complex **5A-1** is of added interest. In presence of neutral *trans*-directing metal-unit, such as *trans*-PtR₂Cl₂ (R = 1-pyrenylacetylde), complex **6-8** can give rise to a self-assembled supramolecular cube, where the Re(I)-chromophores occupy the corners of the cube, and the neutral Pt-acetylde units occupy the middle of each side of the cube (Scheme 6.4). The complex **6-8** can be synthesized by reaction of 1 equivalent of **dgpy** ligand Re(I)(PyNC)₆ precursor, while the latter can be synthesized following literature procedure.¹⁴



Scheme 6.4. Proposed scheme of supramolecular cube formation using vacant coordination sites of a *trans*-PtR₂ unit.

While Chapter 5A opens up a possibility of formation of supramolecular assemblies based on tridentate ligands, Chapter 5B includes a terpyridine ligand grafted at the 4'-position with a 3-pyridyl group (**5B-L**). This Chapter describes the syntheses and characterisation of a series of homoleptic complexes of **5B-L** with 1st row divalent transition metal-ions. The redox and UV-vis electronic absorption properties have been shown to be dependent on the electron-withdrawing nature of the pendant 3-pyridyl moiety. An interesting phenomena of transformation of 2D-terpyridine embrace to 1D-ribbon structure, based on the nature of counter anion in the crystal packing of complexes **5B-1a**, **5B-2** with respect to **5B-1b** has also been investigated.

The scope of the Chapter 5B has been demonstrated in Chapter 5C. In the later Chapter, the chromophoric metallo-ligands (actually complexes **5B-1a** and **5B-2** in Chapter 5B) have been successfully assembled into a supramolecular triangle using neutral PdCl₂ as the binder. The formation of discrete self-assembled products **5C-1** and **5C-2** has been evidenced by downfield CIS in the ¹H NMR spectra of the self-assembled products

compared to that of their synthons, HR-MS, elemental analyses and electrochemistry. The self-assembled complex **5C-2** do not exhibit room temperature luminescence. The quenching of the luminescence may be overcome by introducing photophysically active metal unit as a neutral binder, for e.g., *trans*-PtR₂Cl₂ (R = 1-pyrenylacetylde) (complex **6-10**, Figure 6.4).¹⁵

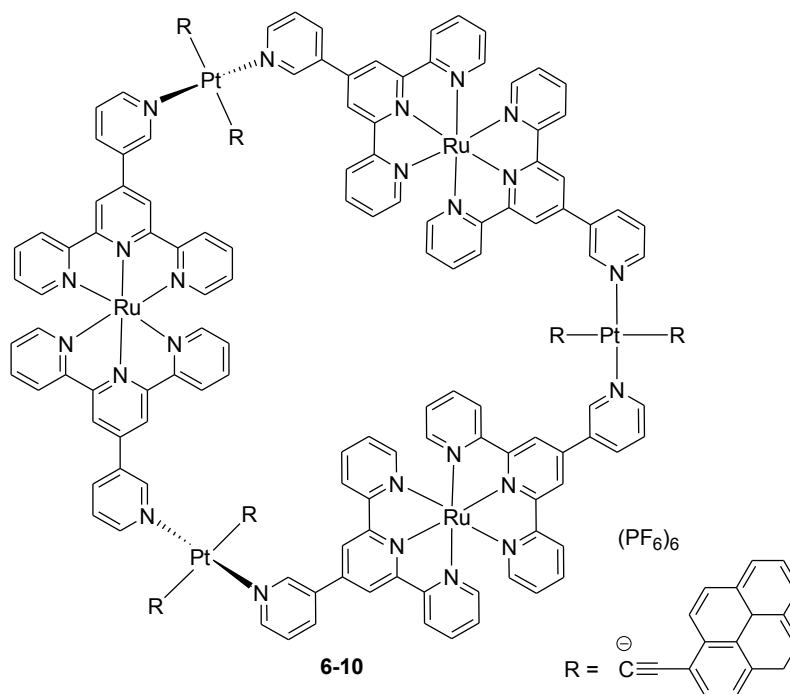


Figure 6.4. Proposed structure of self-assembly of complex **5B-2**, using neutral, *trans*-PtR₂Cl₂ (R = 1-pyrenylacetylde) as binder.

In summary this thesis describes the synthesis, characterization and properties of a series of bidentate and tridentate polypyridyl-based ligands and their metal-complexes. While Chapter 2 introduces the importance of **hpp** unit to affect the electrochemical and photophysical properties of the Ru(II)-polypyridyl complexes, the potential problem of stereopurity has been overcome in Chapter 3, by special ligand-design and in Chapter 4, by synthesizing achiral tridentate Ru(II)-polypyridyl chromophores. Chapter 4 further improves the redox and photophysical properties of the complexes. While Chapter 2, 3 and 4 include Ru(II) complexes as red and NIR-emitters, Chapter 5A covers blue-emitters as Re(I) complexes. Chapters 5B and 5C provide ideas to incorporate the metal-chromophores or metallo-ligands, which exhibit angular separation of coordination of vectors to form discrete supramolecular assemblies. The overall properties of these assemblies can be

further tuned by the electronic nature of the ligands employed and by changing the coordinated metal-ion.

6.5. References

- (1) Pal, A. K.; Nag, S.; Ferreira, J. G.; Brochery, V.; Ganga, G. L.; Santoro, A.; Serroni, S.; Campagna, S., Hanan, G. S. *Inorg. Chem.* **2014**, *53*, 1679.
- (2) (a) Johansson, K. O.; Lotoski, J. A.; Tong, C. C.; Hanan, G. S. *Chem. Commun.* 2000, 819. (b) Polson, M. I. J.; Loiseau, F.; Campagna, S.; Hanan, G. S. *Chem. Commun.* 2006, 1301.
- (3) Gill, M. R.; Garcia-Lara, J.; Foster, S. J.; Smythe, C.; Battaglia, G.; Thomas, J. A. *Nat. Chem.* 2009, **1**, 662.
- (4) Pal, A. K.; Ducharme, P. D.; Hanan, G. S. *Chem. Commun.* 2014, DOI 10.1039/C3CC47856D.
- (5) Pal, A. K.; Hanan, G. S. *Dalton Trans.* 2014, accepted for publication.
- (6) Keene, F. R. *Chem. Soc. Rev.* **1998**, *27*, 185 and references cited therein.
- (7) Janaratne, T. K.; Yadav, A.; Onger, F.; MacDonnell, F. M. *Inorg. Chem.* **2007**, *46*, 3420.
- (8) Browne, W. R.; O'Connor, C. M.; Villani, C.; Vos, J. G. *Inorg. Chem.* **2001**, *40*, 5461.
- (9) MacDonnell, F. M.; Kim, M.-J.; Bodige, S. *Coord. Chem. Rev.* **1999**, *185*, 535.
- (10) Pal, A. K.; Zaccheroni, N.; Campagna, S., Hanan, G. S. *Chem. Commun.* 2014, accepted for publication.
- (11) Pal, A. K.; Zaccheroni, N.; Campagna, S., Hanan, G. S. *Inorg. Chem.* 2014, submitted for publication.
- (12) Liu, Y.; Harlang, T.; Canton, S. E.; Chábera, P.; Suárez-Alcántara, K.; Fleckhaus, A.; Vithanage, D. A.; Göransson, E.; Corani, A.; Lomoth, R.; Sundström V.; Wärnmark, K. *Chem. Commun.* **2013**, *49*, 6412.
- (13) Ragazzon, G.; Verwilst, P.; Denisov, S. A.; Credi, A.; Jonusauskas, G.; McClenaghan, N. D. *Chem. Commun.* 2013, **49**, 9110.
- (14) Allison, J. D.; Wood, T. E.; Wild, R. E.; Walton, R. A. *Inorg. Chem.* **1982**, *21*, 3540.
- (15) Sun, S.-S.; Lees, A. J. *Inorg. Chem.* **2001**, *40*, 3154.

Annexes

SI – Chapter 2 : Supplementary Information

Supplementary Information

Red Emitting $[\text{Ru}(\text{bpy})_2(\text{N-N})]^{2+}$ Photosensitizers: Emission from a Ruthenium(II)-to-2,2'-Bipyridine $^3\text{MLCT}$ State in the Presence of Neutral Ancillary ‘Super Donor’ Ligands

Amlan K. Pal,[†] Samik Nag,[‡] Janaina G. Ferreira,[†] Victor Brochery,[†] Giuseppina La Ganga,[§] Antonio Santoro,[§] Scolastica Serroni,[§] Sebastiano Campagna,^{§} and Garry S. Hanan^{*†}*

[†]*Département of Chemistry, Université de Montréal, Montréal, Québec, H3T-1J4, Canada,*
[‡]*Department of Chemical Sciences, Sikkim University, Sixth Mile, Tadong, Gangtok, Sikkim, India 737102, and*
[§]*Dipartimento di Scienze Chimiche, Università di Messina, Via Sperone 31, I-98166 Messina, Italy.*

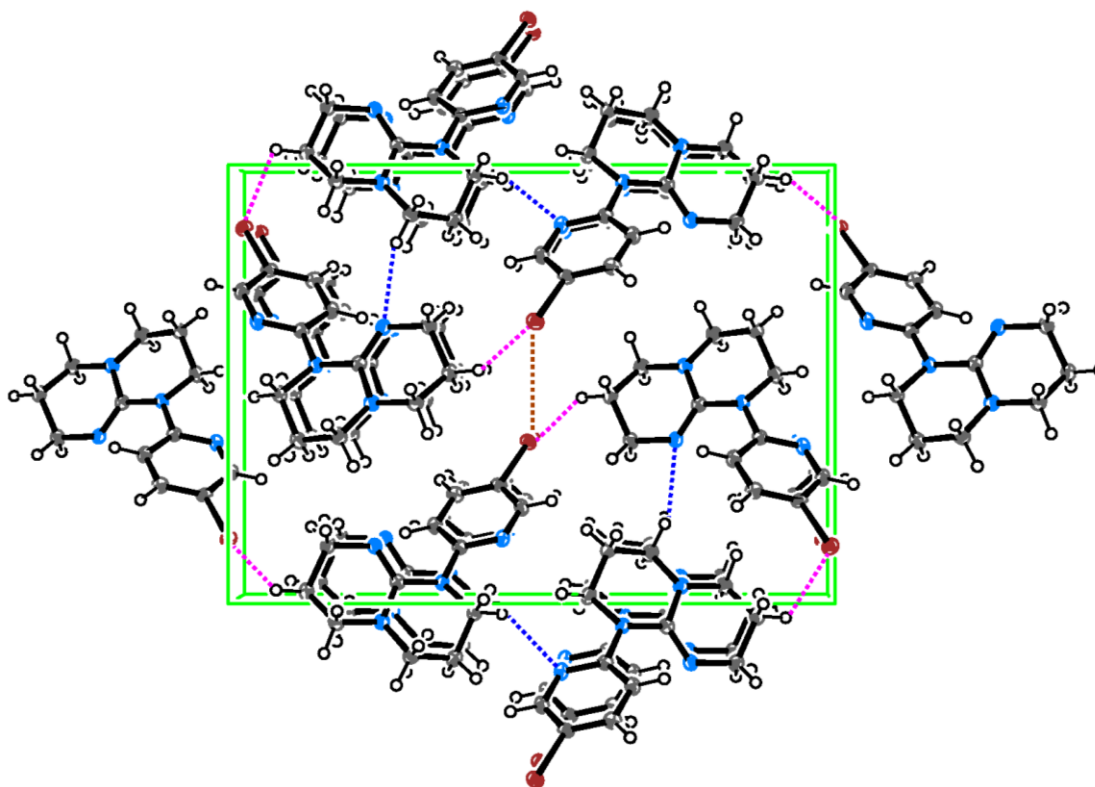


Figure 2.S1. Packing diagram of ligand **2-2a** along normal to 100 plane. Dashed lines indicate Br-Br solid state non-covalent interactions, C-H-Br interactions and C-H-N interactions.

Table II-S1. Comparison of bond distances and angles in **2-1b**, **2-3b** and **2-4b** from X-ray and DFT studies

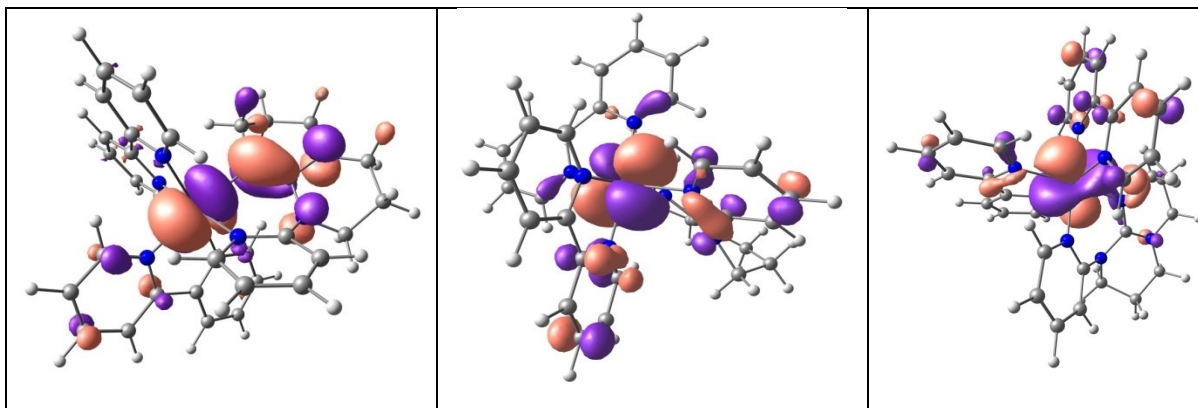
Compound	Bond Length			Angle		
		Obs. (x-ray)	Calc. (DFT)		Obs. (x-ray)	Calc. (DFT)
2-1b	N1-Ru	2.036(6)	2.11173	N1-Ru1-N2	81.6(3)	77.846
	N2-Ru	1.992(6)	2.10267	N3-Ru1-N4	79.3(3)	77.585
	N3-Ru	2.147(7)	2.10672	N5-Ru1-N8	82.8(3)	84.376
	N4-Ru	2.052(7)	2.11307			
	N5-Ru	2.011(6)	2.13536			
	N8-Ru	2.187(7)	2.13874			
	N6-C25	1.418(10)	1.41241			
	N6-C29A	1.498(25)	1.40716			
	N8-C29A	1.349(2)	1.31415			
	N7A-C29A	1.409(25)	1.36561			
	2-3b	N101-Ru1	2.066(2)	2.11029	N101-Ru1-N102	78.88(9)
N102-Ru1		2.060(2)	2.10063	N103-Ru1-N104	78.77(8)	77.648
N103-Ru1		2.051(2)	2.11273	N105-Ru1-N109	84.98(8)	83.778
N104-Ru1		2.066(2)	2.11153			
N105-Ru1		2.090(2)	2.12812			
N109-Ru1		2.087(2)	2.13735			
N107-C124		1.392(3)	1.40395			
N107-C131		1.408(3)	1.40614			
N109-C131		1.314(4)	1.31549			
2-4b	N1-Ru1	2.062(4)	2.11214	N1-Ru1-N2	79.1(2)	77.907
	N2-Ru1	2.054(4)	2.10217	N3-Ru1-N4	78.6(2)	77.664
	N3-Ru1	2.054(4)	2.10993	N5-Ru1-N9	85.2(1)	84.000
	N4-Ru1	2.069(4)	2.11381			
	N5-Ru1	2.089(4)	2.13221			
	N9-Ru1	2.090(4)	2.14098			
	N7-C24	1.377(6)	1.39695			
	N7-C31	1.421(6)	1.41699			
	N9-C31	1.301(6)	1.31194			
	N8-C31	1.336(6)	1.36465			

Table II-S2. Electronic absorption data of ligands (2-1a)-(2-5a).

Compound	λ_{\max} , nm ($\epsilon \times 10^3$, $M^{-1}cm^{-1}$)	
2-1a	238 (13.7)	
2-2a	249 (18.9)	288 (5.5)
2-3a	241 (22.3)	
2-4a	250 (9.8)	280 (6.1)
2-5a	234 (11.7)	268(6.6)

DFT Calculations:**Table II-S3.** MO Composition of **2-1b²⁺** in Singlet ($S=0$) Ground State (b3lyp/LanL2DZ(f)[Ru]6-31G**[C,H,N]).

MO	Energy (eV)	Composition			
		Ru	BPy	Py	hpp
LUMO+5	-1.32	2	92	5	1
LUMO+4	-1.39	3	94	3	0
LUMO+3	-1.52	4	25	69	3
LUMO+2	-1.60	2	78	19	1
LUMO+1	-2.37	6	93	1	1
LUMO	-2.43	3	97	0	0
HOMO	-5.51	61	10	2	27
HOMO-1	-5.99	79	13	6	2
HOMO-2	-6.04	80	16	1	4
HOMO-3	-6.89	3	3	44	50
HOMO-4	-7.01	20	9	3	69
HOMO-5	-7.24	1	98	1	1



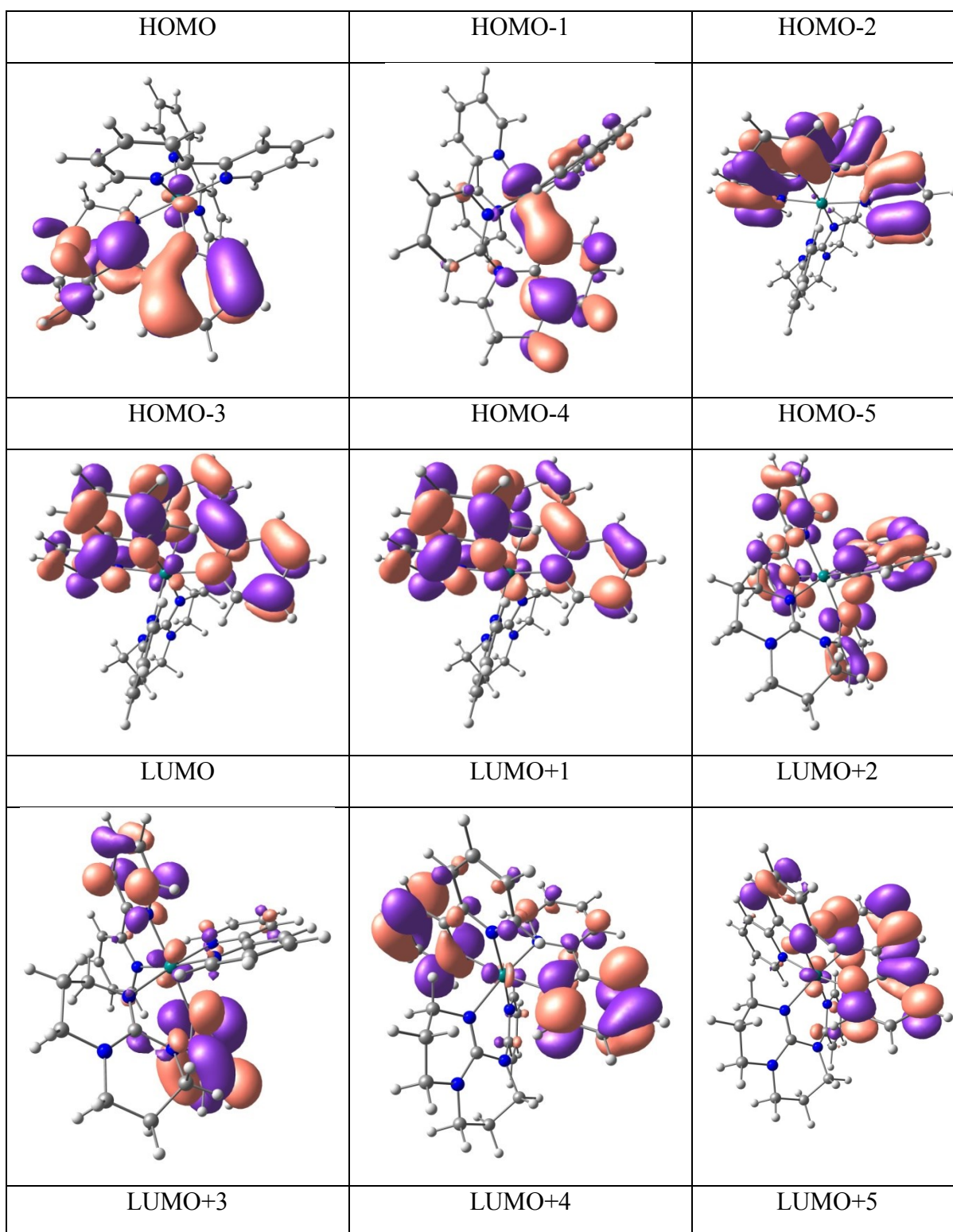


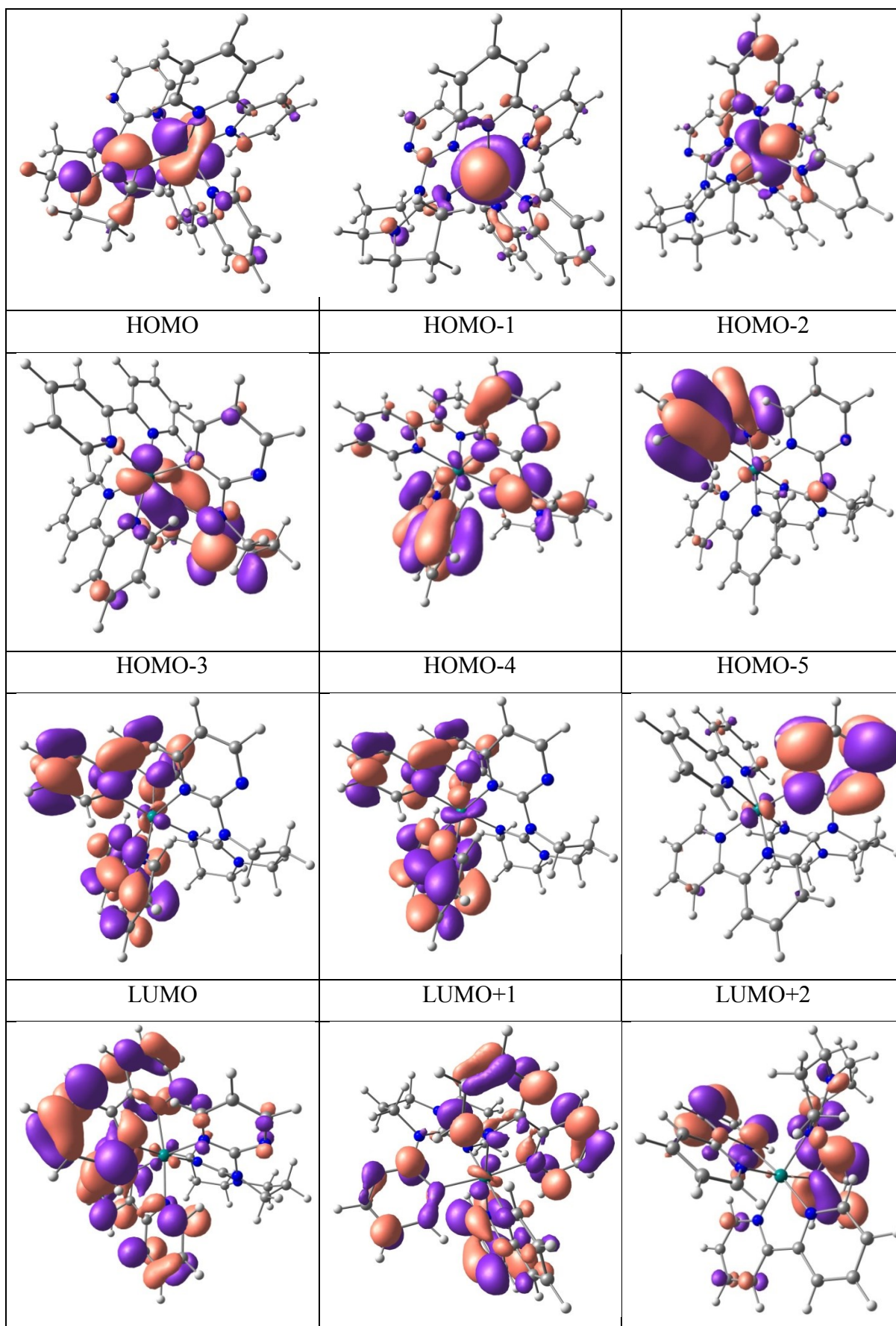
Figure 2.S2. Kohn-Sham orbital sketches in different MOs for **2-1b²⁺** in ($S=0$) ground state.

Table II-S4. Selected Transitions from TD-DFT calculations of **2-1b²⁺** in the Singlet Ground State (b3lyp/LanL2DZ(f)[Ru]6-31G**[C,H,N], CPCM (CH₃CN)).

energy (eV)	λ/nm	λ/nm ($\times 10^3$ M ⁻¹ cm ⁻¹) [expt.]	f	transition	character
5.03	245	242 (34.6)	0.0964	H-3 -> L+5 (55%) H -> L+12 (15%)	hpp/Py(π) to Bpy(π^*)
4.44	279	293 (53.2)	0.6001	H-6 -> L (28%) H-5 -> L+1 (36%)	Bpy(π) to Bpy(π^*)
3.53	351	357 (9.5)	0.0442	H -> L+6 (64%)	Ru(d π) to Bpy(π^*)
2.81	440	487 (7.1)	0.0981	H-2 -> L (36%) H-1 -> L (29%) H-1 -> L+1 (26%)	Ru(d π) to Bpy(π^*)
2.35	527	560 (3.9)	0.0286	H -> L (32%) H -> L+1 (57%)	Ru(d π) to Bpy(π^*)

Table II-S5. MO Composition of **2-3b²⁺** in Singlet (S=0) Ground State (b3lyp/LanL2DZ(f)[Ru]6-31G**[C,H,N]).

MO	Energy (eV)	Composition			
		Ru	BPy	Pyrm	hpp
LUMO+5	-1.39	1	40	49	9
LUMO+4	-1.41	3	82	13	2
LUMO+3	-1.59	3	93	4	0
LUMO+2	-1.94	2	7	89	1
LUMO+1	-2.40	6	92	1	1
LUMO	-2.48	3	97	0	0
HOMO	-5.64	57	12	2	29
HOMO-1	-5.96	83	11	3	3
HOMO-2	-6.19	82	15	3	1
HOMO-3	-7.03	14	7	3	76
HOMO-4	-7.23	4	59	12	25
HOMO-5	-7.28	2	94	2	3



LUMO+3	LUMO+4	LUMO+5
--------	--------	--------

Figure 2.S3. Kohn-Sham orbital sketches in different MOs for **2-3b²⁺** in (*S*=0) ground state.

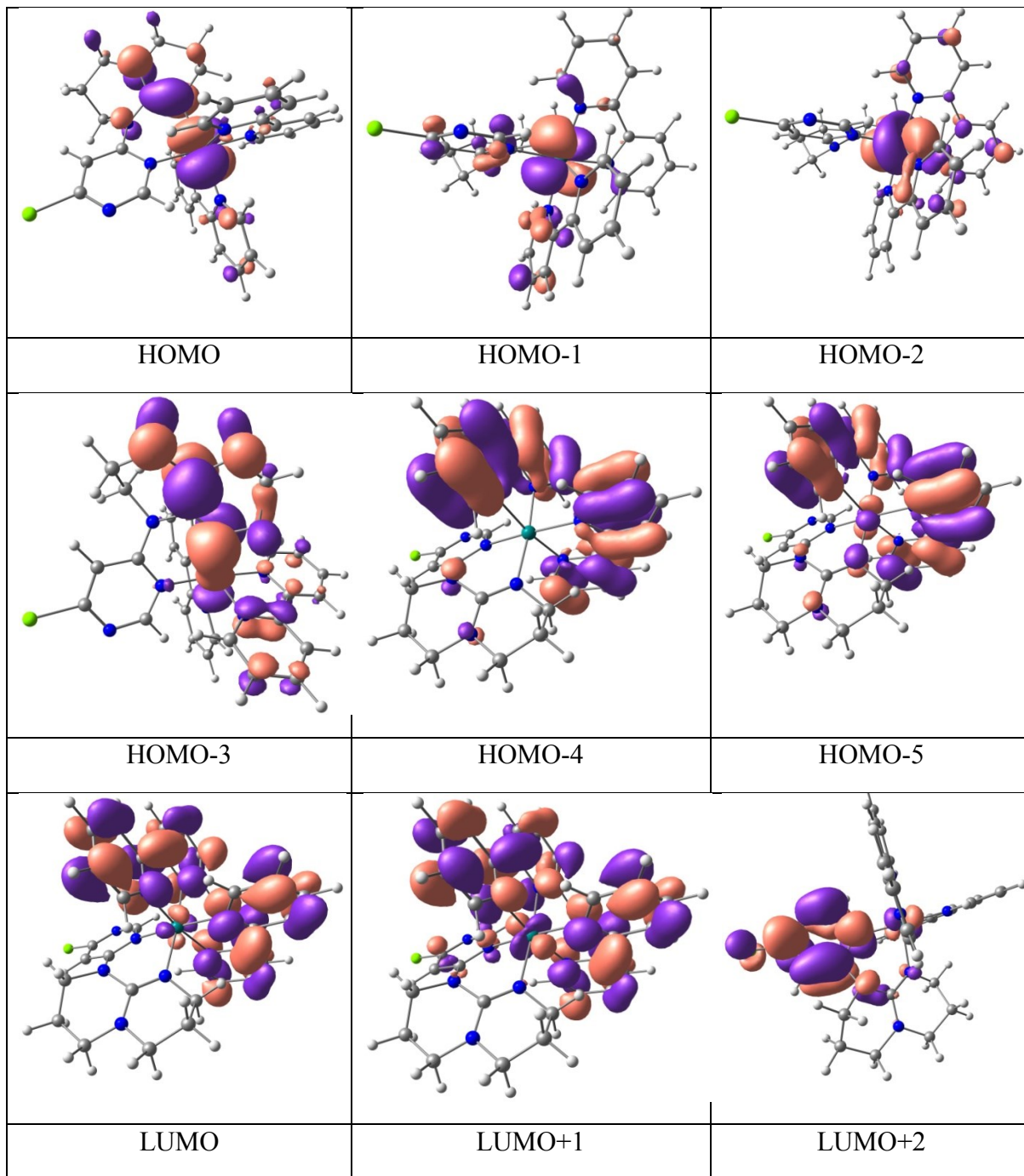
Table II-S6. Selected Transitions from TD-DFT Calculations of **2-3b²⁺** in the Singlet Ground State (b3lyp/LanL2DZ(f)[Ru]6-31G**[C,H,N], CPCM (CH₃CN)).

energy (eV)	λ/nm	λ/nm ($\epsilon \times 10^3 \text{ M}^{-1} \text{ cm}^{-1}$) [expt.]	f	major transition	character
5.21	237	241 (30.5)	0.0575	H-4 -> L+4 (10%) H-3 -> L+6 (10%) H-3 -> L+7 (29%) H-1 -> L+10 (15%)	hpp/Pyrm(π) to Bpy(π^*)
4.46	278	293 (41.4)	0.5211	H-5 -> L (20%) H-5 -> L+1 (23%)	Bpy(π) to Bpy(π^*)
3.51	353	350 (6.7)	0.0125	H-2 -> L+2 (14%) H-1 -> L+8 (12%) H-> L+4 (20%) H-> L+5 (18%) H-> L+8 (17%)	Ru(d π) to Bpy(π^*)
2.55	485	474 (6.4)	0.074	H -> L (13%) H-> L+1 (71%)	Ru(d π) to Bpy(π^*)
2.40	516	550 (2.9)	0.0227	H -> L (82%) H -> L+1 (13%)	Ru(d π) to Bpy(π^*)

Table II-S7. MO Composition of **2-4b²⁺** in Singlet (*S*=0) Ground State (b3lyp/LanL2DZ(f)[Ru]6-31G**[C,H,N]).

MO	Energy (eV)	Composition			
		Ru	BPy	Cl-Pyrm	hpp
LUMO+5	-1.44	4	95	1	1
LUMO+4	-1.63	3	91	6	1
LUMO+3	-1.86	0	13	79	7
LUMO+2	-2.12	4	6	86	4
LUMO+1	-2.46	5	89	5	1
LUMO	-2.50	3	97	0	0
HOMO	-5.72	63	10	1	27
HOMO-1	-6.19	79	14	5	2
HOMO-2	-6.21	80	16	1	3
HOMO-3	-7.17	17	13	1	69
HOMO-4	-7.30	0	96	1	3
HOMO-5	-7.33	3	90	1	5

SI – Chapter 2



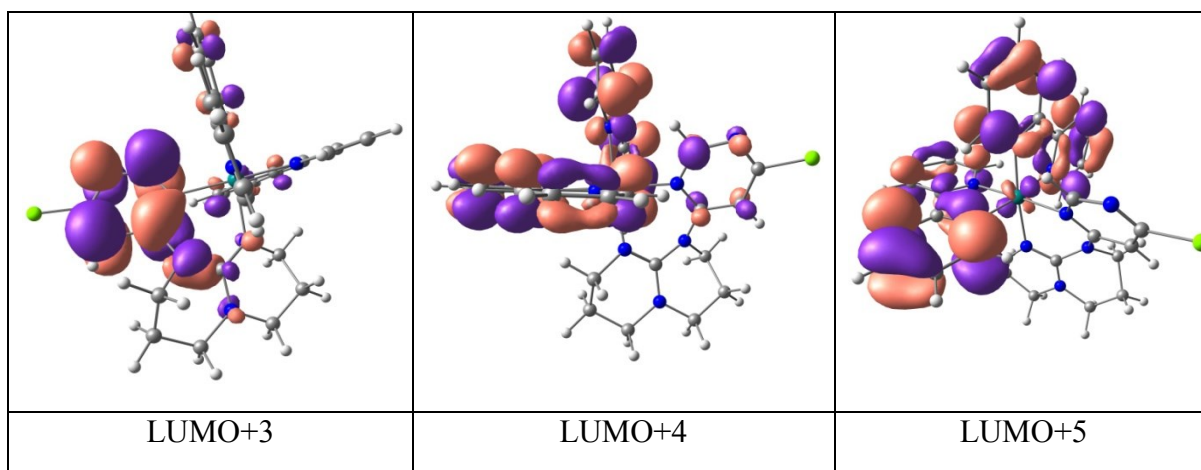


Figure 2.S4. Kohn-Sham orbital sketches in different MOs for **2-4b²⁺** in ($S=0$) ground state.

Table II-S8. Selected Transitions from TD-DFT Calculations of **2-4b²⁺** in the Singlet Ground State (b3lyp/LanL2DZ(f)[Ru]6-31G**[C,H,N], CPCM (CH₃CN)).

energy (eV)	λ/nm	λ/nm ($\times 10^3$ M ⁻¹ cm ⁻¹) [expt.]	f	major transition	character
5.08	244	246 (16.4)	0.2415	H-6 -> L+3 (72%)	hpp (π) to Cl-Pyrm(π^*)
4.44	279	292 (26.6)	0.4648	H-5 -> L (18%) H-5 -> L+1 (18%) H-4 -> L+1 (18%) H-2 -> L+7 (10%)	Bpy(π) to Bpy(π^*)
3.38	367	356 (4.1)	0.0437	H-1 -> L+2 (39%) H -> L+4 (24%) H-> L+9 (15%)	Ru(d π) to Cl-Pyrm(π^*)/Bpy(π^*)
2.91	425	463 (4.1)	0.0998	H-2 -> L (19%) H-1-> L (54%) H-1-> L+1 (19%)	Ru(d π) to Bpy(π^*)
2.45	505	532 (2.1)	0.0252	H -> L (48%) H -> L+1 (43%)	Ru(d π) to Bpy(π^*)

Table II-S9. Comparison in bond distances and angles of two geometry optimized models of **2-1b²⁺** obtained by DFT calculations with and without the effect of CPCM (acetonitrile).

Compound	Bond Length			Angle		
		Calc. (without CPCM)	Calc. (with CPCM)		Calc. (without CPCM)	Calc. (with CPCM)
2-1b	N1-Ru	2.11173	2.10319	N1-Ru1-N2	77.846	77.985
	N2-Ru	2.10267	2.10753	N3-Ru1-N4	77.585	77.707
	N3-Ru	2.10672	2.09865	N5-Ru1-N8	84.376	84.413
	N4-Ru	2.11307	2.10879			
	N5-Ru	2.13536	2.13040			
	N8-Ru	2.13874	2.13235			
	N6-C25	1.41241	1.41148			
	N6-C29A	1.40716	1.40618			
	N8-C29A	1.31415	1.31301			
	N7A-C29A	1.36561	1.36463			

Table II-S10. TD-DFT calculation of **2-1b²⁺** including CPCM (acetonitrile) starting with geometry optimized model, which was performed excluding CPCM.

Wavelength (nm)	Osc. Strength	Major contribution(s)
527.49	0.0286	HOMO->LUMO (32%), HOMO->L+1 (57%)
440.33	0.0981	H-2->LUMO (36%), H-1->LUMO (29%), H-1->L+1 (26%)
351.47	0.0442	HOMO->L+6 (64%)
278.93	0.6001	H-6->LUMO (28%), H-5->L+1 (36%)
245.29	0.0964	H-3 -> L+5 (55%), H -> L+12 (15%)

Table II-S11. TD-DFT calculation of **2-1b²⁺** including CPCM (acetonitrile) starting with geometry optimized model, which was performed including CPCM (acetonitrile).

Wavelength (nm)	Osc. Strength	Major contribution(s)
528.93	0.0294	HOMO->LUMO (30%), HOMO->L+1 (59%)
441.19	0.0984	H-2->LUMO (31%), H-1->LUMO (32%), H-1->L+1 (29%)
351.84	0.0676	HOMO->L+6 (62%)
278.66	0.5841	H-6->LUMO (27%), H-5->L+1 (35%)
247.63	0.0804	H-4->L+4 (46%), HOMO->L+12 (29%)

Table II-S12. TD-DFT calculation of **2-1b²⁺** excluding CPCM starting with geometry optimized model, which was performed excluding CPCM.

Wavelength (nm)	Osc. Strength	Major contribution(s)
529.07	0.0207	HOMO->LUMO (46%), HOMO->L+1 (42%)
438.54	0.071	H-2->LUMO (18%), H-1->LUMO (51%), H-1->L+1 (20%)
350.16	0.0427	HOMO->L+6 (65%)
273.68	0.3656	H-6->LUMO (19%), H-5->L+1 (35%)
244.93	0.0851	H-3->L+5 (20%), HOMO->L+12 (32%)

Table II-S13. Optimized Atomic coordinates obtained from DFT for **2-1b²⁺** in singlet ground state (b3lyp/LanL2DZ(f)[Ru]6-31G**[C,H,N]).

Center Number	Atomic Number	Atomic Type	Coordinates (Angstroms)		
			X	Y	Z
1	44	0	0.399087	0.005432	0.045969
2	7	0	1.244437	-1.485170	1.280020
3	7	0	1.783142	-0.907426	-1.247205
4	7	0	1.847526	1.492853	0.403575
5	7	0	-0.182923	1.536573	-1.288926
6	7	0	-0.915385	0.818437	1.519385
7	7	0	-2.847954	0.252769	0.233651
8	7	0	-1.213293	-1.344559	-0.343833
9	6	0	0.850487	-1.798901	2.530123
10	1	0	0.014361	-1.232556	2.920257
11	6	0	1.464923	-2.786275	3.292568
12	1	0	1.106109	-2.994051	4.294467
13	6	0	2.534629	-3.490587	2.741294
14	1	0	3.041519	-4.266205	3.305664
15	6	0	2.935880	-3.189467	1.443118
16	1	0	3.751974	-3.740457	0.992362
17	6	0	2.274858	-2.187582	0.724219
18	6	0	2.596617	-1.841118	-0.674909
19	6	0	3.633504	-2.436622	-1.401440
20	1	0	4.279808	-3.169840	-0.935184
21	6	0	3.836213	-2.085381	-2.732686
22	1	0	4.638052	-2.541326	-3.303770
23	6	0	2.989082	-1.142765	-3.314421
24	1	0	3.102963	-0.841647	-4.349806
25	6	0	1.982505	-0.579409	-2.538345
26	1	0	1.307383	0.161198	-2.948654

SI – Chapter 2

27	6	0	2.915194	1.372933	1.219054
28	1	0	3.045990	0.406093	1.690439
29	6	0	3.800673	2.415568	1.466435
30	1	0	4.642052	2.261717	2.132916
31	6	0	3.575593	3.645630	0.848590
32	1	0	4.237888	4.486768	1.023985
33	6	0	2.486682	3.774666	-0.007657
34	1	0	2.304235	4.719436	-0.504376
35	6	0	1.638880	2.683182	-0.227468
36	6	0	0.510849	2.704845	-1.178324
37	6	0	0.194318	3.811479	-1.975244
38	1	0	0.744701	4.738102	-1.870644
39	6	0	-0.821316	3.715928	-2.920562
40	1	0	-1.070801	4.567085	-3.545323
41	6	0	-1.494204	2.501744	-3.060798
42	1	0	-2.274260	2.370455	-3.802602
43	6	0	-1.146776	1.445682	-2.226649
44	1	0	-1.638764	0.484146	-2.300508
45	6	0	-0.382459	1.378505	2.634609
46	1	0	0.697814	1.362719	2.692533
47	6	0	-1.130924	1.952498	3.646399
48	1	0	-0.636724	2.396070	4.502949
49	6	0	-2.521006	1.928309	3.526912
50	1	0	-3.157382	2.343862	4.301445
51	6	0	-3.084964	1.338299	2.406046
52	1	0	-4.161282	1.278471	2.323474
53	6	0	-2.263734	0.795110	1.399609
54	6	0	-4.178243	0.747142	-0.177232
55	1	0	-4.167421	0.874098	-1.265939
56	1	0	-4.331662	1.734829	0.254304
57	6	0	-5.242575	-0.264078	0.228617
58	1	0	-5.218883	-0.417416	1.311947
59	1	0	-6.246515	0.083192	-0.030613
60	6	0	-4.941308	-1.563517	-0.512641
61	1	0	-5.323859	-2.434013	0.033699
62	1	0	-5.438686	-1.556084	-1.489976
63	6	0	-2.480465	-1.000480	-0.290206
64	7	0	-3.501389	-1.767010	-0.774999
65	6	0	-3.251513	-2.979016	-1.578902
66	1	0	-3.891083	-2.932014	-2.467946
67	1	0	-3.576981	-3.848653	-0.993905
68	6	0	-1.786132	-3.111757	-1.959732
69	1	0	-1.583319	-4.136599	-2.282998
70	1	0	-1.539342	-2.448874	-2.796713
71	6	0	-0.941642	-2.734882	-0.747102
72	1	0	0.117831	-2.825625	-0.974278
73	1	0	-1.156421	-3.415278	0.088824

SI - Chapter 2

Table II-S14. Optimized Atomic coordinates obtained from DFT for **2-3b²⁺** in singlet ground state (b3lyp/LanL2DZ(f)[Ru]6-31G**[C,H,N]).

Center Number	Atomic Number	Atomic Type	Coordinates (Angstroms)		
			X	Y	Z
1	44	0	-0.414887	-0.040356	-0.031983
2	7	0	0.401730	1.387972	-1.353479
3	7	0	-1.193040	1.757581	0.725998
4	7	0	-2.238733	-0.275174	-1.072220
5	7	0	-1.490558	-1.346276	1.231365
6	7	0	0.548353	-1.759038	-0.836472
7	7	0	2.527572	-2.940036	-1.435236
8	7	0	2.729520	-0.844910	-0.466841
9	7	0	3.676873	0.195689	1.412367
10	7	0	1.330214	0.075753	1.196604
11	6	0	1.128410	1.126004	-2.458723
12	1	0	1.299378	0.079654	-2.676503
13	6	0	1.632898	2.119740	-3.289387
14	1	0	2.207361	1.847529	-4.167853
15	6	0	1.382313	3.453607	-2.966695
16	1	0	1.764920	4.258407	-3.585510
17	6	0	0.615816	3.735314	-1.840827
18	1	0	0.394023	4.764337	-1.587015
19	6	0	0.124302	2.688773	-1.051581
20	6	0	-0.760616	2.894643	0.110684
21	6	0	-1.178274	4.155610	0.551150
22	1	0	-0.823109	5.053184	0.060491
23	6	0	-2.061119	4.259396	1.621514
24	1	0	-2.391016	5.233215	1.967626
25	6	0	-2.514619	3.090613	2.232227
26	1	0	-3.207969	3.118577	3.065371
27	6	0	-2.055689	1.867771	1.756335
28	1	0	-2.373313	0.937729	2.211954
29	6	0	-2.539798	0.273474	-2.265522
30	1	0	-1.734670	0.800709	-2.762291
31	6	0	-3.802286	0.185271	-2.841305
32	1	0	-3.987500	0.644597	-3.805869
33	6	0	-4.807535	-0.492947	-2.152838
34	1	0	-5.807562	-0.574722	-2.565451
35	6	0	-4.505422	-1.069674	-0.922823
36	1	0	-5.273815	-1.602330	-0.376240
37	6	0	-3.212003	-0.956974	-0.400914
38	6	0	-2.784549	-1.584645	0.866370
39	6	0	-3.610046	-2.410405	1.637807
40	1	0	-4.635530	-2.592219	1.341027
41	6	0	-3.106772	-3.013606	2.786813
42	1	0	-3.740259	-3.654402	3.391113

SI – Chapter 2

43	6	0	-1.774395	-2.791364	3.133888
44	1	0	-1.332759	-3.253957	4.009463
45	6	0	-1.004919	-1.957518	2.330233
46	1	0	0.035760	-1.761531	2.552893
47	6	0	-0.173642	-2.809625	-1.295064
48	1	0	-1.248921	-2.709041	-1.227251
49	6	0	0.406036	-3.936956	-1.849043
50	1	0	-0.196941	-4.756184	-2.221148
51	6	0	1.799166	-3.947557	-1.912625
52	1	0	2.347370	-4.781650	-2.343687
53	6	0	1.898757	-1.888785	-0.904148
54	6	0	4.095428	-0.782320	-1.042721
55	1	0	4.295925	0.264547	-1.297628
56	1	0	4.104854	-1.374678	-1.953006
57	6	0	5.089289	-1.296760	-0.014314
58	1	0	6.105715	-1.313272	-0.416746
59	1	0	4.823359	-2.323334	0.253712
60	6	0	5.028844	-0.359672	1.186032
61	1	0	5.355361	-0.858370	2.106455
62	1	0	5.697682	0.494906	1.027957
63	6	0	3.653018	1.191383	2.502447
64	1	0	4.382140	1.973919	2.261407
65	1	0	4.001396	0.696593	3.417485
66	6	0	2.262054	1.771610	2.710939
67	1	0	2.044740	2.548476	1.970080
68	1	0	2.201251	2.231070	3.701522
69	6	0	1.260441	0.630721	2.558492
70	1	0	1.488562	-0.150684	3.298606
71	1	0	0.241335	0.964063	2.744499
72	6	0	2.543873	-0.176856	0.756465

Table II-S15. Optimized Atomic coordinates obtained from DFT for **2-4b²⁺** in singlet ground state (b3lyp/LanL2DZ(f)[Ru]6-31G**[C,H,N]).

Center Number	Atomic Number	Atomic Type	Coordinates (Angstroms)		
			X	Y	Z
1	44	0	0.600042	0.022845	0.010866
2	17	0	-5.013900	2.744712	-2.164773
3	7	0	1.377859	-0.537989	-1.871048
4	7	0	2.512745	-0.686392	0.518483
5	7	0	1.417916	1.967401	0.050548
6	7	0	0.086256	0.689378	1.949920
7	7	0	-1.281169	0.737912	-0.693443
8	7	0	-2.384601	2.458113	-1.940701
9	7	0	-2.520617	-0.907539	0.509332
10	7	0	-2.271737	-3.242515	0.543418
11	7	0	-0.399151	-1.869371	0.081078

SI - Chapter 2

12	6	0	2.680282	-0.947357	-1.863967
13	6	0	3.326060	-1.317103	-3.048735
14	1	0	4.359502	-1.640269	-3.032369
15	6	0	2.634651	-1.279436	-4.256180
16	1	0	3.128426	-1.563754	-5.179428
17	6	0	1.298645	-0.880139	-4.252228
18	1	0	0.714757	-0.844277	-5.165178
19	6	0	0.712701	-0.522018	-3.043081
20	1	0	-0.323350	-0.210283	-2.998622
21	6	0	3.321828	-0.999479	-0.534679
22	6	0	4.655771	-1.370006	-0.333293
23	1	0	5.293213	-1.606111	-1.176272
24	6	0	5.168691	-1.434906	0.958830
25	1	0	6.202103	-1.720639	1.124356
26	6	0	4.330104	-1.128968	2.029914
27	1	0	4.682002	-1.170642	3.054644
28	6	0	3.016477	-0.757818	1.765837
29	1	0	2.335401	-0.504408	2.568649
30	6	0	1.128743	2.704090	1.160974
31	6	0	1.551001	4.033261	1.274729
32	1	0	1.305088	4.613658	2.155171
33	6	0	2.294296	4.615130	0.252467
34	1	0	2.623318	5.645797	0.332042
35	6	0	2.608688	3.847398	-0.868395
36	1	0	3.191036	4.252857	-1.688228
37	6	0	2.151190	2.536050	-0.928323
38	1	0	2.360553	1.912538	-1.789193
39	6	0	0.394329	1.989076	2.223144
40	6	0	0.073610	2.561981	3.459542
41	1	0	0.313856	3.597984	3.662897
42	6	0	-0.543730	1.792337	4.440093
43	1	0	-0.792568	2.227414	5.402299
44	6	0	-0.818099	0.451870	4.166900
45	1	0	-1.276070	-0.193643	4.908194
46	6	0	-0.490667	-0.054343	2.914562
47	1	0	-0.680768	-1.088524	2.656506
48	6	0	-1.313353	1.826755	-1.494753
49	1	0	-0.350989	2.227497	-1.787950
50	6	0	-3.549944	1.941528	-1.573938
51	6	0	-3.667283	0.809162	-0.780754
52	1	0	-4.643009	0.406208	-0.555507
53	6	0	-2.479497	0.207122	-0.331694
54	6	0	-3.757040	-1.159738	1.282713
55	1	0	-4.289387	-0.218890	1.410577
56	1	0	-3.457628	-1.493780	2.281915
57	6	0	-4.574035	-2.235024	0.580551
58	1	0	-5.516368	-2.426600	1.100776
59	1	0	-4.821902	-1.911918	-0.435431
60	6	0	-3.727363	-3.505739	0.562587
61	1	0	-3.922991	-4.093049	1.467247

SI – Chapter 2

62	1	0	-3.978603	-4.143008	-0.293524
63	6	0	-1.484255	-4.486283	0.660366
64	1	0	-1.689387	-5.104345	-0.222791
65	1	0	-1.854441	-5.036663	1.532702
66	6	0	0.002917	-4.199668	0.778142
67	1	0	0.258017	-3.873128	1.792463
68	1	0	0.569318	-5.112918	0.576115
69	6	0	0.357785	-3.099389	-0.215332
70	1	0	0.141063	-3.429069	-1.240801
71	1	0	1.418558	-2.865465	-0.166784
72	6	0	-1.673636	-2.031816	0.346578

SI – Chapter 3 : Supplementary Informations

Supplementary Information

Stereoselective formation of a meso-diruthenium(II,II) complex and tuning the properties of its monoruthenium analogues

*Amlan K. Pal, Garry S. Hanan**

Département de Chimie, Université de Montréal, Montréal, Québec, H3T-1J4, Canada

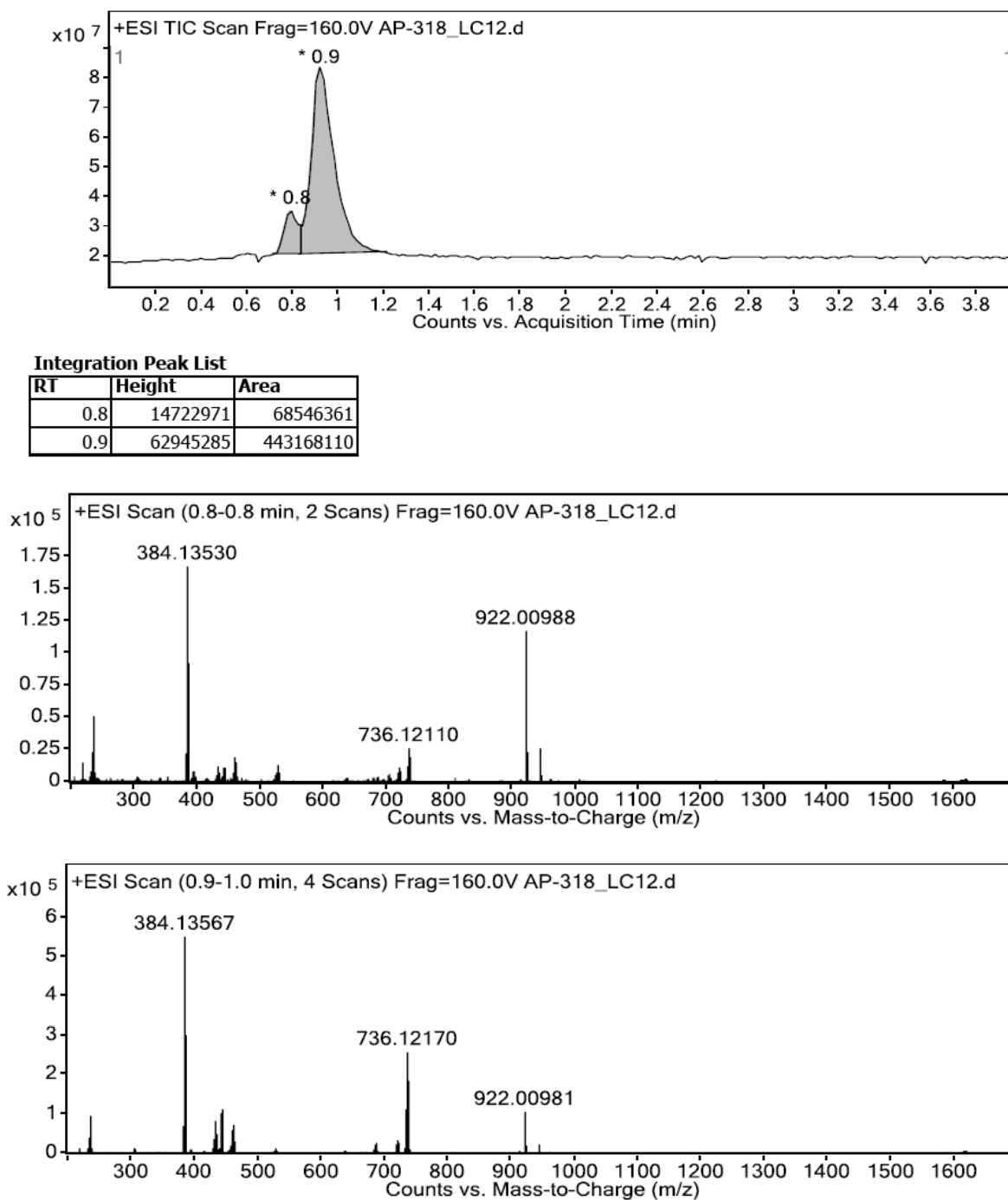


Figure 3.S1. LC-MS of reaction ii (see Scheme 3.1 in main text) using an achiral support, showing the separation of the *rac*- $\Delta\Delta$ or $\Lambda\Lambda$ -isomer (retention time at 0.8 min) and the *meso*- $\Delta\Lambda$ or $\Lambda\Delta$ -isomer (retention time at 0.9-1.0 min) (Figure adopted from ref 1).

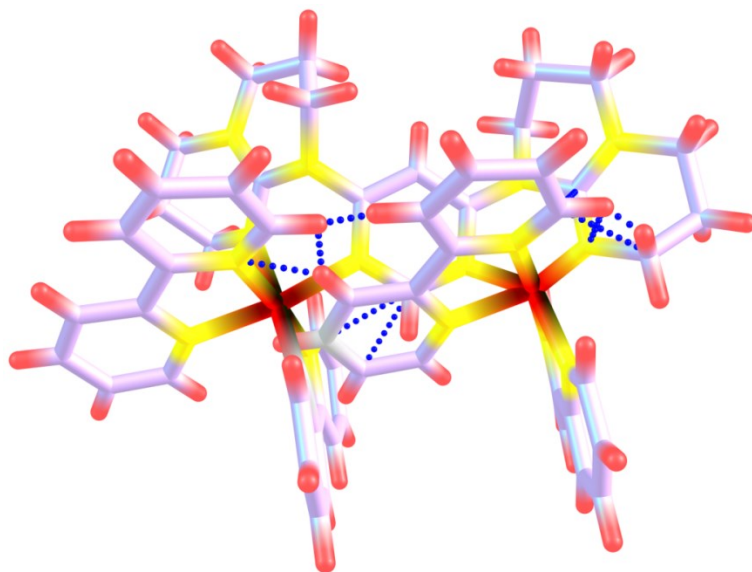


Figure 3.S2. View of capped stick model of *rac*- $\Lambda\Lambda$ or $\Delta\Delta$ -diastereomer, as the initial coordinates for DFT calculation, sketched using Chemcraft. The blue dots show the severe steric interactions between the colliding atoms.

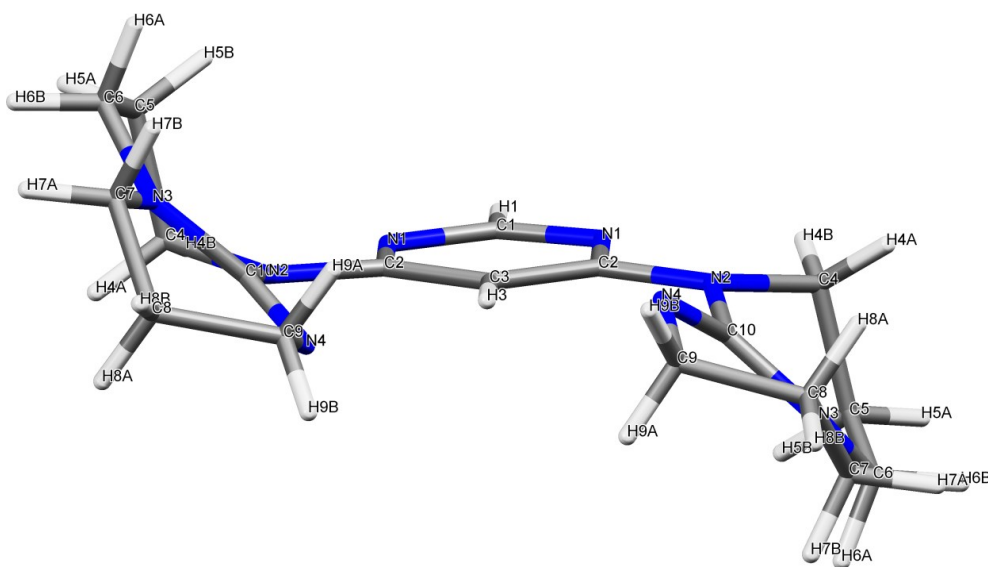


Figure 3.S3. View of capped stick model of **3-L1**, along the plane consisting of pyrimidine, showing the chair conformation of **3-L1**. The pyrimidine ring is twisted with respect to the **hpp** units to minimize the lone pair-lone pair interactions on the hetero atoms.

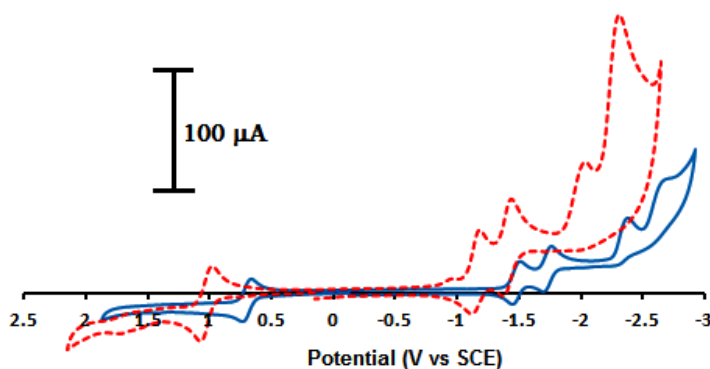
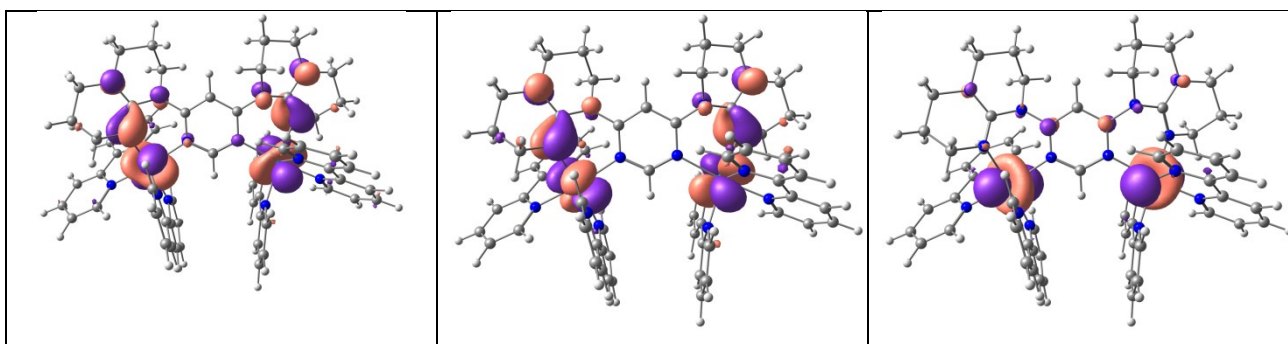


Figure 3.S4. Cyclic voltammogram of **3-3** (blue, bold line) and **3-4** (red, dotted line) in dry, degassed CH₃CN, recorded at a scan rate of 50 mV/s.

DFT calculations:

Table III-S1. MO Composition of **3-(1-meso)⁴⁺** in Singlet ($S=0$) Ground State (b3lyp/LanL2DZ(f)[Ru]6-31G**[C,H,N]).

MO	Energy (eV)	Composition			
		Ru	BPy	Pyrimidine	Hpp
LUMO+6	-1.82	4	95	1	1
LUMO+5	-2.35	4	13	79	5
LUMO+4	-2.59	4	8	73	15
LUMO+3	-2.61	6	92	2	0
LUMO+2	-2.64	5	85	8	2
LUMO+1	-2.71	2	96	1	1
LUMO	-2.72	2	92	4	2
HOMO	-5.94	60	12	2	26
HOMO-1	-5.99	57	12	1	30
HOMO-2	-6.26	82	11	3	4
HOMO-3	-6.30	85	12	2	1
HOMO-4	-6.50	82	14	3	1
HOMO-5	-6.52	82	15	2	1



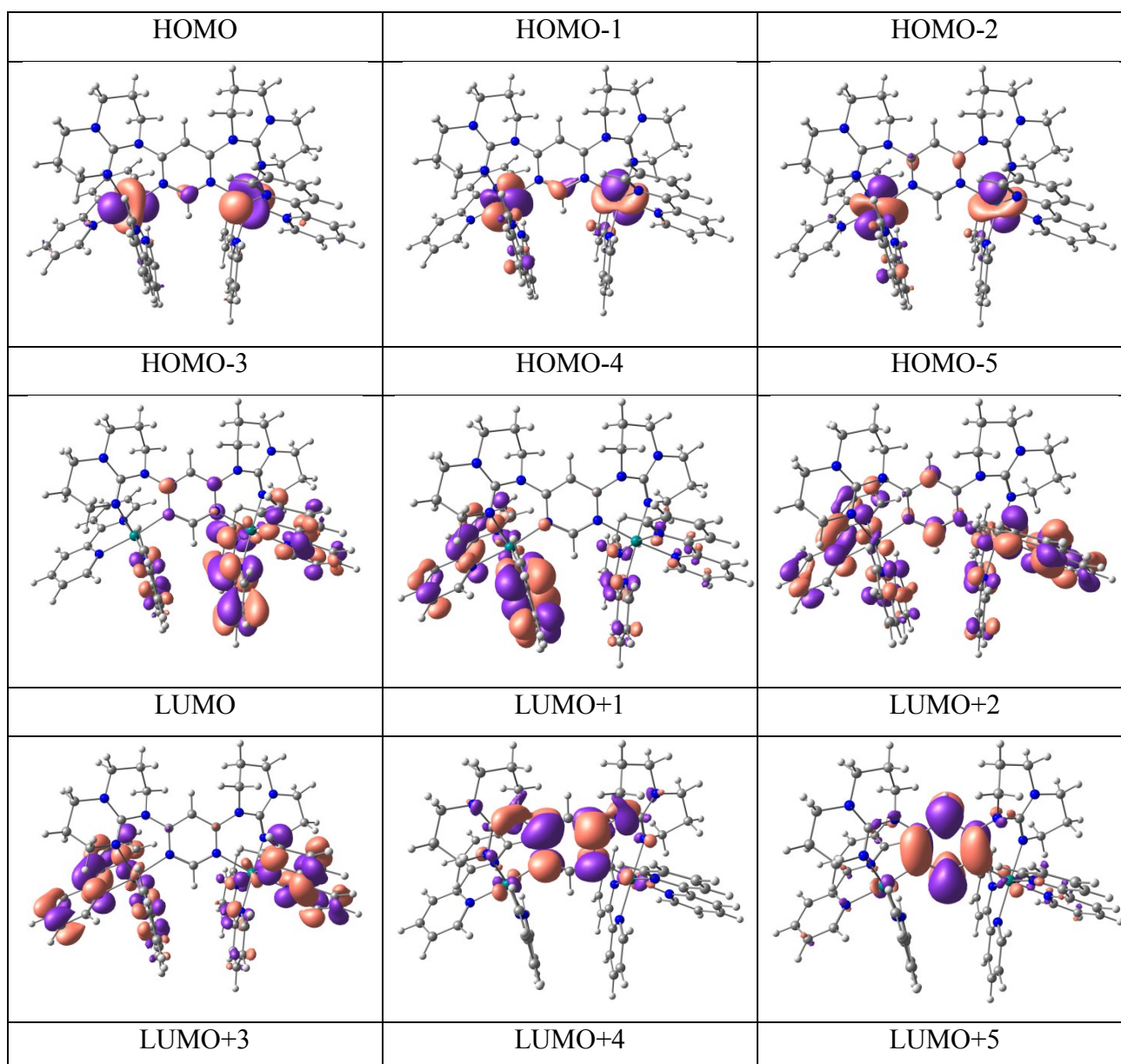


Figure 3.S5. Kohn-Sham molecular orbital sketches for $3-(1\text{-}meso)^{4+}$ in ($S=0$) ground state

Figure 3.S6.

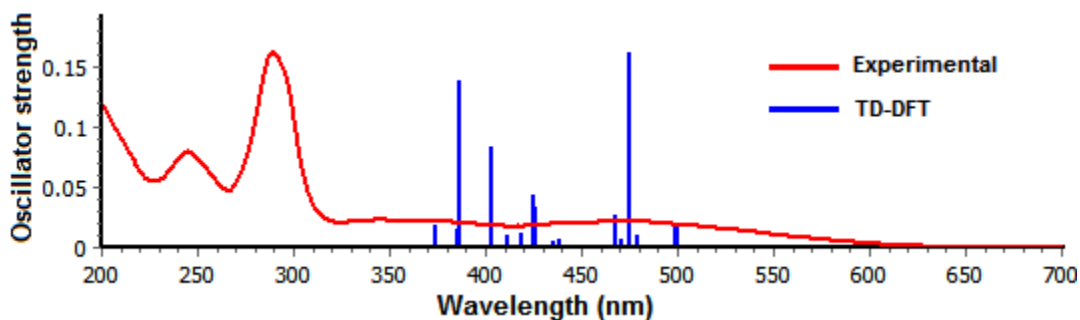


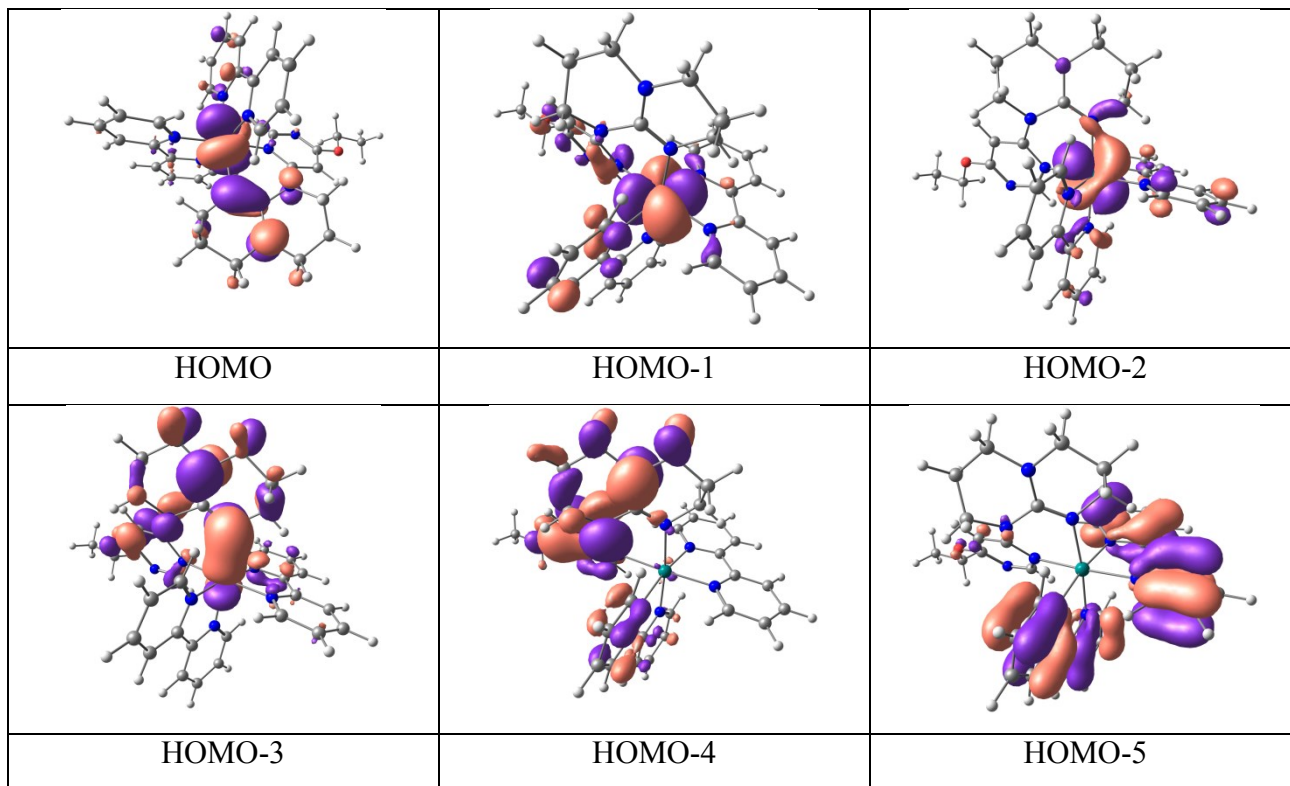
Figure 3.S7. Overlap of experimental electronic absorption spectra with oscillator strength from TD-DFT calculation of **3-(1-meso)⁴⁺** in ($S=0$) ground state. Due to memory allocation problem only the first thirty transitions were calculated.

Table III-S2. Selected Transitions from TD-DFT calculations of **3-(1-meso)⁴⁺** in the Singlet Ground State (b3lyp/LanL2DZ(f)[Ru]6-31G**[C,H,N], CPCM (CH₃CN)).

energy (eV)	λ/nm	λ/nm ($\epsilon \times 10^3 \text{ M}^{-1} \text{ cm}^{-1}$) [expt.]	f	Major transition(s)	character
3.22	384	368 (7.0)	0.1385	H-4->L+4 (52%)	Ru(d π) to Pyrimidine(π^*)
2.62	473	470 (6.8)	0.1615	H->L+2 (52%), H-1->L+3 (25%)	Ru(d π) to Bpy(π^*) (major) + hpp(n/ π) to Bpy(π^*) (minor)
2.49	498	511 (5.6)	0.0198	H-1->L+1 (32%), H->L (38%), H->L+1 (17%)	Ru(d π) to Bpy(π^*) (major) + hpp(n/ π) to Bpy(π^*) (minor)

Table III-S3. MO Composition of $3\text{-}2^{2+}$ in Singlet ($S=0$) Ground State (b3lyp/LanL2DZ(f)[Ru]6-31G**[C,H,N,O]).

MO	Energy (eV)	Composition				
		Ru	BPy	Pyrimidine	Hpp	Adduct (OEt)
LUMO+6	-1.25	2	68	25	2	2
LUMO+5	-1.36	2	53	37	5	3
LUMO+4	-1.38	3	75	20	1	2
LUMO+3	-1.48	2	50	46	2	0
LUMO+2	-1.62	2	83	14	1	0
LUMO+1	-2.39	6	93	1	0	0
LUMO	-2.45	3	97	0	0	0
HOMO	-5.58	63	10	1	26	0
HOMO-1	-6.01	79	13	6	1	1
HOMO-2	-6.08	80	16	1	3	0
HOMO-3	-7.03	18	8	10	61	3
HOMO-4	-7.13	1	12	27	55	5
HOMO-5	-7.26	1	96	2	1	1
HOMO-6	-7.29	1	89	2	6	1



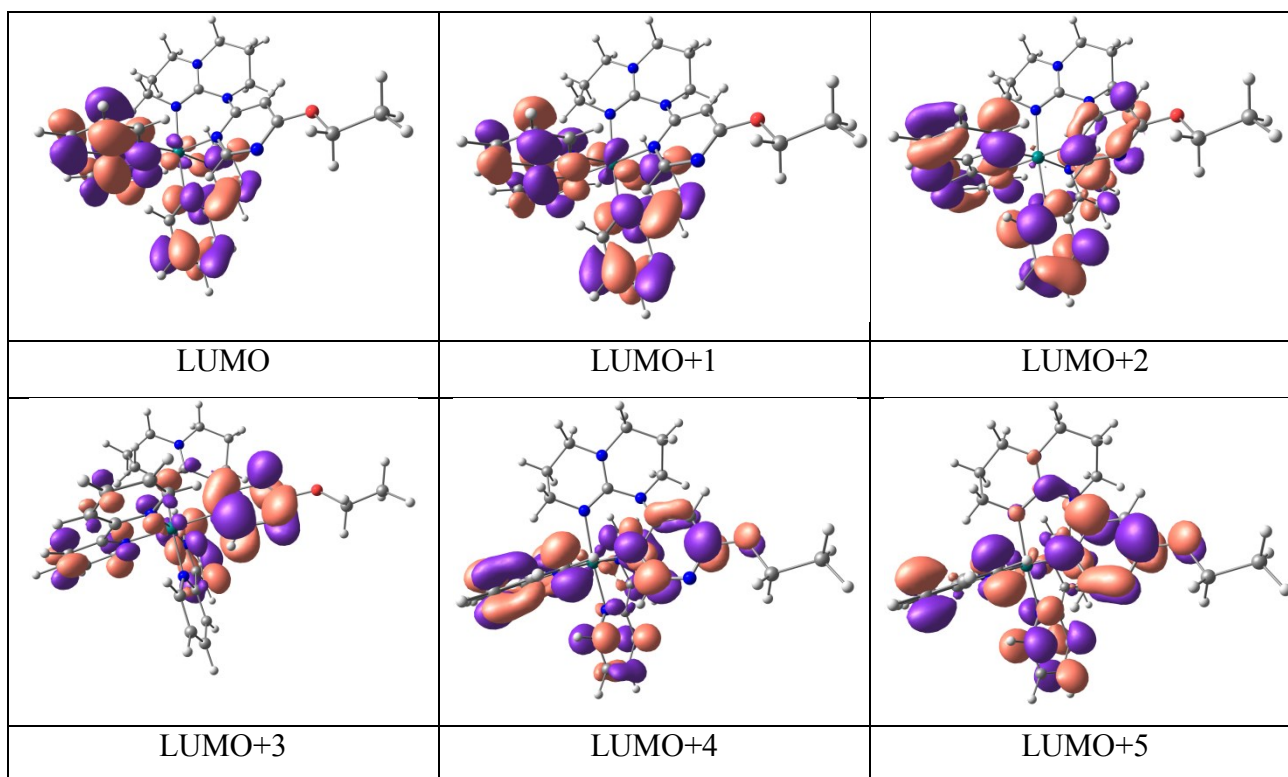


Figure 3.S8. Kohn-Sham molecular orbital sketches for $3-2^{2+}$ in ($S=0$) ground state

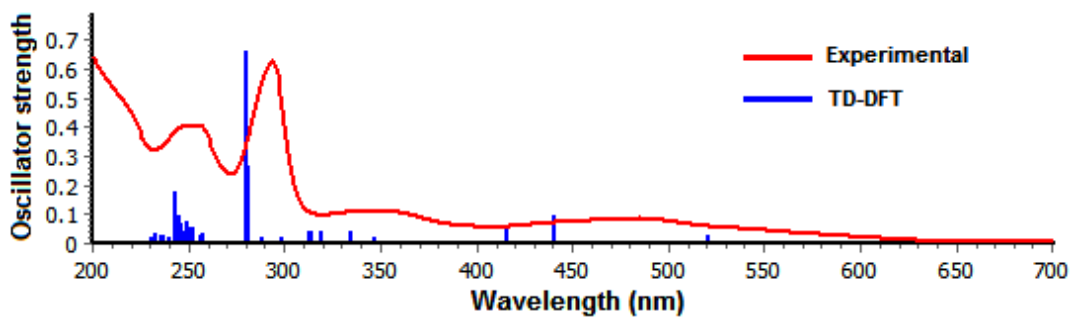


Figure 3.S9. Overlap of experimental electronic absorption spectrum with oscillator strength from TD-DFT calculation of $3-2^{2+}$ in ($S=0$) ground state with first seventy calculated transitions.

Table III-S4. Selected Transitions from TD-DFT calculations of **3-2²⁺** in the Singlet Ground State (b3lyp/LanL2DZ(f)[Ru]6–31G**[C,H,N,O], CPCM (CH₃CN)).

energy (eV)	λ/nm	λ/nm ($\epsilon \times 10^3 \text{ M}^{-1} \text{ cm}^{-1}$) [expt.]	f	Major transition(s)	character
5.13	242	246 (33.1)	0.1757	H-6->L+2 (37%), H-4->L+5 (10%)	Bpy/Pyrimidine/hpp(n/ π) to Bpy/Pyrimidine/hpp(π^*)
5.08	244	255 (33.5)	0.0928	H-4->L+3 (64%)	Pyrimidine/hpp(n/ π) to Bpy/Pyrimidine/hpp(π^*)
4.45	278	293 (51.6)	0.658	H-6->L (28%), H-5->L+1 (37%)	Bpy(π) to Bpy (π^*)
3.72	333	353 (9.4)	0.0406	H-2->L+2 (82%)	Ru(d π) to Bpy(π^*)
2.82	439	493 (6.9)	0.0953	H-2->L (42%), H-1->L (27%), H-1->L+1 (24%)	Ru(d π) to Bpy(π^*)
2.39	519	542 (3.9)	0.0259	H->L (33%), H->L+1 (56%)	Ru(d π) to Bpy(π^*) (major) + hpp(n/ π) to Bpy(π^*) (minor)

Table III-S5. MO Composition of **3-3²⁺** in Singlet ($S=0$) Ground State (b3lyp/LanL2DZ(f)[Ru]6–31G**[C,H,N,O]).

MO	Energy (eV)	Composition				
		Ru	BPy	Pyrimidine	Hpp	Adduct (Butoxy)
LUMO+6	-1.24	2	64	28	3	3
LUMO+5	-1.35	2	53	37	5	3
LUMO+4	-1.38	3	76	19	1	2
LUMO+3	-1.48	2	50	45	3	0
LUMO+2	-1.62	2	83	14	1	0
LUMO+1	-2.38	6	93	1	0	0
LUMO	-2.45	3	97	0	0	0
HOMO	-5.56	63	10	1	26	0
HOMO-1	-6.01	79	13	6	1	2
HOMO-2	-6.08	80	16	1	3	0
HOMO-3	-7.03	18	8	10	60	4
HOMO-4	-7.13	1	12	27	55	6
HOMO-5	-7.25	1	96	2	1	1
HOMO-6	-7.29	1	89	2	7	1

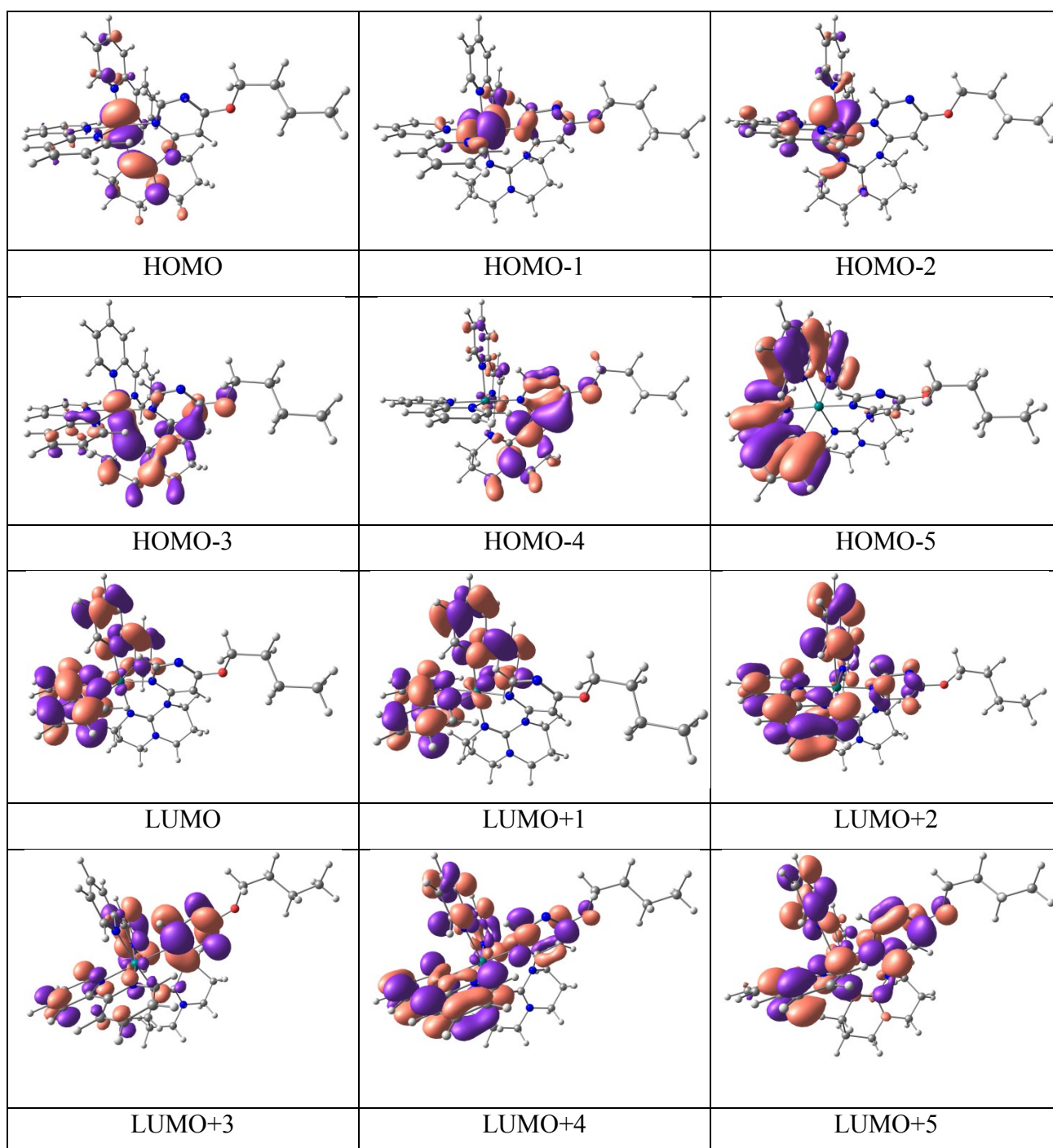


Figure 3.S10. Kohn-Sham molecular orbital sketches for $3\text{-}3^{2+}$ in ($S=0$) ground state

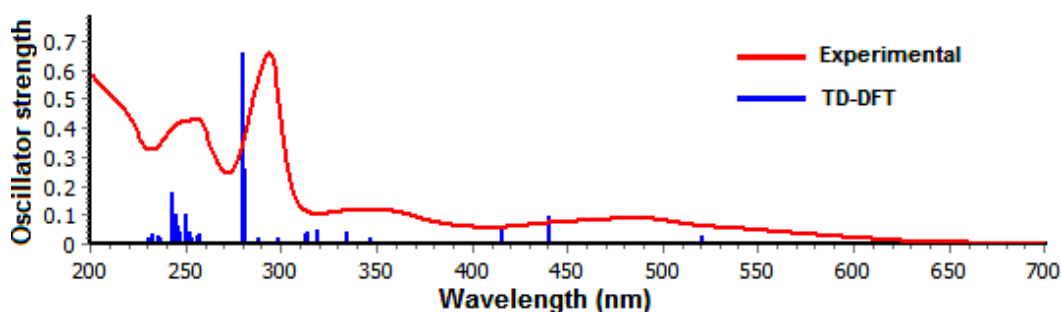


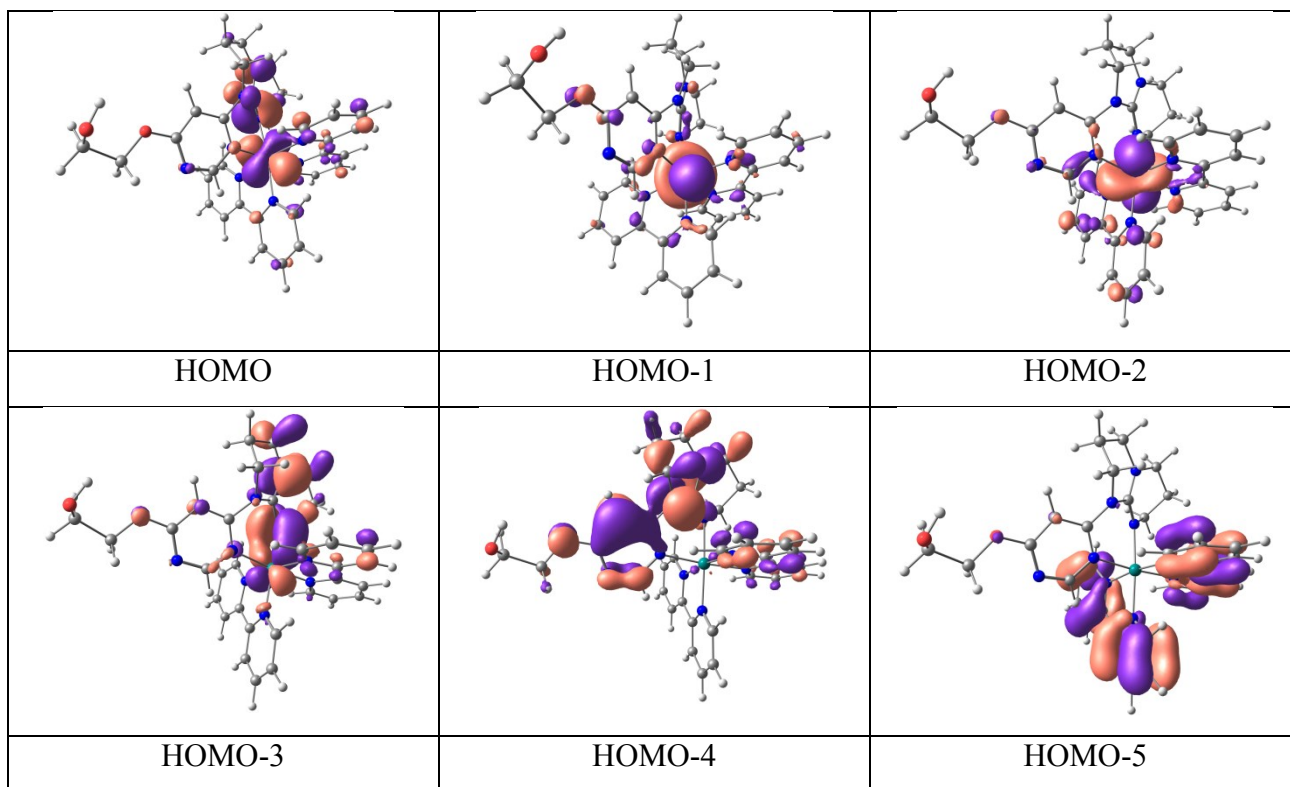
Figure 3.S11. Overlap of experimental electronic absorption spectrum with oscillator strength from TD-DFT calculation of $3-3^{2+}$ in ($S=0$) ground state with first seventy calculated transitions.

Table III-S6. Selected Transitions from TD-DFT calculations of $3-3^{2+}$ in the Singlet Ground State (b3lyp/LanL2DZ(f)[Ru]6–31G**[C,H,N,O], CPCM (CH₃CN)).

energy (eV)	λ /nm	λ /nm ($\epsilon \times 10^3$ M ⁻¹ cm ⁻¹) [expt.]	f	Major transition(s)	character
5.13	242	248 (25.2)	0.1761	H-6->L+2 (30%), H-4->L+5 (12%)	Bpy/Pyrimidine/hpp(n/ π) to Bpy/Pyrimidine/hpp(π^*)
4.98	249	255 (25.7)	0.1048	H-7->L (38%), H-4->L+5 (10%), H->L+12 (11%)	Pyrimidine/hpp(n/ π) to Bpy/Pyrimidine/hpp(π^*)
4.45	279	294 (39.1)	0.6574	H-6->L (28%), H-5->L+1 (38%)	Bpy(π) to Bpy (π^*)
3.72	334	354 (6.9)	0.0406	H-2->L+2 (82%)	Ru(d π) to Bpy(π^*)
2.82	440	494 (5.3)	0.0939	H-2->L (43%), H-1->L (27%), H-1->L+1 (23%)	Ru(d π) to Bpy(π^*)
2.38	520	552 (2.8)	0.0254	H->L (32%), H->L+1 (57%)	Ru(d π) to Bpy(π^*) (major) + hpp(n/ π) to Bpy(π^*) (minor)

Table III-S7. MO Composition of $3\text{-}4^{2+}$ in Singlet ($S=0$) Ground State (b3lyp/LanL2DZ(f)[Ru]6-31G**[C,H,N,O]).

MO	Energy (eV)	Composition				
		Ru	BPy	Pyrimidine	Hpp	Adduct (ethylene glycol)
LUMO+6	-1.3	2	83	13	1	1
LUMO+5	-1.38	4	61	30	1	3
LUMO+4	-1.39	1	68	24	4	2
LUMO+3	-1.48	1	17	75	7	0
LUMO+2	-1.62	2	87	10	0	1
LUMO+1	-2.38	6	92	1	1	0
LUMO	-2.47	3	97	0	0	0
HOMO	-5.65	59	12	2	27	0
HOMO-1	-5.90	82	10	4	3	1
HOMO-2	-6.14	81	15	3	1	1
HOMO-3	-7.04	18	9	3	69	1
HOMO-4	-7.16	1	11	29	53	6
HOMO-5	-7.26	0	97	1	1	0



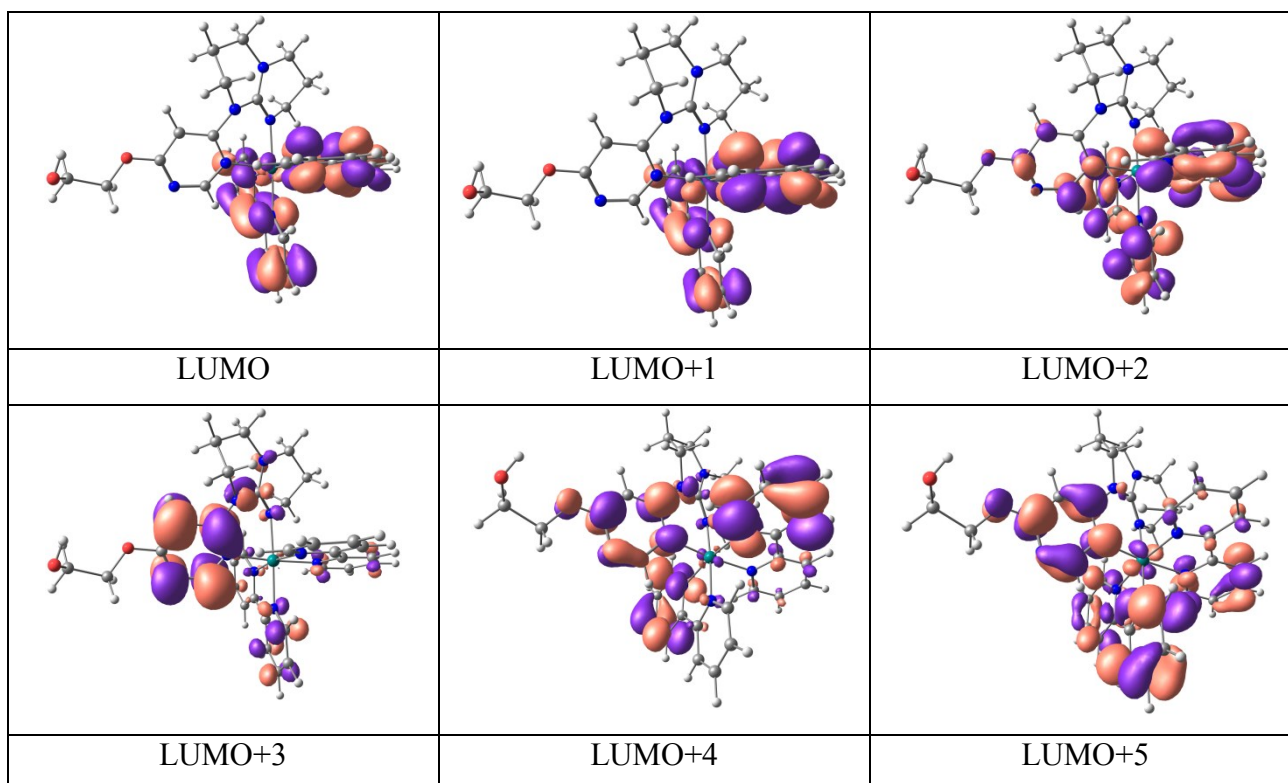


Figure 3.S12. Kohn-Sham Electron density sketches for $3-4^{2+}$ in ($S=0$) ground state

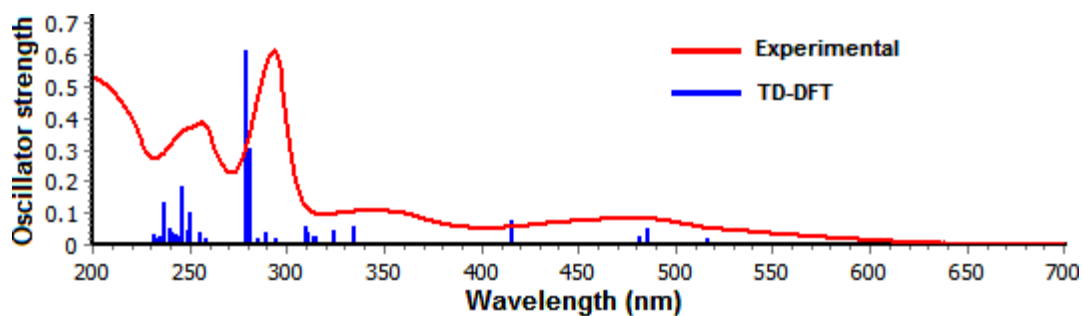


Figure 3.S13. Overlap of experimental electronic absorption spectra with oscillator strength from TD-DFT calculation of $3-4^{2+}$ in ($S=0$) ground state with first seventy calculated transitions.

Table III-S8. Selected Transitions from TD-DFT calculations of **3-4²⁺** in the Singlet Ground State (b3lyp/LanL2DZ(f)[Ru]6-31G**[C,H,N,O], CPCM (CH₃CN)).

energy (eV)	λ/nm	λ/nm ($\epsilon \times 10^3 \text{ M}^{-1} \text{ cm}^{-1}$) [expt.]	f	Major transition(s)	character
5.06	245	248 (15.2)	0.1819	H-4->L+2 (21%), H-4->L+3 (12%), H-3->L+5 (15%)	Bpy/Pyrimidine/hpp(n/ π) to Bpy/Pyrimidine/hpp(π^*)
4.98	249	256 (15.9)	0.1039	H-4->L+3 (19%), H-3->L+4 (28%)	Pyrimidine/hpp(n/ π) to Bpy/Pyrimidine/hpp(π^*)
4.45	278	293 (25.4)	0.6113	H-6->L (18%), H-5->L+1 (38%)	Bpy(π) to Bpy (π^*)
3.72	333	346 (4.5)	0.0589	H-1->L+4 (59%), H-1->L+5 (24%)	Ru(d π) to Bpy(π^*) + Ru(d π) to Pyrm(π^*)
2.56	484	483 (3.5)	0.0486	H-1->L+1 (44%), H->L+1 (39%)	Ru(d π) to Bpy(π^*) (major) + hpp(n/ π) to Bpy(π^*) (minor)
2.40	515	538 (1.6)	0.0208	H->L (80%), H->L+1 (15%)	Ru(d π) to Bpy(π^*) (major) + hpp(n/ π) to Bpy(π^*) (minor)

Table III-S9. Optimized Atomic coordinates obtained from DFT for **3-(1-meso)⁴⁺** in singlet ground state (b3lyp/LanL2DZ(f)[Ru]6-31G**[C,H,N]).

Center Number	Atomic Number	Atomic Type	Coordinates (Angstroms)		
			X	Y	Z
1	44	0	3.062815	-0.294443	-0.175592
2	44	0	-3.062849	-0.294442	0.175534
3	7	0	1.208079	0.821462	-0.008900
4	7	0	-1.208136	0.821497	0.008645
5	7	0	3.915198	0.286553	1.674917
6	7	0	4.971169	-1.179067	-0.265964
7	7	0	2.403549	-2.193621	0.485164
8	7	0	2.347910	-1.165087	-1.958012
9	7	0	2.408895	2.890531	0.204154
10	7	0	4.295256	3.791470	-0.882977
11	7	0	3.791440	1.494823	-1.094408
12	7	0	-3.915447	0.286585	-1.674857
13	7	0	-4.971121	-1.179297	0.266003
14	7	0	-2.347894	-1.165033	1.957975
15	7	0	-2.403431	-2.193518	-0.485242
16	7	0	-2.408898	2.890651	-0.204082
17	7	0	-4.295359	3.791421	0.883026
18	7	0	-3.791368	1.494829	1.094418
19	6	0	-0.000045	0.230738	-0.000177
20	1	0	-0.000060	-0.850880	-0.000258
21	6	0	-1.214876	2.187948	-0.037896
22	6	0	0.000000	2.877512	0.000010
23	1	0	0.000028	3.956027	0.000144
24	6	0	1.214853	2.187907	0.037793
25	6	0	3.294753	0.962661	2.663209
26	1	0	2.260813	1.225420	2.476820
27	6	0	3.916191	1.306938	3.857932
28	1	0	3.365954	1.848614	4.619502
29	6	0	5.249199	0.940254	4.048872
30	1	0	5.773406	1.195802	4.963949
31	6	0	5.893720	0.224360	3.045393
32	1	0	6.922106	-0.084026	3.186087
33	6	0	5.207945	-0.102456	1.868898
34	6	0	5.796716	-0.914541	0.786823

SI – Chapter 3

35	6	0	7.101228	-1.419237	0.825213	84	1	0	-1.343316	-3.147598	5.138701
36	1	0	7.751636	-1.199598	1.662595	85	6	0	-1.676704	-3.221754	3.010400
37	6	0	7.570397	-2.214262	-0.217057	86	1	0	-1.453934	-4.279145	2.936841
38	1	0	8.580946	-2.608860	-0.194372	87	6	0	-2.045859	-2.493964	1.873267
39	6	0	6.715671	-2.492458	-1.282632	88	6	0	-2.134566	-3.079080	0.518727
40	1	0	7.032394	-3.108925	-2.116703	89	6	0	-1.968368	-4.442867	0.252073
41	6	0	5.432299	-1.956565	-1.266847	90	1	0	-1.795082	-5.142792	1.060318
42	1	0	4.747411	-2.141291	-2.084912	91	6	0	-2.062679	-4.909034	-1.056716
43	6	0	2.465887	-2.650433	1.751523	92	1	0	-1.965837	-5.968833	-1.269850
44	1	0	2.681243	-1.909600	2.512205	93	6	0	-2.300692	-3.991754	-2.080752
45	6	0	2.301244	-3.991967	2.080583	94	1	0	-2.387919	-4.307980	-3.114562

Center	Atomic	Atomic	Coordinates (Angstroms)								
Number	Number	Type	X	Y	Z						

46	1	0	2.388586	-4.308247	3.114367	95	6	0	-2.465621	-2.650269	-1.751626
47	6	0	2.063326	-4.909237	1.056516	96	1	0	-2.681141	-1.909444	-2.512270
48	1	0	1.966690	-5.969062	1.269615	97	6	0	2.386939	4.159620	0.972940
49	6	0	1.968833	-4.443020	-0.252237	98	1	0	1.470437	4.195436	1.560429
50	1	0	1.795585	-5.142926	-1.060509	99	1	0	3.220941	4.124547	1.682765
51	6	0	2.134785	-3.079189	-0.518833	100	6	0	2.546920	5.336901	0.021538
52	6	0	2.045957	-2.494031	-1.873342	101	1	0	1.744878	5.332349	-0.725072
53	6	0	1.676777	-3.221789	-3.010492	102	1	0	2.494108	6.289765	0.555006
54	1	0	1.454063	-4.279193	-2.936953	103	6	0	3.911846	5.199441	-0.641849
55	6	0	1.607179	-2.586667	-4.247998	104	1	0	3.951269	5.735833	-1.596400
56	1	0	1.343263	-3.147551	-5.138771	105	1	0	4.683376	5.635197	0.003574
57	6	0	1.884373	-1.220925	-4.319003	106	6	0	5.648847	3.678949	-1.479299
58	1	0	1.839643	-0.683289	-5.259847	107	1	0	6.345320	4.222642	-0.831641
59	6	0	2.244645	-0.551185	-3.154288	108	1	0	5.628191	4.198906	-2.444063
60	1	0	2.480078	0.505705	-3.160144	109	6	0	6.072518	2.229273	-1.660373
61	6	0	-3.295231	0.963092	-2.663023	110	1	0	6.882158	2.176079	-2.393196
62	1	0	-2.261286	1.225893	-2.476707	111	1	0	6.448271	1.810339	-0.721133
63	6	0	-3.916900	1.307713	-3.857524	112	6	0	4.850756	1.439776	-2.120871
64	1	0	-3.366843	1.849705	-4.618998	113	1	0	5.094325	0.397233	-2.311442
65	6	0	-5.249895	0.940941	-4.048371	114	1	0	4.475497	1.865855	-3.062440
66	1	0	-5.774296	1.196777	-4.963257	115	6	0	3.539212	2.694252	-0.626249
67	6	0	-5.894168	0.224611	-3.045042	116	6	0	-2.387011	4.159830	-0.972728
68	1	0	-6.922550	-0.083810	-3.185667	117	1	0	-3.221045	4.124824	-1.682511
69	6	0	-5.208164	-0.102554	-1.868775	118	1	0	-1.470544	4.195775	-1.560260
70	6	0	-5.796691	-0.914983	-0.786825	119	6	0	-2.546976	5.336986	-0.021166
71	6	0	-7.100995	-1.420188	-0.825380	120	1	0	-1.744901	5.332339	0.725407
72	1	0	-7.751394	-1.200813	-1.662838	121	1	0	-2.494181	6.289910	-0.554523
73	6	0	-7.569978	-2.215415	0.216830	122	6	0	-3.911884	5.199428	0.642269
74	1	0	-8.580369	-2.610409	0.194010	123	1	0	-3.951220	5.735582	1.596965
75	6	0	-6.715285	-2.493276	1.282500	124	1	0	-4.683419	5.635415	-0.002999
76	1	0	-7.031867	-3.109844	2.116549	125	6	0	-5.649113	3.678764	1.478940
77	6	0	-5.432080	-1.956949	1.266831	126	1	0	-6.345503	4.222093	0.830880
78	1	0	-4.747226	-2.141465	2.084975	127	1	0	-5.628889	4.199021	2.443551
79	6	0	-2.244698	-0.551184	3.154275	128	6	0	-6.072549	2.229034	1.660294
80	1	0	-2.480149	0.505702	3.160171	129	1	0	-6.448277	1.809888	0.721143
81	6	0	-1.884452	-1.220958	4.318986	130	1	0	-6.882157	2.175818	2.393155
82	1	0	-1.839776	-0.683351	5.259849	131	6	0	-4.850670	1.439788	2.120907
83	6	0	-1.607193	-2.586681	4.247938	132	1	0	-4.475448	1.866100	3.062380
						133	1	0	-5.094095	0.397242	2.311662
						134	6	0	-3.539226	2.694274	0.626257

Table III-S10. Optimized Atomic coordinates obtained from DFT for $3-2^{2+}$ in singlet ground state (b3lyp/LanL2DZ(f)[Ru]6-31G**[C,H,N,O]).

Center Number	Atomic Number	Atomic Type	Coordinates (Angstroms)		
			X	Y	Z
1	44	0	0.733662	-0.117171	0.010315
2	8	0	-5.288412	-1.226899	-0.873688
3	7	0	0.989790	-2.156665	0.468786
4	7	0	0.361377	-0.162320	2.088702
5	7	0	2.820372	0.089615	0.155925
6	7	0	1.331538	-0.239909	-2.008362
7	7	0	-1.359282	-0.373592	-0.334468
8	7	0	-3.077730	-1.886520	-1.042343
9	7	0	-1.887763	1.781727	0.553154
10	7	0	-1.020024	3.891014	-0.010482
11	7	0	0.305227	1.953773	-0.314201
12	6	0	1.392720	-3.113880	-0.391797
13	1	0	1.639421	-2.779801	-1.392608
14	6	0	1.481240	-4.456688	-0.044051
15	1	0	1.809277	-5.183112	-0.779156
16	6	0	1.134387	-4.836976	1.252213
17	1	0	1.180267	-5.876504	1.559022
18	6	0	0.732885	-3.855103	2.152314
19	1	0	0.469717	-4.131637	3.165630
20	6	0	0.676450	-2.517163	1.745860
21	6	0	0.334002	-1.403797	2.651516
22	6	0	0.058374	-1.572569	4.013610
23	1	0	0.028541	-2.563732	4.448580
24	6	0	-0.162727	-0.459890	4.818263
25	1	0	-0.373159	-0.581367	5.875619
26	6	0	-0.089863	0.809123	4.243070
27	1	0	-0.230437	1.706781	4.834987
28	6	0	0.169656	0.910610	2.881370
29	1	0	0.237181	1.872535	2.389308
30	6	0	0.512507	-0.313395	-3.076089
31	1	0	-0.548603	-0.286721	-2.862824
32	6	0	0.977658	-0.417366	-4.382267
33	1	0	0.270629	-0.476941	-5.202170
34	6	0	2.354221	-0.440228	-4.603974
35	1	0	2.755880	-0.522633	-5.608400
36	6	0	3.209482	-0.343990	-3.510221
37	1	0	4.281236	-0.342489	-3.665251
38	6	0	2.680519	-0.238777	-2.219138
39	6	0	3.511101	-0.085106	-1.007731
40	6	0	4.910107	-0.084527	-1.023114
41	1	0	5.448684	-0.234202	-1.950610
42	6	0	5.615371	0.108376	0.160903
43	1	0	6.700234	0.109849	0.158554
44	6	0	4.901384	0.300216	1.343210
45	1	0	5.405594	0.458976	2.289905
46	6	0	3.512040	0.279873	1.296223
47	1	0	2.920737	0.415821	2.193205
48	6	0	-2.300840	0.562168	-0.009979
49	6	0	-3.650257	0.285706	-0.198864
50	1	0	-4.433656	1.000872	0.003295
51	6	0	-4.005807	-0.974916	-0.710009
52	6	0	-1.820792	-1.533406	-0.846940
53	1	0	-1.064223	-2.260438	-1.118941
54	6	0	-2.866528	2.546042	1.354452
55	1	0	-2.332442	2.975023	2.209427
56	1	0	-3.605196	1.853846	1.754488
57	6	0	-3.468404	3.649384	0.494773
58	1	0	-4.226373	4.217100	1.041344
59	1	0	-3.955780	3.213581	-0.382733
60	6	0	-2.326529	4.576607	0.084092
61	1	0	-2.534130	5.068582	-0.873823
62	1	0	-2.206219	5.369924	0.831206
63	6	0	0.082405	4.835778	-0.274565
64	1	0	0.028818	5.633634	0.475046
65	1	0	-0.092701	5.300439	-1.253321

SI – Chapter 3

66	6	0	1.434305	4.142568	-0.248846
67	1	0	2.183644	4.782553	-0.722909
68	1	0	1.760742	3.962672	0.781564
69	6	0	1.301473	2.811216	-0.979608
70	1	0	1.008697	2.980613	-2.025260
71	1	0	2.252443	2.283861	-0.990596
72	6	0	-0.816590	2.541071	0.033107
73	6	0	-5.702454	-2.516273	-1.434098
74	1	0	-5.327335	-3.306839	-0.778843
75	1	0	-5.229256	-2.628716	-2.413220
76	6	0	-7.213677	-2.498876	-1.517462
77	1	0	-7.662444	-2.373619	-0.528747
78	1	0	-7.561034	-3.449038	-1.933133
79	1	0	-7.564019	-1.692894	-2.167324

Table III-S11. Optimized Atomic coordinates obtained from DFT for $3\text{-}3^{2+}$ in singlet ground state (b3lyp/LanL2DZ(f)[Ru]6-31G**[C,H,N,O]).

Center Number	Atomic Number	Atomic Type	Coordinates (Angstroms)		
			X	Y	Z
1	44	0	-1.108242	-0.157866	-0.022975
2	8	0	5.050487	-0.700974	0.042926
3	7	0	1.024975	-0.219568	-0.044933
4	7	0	2.958915	-1.594508	-0.377584
5	7	0	-1.382810	-0.477810	-2.089406
6	7	0	-3.203983	-0.162249	-0.193769
7	7	0	-1.242735	-2.177792	0.560473
8	7	0	-1.050144	-0.023627	2.084739
9	7	0	1.215435	2.034330	0.726553
10	7	0	0.246998	3.999094	-0.123260
11	7	0	-0.829168	1.918042	-0.455835
12	6	0	1.660354	-1.358795	-0.389833
13	1	0	1.019276	-2.174995	-0.703237
14	6	0	3.741219	-0.571609	0.004171
15	6	0	3.199905	0.678289	0.355662
16	1	0	3.876814	1.481506	0.606032
17	6	0	1.818110	0.827750	0.330302
18	6	0	-0.409537	-0.528195	-3.019908
19	1	0	0.598277	-0.365439	-2.659325
20	6	0	-0.660520	-0.771304	-4.365682
21	1	0	0.163467	-0.804685	-5.069646
22	6	0	-1.978790	-0.965697	-4.777049
23	1	0	-2.214807	-1.160813	-5.817826
24	6	0	-2.994046	-0.893311	-3.827672
25	1	0	-4.024885	-1.023434	-4.132907
26	6	0	-2.678256	-0.642331	-2.487905
27	6	0	-3.691845	-0.497166	-1.423355
28	6	0	-5.065966	-0.651837	-1.635764
29	1	0	-5.442605	-0.928912	-2.612577
30	6	0	-5.955891	-0.448783	-0.585295
31	1	0	-7.023051	-0.566876	-0.740748
32	6	0	-5.449645	-0.089433	0.663292
33	1	0	-6.103371	0.085700	1.510408
34	6	0	-4.073581	0.038808	0.815037
35	1	0	-3.638157	0.308233	1.769241
36	6	0	-1.418268	-3.227901	-0.267452
37	1	0	-1.538043	-2.989638	-1.317490
38	6	0	-1.434685	-4.546026	0.173169
39	1	0	-1.576903	-5.350666	-0.539564
40	6	0	-1.258537	-4.799493	1.533286
41	1	0	-1.255329	-5.814922	1.915057
42	6	0	-1.092880	-3.722450	2.398115
43	1	0	-0.964916	-3.901037	3.458420
44	6	0	-1.097735	-2.416565	1.894945
45	6	0	-1.000580	-1.215025	2.745882
46	6	0	-0.924161	-1.262918	4.142907
47	1	0	-0.874905	-2.214488	4.657257
48	6	0	-0.927411	-0.082126	4.877734

SI - Chapter 3

49	1	0	-0.873047	-0.110295	5.960907
50	6	0	-1.018837	1.131446	4.195651
51	1	0	-1.048019	2.076947	4.725862
52	6	0	-1.074002	1.114081	2.806961
53	1	0	-1.145974	2.030059	2.234800
54	6	0	1.989996	2.948183	1.592163
55	1	0	2.723755	2.364742	2.145295
56	1	0	1.298898	3.374365	2.328049
57	6	0	2.604883	4.048727	0.737790
58	1	0	3.250863	3.607574	-0.027415
59	1	0	3.220713	4.726255	1.335500
60	6	0	1.452609	4.823963	0.103383
61	1	0	1.750647	5.278275	-0.849269
62	1	0	1.148265	5.642536	0.766272
63	6	0	-0.889157	4.803617	-0.612886
64	1	0	-0.614390	5.224272	-1.588625
65	1	0	-1.025842	5.646578	0.074234
66	6	0	-2.157065	3.974290	-0.729775
67	1	0	-2.882923	4.500392	-1.356001
68	1	0	-2.618050	3.825154	0.253051
69	6	0	-1.787479	2.620704	-1.326588
70	1	0	-2.670469	1.995737	-1.436822
71	1	0	-1.353555	2.753636	-2.327539
72	6	0	0.167715	2.641174	-0.000100
73	6	0	5.663311	-1.977726	-0.341594
74	1	0	5.296271	-2.744737	0.345727
75	1	0	5.323230	-2.225620	-1.351360
76	6	0	7.169204	-1.804079	-0.265588
77	1	0	7.608958	-2.796515	-0.428846
78	1	0	7.444494	-1.510132	0.754857
79	6	0	7.743688	-0.807413	-1.281757
80	1	0	7.280388	0.174707	-1.126687
81	1	0	7.462894	-1.126328	-2.294844
82	6	0	9.266981	-0.680897	-1.185505
83	1	0	9.574976	-0.333349	-0.193420
84	1	0	9.650636	0.031741	-1.921157
85	1	0	9.758142	-1.642737	-1.367494

Table III-S12. Optimized Atomic coordinates obtained from DFT for $3\text{-}4^{2+}$ in singlet ground state (b3lyp/LanL2DZ(f)[Ru]6-31G**[C,H,N,O]).

Center Number	Atomic Number	Atomic Type	Coordinates (Angstroms)		
			X	Y	Z
1	44	0	0.797102	-0.293863	-0.021913
2	8	0	-5.395153	-0.343404	0.101943
3	8	0	-7.842996	-0.616654	1.603912
4	1	0	-7.605172	0.310298	1.479784
5	7	0	-1.337007	-0.207269	0.066891
6	7	0	-3.373793	-1.459714	0.205003
7	7	0	1.205926	0.895715	1.667011
8	7	0	2.894848	-0.189865	-0.052006
9	7	0	1.007168	-2.146964	0.966344
10	7	0	0.579598	-1.674098	-1.602837
11	7	0	-1.361293	2.180883	-0.090587
12	7	0	-0.187220	3.682607	-1.464407
13	7	0	0.578581	1.462542	-1.226731
14	6	0	-2.059252	-1.341930	0.171761
15	1	0	-1.487425	-2.257874	0.254642
16	6	0	-4.075751	-0.322976	0.093024
17	6	0	-3.439611	0.922810	-0.052354
18	1	0	-4.043494	1.809302	-0.182487
19	6	0	-2.050168	0.952980	-0.048118
20	6	0	0.298970	1.337374	2.561770
21	1	0	-0.726328	1.044672	2.375451
22	6	0	0.637111	2.111185	3.665898
23	1	0	-0.134980	2.432164	4.356381
24	6	0	1.975811	2.453495	3.859897
25	1	0	2.279180	3.060769	4.706195

SI – Chapter 3

26	6	0	2.922455	1.986288	2.954168
27	1	0	3.968581	2.224718	3.100381
28	6	0	2.520275	1.199018	1.868659
29	6	0	3.462163	0.597787	0.905504
30	6	0	4.849212	0.773054	0.966235
31	1	0	5.289190	1.406677	1.726281
32	6	0	5.671019	0.124997	0.049370
33	1	0	6.747341	0.254508	0.090477
34	6	0	5.084404	-0.694970	-0.914122
35	1	0	5.682259	-1.226850	-1.645798
36	6	0	3.700086	-0.821968	-0.929415
37	1	0	3.204462	-1.440321	-1.667997
38	6	0	1.175734	-2.317206	2.292098
39	1	0	1.107743	-1.422025	2.898020
40	6	0	1.426173	-3.557128	2.869151
41	1	0	1.551136	-3.635646	3.943317
42	6	0	1.514900	-4.676192	2.042049
43	1	0	1.717098	-5.659001	2.454510
44	6	0	1.333209	-4.512768	0.671992
45	1	0	1.393100	-5.372344	0.015926
46	6	0	1.072437	-3.240385	0.151969
47	6	0	0.801696	-2.981082	-1.276842
48	6	0	0.721887	-3.988391	-2.244880
49	1	0	0.902314	-5.022028	-1.977069
50	6	0	0.394003	-3.662550	-3.557620
51	1	0	0.330471	-4.437276	-4.314452
52	6	0	0.133080	-2.329506	-3.873880
53	1	0	-0.145308	-2.030071	-4.878120
54	6	0	0.233387	-1.372866	-2.869992
55	1	0	0.030874	-0.327455	-3.062840
56	6	0	-2.039009	3.385050	0.436783
57	1	0	-1.315107	3.932169	1.051783
58	1	0	-2.846538	3.068234	1.094214
59	6	0	-2.510789	4.248942	-0.724894
60	1	0	-3.059075	5.127798	-0.374866
61	1	0	-3.185822	3.674086	-1.366971
62	6	0	-1.266764	4.690803	-1.488432
63	1	0	-1.498961	4.928396	-2.533466
64	1	0	-0.858582	5.602141	-1.034928
65	6	0	1.051929	4.176435	-2.099224
66	1	0	0.818870	4.422890	-3.142515
67	1	0	1.337156	5.111463	-1.602742
68	6	0	2.172383	3.148954	-2.034594
69	1	0	2.655616	3.157620	-1.051911
70	1	0	2.933754	3.390093	-2.781716
71	6	0	1.555240	1.775964	-2.283236
72	1	0	2.311446	0.993671	-2.297934
73	1	0	1.062414	1.772583	-3.266706
74	6	0	-0.281676	2.419748	-0.959678
75	6	0	-6.088254	-1.624731	0.255786
76	1	0	-5.701600	-2.123021	1.146904
77	1	0	-5.882129	-2.240509	-0.624882
78	6	0	-7.565923	-1.309111	0.404912
79	1	0	-7.925652	-0.771194	-0.483927
80	1	0	-8.103978	-2.261817	0.451169

3.S2. References

- (1) A. K. Pal, P. D. Ducharme, G. S. Hanan, *Chem. Commun.*, 2014, **50**, 3303.

SI – Chapter 4 : Supplementary Informations

Supplementary Information

Near Infra-Red emitting Ru(II) complexes: structural,
electrochemical and photophysical investigations

*Amlan K. Pal,^a Nelsi Zaccheroni,^{*b} Sebastiano Campagna,^{*c} and Garry S. Hanan^{*a}*

^aDépartement de Chimie, Université de Montréal, Montréal, Québec, H3T 1J4, Canada

^bDipartimento di Chimica «G. Ciamician», Università di Bologna, 40126 Bologna, Italia

^cDipartimento di Scienze Chimiche, Università di Messina, 98166 Messina, Italia

<http://www.bib.umontreal.ca/theses/produire-PDF.htm>

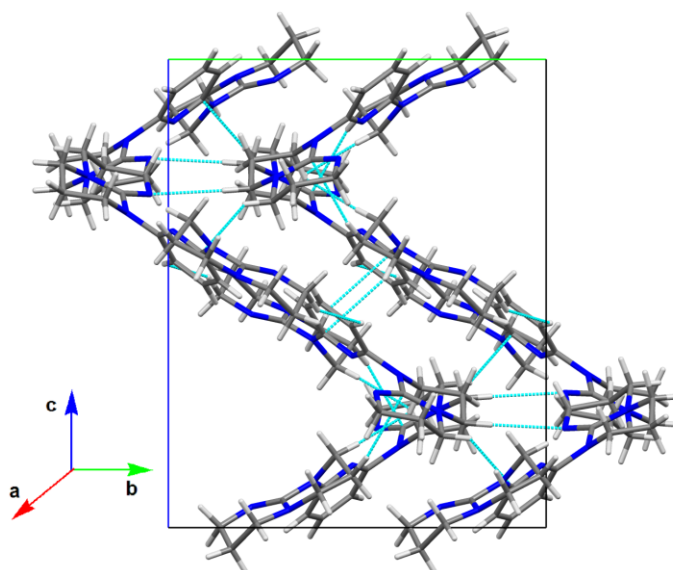


Figure 4.S1. Packing diagram of ligand 4-L1 along crystallographic *a*-axis.

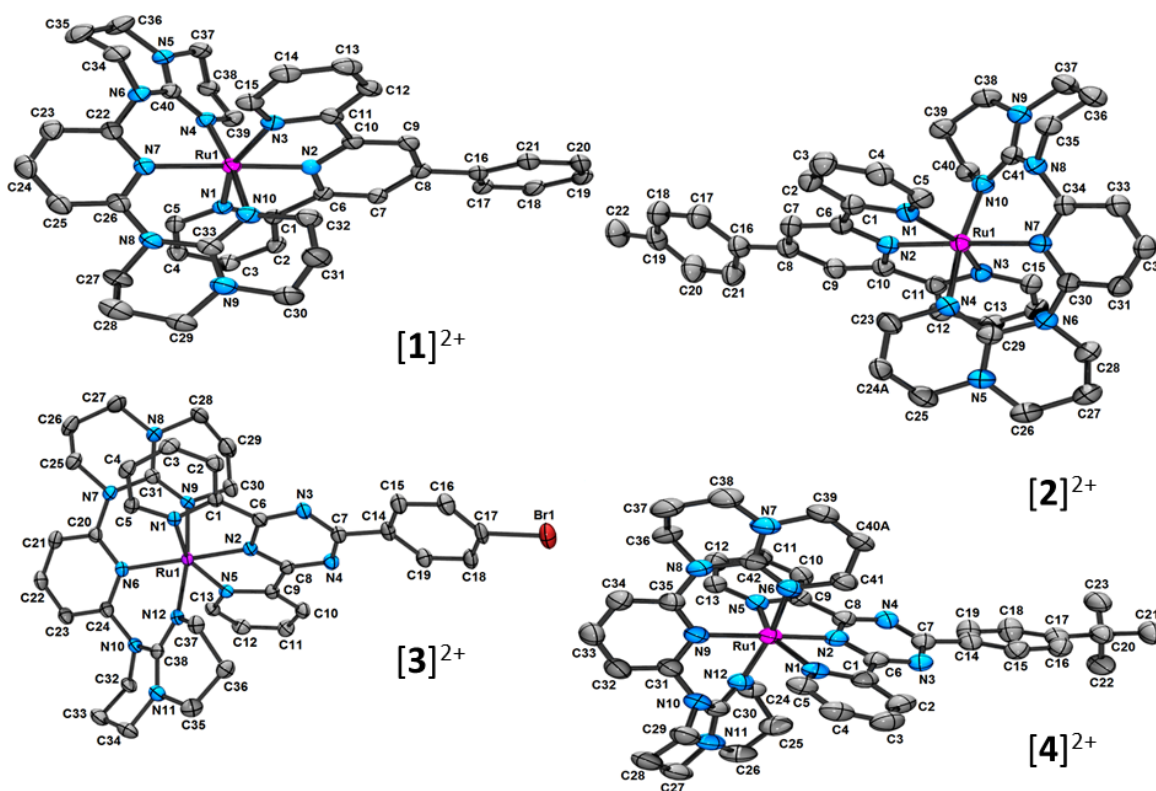


Figure 4.S2. Perspective views of complexes 4-1 to 4-4, as cations only, with complete labeling. Ellipsoids correspond to a 50% probability level. Hydrogen atoms, anions, solvent molecules and disordered components of 4-2 and 4-4 are omitted for clarity.

Table IV-S1. Comparison of bond distances and angles in **4-1** to **4-4** from X-ray and DFT studies

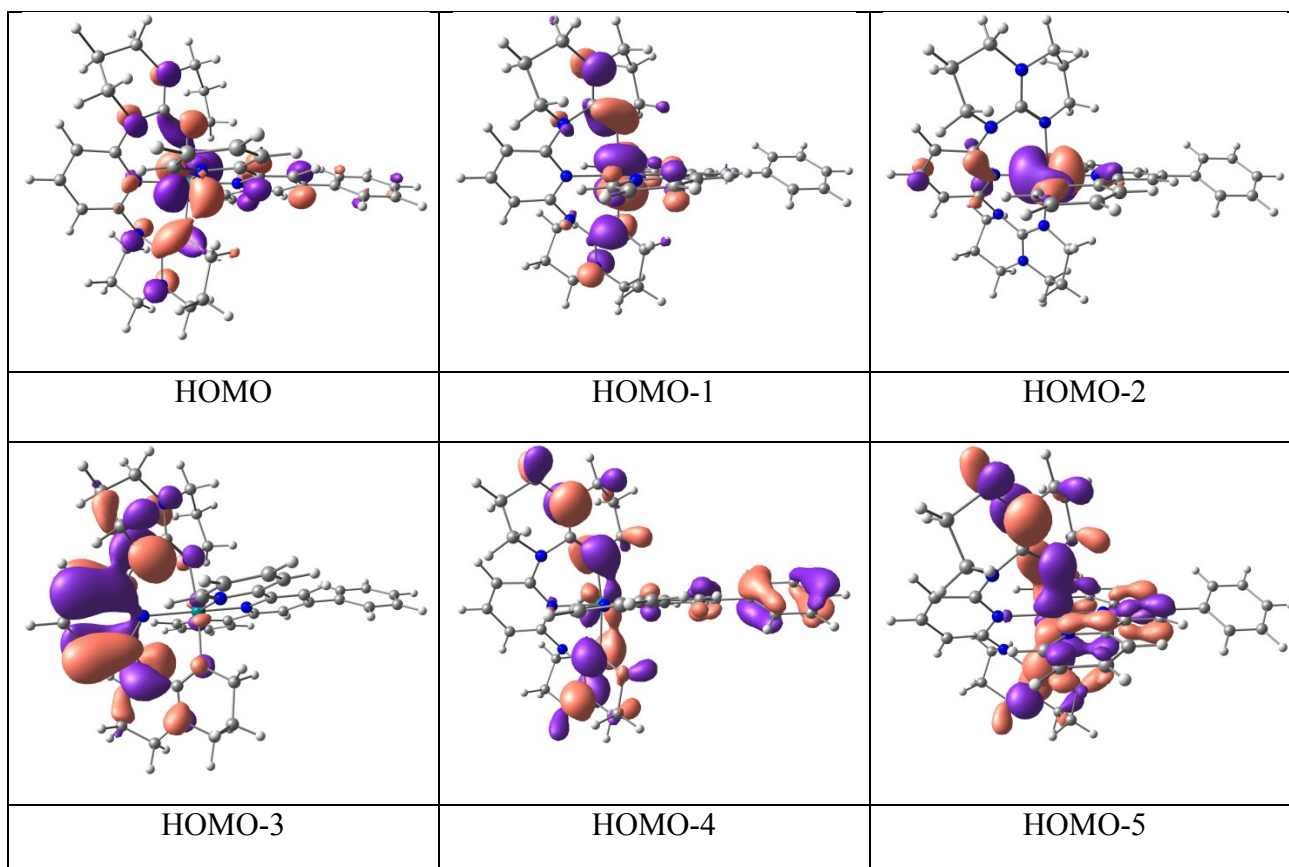
Compound	Bond Length			Angle		
		Obs. (x-ray)	Calc. (DFT)		Obs. (x-ray)	Calc. (DFT)
4-1	N1-Ru1	2.0646 (0.0024)	2.12887	N1-Ru1-N3	159.28 (0.10)	157.256
	N2-Ru1	1.9462 (0.0024)	1.98758	N4-Ru1-N10	173.83 (0.10)	172.513
	N3-Ru1	2.0761 (0.0025)	2.12874			
	N4-Ru1	2.0711 (0.0025)	2.13996			
	N7-Ru1	2.0720 (0.0025)	2.11279			
	N10-Ru1	2.0919 (0.0026)	2.13997			
	N4-C40	1.3050 (0.0039)	1.31063			
	N5-C40	1.3498 (0.0043)	1.36487			
	N6-C40	1.4072 (0.0040)	1.40913			
	N10-C33	1.3102 (0.0043)	1.31062			
	N9-C33	1.3430 (0.0045)	1.36485			
	N8-C33	1.3998 (0.0043)	1.40917			
	4-2	N1-Ru1	2.0859 (0.0019)	2.12784	N1-Ru1-N3	158.89 (0.08)
N2-Ru1		1.9307 (0.0018)	1.98638	N4-Ru1-N10	172.68 (0.07)	171.592
N3-Ru1		2.0722 (0.0019)	2.12795			
N4-Ru1		2.0947 (0.0019)	2.13422			
N7-Ru1		2.0707 (0.0018)	2.11501			
N10-Ru1		2.0639 (0.0018)	2.13415			
N4-C29		1.3080 (0.0030)	1.31024			
N5-C29		1.3502 (0.0030)	1.36492			
N6-C29		1.3842 (0.0030)	1.40789			
N10-C41		1.3042 (0.0029)	1.31024			
N9-C41		1.3434 (0.0029)	1.36494			
N8-C41	1.4044 (0.0028)	1.40794				
4-3	N1-Ru1	2.0789 (0.0029)	2.10617	N1-Ru1-N5	157.19 (0.15)	157.189

SI – Chapter 3

	N2-Ru1	1.9247 (0.0028)	1.91497	N9-Ru1-N12	171.51 (0.13)	171.637
	N5-Ru1	2.0876 (0.0027)	2.07686			
	N6-Ru1	2.0688 (0.0028)	2.06985			
	N9-Ru1	2.0874 (0.0029)	2.09241			
	N12-Ru1	2.0628 (0.0029)	2.06290			
	N9-C31	1.3082 (0.0058)	1.31015			
	N8-C31	1.3563 (0.0060)	1.34625			
	N7-C31	1.3778 (0.0059)	1.38473			
	N12-C38	1.3040 (0.0054)	1.30261			
	N11-C38	1.3433 (0.0055)	1.34104			
	N10-C38	1.4041 (0.0052)	1.40823			
4-4	N1-Ru1	2.0897 (0.0020)	2.15308	N1-Ru1-N5	156.29 (0.09)	154.942
	N2-Ru1	1.9297 (0.0022)	1.97508	N6-Ru1-N12	171.02 (0.08)	171.488
	N5-Ru1	2.1074 (0.0020)	2.15333			
	N6-Ru1	2.0784 (0.0020)	2.13339			
	N9-Ru1	2.0857 (0.0021)	2.11261			
	N12-Ru1	2.0888 (0.0020)	2.13352			
	N12-C30	1.3075 (0.0032)	1.31100			
	N11-C30	1.3396 (0.0031)	1.36403			
	N10-C30	1.3945 (0.0032)	1.40833			
	N6-C42	1.2966 (0.0032)	1.31096			
	N7-C42	1.3481 (0.0032)	1.36409			
	N8-C42	1.3988 (0.0032)	1.40847			

DFT Calculations:**Table IV-S2.** MO composition of $4-1^{2+}$ in singlet ($S=0$) ground state (b3lyp/LanL2DZ(f)[Ru]6-31G**[C,H,N]).

MO	Energy (eV)	Approximate Composition (%)		
		Ru	Ph-tpy	hpp
LUMO+5	-0.99	1	1	98
LUMO+4	-1.25	3	95	2
LUMO+3	-1.36	1	99	0
LUMO+2	-1.43	4	2	94
LUMO+1	-2.27	2	98	0
LUMO	-2.46	9	88	2
HOMO	-5.37	57	18	25
HOMO-1	-5.37	61	10	29
HOMO-2	-5.86	84	10	6
HOMO-3	-6.56	2	1	97
HOMO-4	-6.69	5	26	70
HOMO-5	-6.85	13	22	66



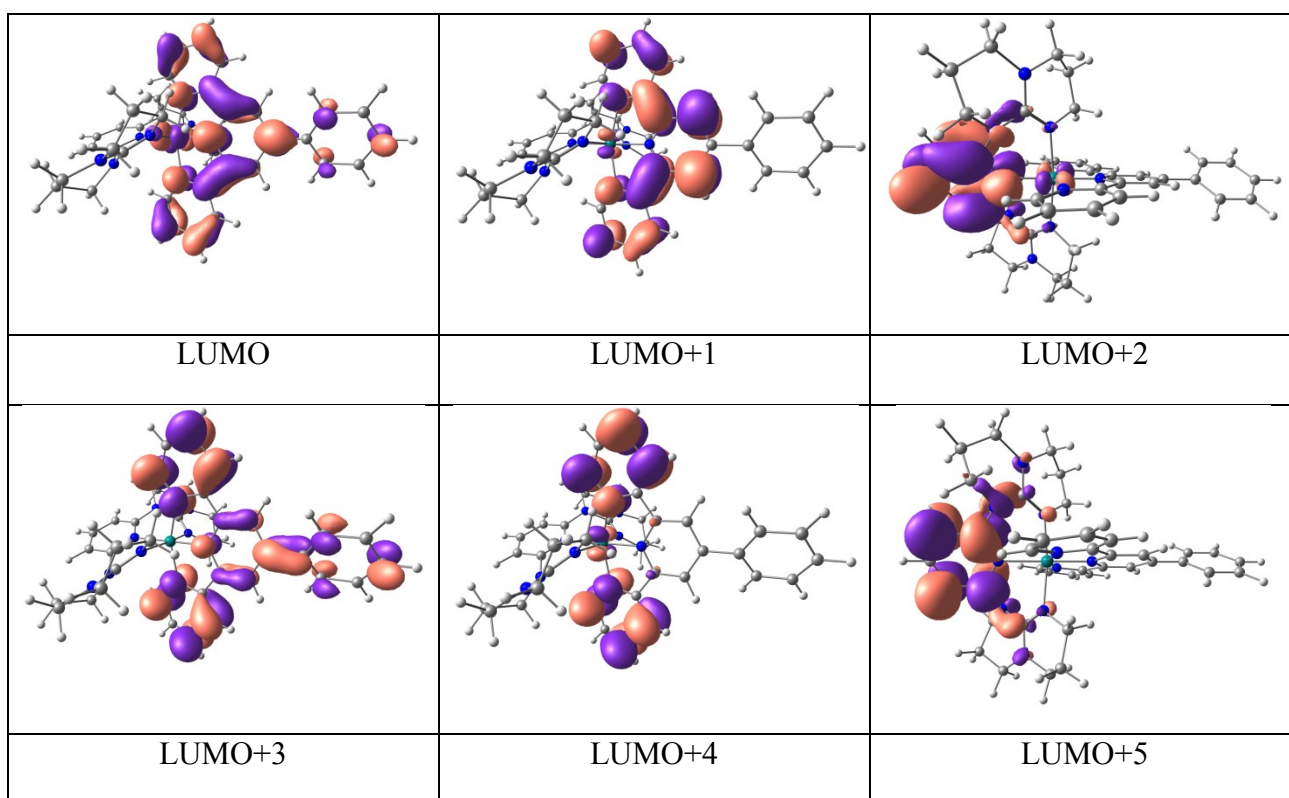


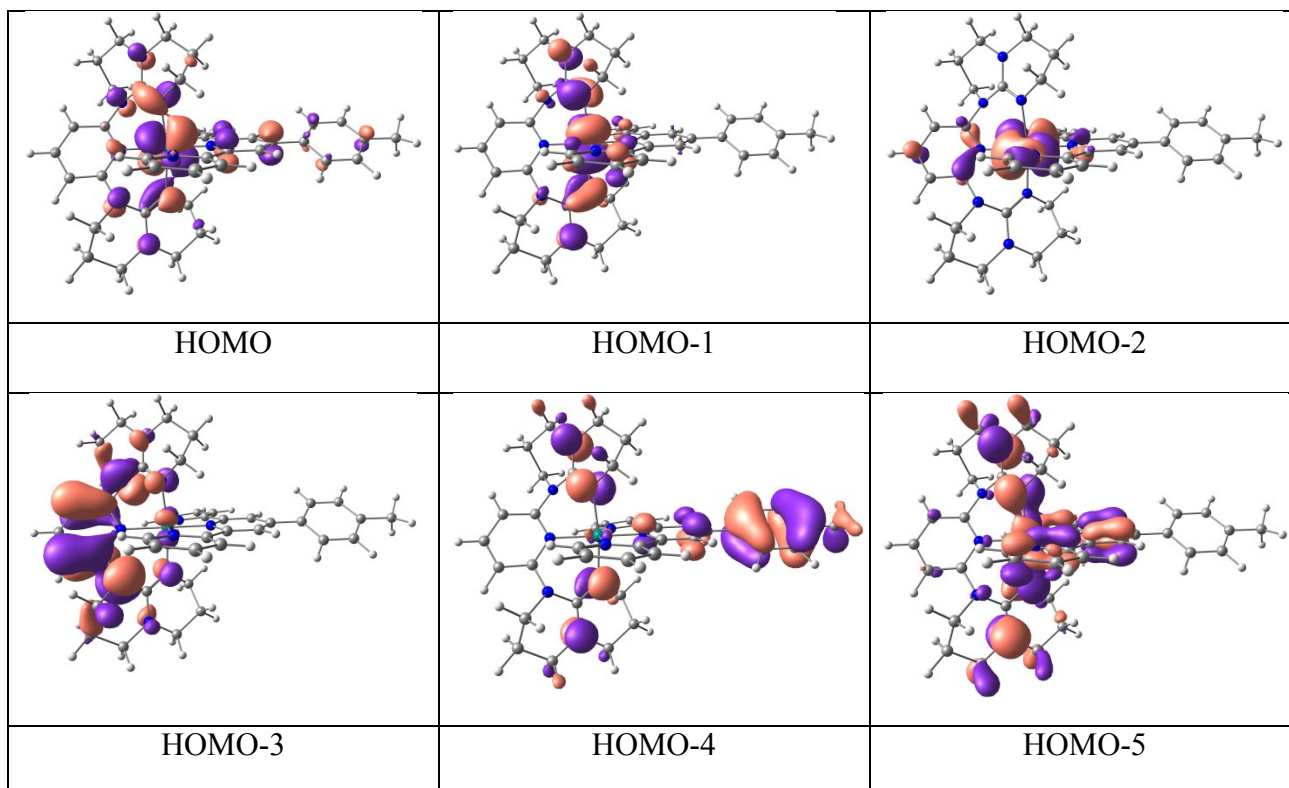
Figure 4.S3. Kohn-Sham Electron density sketches for different MOs for 4-I^{2+} in ($S=0$) ground state.

Table IV-S3. Selected transitions from TD-DFT calculations of **4-1²⁺** in the singlet ground state (b3lyp/LanL2DZ(f)[Ru]6-31G**[C,H,N], CPCM (CH₃CN)).

state	energy (eV)	λ/n m	λ/nm ($\epsilon \times 10^3 \text{ M}^{-1} \text{ cm}^{-1}$) [expt.]	f	Major transition(s)	Character
58	5.03	246	244 (22.6)	0.2525	H-3->L+5 (68%)	Hpp (n/ π) to Hpp (n/ π^*)
41	4.44	279	289 (26.9)	0.3477	H-7->L+1 (61%), H-8->L+1 (13%)	Ph-tpy(π) to Ph-tpy(π^*)
29	4.02	308	317 (13.3)	0.2449	H-7->L (51%)	Ph-tpy(π) to Ph-tpy(π^*)
11	3.34	371	379 (6.1)	0.0632	H-1->L+3 (92%)	Ru(d π) to Ph-tpy(π^*) (major) + hpp(n/ π) to Ph-tpy(π^*) (minor)
2	2.20	562	541 (5.0)	0.0444	H->L (64%), H-1->L+1 (20%), H-2->L (10%)	Ru(d π) to Ph-tpy(π^*) + (major) + hpp(n/ π) to Ph-tpy(π^*) (minor)
1	2.01	616	622 (3.3)	0.0117	H-1->L (94%)	Ru(d π) to Ph-tpy(π^*) + (major) + hpp(n/ π) to Ph-tpy(π^*) (minor)

Table IV-S4. MO composition of $4\text{-}2^{2+}$ in singlet ($S=0$) ground state (b3lyp/LanL2DZ(f)[Ru]6-31G**[C,H,N]).

MO	Energy (eV)	Approximate Composition (%)		
		Ru	Tolyl-tpy	hpp
LUMO+5	-1.01	1	1	99
LUMO+4	-1.22	3	95	1
LUMO+3	-1.35	1	98	1
LUMO+2	-1.44	3	2	95
LUMO+1	-2.26	2	97	1
LUMO	-2.45	9	88	3
HOMO	-5.34	57	19	24
HOMO-1	-5.35	62	10	28
HOMO-2	-5.85	83	11	6
HOMO-3	-6.58	4	3	93
HOMO-4	-6.61	1	63	36
HOMO-5	-6.88	9	29	63



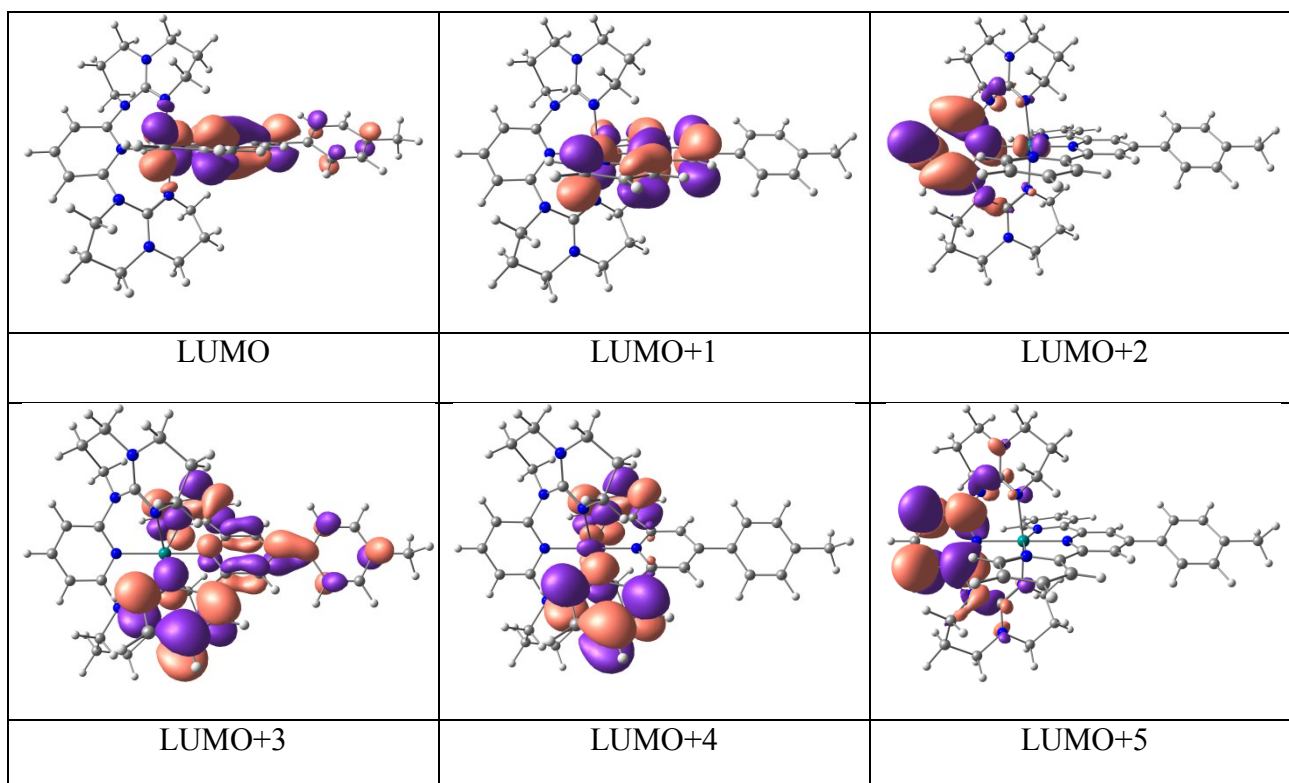


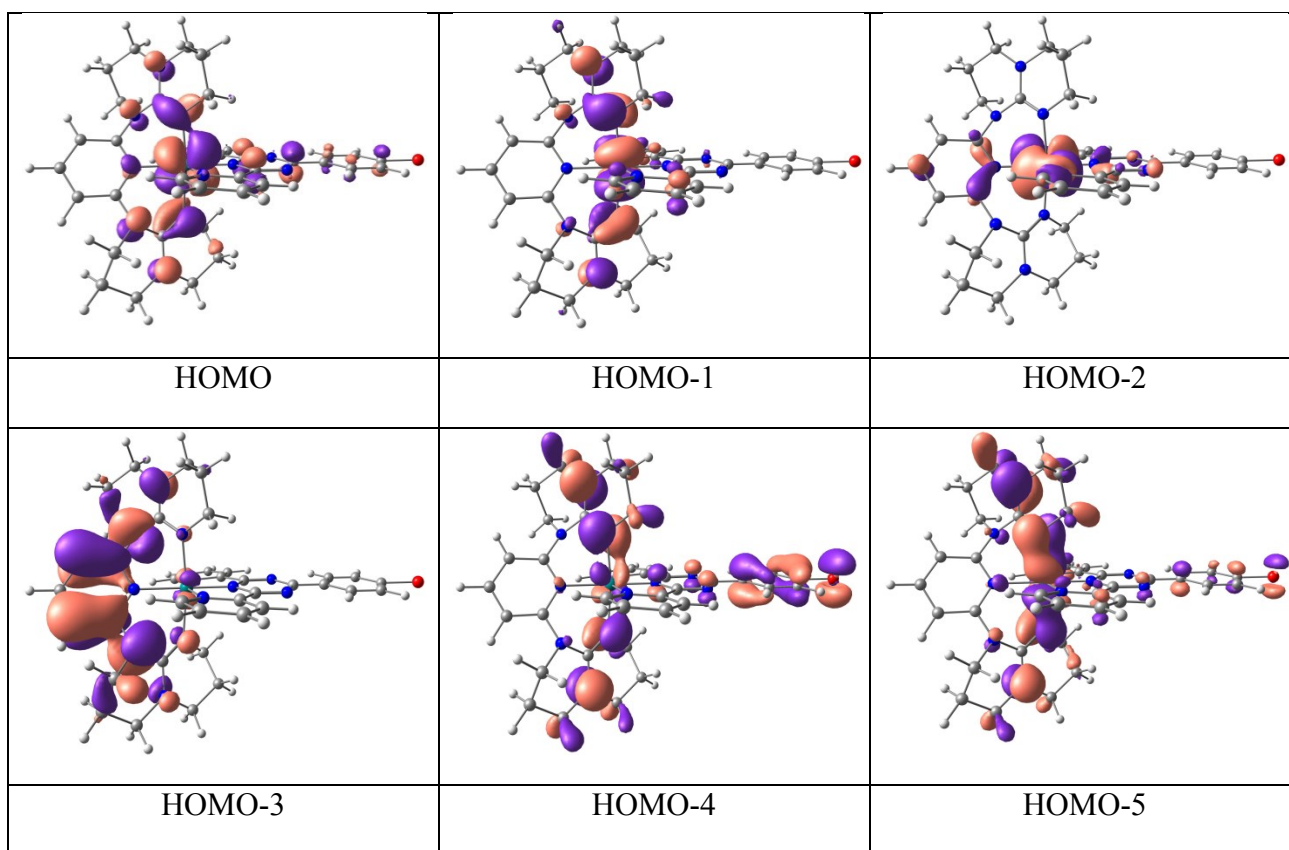
Figure 4.S4. Kohn-Sham electron density sketches for different MOs for $4\text{-}2^{2+}$ in ($S=0$) ground state.

Table IV-S5. Selected transitions from TD-DFT calculations of **4-2²⁺** in the singlet ground state (b3lyp/LanL2DZ(f)[Ru]6-31G**[C,H,N], CPCM (CH₃CN)).

state	energy (eV)	λ/nm	λ/nm ($\epsilon \times 10^3 \text{ M}^{-1} \text{ cm}^{-1}$) [expt.]	f	Major transition(s)	Character
59	5.04	246	247 (39.7)	0.2134	H-10->L+1 (46%), H-5->L+3 (24%)	Tolyl-tpy(π) to Tolyl-tpy(π^*) (major) + hpp(n/ π) to Tolyl-tpy(π^*) (minor)
41	4.44	279	288 (45.1)	0.3339	H-8->L+1 (41%), H-7->L+1 (19%), H-9->L (16%)	Tolyl-tpy(π) to Tolyl-tpy(π^*) (major) + hpp(n/ π) to Tolyl-tpy(π^*) (minor)
32	4.06	305	313 (27.9)	0.1566	H-7->L (34%), H-6->L+1 (33%), H-8->L (20%)	Tolyl-tpy(π) to Tolyl-tpy(π^*) (major) + hpp(n/ π) to Tolyl-tpy(π^*) (minor)
10	3.31	375	383 (11.3)	0.0631	H->L+3 (93%)	Ru(d π) to Tolyl-tpy(π^*) (major) + hpp(n/ π) to Tolyl-tpy(π^*) (minor)
2	2.19	565	538 (9.4)	0.0485	H->L (63%), H-1->L+1 (22%)	Ru(d π) to Tolyl-tpy(π^*) (major) + hpp(n/ π) to Tolyl-tpy(π^*) (minor)
1	2.00	620	620 (6.2)	0.0119	H-1->L (94%)	Ru(d π) to Tolyl-tpy(π^*) (major) + hpp(n/ π) to Tolyl-tpy(π^*) (minor)

Table IV-S6. MO composition of $4\text{-}3^{2+}$ in singlet ($S=0$) ground state (b3lyp/LanL2DZ(f)[Ru]6-31G**[C,H,N,Br]).

MO	Energy (eV)	Approximate Composition (%)		
		Ru	Br-Ph-trz	hpp
LUMO+5	-1.31	1	96	3
LUMO+4	-1.44	3	96	1
LUMO+3	-1.52	1	3	94
LUMO+2	-1.80	1	99	0
LUMO+1	-2.90	10	87	3
LUMO	-2.99	2	97	1
HOMO	-5.58	53	19	28
HOMO-1	-5.62	57	9	34
HOMO-2	-6.09	81	13	6
HOMO-3	-6.66	2	1	97
HOMO-4	-6.81	5	33	62
HOMO-5	-7.05	20	17	63



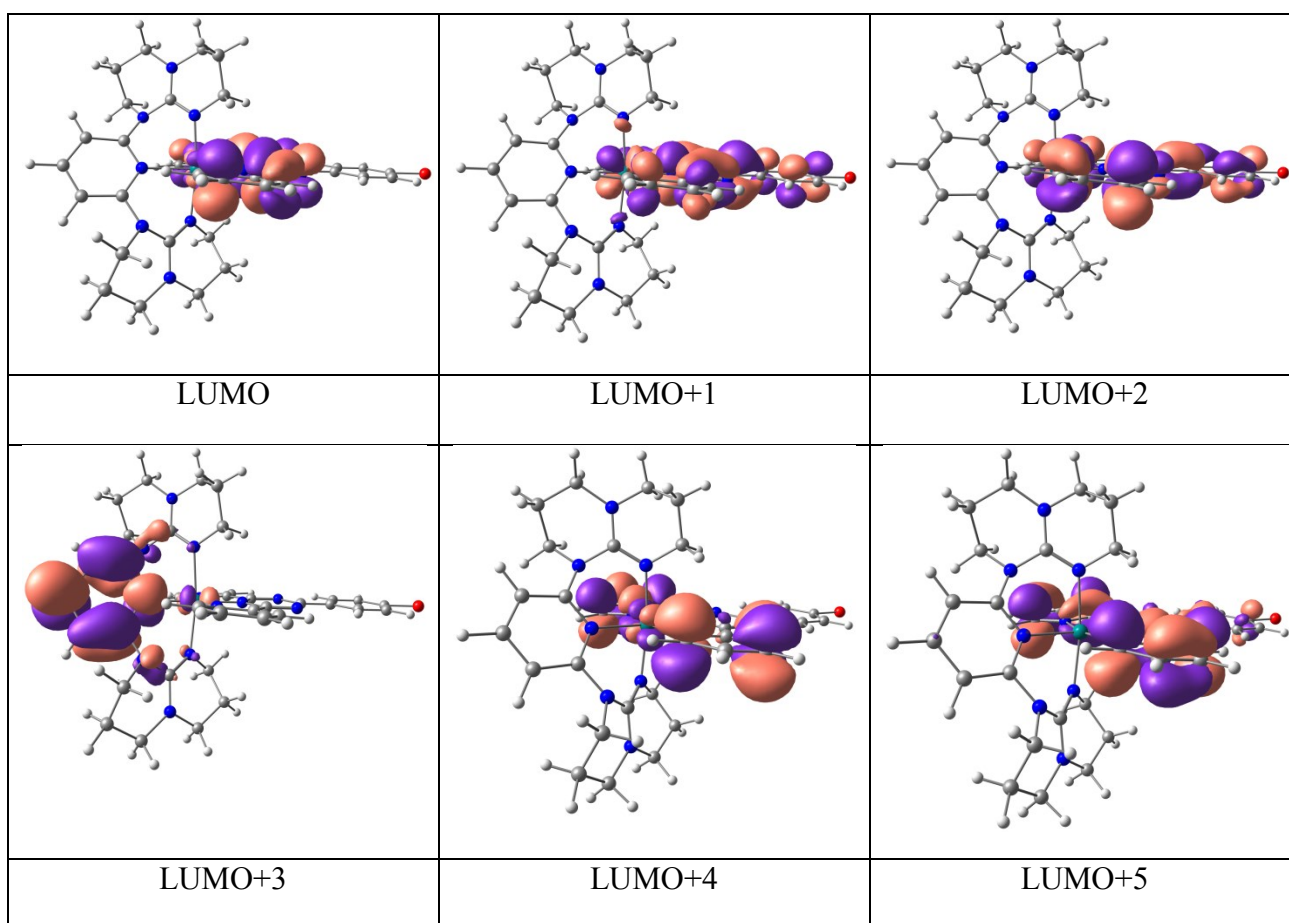


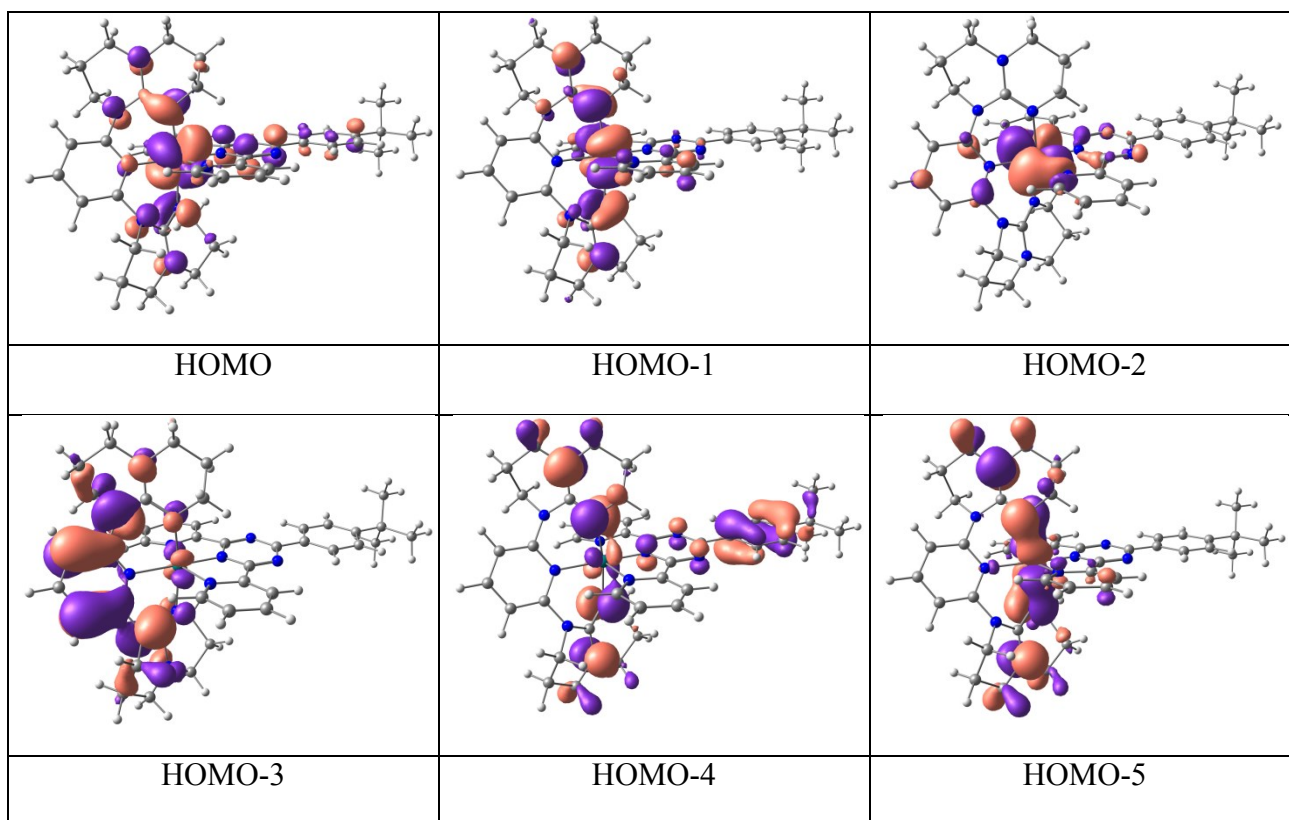
Figure 4.S5. Kohn-Sham electron density sketches for different M.O.s for $4\text{-}\mathbf{3}^{2+}$ in ($S=0$) ground state.

Table IV-S7. Selected transitions from TD-DFT calculations of **4-3²⁺** in the singlet ground state (b3lyp/LanL2DZ(f)[Ru]6-31G**[C,H,N], CPCM (CH₃CN)).

state	energy (eV)	λ/nm	λ/nm ($\epsilon \times 10^3$ M ⁻¹ cm ⁻¹) [expt.]	f	Major transition(s)	Character
67	5.02	247	244 (33.3)	0.0715	H-1->L+12 (61%)	hpp (n/ π) to hpp (n/ π^*)
46	4.49	276	291 (35.3)	0.2777	H-11->L (49%), H-10->L (17%)	Br-Ph-trz(π) to Br-Ph-trz (π^*)
22	3.57	347	380 (7.0)	0.3221	H-2->L+2 (28%), H-1->L+4 (34%)	Ru(d π) to Br-Ph-trz (π^*)(major) + hpp(n/ π) to Br-Ph-trz(π^*)(minor)
8	3.15	394	411 (8.6)	0.0985	H->L+2 (93%)	Ru(d π) to Br-Ph-trz (π^*)(major) + hpp(n/ π) to Br-Ph-trz(π^*)(minor)
6	2.38	520	560 (11.8)	0.2337	H-2->L+1 (44%), H->L+1 (32%)	Ru(d π) to Br-Ph-trz (π^*)(major) + hpp(n/ π) to Br-Ph-trz(π^*)(minor)
1	1.84	675	740 (3.8)	0.0017	H-1->L+1 (47%), H->L(44%)	Ru(d π) to Br-Ph-trz (π^*)(major) + hpp(n/ π) to Br-Ph-trz(π^*)(minor)

Table IV-S8. MO composition of $4\text{-}4^{2+}$ in singlet ($S=0$) ground state (b3lyp/LanL2DZ(f)[Ru]6-31G**[C,H,N]).

MO	Energy (eV)	Approximate Composition (%)		
		Ru	<i>t</i> Bu-Ph-Trz	hpp
LUMO+5	-1.23	1	97	1
LUMO+4	-1.38	3	96	1
LUMO+3	-1.51	3	2	95
LUMO+2	-1.71	1	99	1
LUMO+1	-2.85	12	86	3
LUMO	-2.98	3	97	1
HOMO	-5.5	54	20	25
HOMO-1	-5.53	59	9	32
HOMO-2	-5.99	81	13	6
HOMO-3	-6.69	3	1	96
HOMO-4	-6.79	4	33	64
HOMO-5	-7.04	19	8	72



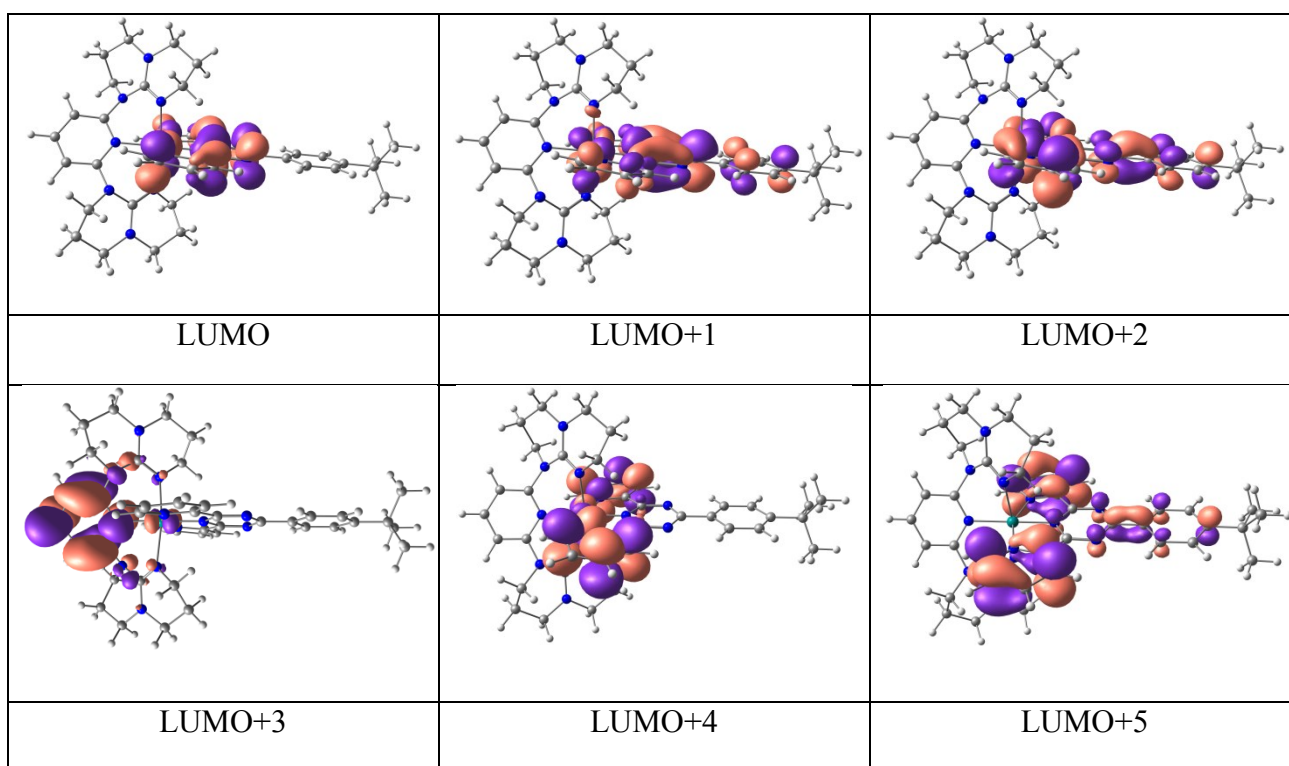


Figure 4.S6. Kohn-Sham electron density sketches for different M.O.s for $4\text{-}4^{2+}$ in ($S=0$) ground state.

Table IV-S9. Selected transitions from TD-DFT calculations of **4-4²⁺** in the singlet ground state (b3lyp/LanL2DZ(f)[Ru], 6-31G**[C,H,N], CPCM (CH₃CN)).

state	energy (eV)	λ/nm	λ/nm ($\epsilon \times 10^3 \text{ M}^{-1} \text{ cm}^{-1}$) [expt.]	f	Major transition(s)	Character
72	5.16	240	243 (29.1)	0.1502	H-4->L+6 (65%)	hpp (n/ π) to hpp (π^*) (major) + ^t Bu-Ph-trz(π) to hpp (π^*) (minor)
47	4.56	271	288 (27.8)	0.2940	H-11->L (76%)	^t Bu-Ph-trz(π) to ^t Bu-Ph-trz(π^*)
21	3.54	350	373 (6.7)	0.3102	H-2->L+2 (27%), H-1->L+4 (27%), H-2->L+3 (18%)	Ru(d π) to ^t Bu-Ph-trz(π^*) (major) + hpp(n/ π) to ^t Bu-Ph-trz(π) (minor)
8	3.14	394	405 (7.0)	0.1027	H->L+2 (92%)	Ru(d π) to ^t Bu-Ph-trz(π^*) (major) + hpp(n/ π) to ^t Bu-Ph-trz(π) (minor)
6	2.37	523	558 (9.3)	0.2879	H->L+1 (37%), H-2->L+1 (34%)	Ru(d π) to ^t Bu-Ph-trz(π^*) (major) + hpp(n/ π) to ^t Bu-Ph-trz(π) (minor)
3	1.84	674	740 (3.0)	0.0419	H->L(53%), H-1->L+1(41%)	Ru(d π) to ^t Bu-Ph-trz(π^*) (major) + hpp(n/ π) to ^t Bu-Ph-trz(π) (minor)

SI - Chapter 4

Table IV-S10. Optimized Atomic coordinates obtained from DFT for 4-I^{2+} in singlet ground state (b3lyp/LanL2DZ(f)[Ru]6-31G**[C,H,N]).

Center Number	Atomic Number	Atomic Type	Coordinates (Angstroms)		
			X	Y	Z
1	44	0	-0.545664	0.000015	0.000029
2	7	0	-0.125997	-0.992801	-1.835809
3	7	0	1.441919	-0.000293	0.000095
4	7	0	-0.125823	0.992635	1.835781
5	7	0	-0.685039	1.879629	-1.013404
6	7	0	-1.557872	4.078253	-1.035268
7	7	0	-2.632296	2.381660	0.198591
8	7	0	-2.658451	0.000291	-0.000208
9	7	0	-2.632879	-2.381065	-0.198906
10	7	0	-1.559575	-4.077736	1.035804
11	7	0	-0.685736	-1.879521	1.013545
12	6	0	1.215531	-1.205606	-2.029274
13	6	0	1.683070	-1.874469	-3.164219
14	1	0	2.745061	-2.044867	-3.295426
15	6	0	0.783095	-2.310952	-4.132485
16	1	0	1.137914	-2.829022	-5.017247
17	6	0	-0.575421	-2.054084	-3.949415
18	1	0	-1.311835	-2.352853	-4.687259
19	6	0	-0.981762	-1.397838	-2.791368
20	1	0	-2.026384	-1.177505	-2.609378
21	6	0	2.107587	-0.628445	-1.001251
22	6	0	3.500601	-0.648214	-1.013787
23	1	0	4.033544	-1.176265	-1.794746
24	6	0	4.232029	-0.000458	0.000019
25	6	0	3.500739	0.647372	1.013878
26	1	0	4.033778	1.175389	1.794796
27	6	0	2.107723	0.627761	1.001416
28	6	0	1.215752	1.205071	2.029420
29	6	0	1.683342	1.873669	3.164492
30	1	0	2.745375	2.043705	3.295850
31	6	0	0.783382	2.310310	4.132703
32	1	0	1.138248	2.828196	5.017553
33	6	0	-0.575185	2.053844	3.949446
34	1	0	-1.311602	2.352737	4.687237
35	6	0	-0.981583	1.397818	2.791295
36	1	0	-2.026237	1.177782	2.609166
37	6	0	5.710344	-0.000517	-0.000054
38	6	0	6.427415	0.049301	-1.209224
39	1	0	5.896264	0.124435	-2.153750
40	6	0	7.820229	0.052787	-1.207627
41	1	0	8.359749	0.105880	-2.147907
42	6	0	8.520394	-0.000641	-0.000197
43	1	0	9.605732	-0.000690	-0.000255
44	6	0	7.820349	-0.054003	1.207305
45	1	0	8.359957	-0.107143	2.147531
46	6	0	6.427534	-0.050395	1.209041
47	1	0	5.896471	-0.125471	2.153621
48	6	0	-3.348245	1.170337	0.050467
49	6	0	-4.747245	1.198068	0.013790
50	1	0	-5.279232	2.138914	-0.009551
51	6	0	-5.449020	0.000742	-0.001062
52	1	0	-6.534046	0.000896	-0.001430
53	6	0	-4.747612	-1.196815	-0.015457
54	1	0	-5.279963	-2.137458	0.007572
55	6	0	-3.348583	-1.169566	-0.051243
56	6	0	-3.271660	-3.476228	-0.959430
57	1	0	-2.518399	-3.898114	-1.636251
58	1	0	-4.058349	-3.050662	-1.581165
59	6	0	-3.784006	-4.545603	-0.004833
60	1	0	-4.512594	-4.112064	0.687692
61	1	0	-4.283864	-5.355724	-0.543260
62	6	0	-2.583733	-5.099862	0.752223
63	1	0	-2.893187	-5.553467	1.700507
64	1	0	-2.102096	-5.888222	0.159208
65	6	0	-0.391239	-4.570924	1.779657

SI – Chapter 3

66	1	0	0.423413	-4.814073	1.083522
67	1	0	-0.683072	-5.496891	2.279690
68	6	0	0.040204	-3.511660	2.781920
69	1	0	-0.760307	-3.359666	3.514395
70	1	0	0.930867	-3.833960	3.328886
71	6	0	0.331589	-2.222815	2.021853
72	1	0	0.414511	-1.386817	2.720554
73	1	0	1.299327	-2.306988	1.512104
74	6	0	-1.584556	-2.765697	0.660654
75	6	0	-3.271059	3.476777	0.959209
76	1	0	-2.518006	3.898102	1.636619
77	1	0	-4.058266	3.051268	1.580322
78	6	0	-3.782431	4.546739	0.004756
79	1	0	-4.282251	5.356848	0.543233
80	1	0	-4.510812	4.113789	-0.688361
81	6	0	-2.581520	5.100802	-0.751417
82	1	0	-2.890331	5.555206	-1.699527
83	1	0	-2.099683	5.888518	-0.157691
84	6	0	-0.389181	4.571063	-1.778811
85	1	0	0.425486	4.813658	-1.082502
86	1	0	-0.680501	5.497293	-2.278662
87	6	0	0.041902	3.511833	-2.781274
88	1	0	-0.758605	3.360364	-3.513858
89	1	0	0.932764	3.833862	-3.328076
90	6	0	0.332619	2.222704	-2.021441
91	1	0	0.415327	1.386798	-2.720289
92	1	0	1.300305	2.306385	-1.511509
93	6	0	-1.583561	2.766106	-0.660472

Table IV-S11. Optimized Atomic coordinates obtained from DFT for $4\text{-}2^{2+}$ in singlet ground state (b3lyp/LanL2DZ(f)[Ru]6-31G**[C,H,N]).

Center Number	Atomic Number	Atomic Type	Coordinates (Angstroms)		
			X	Y	Z
1	44	0	-0.773882	-0.000117	-0.000185
2	7	0	-0.353309	1.045790	-1.804878
3	7	0	1.212502	-0.000742	0.000247
4	7	0	-0.354649	-1.046556	1.804631
5	7	0	-0.930902	-1.820646	-1.102864
6	7	0	-1.765263	-4.027989	-1.185942
7	7	0	-2.863072	-2.389806	0.106542
8	7	0	-2.888895	0.000857	-0.000872
9	7	0	-2.860725	2.391500	-0.107928
10	7	0	-1.763712	4.027834	1.187598
11	7	0	-0.929779	1.820369	1.102590
12	6	0	0.988375	1.255556	-1.997969
13	6	0	1.456820	1.940963	-3.122848
14	1	0	2.519565	2.105878	-3.254841
15	6	0	0.556830	2.399774	-4.080312
16	1	0	0.912178	2.930095	-4.957574
17	6	0	-0.802991	2.150107	-3.896221
18	1	0	-1.540007	2.468223	-4.625317
19	6	0	-1.209580	1.475090	-2.749492
20	1	0	-2.255237	1.259865	-2.567370
21	6	0	1.880313	0.660004	-0.979374
22	6	0	3.273095	0.673983	-0.994832
23	1	0	3.805360	1.175366	-1.793459
24	6	0	4.006324	-0.000490	0.001486
25	6	0	3.272375	-0.675225	0.997068
26	1	0	3.803925	-1.176270	1.796364
27	6	0	1.879570	-0.661469	0.980353
28	6	0	0.986853	-1.256936	1.998333
29	6	0	1.454450	-1.942898	3.123226
30	1	0	2.517053	-2.108367	3.255659
31	6	0	0.553794	-2.401611	4.080114
32	1	0	0.908487	-2.932341	4.957395
33	6	0	-0.805832	-2.151346	3.895410

SI - Chapter 4

34	1	0	-1.543344	-2.469381	4.624037
35	6	0	-1.211568	-1.475835	2.748664
36	1	0	-2.257051	-1.260187	2.566042
37	6	0	5.481594	0.000008	0.001769
38	6	0	6.205040	1.113056	-0.463481
39	1	0	5.680143	2.004407	-0.795455
40	6	0	7.595759	1.112925	-0.454418
41	1	0	8.130408	1.992723	-0.801054
42	6	0	8.320880	0.003373	0.006225
43	6	0	7.596793	-1.106374	0.468847
44	1	0	8.132579	-1.981420	0.825841
45	6	0	6.206298	-1.110764	0.471117
46	1	0	5.682418	-2.000836	0.808083
47	6	0	9.827812	-0.006635	-0.017133
48	1	0	10.196953	-0.431961	-0.958499
49	1	0	10.237693	-0.612499	0.795453
50	1	0	10.237157	1.003462	0.066522
51	6	0	0.016728	-2.196546	-2.160827
52	1	0	0.814547	-1.457387	-2.192127
53	1	0	-0.485588	-2.171279	-3.138343
54	6	0	0.576047	-3.590952	-1.894803
55	1	0	1.296597	-3.886591	-2.662673
56	1	0	1.097816	-3.594226	-0.931640
57	6	0	-0.584373	-4.574456	-1.882151
58	1	0	-0.304718	-5.512157	-1.387604
59	1	0	-0.883440	-4.827745	-2.907350
60	6	0	-2.839823	-5.028115	-1.044947
61	1	0	-2.403986	-5.891521	-0.526788
62	1	0	-3.133048	-5.370857	-2.044679
63	6	0	-4.041781	-4.511827	-0.261207
64	1	0	-4.563182	-5.351721	0.206444
65	1	0	-4.754394	-4.012789	-0.925058
66	6	0	-3.521302	-3.528395	0.780244
67	1	0	-4.304586	-3.141588	1.430803
68	1	0	-2.776433	-4.012338	1.423131
69	6	0	-1.812142	-2.730000	-0.766373
70	6	0	-3.579072	-1.170789	0.007742
71	6	0	-4.978255	-1.195712	-0.027071
72	1	0	-5.513725	-2.132873	-0.080945
73	6	0	-5.678451	0.002086	-0.003343
74	1	0	-6.763459	0.002575	-0.004325
75	6	0	-4.977240	1.199255	0.021691
76	1	0	-5.512037	2.136847	0.074634
77	6	0	-3.577993	1.173136	-0.010573
78	6	0	-3.517080	3.531128	-0.781678
79	1	0	-4.299534	3.145479	-1.433925
80	1	0	-2.770797	4.015124	-1.422871
81	6	0	-4.038573	4.513985	0.259807
82	1	0	-4.558586	5.354691	-0.207932
83	1	0	-4.752636	4.014886	0.922042
84	6	0	-2.837515	5.028690	1.045974
85	1	0	-2.400354	5.892391	0.529417
86	1	0	-3.132091	5.370554	2.045608
87	6	0	-0.583543	4.573108	1.885947
88	1	0	-0.883669	4.824863	2.911213
89	1	0	-0.303262	5.511538	1.393144
90	6	0	0.576756	3.589491	1.898240
91	1	0	1.296609	3.883908	2.667230
92	1	0	1.099444	3.594182	0.935581
93	6	0	0.017166	2.194738	2.161743
94	1	0	0.814989	1.455572	2.192443
95	1	0	-0.485796	2.167973	3.138885
96	6	0	-1.810482	2.730351	0.766411

SI – Chapter 3

Table IV-S12. Optimized Atomic coordinates obtained from DFT for $4\text{-}3^{2+}$ in singlet ground state (b3lyp/LanL2DZ(f)[Ru]6-31G**[C,H,N]).

Center Number	Atomic Number	Atomic Type	Coordinates (Angstroms)		
			X	Y	Z
1	35	0	-8.898623	0.103425	-0.209417
2	44	0	1.308804	0.055589	0.023965
3	7	0	0.882670	1.153329	1.770456
4	7	0	-0.601138	-0.063705	0.097415
5	7	0	-2.634610	0.526029	1.129263
6	7	0	-2.603097	-0.967413	-0.746190
7	7	0	0.913819	-1.113919	-1.646515
8	7	0	3.376583	0.133682	-0.029054
9	7	0	3.417803	-2.244492	-0.152888
10	7	0	2.233499	-3.933336	0.936518
11	7	0	1.568613	-1.695710	1.139283
12	7	0	3.273680	2.495388	-0.009990
13	7	0	2.126387	3.953522	-1.425759
14	7	0	1.348826	1.767836	-1.126022
15	6	0	-0.392048	-1.561817	-1.682270
16	6	0	-0.805765	-2.555992	-2.557942
17	1	0	-1.683897	-2.868187	-2.545668
18	6	0	0.119719	-3.071196	-3.450438
19	1	0	-0.119827	-3.769065	-4.019013
20	6	0	1.394721	-2.551415	-3.496755
21	1	0	2.005189	-2.857575	-4.129235
22	6	0	1.752690	-1.571090	-2.591401
23	1	0	2.611157	-1.211696	-2.638342
24	6	0	-1.281810	-0.877530	-0.747135
25	6	0	-3.242679	-0.228328	0.189115
26	6	0	-1.313427	0.587166	1.057634
27	6	0	-0.459122	1.289945	2.004005
28	6	0	-0.961387	1.978024	3.106358
29	1	0	-1.880153	2.070517	3.229003
30	6	0	-0.072303	2.516716	4.012757
31	1	0	-0.380702	2.993310	4.751368
32	6	0	1.278356	2.338686	3.808242
33	1	0	1.892288	2.664164	4.428773
34	6	0	1.714461	1.679232	2.681047
35	1	0	2.632773	1.593008	2.544834
36	6	0	-4.704502	-0.195703	0.142200
37	6	0	-5.394090	-0.833951	-0.865662
38	1	0	-4.930391	-1.351959	-1.485478
39	6	0	-6.753920	-0.703831	-0.949398
40	1	0	-7.234669	-1.106479	-1.635366
41	6	0	-7.381296	0.007593	-0.042830
42	6	0	-6.788352	0.638762	0.946402
43	1	0	-7.291626	1.135531	1.549012
44	6	0	-5.422445	0.548208	1.065132
45	1	0	-4.978551	0.980010	1.759044
46	6	0	0.615913	-2.086949	2.178216
47	1	0	0.643216	-1.409637	2.873944
48	1	0	-0.271833	-2.060527	1.789506
49	6	0	0.777927	-3.336172	2.792611
50	1	0	-0.019002	-3.568444	3.297181
51	1	0	1.533614	-3.315012	3.402444
52	6	0	1.031747	-4.417178	1.631963
53	1	0	1.182985	-5.300170	2.007859
54	1	0	0.275857	-4.457485	1.025356
55	6	0	3.371903	-4.885711	0.805409
56	1	0	3.735819	-5.052968	1.690045
57	1	0	3.027596	-5.729725	0.468396
58	6	0	4.445308	-4.454260	-0.055251
59	1	0	4.718580	-5.202272	-0.610627
60	1	0	5.204367	-4.203051	0.495060
61	6	0	4.090638	-3.305011	-0.937045
62	1	0	4.894572	-2.947000	-1.344664
63	1	0	3.500087	-3.608767	-1.645966
64	6	0	2.371378	-2.620085	0.672773
65	6	0	4.097865	-1.010613	-0.001865

SI - Chapter 4

66	6	0	5.474016	-1.009657	0.138306
67	1	0	5.943378	-1.811247	0.191160
68	6	0	6.139175	0.191518	0.198975
69	1	0	7.062839	0.211559	0.305555
70	6	0	5.421719	1.372523	0.100376
71	1	0	5.862218	2.192269	0.105531
72	6	0	4.040633	1.317942	-0.005215
73	6	0	3.886122	3.729815	0.508128
74	1	0	4.612791	3.507235	1.111351
75	1	0	3.226557	4.242746	1.001915
76	6	0	4.411137	4.548745	-0.649710
77	1	0	4.840791	5.354889	-0.319833
78	1	0	5.065774	4.036561	-1.151758
79	6	0	3.244073	4.908674	-1.532926
80	1	0	2.926347	5.793330	-1.292678
81	1	0	3.543994	4.941326	-2.455385
82	6	0	0.914620	4.411969	-2.102965
83	1	0	1.113883	4.568367	-3.040205
84	1	0	0.632595	5.255287	-1.713711
85	6	0	-0.212133	3.415079	-1.995121
86	1	0	-0.881419	3.594172	-2.674871
87	1	0	-0.633614	3.483152	-1.123428
88	6	0	0.367941	2.029819	-2.186858
89	1	0	-0.341468	1.366937	-2.151511
90	1	0	0.797807	1.969682	-3.055355
91	6	0	2.207093	2.721563	-0.901318

Table IV-S13. Optimized Atomic coordinates obtained from DFT for $4\text{-}4^{2+}$ in singlet ground state (b3lyp/LanL2DZ(f)[Ru]6-31G**[C,H,N]).

Center Number	Atomic Number	Atomic Type	Coordinates (Angstroms)		
			X	Y	Z
1	44	0	-1.348493	0.000183	0.000581
2	7	0	-0.888845	-1.079414	1.805836
3	7	0	0.626580	-0.004275	0.005955
4	7	0	-0.873940	1.077575	-1.802426
5	7	0	-1.505872	1.810089	1.118981
6	7	0	-2.335143	4.018621	1.212590
7	7	0	-3.422842	2.394636	-0.107689
8	7	0	-3.461086	0.005110	-0.006121
9	7	0	-3.435034	-2.384529	0.096563
10	7	0	-2.342875	-4.015666	-1.211278
11	7	0	-1.507773	-1.809496	-1.118164
12	6	0	0.458186	-1.271899	1.986673
13	6	0	0.976348	-1.950228	3.088527
14	1	0	2.051122	-2.066425	3.168695
15	6	0	0.102336	-2.441409	4.055672
16	1	0	0.480175	-2.971399	4.923658
17	6	0	-1.265623	-2.222552	3.890473
18	1	0	-1.982946	-2.568064	4.627080
19	6	0	-1.715504	-1.543035	2.759110
20	1	0	-2.770423	-1.354499	2.601701
21	6	0	1.325554	-0.653542	0.964003
22	7	0	2.644104	-0.686729	0.998612
23	6	0	3.299855	-0.010804	0.013147
24	7	0	2.652683	0.668238	-0.975731
25	6	0	1.333671	0.641458	-0.948197
26	6	0	0.474959	1.263890	-1.975632
27	6	0	1.002479	1.939866	-3.074487
28	1	0	2.078211	2.051091	-3.148553
29	6	0	0.136213	2.435057	-4.046529
30	1	0	0.521357	2.963396	-4.912308
31	6	0	-1.233637	2.222351	-3.889159
32	1	0	-1.945177	2.571121	-4.629827
33	6	0	-1.693040	1.544845	-2.760414
34	1	0	-2.749695	1.361035	-2.609097
35	6	0	4.756211	-0.013801	0.016509

SI – Chapter 3

36	6	0	5.473891	-0.695710	1.016920
37	1	0	4.932934	-1.224165	1.793151
38	6	0	6.863208	-0.694925	1.015749
39	1	0	7.380241	-1.230364	1.802273
40	6	0	7.598935	-0.019935	0.025162
41	6	0	6.866833	0.659104	-0.971739
42	1	0	7.395571	1.192362	-1.754305
43	6	0	5.482097	0.667230	-0.983168
44	1	0	4.946587	1.197577	-1.761743
45	6	0	9.133435	-0.000104	-0.004300
46	6	0	9.753916	-0.790021	1.163408
47	1	0	9.470620	-1.847476	1.140516
48	1	0	9.470523	-0.375419	2.136445
49	1	0	10.844453	-0.743896	1.095332
50	6	0	9.621733	-0.627504	-1.334174
51	1	0	10.715623	-0.616684	-1.368716
52	1	0	9.258479	-0.078030	-2.207625
53	1	0	9.291054	-1.666942	-1.426656
54	6	0	9.622284	1.467496	0.082643
55	1	0	10.716167	1.495622	0.059159
56	1	0	9.292093	1.939533	1.013471
57	1	0	9.258506	2.074037	-0.751937
58	6	0	-0.565648	-2.179163	-2.183230
59	1	0	0.231381	-1.438930	-2.216750
60	1	0	-1.072855	-2.147802	-3.157978
61	6	0	-0.004025	-3.574763	-1.928654
62	1	0	0.712211	-3.865296	-2.702377
63	1	0	0.523660	-3.585269	-0.968711
64	6	0	-1.164398	-4.558335	-1.915695
65	1	0	-1.468636	-4.806458	-2.940531
66	1	0	-0.882290	-5.498192	-1.426931
67	6	0	-3.416331	-5.017349	-1.070426
68	1	0	-2.979194	-5.881188	-0.554163
69	1	0	-3.709858	-5.358254	-2.070598
70	6	0	-4.617797	-4.502878	-0.285209
71	1	0	-5.141147	-5.344267	0.177499
72	1	0	-5.328851	-3.999096	-0.947135
73	6	0	-4.096264	-3.526342	0.762267
74	1	0	-4.879126	-3.141826	1.414776
75	1	0	-3.352694	-4.015928	1.402370
76	6	0	-2.388154	-2.721339	-0.783205
77	6	0	-4.152183	-1.165367	-0.000988
78	6	0	-5.551069	-1.187947	-0.039609
79	1	0	-6.088501	-2.123948	-0.094044
80	6	0	-6.248702	0.011611	-0.019727
81	1	0	-7.333692	0.014176	-0.025108
82	6	0	-5.545705	1.207886	0.007169
83	1	0	-6.079430	2.146284	0.056353
84	6	0	-4.146580	1.178886	-0.017596
85	6	0	-4.073027	3.540753	-0.776799
86	1	0	-4.851230	3.161242	-1.437771
87	1	0	-3.321293	4.028720	-1.408513
88	6	0	-4.600318	4.516985	0.268073
89	1	0	-5.115546	5.361778	-0.197540
90	1	0	-5.319890	4.014750	0.921893
91	6	0	-3.404194	5.024250	1.066141
92	1	0	-2.959489	5.888671	0.557374
93	1	0	-3.705610	5.362164	2.064988
94	6	0	-1.161256	4.555027	1.929246
95	1	0	-0.873526	5.496998	1.447916
96	1	0	-1.472816	4.798082	2.953115
97	6	0	-0.003089	3.569073	1.945415
98	1	0	0.708904	3.854901	2.724783
99	1	0	0.530575	3.582512	0.988815
100	6	0	-0.568986	2.173621	2.190870
101	1	0	0.226526	1.431812	2.225655
102	1	0	-1.081620	2.139057	3.162652
103	6	0	-2.381189	2.725520	0.780721

SI – Chapter 5 : (A) Supplementary Informations

Tuning the structural and electronic properties of rare Re(I)-
complexes of κ^3N -tridentate heterocyclic ligands

Table V-S1. Comparison of bond distances and angles in **5A-1** and **5A-2**.

Compound	Bond Length			Angle		
		Obs. (x-ray)	Calc. (DFT)		Obs. (x-ray)	Calc. (DFT)
5A-1	Re1-N1	2.175(3)	2.21295	N1-Re1-N4	78.14(11)	78.048
	Re1-N4	2.199(3)	2.24161	N1-Re1-N7	78.75(11)	78.049
	Re1-N7	2.183(3)	2.22573	N4-Re1-N7	88.41(11)	89.895
	Re1-C21	1.901(5)	1.92552			
	Re1-C20	1.922(4)	1.92647			
	Re1-C22	1.933(4)	1.92743			
	O2-C21	1.170(6)	1.16266			
	O1-C20	1.144(6)	1.16305			
	O3-C22	1.153(5)	1.16318			
5A-2	Re1-N1	2.163(4)	2.19737	N1-Re1-N5	77.95(15)	77.893
	Re1-N8	2.194(4)	2.24680	N1-Re1-N8	78.61(14)	78.298
	Re1-N5	2.195(4)	2.25059	N5-Re1-N8	89.05(15)	91.413
	Re1-C19	1.934(6)	1.92749			
	Re1-C20	1.931(5)	1.92935			
	Re1-C21	1.900(6)	1.92698			
	O1-C19	1.135(7)	1.16226			
	O2-C20	1.140(7)	1.16149			
	O3-C21	1.184(7)	1.16254			

DFT Calculations**Table VA-S2.** MO Composition of **5A-1¹⁺** in Singlet ($S=0$) Ground State (b3lyp/LanL2DZ(f)[Re]6-31G**[C,H,N,O]).

MO	Energy (eV)	Composition				
		Re	Py	Hpp	CO (trans to Py)	CO (trans to Hpp)
LUMO+5	-0.04	8	3	69	1	19
LUMO+4	-0.12	0	2	3	25	70
LUMO+3	-0.87	22	9	8	17	43
LUMO+2	-0.91	22	16	5	22	36
LUMO+1	-1.05	2	75	18	2	3
LUMO	-1.70	6	75	8	9	2
HOMO	-5.97	34	0	48	1	17
HOMO-1	-6.14	22	14	55	6	5
HOMO-2	-6.62	61	5	4	13	17
HOMO-3	-6.78	6	31	59	1	2
HOMO-4	-7.05	40	3	40	9	8
HOMO-5	-7.30	23	5	61	0	10

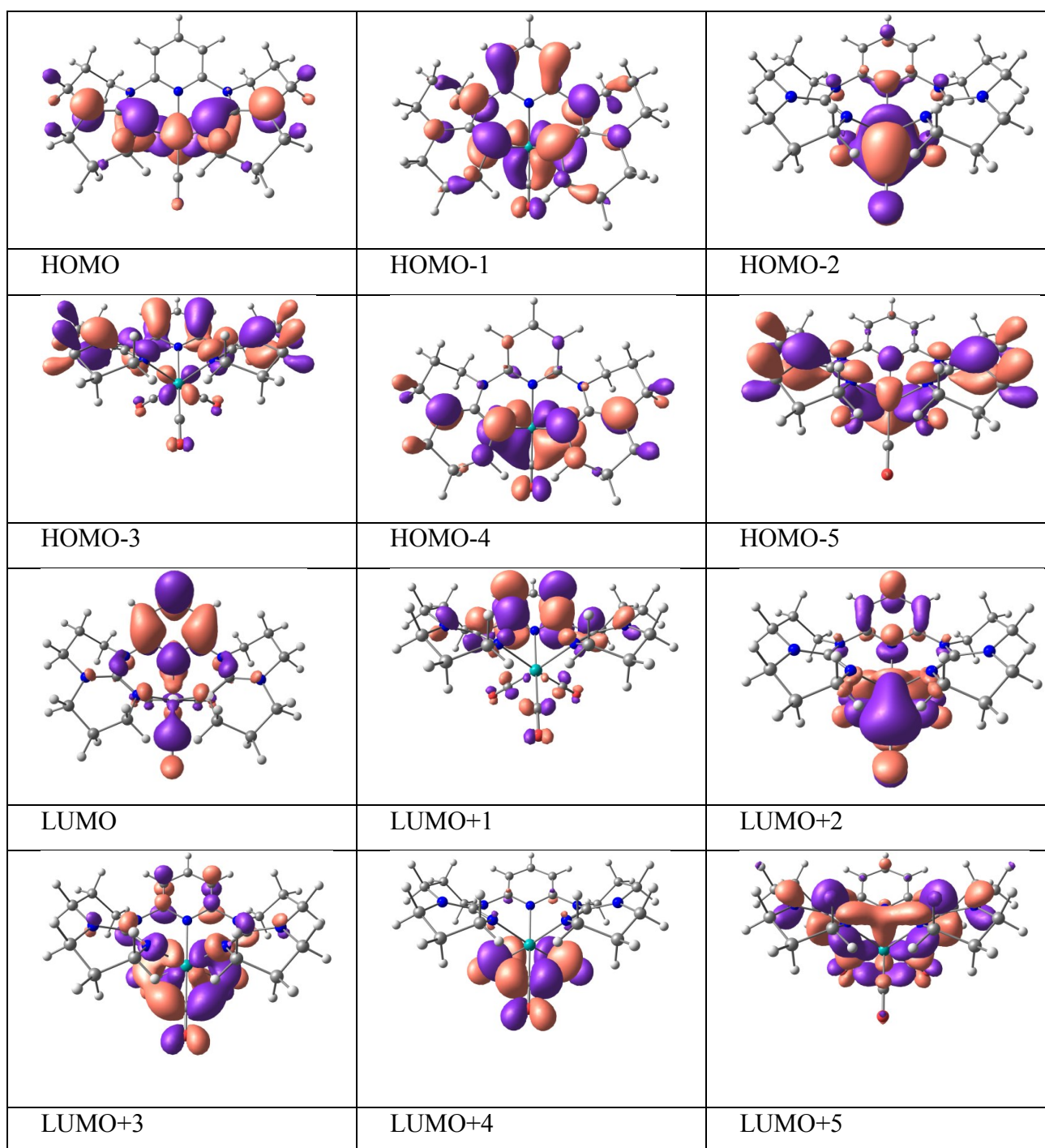


Figure 5.S1. Kohn-Sham molecular orbital diagrams of $5A-1^{1+}$ in ($S=0$) ground state.

Table VA-S3. Selected Transitions from TD-DFT calculations of **5A-1¹⁺** in the Singlet Ground State (b3lyp/LanL2DZ(f)[Re]6-31G**[C,H,N,O], CPCM (CH₃CN)).

energy (eV)	λ/nm	λ/nm ($\epsilon \times 10^3$ $\text{M}^{-1}\text{cm}^{-1}$ [expt.]	f	Major transition(s)	character
5.55	223	218 (64.7)	0.1553	H-5 \rightarrow L+1 (33%), H-1 \rightarrow L+7 (26%), H \rightarrow L+6 (16%)	[hpp(n/ π) (major) + Re(d π) (minor) to Py(π^*)] + [hpp(n/ π) (major) + Re(d π) (minor) to hpp(π^*)]
4.39	282	282 (19.2)	0.1143	H-3 \rightarrow L (75%), H \rightarrow L+3 (10%)	hpp(n/ π) (major) + Py(π) (minor) to Py(π^*)
3.61	343	346 (3.5)	0.0199	H-1 \rightarrow L (94%)	hpp(n/ π) (major) + Re(d π) (minor) to Py(π^*)

Table VA-S4. MO Composition of **5A-2¹⁺** in Singlet ($S=0$) Ground State (b3lyp/LanL2DZ(f)[Re]6-31G**[C,H,N,O]).

MO	Energy (eV)	Composition				
		Re	Pz	Hpp	CO (trans to Pz)	CO (trans to Hpp)
LUMO+6	+0.11	8	5	70	15	2
LUMO+5	-0.14	11	3	68	0	18
LUMO+4	-0.20	1	1	4	25	69
LUMO+3	-0.97	25	1	10	19	45
LUMO+2	-1.05	26	6	3	26	38
LUMO+1	-1.36	0	84	15	0	1
LUMO	-2.35	3	85	7	4	0
HOMO	-6.06	33	0	50	1	16
HOMO-1	-6.31	24	9	56	6	5
HOMO-2	-6.74	62	4	5	12	17
HOMO-3	-6.91	1	27	71	0	1
HOMO-4	-7.13	43	9	30	9	9
HOMO-5	-7.32	18	14	60	0	8

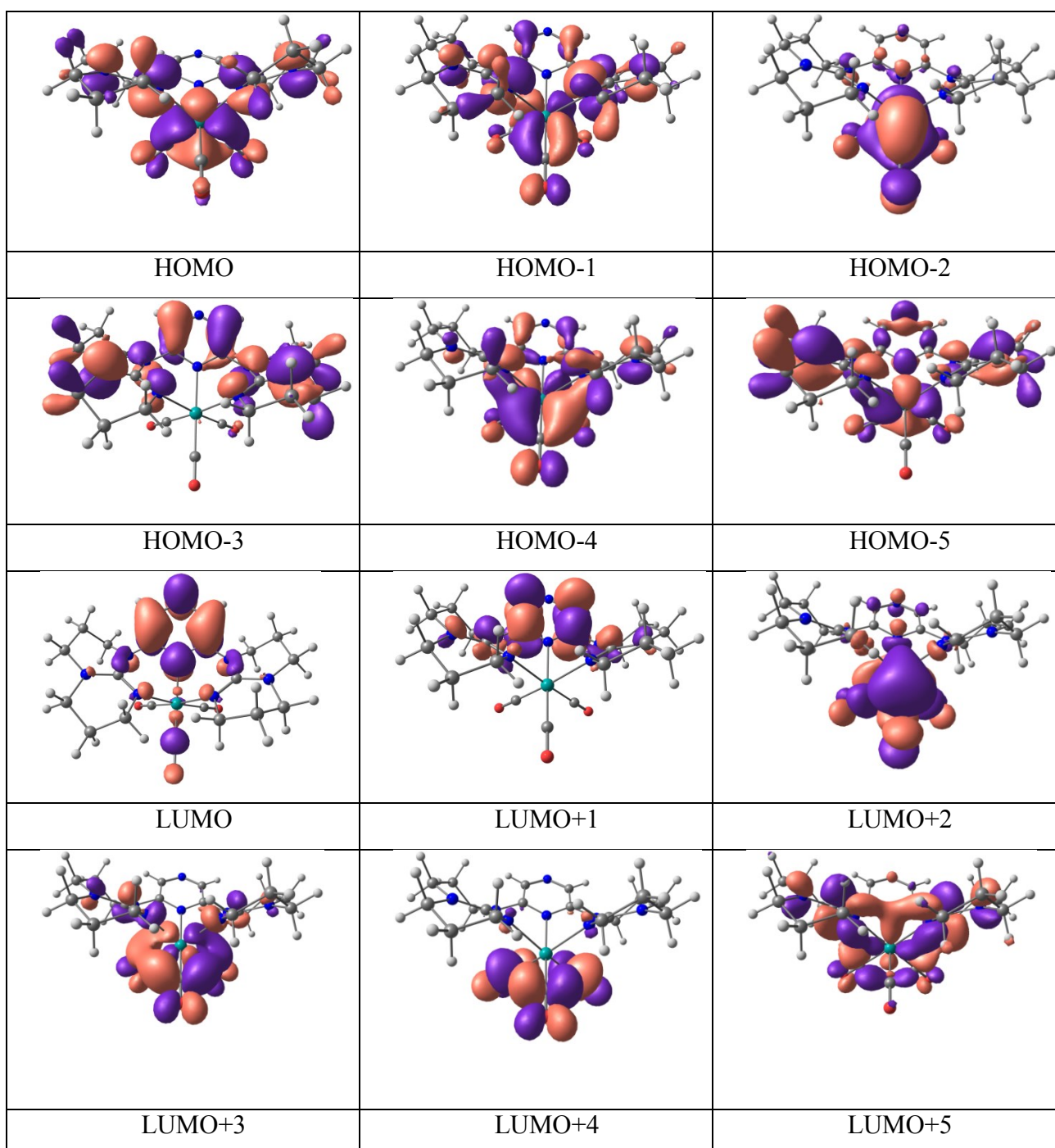


Figure 5.S2. Kohn-Sham molecular orbital diagrams of $5A-2^{1+}$ in ($S=0$) ground state.

Table VA-S5. Selected Transitions from TD-DFT calculations of **5A-2¹⁺** in the Singlet Ground State (b3lyp/LanL2DZ(f)[Re]6-31G**[C,H,N,O], CPCM (CH₃CN)).

energy (eV)	λ/nm	λ/nm ($\times 10^3$ $\text{M}^{-1}\text{cm}^{-1}$ [expt.]	f	Major transition(s)	character
5.42	228	219 (44.5)	0.1714	H ->L+6 (49%)	hpp(n/ π) (major) + Re(d π) (minor) to hpp(π^*)
4.41	281	283 (12.4)	0.0972	H-1 -> L+2 (51%), H -> L+3 (27%)	hpp(n/ π) (major) + Re(d π) (minor) to CO(π^*) (major) + Re(d π^*) (minor)
3.90	318	318 (7.3)	0.0773	H-3 -> L (87%)	hpp(n/ π) (major) + Pz(n/ π) (minor) to Pz(π^*)
3.19	389	377 (3.4)	0.0238	H-1 -> L (96%)	hpp(n/ π) (major) + Re(d π) (minor) to Pz(π^*)

Table VA-S6. Optimized Atomic coordinates obtained from DFT calculations of **5A-1¹⁺**

Center Number	Atomic Number	Atomic Type	Coordinates (Angstroms)		
			X	Y	Z
1	75	0	-0.000045	-0.766037	0.748959
2	8	0	2.188434	-0.566095	2.920411
3	8	0	-0.000405	-3.842376	1.013527
4	8	0	-2.188380	-0.565700	2.920517
5	7	0	0.000051	1.378688	0.203710
6	7	0	-2.372700	1.310015	0.106480
7	7	0	-3.808899	0.007507	-1.228912
8	7	0	-1.583576	-0.689864	-0.835788
9	7	0	2.372806	1.309799	0.106686
10	7	0	3.808871	0.007474	-1.229120
11	7	0	1.583642	-0.690019	-0.835651
12	6	0	1.171421	2.044684	0.047251
13	6	0	1.200860	3.433053	-0.125057
14	1	0	2.138792	3.956448	-0.246695
15	6	0	0.000183	4.127549	-0.182576
16	1	0	0.000237	5.202897	-0.328043
17	6	0	-1.200557	3.433156	-0.125164
18	1	0	-2.138440	3.956621	-0.246890
19	6	0	-1.171247	2.044787	0.047151
20	6	0	-3.591981	1.971280	0.607391
21	1	0	-3.297707	2.833920	1.203264
22	1	0	-4.096619	1.273049	1.284454
23	6	0	-4.488526	2.329014	-0.571917
24	1	0	-5.393873	2.848361	-0.245068

SI-Chapter 5

25	1	0	-3.954986	2.995714	-1.257380
26	6	0	-4.873024	1.026997	-1.267912
27	1	0	-5.749651	0.590708	-0.772516
28	1	0	-5.150706	1.200721	-2.314950
29	6	0	-4.227442	-1.272753	-1.831391
30	1	0	-4.375594	-1.109589	-2.906950
31	1	0	-5.201968	-1.541089	-1.406793
32	6	0	-3.204339	-2.372643	-1.591533
33	1	0	-3.389998	-3.202162	-2.279635
34	1	0	-3.285597	-2.762794	-0.571586
35	6	0	-1.811660	-1.782734	-1.792001
36	1	0	-1.046174	-2.540535	-1.635537
37	1	0	-1.698420	-1.410460	-2.820329
38	6	0	-2.568090	0.164973	-0.688246
39	6	0	3.592088	1.971028	0.607646
40	1	0	4.096694	1.272771	1.284707
41	1	0	3.297812	2.833651	1.203542
42	6	0	4.488673	2.328752	-0.571634
43	1	0	5.393977	2.848187	-0.244803
44	1	0	3.955112	2.995330	-1.257202
45	6	0	4.873277	1.026692	-1.267428
46	1	0	5.151630	1.200360	-2.314293
47	1	0	5.749511	0.590202	-0.771496
48	6	0	4.227259	-1.272631	-1.832038
49	1	0	5.201968	-1.540993	-1.407879
50	1	0	4.374980	-1.109234	-2.907619
51	6	0	3.204332	-2.372635	-1.591994
52	1	0	3.285958	-2.762904	-0.572121
53	1	0	3.389842	-3.202050	-2.280261
54	6	0	1.811532	-1.782848	-1.791953
55	1	0	1.697871	-1.410583	-2.820239
56	1	0	1.046192	-2.540742	-1.635217
57	6	0	2.568162	0.164819	-0.688171
58	6	0	1.363340	-0.652279	2.105257
59	6	0	-0.000239	-2.682021	0.940370
60	6	0	-1.363364	-0.652046	2.105299

Table VA-S7. Optimized Atomic coordinates obtained from DFT calculations of **5A-2¹⁺**

Center Number	Atomic Number	Atomic Type	Coordinates (Angstroms)		
			X	Y	Z
1	75	0	0.013673	-0.781041	0.765764
2	8	0	2.208585	-0.519033	2.924365
3	8	0	0.096155	-3.857669	1.046418
4	8	0	-2.171290	-0.642276	2.945522
5	7	0	-0.046399	1.346319	0.218823
6	7	0	-0.144445	4.082819	-0.260951
7	7	0	-2.417824	1.237299	0.161365
8	7	0	-3.847517	-0.079514	-1.170717
9	7	0	-1.605078	-0.741036	-0.797316
10	7	0	2.325374	1.390874	0.073640
11	7	0	3.821388	0.088320	-1.189715
12	7	0	1.613223	-0.669826	-0.808140
13	6	0	1.090000	2.052573	0.016700
14	6	0	1.016599	3.437656	-0.206297
15	1	0	1.911068	4.029168	-0.365182

SI - Chapter 5

16	6	0	-1.259096	3.367299	-0.147574
17	1	0	-2.197402	3.900145	-0.255242
18	6	0	-1.233113	1.980606	0.068206
19	6	0	-3.624040	1.867339	0.734740
20	1	0	-3.318771	2.759290	1.280660
21	1	0	-4.045558	1.172361	1.470187
22	6	0	-4.623193	2.160088	-0.375805
23	1	0	-4.180180	2.845793	-1.105987
24	1	0	-5.526276	2.634742	0.018213
25	6	0	-4.993555	0.836615	-1.034718
26	1	0	-5.758484	0.324627	-0.435609
27	1	0	-5.419224	1.001961	-2.030683
28	6	0	-4.135024	-1.350955	-1.851121
29	1	0	-5.019820	-1.200018	-2.473637
30	1	0	-4.375362	-2.127471	-1.112258
31	6	0	-2.925807	-1.743631	-2.688464
32	1	0	-3.095007	-2.702359	-3.187105
33	1	0	-2.767451	-0.989075	-3.466964
34	6	0	-1.711602	-1.842393	-1.769686
35	1	0	-1.745336	-2.784636	-1.209270
36	1	0	-0.793484	-1.857611	-2.362819
37	6	0	-2.607203	0.090178	-0.636864
38	6	0	3.512283	2.134285	0.541743
39	1	0	4.045725	1.497041	1.255900
40	1	0	3.175792	3.013269	1.089441
41	6	0	4.392846	2.469258	-0.655082
42	1	0	5.270596	3.049368	-0.356832
43	1	0	3.828712	3.070944	-1.375418
44	6	0	4.841876	1.149961	-1.275313
45	1	0	5.121886	1.278010	-2.328100
46	1	0	5.730644	0.780119	-0.748951
47	6	0	4.301609	-1.204010	-1.717617
48	1	0	5.272605	-1.415143	-1.254489
49	1	0	4.473726	-1.086845	-2.795376
50	6	0	3.310660	-2.326668	-1.451067
51	1	0	3.378611	-2.667821	-0.412792
52	1	0	3.540598	-3.179620	-2.095691
53	6	0	1.905176	-1.793574	-1.712645
54	1	0	1.812506	-1.465950	-2.758315
55	1	0	1.160502	-2.569919	-1.545686
56	6	0	2.568128	0.222340	-0.675118
57	6	0	1.381640	-0.630186	2.115261
58	6	0	0.063254	-2.699652	0.962882
59	6	0	-1.348895	-0.705005	2.126232

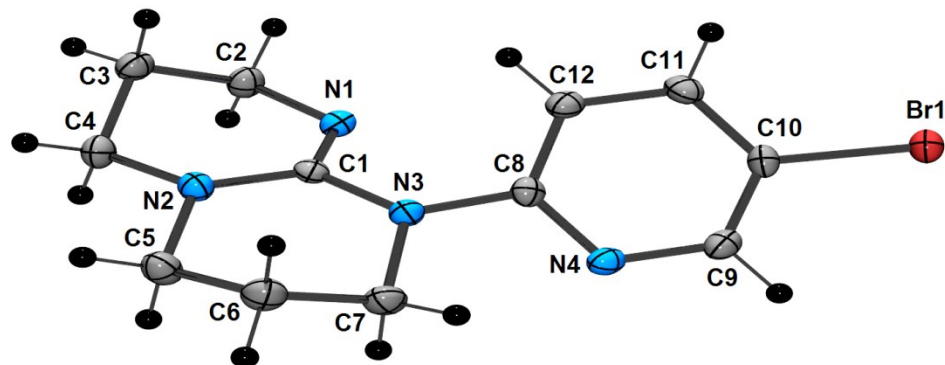
Appendix

Appendix 1 : CCDC numbers for Chapters 2, 3, 4, 5A and 5B

The crystallographic reports and cif files of the structures listed below are available from the Cambridge Crystallographic Data Centre (CCDC) and may be downloaded electronically from the internet site : www.ccdc.cam.ac.uk/data_request/cif.

Chapter	Complex/ Ligand	CCDC N°
Chapter 2	2-2a [C ₁₂ H ₁₅ BrN ₄]	954083
	2-1b [C ₃₂ H ₃₂ F ₁₂ N ₈ P ₂ Ru]	954084
	2-3b [C ₃₁ H ₃₁ F ₁₂ N ₉ P ₂ Ru]	954085
	2-4b [C ₄₆ H ₆₄ ClF ₁₂ N ₉ O ₇ P ₂ Ru]	954086
Chapter 3	3-L1 [C ₁₈ H ₂₆ N ₈]	964843
	3-(1-meso) [C ₆₂ H ₆₄ F ₂₄ N ₁₈ P ₄ Ru ₂]	964842
	3-2 [C ₃₉ H ₄₇ F ₁₂ N ₉ O ₃ P ₂ Ru]	972273
	3-3 [C ₃₅ H ₃₉ F ₁₂ N ₉ OP ₂ Ru]	972274
	3-4 [C ₃₆ H ₄₁ F ₁₂ N ₉ O ₃ P ₂ Ru]	972275
Chapter 4	4-L1 [C ₁₉ H ₂₇ N ₇]	988217
	4-1 [C ₄₂ H ₄₅ F ₁₂ N ₁₁ P ₂ Ru]	978431
	4-2 [C ₄₄ H ₅₀ F ₁₂ N ₁₀ OP ₂ Ru]	988218
	4-3 [C ₄₁ H ₄₅ BrF ₁₂ N ₁₂ OP ₂ Ru]	988219
	4-4 [C ₆₆ H ₉₈ F ₁₂ N ₁₂ O ₉ P ₂ Ru]	988220
Chapter 5A	5A-1 [C ₂₂ H ₂₇ BrN ₇ O ₃ Re]	922649
	5A-2 [C ₂₁ H ₂₆ BrN ₈ O ₃ Re]	975057
Chapter 5B	5B-1b [C ₈₈ H ₆₈ B ₂ FeN ₈]	962834
	5B-3 [C ₄₀ H ₃₂ CoF ₁₂ N ₈ O ₂ P ₂]	962835
	5B-5 [C ₄₂ H ₃₁ CuF ₁₂ N ₉ P ₂]	962836

Appendix 2 : Crystal Data for Chapter 2

2-2a [C₁₂H₁₅BrN₄]Table 1. Crystal data and structure refinement for C₁₂H₁₅BrN₄ (2-2a)

Empirical formula	C ₁₂ H ₁₅ Br N ₄
Formula weight	295.19
Temperature	100(2) K
Wavelength	1.54178 Å
Crystal system	Monoclinic
Space group	P2 ₁ /n
Unit cell dimensions	a = 5.0181(2) Å α = 90° b = 18.1139(6) Å β = 92.255(2)° c = 13.0979(4) Å γ = 90°
Volume	1189.64(7) Å ³
Z	4
Density (calculated)	1.648 g/cm ³
Absorption coefficient	4.566 mm ⁻¹
F(000)	600
Crystal size	0.13 x 0.03 x 0.01 mm
Theta range for data collection	4.167 to 70.952°
Index ranges	-6 ≤ h ≤ 6, -22 ≤ k ≤ 21, -15 ≤ l ≤ 16
Reflections collected	7733
Independent reflections	2237 [R(int) = 0.069]

Absorption correction	Semi-empirical from equivalents
Max. and min. transmission	0.7534 and 0.5344
Refinement method	Full-matrix least-squares on F ²
Data / restraints / parameters	2237 / 0 / 154
Goodness-of-fit on F ²	1.028
Final R indices [I>2sigma(I)]	R1 = 0.0366, wR2 = 0.0899
R indices (all data)	R1 = 0.0442, wR2 = 0.0950
Largest diff. peak and hole	0.936 and -0.762 e/Å ³

Table 2. Bond lengths [Å] and angles [°] for C12H15BrN4 (**2-2a**)

Br(1)-C(10)	1.903(3)
N(1)-C(1)	1.283(4)
N(1)-C(2)	1.458(4)
N(2)-C(1)	1.391(4)
N(2)-C(4)	1.459(4)
N(2)-C(5)	1.463(4)
N(3)-C(8)	1.412(4)
N(3)-C(1)	1.413(4)
N(3)-C(7)	1.472(4)
N(4)-C(8)	1.342(4)
N(4)-C(9)	1.344(4)
C(2)-C(3)	1.521(4)
C(3)-C(4)	1.510(4)
C(5)-C(6)	1.501(4)
C(6)-C(7)	1.514(4)
C(8)-C(12)	1.404(4)
C(9)-C(10)	1.368(4)
C(10)-C(11)	1.392(4)
C(11)-C(12)	1.373(4)
C(1)-N(1)-C(2)	118.9(2)
C(1)-N(2)-C(4)	117.3(2)
C(1)-N(2)-C(5)	122.8(2)
C(4)-N(2)-C(5)	113.3(2)
C(8)-N(3)-C(1)	121.1(2)
C(8)-N(3)-C(7)	116.4(2)
C(1)-N(3)-C(7)	119.8(2)
C(8)-N(4)-C(9)	117.9(3)
N(1)-C(1)-N(2)	126.2(3)
N(1)-C(1)-N(3)	118.5(2)
N(2)-C(1)-N(3)	115.2(2)
N(1)-C(2)-C(3)	113.2(2)
C(4)-C(3)-C(2)	108.1(2)
N(2)-C(4)-C(3)	110.2(2)
N(2)-C(5)-C(6)	110.3(2)
C(5)-C(6)-C(7)	109.6(2)
N(3)-C(7)-C(6)	109.5(2)

N(4)-C(8)-C(12)	122.2(3)
N(4)-C(8)-N(3)	114.9(3)
C(12)-C(8)-N(3)	122.6(3)
N(4)-C(9)-C(10)	122.9(3)
C(9)-C(10)-C(11)	119.5(3)
C(9)-C(10)-BR1	119.5(2)
C(11)-C(10)-BR1	121.0(2)
C(12)-C(11)-C(10)	118.4(3)
C(11)-C(12)-C(8)	118.9(3)

2-1b [C₃₂H₃₂F₁₂N₈P₂Ru]

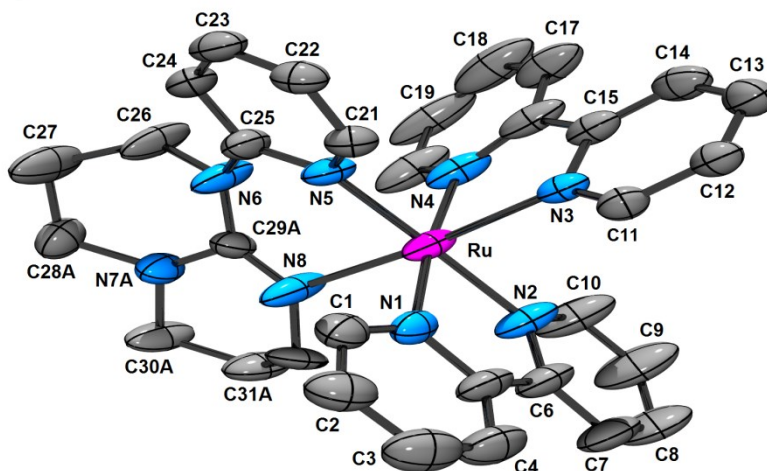


Table 3. Crystal data and structure refinement for C₃₂H₃₂F₁₂N₈P₂Ru (**2-1b**)

Empirical formula	C ₃₂ H ₃₂ F ₁₂ N ₈ P ₂ Ru
Formula weight	919.66
Temperature	150(2) K
Wavelength	1.54178 Å
Crystal system	Monoclinic
Space group	C2/c
Unit cell dimensions	a = 35.6514(10) Å α = 90° b = 10.1520(3) Å β = 130.121(1)° c = 26.1512(12) Å γ = 90°
Volume	7237.7(5) Å ³
Z	8
Density (calculated)	1.688 g/cm ³

Absorption coefficient	5.252 mm ⁻¹
F(000)	3696
Crystal size	0.13 x 0.09 x 0.04 mm
Theta range for data collection	3.242 to 87.566 deg.
Index ranges	-44<=h<=43, -12<=k<=12, -33<=l<=33
Reflections collected	48623
Independent reflections	7142 [R(int) = 0.070]
Absorption correction	Semi-empirical from equivalents
Max. and min. transmission	0.8584 and 0.4935
Refinement method	Full-matrix least-squares on F ²
Data / restraints / parameters	7142 / 1087 / 676
Goodness-of-fit on F ²	0.983
Final R indices [I>2sigma(I)]	R1 = 0.0642, wR2 = 0.1771
R indices (all data)	R1 = 0.0814, wR2 = 0.1895
Largest diff. peak and hole	3.298 and -1.093 e/A ³

Table 4. Bond lengths [Å] and angles [°] for C32H32F12N8P2Ru (**2-1b**)

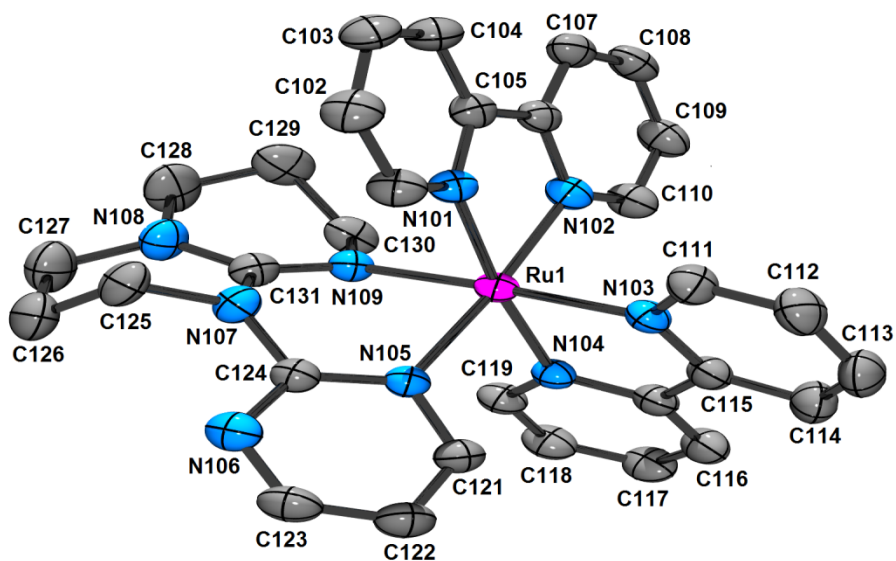
Ru-N(2)	1.992(4)
Ru-N(5)	2.011(4)
Ru-N(1)	2.036(4)
Ru-N(4)	2.052(5)
Ru-N(3)	2.147(5)
Ru-N(8)	2.187(5)
N(1)-C(5)	1.327(6)
N(1)-C(1)	1.336(7)
N(2)-C(10)	1.329(9)
N(2)-C(6)	1.353(7)
N(3)-C(15)	1.336(6)
N(3)-C(11)	1.379(6)
N(4)-C(20)	1.390(7)
N(4)-C(16)	1.395(9)
N(5)-C(21)	1.379(6)
N(5)-C(25)	1.376(6)
N(6)-C(29b)	1.305(19)
N(6)-C(25)	1.418(7)
N(6)-C(26)	1.484(6)
N(6)-C(29a)	1.497(17)
N(8)-C(29b)	1.294(15)
N(8)-C(32b)	1.33(2)
N(8)-C(29a)	1.348(13)
N(8)-C(32a)	1.567(15)
C(1)-C(2)	1.356(8)
C(2)-C(3)	1.356(10)

C (3) -C (4)	1.357 (10)
C (4) -C (5)	1.366 (8)
C (5) -C (6)	1.460 (9)
C (6) -C (7)	1.336 (8)
C (7) -C (8)	1.371 (10)
C (8) -C (9)	1.329 (10)
C (9) -C (10)	1.322 (8)
C (11) -C (12)	1.412 (7)
C (12) -C (13)	1.344 (7)
C (13) -C (14)	1.428 (8)
C (14) -C (15)	1.423 (9)
C (15) -C (16)	1.497 (8)
C (16) -C (17)	1.365 (8)
C (17) -C (18)	1.420 (12)
C (18) -C (19)	1.364 (13)
C (19) -C (20)	1.364 (11)
C (21) -C (22)	1.318 (6)
C (22) -C (23)	1.409 (7)
C (23) -C (24)	1.387 (8)
C (24) -C (25)	1.348 (6)
C (26) -C (27)	1.568 (11)
C (27) -C (28a)	1.519 (13)
C (27) -C (28b)	1.533 (14)
C (28a) -N (7a)	1.470 (17)
C (29a) -N (7a)	1.410 (17)
N (7a) -C (30a)	1.438 (12)
C (30a) -C (31a)	1.54 (2)
C (31a) -C (32a)	1.53 (2)
C (28b) -N (7b)	1.512 (18)
C (29b) -N (7b)	1.38 (2)
N (7b) -C (30b)	1.432 (13)
C (30b) -C (31b)	1.49 (2)
C (31b) -C (32b)	1.55 (3)
P (1) -F (14)	1.553 (3)
P (1) -F (12)	1.556 (4)
P (1) -F (11)	1.566 (3)
P (1) -F (15)	1.573 (3)
P (1) -F (13)	1.608 (4)
P (1) -F (16)	1.628 (4)
P (2) -F (23)	1.527 (10)
P (2) -F (25)	1.553 (11)
P (2) -F (22)	1.561 (11)
P (2) -F (21)	1.558 (10)
P (2) -F (24)	1.586 (10)
P (2) -F (26)	1.595 (11)
F (22) -F (23)	2.030 (18)
P (3) -F (33)	1.540 (11)
P (3) -F (31)	1.545 (11)
P (3) -F (36)	1.551 (11)
P (3) -F (32)	1.562 (11)
P (3) -F (35)	1.562 (11)
P (3) -F (34)	1.603 (11)
P (4) -F (46)	1.546 (12)
P (4) -F (43)	1.550 (13)
P (4) -F (44)	1.564 (12)
P (4) -F (45)	1.566 (12)
P (4) -F (41)	1.571 (12)
P (4) -F (42)	1.585 (12)

N (2) -RU-N (5)	173.83 (18)
N (2) -RU-N (1)	81.58 (18)
N (5) -RU-N (1)	92.67 (16)
N (2) -RU-N (4)	94.10 (18)
N (5) -RU-N (4)	91.47 (17)
N (1) -RU-N (4)	174.05 (18)
N (2) -RU-N (3)	85.04 (18)
N (5) -RU-N (3)	93.39 (15)
N (1) -RU-N (3)	96.16 (15)
N (4) -RU-N (3)	79.32 (18)
N (2) -RU-N (8)	99.23 (19)
N (5) -RU-N (8)	82.76 (17)
N (1) -RU-N (8)	88.37 (18)
N (4) -RU-N (8)	96.4 (2)
N (3) -RU-N (8)	174.20 (15)
C (5) -N (1) -C (1)	118.5 (5)
C (5) -N (1) -RU	113.0 (4)
C (1) -N (1) -RU	128.5 (3)
C (10) -N (2) -C (6)	118.6 (5)
C (10) -N (2) -RU	128.4 (4)
C (6) -N (2) -RU	112.9 (4)
C (15) -N (3) -C (11)	116.0 (5)
C (15) -N (3) -RU	115.1 (4)
C (11) -N (3) -RU	128.8 (3)
C (20) -N (4) -C (16)	120.8 (6)
C (20) -N (4) -RU	125.7 (5)
C (16) -N (4) -RU	113.5 (3)
C (21) -N (5) -C (25)	120.7 (4)
C (21) -N (5) -RU	117.0 (3)
C (25) -N (5) -RU	122.1 (3)
C (29B) -N (6) -C (25)	127.8 (8)
C (29B) -N (6) -C (26)	108.2 (7)
C (25) -N (6) -C (26)	121.8 (4)
C (25) -N (6) -C (29A)	114.4 (7)
C (26) -N (6) -C (29A)	110.5 (6)
C (29B) -N (8) -C (32B)	118.0 (12)
C (29A) -N (8) -C (32A)	100.5 (10)
C (29B) -N (8) -RU	119.9 (8)
C (32B) -N (8) -RU	117.2 (9)
C (29A) -N (8) -RU	130.2 (8)
C (32A) -N (8) -RU	122.9 (6)
N (1) -C (1) -C (2)	124.4 (6)
C (1) -C (2) -C (3)	117.1 (7)
C (4) -C (3) -C (2)	118.8 (6)
C (3) -C (4) -C (5)	122.2 (6)
N (1) -C (5) -C (4)	118.9 (6)
N (1) -C (5) -C (6)	115.3 (5)
C (4) -C (5) -C (6)	125.8 (5)
C (7) -C (6) -N (2)	119.1 (6)
C (7) -C (6) -C (5)	124.2 (6)
N (2) -C (6) -C (5)	116.6 (5)
C (6) -C (7) -C (8)	120.5 (6)
C (9) -C (8) -C (7)	119.7 (6)
C (10) -C (9) -C (8)	118.4 (8)
C (9) -C (10) -N (2)	123.6 (7)
N (3) -C (11) -C (12)	125.3 (4)
C (13) -C (12) -C (11)	119.7 (5)
C (12) -C (13) -C (14)	115.7 (5)
C (15) -C (14) -C (13)	122.8 (5)

N(3)-C(15)-C(14)	120.5(5)
N(3)-C(15)-C(16)	113.6(5)
C(14)-C(15)-C(16)	125.9(5)
C(17)-C(16)-N(4)	119.5(6)
C(17)-C(16)-C(15)	122.8(7)
N(4)-C(16)-C(15)	117.7(5)
C(16)-C(17)-C(18)	117.9(8)
C(19)-C(18)-C(17)	122.4(8)
C(20)-C(19)-C(18)	118.6(8)
C(19)-C(20)-N(4)	120.2(8)
C(22)-C(21)-N(5)	122.5(5)
C(21)-C(22)-C(23)	115.8(5)
C(24)-C(23)-C(22)	123.3(4)
C(25)-C(24)-C(23)	118.0(5)
C(24)-C(25)-N(5)	119.2(5)
C(24)-C(25)-N(6)	119.7(5)
N(5)-C(25)-N(6)	121.0(4)
N(6)-C(26)-C(27)	111.6(6)
C(28A)-C(27)-C(26)	118.4(8)
C(28B)-C(27)-C(26)	95.3(8)
N(7A)-C(28A)-C(27)	104.7(9)
N(8)-C(29A)-N(7A)	134.0(14)
N(8)-C(29A)-N(6)	104.6(9)
N(7A)-C(29A)-N(6)	116.5(10)
C(29A)-N(7A)-C(30A)	121.1(12)
C(29A)-N(7A)-C(28A)	129.3(11)
C(30A)-N(7A)-C(28A)	107.4(11)
N(7A)-C(30A)-C(31A)	104.1(13)
C(32A)-C(31A)-C(30A)	111.5(15)
C(31A)-C(32A)-N(8)	108.5(12)
N(7B)-C(28B)-C(27)	111.1(11)
N(8)-C(29B)-N(6)	120.2(13)
N(8)-C(29B)-N(7B)	123.0(15)
N(6)-C(29B)-N(7B)	113.9(12)
C(29B)-N(7B)-C(30B)	123.5(13)
C(29B)-N(7B)-C(28B)	129.6(13)
C(30B)-N(7B)-C(28B)	105.8(12)
N(7B)-C(30B)-C(31B)	105.7(12)
C(30B)-C(31B)-C(32B)	112.6(15)
N(8)-C(32B)-C(31B)	114.3(13)
F(14)-P(1)-F(12)	90.8(2)
F(14)-P(1)-F(11)	179.6(2)
F(12)-P(1)-F(11)	88.8(2)
F(14)-P(1)-F(15)	89.4(2)
F(12)-P(1)-F(15)	179.0(3)
F(11)-P(1)-F(15)	91.0(2)
F(14)-P(1)-F(13)	86.2(2)
F(12)-P(1)-F(13)	88.1(3)
F(11)-P(1)-F(13)	93.8(2)
F(15)-P(1)-F(13)	92.9(2)
F(14)-P(1)-F(16)	93.1(2)
F(12)-P(1)-F(16)	93.5(3)
F(11)-P(1)-F(16)	86.9(2)
F(15)-P(1)-F(16)	85.4(2)
F(13)-P(1)-F(16)	178.2(3)
F(23)-P(2)-F(25)	169.1(11)
F(23)-P(2)-F(22)	82.2(9)
F(25)-P(2)-F(22)	106.9(12)
F(23)-P(2)-F(21)	88.6(7)

F(25)-P(2)-F(21)	97.1(10)
F(22)-P(2)-F(21)	90.3(10)
F(23)-P(2)-F(24)	91.8(9)
F(25)-P(2)-F(24)	83.0(10)
F(22)-P(2)-F(24)	86.0(7)
F(21)-P(2)-F(24)	176.1(11)
F(23)-P(2)-F(26)	89.1(10)
F(25)-P(2)-F(26)	82.8(8)
F(22)-P(2)-F(26)	167.2(12)
F(21)-P(2)-F(26)	80.2(9)
F(24)-P(2)-F(26)	103.7(10)
P(2)-F(22)-F(23)	48.2(5)
P(2)-F(23)-F(22)	49.6(6)
F(33)-P(3)-F(31)	89.7(8)
F(33)-P(3)-F(36)	167.7(12)
F(31)-P(3)-F(36)	79.1(11)
F(33)-P(3)-F(32)	87.2(9)
F(31)-P(3)-F(32)	93.1(9)
F(36)-P(3)-F(32)	98.3(11)
F(33)-P(3)-F(35)	89.3(10)
F(31)-P(3)-F(35)	93.9(10)
F(36)-P(3)-F(35)	86.6(8)
F(32)-P(3)-F(35)	172.1(12)
F(33)-P(3)-F(34)	90.7(10)
F(31)-P(3)-F(34)	179.2(12)
F(36)-P(3)-F(34)	100.6(12)
F(32)-P(3)-F(34)	86.2(7)
F(35)-P(3)-F(34)	86.8(11)
F(46)-P(4)-F(43)	165.4(14)
F(46)-P(4)-F(44)	111.2(14)
F(43)-P(4)-F(44)	83.5(12)
F(46)-P(4)-F(45)	86.8(8)
F(43)-P(4)-F(45)	92.8(13)
F(44)-P(4)-F(45)	89.9(13)
F(46)-P(4)-F(41)	77.5(11)
F(43)-P(4)-F(41)	88.0(9)
F(44)-P(4)-F(41)	170.7(13)
F(45)-P(4)-F(41)	94.1(14)
F(46)-P(4)-F(42)	99.8(13)
F(43)-P(4)-F(42)	81.6(12)
F(44)-P(4)-F(42)	84.8(8)
F(45)-P(4)-F(42)	172.7(14)
F(41)-P(4)-F(42)	90.4(11)

2-3b [C₃₁H₃₁F₁₂N₉P₂Ru]**Table 5.** Crystal data and structure refinement for C₃₁H₃₁F₁₂N₉P₂Ru (**2-3b**)

Empirical formula	C ₃₁ H ₃₁ F ₁₂ N ₉ P ₂ Ru
Formula weight	920.66
Temperature	150(2) K
Wavelength	1.54178 Å
Crystal system	Monoclinic
Space group	P2 ₁ /c
Unit cell dimensions	a = 20.4021(8) Å α = 90° b = 10.5565(4) Å β = 95.787(2)° c = 16.4117(7) Å γ = 90°
Volume	3516.7(2) Å ³
Z	4
Density (calculated)	1.739 g/cm ³
Absorption coefficient	5.414 mm ⁻¹
F(000)	1848
Crystal size	0.23 x 0.21 x 0.01 mm
Theta range for data collection	2.18 to 72.54°

Index ranges	$-25 \leq h \leq 25, -13 \leq k \leq 13, -19 \leq l \leq 16$
Reflections collected	45600
Independent reflections	6818 [R _{int} = 0.057]
Absorption correction	Semi-empirical from equivalents
Max. and min. transmission	0.9473 and 0.5329
Refinement method	Full-matrix least-squares on F ²
Data / restraints / parameters	6818 / 672 / 623
Goodness-of-fit on F ²	1.038
Final R indices [I>2sigma(I)]	R1 = 0.0362, wR2 = 0.0971
R indices (all data)	R1 = 0.0415, wR2 = 0.0999
Extinction coefficient	0.00025(4)
Largest diff. peak and hole	0.882 and -0.827 e/Å ³

Table 6. Bond lengths [Å] and angles [°] for C₃₁H₃₁F₁₂N₉P₂Ru (**2-3b**)

		C(104)-C(105)	1.388(4)
Ru(1)-N(103)	2.051(2)	C(105)-C(106)	1.472(3)
Ru(1)-N(102)	2.060(2)	C(106)-C(107)	1.392(4)
Ru(1)-N(101)	2.0663(19)	C(107)-C(108)	1.385(4)
Ru(1)-N(104)	2.0665(19)	C(108)-C(109)	1.378(4)
Ru(1)-N(109)	2.087(2)	C(109)-C(110)	1.385(4)
Ru(1)-N(105)	2.0900(19)	C(111)-C(112)	1.373(4)
N(101)-C(101)	1.344(3)	C(112)-C(113)	1.387(4)
N(101)-C(105)	1.360(3)	C(113)-C(114)	1.385(4)
N(102)-C(110)	1.347(3)	C(114)-C(115)	1.385(4)
N(102)-C(106)	1.365(3)	C(115)-C(116)	1.483(3)
N(103)-C(111)	1.353(3)	C(116)-C(117)	1.389(3)
N(103)-C(115)	1.364(3)	C(117)-C(118)	1.389(4)
N(104)-C(120)	1.346(3)	C(118)-C(119)	1.375(4)
N(104)-C(116)	1.358(3)	C(119)-C(120)	1.382(3)
N(105)-C(124)	1.351(3)	C(121)-C(122)	1.376(4)
N(105)-C(121)	1.362(3)	C(122)-C(123)	1.374(4)
N(106)-C(124)	1.331(3)	C(125)-C(126)	1.506(4)
N(106)-C(123)	1.343(4)	C(126)-C(127)	1.531(4)
N(107)-C(124)	1.392(3)	C(128)-C(129)	1.503(5)
N(107)-C(131)	1.408(3)	C(129)-C(130)	1.509(4)
N(107)-C(125)	1.486(3)	P(1)-F(103)	1.576(2)
N(108)-C(131)	1.352(4)	P(1)-F(106)	1.5889(18)
N(108)-C(128)	1.463(4)	P(1)-F(104)	1.5925(18)
N(108)-C(127)	1.475(4)	P(1)-F(105)	1.596(2)
N(109)-C(131)	1.314(4)	P(1)-F(102)	1.5999(19)
N(109)-C(130)	1.466(3)	P(1)-F(101)	1.602(2)
C(101)-C(102)	1.382(4)	P(2)-F(203)	1.573(9)
C(102)-C(103)	1.379(4)	P(2)-F(202)	1.594(8)
C(103)-C(104)	1.381(4)	P(2)-F(205)	1.594(8)

P(2)-F(204)	1.595(9)	C(103)-C(104)-C(105)	
P(2)-F(206)	1.599(9)	119.4(3)	
P(2)-F(201)	1.621(8)	N(101)-C(105)-C(104)	121.1(2)
P(3)-F(303)	1.570(10)	N(101)-C(105)-C(106)	115.0(2)
P(3)-F(305)	1.591(9)	C(104)-C(105)-C(106)	123.9(2)
P(3)-F(304)	1.592(10)	N(102)-C(106)-C(107)	121.0(2)
P(3)-F(302)	1.597(10)	N(102)-C(106)-C(105)	114.9(2)
P(3)-F(306)	1.600(10)	C(107)-C(106)-C(105)	124.0(2)
P(3)-F(301)	1.613(10)	C(108)-C(107)-C(106)	119.3(3)
P(4)-F(403)	1.579(11)	C(109)-C(108)-C(107)	119.5(3)
P(4)-F(405)	1.591(11)	C(108)-C(109)-C(110)	119.1(3)
P(4)-F(404)	1.594(12)	N(102)-C(110)-C(109)	122.2(3)
P(4)-F(406)	1.599(11)	N(103)-C(111)-C(112)	122.4(3)
P(4)-F(401)	1.601(11)	C(111)-C(112)-C(113)	119.2(3)
P(4)-F(402)	1.605(11)	C(114)-C(113)-C(112)	119.2(3)
		C(113)-C(114)-C(115)	119.2(3)
N(103)-RU1-N(102)	89.61(8)	N(103)-C(115)-C(114)	121.6(2)
N(103)-RU1-N(101)	97.84(8)	N(103)-C(115)-C(116)	114.3(2)
N(102)-RU1-N(101)	78.88(9)	C(114)-C(115)-C(116)	124.1(2)
N(103)-RU1-N(104)	78.77(8)	N(104)-C(116)-C(117)	121.4(2)
N(102)-RU1-N(104)	94.84(8)	N(104)-C(116)-C(115)	114.6(2)
N(101)-RU1-N(104)	172.95(8)	C(117)-C(116)-C(115)	124.0(2)
N(103)-RU1-N(109)	176.15(8)	C(116)-C(117)-C(118)	118.8(3)
N(102)-RU1-N(109)	91.57(8)	C(119)-C(118)-C(117)	119.5(2)
N(101)-RU1-N(109)	85.99(8)	C(118)-C(119)-C(120)	119.2(3)
N(104)-RU1-N(109)	97.47(8)	N(104)-C(120)-C(119)	121.9(3)
N(103)-RU1-N(105)	94.05(8)	N(105)-C(121)-C(122)	122.4(2)
N(102)-RU1-N(105)	175.21(8)	C(123)-C(122)-C(121)	116.8(3)
N(101)-RU1-N(105)	97.53(8)	N(106)-C(123)-C(122)	122.2(2)
N(104)-RU1-N(105)	88.91(8)	N(106)-C(124)-N(105)	125.0(2)
N(109)-RU1-N(105)	84.98(8)	N(106)-C(124)-N(107)	115.8(2)
C(101)-N(101)-C(105)	118.7(2)	N(105)-C(124)-N(107)	119.0(2)
C(101)-N(101)-RU1	126.52(17)	N(107)-C(125)-C(126)	108.1(2)
C(105)-N(101)-RU1	114.49(16)	C(125)-C(126)-C(127)	105.9(3)
C(110)-N(102)-C(106)	118.9(2)	N(108)-C(127)-C(126)	113.0(3)
C(110)-N(102)-RU1	126.33(18)	N(108)-C(128)-C(129)	111.4(2)
C(106)-N(102)-RU1	114.63(17)	C(128)-C(129)-C(130)	107.8(3)
C(111)-N(103)-C(115)	118.3(2)	N(109)-C(130)-C(129)	109.9(2)
C(111)-N(103)-RU1	125.41(18)	N(109)-C(131)-N(108)	125.1(2)
C(115)-N(103)-RU1	116.25(17)	N(109)-C(131)-N(107)	120.5(2)
C(120)-N(104)-C(116)	119.0(2)	N(108)-C(131)-N(107)	114.3(2)
C(120)-N(104)-RU1	125.32(17)	F(103)-P(1)-F(106)	90.01(12)
C(116)-N(104)-RU1	115.53(16)	F(103)-P(1)-F(104)	91.72(13)
C(124)-N(105)-C(121)	115.6(2)	F(106)-P(1)-F(104)	90.45(10)
C(124)-N(105)-RU1	123.44(16)	F(103)-P(1)-F(105)	90.98(14)
C(121)-N(105)-RU1	120.93(16)	F(106)-P(1)-F(105)	178.98(15)
C(124)-N(106)-C(123)	117.4(2)	F(104)-P(1)-F(105)	89.74(12)
C(124)-N(107)-C(131)	124.5(2)	F(103)-P(1)-F(102)	89.58(13)
C(124)-N(107)-C(125)	117.1(2)	F(106)-P(1)-F(102)	89.52(11)
C(131)-N(107)-C(125)	115.1(2)	F(104)-P(1)-F(102)	178.70(13)
C(131)-N(108)-C(128)	121.0(3)	F(105)-P(1)-F(102)	90.28(13)
C(131)-N(108)-C(127)	125.2(2)	F(103)-P(1)-F(101)	179.46(14)
C(128)-N(108)-C(127)	113.1(2)	F(106)-P(1)-F(101)	89.50(12)
C(131)-N(109)-C(130)	114.4(2)	F(104)-P(1)-F(101)	88.51(11)
C(131)-N(109)-RU1	123.01(18)	F(105)-P(1)-F(101)	89.50(15)
C(130)-N(109)-RU1	122.10(18)	F(102)-P(1)-F(101)	90.19(12)
N(101)-C(101)-C(102)	122.3(3)	F(203)-P(2)-F(202)	91.3(7)
C(103)-C(102)-C(101)	118.9(3)	F(203)-P(2)-F(205)	92.2(8)
C(102)-C(103)-C(104)	119.3(3)	F(202)-P(2)-F(205)	90.3(7)

F(203)-P(2)-F(204)	90.4(8)
F(202)-P(2)-F(204)	178.2(9)
F(205)-P(2)-F(204)	89.4(7)
F(203)-P(2)-F(206)	89.6(8)
F(202)-P(2)-F(206)	90.4(8)
F(205)-P(2)-F(206)	178.1(9)
F(204)-P(2)-F(206)	89.9(8)
F(203)-P(2)-F(201)	178.1(8)
F(202)-P(2)-F(201)	90.1(7)
F(205)-P(2)-F(201)	89.1(7)
F(204)-P(2)-F(201)	88.2(7)
F(206)-P(2)-F(201)	89.1(7)
F(303)-P(3)-F(305)	92.5(9)
F(303)-P(3)-F(304)	91.8(9)
F(305)-P(3)-F(304)	90.8(9)
F(303)-P(3)-F(302)	92.6(8)
F(305)-P(3)-F(302)	89.9(8)
F(304)-P(3)-F(302)	175.5(9)
F(303)-P(3)-F(306)	89.7(9)
F(305)-P(3)-F(306)	177.7(10)
F(304)-P(3)-F(306)	89.8(9)
F(302)-P(3)-F(306)	89.4(8)
F(303)-P(3)-F(301)	177.8(11)
F(305)-P(3)-F(301)	89.1(8)
F(304)-P(3)-F(301)	86.8(8)
F(302)-P(3)-F(301)	88.8(8)
F(306)-P(3)-F(301)	88.7(8)
F(403)-P(4)-F(405)	90.4(9)
F(403)-P(4)-F(404)	89.6(10)
F(405)-P(4)-F(404)	93.0(10)
F(403)-P(4)-F(406)	90.1(10)
F(405)-P(4)-F(406)	177.3(13)
F(404)-P(4)-F(406)	89.6(11)
F(403)-P(4)-F(401)	179.2(10)
F(405)-P(4)-F(401)	89.8(9)
F(404)-P(4)-F(401)	89.6(9)
F(406)-P(4)-F(401)	89.8(10)
F(403)-P(4)-F(402)	90.0(8)
F(405)-P(4)-F(402)	88.5(9)
F(404)-P(4)-F(402)	178.4(11)
F(406)-P(4)-F(402)	88.9(11)
F(401)-P(4)-F(402)	90.8(9)

2-4b [C₄₆H₆₄ClF₁₂N₉O₇P₂Ru]

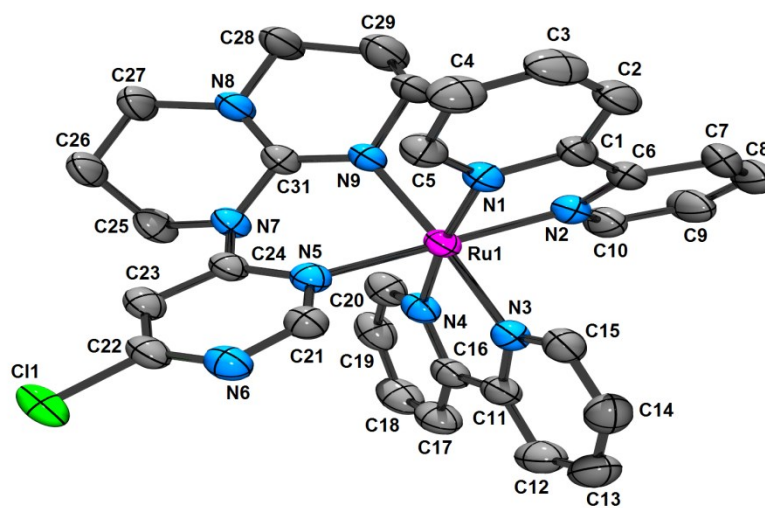


Table 7. Crystal data and structure refinement for C₃₄H₃₆ClF₁₂N₉O₇P₂Ru (**2-4b**).

Empirical formula	C ₃₄ H ₃₆ Cl F ₁₂ N ₉ O ₇ P ₂ Ru
Formula weight	1013.18
Temperature	150(2) K
Wavelength	1.54178 Å
Crystal system	Triclinic
Space group	P-1
Unit cell dimensions	a = 12.0837(5) Å α = 88.110(2) b = 12.3164(4) Å β = 81.464(2) c = 14.5069(5) Å γ = 82.341(2)
Volume	2115.87(13) Å ³
Z	2
Density (calculated)	1.590 g/cm ³
Absorption coefficient	5.144 mm ⁻¹
F(000)	1020
Crystal size	0.23 x 0.13 x 0.07 mm
Theta range for data collection	3.081 to 69.724 deg.
Index ranges	-14 ≤ h ≤ 12, -14 ≤ k ≤ 14, -17 ≤ l ≤ 17

Appendix

Reflections collected	43073
Independent reflections	7827 [R(int) = 0.045]
Absorption correction	Semi-empirical from equivalents
Max. and min. transmission	0.5047 and 0.2910
Refinement method	Full-matrix least-squares on F ²
Data / restraints / parameters	7827 / 0 / 543
Goodness-of-fit on F ²	1.089
Final R indices [I>2sigma(I)]	R1 = 0.0611, wR2 = 0.1853
R indices (all data)	R1 = 0.0623, wR2 = 0.1867
Largest diff. peak and hole	1.532 and -1.016 e/A ³

Table 8. Bond lengths [Å] and angles [°] for C₃₄H₃₆ClF₁₂N₉OP₂Ru (**2-4b**)

Ru(1)-N(2)	2.054(4)
Ru(1)-N(3)	2.054(4)
Ru(1)-N(1)	2.062(4)
Ru(1)-N(4)	2.070(4)
Ru(1)-N(5)	2.089(4)
Ru(1)-N(9)	2.090(4)
Cl(1)-C(22)	1.732(5)
P(1)-F(6)	1.550(5)
P(1)-F(5)	1.557(5)
P(1)-F(2)	1.564(5)
P(1)-F(1)	1.575(5)
P(1)-F(3)	1.589(5)
P(1)-F(4)	1.595(4)
P(2)-F(11)	1.547(5)
P(2)-F(8)	1.563(5)
P(2)-F(7)	1.573(5)
P(2)-F(9)	1.592(4)
P(2)-F(12)	1.594(4)
P(2)-F(10)	1.595(4)
O(1)-C(33)	1.203(11)
N(1)-C(5)	1.335(6)
N(1)-C(1)	1.359(6)
N(2)-C(10)	1.352(7)
N(2)-C(6)	1.352(7)
N(3)-C(15)	1.349(6)
N(3)-C(11)	1.354(6)
N(4)-C(20)	1.343(7)
N(4)-C(16)	1.355(6)
N(5)-C(21)	1.338(6)
N(5)-C(24)	1.353(6)
N(6)-C(22)	1.322(7)
N(6)-C(21)	1.322(6)
N(7)-C(24)	1.377(6)
N(7)-C(31)	1.421(6)
N(7)-C(25)	1.476(6)

Appendix

N(8)-C(31)	1.336(6)
N(8)-C(27)	1.466(6)
N(8)-C(28)	1.473(6)
N(9)-C(31)	1.301(6)
N(9)-C(30)	1.471(6)
C(1)-C(2)	1.384(7)
C(1)-C(6)	1.474(7)
C(2)-C(3)	1.391(9)
C(3)-C(4)	1.367(9)
C(4)-C(5)	1.387(7)
C(6)-C(7)	1.397(7)
C(7)-C(8)	1.365(10)
C(8)-C(9)	1.404(10)
C(9)-C(10)	1.371(8)
C(11)-C(12)	1.382(7)
C(11)-C(16)	1.484(7)
C(12)-C(13)	1.371(9)
C(13)-C(14)	1.381(9)
C(14)-C(15)	1.379(7)
C(16)-C(17)	1.381(7)
C(17)-C(18)	1.387(9)
C(18)-C(19)	1.396(9)
C(19)-C(20)	1.383(7)
C(22)-C(23)	1.371(7)
C(23)-C(24)	1.405(6)
C(25)-C(26)	1.518(8)
C(26)-C(27)	1.508(7)
C(28)-C(29)	1.526(9)
C(29)-C(30)	1.456(9)
C(32)-C(33)	1.504(14)
C(33)-C(34)	1.500(16)
N(2)-RU1-N(3)	86.95(15)
N(2)-RU1-N(1)	79.10(16)
N(3)-RU1-N(1)	97.10(15)
N(2)-RU1-N(4)	95.26(15)
N(3)-RU1-N(4)	78.59(16)
N(1)-RU1-N(4)	173.14(14)
N(2)-RU1-N(5)	175.79(15)
N(3)-RU1-N(5)	91.79(15)
N(1)-RU1-N(5)	97.09(15)
N(4)-RU1-N(5)	88.42(14)
N(2)-RU1-N(9)	96.28(15)
N(3)-RU1-N(9)	175.95(14)
N(1)-RU1-N(9)	85.94(15)
N(4)-RU1-N(9)	98.64(16)
N(5)-RU1-N(9)	85.16(15)
F(6)-P(1)-F(5)	93.0(4)
F(6)-P(1)-F(2)	90.4(4)
F(5)-P(1)-F(2)	176.6(4)
F(6)-P(1)-F(1)	89.6(4)
F(5)-P(1)-F(1)	89.4(3)
F(2)-P(1)-F(1)	90.2(3)
F(6)-P(1)-F(3)	178.5(4)
F(5)-P(1)-F(3)	87.3(4)
F(2)-P(1)-F(3)	89.4(4)
F(1)-P(1)-F(3)	91.9(3)
F(6)-P(1)-F(4)	91.5(3)
F(5)-P(1)-F(4)	92.0(3)

Appendix

F(2)-P(1)-F(4)	88.4(3)
F(1)-P(1)-F(4)	178.2(3)
F(3)-P(1)-F(4)	87.0(2)
F(11)-P(2)-F(8)	92.2(5)
F(11)-P(2)-F(7)	89.8(5)
F(8)-P(2)-F(7)	177.8(4)
F(11)-P(2)-F(9)	92.6(3)
F(8)-P(2)-F(9)	90.1(3)
F(7)-P(2)-F(9)	91.0(3)
F(11)-P(2)-F(12)	178.4(4)
F(8)-P(2)-F(12)	88.9(4)
F(7)-P(2)-F(12)	89.1(4)
F(9)-P(2)-F(12)	88.6(2)
F(11)-P(2)-F(10)	88.2(3)
F(8)-P(2)-F(10)	90.2(2)
F(7)-P(2)-F(10)	88.8(3)
F(9)-P(2)-F(10)	179.2(3)
F(12)-P(2)-F(10)	90.7(2)
C(5)-N(1)-C(1)	119.0(4)
C(5)-N(1)-RU1	126.1(3)
C(1)-N(1)-RU1	114.6(3)
C(10)-N(2)-C(6)	118.5(4)
C(10)-N(2)-RU1	126.5(4)
C(6)-N(2)-RU1	114.7(3)
C(15)-N(3)-C(11)	118.0(4)
C(15)-N(3)-RU1	125.7(3)
C(11)-N(3)-RU1	116.3(3)
C(20)-N(4)-C(16)	118.4(4)
C(20)-N(4)-RU1	126.0(3)
C(16)-N(4)-RU1	115.6(3)
C(21)-N(5)-C(24)	117.2(4)
C(21)-N(5)-RU1	119.3(3)
C(24)-N(5)-RU1	122.9(3)
C(22)-N(6)-C(21)	114.3(4)
C(24)-N(7)-C(31)	122.5(4)
C(24)-N(7)-C(25)	118.8(4)
C(31)-N(7)-C(25)	114.2(4)
C(31)-N(8)-C(27)	126.6(4)
C(31)-N(8)-C(28)	121.3(4)
C(27)-N(8)-C(28)	112.1(4)
C(31)-N(9)-C(30)	116.4(4)
C(31)-N(9)-RU1	124.1(3)
C(30)-N(9)-RU1	119.0(3)
N(1)-C(1)-C(2)	121.2(5)
N(1)-C(1)-C(6)	115.0(4)
C(2)-C(1)-C(6)	123.4(5)
C(1)-C(2)-C(3)	119.1(5)
C(4)-C(3)-C(2)	119.4(5)
C(3)-C(4)-C(5)	119.1(5)
N(1)-C(5)-C(4)	122.2(5)
N(2)-C(6)-C(7)	121.3(5)
N(2)-C(6)-C(1)	114.7(4)
C(7)-C(6)-C(1)	123.9(5)
C(8)-C(7)-C(6)	119.5(6)
C(7)-C(8)-C(9)	119.2(5)
C(10)-C(9)-C(8)	118.5(6)
N(2)-C(10)-C(9)	122.7(6)
N(3)-C(11)-C(12)	122.0(5)
N(3)-C(11)-C(16)	114.4(4)

Appendix

C (12) -C (11) -C (16)	123.5 (5)
C (13) -C (12) -C (11)	119.5 (5)
C (12) -C (13) -C (14)	118.9 (5)
C (15) -C (14) -C (13)	119.3 (5)
N (3) -C (15) -C (14)	122.2 (5)
N (4) -C (16) -C (17)	121.3 (5)
N (4) -C (16) -C (11)	114.8 (4)
C (17) -C (16) -C (11)	123.8 (5)
C (16) -C (17) -C (18)	120.1 (5)
C (17) -C (18) -C (19)	118.5 (5)
C (20) -C (19) -C (18)	118.3 (5)
N (4) -C (20) -C (19)	123.2 (5)
N (6) -C (21) -N (5)	127.4 (4)
N (6) -C (22) -C (23)	124.8 (4)
N (6) -C (22) -CL1	116.2 (4)
C (23) -C (22) -CL1	118.9 (4)
C (22) -C (23) -C (24)	116.9 (4)
N (5) -C (24) -N (7)	119.4 (4)
N (5) -C (24) -C (23)	119.1 (4)
N (7) -C (24) -C (23)	121.4 (4)
N (7) -C (25) -C (26)	108.4 (4)
C (27) -C (26) -C (25)	106.6 (4)
N (8) -C (27) -C (26)	113.9 (4)
N (8) -C (28) -C (29)	110.9 (5)
C (30) -C (29) -C (28)	108.5 (5)
C (29) -C (30) -N (9)	111.1 (5)
N (9) -C (31) -N (8)	124.4 (4)
N (9) -C (31) -N (7)	120.0 (4)
N (8) -C (31) -N (7)	115.5 (4)
O (1) -C (33) -C (34)	118.1 (10)
O (1) -C (33) -C (32)	125.3 (11)
C (34) -C (33) -C (32)	116.5 (10)

Appendix

Appendix 3 : Crystal Data for Chapter 3

3-L1 [C₁₈H₂₆N₈]

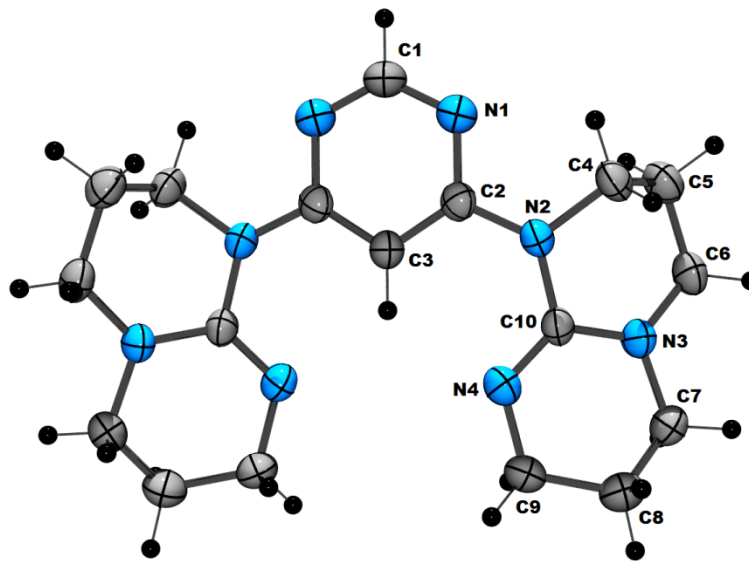


Table 1. Crystal data and structure refinement for C₁₈H₂₆N₈ (**3-L1**).

Empirical formula	C ₁₈ H ₂₆ N ₈
Formula weight	354.47
Temperature	150(2) K
Wavelength	1.54178 Å
Crystal system	Orthorhombic
Space group	Fdd2
Unit cell dimensions	a = 16.2300(2) Å α = 90° b = 23.4755(4) Å β = 90° c = 8.9782(1) Å γ = 90°
Volume	3420.76(8) Å ³
Z	8
Density (calculated)	1.377 g/cm ³
Absorption coefficient	0.706 mm ⁻¹
F(000)	1520
Crystal size	0.20 x 0.09 x 0.09 mm
Theta range for data collection	5.939 to 72.230 deg.
Index ranges	-19<=h<=19, -28<=k<=28, -10<=l<=11

Appendix

Reflections collected	10526
Independent reflections	1668 [R(int) = 0.038]
Absorption correction	Semi-empirical from equivalents
Max. and min. transmission	0.9392 and 0.8717
Refinement method	Full-matrix least-squares on F ²
Data / restraints / parameters	1668 / 1 / 120
Goodness-of-fit on F ²	1.050
Final R indices [I>2sigma(I)]	R1 = 0.0330, wR2 = 0.0846
R indices (all data)	R1 = 0.0335, wR2 = 0.0850
Absolute structure parameter	0.47(18)
Extinction coefficient	0.00074(13)
Largest diff. peak and hole	0.220 and -0.260 e.Å ³

Table 2. Bond lengths [Å] and angles [°] for C₁₈H₂₆N₈ (**3-L1**)

N(1)-C(1)	1.3266(19)
N(1)-C(2)	1.351(2)
N(2)-C(2)	1.395(2)
N(2)-C(10)	1.416(2)
N(2)-C(4)	1.472(2)
N(3)-C(10)	1.375(2)
N(3)-C(6)	1.466(2)
N(3)-C(7)	1.466(2)
N(4)-C(10)	1.284(2)
N(4)-C(9)	1.457(2)
C(1)-N(1)#1	1.3266(19)
C(2)-C(3)	1.402(2)
C(3)-C(2)#1	1.402(2)
C(4)-C(5)	1.515(2)
C(5)-C(6)	1.522(3)
C(7)-C(8)	1.513(3)
C(8)-C(9)	1.519(3)
C(1)-N(1)-C(2)	115.44(17)
C(2)-N(2)-C(10)	123.10(14)
C(2)-N(2)-C(4)	119.20(15)
C(10)-N(2)-C(4)	114.35(13)
C(10)-N(3)-C(6)	125.74(15)
C(10)-N(3)-C(7)	119.12(14)
C(6)-N(3)-C(7)	113.72(14)
C(10)-N(4)-C(9)	116.56(15)
N(1)-C(1)-N(1)#1	128.9(3)
N(1)-C(2)-N(2)	114.39(15)
N(1)-C(2)-C(3)	121.69(17)
N(2)-C(2)-C(3)	123.91(17)

Appendix

C (2) #1-C (3)-C (2)	116.8 (2)
N (2)-C (4)-C (5)	108.13 (14)
C (4)-C (5)-C (6)	108.22 (15)
N (3)-C (6)-C (5)	113.59 (15)
N (3)-C (7)-C (8)	111.16 (15)
C (7)-C (8)-C (9)	108.17 (17)
N (4)-C (9)-C (8)	112.12 (17)
N (4)-C (10)-N (3)	126.89 (17)
N (4)-C (10)-N (2)	119.22 (15)
N (3)-C (10)-N (2)	113.82 (14)

3-(1-meso) [C₆₂H₆₄F₂₄N₁₈P₄Ru₂]

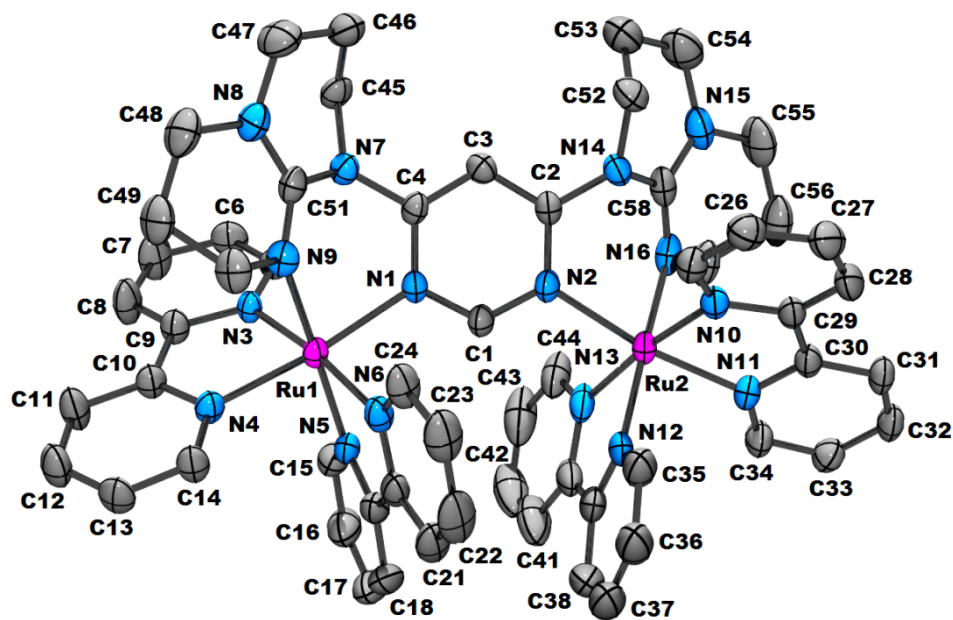


Table 3. Crystal data and structure refinement for C₆₂H₆₄F₂₄N₁₈P₄Ru₂ (**3-(1-meso)**).

Empirical formula	C ₆₂ H ₆₄ F ₂₄ N ₁₈ P ₄ Ru ₂
Formula weight	1843.33
Temperature	150 (2) K
Wavelength	1.54178 Å
Crystal system	Monoclinic
Space group	Cc
Unit cell dimensions	a = 22.038 (2) Å α = 90°. b = 14.0363 (13) Å β = 12.384 (2)°. c = 25.925 (3) Å γ = 90°.

Appendix

Volume	7415.2(13) Å ³
Z	4
Density (calculated)	1.651 g/cm ³
Absorption coefficient	5.136 mm ⁻¹
F(000)	3704
Crystal size	0.36 x 0.16 x 0.16 mm
Theta range for data collection	3.688 to 69.687 deg.
Index ranges	-26<=h<=26, -12<=k<=16, -31<=l<=31
Reflections collected	123531
Independent reflections	13692 [R(int) = 0.060]
Absorption correction	Semi-empirical from equivalents
Max. and min. transmission	0.7533 and 0.4347
Refinement method	Full-matrix least-squares on F ²
Data / restraints / parameters	13692 / 2 / 993
Goodness-of-fit on F ²	1.052
Final R indices [I>2sigma(I)]	R1 = 0.0382, wR2 = 0.1008
R indices (all data)	R1 = 0.0384, wR2 = 0.1011
Absolute structure parameter	0.122(3)
Largest diff. peak and hole	0.980 and -0.454 e Å ³

Table 4. Bond lengths [Å] and angles [°] for C62H64F24N18P4Ru2 (**3-(1-meso)**)

Ru(1)-N(5)	2.053(5)
Ru(1)-N(4)	2.059(4)
Ru(1)-N(3)	2.069(4)
Ru(1)-N(6)	2.078(4)
Ru(1)-N(1)	2.089(4)
Ru(1)-N(9)	2.096(5)
Ru(2)-N(11)	2.058(5)
Ru(2)-N(13)	2.061(5)
Ru(2)-N(10)	2.063(5)
Ru(2)-N(12)	2.064(5)
Ru(2)-N(2)	2.085(4)
Ru(2)-N(16)	2.096(6)
N(1)-C(1)	1.328(7)
N(1)-C(4)	1.356(7)
N(2)-C(1)	1.330(7)
N(2)-C(2)	1.357(7)
N(3)-C(5)	1.351(7)

Appendix

N(3) -C(9)	1.351(7)
N(4) -C(14)	1.345(7)
N(4) -C(10)	1.360(7)
N(5) -C(15)	1.335(9)
N(5) -C(19)	1.359(8)
N(6) -C(24)	1.332(8)
N(6) -C(20)	1.352(8)
N(7) -C(4)	1.402(7)
N(7) -C(51)	1.402(7)
N(7) -C(45)	1.465(7)
N(8) -C(51)	1.347(7)
N(8) -C(47)	1.463(9)
N(8) -C(48)	1.475(8)
N(9) -C(51)	1.304(8)
N(9) -C(50)	1.465(7)
N(10) -C(25)	1.339(7)
N(10) -C(29)	1.356(7)
N(11) -C(34)	1.344(8)
N(11) -C(30)	1.359(7)
N(12) -C(35)	1.353(11)
N(12) -C(39)	1.368(9)
N(13) -C(44)	1.313(11)
N(13) -C(40)	1.389(10)
N(14) -C(2)	1.394(7)
N(14) -C(58)	1.406(7)
N(14) -C(52)	1.478(7)
N(15) -C(58)	1.343(8)
N(15) -C(54)	1.458(10)
N(15) -C(55)	1.481(9)
N(16) -C(58)	1.290(9)
N(16) -C(57)	1.463(7)
C(2) -C(3)	1.386(8)
C(3) -C(4)	1.378(8)
C(5) -C(6)	1.366(8)
C(6) -C(7)	1.384(9)
C(7) -C(8)	1.380(10)
C(8) -C(9)	1.380(8)
C(9) -C(10)	1.467(7)
C(10) -C(11)	1.393(9)
C(11) -C(12)	1.366(9)
C(12) -C(13)	1.391(9)
C(13) -C(14)	1.378(8)
C(15) -C(16)	1.399(9)
C(16) -C(17)	1.379(12)
C(17) -C(18)	1.374(13)
C(18) -C(19)	1.390(9)
C(19) -C(20)	1.479(10)
C(20) -C(21)	1.393(8)
C(21) -C(22)	1.373(14)
C(22) -C(23)	1.380(14)
C(23) -C(24)	1.382(9)
C(25) -C(26)	1.387(8)
C(26) -C(27)	1.376(9)
C(27) -C(28)	1.373(10)
C(28) -C(29)	1.392(8)
C(29) -C(30)	1.465(8)
C(30) -C(31)	1.396(7)
C(31) -C(32)	1.384(9)
C(32) -C(33)	1.379(9)

Appendix

C (33) -C (34)	1.366 (9)
C (35) -C (36)	1.370 (11)
C (36) -C (37)	1.347 (16)
C (37) -C (38)	1.372 (17)
C (38) -C (39)	1.416 (12)
C (39) -C (40)	1.449 (13)
C (40) -C (41)	1.384 (11)
C (41) -C (42)	1.336 (16)
C (42) -C (43)	1.416 (17)
C (43) -C (44)	1.393 (11)
C (45) -C (46)	1.514 (9)
C (46) -C (47)	1.508 (10)
C (48) -C (49)	1.499 (11)
C (49) -C (50)	1.506 (9)
C (52) -C (53)	1.506 (11)
C (53) -C (54)	1.507 (12)
C (55) -C (56)	1.485 (13)
C (56) -C (57)	1.519 (10)
P (1) -F (5)	1.575 (6)
P (1) -F (1)	1.583 (5)
P (1) -F (3)	1.583 (4)
P (1) -F (6)	1.585 (5)
P (1) -F (4)	1.590 (6)
P (1) -F (2)	1.611 (5)
P (2) -F (11)	1.580 (5)
P (2) -F (12)	1.584 (5)
P (2) -F (8)	1.588 (5)
P (2) -F (7)	1.592 (5)
P (2) -F (9)	1.609 (5)
P (2) -F (10)	1.611 (6)
P (3) -F (13)	1.566 (6)
P (3) -F (17)	1.571 (5)
P (3) -F (18)	1.596 (5)
P (3) -F (16)	1.601 (6)
P (3) -F (15)	1.605 (5)
P (3) -F (14)	1.607 (5)
P (4) -F (22)	1.536 (6)
P (4) -F (21)	1.567 (6)
P (4) -F (20)	1.569 (6)
P (4) -F (24)	1.585 (6)
P (4) -F (23)	1.595 (6)
P (4) -F (19)	1.607 (6)
N (17) -C (60)	1.120 (15)
C (59) -C (60)	1.359 (18)
N (18) -C (62)	1.22 (2)
C (61) -C (62)	1.40 (2)
N (5) -RU1-N (4)	87.09 (18)
N (5) -RU1-N (3)	95.36 (19)
N (4) -RU1-N (3)	78.87 (17)
N (5) -RU1-N (6)	79.3 (2)
N (4) -RU1-N (6)	96.06 (17)
N (3) -RU1-N (6)	172.89 (19)
N (5) -RU1-N (1)	97.99 (17)
N (4) -RU1-N (1)	173.76 (17)
N (3) -RU1-N (1)	96.97 (17)
N (6) -RU1-N (1)	88.48 (17)
N (5) -RU1-N (9)	173.91 (18)
N (4) -RU1-N (9)	90.72 (19)

Appendix

N(3)-RU1-N(9)	89.79(18)
N(6)-RU1-N(9)	95.30(19)
N(1)-RU1-N(9)	84.57(18)
N(11)-RU2-N(13)	96.72(19)
N(11)-RU2-N(10)	79.23(18)
N(13)-RU2-N(10)	173.2(2)
N(11)-RU2-N(12)	88.36(19)
N(13)-RU2-N(12)	79.5(3)
N(10)-RU2-N(12)	94.8(2)
N(11)-RU2-N(2)	171.27(18)
N(13)-RU2-N(2)	89.55(18)
N(10)-RU2-N(2)	95.08(17)
N(12)-RU2-N(2)	98.78(19)
N(11)-RU2-N(16)	88.92(19)
N(13)-RU2-N(16)	96.4(2)
N(10)-RU2-N(16)	89.07(18)
N(12)-RU2-N(16)	174.8(2)
N(2)-RU2-N(16)	84.34(18)
C(1)-N(1)-C(4)	116.7(4)
C(1)-N(1)-RU1	120.7(4)
C(4)-N(1)-RU1	122.6(3)
C(1)-N(2)-C(2)	117.5(4)
C(1)-N(2)-RU2	121.3(4)
C(2)-N(2)-RU2	121.2(3)
C(5)-N(3)-C(9)	118.3(4)
C(5)-N(3)-RU1	126.4(4)
C(9)-N(3)-RU1	115.2(3)
C(14)-N(4)-C(10)	118.5(5)
C(14)-N(4)-RU1	126.5(4)
C(10)-N(4)-RU1	115.0(3)
C(15)-N(5)-C(19)	119.2(5)
C(15)-N(5)-RU1	126.0(4)
C(19)-N(5)-RU1	114.1(4)
C(24)-N(6)-C(20)	120.3(5)
C(24)-N(6)-RU1	125.8(4)
C(20)-N(6)-RU1	113.9(4)
C(4)-N(7)-C(51)	121.7(4)
C(4)-N(7)-C(45)	118.5(4)
C(51)-N(7)-C(45)	115.5(4)
C(51)-N(8)-C(47)	125.6(5)
C(51)-N(8)-C(48)	120.5(5)
C(47)-N(8)-C(48)	113.3(5)
C(51)-N(9)-C(50)	115.6(5)
C(51)-N(9)-RU1	122.6(4)
C(50)-N(9)-RU1	121.0(4)
C(25)-N(10)-C(29)	118.7(5)
C(25)-N(10)-RU2	126.6(4)
C(29)-N(10)-RU2	114.7(4)
C(34)-N(11)-C(30)	119.1(5)
C(34)-N(11)-RU2	126.7(4)
C(30)-N(11)-RU2	113.5(4)
C(35)-N(12)-C(39)	119.1(6)
C(35)-N(12)-RU2	126.3(5)
C(39)-N(12)-RU2	114.1(5)
C(44)-N(13)-C(40)	119.8(6)
C(44)-N(13)-RU2	126.9(5)
C(40)-N(13)-RU2	113.3(5)
C(2)-N(14)-C(58)	122.0(5)
C(2)-N(14)-C(52)	119.0(5)

Appendix

C (58) -N (14) -C (52)	116.3 (5)
C (58) -N (15) -C (54)	126.4 (6)
C (58) -N (15) -C (55)	119.8 (6)
C (54) -N (15) -C (55)	113.7 (6)
C (58) -N (16) -C (57)	115.4 (6)
C (58) -N (16) -RU2	121.8 (4)
C (57) -N (16) -RU2	121.7 (4)
N (1) -C (1) -N (2)	126.4 (5)
N (2) -C (2) -C (3)	119.3 (5)
N (2) -C (2) -N (14)	119.6 (5)
C (3) -C (2) -N (14)	121.0 (5)
C (4) -C (3) -C (2)	119.6 (5)
N (1) -C (4) -C (3)	120.4 (5)
N (1) -C (4) -N (7)	118.9 (5)
C (3) -C (4) -N (7)	120.6 (5)
N (3) -C (5) -C (6)	122.9 (5)
C (5) -C (6) -C (7)	119.0 (5)
C (8) -C (7) -C (6)	118.5 (6)
C (7) -C (8) -C (9)	120.2 (6)
N (3) -C (9) -C (8)	121.1 (5)
N (3) -C (9) -C (10)	115.1 (5)
C (8) -C (9) -C (10)	123.7 (6)
N (4) -C (10) -C (11)	120.5 (5)
N (4) -C (10) -C (9)	115.3 (5)
C (11) -C (10) -C (9)	124.1 (5)
C (12) -C (11) -C (10)	120.6 (6)
C (11) -C (12) -C (13)	118.6 (6)
C (14) -C (13) -C (12)	118.8 (5)
N (4) -C (14) -C (13)	122.9 (5)
N (5) -C (15) -C (16)	122.9 (7)
C (17) -C (16) -C (15)	117.2 (7)
C (18) -C (17) -C (16)	120.6 (6)
C (17) -C (18) -C (19)	119.4 (7)
N (5) -C (19) -C (18)	120.7 (6)
N (5) -C (19) -C (20)	115.3 (5)
C (18) -C (19) -C (20)	124.0 (6)
N (6) -C (20) -C (21)	120.1 (7)
N (6) -C (20) -C (19)	115.2 (5)
C (21) -C (20) -C (19)	124.6 (6)
C (22) -C (21) -C (20)	119.9 (7)
C (21) -C (22) -C (23)	118.7 (6)
C (22) -C (23) -C (24)	119.6 (8)
N (6) -C (24) -C (23)	121.2 (7)
N (10) -C (25) -C (26)	122.7 (5)
C (27) -C (26) -C (25)	118.4 (6)
C (28) -C (27) -C (26)	119.6 (6)
C (27) -C (28) -C (29)	119.6 (6)
N (10) -C (29) -C (28)	120.9 (5)
N (10) -C (29) -C (30)	114.6 (5)
C (28) -C (29) -C (30)	124.4 (5)
N (11) -C (30) -C (31)	120.2 (5)
N (11) -C (30) -C (29)	116.1 (5)
C (31) -C (30) -C (29)	123.7 (5)
C (32) -C (31) -C (30)	119.8 (5)
C (33) -C (32) -C (31)	118.8 (5)
C (34) -C (33) -C (32)	119.4 (6)
N (11) -C (34) -C (33)	122.6 (6)
N (12) -C (35) -C (36)	122.5 (9)
C (37) -C (36) -C (35)	120.6 (11)

Appendix

C (36) -C (37) -C (38)	118.0 (8)
C (37) -C (38) -C (39)	122.0 (8)
N (12) -C (39) -C (38)	117.8 (8)
N (12) -C (39) -C (40)	115.1 (6)
C (38) -C (39) -C (40)	127.0 (8)
C (41) -C (40) -N (13)	119.3 (9)
C (41) -C (40) -C (39)	124.7 (8)
N (13) -C (40) -C (39)	115.9 (6)
C (42) -C (41) -C (40)	120.5 (10)
C (41) -C (42) -C (43)	120.7 (8)
C (44) -C (43) -C (42)	116.5 (10)
N (13) -C (44) -C (43)	123.0 (9)
N (7) -C (45) -C (46)	108.8 (5)
C (47) -C (46) -C (45)	107.4 (5)
N (8) -C (47) -C (46)	112.8 (5)
N (8) -C (48) -C (49)	111.9 (5)
C (48) -C (49) -C (50)	107.7 (5)
N (9) -C (50) -C (49)	108.8 (5)
N (9) -C (51) -N (8)	124.4 (5)
N (9) -C (51) -N (7)	119.7 (5)
N (8) -C (51) -N (7)	115.8 (5)
N (14) -C (52) -C (53)	107.5 (5)
C (52) -C (53) -C (54)	108.9 (6)
N (15) -C (54) -C (53)	112.4 (6)
N (15) -C (55) -C (56)	113.4 (6)
C (55) -C (56) -C (57)	107.3 (6)
N (16) -C (57) -C (56)	109.3 (6)
N (16) -C (58) -N (15)	124.9 (6)
N (16) -C (58) -N (14)	119.3 (5)
N (15) -C (58) -N (14)	115.7 (6)
F (5) -P (1) -F (1)	89.1 (4)
F (5) -P (1) -F (3)	90.2 (3)
F (1) -P (1) -F (3)	89.7 (3)
F (5) -P (1) -F (6)	90.2 (4)
F (1) -P (1) -F (6)	90.3 (3)
F (3) -P (1) -F (6)	179.5 (4)
F (5) -P (1) -F (4)	91.6 (4)
F (1) -P (1) -F (4)	178.3 (3)
F (3) -P (1) -F (4)	88.7 (3)
F (6) -P (1) -F (4)	91.3 (3)
F (5) -P (1) -F (2)	178.6 (4)
F (1) -P (1) -F (2)	89.8 (3)
F (3) -P (1) -F (2)	89.0 (3)
F (6) -P (1) -F (2)	90.5 (3)
F (4) -P (1) -F (2)	89.5 (3)
F (11) -P (2) -F (12)	91.0 (3)
F (11) -P (2) -F (8)	178.0 (3)
F (12) -P (2) -F (8)	91.0 (3)
F (11) -P (2) -F (7)	89.3 (3)
F (12) -P (2) -F (7)	90.7 (3)
F (8) -P (2) -F (7)	90.6 (3)
F (11) -P (2) -F (9)	88.8 (3)
F (12) -P (2) -F (9)	179.5 (3)
F (8) -P (2) -F (9)	89.2 (3)
F (7) -P (2) -F (9)	89.7 (3)
F (11) -P (2) -F (10)	90.4 (3)
F (12) -P (2) -F (10)	90.2 (3)
F (8) -P (2) -F (10)	89.6 (3)
F (7) -P (2) -F (10)	179.0 (3)

Appendix

F(9)-P(2)-F(10)	89.4(3)
F(13)-P(3)-F(17)	92.5(4)
F(13)-P(3)-F(18)	90.3(3)
F(17)-P(3)-F(18)	90.3(3)
F(13)-P(3)-F(16)	175.9(4)
F(17)-P(3)-F(16)	91.7(4)
F(18)-P(3)-F(16)	90.0(3)
F(13)-P(3)-F(15)	90.8(3)
F(17)-P(3)-F(15)	89.8(3)
F(18)-P(3)-F(15)	178.9(3)
F(16)-P(3)-F(15)	88.9(3)
F(13)-P(3)-F(14)	89.1(4)
F(17)-P(3)-F(14)	178.3(4)
F(18)-P(3)-F(14)	90.2(3)
F(16)-P(3)-F(14)	86.7(3)
F(15)-P(3)-F(14)	89.7(3)
F(22)-P(4)-F(21)	88.4(5)
F(22)-P(4)-F(20)	92.1(5)
F(21)-P(4)-F(20)	91.7(4)
F(22)-P(4)-F(24)	93.4(5)
F(21)-P(4)-F(24)	178.1(5)
F(20)-P(4)-F(24)	87.8(4)
F(22)-P(4)-F(23)	89.7(5)
F(21)-P(4)-F(23)	90.5(4)
F(20)-P(4)-F(23)	177.2(4)
F(24)-P(4)-F(23)	89.9(4)
F(22)-P(4)-F(19)	179.4(5)
F(21)-P(4)-F(19)	91.2(4)
F(20)-P(4)-F(19)	88.4(4)
F(24)-P(4)-F(19)	86.9(4)
F(23)-P(4)-F(19)	89.7(4)
N(17)-C(60)-C(59)	174.7(17)
N(18)-C(62)-C(61)	174.6(17)

3-2 [C₃₉H₄₇F₁₂N₉O₃P₂Ru]

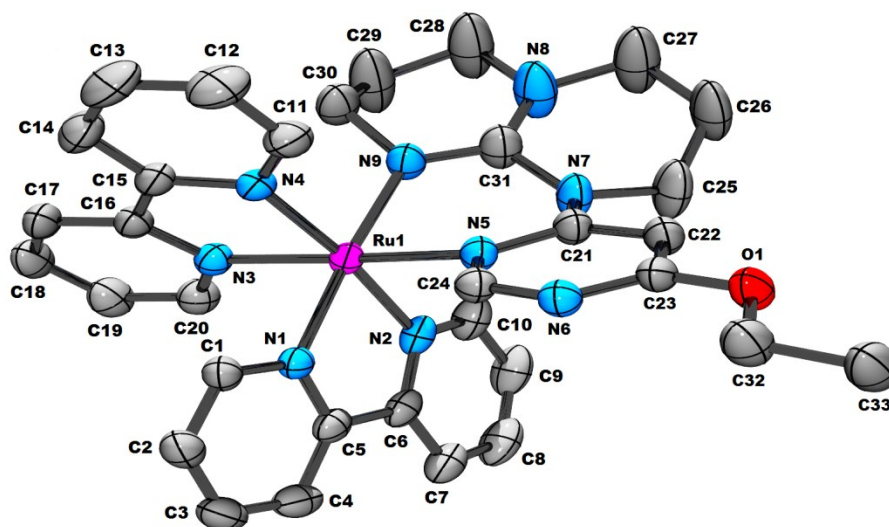


Table 5. Crystal data and structure refinement for C₆₀H₈₉F₁₂N₉O₂P₂Ru (**3-2**).

Appendix

Empirical formula	C36 H41 F12 N9 O2 P2 Ru
Formula weight	1022.79
Temperature	150(2) K
Wavelength	1.54178 Å
Crystal system	Monoclinic
Space group	C2/c
Unit cell dimensions	a = 42.0995(16) Å $\alpha = 90^\circ$ b = 9.7518(4) Å $\beta = 125.664(2)^\circ$ c = 25.0993(9) Å $\gamma = 90^\circ$
Volume	8371.8(6) Å ³
Z	8
Density (calculated)	1.623 g/cm ³
Absorption coefficient	4.650 mm ⁻¹
F(000)	4144
Crystal size	0.13 x 0.10 x 0.03 mm
Theta range for data collection	2.584 to 69.748 deg.
Index ranges	-51<=h<=43, -11<=k<=11, -24<=l<=30
Reflections collected	70224
Independent reflections	7827 [R(int) = 0.044]
Absorption correction	Semi-empirical from equivalents
Max. and min. transmission	0.7533 and 0.5239
Refinement method	Full-matrix least-squares on F ²
Data / restraints / parameters	7827 / 0 / 540
Goodness-of-fit on F ²	1.086
Final R indices [I>2sigma(I)]	R1 = 0.0489, wR2 = 0.1368
R indices (all data)	R1 = 0.0505, wR2 = 0.1388
Largest diff. peak and hole	1.218 and -0.959 e/Å ³

Table 6. Bond lengths [Å] and angles [°] for C60H89F12N9O2P2Ru (**3-2**)

Ru(1)-N(3)	2.057(3)
Ru(1)-N(4)	2.061(3)

Appendix

Ru (1) -N (1)	2.061 (3)
Ru (1) -N (2)	2.083 (3)
Ru (1) -N (5)	2.085 (3)
Ru (1) -N (9)	2.088 (3)
P (1) -F (1b)	1.49 (2)
P (1) -F (3a)	1.501 (16)
P (1) -F (2b)	1.504 (18)
P (1) -F (5)	1.560 (4)
P (1) -F (4)	1.592 (4)
P (1) -F (1a)	1.610 (12)
P (1) -F (6)	1.615 (5)
P (1) -F (2a)	1.634 (14)
P (1) -F (3b)	1.74 (2)
P (2) -F (11)	1.575 (3)
P (2) -F (12)	1.586 (3)
P (2) -F (7)	1.588 (3)
P (2) -F (8)	1.593 (3)
P (2) -F (10)	1.598 (3)
P (2) -F (9)	1.615 (3)
F (2a) -F (2b)	1.04 (5)
F (2b) -F (3a)	1.30 (4)
F (3a) -F (3b)	0.76 (3)
O (1) -C (23)	1.329 (4)
O (1) -C (32)	1.461 (4)
N (1) -C (5)	1.351 (4)
N (1) -C (1)	1.356 (4)
N (2) -C (10)	1.346 (4)
N (2) -C (6)	1.346 (4)
N (3) -C (20)	1.341 (5)
N (3) -C (16)	1.364 (4)
N (4) -C (11)	1.343 (4)
N (4) -C (15)	1.362 (4)
N (5) -C (24)	1.343 (4)
N (5) -C (21)	1.360 (4)
N (6) -C (24)	1.315 (4)
N (6) -C (23)	1.337 (4)
N (7) -C (21)	1.381 (5)
N (7) -C (31)	1.406 (5)
N (7) -C (25)	1.487 (4)
N (8) -C (31)	1.347 (5)
N (8) -C (28)	1.472 (6)
N (8) -C (27)	1.477 (6)
N (9) -C (31)	1.298 (5)
N (9) -C (30)	1.476 (5)
C (1) -C (2)	1.382 (5)
C (2) -C (3)	1.380 (5)
C (3) -C (4)	1.364 (6)
C (4) -C (5)	1.398 (5)
C (5) -C (6)	1.470 (5)
C (6) -C (7)	1.394 (5)
C (7) -C (8)	1.376 (6)
C (8) -C (9)	1.367 (7)
C (9) -C (10)	1.389 (6)
C (11) -C (12)	1.377 (5)
C (12) -C (13)	1.370 (6)
C (13) -C (14)	1.377 (6)
C (14) -C (15)	1.382 (5)
C (15) -C (16)	1.466 (5)
C (16) -C (17)	1.384 (5)

Appendix

C (17) -C (18)	1.378 (6)
C (18) -C (19)	1.376 (6)
C (19) -C (20)	1.379 (5)
C (21) -C (22)	1.385 (5)
C (22) -C (23)	1.378 (5)
C (25) -C (26)	1.501 (8)
C (26) -C (27)	1.520 (7)
C (28) -C (29)	1.524 (8)
C (29) -C (30)	1.489 (7)
C (32) -C (33)	1.498 (5)
N (3) -RU1-N (4)	79.01 (11)
N (3) -RU1-N (1)	84.99 (10)
N (4) -RU1-N (1)	97.64 (10)
N (3) -RU1-N (2)	95.68 (10)
N (4) -RU1-N (2)	173.51 (10)
N (1) -RU1-N (2)	78.05 (10)
N (3) -RU1-N (5)	173.59 (11)
N (4) -RU1-N (5)	95.03 (11)
N (1) -RU1-N (5)	93.55 (10)
N (2) -RU1-N (5)	90.11 (10)
N (3) -RU1-N (9)	97.46 (11)
N (4) -RU1-N (9)	86.81 (11)
N (1) -RU1-N (9)	175.28 (11)
N (2) -RU1-N (9)	97.65 (12)
N (5) -RU1-N (9)	84.46 (11)
F (1B) -P (1) -F (3A)	85.8 (14)
F (1B) -P (1) -F (2B)	86.6 (13)
F (3A) -P (1) -F (2B)	51.3 (16)
F (1B) -P (1) -F (5)	177.3 (14)
F (3A) -P (1) -F (5)	91.8 (8)
F (2B) -P (1) -F (5)	92.8 (10)
F (1B) -P (1) -F (4)	90.4 (11)
F (3A) -P (1) -F (4)	100.7 (7)
F (2B) -P (1) -F (4)	152.1 (17)
F (5) -P (1) -F (4)	88.8 (3)
F (1B) -P (1) -F (1A)	5.6 (14)
F (3A) -P (1) -F (1A)	91.4 (9)
F (2B) -P (1) -F (1A)	90.6 (10)
F (5) -P (1) -F (1A)	176.3 (4)
F (4) -P (1) -F (1A)	88.7 (4)
F (1B) -P (1) -F (6)	93.0 (13)
F (3A) -P (1) -F (6)	170.5 (8)
F (2B) -P (1) -F (6)	119.2 (17)
F (5) -P (1) -F (6)	89.6 (3)
F (4) -P (1) -F (6)	88.6 (3)
F (1A) -P (1) -F (6)	87.6 (4)
F (1B) -P (1) -F (2A)	90.8 (13)
F (3A) -P (1) -F (2A)	89.7 (10)
F (2B) -P (1) -F (2A)	38.3 (18)
F (5) -P (1) -F (2A)	90.4 (6)
F (4) -P (1) -F (2A)	169.6 (7)
F (1A) -P (1) -F (2A)	91.4 (7)
F (6) -P (1) -F (2A)	81.0 (7)
F (1B) -P (1) -F (3B)	89.1 (15)
F (3A) -P (1) -F (3B)	25.7 (9)
F (2B) -P (1) -F (3B)	76.9 (15)
F (5) -P (1) -F (3B)	88.2 (8)
F (4) -P (1) -F (3B)	75.3 (7)

Appendix

F (1A) -P (1) -F (3B)	93.9 (8)
F (6) -P (1) -F (3B)	163.8 (7)
F (2A) -P (1) -F (3B)	115.1 (9)
F (11) -P (2) -F (12)	94.15 (19)
F (11) -P (2) -F (7)	92.74 (18)
F (12) -P (2) -F (7)	90.92 (18)
F (11) -P (2) -F (8)	176.11 (19)
F (12) -P (2) -F (8)	89.39 (18)
F (7) -P (2) -F (8)	88.82 (19)
F (11) -P (2) -F (10)	89.85 (17)
F (12) -P (2) -F (10)	92.17 (18)
F (7) -P (2) -F (10)	175.8 (2)
F (8) -P (2) -F (10)	88.41 (18)
F (11) -P (2) -F (9)	88.30 (18)
F (12) -P (2) -F (9)	177.2 (2)
F (7) -P (2) -F (9)	87.61 (17)
F (8) -P (2) -F (9)	88.20 (18)
F (10) -P (2) -F (9)	89.18 (16)
F (2B) -F (2A) -P (1)	64.0 (14)
F (2A) -F (2B) -F (3A)	142 (3)
F (2A) -F (2B) -P (1)	78 (2)
F (3A) -F (2B) -P (1)	64.2 (11)
F (3B) -F (3A) -F (2B)	159 (3)
F (3B) -F (3A) -P (1)	95 (2)
F (2B) -F (3A) -P (1)	64.4 (13)
F (3A) -F (3B) -P (1)	59 (2)
C (23) -O (1) -C (32)	117.5 (3)
C (5) -N (1) -C (1)	118.4 (3)
C (5) -N (1) -RU1	116.3 (2)
C (1) -N (1) -RU1	125.2 (2)
C (10) -N (2) -C (6)	118.0 (3)
C (10) -N (2) -RU1	126.3 (3)
C (6) -N (2) -RU1	115.6 (2)
C (20) -N (3) -C (16)	118.3 (3)
C (20) -N (3) -RU1	126.2 (2)
C (16) -N (3) -RU1	115.2 (2)
C (11) -N (4) -C (15)	118.1 (3)
C (11) -N (4) -RU1	126.5 (2)
C (15) -N (4) -RU1	115.3 (2)
C (24) -N (5) -C (21)	116.7 (3)
C (24) -N (5) -RU1	118.4 (2)
C (21) -N (5) -RU1	124.8 (2)
C (24) -N (6) -C (23)	115.8 (3)
C (21) -N (7) -C (31)	123.2 (3)
C (21) -N (7) -C (25)	118.1 (3)
C (31) -N (7) -C (25)	114.2 (3)
C (31) -N (8) -C (28)	121.9 (4)
C (31) -N (8) -C (27)	126.7 (4)
C (28) -N (8) -C (27)	111.2 (4)
C (31) -N (9) -C (30)	115.8 (3)
C (31) -N (9) -RU1	124.7 (3)
C (30) -N (9) -RU1	119.4 (2)
N (1) -C (1) -C (2)	122.3 (3)
C (3) -C (2) -C (1)	118.9 (3)
C (4) -C (3) -C (2)	119.5 (3)
C (3) -C (4) -C (5)	119.7 (3)
N (1) -C (5) -C (4)	121.2 (3)
N (1) -C (5) -C (6)	114.9 (3)
C (4) -C (5) -C (6)	123.9 (3)

Appendix

N(2) -C(6) -C(7)	122.4(3)
N(2) -C(6) -C(5)	115.0(3)
C(7) -C(6) -C(5)	122.5(3)
C(8) -C(7) -C(6)	118.7(4)
C(9) -C(8) -C(7)	119.3(4)
C(8) -C(9) -C(10)	119.7(4)
N(2) -C(10) -C(9)	121.9(4)
N(4) -C(11) -C(12)	122.6(3)
C(13) -C(12) -C(11)	119.3(4)
C(12) -C(13) -C(14)	118.8(4)
C(13) -C(14) -C(15)	119.9(3)
N(4) -C(15) -C(14)	121.0(3)
N(4) -C(15) -C(16)	114.9(3)
C(14) -C(15) -C(16)	124.0(3)
N(3) -C(16) -C(17)	121.0(3)
N(3) -C(16) -C(15)	115.1(3)
C(17) -C(16) -C(15)	123.8(3)
C(18) -C(17) -C(16)	120.0(4)
C(19) -C(18) -C(17)	118.7(3)
C(18) -C(19) -C(20)	119.4(4)
N(3) -C(20) -C(19)	122.5(3)
N(5) -C(21) -N(7)	117.8(3)
N(5) -C(21) -C(22)	119.6(3)
N(7) -C(21) -C(22)	122.5(3)
C(23) -C(22) -C(21)	118.2(3)
O(1) -C(23) -N(6)	119.3(3)
O(1) -C(23) -C(22)	118.2(3)
N(6) -C(23) -C(22)	122.5(3)
N(6) -C(24) -N(5)	127.0(3)
N(7) -C(25) -C(26)	108.3(4)
C(25) -C(26) -C(27)	107.9(5)
N(8) -C(27) -C(26)	111.8(4)
N(8) -C(28) -C(29)	111.0(4)
C(30) -C(29) -C(28)	106.9(6)
N(9) -C(30) -C(29)	110.4(4)
N(9) -C(31) -N(8)	123.9(4)
N(9) -C(31) -N(7)	120.4(3)
N(8) -C(31) -N(7)	115.6(3)
O(1) -C(32) -C(33)	106.8(3)

Appendix

3-3 [C₃₅H₃₉F₁₂N₉OP₂Ru]

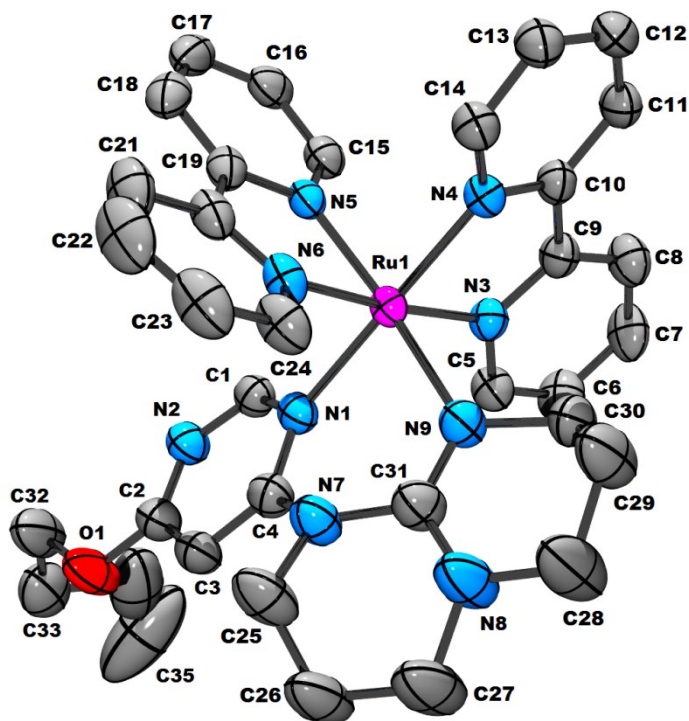


Table 7. Crystal data and structure refinement for C₃₅H₃₉F₁₂N₉OP₂Ru (**3-3**).

Empirical formula	C ₃₅ H ₃₉ F ₁₂ N ₉ O ₂ Ru
Formula weight	992.76
Temperature	100(2) K
Wavelength	0.71073 Å
Crystal system	Monoclinic
Space group	C2/c
Unit cell dimensions	a = 41.763(2) Å α = 90° b = 9.6049(6) Å β = 122.787(2)° c = 24.2324(14) Å γ = 90°
Volume	8171.8(9) Å ³
Z	8
Density (calculated)	1.614 g/cm ³
Absorption coefficient	0.559 mm ⁻¹
F(000)	4016
Crystal size	0.42 x 0.06 x 0.04 mm
Theta range for data collection	1.160 to 25.856 deg.

Appendix

Index ranges	-51<=h<=50, -10<=k<=11, -29<=l<=29
Reflections collected	54092
Independent reflections	7846 [R(int) = 0.045]
Absorption correction	Semi-empirical from equivalents
Max. and min. transmission	0.7534 and 0.4922
Refinement method	Full-matrix least-squares on F ²
Data / restraints / parameters	7846 / 0 / 541
Goodness-of-fit on F ²	1.089
Final R indices [I>2sigma(I)]	R1 = 0.0616, wR2 = 0.1716
R indices (all data)	R1 = 0.0675, wR2 = 0.1774
Largest diff. peak and hole	1.833 and -0.813 e/A ³

Table 8. Bond lengths [Å] and angles [°] for C35H39F12N9OP2Ru (**3-3**)

Ru(1)-N(5)	2.049(4)
Ru(1)-N(4)	2.049(4)
Ru(1)-N(3)	2.062(4)
Ru(1)-N(9)	2.074(4)
Ru(1)-N(1)	2.078(4)
Ru(1)-N(6)	2.078(4)
P(1)-F(6)	1.565(4)
P(1)-F(1)	1.582(4)
P(1)-F(3)	1.589(5)
P(1)-F(5)	1.589(4)
P(1)-F(2)	1.610(4)
P(1)-F(4)	1.611(4)
P(2)-F(10)	1.550(7)
P(2)-F(8)	1.580(6)
P(2)-F(9)	1.581(6)
P(2)-F(7)	1.592(6)
P(2)-F(11)	1.599(5)
P(2)-F(12)	1.604(6)
O(1)-C(2)	1.342(7)
O(1)-C(32)	1.463(7)
N(1)-C(4)	1.346(6)
N(1)-C(1)	1.346(6)
N(2)-C(1)	1.313(6)
N(2)-C(2)	1.327(7)
N(3)-C(5)	1.346(6)
N(3)-C(9)	1.358(6)
N(4)-C(14)	1.352(6)
N(4)-C(10)	1.360(6)
N(5)-C(15)	1.345(6)
N(5)-C(19)	1.378(6)
N(6)-C(20)	1.338(7)
N(6)-C(24)	1.345(7)

Appendix

N(7) -C(4)	1.387(7)
N(7) -C(31)	1.405(7)
N(7) -C(25)	1.486(7)
N(8) -C(31)	1.354(8)
N(8) -C(28)	1.463(9)
N(8) -C(27)	1.476(8)
N(9) -C(31)	1.306(7)
N(9) -C(30)	1.471(7)
C(2) -C(3)	1.383(8)
C(3) -C(4)	1.391(7)
C(5) -C(6)	1.368(7)
C(6) -C(7)	1.362(8)
C(7) -C(8)	1.386(8)
C(8) -C(9)	1.389(7)
C(9) -C(10)	1.469(7)
C(10) -C(11)	1.389(7)
C(11) -C(12)	1.377(7)
C(12) -C(13)	1.385(7)
C(13) -C(14)	1.374(7)
C(15) -C(16)	1.373(7)
C(16) -C(17)	1.389(8)
C(17) -C(18)	1.362(8)
C(18) -C(19)	1.382(7)
C(19) -C(20)	1.458(7)
C(20) -C(21)	1.394(7)
C(21) -C(22)	1.374(10)
C(22) -C(23)	1.349(10)
C(23) -C(24)	1.386(8)
C(25) -C(26)	1.519(11)
C(26) -C(27)	1.505(10)
C(28) -C(29)	1.519(10)
C(29) -C(30)	1.509(9)
C(32) -C(33)	1.481(11)
C(33) -C(34)	1.510(12)
C(34) -C(35)	1.524(19)
N(5) -RU1-N(4)	84.86(14)
N(5) -RU1-N(3)	99.34(15)
N(4) -RU1-N(3)	78.68(15)
N(5) -RU1-N(9)	174.72(15)
N(4) -RU1-N(9)	98.51(16)
N(3) -RU1-N(9)	85.35(16)
N(5) -RU1-N(1)	92.85(15)
N(4) -RU1-N(1)	173.96(15)
N(3) -RU1-N(1)	96.22(15)
N(9) -RU1-N(1)	84.19(16)
N(5) -RU1-N(6)	78.45(16)
N(4) -RU1-N(6)	96.55(15)
N(3) -RU1-N(6)	174.96(15)
N(9) -RU1-N(6)	97.06(17)
N(1) -RU1-N(6)	88.45(15)
F(6) -P(1) -F(1)	91.4(3)
F(6) -P(1) -F(3)	174.0(3)
F(1) -P(1) -F(3)	92.7(3)
F(6) -P(1) -F(5)	89.7(2)
F(1) -P(1) -F(5)	91.6(2)
F(3) -P(1) -F(5)	94.6(3)
F(6) -P(1) -F(2)	89.3(2)
F(1) -P(1) -F(2)	87.6(2)

Appendix

F(3)-P(1)-F(2)	86.5(3)
F(5)-P(1)-F(2)	178.7(3)
F(6)-P(1)-F(4)	87.6(3)
F(1)-P(1)-F(4)	176.4(3)
F(3)-P(1)-F(4)	88.1(3)
F(5)-P(1)-F(4)	91.9(2)
F(2)-P(1)-F(4)	88.9(2)
F(10)-P(2)-F(8)	90.4(4)
F(10)-P(2)-F(9)	90.8(4)
F(8)-P(2)-F(9)	90.0(4)
F(10)-P(2)-F(7)	179.9(4)
F(8)-P(2)-F(7)	89.5(4)
F(9)-P(2)-F(7)	89.3(4)
F(10)-P(2)-F(11)	90.9(4)
F(8)-P(2)-F(11)	178.6(4)
F(9)-P(2)-F(11)	89.5(3)
F(7)-P(2)-F(11)	89.2(3)
F(10)-P(2)-F(12)	90.2(4)
F(8)-P(2)-F(12)	91.6(4)
F(9)-P(2)-F(12)	178.2(3)
F(7)-P(2)-F(12)	89.8(3)
F(11)-P(2)-F(12)	89.0(3)
C(2)-O(1)-C(32)	119.8(5)
C(4)-N(1)-C(1)	115.7(4)
C(4)-N(1)-RU1	125.3(3)
C(1)-N(1)-RU1	118.6(3)
C(1)-N(2)-C(2)	115.2(4)
C(5)-N(3)-C(9)	118.0(4)
C(5)-N(3)-RU1	126.0(3)
C(9)-N(3)-RU1	115.6(3)
C(14)-N(4)-C(10)	117.3(4)
C(14)-N(4)-RU1	126.3(3)
C(10)-N(4)-RU1	115.9(3)
C(15)-N(5)-C(19)	117.6(4)
C(15)-N(5)-RU1	126.9(3)
C(19)-N(5)-RU1	115.4(3)
C(20)-N(6)-C(24)	119.0(5)
C(20)-N(6)-RU1	115.6(3)
C(24)-N(6)-RU1	125.4(4)
C(4)-N(7)-C(31)	123.8(4)
C(4)-N(7)-C(25)	118.6(5)
C(31)-N(7)-C(25)	114.7(5)
C(31)-N(8)-C(28)	121.6(5)
C(31)-N(8)-C(27)	125.8(5)
C(28)-N(8)-C(27)	112.2(5)
C(31)-N(9)-C(30)	115.6(5)
C(31)-N(9)-RU1	124.0(4)
C(30)-N(9)-RU1	120.4(3)
N(2)-C(1)-N(1)	128.1(4)
N(2)-C(2)-O(1)	119.9(5)
N(2)-C(2)-C(3)	122.8(5)
O(1)-C(2)-C(3)	117.3(5)
C(2)-C(3)-C(4)	117.5(5)
N(1)-C(4)-N(7)	117.8(4)
N(1)-C(4)-C(3)	120.5(5)
N(7)-C(4)-C(3)	121.7(5)
N(3)-C(5)-C(6)	122.7(5)
C(7)-C(6)-C(5)	119.6(5)
C(6)-C(7)-C(8)	119.2(5)

Appendix

C (7) -C (8) -C (9)	119.0 (5)
N (3) -C (9) -C (8)	121.4 (5)
N (3) -C (9) -C (10)	114.8 (4)
C (8) -C (9) -C (10)	123.8 (5)
N (4) -C (10) -C (11)	121.7 (4)
N (4) -C (10) -C (9)	114.6 (4)
C (11) -C (10) -C (9)	123.7 (4)
C (12) -C (11) -C (10)	120.1 (5)
C (11) -C (12) -C (13)	118.3 (5)
C (14) -C (13) -C (12)	119.3 (5)
N (4) -C (14) -C (13)	123.3 (5)
N (5) -C (15) -C (16)	123.2 (5)
C (15) -C (16) -C (17)	118.8 (5)
C (18) -C (17) -C (16)	119.0 (5)
C (17) -C (18) -C (19)	120.4 (5)
N (5) -C (19) -C (18)	120.9 (5)
N (5) -C (19) -C (20)	114.8 (4)
C (18) -C (19) -C (20)	124.1 (5)
N (6) -C (20) -C (21)	121.2 (5)
N (6) -C (20) -C (19)	115.4 (4)
C (21) -C (20) -C (19)	123.3 (5)
C (22) -C (21) -C (20)	118.7 (6)
C (23) -C (22) -C (21)	120.5 (6)
C (22) -C (23) -C (24)	118.7 (6)
N (6) -C (24) -C (23)	122.0 (6)
N (7) -C (25) -C (26)	107.0 (6)
C (27) -C (26) -C (25)	107.6 (6)
N (8) -C (27) -C (26)	112.6 (6)
N (8) -C (28) -C (29)	111.6 (6)
C (30) -C (29) -C (28)	106.8 (6)
N (9) -C (30) -C (29)	109.9 (5)
N (9) -C (31) -N (8)	124.0 (5)
N (9) -C (31) -N (7)	121.0 (5)
N (8) -C (31) -N (7)	114.9 (5)
O (1) -C (32) -C (33)	111.7 (6)
C (32) -C (33) -C (34)	110.2 (8)
C (33) -C (34) -C (35)	113.0 (11)

Appendix

3-4 [C₃₆H₄₁F₁₂N₉O₃P₂Ru]

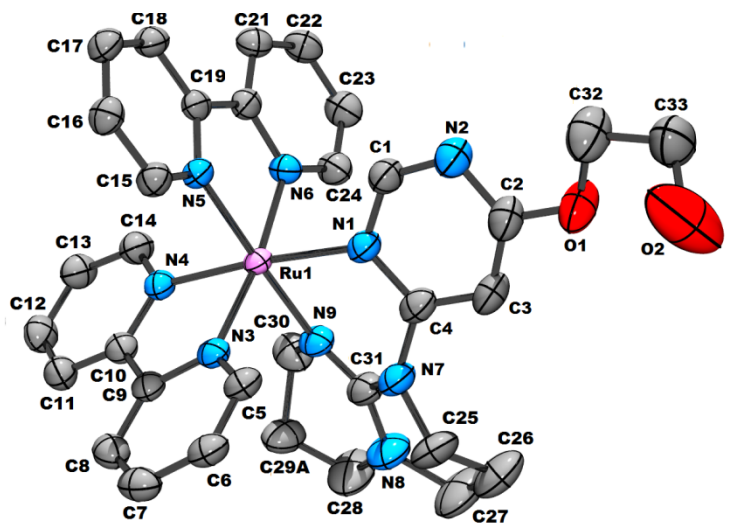


Table 9. Crystal data and structure refinement for C₃₆H₄₁F₁₂N₉O₃P₂Ru (**3-4**).

Empirical formula	C ₃₆ H ₄₁ F ₁₂ N ₉ O ₃ P ₂ Ru
Formula weight	1038.79
Temperature	100(2) K
Wavelength	0.71073 Å
Crystal system	Monoclinic
Space group	P2 ₁ /c
Unit cell dimensions	a = 19.5419(9) Å α = 90° b = 12.9232(6) Å β = 112.899(2)° c = 17.6430(9) Å γ = 90°.
Volume	4104.5(3) Å ³
Z	4
Density (calculated)	1.681 g/cm ³
Absorption coefficient	0.564 mm ⁻¹
F(000)	2104
Crystal size	0.46 x 0.25 x 0.08 mm
Theta range for data collection	1.131 to 25.860 deg.
Index ranges	-23 ≤ h ≤ 23, -15 ≤ k ≤ 14, -21 ≤ l ≤ 21
Reflections collected	81310

Appendix

Independent reflections	7912 [R(int) = 0.063]
Absorption correction	Semi-empirical from equivalents
Max. and min. transmission	0.7534 and 0.4786
Refinement method	Full-matrix least-squares on F ²
Data / restraints / parameters	7912 / 1 / 614
Goodness-of-fit on F ²	1.101
Final R indices [I>2sigma(I)]	R1 = 0.0539, wR2 = 0.1267
R indices (all data)	R1 = 0.0567, wR2 = 0.1283
Largest diff. peak and hole	1.361 and -0.929 e/A ³

Table 10. Bond lengths [Å] and angles [°] for C₃₆H₄₁F₁₂N₉O₃P₂Ru (3-4)

Ru(1)-N(4)	2.053(3)
Ru(1)-N(6)	2.059(3)
Ru(1)-N(3)	2.063(3)
Ru(1)-N(5)	2.063(3)
Ru(1)-N(1)	2.083(4)
Ru(1)-N(9)	2.098(3)
P(1)-F(2)	1.580(3)
P(1)-F(5)	1.586(3)
P(1)-F(1)	1.591(3)
P(1)-F(3)	1.595(3)
P(1)-F(6)	1.596(3)
P(1)-F(4)	1.609(3)
P(2)-F(10a)	1.466(6)
P(2)-F(12)	1.560(4)
P(2)-F(9a)	1.573(9)
P(2)-F(11)	1.583(4)
P(2)-F(7)	1.603(5)
P(2)-F(8)	1.607(4)
P(2)-F(9b)	1.687(7)
P(2)-F(10b)	1.977(13)
F(9a)-F(9b)	1.214(14)
F(9a)-F(10a)	1.297(13)
F(10a)-F(10b)	1.102(13)
O(1)-C(2)	1.338(6)
O(1)-C(32)	1.437(7)
O(2)-C(33)	1.404(8)
O(3)-C(35)	1.210(6)
N(1)-C(1)	1.342(5)
N(1)-C(4)	1.362(5)
N(2)-C(1)	1.328(6)
N(2)-C(2)	1.336(6)
N(3)-C(5)	1.353(6)
N(3)-C(9)	1.360(5)
N(4)-C(14)	1.343(6)
N(4)-C(10)	1.350(5)
N(5)-C(15)	1.350(5)
N(5)-C(19)	1.355(5)

Appendix

N(6) -C(24)	1.341(5)
N(6) -C(20)	1.367(5)
N(7) -C(31)	1.400(6)
N(7) -C(4)	1.401(6)
N(7) -C(25)	1.477(6)
N(8) -C(31)	1.348(6)
N(8) -C(28)	1.463(9)
N(8) -C(27)	1.474(7)
N(9) -C(31)	1.297(6)
N(9) -C(30)	1.472(7)
C(2) -C(3)	1.376(7)
C(3) -C(4)	1.385(7)
C(5) -C(6)	1.372(6)
C(6) -C(7)	1.376(7)
C(7) -C(8)	1.377(7)
C(8) -C(9)	1.386(6)
C(9) -C(10)	1.474(6)
C(10) -C(11)	1.392(6)
C(11) -C(12)	1.382(7)
C(12) -C(13)	1.373(7)
C(13) -C(14)	1.376(6)
C(15) -C(16)	1.382(6)
C(16) -C(17)	1.374(6)
C(17) -C(18)	1.384(6)
C(18) -C(19)	1.384(5)
C(19) -C(20)	1.473(6)
C(20) -C(21)	1.378(6)
C(21) -C(22)	1.385(6)
C(22) -C(23)	1.384(7)
C(23) -C(24)	1.376(6)
C(25) -C(26)	1.509(8)
C(26) -C(27)	1.527(9)
C(28) -C(29b)	1.413(12)
C(28) -C(29a)	1.711(19)
C(29a) -C(30)	1.475(12)
C(29b) -C(30)	1.552(10)
C(32) -C(33)	1.466(8)
C(34) -C(35)	1.487(8)
C(35) -C(36)	1.489(7)
N(4) -RU1-N(6)	95.29(14)
N(4) -RU1-N(3)	78.88(14)
N(6) -RU1-N(3)	172.36(13)
N(4) -RU1-N(5)	88.08(13)
N(6) -RU1-N(5)	78.80(13)
N(3) -RU1-N(5)	95.94(13)
N(4) -RU1-N(1)	175.12(13)
N(6) -RU1-N(1)	87.96(14)
N(3) -RU1-N(1)	98.19(14)
N(5) -RU1-N(1)	96.14(13)
N(4) -RU1-N(9)	90.78(14)
N(6) -RU1-N(9)	96.93(14)
N(3) -RU1-N(9)	88.16(13)
N(5) -RU1-N(9)	175.45(14)
N(1) -RU1-N(9)	85.20(14)
F(2) -P(1) -F(5)	178.73(18)
F(2) -P(1) -F(1)	90.59(18)
F(5) -P(1) -F(1)	90.59(16)
F(2) -P(1) -F(3)	89.9(2)

Appendix

F(5)-P(1)-F(3)	89.59(18)
F(1)-P(1)-F(3)	90.82(17)
F(2)-P(1)-F(6)	90.5(2)
F(5)-P(1)-F(6)	90.0(2)
F(1)-P(1)-F(6)	89.26(16)
F(3)-P(1)-F(6)	179.5(2)
F(2)-P(1)-F(4)	90.39(19)
F(5)-P(1)-F(4)	88.44(17)
F(1)-P(1)-F(4)	178.79(19)
F(3)-P(1)-F(4)	89.90(17)
F(6)-P(1)-F(4)	90.01(17)
F(10A)-P(2)-F(12)	102.4(5)
F(10A)-P(2)-F(9A)	50.4(6)
F(12)-P(2)-F(9A)	152.8(6)
F(10A)-P(2)-F(11)	90.4(3)
F(12)-P(2)-F(11)	90.2(2)
F(9A)-P(2)-F(11)	88.8(4)
F(10A)-P(2)-F(7)	169.5(5)
F(12)-P(2)-F(7)	88.0(3)
F(9A)-P(2)-F(7)	119.2(6)
F(11)-P(2)-F(7)	90.7(3)
F(10A)-P(2)-F(8)	88.8(3)
F(12)-P(2)-F(8)	88.4(2)
F(9A)-P(2)-F(8)	91.8(4)
F(11)-P(2)-F(8)	178.2(3)
F(7)-P(2)-F(8)	90.4(2)
F(10A)-P(2)-F(9B)	93.7(5)
F(12)-P(2)-F(9B)	163.5(3)
F(9A)-P(2)-F(9B)	43.6(5)
F(11)-P(2)-F(9B)	93.2(4)
F(7)-P(2)-F(9B)	75.8(3)
F(8)-P(2)-F(9B)	88.4(4)
F(10A)-P(2)-F(10B)	33.3(5)
F(12)-P(2)-F(10B)	69.2(4)
F(9A)-P(2)-F(10B)	83.7(6)
F(11)-P(2)-F(10B)	92.5(6)
F(7)-P(2)-F(10B)	156.9(4)
F(8)-P(2)-F(10B)	86.0(5)
F(9B)-P(2)-F(10B)	126.8(4)
F(9B)-F(9A)-F(10A)	133.2(9)
F(9B)-F(9A)-P(2)	73.2(7)
F(10A)-F(9A)-P(2)	60.5(4)
F(9A)-F(9B)-P(2)	63.2(5)
F(10B)-F(10A)-F(9A)	168.6(11)
F(10B)-F(10A)-P(2)	99.7(9)
F(9A)-F(10A)-P(2)	69.1(6)
F(10A)-F(10B)-P(2)	47.0(6)
C(2)-O(1)-C(32)	117.9(4)
C(1)-N(1)-C(4)	115.3(4)
C(1)-N(1)-RU1	121.7(3)
C(4)-N(1)-RU1	123.1(3)
C(1)-N(2)-C(2)	115.0(4)
C(5)-N(3)-C(9)	117.8(4)
C(5)-N(3)-RU1	126.8(3)
C(9)-N(3)-RU1	115.4(3)
C(14)-N(4)-C(10)	118.8(4)
C(14)-N(4)-RU1	125.6(3)
C(10)-N(4)-RU1	115.4(3)
C(15)-N(5)-C(19)	118.6(3)

Appendix

C (15) -N (5) -RU1	126.1 (3)
C (19) -N (5) -RU1	115.1 (3)
C (24) -N (6) -C (20)	118.3 (4)
C (24) -N (6) -RU1	126.6 (3)
C (20) -N (6) -RU1	115.1 (3)
C (31) -N (7) -C (4)	123.6 (4)
C (31) -N (7) -C (25)	115.9 (4)
C (4) -N (7) -C (25)	117.3 (4)
C (31) -N (8) -C (28)	119.7 (5)
C (31) -N (8) -C (27)	125.4 (5)
C (28) -N (8) -C (27)	113.7 (5)
C (31) -N (9) -C (30)	117.4 (4)
C (31) -N (9) -RU1	122.1 (3)
C (30) -N (9) -RU1	119.7 (3)
N (2) -C (1) -N (1)	128.0 (4)
N (2) -C (2) -O (1)	119.7 (5)
N (2) -C (2) -C (3)	123.0 (5)
O (1) -C (2) -C (3)	117.3 (4)
C (2) -C (3) -C (4)	117.7 (4)
N (1) -C (4) -C (3)	120.9 (4)
N (1) -C (4) -N (7)	117.8 (4)
C (3) -C (4) -N (7)	121.2 (4)
N (3) -C (5) -C (6)	123.3 (4)
C (5) -C (6) -C (7)	118.6 (4)
C (6) -C (7) -C (8)	119.5 (4)
C (7) -C (8) -C (9)	119.7 (4)
N (3) -C (9) -C (8)	121.2 (4)
N (3) -C (9) -C (10)	114.4 (4)
C (8) -C (9) -C (10)	124.3 (4)
N (4) -C (10) -C (11)	120.8 (4)
N (4) -C (10) -C (9)	115.3 (4)
C (11) -C (10) -C (9)	123.9 (4)
C (12) -C (11) -C (10)	119.9 (4)
C (13) -C (12) -C (11)	118.5 (4)
C (12) -C (13) -C (14)	119.5 (4)
N (4) -C (14) -C (13)	122.4 (4)
N (5) -C (15) -C (16)	122.2 (4)
C (17) -C (16) -C (15)	119.3 (4)
C (16) -C (17) -C (18)	119.0 (4)
C (17) -C (18) -C (19)	119.6 (4)
N (5) -C (19) -C (18)	121.3 (4)
N (5) -C (19) -C (20)	115.1 (3)
C (18) -C (19) -C (20)	123.5 (4)
N (6) -C (20) -C (21)	121.6 (4)
N (6) -C (20) -C (19)	114.5 (4)
C (21) -C (20) -C (19)	123.8 (4)
C (20) -C (21) -C (22)	119.5 (4)
C (23) -C (22) -C (21)	118.7 (4)
C (24) -C (23) -C (22)	119.4 (4)
N (6) -C (24) -C (23)	122.4 (4)
N (7) -C (25) -C (26)	108.1 (5)
C (25) -C (26) -C (27)	107.1 (5)
N (8) -C (27) -C (26)	113.0 (5)
C (29B) -C (28) -N (8)	109.2 (6)
N (8) -C (28) -C (29A)	107.2 (7)
C (30) -C (29A) -C (28)	99.7 (9)
C (28) -C (29B) -C (30)	110.7 (8)
N (9) -C (30) -C (29A)	120.6 (7)
N (9) -C (30) -C (29B)	103.5 (6)

Appendix

N (9) -C (31) -N (8)	125.2 (5)
N (9) -C (31) -N (7)	120.3 (4)
N (8) -C (31) -N (7)	114.5 (4)
O (1) -C (32) -C (33)	107.2 (5)
O (2) -C (33) -C (32)	113.9 (6)
O (3) -C (35) -C (34)	121.5 (5)
O (3) -C (35) -C (36)	120.6 (5)
C (34) -C (35) -C (36)	117.9 (5)

Appendix

Appendix 4 : Crystal Data for Chapter 4

4-L1 [C₁₉H₂₇N₇]

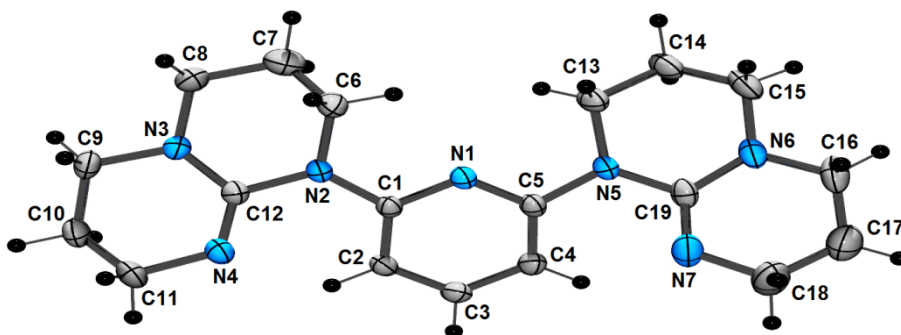


Table 1. Crystal data and structure refinement for C₁₉H₂₇N₇ (**4-L1**).

Empirical formula	C ₁₉ H ₂₇ N ₇
Formula weight	353.47
Temperature	200(2) K
Wavelength	1.54178 Å
Crystal system	Monoclinic
Space group	C ₂ /c
Unit cell dimensions	a = 16.6894(3) Å α = 90° b = 13.1912(2) Å β = 107.752(1)° c = 17.1396(3) Å γ = 90°
Volume	3593.67(11) Å ³
Z	8
Density (calculated)	1.307 g/cm ³
Absorption coefficient	0.654 mm ⁻¹
F(000)	1520
Crystal size	0.20 x 0.14 x 0.06 mm
Theta range for data collection	4.355 to 72.436 deg.
Index ranges	-20 ≤ h ≤ 20, -12 ≤ k ≤ 16, -21 ≤ l ≤ 19
Reflections collected	23763
Independent reflections	3481 [R(int) = 0.039]
Absorption correction	Semi-empirical from equivalents

Appendix

Max. and min. transmission	0.7536 and 0.6350
Refinement method	Full-matrix least-squares on F ²
Data / restraints / parameters	3481 / 0 / 238
Goodness-of-fit on F ²	1.046
Final R indices [I>2sigma(I)]	R1 = 0.0727, wR2 = 0.1959
R indices (all data)	R1 = 0.0817, wR2 = 0.2055
Extinction coefficient	0.0018(2)
Largest diff. peak and hole	1.304 and -0.392 e/A ³

Table 2. Bond lengths [Å] and angles [°] for C19H27N7

N(1)-C(5)	1.335(3)
N(1)-C(1)	1.340(3)
N(2)-C(1)	1.402(3)
N(2)-C(12)	1.409(3)
N(2)-C(6)	1.470(3)
N(3)-C(12)	1.383(3)
N(3)-C(9)	1.460(3)
N(3)-C(8)	1.463(3)
N(4)-C(12)	1.278(3)
N(4)-C(11)	1.462(3)
N(5)-C(19)	1.409(3)
N(5)-C(5)	1.420(3)
N(5)-C(13)	1.468(3)
N(6)-C(19)	1.388(3)
N(6)-C(16)	1.453(3)
N(6)-C(15)	1.457(4)
N(7)-C(19)	1.260(3)
N(7)-C(18)	1.457(4)
C(1)-C(2)	1.399(3)
C(2)-C(3)	1.380(3)
C(3)-C(4)	1.383(3)
C(4)-C(5)	1.394(3)
C(6)-C(7)	1.470(4)
C(7)-C(8)	1.514(4)
C(9)-C(10)	1.510(4)
C(10)-C(11)	1.514(4)
C(13)-C(14)	1.516(3)
C(14)-C(15)	1.494(4)
C(16)-C(17)	1.460(5)
C(17)-C(18)	1.499(5)
C(5)-N(1)-C(1)	119.86(19)
C(1)-N(2)-C(12)	124.24(19)
C(1)-N(2)-C(6)	119.15(19)
C(12)-N(2)-C(6)	116.60(19)
C(12)-N(3)-C(9)	117.1(2)
C(12)-N(3)-C(8)	124.0(2)
C(9)-N(3)-C(8)	113.40(19)
C(12)-N(4)-C(11)	118.8(2)

Appendix

C (19) -N (5) -C (5)	121.19 (19)
C (19) -N (5) -C (13)	119.08 (19)
C (5) -N (5) -C (13)	116.23 (18)
C (19) -N (6) -C (16)	117.0 (2)
C (19) -N (6) -C (15)	123.5 (2)
C (16) -N (6) -C (15)	112.5 (2)
C (19) -N (7) -C (18)	118.5 (2)
N (1) -C (1) -C (2)	121.5 (2)
N (1) -C (1) -N (2)	114.11 (19)
C (2) -C (1) -N (2)	124.3 (2)
C (3) -C (2) -C (1)	117.6 (2)
C (2) -C (3) -C (4)	121.7 (2)
C (3) -C (4) -C (5)	116.7 (2)
N (1) -C (5) -C (4)	122.7 (2)
N (1) -C (5) -N (5)	114.34 (19)
C (4) -C (5) -N (5)	122.8 (2)
N (2) -C (6) -C (7)	109.4 (2)
C (6) -C (7) -C (8)	109.2 (2)
N (3) -C (8) -C (7)	113.6 (2)
N (3) -C (9) -C (10)	109.69 (19)
C (9) -C (10) -C (11)	108.5 (2)
N (4) -C (11) -C (10)	114.3 (2)
N (4) -C (12) -N (3)	126.4 (2)
N (4) -C (12) -N (2)	119.0 (2)
N (3) -C (12) -N (2)	114.6 (2)
N (5) -C (13) -C (14)	109.6 (2)
C (15) -C (14) -C (13)	108.9 (2)
N (6) -C (15) -C (14)	110.7 (2)
N (6) -C (16) -C (17)	110.6 (2)
C (16) -C (17) -C (18)	109.8 (3)
N (7) -C (18) -C (17)	114.6 (3)
N (7) -C (19) -N (6)	126.2 (2)
N (7) -C (19) -N (5)	118.6 (2)
N (6) -C (19) -N (5)	115.2 (2)

Appendix

4-1 [$C_{42}H_{45}F_{12}N_{11}P_2Ru$]

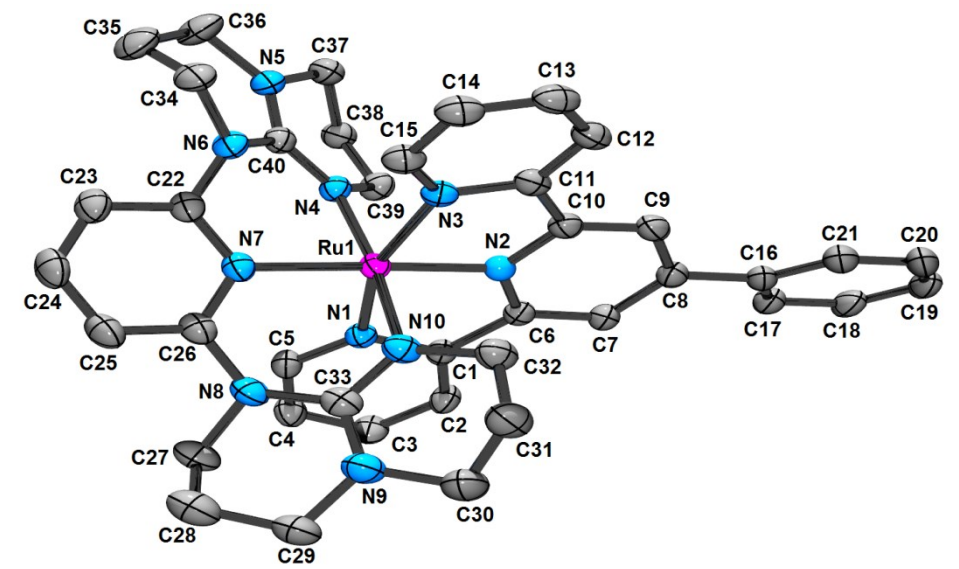


Table 3. Crystal data and structure refinement for $C_{58}H_{78}F_{12}N_{10}O_6P_2Ru$ (**4-1**).

Empirical formula	C ₅₈ H ₇₈ F ₁₂ N ₁₀ O ₆ P ₂ Ru	
Formula weight	1402.31	
Temperature	100(2) K	
Wavelength	1.54178 Å	
Crystal system	Monoclinic	
Space group	C2/c	
Unit cell dimensions	a = 40.9186(5) Å	alpha = 90°
	b = 12.9990(2) Å	beta = 116.184(1)°
	c = 19.2466(2) Å	gamma = 90°.
Volume	9186.7(2) Å ³	
Z	8	
Density (calculated)	2.028 g/cm ³	
Absorption coefficient	4.533 mm ⁻¹	
F(000)	5808	
Crystal size	0.21 x 0.17 x 0.15 mm	
Theta range for data collection	2.406 to 71.231 deg.	
Index ranges	-50<=h<=50, -15<=k<=15, -23<=l<=23	

Appendix

Reflections collected	182676
Independent reflections	8880 [R(int) = 0.027]
Absorption correction	Semi-empirical from equivalents
Max. and min. transmission	0.7534 and 0.6210
Refinement method	Full-matrix least-squares on F ²
Data / restraints / parameters	8880 / 0 / 606
Goodness-of-fit on F ²	1.038
Final R indices [I>2sigma(I)]	R1 = 0.0468, wR2 = 0.1295
R indices (all data)	R1 = 0.0472, wR2 = 0.1299
Largest diff. peak and hole	1.914 and -0.777 e/Å ³

Table 4. Bond lengths [Å] and angles [°] for C58H78F12N10O6P2Ru (**4-1**)

Ru(1)-N(2)	1.946(2)
Ru(1)-N(1)	2.065(2)
Ru(1)-N(4)	2.071(2)
Ru(1)-N(7)	2.072(2)
Ru(1)-N(3)	2.076(2)
Ru(1)-N(10)	2.092(3)
P(1)-F(1a)	1.527(4)
P(1)-F(3)	1.562(3)
P(1)-F(2b)	1.566(10)
P(1)-F(6a)	1.584(4)
P(1)-F(2a)	1.605(5)
P(1)-F(4)	1.607(4)
P(1)-F(5)	1.616(3)
P(1)-F(6b)	1.732(13)
P(1)-F(1b)	1.88(2)
P(2)-F(9)	1.592(2)
P(2)-F(9)#1	1.592(2)
P(2)-F(7)#1	1.595(2)
P(2)-F(7)	1.595(2)
P(2)-F(8)#1	1.602(2)
P(2)-F(8)	1.602(2)
P(3)-F(10b)#2	1.460(17)
P(3)-F(10b)	1.460(17)
P(3)-F(12)#2	1.572(3)
P(3)-F(12)	1.572(3)
P(3)-F(11)#2	1.592(3)
P(3)-F(11)	1.592(3)
P(3)-F(10a)#2	1.659(6)
P(3)-F(10a)	1.659(6)
F(1a)-F(1b)	0.990(18)
F(1a)-F(2b)	1.484(11)
F(1a)-F(6b)	1.570(14)
F(2a)-F(2b)	1.077(12)
F(6a)-F(6b)	0.979(17)

Appendix

F(10a) -F(10b)	1.07(3)
F(10b) -F(10b) #2	1.20(5)
N(1) -C(5)	1.346(4)
N(1) -C(1)	1.376(4)
N(2) -C(10)	1.353(4)
N(2) -C(6)	1.355(4)
N(3) -C(15)	1.347(4)
N(3) -C(11)	1.374(4)
N(4) -C(40)	1.305(4)
N(4) -C(39)	1.476(4)
N(5) -C(40)	1.350(4)
N(5) -C(37)	1.461(4)
N(5) -C(36)	1.466(4)
N(6) -C(22)	1.399(4)
N(6) -C(40)	1.407(4)
N(6) -C(34)	1.473(4)
N(7) -C(22)	1.352(4)
N(7) -C(26)	1.360(4)
N(8) -C(33)	1.400(4)
N(8) -C(26)	1.409(4)
N(8) -C(27)	1.476(4)
N(9) -C(33)	1.343(4)
N(9) -C(30)	1.467(5)
N(9) -C(29)	1.470(5)
N(10) -C(33)	1.310(4)
N(10) -C(32)	1.465(4)
C(1) -C(2)	1.391(4)
C(1) -C(6)	1.472(4)
C(2) -C(3)	1.384(5)
C(3) -C(4)	1.384(5)
C(4) -C(5)	1.384(5)
C(6) -C(7)	1.384(4)
C(7) -C(8)	1.400(4)
C(8) -C(9)	1.399(5)
C(8) -C(16)	1.483(4)
C(9) -C(10)	1.387(4)
C(10) -C(11)	1.472(4)
C(11) -C(12)	1.394(4)
C(12) -C(13)	1.379(5)
C(13) -C(14)	1.383(5)
C(14) -C(15)	1.387(5)
C(16) -C(21)	1.396(5)
C(16) -C(17)	1.401(5)
C(17) -C(18)	1.390(5)
C(18) -C(19)	1.381(6)
C(19) -C(20)	1.391(6)
C(20) -C(21)	1.384(5)
C(22) -C(23)	1.397(4)
C(23) -C(24)	1.374(6)
C(24) -C(25)	1.375(6)
C(25) -C(26)	1.387(5)
C(27) -C(28)	1.497(6)
C(28) -C(29)	1.505(6)
C(30) -C(31)	1.510(6)
C(31) -C(32)	1.511(5)
C(34) -C(35)	1.501(6)
C(35) -C(36)	1.507(6)
C(37) -C(38)	1.512(5)
C(38) -C(39)	1.513(4)

Appendix

N(2) -RU1-N(1)	79.98(10)
N(2) -RU1-N(4)	94.11(10)
N(1) -RU1-N(4)	90.87(10)
N(2) -RU1-N(7)	178.33(10)
N(1) -RU1-N(7)	98.96(10)
N(4) -RU1-N(7)	87.18(10)
N(2) -RU1-N(3)	79.30(10)
N(1) -RU1-N(3)	159.28(10)
N(4) -RU1-N(3)	90.81(10)
N(7) -RU1-N(3)	101.75(10)
N(2) -RU1-N(10)	92.04(10)
N(1) -RU1-N(10)	89.78(10)
N(4) -RU1-N(10)	173.83(10)
N(7) -RU1-N(10)	86.66(11)
N(3) -RU1-N(10)	90.74(10)
F(1A) -P(1) -F(3)	95.5(2)
F(1A) -P(1) -F(2B)	57.3(4)
F(3) -P(1) -F(2B)	85.1(4)
F(1A) -P(1) -F(6A)	91.1(3)
F(3) -P(1) -F(6A)	173.2(2)
F(2B) -P(1) -F(6A)	99.9(4)
F(1A) -P(1) -F(2A)	95.2(2)
F(3) -P(1) -F(2A)	92.4(3)
F(2B) -P(1) -F(2A)	39.7(4)
F(6A) -P(1) -F(2A)	88.7(3)
F(1A) -P(1) -F(4)	177.3(2)
F(3) -P(1) -F(4)	85.95(19)
F(2B) -P(1) -F(4)	125.2(4)
F(6A) -P(1) -F(4)	87.4(3)
F(2A) -P(1) -F(4)	87.0(2)
F(1A) -P(1) -F(5)	92.6(2)
F(3) -P(1) -F(5)	91.8(2)
F(2B) -P(1) -F(5)	149.1(5)
F(6A) -P(1) -F(5)	86.2(2)
F(2A) -P(1) -F(5)	170.7(3)
F(4) -P(1) -F(5)	85.05(17)
F(1A) -P(1) -F(6B)	57.2(6)
F(3) -P(1) -F(6B)	152.3(6)
F(2B) -P(1) -F(6B)	83.1(6)
F(6A) -P(1) -F(6B)	34.0(5)
F(2A) -P(1) -F(6B)	94.3(4)
F(4) -P(1) -F(6B)	121.2(6)
F(5) -P(1) -F(6B)	85.8(4)
F(1A) -P(1) -F(1B)	31.6(5)
F(3) -P(1) -F(1B)	78.2(5)
F(2B) -P(1) -F(1B)	82.2(7)
F(6A) -P(1) -F(1B)	106.8(6)
F(2A) -P(1) -F(1B)	121.9(5)
F(4) -P(1) -F(1B)	147.2(5)
F(5) -P(1) -F(1B)	67.1(5)
F(6B) -P(1) -F(1B)	75.4(7)
F(9) -P(2) -F(9) #1	180.0
F(9) -P(2) -F(7) #1	90.78(13)
F(9) #1 -P(2) -F(7) #1	89.22(13)
F(9) -P(2) -F(7)	89.22(13)
F(9) #1 -P(2) -F(7)	90.78(13)
F(7) #1 -P(2) -F(7)	180.00(16)
F(9) -P(2) -F(8) #1	90.23(12)

Appendix

F (9) #1-P (2) -F (8) #1	89.78 (12)
F (7) #1-P (2) -F (8) #1	89.60 (13)
F (7) -P (2) -F (8) #1	90.40 (13)
F (9) -P (2) -F (8)	89.77 (12)
F (9) #1-P (2) -F (8)	90.22 (12)
F (7) #1-P (2) -F (8)	90.40 (13)
F (7) -P (2) -F (8)	89.60 (13)
F (8) #1-P (2) -F (8)	180.00 (9)
F (10B) #2-P (3) -F (10B)	48.6 (18)
F (10B) #2-P (3) -F (12) #2	116.4 (7)
F (10B) -P (3) -F (12) #2	147.8 (14)
F (10B) #2-P (3) -F (12)	147.8 (14)
F (10B) -P (3) -F (12)	116.4 (7)
F (12) #2-P (3) -F (12)	89.8 (2)
F (10B) #2-P (3) -F (11) #2	107.8 (16)
F (10B) -P (3) -F (11) #2	72.8 (16)
F (12) #2-P (3) -F (11) #2	90.26 (18)
F (12) -P (3) -F (11) #2	89.32 (14)
F (10B) #2-P (3) -F (11)	72.8 (16)
F (10B) -P (3) -F (11)	107.8 (16)
F (12) #2-P (3) -F (11)	89.32 (14)
F (12) -P (3) -F (11)	90.26 (18)
F (11) #2-P (3) -F (11)	179.4 (2)
F (10B) #2-P (3) -F (10A) #2	39.5 (12)
F (10B) -P (3) -F (10A) #2	69.5 (9)
F (12) #2-P (3) -F (10A) #2	83.1 (3)
F (12) -P (3) -F (10A) #2	172.5 (3)
F (11) #2-P (3) -F (10A) #2	88.2 (2)
F (11) -P (3) -F (10A) #2	92.2 (2)
F (10B) #2-P (3) -F (10A)	69.5 (9)
F (10B) -P (3) -F (10A)	39.5 (12)
F (12) #2-P (3) -F (10A)	172.5 (3)
F (12) -P (3) -F (10A)	83.1 (3)
F (11) #2-P (3) -F (10A)	92.2 (2)
F (11) -P (3) -F (10A)	88.2 (2)
F (10A) #2-P (3) -F (10A)	104.0 (6)
F (1B) -F (1A) -F (2B)	133.5 (11)
F (1B) -F (1A) -P (1)	94.4 (10)
F (2B) -F (1A) -P (1)	62.7 (4)
F (1B) -F (1A) -F (6B)	118.0 (12)
F (2B) -F (1A) -F (6B)	91.6 (7)
P (1) -F (1A) -F (6B)	68.0 (7)
F (1A) -F (1B) -P (1)	54.0 (10)
F (2B) -F (2A) -P (1)	68.2 (6)
F (2A) -F (2B) -F (1A)	128.6 (9)
F (2A) -F (2B) -P (1)	72.1 (6)
F (1A) -F (2B) -P (1)	60.0 (4)
F (6B) -F (6A) -P (1)	81.3 (8)
F (6A) -F (6B) -F (1A)	119.3 (12)
F (6A) -F (6B) -P (1)	64.7 (9)
F (1A) -F (6B) -P (1)	54.8 (4)
F (10B) -F (10A) -P (3)	60.2 (10)
F (10A) -F (10B) -F (10B) #2	103 (5)
F (10A) -F (10B) -P (3)	80.3 (15)
F (10B) #2-F (10B) -P (3)	65.7 (9)
C (5) -N (1) -C (1)	118.0 (3)
C (5) -N (1) -RU1	129.1 (2)
C (1) -N (1) -RU1	112.81 (19)
C (10) -N (2) -C (6)	121.1 (3)

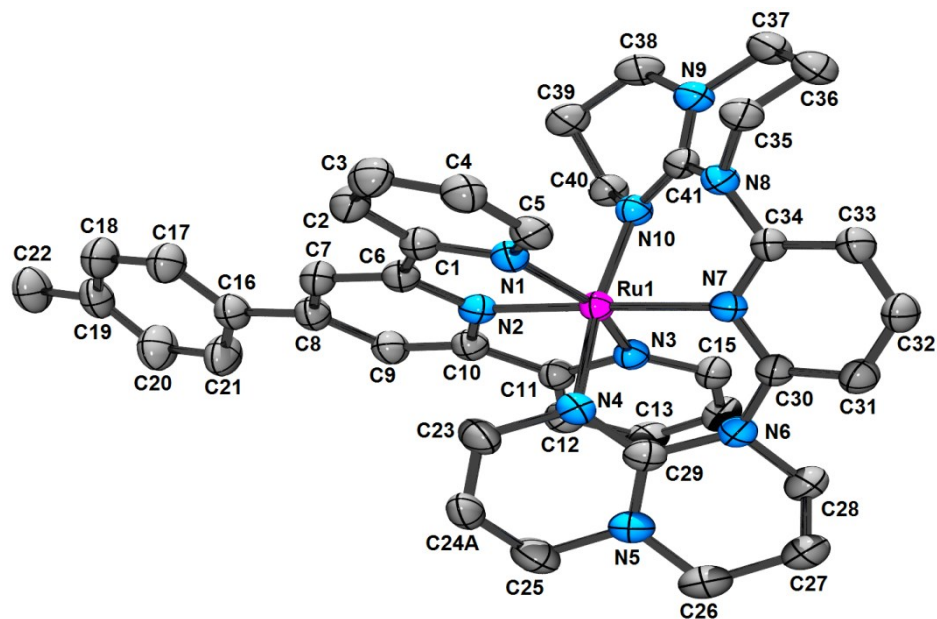
Appendix

C (10) -N (2) -RU1	120.0 (2)
C (6) -N (2) -RU1	118.8 (2)
C (15) -N (3) -C (11)	117.9 (3)
C (15) -N (3) -RU1	128.8 (2)
C (11) -N (3) -RU1	113.1 (2)
C (40) -N (4) -C (39)	120.0 (3)
C (40) -N (4) -RU1	121.2 (2)
C (39) -N (4) -RU1	118.54 (18)
C (40) -N (5) -C (37)	118.3 (3)
C (40) -N (5) -C (36)	126.9 (3)
C (37) -N (5) -C (36)	114.8 (3)
C (22) -N (6) -C (40)	123.5 (3)
C (22) -N (6) -C (34)	118.0 (3)
C (40) -N (6) -C (34)	115.0 (3)
C (22) -N (7) -C (26)	119.2 (3)
C (22) -N (7) -RU1	120.8 (2)
C (26) -N (7) -RU1	120.0 (2)
C (33) -N (8) -C (26)	122.9 (3)
C (33) -N (8) -C (27)	116.1 (3)
C (26) -N (8) -C (27)	118.0 (3)
C (33) -N (9) -C (30)	118.8 (3)
C (33) -N (9) -C (29)	126.3 (3)
C (30) -N (9) -C (29)	114.9 (3)
C (33) -N (10) -C (32)	119.8 (3)
C (33) -N (10) -RU1	120.0 (2)
C (32) -N (10) -RU1	119.4 (2)
N (1) -C (1) -C (2)	121.3 (3)
N (1) -C (1) -C (6)	114.8 (3)
C (2) -C (1) -C (6)	123.8 (3)
C (3) -C (2) -C (1)	119.6 (3)
C (4) -C (3) -C (2)	118.7 (3)
C (3) -C (4) -C (5)	119.6 (3)
N (1) -C (5) -C (4)	122.4 (3)
N (2) -C (6) -C (7)	120.4 (3)
N (2) -C (6) -C (1)	113.0 (3)
C (7) -C (6) -C (1)	126.6 (3)
C (6) -C (7) -C (8)	120.0 (3)
C (9) -C (8) -C (7)	118.0 (3)
C (9) -C (8) -C (16)	121.6 (3)
C (7) -C (8) -C (16)	120.3 (3)
C (10) -C (9) -C (8)	120.2 (3)
N (2) -C (10) -C (9)	120.1 (3)
N (2) -C (10) -C (11)	112.4 (3)
C (9) -C (10) -C (11)	127.4 (3)
N (3) -C (11) -C (12)	121.4 (3)
N (3) -C (11) -C (10)	115.0 (3)
C (12) -C (11) -C (10)	123.4 (3)
C (13) -C (12) -C (11)	119.4 (3)
C (12) -C (13) -C (14)	119.5 (3)
C (13) -C (14) -C (15)	118.9 (3)
N (3) -C (15) -C (14)	122.9 (3)
C (21) -C (16) -C (17)	118.0 (3)
C (21) -C (16) -C (8)	121.5 (3)
C (17) -C (16) -C (8)	120.5 (3)
C (18) -C (17) -C (16)	120.9 (3)
C (19) -C (18) -C (17)	120.5 (4)
C (18) -C (19) -C (20)	119.0 (3)
C (21) -C (20) -C (19)	120.8 (4)
C (20) -C (21) -C (16)	120.8 (4)

Appendix

N(7) -C(22) -C(23)	121.2(3)
N(7) -C(22) -N(6)	118.6(3)
C(23) -C(22) -N(6)	120.2(3)
C(24) -C(23) -C(22)	118.9(3)
C(23) -C(24) -C(25)	120.3(3)
C(24) -C(25) -C(26)	118.8(3)
N(7) -C(26) -C(25)	121.5(3)
N(7) -C(26) -N(8)	118.5(3)
C(25) -C(26) -N(8)	120.0(3)
N(8) -C(27) -C(28)	109.3(3)
C(27) -C(28) -C(29)	107.4(3)
N(9) -C(29) -C(28)	112.3(3)
N(9) -C(30) -C(31)	108.3(3)
C(30) -C(31) -C(32)	108.9(3)
N(10) -C(32) -C(31)	114.0(3)
N(10) -C(33) -N(9)	124.2(3)
N(10) -C(33) -N(8)	118.7(3)
N(9) -C(33) -N(8)	117.0(3)
N(6) -C(34) -C(35)	109.4(3)
C(34) -C(35) -C(36)	107.2(3)
N(5) -C(36) -C(35)	112.3(3)
N(5) -C(37) -C(38)	109.1(3)
C(37) -C(38) -C(39)	108.3(3)
N(4) -C(39) -C(38)	114.1(3)
N(4) -C(40) -N(5)	124.3(3)
N(4) -C(40) -N(6)	119.4(3)
N(5) -C(40) -N(6)	116.2(3)

Appendix

4-2 [C₄₄H₅₀F₁₂N₁₀OP₂Ru]Table 5. Crystal data and structure refinement for C₄₄H₅₀F₁₂N₁₀OP₂Ru (**4-2**)

Empirical formula	C ₄₄ H ₅₀ F ₁₂ N ₁₀ O ₂ P ₂ Ru
Formula weight	1125.95
Temperature	150(2) K
Wavelength	1.54178 Å
Crystal system	Triclinic
Space group	P-1
Unit cell dimensions	a = 8.5139(2) Å α = 96.631(1)° b = 13.5117(4) Å β = 94.882(1)° c = 21.1951(6) Å γ = 106.466(1)°
Volume	2304.75(11) Å ³
Z	2
Density (calculated)	1.622 g/cm ³
Absorption coefficient	4.275 mm ⁻¹
F(000)	1148
Crystal size	0.23 x 0.13 x 0.03 mm
Theta range for data collection	3.448 to 69.670 deg.

Appendix

Index ranges	-10<=h<=10, -16<=k<=16, -20<=l<=25
Reflections collected	70005
Independent reflections	8591 [R(int) = 0.037]
Absorption correction	Semi-empirical from equivalents
Max. and min. transmission	0.7533 and 0.5303
Refinement method	Full-matrix least-squares on F ²
Data / restraints / parameters	8591 / 0 / 656
Goodness-of-fit on F ²	1.039
Final R indices [I>2sigma(I)]	R1 = 0.0345, wR2 = 0.0946
R indices (all data)	R1 = 0.0347, wR2 = 0.0950
Largest diff. peak and hole	0.713 and -0.818 e/A ³

Table 6. Bond lengths [Å] and angles [°] for C₄₄H₅₀F₁₂N₁₀OP₂Ru (**4-2**)

Ru(1)-N(2)	1.9307(19)
Ru(1)-N(10)	2.0639(18)
Ru(1)-N(7)	2.0707(18)
Ru(1)-N(3)	2.0722(19)
Ru(1)-N(1)	2.0859(19)
Ru(1)-N(4)	2.0947(19)
P(1)-F(5)	1.5805(19)
P(1)-F(3)	1.582(2)
P(1)-F(4)	1.5933(16)
P(1)-F(2)	1.5981(18)
P(1)-F(6)	1.6011(18)
P(1)-F(1)	1.6047(16)
P(2)-F(9)#1	1.5916(18)
P(2)-F(9)	1.5917(18)
P(2)-F(8)#1	1.5961(17)
P(2)-F(8)	1.5961(17)
P(2)-F(7)	1.6038(17)
P(2)-F(7)#1	1.6038(17)
P(3)-F(10)	1.568(2)
P(3)-F(10)#2	1.568(2)
P(3)-F(11)	1.570(2)
P(3)-F(11)#2	1.570(2)
P(3)-F(12)#2	1.5784(15)
P(3)-F(12)	1.5784(15)
O(1)-C(43)	1.185(4)
N(1)-C(5)	1.347(3)
N(1)-C(1)	1.369(3)
N(2)-C(10)	1.361(3)
N(2)-C(6)	1.364(3)
N(3)-C(15)	1.349(3)
N(3)-C(11)	1.371(3)
N(4)-C(29)	1.308(3)
N(4)-C(23)	1.465(3)

Appendix

N(5) -C(29)	1.350(3)
N(5) -C(26)	1.456(3)
N(5) -C(25)	1.458(4)
N(6) -C(29)	1.384(3)
N(6) -C(30)	1.417(3)
N(6) -C(28)	1.475(3)
N(7) -C(34)	1.360(3)
N(7) -C(30)	1.361(3)
N(8) -C(34)	1.404(3)
N(8) -C(41)	1.404(3)
N(8) -C(35)	1.474(3)
N(9) -C(41)	1.343(3)
N(9) -C(38)	1.469(3)
N(9) -C(37)	1.471(3)
N(10) -C(41)	1.304(3)
N(10) -C(40)	1.466(3)
C(1) -C(2)	1.391(3)
C(1) -C(6)	1.472(3)
C(2) -C(3)	1.375(4)
C(3) -C(4)	1.382(4)
C(4) -C(5)	1.380(3)
C(6) -C(7)	1.382(3)
C(7) -C(8)	1.407(3)
C(8) -C(9)	1.410(3)
C(8) -C(16)	1.478(3)
C(9) -C(10)	1.378(3)
C(10) -C(11)	1.477(3)
C(11) -C(12)	1.391(3)
C(12) -C(13)	1.390(4)
C(13) -C(14)	1.389(4)
C(14) -C(15)	1.381(3)
C(16) -C(21)	1.384(4)
C(16) -C(17)	1.390(4)
C(17) -C(18)	1.387(4)
C(18) -C(19)	1.380(4)
C(19) -C(20)	1.388(4)
C(19) -C(22)	1.513(4)
C(20) -C(21)	1.386(4)
C(23) -C(24b)	1.419(6)
C(23) -C(24a)	1.498(5)
C(24a) -C(25)	1.408(6)
C(24b) -C(25)	1.560(7)
C(26) -C(27)	1.503(4)
C(27) -C(28)	1.510(4)
C(30) -C(31)	1.376(3)
C(31) -C(32)	1.380(3)
C(32) -C(33)	1.381(3)
C(33) -C(34)	1.392(3)
C(35) -C(36)	1.519(3)
C(36) -C(37)	1.517(4)
C(38) -C(39)	1.508(4)
C(39) -C(40)	1.516(3)
C(42) -C(43)	1.509(7)
C(43) -C(44b)	1.397(14)
C(43) -C(44a)	1.656(13)
N(2) -RU1-N(10)	95.57(7)
N(2) -RU1-N(7)	178.06(7)
N(10) -RU1-N(7)	86.36(7)

Appendix

N(2)-RU1-N(3)	79.86(7)
N(10)-RU1-N(3)	91.95(7)
N(7)-RU1-N(3)	100.31(7)
N(2)-RU1-N(1)	79.03(7)
N(10)-RU1-N(1)	90.37(7)
N(7)-RU1-N(1)	100.78(7)
N(3)-RU1-N(1)	158.89(8)
N(2)-RU1-N(4)	91.37(8)
N(10)-RU1-N(4)	172.68(7)
N(7)-RU1-N(4)	86.71(7)
N(3)-RU1-N(4)	86.99(7)
N(1)-RU1-N(4)	93.23(7)
F(5)-P(1)-F(3)	91.82(15)
F(5)-P(1)-F(4)	90.57(10)
F(3)-P(1)-F(4)	90.79(10)
F(5)-P(1)-F(2)	177.53(14)
F(3)-P(1)-F(2)	90.44(14)
F(4)-P(1)-F(2)	90.37(10)
F(5)-P(1)-F(6)	89.47(13)
F(3)-P(1)-F(6)	178.33(13)
F(4)-P(1)-F(6)	90.25(10)
F(2)-P(1)-F(6)	88.25(12)
F(5)-P(1)-F(1)	89.88(9)
F(3)-P(1)-F(1)	89.44(10)
F(4)-P(1)-F(1)	179.49(10)
F(2)-P(1)-F(1)	89.17(9)
F(6)-P(1)-F(1)	89.50(10)
F(9)#1-P(2)-F(9)	180.0
F(9)#1-P(2)-F(8)#1	89.81(10)
F(9)-P(2)-F(8)#1	90.19(10)
F(9)#1-P(2)-F(8)	90.19(10)
F(9)-P(2)-F(8)	89.81(10)
F(8)#1-P(2)-F(8)	180.0
F(9)#1-P(2)-F(7)	90.45(10)
F(9)-P(2)-F(7)	89.55(10)
F(8)#1-P(2)-F(7)	89.76(9)
F(8)-P(2)-F(7)	90.24(9)
F(9)#1-P(2)-F(7)#1	89.55(10)
F(9)-P(2)-F(7)#1	90.45(10)
F(8)#1-P(2)-F(7)#1	90.24(9)
F(8)-P(2)-F(7)#1	89.76(9)
F(7)-P(2)-F(7)#1	180.0
F(10)-P(3)-F(10)#2	180.0
F(10)-P(3)-F(11)	92.81(18)
F(10)#2-P(3)-F(11)	87.19(18)
F(10)-P(3)-F(11)#2	87.19(18)
F(10)#2-P(3)-F(11)#2	92.81(18)
F(11)-P(3)-F(11)#2	180.0
F(10)-P(3)-F(12)#2	91.81(12)
F(10)#2-P(3)-F(12)#2	88.18(12)
F(11)-P(3)-F(12)#2	90.15(12)
F(11)#2-P(3)-F(12)#2	89.85(12)
F(10)-P(3)-F(12)	88.19(12)
F(10)#2-P(3)-F(12)	91.81(12)
F(11)-P(3)-F(12)	89.85(12)
F(11)#2-P(3)-F(12)	90.15(12)
F(12)#2-P(3)-F(12)	180.0
C(5)-N(1)-C(1)	117.67(19)
C(5)-N(1)-RU1	129.39(15)

Appendix

C (1) -N (1) -RU1	112.90 (15)
C (10) -N (2) -C (6)	120.1 (2)
C (10) -N (2) -RU1	119.32 (15)
C (6) -N (2) -RU1	120.50 (15)
C (15) -N (3) -C (11)	118.19 (19)
C (15) -N (3) -RU1	129.52 (15)
C (11) -N (3) -RU1	111.85 (14)
C (29) -N (4) -C (23)	117.4 (2)
C (29) -N (4) -RU1	118.89 (15)
C (23) -N (4) -RU1	121.76 (16)
C (29) -N (5) -C (26)	125.9 (2)
C (29) -N (5) -C (25)	119.9 (2)
C (26) -N (5) -C (25)	113.8 (2)
C (29) -N (6) -C (30)	122.62 (18)
C (29) -N (6) -C (28)	116.75 (19)
C (30) -N (6) -C (28)	117.80 (18)
C (34) -N (7) -C (30)	117.99 (18)
C (34) -N (7) -RU1	121.87 (14)
C (30) -N (7) -RU1	119.86 (14)
C (34) -N (8) -C (41)	123.90 (17)
C (34) -N (8) -C (35)	118.37 (18)
C (41) -N (8) -C (35)	113.94 (18)
C (41) -N (9) -C (38)	121.43 (19)
C (41) -N (9) -C (37)	125.2 (2)
C (38) -N (9) -C (37)	113.01 (19)
C (41) -N (10) -C (40)	115.53 (18)
C (41) -N (10) -RU1	122.02 (15)
C (40) -N (10) -RU1	122.42 (14)
N (1) -C (1) -C (2)	121.4 (2)
N (1) -C (1) -C (6)	115.04 (19)
C (2) -C (1) -C (6)	123.5 (2)
C (3) -C (2) -C (1)	119.5 (2)
C (2) -C (3) -C (4)	119.5 (2)
C (5) -C (4) -C (3)	118.6 (2)
N (1) -C (5) -C (4)	123.3 (2)
N (2) -C (6) -C (7)	120.7 (2)
N (2) -C (6) -C (1)	111.75 (19)
C (7) -C (6) -C (1)	127.4 (2)
C (6) -C (7) -C (8)	120.5 (2)
C (7) -C (8) -C (9)	117.1 (2)
C (7) -C (8) -C (16)	122.2 (2)
C (9) -C (8) -C (16)	120.5 (2)
C (10) -C (9) -C (8)	120.6 (2)
N (2) -C (10) -C (9)	120.8 (2)
N (2) -C (10) -C (11)	112.04 (19)
C (9) -C (10) -C (11)	127.1 (2)
N (3) -C (11) -C (12)	121.4 (2)
N (3) -C (11) -C (10)	114.90 (19)
C (12) -C (11) -C (10)	123.7 (2)
C (13) -C (12) -C (11)	119.3 (2)
C (14) -C (13) -C (12)	119.0 (2)
C (15) -C (14) -C (13)	119.1 (2)
N (3) -C (15) -C (14)	122.7 (2)
C (21) -C (16) -C (17)	117.4 (2)
C (21) -C (16) -C (8)	121.1 (2)
C (17) -C (16) -C (8)	121.5 (2)
C (18) -C (17) -C (16)	120.6 (3)
C (19) -C (18) -C (17)	122.4 (3)
C (18) -C (19) -C (20)	116.4 (2)

Appendix

C (18) -C (19) -C (22)	122.9 (3)
C (20) -C (19) -C (22)	120.7 (3)
C (21) -C (20) -C (19)	121.9 (3)
C (16) -C (21) -C (20)	121.1 (3)
C (24B) -C (23) -N (4)	120.0 (3)
N (4) -C (23) -C (24A)	108.1 (3)
C (25) -C (24A) -C (23)	114.2 (4)
C (23) -C (24B) -C (25)	109.9 (4)
C (24A) -C (25) -N (5)	113.4 (3)
N (5) -C (25) -C (24B)	108.6 (3)
N (5) -C (26) -C (27)	113.6 (2)
C (26) -C (27) -C (28)	108.0 (2)
N (6) -C (28) -C (27)	109.5 (2)
N (4) -C (29) -N (5)	124.3 (2)
N (4) -C (29) -N (6)	119.5 (2)
N (5) -C (29) -N (6)	116.2 (2)
N (7) -C (30) -C (31)	122.7 (2)
N (7) -C (30) -N (6)	118.38 (19)
C (31) -C (30) -N (6)	118.9 (2)
C (30) -C (31) -C (32)	118.6 (2)
C (31) -C (32) -C (33)	120.0 (2)
C (32) -C (33) -C (34)	118.8 (2)
N (7) -C (34) -C (33)	121.7 (2)
N (7) -C (34) -N (8)	117.73 (18)
C (33) -C (34) -N (8)	120.52 (19)
N (8) -C (35) -C (36)	108.76 (19)
C (37) -C (36) -C (35)	108.1 (2)
N (9) -C (37) -C (36)	113.0 (2)
N (9) -C (38) -C (39)	111.68 (19)
C (38) -C (39) -C (40)	108.2 (2)
N (10) -C (40) -C (39)	109.02 (18)
N (10) -C (41) -N (9)	124.3 (2)
N (10) -C (41) -N (8)	119.99 (19)
N (9) -C (41) -N (8)	115.63 (19)
O (1) -C (43) -C (44B)	131.4 (8)
O (1) -C (43) -C (42)	120.1 (4)
C (44B) -C (43) -C (42)	107.7 (7)
O (1) -C (43) -C (44A)	110.4 (6)
C (42) -C (43) -C (44A)	127.5 (6)

Appendix

4-3 [C₄₁H₄₅BrF₁₂N₁₂OP₂Ru]

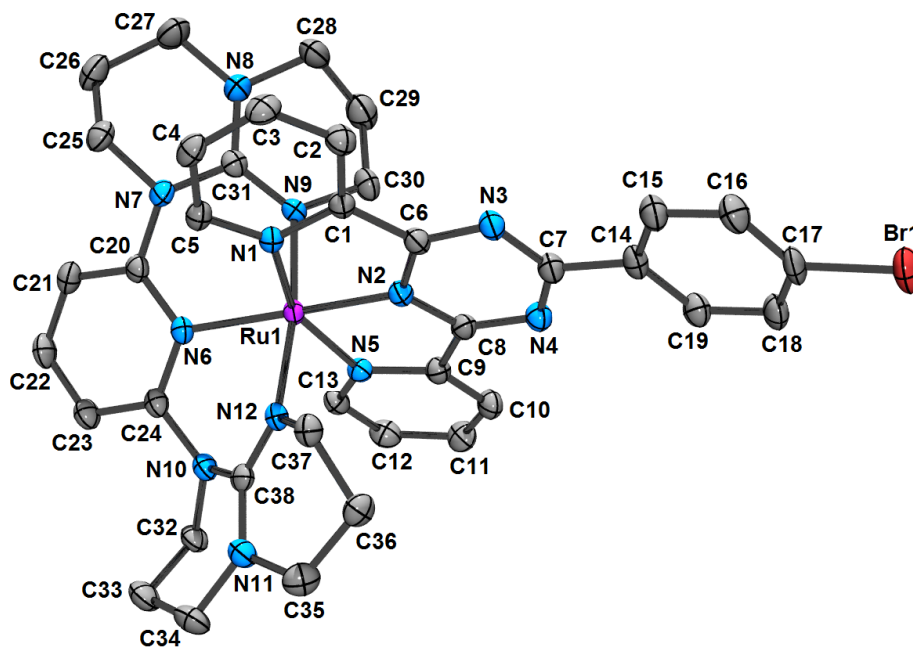


Table 7. Crystal data and structure refinement for C₄₁H₄₅BrF₁₂N₁₂OP₂Ru (**4-3**)

Empirical formula	C ₄₁ H ₄₅ Br F ₁₂ N ₁₂ O ₂ Ru
Formula weight	1192.81
Temperature	100(2) K
Wavelength	1.54178 Å
Crystal system	Monoclinic
Space group	P2 ₁ /n
Unit cell dimensions	a = 8.5505(3) Å α = 90° b = 44.2040(14) Å β = 96.705(2)° c = 12.3222(4) Å γ = 90°
Volume	4625.5(3) Å ³
Z	4
Density (calculated)	1.713 g/cm ³
Absorption coefficient	5.286 mm ⁻¹
F(000)	2400
Crystal size	0.15 x 0.06 x 0.04 mm

Appendix

Theta range for data collection	1.999 to 71.401 deg.
Index ranges	-10<=h<=10, -49<=k<=53, -15<=l<=15
Reflections collected	62839
Independent reflections	8973 [R(int) = 0.103]
Absorption correction	Semi-empirical from equivalents
Max. and min. transmission	0.7535 and 0.4685
Refinement method	Full-matrix least-squares on F ²
Data / restraints / parameters	8973 / 0 / 633
Goodness-of-fit on F ²	1.036
Final R indices [I>2sigma(I)]	R1 = 0.0457, wR2 = 0.1142
R indices (all data)	R1 = 0.0564, wR2 = 0.1239
Largest diff. peak and hole	1.220 and -0.665 e/Å ³

Table 8. Bond lengths [Å] and angles [°] for C41H45BrF12N12OP2Ru (**4-3**)

Br(1)-C(17)	1.900(4)
Ru(1)-N(2)	1.925(3)
Ru(1)-N(12)	2.063(3)
Ru(1)-N(6)	2.069(3)
Ru(1)-N(1)	2.079(3)
Ru(1)-N(9)	2.087(3)
Ru(1)-N(5)	2.088(3)
P(1)-F(1)	1.586(3)
P(1)-F(5)	1.598(3)
P(1)-F(2)	1.600(3)
P(1)-F(6)	1.601(3)
P(1)-F(3)	1.602(3)
P(1)-F(4)	1.613(3)
P(2)-F(9)	1.580(3)
P(2)-F(8)	1.585(3)
P(2)-F(10)	1.588(2)
P(2)-F(7)	1.591(3)
P(2)-F(11)	1.599(3)
P(2)-F(12)	1.610(3)
O(1)-C(40)	1.205(7)
N(1)-C(5)	1.350(4)
N(1)-C(1)	1.382(4)
N(2)-C(6)	1.349(5)
N(2)-C(8)	1.358(4)
N(3)-C(6)	1.321(5)
N(3)-C(7)	1.356(5)
N(4)-C(8)	1.322(5)
N(4)-C(7)	1.351(5)
N(5)-C(13)	1.351(4)
N(5)-C(9)	1.370(4)
N(6)-C(24)	1.354(5)
N(6)-C(20)	1.358(5)

Appendix

N(7) -C(31)	1.392(5)
N(7) -C(20)	1.409(5)
N(7) -C(25)	1.480(4)
N(8) -C(31)	1.342(5)
N(8) -C(27)	1.456(5)
N(8) -C(28)	1.476(5)
N(9) -C(31)	1.309(5)
N(9) -C(30)	1.477(4)
N(10) -C(38)	1.404(5)
N(10) -C(24)	1.414(5)
N(10) -C(32)	1.470(4)
N(11) -C(38)	1.346(5)
N(11) -C(34)	1.469(5)
N(11) -C(35)	1.474(5)
N(12) -C(38)	1.306(5)
N(12) -C(37)	1.463(4)
C(1) -C(2)	1.378(5)
C(1) -C(6)	1.470(5)
C(2) -C(3)	1.394(5)
C(3) -C(4)	1.383(6)
C(4) -C(5)	1.384(5)
C(7) -C(14)	1.479(5)
C(8) -C(9)	1.469(5)
C(9) -C(10)	1.391(5)
C(10) -C(11)	1.386(5)
C(11) -C(12)	1.382(6)
C(12) -C(13)	1.373(5)
C(14) -C(19)	1.397(5)
C(14) -C(15)	1.398(5)
C(15) -C(16)	1.391(5)
C(16) -C(17)	1.390(6)
C(17) -C(18)	1.379(6)
C(18) -C(19)	1.386(5)
C(20) -C(21)	1.383(5)
C(21) -C(22)	1.379(6)
C(22) -C(23)	1.380(6)
C(23) -C(24)	1.396(5)
C(25) -C(26)	1.500(6)
C(26) -C(27)	1.519(6)
C(28) -C(29)	1.544(7)
C(29) -C(30)	1.481(6)
C(32) -C(33)	1.529(5)
C(33) -C(34)	1.508(6)
C(35) -C(36)	1.510(6)
C(36) -C(37)	1.528(5)
C(39) -C(40)	1.487(7)
C(40) -C(41)	1.480(9)
N(2) -RU1-N(12)	95.11(12)
N(2) -RU1-N(6)	178.44(12)
N(12) -RU1-N(6)	86.20(11)
N(2) -RU1-N(1)	78.67(11)
N(12) -RU1-N(1)	92.28(11)
N(6) -RU1-N(1)	102.14(11)
N(2) -RU1-N(9)	92.53(12)
N(12) -RU1-N(9)	172.14(11)
N(6) -RU1-N(9)	86.18(11)
N(1) -RU1-N(9)	87.42(11)
N(2) -RU1-N(5)	78.53(11)

Appendix

N(12)-RU1-N(5)	91.74(11)
N(6)-RU1-N(5)	100.61(11)
N(1)-RU1-N(5)	157.11(11)
N(9)-RU1-N(5)	91.57(11)
F(1)-P(1)-F(5)	91.43(18)
F(1)-P(1)-F(2)	89.91(17)
F(5)-P(1)-F(2)	178.64(19)
F(1)-P(1)-F(6)	90.69(16)
F(5)-P(1)-F(6)	89.93(17)
F(2)-P(1)-F(6)	89.87(17)
F(1)-P(1)-F(3)	90.23(16)
F(5)-P(1)-F(3)	90.16(16)
F(2)-P(1)-F(3)	90.02(16)
F(6)-P(1)-F(3)	179.08(16)
F(1)-P(1)-F(4)	178.76(18)
F(5)-P(1)-F(4)	89.70(18)
F(2)-P(1)-F(4)	88.96(17)
F(6)-P(1)-F(4)	89.81(16)
F(3)-P(1)-F(4)	89.28(16)
F(9)-P(2)-F(8)	89.47(18)
F(9)-P(2)-F(10)	90.10(18)
F(8)-P(2)-F(10)	89.87(16)
F(9)-P(2)-F(7)	90.13(19)
F(8)-P(2)-F(7)	90.72(17)
F(10)-P(2)-F(7)	179.37(18)
F(9)-P(2)-F(11)	92.1(2)
F(8)-P(2)-F(11)	178.35(18)
F(10)-P(2)-F(11)	89.52(16)
F(7)-P(2)-F(11)	89.88(17)
F(9)-P(2)-F(12)	179.3(2)
F(8)-P(2)-F(12)	89.84(15)
F(10)-P(2)-F(12)	89.89(16)
F(7)-P(2)-F(12)	89.88(17)
F(11)-P(2)-F(12)	88.63(18)
C(5)-N(1)-C(1)	117.1(3)
C(5)-N(1)-RU1	129.6(2)
C(1)-N(1)-RU1	113.0(2)
C(6)-N(2)-C(8)	117.4(3)
C(6)-N(2)-RU1	121.0(2)
C(8)-N(2)-RU1	121.5(2)
C(6)-N(3)-C(7)	115.1(3)
C(8)-N(4)-C(7)	115.3(3)
C(13)-N(5)-C(9)	116.9(3)
C(13)-N(5)-RU1	129.7(2)
C(9)-N(5)-RU1	113.4(2)
C(24)-N(6)-C(20)	119.0(3)
C(24)-N(6)-RU1	121.1(2)
C(20)-N(6)-RU1	119.7(2)
C(31)-N(7)-C(20)	122.7(3)
C(31)-N(7)-C(25)	117.4(3)
C(20)-N(7)-C(25)	117.6(3)
C(31)-N(8)-C(27)	126.1(3)
C(31)-N(8)-C(28)	118.3(3)
C(27)-N(8)-C(28)	114.9(3)
C(31)-N(9)-C(30)	119.5(3)
C(31)-N(9)-RU1	119.5(2)
C(30)-N(9)-RU1	119.4(2)
C(38)-N(10)-C(24)	123.2(3)
C(38)-N(10)-C(32)	114.5(3)

Appendix

C (24) -N (10) -C (32)	118.1 (3)
C (38) -N (11) -C (34)	126.4 (3)
C (38) -N (11) -C (35)	120.9 (3)
C (34) -N (11) -C (35)	112.6 (3)
C (38) -N (12) -C (37)	115.7 (3)
C (38) -N (12) -RU1	121.4 (2)
C (37) -N (12) -RU1	122.7 (2)
C (2) -C (1) -N (1)	122.6 (3)
C (2) -C (1) -C (6)	123.7 (3)
N (1) -C (1) -C (6)	113.7 (3)
C (1) -C (2) -C (3)	118.9 (3)
C (4) -C (3) -C (2)	118.8 (3)
C (3) -C (4) -C (5)	119.7 (3)
N (1) -C (5) -C (4)	122.5 (3)
N (3) -C (6) -N (2)	123.4 (3)
N (3) -C (6) -C (1)	124.3 (3)
N (2) -C (6) -C (1)	112.2 (3)
N (4) -C (7) -N (3)	125.3 (3)
N (4) -C (7) -C (14)	117.9 (3)
N (3) -C (7) -C (14)	116.7 (3)
N (4) -C (8) -N (2)	123.0 (3)
N (4) -C (8) -C (9)	125.3 (3)
N (2) -C (8) -C (9)	111.6 (3)
N (5) -C (9) -C (10)	122.8 (3)
N (5) -C (9) -C (8)	114.8 (3)
C (10) -C (9) -C (8)	122.3 (3)
C (11) -C (10) -C (9)	118.7 (3)
C (10) -C (11) -C (12)	118.8 (3)
C (13) -C (12) -C (11)	119.9 (3)
N (5) -C (13) -C (12)	123.0 (3)
C (19) -C (14) -C (15)	119.9 (3)
C (19) -C (14) -C (7)	119.6 (3)
C (15) -C (14) -C (7)	120.3 (3)
C (16) -C (15) -C (14)	120.3 (4)
C (17) -C (16) -C (15)	118.4 (4)
C (18) -C (17) -C (16)	122.0 (3)
C (18) -C (17) -BR1	119.7 (3)
C (16) -C (17) -BR1	118.3 (3)
C (17) -C (18) -C (19)	119.4 (4)
C (18) -C (19) -C (14)	119.9 (4)
N (6) -C (20) -C (21)	121.9 (3)
N (6) -C (20) -N (7)	118.3 (3)
C (21) -C (20) -N (7)	119.8 (3)
C (22) -C (21) -C (20)	118.8 (4)
C (21) -C (22) -C (23)	120.2 (3)
C (22) -C (23) -C (24)	118.7 (3)
N (6) -C (24) -C (23)	121.4 (3)
N (6) -C (24) -N (10)	117.9 (3)
C (23) -C (24) -N (10)	120.6 (3)
N (7) -C (25) -C (26)	110.4 (3)
C (25) -C (26) -C (27)	107.0 (3)
N (8) -C (27) -C (26)	113.0 (4)
N (8) -C (28) -C (29)	107.9 (3)
C (30) -C (29) -C (28)	108.2 (4)
N (9) -C (30) -C (29)	115.2 (3)
N (9) -C (31) -N (8)	124.3 (3)
N (9) -C (31) -N (7)	118.2 (3)
N (8) -C (31) -N (7)	117.4 (3)
N (10) -C (32) -C (33)	108.0 (3)

Appendix

C (34)-C (33)-C (32)	106.9 (3)
N (11)-C (34)-C (33)	112.5 (3)
N (11)-C (35)-C (36)	111.9 (3)
C (35)-C (36)-C (37)	108.2 (3)
N (12)-C (37)-C (36)	108.3 (3)
N (12)-C (38)-N (11)	124.1 (3)
N (12)-C (38)-N (10)	119.5 (3)
N (11)-C (38)-N (10)	116.4 (3)
O (1)-C (40)-C (41)	121.6 (6)
O (1)-C (40)-C (39)	120.6 (5)
C (41)-C (40)-C (39)	117.8 (6)

4-4 [C₆₆H₉₈F₁₂N₁₂O₉P₂Ru]

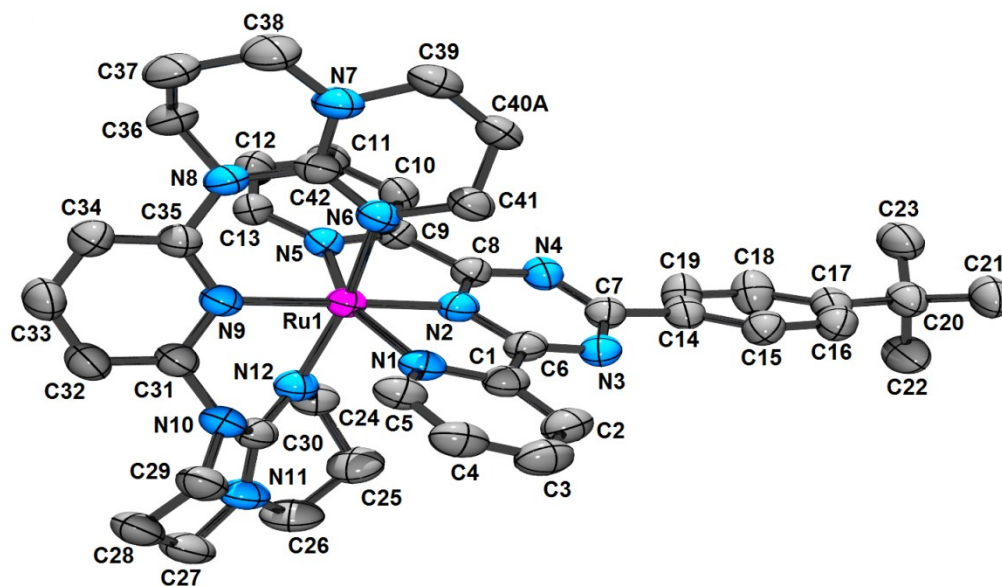


Table 9. Crystal data and structure refinement for C₆₆H₉₈F₁₂N₁₂O₉P₂Ru (**4-4**)

Empirical formula	C ₄₂ H ₄₈ F ₁₂ N ₁₂ O ₀ P ₂ Ru
Formula weight	1111.93
Temperature	150(2) K
Wavelength	1.54178 Å
Crystal system	Monoclinic
Space group	P2 ₁ /c
Unit cell dimensions	a = 9.6046(4) Å α = 90° b = 32.8531(14) Å β = 94.903(2)° c = 17.3497(8) Å γ = 90°
Volume	5454.5(4) Å ³

Appendix

Z	4
Density (calculated)	1.354 g/cm ³
Absorption coefficient	3.602 mm ⁻¹
F(000)	2264
Crystal size	0.23 x 0.16 x 0.03 mm
Theta range for data collection	3.712 to 69.712 deg.
Index ranges	-11<=h<=11, -39<=k<=39, -20<=l<=15
Reflections collected	220993
Independent reflections	10234 [R(int) = 0.043]
Absorption correction	Semi-empirical from equivalents
Max. and min. transmission	0.7533 and 0.5488
Refinement method	Full-matrix least-squares on F ²
Data / restraints / parameters	10234 / 0 / 643
Goodness-of-fit on F ²	1.045
Final R indices [I>2sigma(I)]	R1 = 0.0402, wR2 = 0.1124
R indices (all data)	R1 = 0.0407, wR2 = 0.1129
Largest diff. peak and hole	0.763 and -0.776 e/Å ³

Table 10. Bond lengths [Å] and angles [°] for C66H98F12N12O9P2Ru (**4-4**)

Ru(1)-N(2)	1.930(2)
Ru(1)-N(6)	2.078(2)
Ru(1)-N(9)	2.086(2)
Ru(1)-N(12)	2.089(2)
Ru(1)-N(1)	2.090(2)
Ru(1)-N(5)	2.107(2)
P(1)-F(5b)	1.55(2)
P(1)-F(6)	1.559(2)
P(1)-F(2)	1.581(2)
P(1)-F(1)	1.584(3)
P(1)-F(3)	1.594(2)
P(1)-F(4)	1.613(3)
P(1)-F(5a)	1.640(11)
P(2)-F(8)	1.571(2)
P(2)-F(9)	1.583(2)
P(2)-F(11)	1.589(2)
P(2)-F(7)	1.5933(18)
P(2)-F(12)	1.5956(19)
P(2)-F(10)	1.596(2)

Appendix

F (5a) -F (5b)	0.55 (2)
N (1) -C (5)	1.351 (3)
N (1) -C (1)	1.375 (3)
N (2) -C (8)	1.352 (3)
N (2) -C (6)	1.359 (3)
N (5) -C (13)	1.351 (3)
N (5) -C (9)	1.370 (3)
N (6) -C (42)	1.297 (3)
N (6) -C (41)	1.468 (3)
N (7) -C (42)	1.348 (3)
N (7) -C (38)	1.464 (4)
N (7) -C (39)	1.473 (4)
N (8) -C (42)	1.399 (3)
N (8) -C (35)	1.413 (3)
N (8) -C (36)	1.466 (3)
N (9) -C (35)	1.348 (3)
N (9) -C (31)	1.358 (3)
N (10) -C (30)	1.394 (3)
N (10) -C (31)	1.413 (3)
N (10) -C (29)	1.476 (3)
N (11) -C (30)	1.340 (3)
N (11) -C (26)	1.469 (4)
N (11) -C (27)	1.474 (4)
N (12) -C (30)	1.308 (3)
N (12) -C (24)	1.460 (3)
C (1) -C (2)	1.380 (4)
C (1) -C (6)	1.463 (3)
C (2) -C (3)	1.384 (4)
C (3) -C (4)	1.386 (4)
C (4) -C (5)	1.376 (4)
C (6) -N (3)	1.325 (3)
N (3) -C (7)	1.349 (3)
C (7) -N (4)	1.352 (3)
C (7) -C (14)	1.474 (4)
N (4) -C (8)	1.319 (3)
C (8) -C (9)	1.459 (3)
C (9) -C (10)	1.384 (3)
C (10) -C (11)	1.377 (4)
C (11) -C (12)	1.390 (4)
C (12) -C (13)	1.384 (4)
C (14) -C (19)	1.384 (4)
C (14) -C (15)	1.387 (4)
C (15) -C (16)	1.387 (4)
C (16) -C (17)	1.397 (4)
C (17) -C (18)	1.392 (4)
C (17) -C (20)	1.531 (4)
C (18) -C (19)	1.378 (4)
C (20) -C (21)	1.526 (4)
C (20) -C (22)	1.532 (4)
C (20) -C (23)	1.535 (5)
C (24) -C (25)	1.520 (4)
C (25) -C (26)	1.507 (5)
C (27) -C (28)	1.504 (5)
C (28) -C (29)	1.512 (4)
C (31) -C (32)	1.387 (4)
C (32) -C (33)	1.381 (4)
C (33) -C (34)	1.372 (4)
C (34) -C (35)	1.388 (4)
C (36) -C (37)	1.510 (4)

Appendix

C (37) -C (38)	1.503 (5)
C (39) -C (40a)	1.466 (6)
C (39) -C (40b)	1.487 (9)
C (40a) -C (41)	1.508 (5)
C (40b) -C (41)	1.452 (8)
N (2) -RU1-N (6)	94.91 (7)
N (2) -RU1-N (9)	178.80 (7)
N (6) -RU1-N (9)	85.93 (7)
N (2) -RU1-N (12)	94.06 (7)
N (6) -RU1-N (12)	171.02 (8)
N (9) -RU1-N (12)	85.11 (7)
N (2) -RU1-N (1)	78.07 (8)
N (6) -RU1-N (1)	91.70 (8)
N (9) -RU1-N (1)	101.05 (8)
N (12) -RU1-N (1)	90.55 (8)
N (2) -RU1-N (5)	78.27 (7)
N (6) -RU1-N (5)	88.70 (8)
N (9) -RU1-N (5)	102.63 (7)
N (12) -RU1-N (5)	92.72 (8)
N (1) -RU1-N (5)	156.29 (9)
F (5B) -P (1) -F (6)	80.1 (7)
F (5B) -P (1) -F (2)	167.2 (6)
F (6) -P (1) -F (2)	92.39 (14)
F (5B) -P (1) -F (1)	79.2 (8)
F (6) -P (1) -F (1)	96.33 (19)
F (2) -P (1) -F (1)	91.50 (13)
F (5B) -P (1) -F (3)	99.1 (7)
F (6) -P (1) -F (3)	175.33 (18)
F (2) -P (1) -F (3)	89.22 (13)
F (1) -P (1) -F (3)	88.00 (15)
F (5B) -P (1) -F (4)	101.0 (7)
F (6) -P (1) -F (4)	87.95 (18)
F (2) -P (1) -F (4)	88.98 (13)
F (1) -P (1) -F (4)	175.67 (17)
F (3) -P (1) -F (4)	87.70 (15)
F (5B) -P (1) -F (5A)	19.6 (8)
F (6) -P (1) -F (5A)	92.1 (4)
F (2) -P (1) -F (5A)	173.2 (4)
F (1) -P (1) -F (5A)	93.1 (5)
F (3) -P (1) -F (5A)	85.9 (4)
F (4) -P (1) -F (5A)	86.0 (5)
F (8) -P (2) -F (9)	90.21 (14)
F (8) -P (2) -F (11)	179.44 (15)
F (9) -P (2) -F (11)	89.52 (13)
F (8) -P (2) -F (7)	90.67 (13)
F (9) -P (2) -F (7)	89.44 (12)
F (11) -P (2) -F (7)	89.82 (10)
F (8) -P (2) -F (12)	90.72 (13)
F (9) -P (2) -F (12)	178.38 (12)
F (11) -P (2) -F (12)	89.56 (12)
F (7) -P (2) -F (12)	89.22 (11)
F (8) -P (2) -F (10)	90.08 (14)
F (9) -P (2) -F (10)	90.86 (13)
F (11) -P (2) -F (10)	89.43 (13)
F (7) -P (2) -F (10)	179.20 (14)
F (12) -P (2) -F (10)	90.47 (12)
F (5B) -F (5A) -P (1)	71 (3)
F (5A) -F (5B) -P (1)	89 (4)

Appendix

C (5) -N (1) -C (1)	117.1 (2)
C (5) -N (1) -RU1	129.11 (18)
C (1) -N (1) -RU1	113.82 (15)
C (8) -N (2) -C (6)	117.2 (2)
C (8) -N (2) -RU1	121.30 (15)
C (6) -N (2) -RU1	121.53 (16)
C (13) -N (5) -C (9)	116.5 (2)
C (13) -N (5) -RU1	130.50 (17)
C (9) -N (5) -RU1	112.86 (15)
C (42) -N (6) -C (41)	117.4 (2)
C (42) -N (6) -RU1	120.93 (17)
C (41) -N (6) -RU1	121.58 (16)
C (42) -N (7) -C (38)	124.9 (2)
C (42) -N (7) -C (39)	119.8 (2)
C (38) -N (7) -C (39)	114.3 (2)
C (42) -N (8) -C (35)	122.7 (2)
C (42) -N (8) -C (36)	115.2 (2)
C (35) -N (8) -C (36)	118.0 (2)
C (35) -N (9) -C (31)	118.5 (2)
C (35) -N (9) -RU1	121.48 (15)
C (31) -N (9) -RU1	120.04 (16)
C (30) -N (10) -C (31)	121.1 (2)
C (30) -N (10) -C (29)	116.2 (2)
C (31) -N (10) -C (29)	118.0 (2)
C (30) -N (11) -C (26)	121.6 (2)
C (30) -N (11) -C (27)	126.1 (2)
C (26) -N (11) -C (27)	112.2 (2)
C (30) -N (12) -C (24)	115.6 (2)
C (30) -N (12) -RU1	119.88 (16)
C (24) -N (12) -RU1	123.79 (16)
N (1) -C (1) -C (2)	123.0 (2)
N (1) -C (1) -C (6)	114.2 (2)
C (2) -C (1) -C (6)	122.7 (2)
C (1) -C (2) -C (3)	118.7 (3)
C (2) -C (3) -C (4)	118.6 (3)
C (5) -C (4) -C (3)	120.3 (3)
N (1) -C (5) -C (4)	122.2 (3)
N (3) -C (6) -N (2)	123.1 (2)
N (3) -C (6) -C (1)	125.0 (2)
N (2) -C (6) -C (1)	111.9 (2)
C (6) -N (3) -C (7)	115.6 (2)
N (3) -C (7) -N (4)	125.0 (2)
N (3) -C (7) -C (14)	119.1 (2)
N (4) -C (7) -C (14)	115.8 (2)
C (8) -N (4) -C (7)	115.7 (2)
N (4) -C (8) -N (2)	123.4 (2)
N (4) -C (8) -C (9)	124.2 (2)
N (2) -C (8) -C (9)	112.4 (2)
N (5) -C (9) -C (10)	123.4 (2)
N (5) -C (9) -C (8)	114.8 (2)
C (10) -C (9) -C (8)	121.8 (2)
C (11) -C (10) -C (9)	119.0 (2)
C (10) -C (11) -C (12)	118.4 (2)
C (13) -C (12) -C (11)	119.9 (2)
N (5) -C (13) -C (12)	122.7 (2)
C (19) -C (14) -C (15)	118.2 (3)
C (19) -C (14) -C (7)	120.4 (2)
C (15) -C (14) -C (7)	121.3 (2)
C (14) -C (15) -C (16)	120.9 (3)

Appendix

C (15) -C (16) -C (17)	121.2 (3)
C (18) -C (17) -C (16)	116.9 (3)
C (18) -C (17) -C (20)	120.4 (3)
C (16) -C (17) -C (20)	122.7 (3)
C (19) -C (18) -C (17)	122.0 (3)
C (18) -C (19) -C (14)	120.8 (3)
C (21) -C (20) -C (17)	112.5 (3)
C (21) -C (20) -C (22)	109.5 (3)
C (17) -C (20) -C (22)	107.5 (2)
C (21) -C (20) -C (23)	107.7 (3)
C (17) -C (20) -C (23)	110.0 (3)
C (22) -C (20) -C (23)	109.6 (3)
N (12) -C (24) -C (25)	108.9 (2)
C (26) -C (25) -C (24)	108.3 (3)
N (11) -C (26) -C (25)	111.6 (2)
N (11) -C (27) -C (28)	113.1 (2)
C (27) -C (28) -C (29)	107.4 (2)
N (10) -C (29) -C (28)	109.0 (2)
N (12) -C (30) -N (11)	124.1 (2)
N (12) -C (30) -N (10)	119.1 (2)
N (11) -C (30) -N (10)	116.9 (2)
N (9) -C (31) -C (32)	121.9 (2)
N (9) -C (31) -N (10)	118.0 (2)
C (32) -C (31) -N (10)	120.0 (2)
C (33) -C (32) -C (31)	118.8 (2)
C (34) -C (33) -C (32)	119.6 (3)
C (33) -C (34) -C (35)	119.4 (3)
N (9) -C (35) -C (34)	121.8 (2)
N (9) -C (35) -N (8)	117.7 (2)
C (34) -C (35) -N (8)	120.5 (2)
N (8) -C (36) -C (37)	109.8 (2)
C (38) -C (37) -C (36)	108.5 (3)
N (7) -C (38) -C (37)	113.9 (2)
C (40A) -C (39) -N (7)	113.6 (3)
N (7) -C (39) -C (40B)	105.8 (4)
C (39) -C (40A) -C (41)	109.6 (3)
C (41) -C (40B) -C (39)	111.6 (6)
C (40B) -C (41) -N (6)	116.4 (4)
N (6) -C (41) -C (40A)	108.4 (3)
N (6) -C (42) -N (7)	124.1 (2)
N (6) -C (42) -N (8)	120.4 (2)
N (7) -C (42) -N (8)	115.4 (2)

Appendix

Appendix 5 : Crystal Data for Chapter 5A

5A-1 [C₂₂H₂₇BrN₇O₃Re]

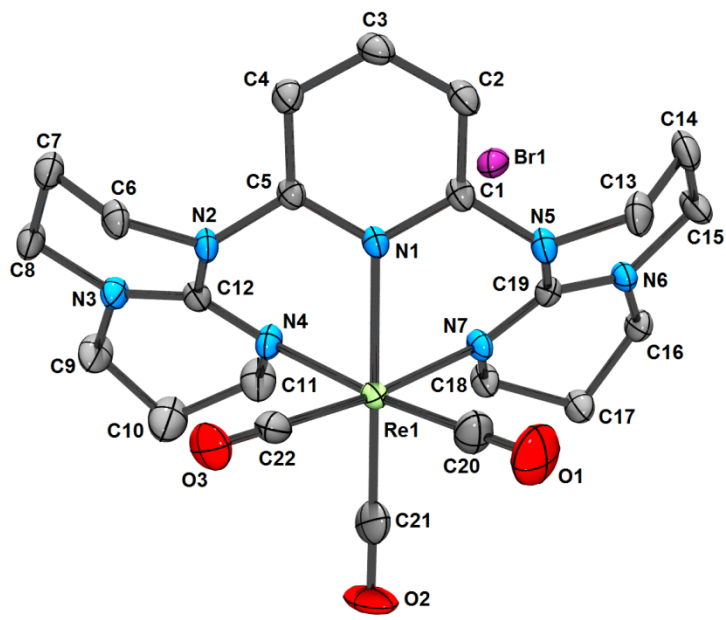


Table 1. Crystal data and structure refinement for C₂₂H₂₇BrN₇O₃Re (**5A-1**)

Empirical formula	C ₂₂ H ₂₇ Br N ₇ O ₃ Re
Formula weight	703.61
Temperature	150(2) K
Wavelength	1.54178 Å
Crystal system	Triclinic
Space group	P-1
Unit cell dimensions	a = 8.1289(3) Å α = 105.115(2)° b = 11.6833(5) Å β = 105.785(2)° c = 13.8021(6) Å γ = 99.199(1)°
Volume	1179.57(9) Å ³
Z	2
Density (calculated)	1.981 g/cm ³
Absorption coefficient	12.397 mm ⁻¹
F(000)	684
Crystal size	0.31 x 0.08 x 0.08 mm
Theta range for data collection	3.513 to 69.654 deg.

Appendix

Index ranges	-9<=h<=9, -14<=k<=14, -16<=l<=15
Reflections collected	74675
Independent reflections	4350 [R(int) = 0.049]
Absorption correction	Semi-empirical from equivalents
Max. and min. transmission	0.7532 and 0.3692
Refinement method	Full-matrix least-squares on F ²
Data / restraints / parameters	4350 / 0 / 307
Goodness-of-fit on F ²	1.105
Final R indices [I>2sigma(I)]	R1 = 0.0271, wR2 = 0.0709
R indices (all data)	R1 = 0.0271, wR2 = 0.0709
Largest diff. peak and hole	1.528 and -0.935 e/Å ³

Table 2. Bond lengths [Å] and angles [°] for C₂₂H₂₇BrN₇O₃Re (**5A-1**)

Re(1)-C(21)	1.901(5)
Re(1)-C(20)	1.922(4)
Re(1)-C(22)	1.933(4)
Re(1)-N(1)	2.175(3)
Re(1)-N(7)	2.183(3)
Re(1)-N(4)	2.199(3)
O(1)-C(20)	1.144(6)
O(2)-C(21)	1.170(6)
O(3)-C(22)	1.153(5)
N(1)-C(5)	1.348(4)
N(1)-C(1)	1.359(4)
N(2)-C(12)	1.402(4)
N(2)-C(5)	1.406(4)
N(2)-C(6)	1.472(4)
N(3)-C(12)	1.339(5)
N(3)-C(8)	1.472(4)
N(3)-C(9)	1.474(5)
N(4)-C(12)	1.311(5)
N(4)-C(11)	1.476(5)
N(5)-C(1)	1.400(5)
N(5)-C(19)	1.413(4)
N(5)-C(13)	1.473(4)
N(6)-C(19)	1.343(4)
N(6)-C(15)	1.462(4)
N(6)-C(16)	1.466(4)
N(7)-C(19)	1.307(4)
N(7)-C(18)	1.462(4)
C(1)-C(2)	1.390(5)
C(2)-C(3)	1.375(5)
C(3)-C(4)	1.389(5)
C(4)-C(5)	1.386(5)
C(6)-C(7)	1.512(5)

Appendix

C (7) -C (8)	1.506 (5)
C (9) -C (10)	1.482 (6)
C (10) -C (11)	1.485 (6)
C (13) -C (14)	1.508 (6)
C (14) -C (15)	1.513 (5)
C (16) -C (17)	1.508 (5)
C (17) -C (18)	1.514 (5)
C (21) -RE1 -C (20)	88.1 (2)
C (21) -RE1 -C (22)	89.23 (16)
C (20) -RE1 -C (22)	89.52 (17)
C (21) -RE1 -N (1)	174.11 (15)
C (20) -RE1 -N (1)	96.24 (16)
C (22) -RE1 -N (1)	94.74 (13)
C (21) -RE1 -N (7)	97.27 (14)
C (20) -RE1 -N (7)	91.04 (15)
C (22) -RE1 -N (7)	173.49 (13)
N (1) -RE1 -N (7)	78.75 (11)
C (21) -RE1 -N (4)	97.52 (17)
C (20) -RE1 -N (4)	174.36 (16)
C (22) -RE1 -N (4)	90.39 (14)
N (1) -RE1 -N (4)	78.14 (11)
N (7) -RE1 -N (4)	88.41 (11)
C (5) -N (1) -C (1)	119.7 (3)
C (5) -N (1) -RE1	119.9 (2)
C (1) -N (1) -RE1	120.3 (2)
C (12) -N (2) -C (5)	121.4 (3)
C (12) -N (2) -C (6)	117.3 (3)
C (5) -N (2) -C (6)	118.5 (3)
C (12) -N (3) -C (8)	126.0 (3)
C (12) -N (3) -C (9)	120.9 (3)
C (8) -N (3) -C (9)	112.4 (3)
C (12) -N (4) -C (11)	116.2 (3)
C (12) -N (4) -RE1	117.0 (2)
C (11) -N (4) -RE1	123.2 (2)
C (1) -N (5) -C (19)	119.6 (3)
C (1) -N (5) -C (13)	118.9 (3)
C (19) -N (5) -C (13)	115.1 (3)
C (19) -N (6) -C (15)	126.7 (3)
C (19) -N (6) -C (16)	121.4 (3)
C (15) -N (6) -C (16)	111.8 (3)
C (19) -N (7) -C (18)	116.4 (3)
C (19) -N (7) -RE1	120.2 (2)
C (18) -N (7) -RE1	122.7 (2)
N (1) -C (1) -C (2)	120.7 (3)
N (1) -C (1) -N (5)	117.1 (3)
C (2) -C (1) -N (5)	122.2 (3)
C (3) -C (2) -C (1)	118.7 (3)
C (2) -C (3) -C (4)	120.7 (3)
C (5) -C (4) -C (3)	117.9 (3)
N (1) -C (5) -C (4)	121.7 (3)
N (1) -C (5) -N (2)	117.6 (3)
C (4) -C (5) -N (2)	120.7 (3)
N (2) -C (6) -C (7)	109.3 (3)
C (8) -C (7) -C (6)	107.4 (3)
N (3) -C (8) -C (7)	113.0 (3)
N (3) -C (9) -C (10)	112.1 (3)
C (9) -C (10) -C (11)	111.5 (4)
N (4) -C (11) -C (10)	110.4 (3)

Appendix

N(4)-C(12)-N(3)	124.9(3)
N(4)-C(12)-N(2)	118.2(3)
N(3)-C(12)-N(2)	116.9(3)
N(5)-C(13)-C(14)	109.7(3)
C(13)-C(14)-C(15)	108.5(3)
N(6)-C(15)-C(14)	113.3(3)
N(6)-C(16)-C(17)	110.5(3)
C(16)-C(17)-C(18)	108.8(3)
N(7)-C(18)-C(17)	110.5(3)
N(7)-C(19)-N(6)	125.3(3)
N(7)-C(19)-N(5)	118.4(3)
N(6)-C(19)-N(5)	116.3(3)
O(1)-C(20)-RE1	179.2(5)
O(2)-C(21)-RE1	178.5(4)
O(3)-C(22)-RE1	178.8(3)

5A-2 [C₂₁H₂₆BrN₈O₃Re]

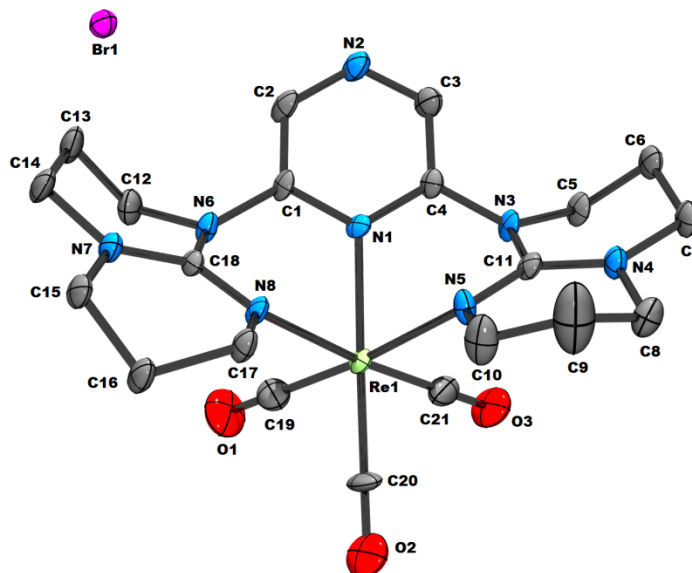


Table 3. Crystal data and structure refinement for C₂₁H₂₆BrN₈O₃Re (**5A-2**)

Empirical formula	C ₂₁ H ₂₆ Br N ₈ O ₃ Re
Formula weight	704.61
Temperature	150(2) K
Wavelength	1.54178 Å
Crystal system	Triclinic
Space group	P-1
Unit cell dimensions	a = 8.2315(6) Å α = 104.882(3)°

Appendix

	$b = 11.7681(6) \text{ \AA}$	$\beta = 105.407(3)^\circ$
	$c = 13.3936(8) \text{ \AA}$	$\gamma = 99.732(3)^\circ$
Volume	1168.99(13) \AA^3	
Z	2	
Density (calculated)	2.002 g/cm ³	
Absorption coefficient	12.524 mm ⁻¹	
F(000)	684	
Crystal size	0.42 x 0.21 x 0.10 mm	
Theta range for data collection	3.610 to 69.808 deg.	
Index ranges	-9<=h<=9, -11<=k<=14, -16<=l<=16	
Reflections collected	48485	
Independent reflections	4333 [R(int) = 0.054]	
Absorption correction	Semi-empirical from equivalents	
Max. and min. transmission	0.7533 and 0.4083	
Refinement method	Full-matrix least-squares on F ²	
Data / restraints / parameters	4333 / 0 / 301	
Goodness-of-fit on F ²	1.082	
Final R indices [I>2sigma(I)]	R1 = 0.0337, wR2 = 0.0908	
R indices (all data)	R1 = 0.0337, wR2 = 0.0908	
Largest diff. peak and hole	2.646 and -1.040 e/ \AA^3	

Table 4. Bond lengths [\AA] and angles [$^\circ$] for C₂₁H₂₆BrN₈O₃Re (**5A-2**)

Re(1)-C(21)	1.900(6)
Re(1)-C(20)	1.931(5)
Re(1)-C(19)	1.934(6)
Re(1)-N(1)	2.163(4)
Re(1)-N(8)	2.194(4)
Re(1)-N(5)	2.195(4)
O(1)-C(19)	1.135(7)
O(2)-C(20)	1.140(7)
O(3)-C(21)	1.184(7)
N(1)-C(4)	1.349(6)
N(1)-C(1)	1.356(6)
N(2)-C(3)	1.328(6)
N(2)-C(2)	1.330(6)
N(3)-C(4)	1.390(6)
N(3)-C(11)	1.404(6)
N(3)-C(5)	1.474(5)

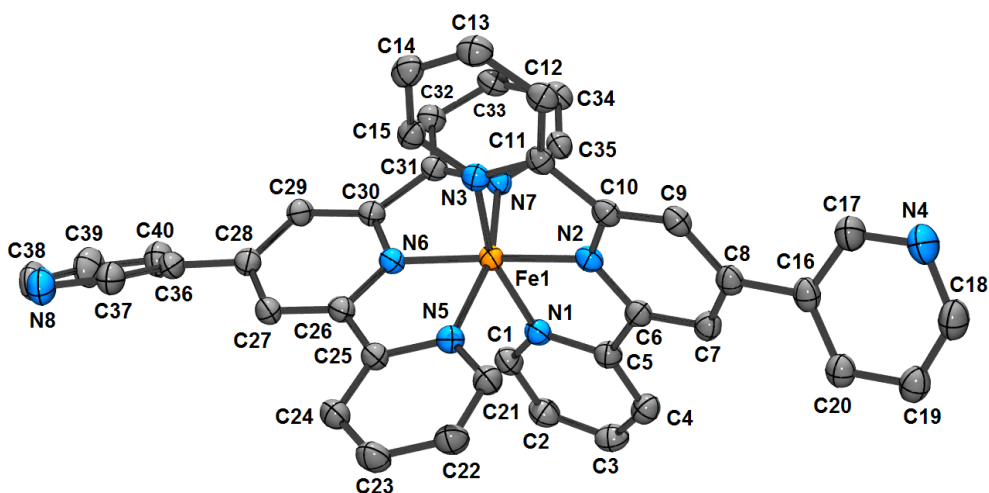
Appendix

N(4) -C(11)	1.338(6)
N(4) -C(8)	1.470(6)
N(4) -C(7)	1.471(6)
N(5) -C(11)	1.312(6)
N(5) -C(10)	1.473(6)
N(6) -C(1)	1.400(6)
N(6) -C(18)	1.414(6)
N(6) -C(12)	1.469(6)
N(7) -C(18)	1.340(6)
N(7) -C(14)	1.465(6)
N(7) -C(15)	1.467(6)
N(8) -C(18)	1.306(6)
N(8) -C(17)	1.461(6)
C(1) -C(2)	1.394(7)
C(3) -C(4)	1.397(7)
C(5) -C(6)	1.509(7)
C(6) -C(7)	1.513(7)
C(8) -C(9)	1.464(9)
C(9) -C(10)	1.446(9)
C(12) -C(13)	1.518(7)
C(13) -C(14)	1.508(7)
C(15) -C(16)	1.506(6)
C(16) -C(17)	1.518(6)
C(21) -RE1 -C(20)	87.9(2)
C(21) -RE1 -C(19)	89.6(2)
C(20) -RE1 -C(19)	88.6(3)
C(21) -RE1 -N(1)	95.77(19)
C(20) -RE1 -N(1)	173.86(19)
C(19) -RE1 -N(1)	96.3(2)
C(21) -RE1 -N(8)	174.34(19)
C(20) -RE1 -N(8)	97.77(18)
C(19) -RE1 -N(8)	90.28(19)
N(1) -RE1 -N(8)	78.61(14)
C(21) -RE1 -N(5)	90.48(18)
C(20) -RE1 -N(5)	97.1(2)
C(19) -RE1 -N(5)	174.25(19)
N(1) -RE1 -N(5)	77.95(15)
N(8) -RE1 -N(5)	89.05(15)
C(4) -N(1) -C(1)	118.5(4)
C(4) -N(1) -RE1	120.7(3)
C(1) -N(1) -RE1	120.8(3)
C(3) -N(2) -C(2)	118.2(4)
C(4) -N(3) -C(11)	121.2(3)
C(4) -N(3) -C(5)	118.8(4)
C(11) -N(3) -C(5)	117.8(4)
C(11) -N(4) -C(8)	118.8(4)
C(11) -N(4) -C(7)	126.2(4)
C(8) -N(4) -C(7)	114.6(4)
C(11) -N(5) -C(10)	118.2(4)
C(11) -N(5) -RE1	117.0(3)
C(10) -N(5) -RE1	121.8(3)
C(1) -N(6) -C(18)	119.6(4)
C(1) -N(6) -C(12)	119.3(4)
C(18) -N(6) -C(12)	116.1(4)
C(18) -N(7) -C(14)	126.6(4)
C(18) -N(7) -C(15)	121.4(4)
C(14) -N(7) -C(15)	112.0(4)
C(18) -N(8) -C(17)	117.3(4)

Appendix

C (18) -N (8) -RE1	119.6 (3)
C (17) -N (8) -RE1	121.7 (3)
N (1) -C (1) -C (2)	119.7 (4)
N (1) -C (1) -N (6)	117.5 (4)
C (2) -C (1) -N (6)	122.9 (4)
N (2) -C (2) -C (1)	121.7 (4)
N (2) -C (3) -C (4)	121.8 (4)
N (1) -C (4) -N (3)	117.8 (4)
N (1) -C (4) -C (3)	119.7 (4)
N (3) -C (4) -C (3)	122.4 (4)
N (3) -C (5) -C (6)	109.2 (4)
C (5) -C (6) -C (7)	107.7 (4)
N (4) -C (7) -C (6)	112.6 (4)
C (9) -C (8) -N (4)	109.3 (5)
C (10) -C (9) -C (8)	114.6 (6)
C (9) -C (10) -N (5)	116.0 (5)
N (5) -C (11) -N (4)	124.7 (4)
N (5) -C (11) -N (3)	118.4 (4)
N (4) -C (11) -N (3)	116.9 (4)
N (6) -C (12) -C (13)	109.5 (4)
C (14) -C (13) -C (12)	108.8 (4)
N (7) -C (14) -C (13)	113.8 (4)
N (7) -C (15) -C (16)	110.3 (4)
C (15) -C (16) -C (17)	108.6 (4)
N (8) -C (17) -C (16)	110.0 (4)
N (8) -C (18) -N (7)	124.9 (4)
N (8) -C (18) -N (6)	118.7 (4)
N (7) -C (18) -N (6)	116.3 (4)
O (1) -C (19) -RE1	179.7 (7)
O (2) -C (20) -RE1	179.6 (5)
O (3) -C (21) -RE1	177.6 (5)

Appendix

5B-1b [C₈₈H₆₈B₂FeN₈]Table 5. Crystal data and structure refinement for C₈₈H₆₈B₂FeN₈ (**5B-1b**)

Empirical formula	C ₈₈ H ₆₈ B ₂ Fe N ₈	
Formula weight	1314.97	
Temperature	150(2) K	
Wavelength	1.54178 Å	
Crystal system	Monoclinic	
Space group	P2 ₁ /c	
Unit cell dimensions	a = 18.0475(12) Å	α = 90°
	b = 17.6434(11) Å	β = 102.510(3)°
	c = 21.3645(14) Å	γ = 90°
Volume	6641.4(7) Å ³	
Z	4	
Density (calculated)	1.315 g/cm ³	
Absorption coefficient	2.254 mm ⁻¹	
F(000)	2752	
Crystal size	0.16 x 0.04 x 0.01 mm	
Theta range for data collection	2.508 to 65.084 deg.	
Index ranges	-17 ≤ h ≤ 21, -20 ≤ k ≤ 20, -25 ≤ l ≤ 25	
Reflections collected	306511	

Appendix

Independent reflections	11334 [R(int) = 0.063]
Absorption correction	Semi-empirical from equivalents
Max. and min. transmission	0.9977 and 0.7144
Refinement method	Full-matrix least-squares on F ²
Data / restraints / parameters	11334 / 0 / 892
Goodness-of-fit on F ²	1.045
Final R indices [I>2sigma(I)]	R1 = 0.0388, wR2 = 0.1077
R indices (all data)	R1 = 0.0403, wR2 = 0.1102
Largest diff. peak and hole	0.744 and -0.352 e/Å ³

Table 6. Bond lengths [Å] and angles [°] for C₈₈H₆₈B₂FeN₈ (**5B-1b**)

Fe(1)-N(2)	1.8722(13)
Fe(1)-N(6)	1.8811(12)
Fe(1)-N(1)	1.9664(14)
Fe(1)-N(3)	1.9698(12)
Fe(1)-N(7)	1.9750(12)
Fe(1)-N(5)	1.9839(13)
N(1)-C(1)	1.342(2)
N(1)-C(5)	1.367(2)
N(2)-C(6)	1.3497(19)
N(2)-C(10)	1.3523(19)
N(3)-C(15)	1.342(2)
N(3)-C(11)	1.368(2)
N(4)-C(18)	1.333(3)
N(4)-C(17)	1.344(2)
N(5)-C(21)	1.341(2)
N(5)-C(25)	1.366(2)
N(6)-C(26)	1.3521(19)
N(6)-C(30)	1.3532(19)
N(7)-C(35)	1.345(2)
N(7)-C(31)	1.3718(19)
N(8)-C(37)	1.334(2)
N(8)-C(38)	1.339(3)
C(1)-C(2)	1.382(2)
C(2)-C(3)	1.380(2)
C(3)-C(4)	1.385(2)
C(4)-C(5)	1.389(2)
C(5)-C(6)	1.467(2)
C(6)-C(7)	1.381(2)
C(7)-C(8)	1.399(2)
C(8)-C(9)	1.404(2)
C(8)-C(16)	1.480(2)
C(9)-C(10)	1.392(2)
C(10)-C(11)	1.468(2)
C(11)-C(12)	1.385(2)
C(12)-C(13)	1.381(2)
C(13)-C(14)	1.389(2)
C(14)-C(15)	1.378(2)

Appendix

C (16) -C (17)	1.388 (2)
C (16) -C (20)	1.395 (2)
C (18) -C (19)	1.377 (3)
C (19) -C (20)	1.377 (2)
C (21) -C (22)	1.385 (2)
C (22) -C (23)	1.378 (2)
C (23) -C (24)	1.383 (2)
C (24) -C (25)	1.387 (2)
C (25) -C (26)	1.471 (2)
C (26) -C (27)	1.385 (2)
C (27) -C (28)	1.396 (2)
C (28) -C (29)	1.404 (2)
C (28) -C (36)	1.481 (2)
C (29) -C (30)	1.392 (2)
C (30) -C (31)	1.475 (2)
C (31) -C (32)	1.381 (2)
C (32) -C (33)	1.384 (2)
C (33) -C (34)	1.382 (2)
C (34) -C (35)	1.382 (2)
C (36) -C (40)	1.379 (2)
C (36) -C (37)	1.399 (2)
C (38) -C (39)	1.368 (3)
C (39) -C (40)	1.389 (3)
C (41) -C (46)	1.396 (2)
C (41) -C (42)	1.405 (2)
C (41) -B (1)	1.646 (2)
C (42) -C (43)	1.382 (2)
C (43) -C (44)	1.381 (3)
C (44) -C (45)	1.381 (3)
C (45) -C (46)	1.394 (2)
C (47) -C (52)	1.401 (2)
C (47) -C (48)	1.404 (2)
C (47) -B (1)	1.649 (2)
C (48) -C (49)	1.380 (2)
C (49) -C (50)	1.395 (3)
C (50) -C (51)	1.385 (3)
C (51) -C (52)	1.387 (2)
C (53) -C (54)	1.401 (2)
C (53) -C (58)	1.405 (2)
C (53) -B (1)	1.644 (2)
C (54) -C (55)	1.391 (2)
C (55) -C (56)	1.381 (2)
C (56) -C (57)	1.385 (2)
C (57) -C (58)	1.391 (2)
C (59) -C (64)	1.398 (2)
C (59) -C (60)	1.403 (2)
C (59) -B (1)	1.648 (2)
C (60) -C (61)	1.395 (2)
C (61) -C (62)	1.378 (2)
C (62) -C (63)	1.388 (2)
C (63) -C (64)	1.385 (2)
C (65) -C (66)	1.398 (2)
C (65) -C (70)	1.403 (2)
C (65) -B (2)	1.646 (2)
C (66) -C (67)	1.384 (2)
C (67) -C (68)	1.382 (2)
C (68) -C (69)	1.380 (3)
C (69) -C (70)	1.387 (3)
C (71) -C (72)	1.399 (2)

Appendix

C (71) -C (76)	1.400 (2)
C (71) -B (2)	1.643 (2)
C (72) -C (73)	1.394 (3)
C (73) -C (74)	1.380 (3)
C (74) -C (75)	1.378 (3)
C (75) -C (76)	1.384 (3)
C (77) -C (78)	1.398 (2)
C (77) -C (82)	1.403 (2)
C (77) -B (2)	1.648 (2)
C (78) -C (79)	1.397 (2)
C (79) -C (80)	1.378 (3)
C (80) -C (81)	1.388 (3)
C (81) -C (82)	1.390 (2)
C (83) -C (84)	1.400 (2)
C (83) -C (88)	1.408 (2)
C (83) -B (2)	1.658 (2)
C (84) -C (85)	1.398 (2)
C (85) -C (86)	1.382 (3)
C (86) -C (87)	1.387 (3)
C (87) -C (88)	1.389 (2)
N (2) -FE1-N (6)	175.35 (5)
N (2) -FE1-N (1)	80.96 (5)
N (6) -FE1-N (1)	100.44 (5)
N (2) -FE1-N (3)	81.33 (5)
N (6) -FE1-N (3)	97.41 (5)
N (1) -FE1-N (3)	162.13 (5)
N (2) -FE1-N (7)	103.60 (5)
N (6) -FE1-N (7)	80.86 (5)
N (1) -FE1-N (7)	90.93 (5)
N (3) -FE1-N (7)	90.95 (5)
N (2) -FE1-N (5)	94.09 (5)
N (6) -FE1-N (5)	81.46 (5)
N (1) -FE1-N (5)	91.74 (5)
N (3) -FE1-N (5)	91.85 (5)
N (7) -FE1-N (5)	162.31 (5)
C (1) -N (1) -C (5)	118.13 (14)
C (1) -N (1) -FE1	127.29 (11)
C (5) -N (1) -FE1	114.58 (10)
C (6) -N (2) -C (10)	120.75 (13)
C (6) -N (2) -FE1	118.94 (10)
C (10) -N (2) -FE1	119.29 (10)
C (15) -N (3) -C (11)	118.16 (13)
C (15) -N (3) -FE1	127.34 (11)
C (11) -N (3) -FE1	114.38 (10)
C (18) -N (4) -C (17)	116.90 (15)
C (21) -N (5) -C (25)	117.60 (13)
C (21) -N (5) -FE1	128.37 (11)
C (25) -N (5) -FE1	114.04 (10)
C (26) -N (6) -C (30)	121.08 (13)
C (26) -N (6) -FE1	118.95 (10)
C (30) -N (6) -FE1	119.86 (10)
C (35) -N (7) -C (31)	118.09 (13)
C (35) -N (7) -FE1	127.01 (10)
C (31) -N (7) -FE1	114.90 (9)
C (37) -N (8) -C (38)	116.25 (16)
N (1) -C (1) -C (2)	122.52 (15)
C (3) -C (2) -C (1)	119.35 (15)
C (2) -C (3) -C (4)	119.17 (15)

Appendix

C (3) -C (4) -C (5)	118.94 (15)
N (1) -C (5) -C (4)	121.78 (14)
N (1) -C (5) -C (6)	112.68 (13)
C (4) -C (5) -C (6)	125.54 (14)
N (2) -C (6) -C (7)	120.97 (14)
N (2) -C (6) -C (5)	111.64 (13)
C (7) -C (6) -C (5)	127.38 (14)
C (6) -C (7) -C (8)	119.80 (14)
C (7) -C (8) -C (9)	118.44 (14)
C (7) -C (8) -C (16)	119.78 (14)
C (9) -C (8) -C (16)	121.76 (14)
C (10) -C (9) -C (8)	119.33 (14)
N (2) -C (10) -C (9)	120.71 (14)
N (2) -C (10) -C (11)	111.49 (13)
C (9) -C (10) -C (11)	127.67 (14)
N (3) -C (11) -C (12)	121.79 (14)
N (3) -C (11) -C (10)	113.04 (13)
C (12) -C (11) -C (10)	125.17 (14)
C (13) -C (12) -C (11)	119.04 (15)
C (12) -C (13) -C (14)	119.33 (15)
C (15) -C (14) -C (13)	118.88 (15)
N (3) -C (15) -C (14)	122.73 (15)
C (17) -C (16) -C (20)	117.20 (14)
C (17) -C (16) -C (8)	122.00 (14)
C (20) -C (16) -C (8)	120.80 (14)
N (4) -C (17) -C (16)	123.76 (16)
N (4) -C (18) -C (19)	124.23 (15)
C (18) -C (19) -C (20)	118.01 (16)
C (19) -C (20) -C (16)	119.88 (15)
N (5) -C (21) -C (22)	123.05 (15)
C (23) -C (22) -C (21)	118.97 (15)
C (22) -C (23) -C (24)	119.22 (15)
C (23) -C (24) -C (25)	119.06 (15)
N (5) -C (25) -C (24)	122.09 (14)
N (5) -C (25) -C (26)	113.46 (13)
C (24) -C (25) -C (26)	124.45 (14)
N (6) -C (26) -C (27)	120.58 (14)
N (6) -C (26) -C (25)	112.08 (13)
C (27) -C (26) -C (25)	127.34 (13)
C (26) -C (27) -C (28)	119.71 (14)
C (27) -C (28) -C (29)	118.85 (14)
C (27) -C (28) -C (36)	119.12 (14)
C (29) -C (28) -C (36)	122.02 (14)
C (30) -C (29) -C (28)	119.11 (14)
N (6) -C (30) -C (29)	120.65 (13)
N (6) -C (30) -C (31)	111.34 (13)
C (29) -C (30) -C (31)	128.01 (14)
N (7) -C (31) -C (32)	121.78 (14)
N (7) -C (31) -C (30)	112.91 (13)
C (32) -C (31) -C (30)	125.30 (14)
C (31) -C (32) -C (33)	119.05 (14)
C (34) -C (33) -C (32)	119.55 (14)
C (33) -C (34) -C (35)	118.88 (14)
N (7) -C (35) -C (34)	122.63 (14)
C (40) -C (36) -C (37)	117.53 (15)
C (40) -C (36) -C (28)	122.63 (15)
C (37) -C (36) -C (28)	119.78 (15)
N (8) -C (37) -C (36)	124.31 (17)
N (8) -C (38) -C (39)	124.16 (17)

Appendix

C (38) -C (39) -C (40)	118.77 (18)
C (36) -C (40) -C (39)	118.96 (17)
C (46) -C (41) -C (42)	115.07 (15)
C (46) -C (41) -B (1)	125.58 (14)
C (42) -C (41) -B (1)	119.31 (14)
C (43) -C (42) -C (41)	123.22 (16)
C (44) -C (43) -C (42)	119.73 (17)
C (43) -C (44) -C (45)	119.20 (17)
C (44) -C (45) -C (46)	120.22 (17)
C (45) -C (46) -C (41)	122.44 (17)
C (52) -C (47) -C (48)	114.95 (14)
C (52) -C (47) -B (1)	124.42 (14)
C (48) -C (47) -B (1)	120.39 (13)
C (49) -C (48) -C (47)	123.50 (15)
C (48) -C (49) -C (50)	119.74 (16)
C (51) -C (50) -C (49)	118.52 (15)
C (50) -C (51) -C (52)	120.72 (15)
C (51) -C (52) -C (47)	122.47 (15)
C (54) -C (53) -C (58)	115.03 (14)
C (54) -C (53) -B (1)	121.68 (13)
C (58) -C (53) -B (1)	122.91 (14)
C (55) -C (54) -C (53)	122.87 (14)
C (56) -C (55) -C (54)	120.26 (15)
C (55) -C (56) -C (57)	118.82 (15)
C (56) -C (57) -C (58)	120.32 (16)
C (57) -C (58) -C (53)	122.62 (15)
C (64) -C (59) -C (60)	114.65 (14)
C (64) -C (59) -B (1)	118.96 (13)
C (60) -C (59) -B (1)	126.39 (14)
C (61) -C (60) -C (59)	122.72 (15)
C (62) -C (61) -C (60)	120.46 (15)
C (61) -C (62) -C (63)	118.56 (15)
C (64) -C (63) -C (62)	120.09 (15)
C (63) -C (64) -C (59)	123.49 (15)
C (66) -C (65) -C (70)	114.02 (15)
C (66) -C (65) -B (2)	120.59 (13)
C (70) -C (65) -B (2)	125.40 (14)
C (67) -C (66) -C (65)	124.02 (15)
C (68) -C (67) -C (66)	119.83 (16)
C (69) -C (68) -C (67)	118.47 (17)
C (68) -C (69) -C (70)	120.66 (16)
C (69) -C (70) -C (65)	122.94 (17)
C (72) -C (71) -C (76)	115.14 (15)
C (72) -C (71) -B (2)	125.75 (14)
C (76) -C (71) -B (2)	119.10 (14)
C (73) -C (72) -C (71)	122.06 (16)
C (74) -C (73) -C (72)	120.77 (18)
C (75) -C (74) -C (73)	118.65 (17)
C (74) -C (75) -C (76)	120.17 (17)
C (75) -C (76) -C (71)	123.15 (17)
C (78) -C (77) -C (82)	115.08 (14)
C (78) -C (77) -B (2)	124.52 (14)
C (82) -C (77) -B (2)	120.36 (13)
C (79) -C (78) -C (77)	122.75 (16)
C (80) -C (79) -C (78)	120.34 (16)
C (79) -C (80) -C (81)	118.79 (15)
C (80) -C (81) -C (82)	120.14 (16)
C (81) -C (82) -C (77)	122.90 (16)
C (84) -C (83) -C (88)	115.08 (15)

Appendix

C (84)–C (83)–B (2)	124.99 (14)
C (88)–C (83)–B (2)	119.93 (14)
C (85)–C (84)–C (83)	122.42 (16)
C (86)–C (85)–C (84)	120.52 (16)
C (85)–C (86)–C (87)	118.93 (15)
C (86)–C (87)–C (88)	119.88 (16)
C (87)–C (88)–C (83)	123.16 (16)
C (53)–B (1)–C (41)	113.75 (13)
C (53)–B (1)–C (59)	109.63 (12)
C (41)–B (1)–C (59)	105.89 (13)
C (53)–B (1)–C (47)	103.81 (12)
C (41)–B (1)–C (47)	111.41 (12)
C (59)–B (1)–C (47)	112.51 (13)
C (71)–B (2)–C (65)	110.89 (12)
C (71)–B (2)–C (77)	111.91 (12)
C (65)–B (2)–C (77)	107.03 (13)
C (71)–B (2)–C (83)	105.64 (13)
C (65)–B (2)–C (83)	111.03 (13)
C (77)–B (2)–C (83)	110.41 (12)

5B-3 [C₄₀H₃₂CoF₁₂N₈O₂P₂]

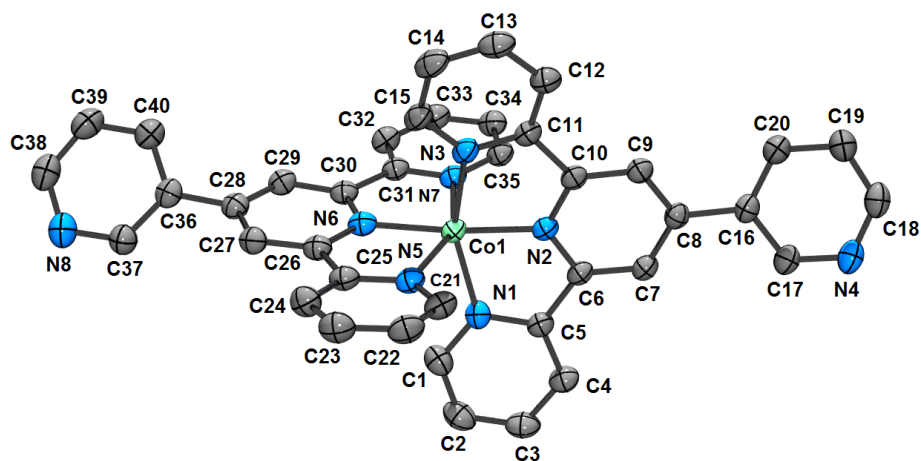


Table 7. Crystal data and structure refinement for C₄₀H₃₂CoF₁₂N₈O₂P₂ (**5B-3**)

Empirical formula	C ₄₀ H ₃₂ Co F ₁₂ N ₈ O ₂ P ₂
Formula weight	1005.60
Temperature	150(2) K
Wavelength	1.54178 Å
Crystal system	Monoclinic
Space group	P2 ₁ /c
Unit cell dimensions	a = 16.6279(5) Å α = 90° b = 14.8960(4) Å β = 101.648(1)°

Appendix

	$c = 16.3103(5) \text{ \AA}$	$\gamma = 90^\circ$
Volume	3956.7(2) \AA^3	
Z	4	
Density (calculated)	1.688 g/cm ³	
Absorption coefficient	5.130 mm ⁻¹	
F(000)	2036	
Crystal size	0.13 x 0.03 x 0.01 mm	
Theta range for data collection	2.713 to 69.517 deg.	
Index ranges	-20<=h<=20, -18<=k<=17, -19<=l<=18	
Reflections collected	72674	
Independent reflections	7385 [R(int) = 0.055]	
Absorption correction	Semi-empirical from equivalents	
Max. and min. transmission	0.6700 and 0.4783	
Refinement method	Full-matrix least-squares on F ²	
Data / restraints / parameters	7385 / 0 / 595	
Goodness-of-fit on F ²	1.052	
Final R indices [I>2sigma(I)]	R1 = 0.0341, wR2 = 0.0899	
R indices (all data)	R1 = 0.0394, wR2 = 0.0931	
Largest diff. peak and hole	0.446 and -0.253 e/ \AA^3	

Table 8. Bond lengths [\AA] and angles [$^\circ$] for C40H32CoF12N8O2P2 (**5B-3**)

Co(1)-N(2)	1.9306(16)
Co(1)-N(6)	1.9728(17)
Co(1)-N(3)	2.0472(17)
Co(1)-N(1)	2.0511(17)
Co(1)-N(5)	2.1719(17)
Co(1)-N(7)	2.1761(16)
P(1)-F(3)	1.5869(15)
P(1)-F(6)	1.5895(15)
P(1)-F(1)	1.5924(15)
P(1)-F(4)	1.5945(14)
P(1)-F(2)	1.5967(15)
P(1)-F(5)	1.6032(14)
P(2)-F(9)	1.5724(17)
P(2)-F(10)	1.5799(16)
P(2)-F(8)	1.5857(15)
P(2)-F(11)	1.5902(16)
P(2)-F(7)	1.5962(17)

Appendix

P (2) -F (12)	1.6027 (17)
N (1) -C (1)	1.346 (3)
N (1) -C (5)	1.355 (3)
N (2) -C (10)	1.345 (2)
N (2) -C (6)	1.347 (2)
N (3) -C (15)	1.342 (3)
N (3) -C (11)	1.351 (3)
N (4) -C (18)	1.335 (3)
N (4) -C (17)	1.342 (3)
N (5) -C (21)	1.337 (3)
N (5) -C (25)	1.352 (3)
N (6) -C (30)	1.352 (3)
N (6) -C (26)	1.356 (3)
N (7) -C (35)	1.335 (3)
N (7) -C (31)	1.353 (3)
N (8) -C (37)	1.338 (3)
N (8) -C (38)	1.341 (3)
C (1) -C (2)	1.376 (3)
C (2) -C (3)	1.386 (3)
C (3) -C (4)	1.379 (3)
C (4) -C (5)	1.388 (3)
C (5) -C (6)	1.477 (3)
C (6) -C (7)	1.386 (3)
C (7) -C (8)	1.402 (3)
C (8) -C (9)	1.393 (3)
C (8) -C (16)	1.482 (3)
C (9) -C (10)	1.380 (3)
C (10) -C (11)	1.472 (3)
C (11) -C (12)	1.385 (3)
C (12) -C (13)	1.383 (3)
C (13) -C (14)	1.377 (3)
C (14) -C (15)	1.379 (3)
C (16) -C (17)	1.392 (3)
C (16) -C (20)	1.396 (3)
C (18) -C (19)	1.377 (3)
C (19) -C (20)	1.376 (3)
C (21) -C (22)	1.386 (3)
C (22) -C (23)	1.377 (3)
C (23) -C (24)	1.384 (3)
C (24) -C (25)	1.390 (3)
C (25) -C (26)	1.481 (3)
C (26) -C (27)	1.385 (3)
C (27) -C (28)	1.392 (3)
C (28) -C (29)	1.393 (3)
C (28) -C (36)	1.479 (3)
C (29) -C (30)	1.382 (3)
C (30) -C (31)	1.479 (3)
C (31) -C (32)	1.387 (3)
C (32) -C (33)	1.382 (3)
C (33) -C (34)	1.381 (3)
C (34) -C (35)	1.383 (3)
C (36) -C (37)	1.388 (3)
C (36) -C (40)	1.392 (3)
C (38) -C (39)	1.374 (4)
C (39) -C (40)	1.381 (3)
N (2) -CO1-N (6)	171.86 (7)
N (2) -CO1-N (3)	79.26 (7)
N (6) -CO1-N (3)	99.63 (7)

Appendix

N(2)-CO1-N(1)	78.72(6)
N(6)-CO1-N(1)	103.41(7)
N(3)-CO1-N(1)	156.27(7)
N(2)-CO1-N(5)	110.65(7)
N(6)-CO1-N(5)	77.30(6)
N(3)-CO1-N(5)	88.82(6)
N(1)-CO1-N(5)	90.72(6)
N(2)-CO1-N(7)	93.87(7)
N(6)-CO1-N(7)	78.12(7)
N(3)-CO1-N(7)	93.41(6)
N(1)-CO1-N(7)	96.80(6)
N(5)-CO1-N(7)	155.34(7)
F(3)-P(1)-F(6)	90.70(9)
F(3)-P(1)-F(1)	89.39(9)
F(6)-P(1)-F(1)	179.10(9)
F(3)-P(1)-F(4)	178.73(9)
F(6)-P(1)-F(4)	90.36(9)
F(1)-P(1)-F(4)	89.55(8)
F(3)-P(1)-F(2)	90.80(9)
F(6)-P(1)-F(2)	90.98(9)
F(1)-P(1)-F(2)	89.92(9)
F(4)-P(1)-F(2)	89.88(8)
F(3)-P(1)-F(5)	89.93(8)
F(6)-P(1)-F(5)	89.14(8)
F(1)-P(1)-F(5)	89.96(8)
F(4)-P(1)-F(5)	89.39(8)
F(2)-P(1)-F(5)	179.26(9)
F(9)-P(2)-F(10)	90.79(11)
F(9)-P(2)-F(8)	89.88(9)
F(10)-P(2)-F(8)	89.58(10)
F(9)-P(2)-F(11)	91.20(10)
F(10)-P(2)-F(11)	90.31(10)
F(8)-P(2)-F(11)	178.92(11)
F(9)-P(2)-F(7)	91.59(11)
F(10)-P(2)-F(7)	177.54(11)
F(8)-P(2)-F(7)	89.85(10)
F(11)-P(2)-F(7)	90.21(10)
F(9)-P(2)-F(12)	179.63(11)
F(10)-P(2)-F(12)	89.09(10)
F(8)-P(2)-F(12)	89.76(9)
F(11)-P(2)-F(12)	89.16(10)
F(7)-P(2)-F(12)	88.52(10)
C(1)-N(1)-C(5)	118.28(18)
C(1)-N(1)-CO1	126.69(15)
C(5)-N(1)-CO1	114.87(13)
C(10)-N(2)-C(6)	120.54(16)
C(10)-N(2)-CO1	118.95(13)
C(6)-N(2)-CO1	120.00(13)
C(15)-N(3)-C(11)	118.73(18)
C(15)-N(3)-CO1	126.74(15)
C(11)-N(3)-CO1	114.43(13)
C(18)-N(4)-C(17)	116.29(19)
C(21)-N(5)-C(25)	118.73(18)
C(21)-N(5)-CO1	127.19(14)
C(25)-N(5)-CO1	113.43(13)
C(30)-N(6)-C(26)	119.68(18)
C(30)-N(6)-CO1	119.58(13)
C(26)-N(6)-CO1	120.61(14)
C(35)-N(7)-C(31)	118.36(17)

Appendix

C (35) -N (7) -CO1	129.26 (14)
C (31) -N (7) -CO1	112.37 (13)
C (37) -N (8) -C (38)	117.2 (2)
N (1) -C (1) -C (2)	122.4 (2)
C (1) -C (2) -C (3)	119.0 (2)
C (4) -C (3) -C (2)	119.3 (2)
C (3) -C (4) -C (5)	118.8 (2)
N (1) -C (5) -C (4)	122.08 (18)
N (1) -C (5) -C (6)	113.56 (16)
C (4) -C (5) -C (6)	124.26 (18)
N (2) -C (6) -C (7)	120.85 (17)
N (2) -C (6) -C (5)	112.01 (16)
C (7) -C (6) -C (5)	127.12 (17)
C (6) -C (7) -C (8)	119.79 (18)
C (9) -C (8) -C (7)	117.63 (18)
C (9) -C (8) -C (16)	120.05 (18)
C (7) -C (8) -C (16)	122.29 (18)
C (10) -C (9) -C (8)	120.32 (18)
N (2) -C (10) -C (9)	120.84 (17)
N (2) -C (10) -C (11)	112.82 (17)
C (9) -C (10) -C (11)	126.29 (18)
N (3) -C (11) -C (12)	121.94 (18)
N (3) -C (11) -C (10)	113.70 (17)
C (12) -C (11) -C (10)	124.23 (18)
C (13) -C (12) -C (11)	118.5 (2)
C (14) -C (13) -C (12)	119.6 (2)
C (13) -C (14) -C (15)	118.9 (2)
N (3) -C (15) -C (14)	122.2 (2)
C (17) -C (16) -C (20)	116.84 (19)
C (17) -C (16) -C (8)	121.73 (18)
C (20) -C (16) -C (8)	121.40 (18)
N (4) -C (17) -C (16)	124.6 (2)
N (4) -C (18) -C (19)	124.1 (2)
C (20) -C (19) -C (18)	118.7 (2)
C (19) -C (20) -C (16)	119.4 (2)
N (5) -C (21) -C (22)	122.5 (2)
C (23) -C (22) -C (21)	118.9 (2)
C (22) -C (23) -C (24)	119.3 (2)
C (23) -C (24) -C (25)	118.9 (2)
N (5) -C (25) -C (24)	121.64 (19)
N (5) -C (25) -C (26)	114.50 (17)
C (24) -C (25) -C (26)	123.81 (19)
N (6) -C (26) -C (27)	120.97 (19)
N (6) -C (26) -C (25)	113.89 (18)
C (27) -C (26) -C (25)	125.02 (18)
C (26) -C (27) -C (28)	119.95 (19)
C (27) -C (28) -C (29)	118.13 (19)
C (27) -C (28) -C (36)	121.98 (19)
C (29) -C (28) -C (36)	119.86 (19)
C (30) -C (29) -C (28)	119.85 (19)
N (6) -C (30) -C (29)	121.32 (18)
N (6) -C (30) -C (31)	114.70 (17)
C (29) -C (30) -C (31)	123.92 (18)
N (7) -C (31) -C (32)	121.84 (18)
N (7) -C (31) -C (30)	115.04 (17)
C (32) -C (31) -C (30)	123.10 (19)
C (33) -C (32) -C (31)	118.7 (2)
C (34) -C (33) -C (32)	119.7 (2)
C (33) -C (34) -C (35)	118.20 (19)

Appendix

N (7) -C (35) -C (34)	123.13 (19)
C (37) -C (36) -C (40)	117.4 (2)
C (37) -C (36) -C (28)	121.7 (2)
C (40) -C (36) -C (28)	120.9 (2)
N (8) -C (37) -C (36)	123.9 (2)
N (8) -C (38) -C (39)	123.3 (2)
C (38) -C (39) -C (40)	118.8 (2)
C (39) -C (40) -C (36)	119.3 (2)

5B-5 [C₄₂H₃₁CuF₁₂N₉P₂]

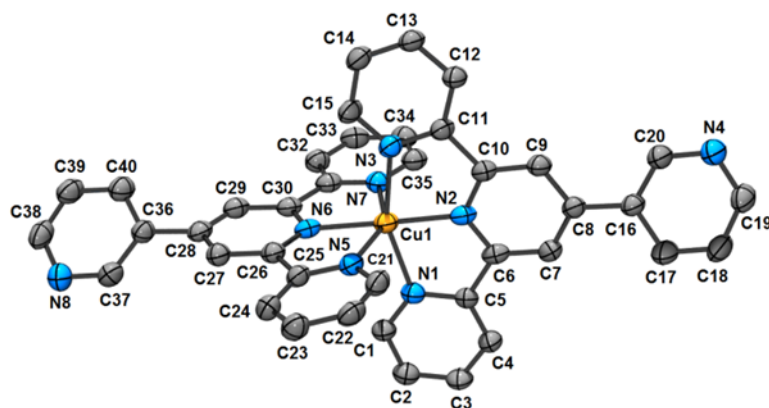


Table 9. Crystal data and structure refinement for C₄₂H₃₁CuF₁₂N₉P₂ (**5B-5**)

Empirical formula	C ₄₂ H ₃₁ Cu F ₁₂ N ₉ P ₂
Formula weight	1015.24
Temperature	150(2) K
Wavelength	1.54178 Å
Crystal system	Triclinic
Space group	P-1
Unit cell dimensions	a = 9.0556(6) Å α = 84.796(4)° b = 10.3716(7) Å β = 78.733(3)° c = 21.8764(14) Å γ = 73.588(3)°
Volume	1931.6(2) Å ³
Z	2
Density (calculated)	1.746 g/cm ³
Absorption coefficient	2.543 mm ⁻¹
F(000)	1026
Crystal size	0.10 x 0.01 x 0.01 mm

Appendix

Theta range for data collection	2.061 to 69.502 deg.
Index ranges	-10<=h<=10, -12<=k<=12, -26<=l<=23
Reflections collected	39288
Independent reflections	7119 [R(int) = 0.104]
Absorption correction	Semi-empirical from equivalents
Max. and min. transmission	0.8287 and 0.6053
Refinement method	Full-matrix least-squares on F ²
Data / restraints / parameters	7119 / 0 / 505
Goodness-of-fit on F ²	0.891
Final R indices [I>2sigma(I)]	R1 = 0.0566, wR2 = 0.1381
R indices (all data)	R1 = 0.0857, wR2 = 0.1483
Largest diff. peak and hole	0.736 and -0.577 e/Å ³

Table 10. Bond lengths [Å] and angles [°] for C₄₂H₃₁CuF₁₂N₉P₂ (**5B-5**)

Cu(1)-N(2)	1.947(3)
Cu(1)-N(6)	2.012(3)
Cu(1)-N(1)	2.090(3)
Cu(1)-N(3)	2.113(3)
Cu(1)-N(5)	2.218(3)
Cu(1)-N(7)	2.262(3)
P(1)-F(5)	1.574(3)
P(1)-F(4)	1.580(3)
P(1)-F(3)	1.592(3)
P(1)-F(1)	1.592(3)
P(1)-F(2)	1.594(3)
P(1)-F(6)	1.595(3)
N(1)-C(5)	1.336(5)
N(1)-C(1)	1.359(5)
N(2)-C(10)	1.340(4)
N(2)-C(6)	1.344(4)
N(3)-C(15)	1.334(4)
N(3)-C(11)	1.355(5)
N(4)-C(17)	1.331(5)
N(4)-C(18)	1.337(5)
N(5)-C(25)	1.330(5)
N(5)-C(21)	1.349(5)
N(6)-C(30)	1.342(5)
N(6)-C(26)	1.358(5)
N(7)-C(31)	1.335(4)
N(7)-C(35)	1.340(5)
N(8)-C(38)	1.333(5)
N(8)-C(37)	1.337(5)
C(1)-C(2)	1.384(5)
C(1)-C(6)	1.475(5)

Appendix

C (2) -C (3)	1.378 (5)
C (3) -C (4)	1.379 (5)
C (4) -C (5)	1.391 (5)
C (6) -C (7)	1.377 (5)
C (7) -C (8)	1.387 (5)
C (8) -C (9)	1.413 (5)
C (8) -C (16)	1.478 (5)
C (9) -C (10)	1.377 (5)
C (10) -C (11)	1.495 (5)
C (11) -C (12)	1.376 (5)
C (12) -C (13)	1.389 (5)
C (13) -C (14)	1.364 (5)
C (14) -C (15)	1.382 (5)
C (16) -C (17)	1.377 (5)
C (16) -C (20)	1.407 (5)
C (18) -C (19)	1.363 (6)
C (19) -C (20)	1.365 (6)
C (21) -C (22)	1.389 (5)
C (21) -C (26)	1.478 (5)
C (22) -C (23)	1.368 (5)
C (23) -C (24)	1.392 (6)
C (24) -C (25)	1.379 (5)
C (26) -C (27)	1.390 (5)
C (27) -C (28)	1.378 (5)
C (28) -C (29)	1.405 (5)
C (28) -C (36)	1.484 (5)
C (29) -C (30)	1.390 (5)
C (30) -C (31)	1.489 (5)
C (31) -C (32)	1.397 (5)
C (32) -C (33)	1.383 (5)
C (33) -C (34)	1.385 (6)
C (34) -C (35)	1.361 (6)
C (36) -C (37)	1.380 (5)
C (36) -C (40)	1.394 (5)
C (38) -C (39)	1.366 (6)
C (39) -C (40)	1.377 (6)
N (2) -CU1-N (6)	176.09 (12)
N (2) -CU1-N (1)	78.95 (12)
N (6) -CU1-N (1)	100.32 (12)
N (2) -CU1-N (3)	78.87 (12)
N (6) -CU1-N (3)	101.81 (11)
N (1) -CU1-N (3)	157.82 (12)
N (2) -CU1-N (5)	99.06 (12)
N (6) -CU1-N (5)	77.13 (11)
N (1) -CU1-N (5)	94.02 (11)
N (3) -CU1-N (5)	89.38 (11)
N (2) -CU1-N (7)	108.19 (12)
N (6) -CU1-N (7)	75.66 (11)
N (1) -CU1-N (7)	94.03 (11)
N (3) -CU1-N (7)	92.93 (11)
N (5) -CU1-N (7)	152.59 (11)
F (5) -P (1) -F (4)	91.82 (18)
F (5) -P (1) -F (3)	90.08 (16)
F (4) -P (1) -F (3)	88.90 (15)
F (5) -P (1) -F (1)	90.68 (15)
F (4) -P (1) -F (1)	91.60 (15)
F (3) -P (1) -F (1)	179.08 (17)
F (5) -P (1) -F (2)	179.4 (2)

Appendix

F (4) -P (1) -F (2)	88.61 (16)
F (3) -P (1) -F (2)	89.56 (15)
F (1) -P (1) -F (2)	89.68 (14)
F (5) -P (1) -F (6)	90.3 (2)
F (4) -P (1) -F (6)	177.81 (18)
F (3) -P (1) -F (6)	90.69 (15)
F (1) -P (1) -F (6)	88.78 (15)
F (2) -P (1) -F (6)	89.23 (18)
C (5) -N (1) -C (1)	119.1 (3)
C (5) -N (1) -CU1	127.2 (2)
C (1) -N (1) -CU1	113.6 (2)
C (10) -N (2) -C (6)	120.3 (3)
C (10) -N (2) -CU1	120.0 (2)
C (6) -N (2) -CU1	119.7 (2)
C (15) -N (3) -C (11)	118.0 (3)
C (15) -N (3) -CU1	128.2 (2)
C (11) -N (3) -CU1	113.4 (2)
C (17) -N (4) -C (18)	116.7 (3)
C (25) -N (5) -C (21)	119.0 (3)
C (25) -N (5) -CU1	128.2 (3)
C (21) -N (5) -CU1	112.9 (2)
C (30) -N (6) -C (26)	119.6 (3)
C (30) -N (6) -CU1	121.3 (2)
C (26) -N (6) -CU1	119.1 (2)
C (31) -N (7) -C (35)	118.5 (3)
C (31) -N (7) -CU1	112.3 (2)
C (35) -N (7) -CU1	129.0 (3)
C (38) -N (8) -C (37)	116.1 (4)
N (1) -C (1) -C (2)	121.0 (3)
N (1) -C (1) -C (6)	114.3 (3)
C (2) -C (1) -C (6)	124.6 (3)
C (3) -C (2) -C (1)	119.5 (3)
C (2) -C (3) -C (4)	119.6 (3)
C (3) -C (4) -C (5)	118.5 (4)
N (1) -C (5) -C (4)	122.3 (4)
N (2) -C (6) -C (7)	121.0 (3)
N (2) -C (6) -C (1)	113.4 (3)
C (7) -C (6) -C (1)	125.6 (3)
C (6) -C (7) -C (8)	120.3 (3)
C (7) -C (8) -C (9)	117.6 (3)
C (7) -C (8) -C (16)	121.9 (3)
C (9) -C (8) -C (16)	120.5 (3)
C (10) -C (9) -C (8)	119.3 (3)
N (2) -C (10) -C (9)	121.4 (3)
N (2) -C (10) -C (11)	113.5 (3)
C (9) -C (10) -C (11)	125.1 (3)
N (3) -C (11) -C (12)	122.5 (3)
N (3) -C (11) -C (10)	113.9 (3)
C (12) -C (11) -C (10)	123.6 (3)
C (11) -C (12) -C (13)	118.2 (3)
C (14) -C (13) -C (12)	119.7 (3)
C (13) -C (14) -C (15)	118.9 (3)
N (3) -C (15) -C (14)	122.6 (4)
C (17) -C (16) -C (20)	116.3 (3)
C (17) -C (16) -C (8)	122.5 (3)
C (20) -C (16) -C (8)	121.1 (3)
N (4) -C (17) -C (16)	125.3 (4)
N (4) -C (18) -C (19)	122.6 (4)
C (18) -C (19) -C (20)	120.4 (4)

Appendix

C (19) -C (20) -C (16)	118.6 (4)
N (5) -C (21) -C (22)	120.9 (3)
N (5) -C (21) -C (26)	115.0 (3)
C (22) -C (21) -C (26)	124.0 (3)
C (23) -C (22) -C (21)	119.7 (4)
C (22) -C (23) -C (24)	119.3 (4)
C (25) -C (24) -C (23)	118.0 (4)
N (5) -C (25) -C (24)	123.1 (4)
N (6) -C (26) -C (27)	120.6 (3)
N (6) -C (26) -C (21)	115.8 (3)
C (27) -C (26) -C (21)	123.6 (3)
C (28) -C (27) -C (26)	120.6 (3)
C (27) -C (28) -C (29)	118.2 (3)
C (27) -C (28) -C (36)	120.4 (3)
C (29) -C (28) -C (36)	121.4 (3)
C (30) -C (29) -C (28)	119.0 (3)
N (6) -C (30) -C (29)	122.0 (3)
N (6) -C (30) -C (31)	114.7 (3)
C (29) -C (30) -C (31)	123.2 (3)
N (7) -C (31) -C (32)	121.9 (3)
N (7) -C (31) -C (30)	115.5 (3)
C (32) -C (31) -C (30)	122.6 (3)
C (33) -C (32) -C (31)	118.6 (4)
C (32) -C (33) -C (34)	118.9 (4)
C (35) -C (34) -C (33)	118.8 (4)
N (7) -C (35) -C (34)	123.2 (4)
C (37) -C (36) -C (40)	117.6 (4)
C (37) -C (36) -C (28)	122.2 (3)
C (40) -C (36) -C (28)	120.2 (3)
N (8) -C (37) -C (36)	124.3 (4)
N (8) -C (38) -C (39)	124.5 (4)
C (38) -C (39) -C (40)	118.5 (4)
C (39) -C (40) -C (36)	118.9 (4)

References

- (1) SAINT (2006) Release 7.34A; Integration Software for Single Crystal Data. Bruker AXS Inc., Madison, WI 53719-1173.
- (2) Sheldrick, G. M. (2004). SADABS, Bruker Area Detector Absorption Corrections. Bruker AXS Inc., Madison, WI 53719-1173.
- (3) Sheldrick, G. M. (2008). Acta Cryst. A64, 112-122.
- (4) SHELXTL (2001) version 6.12; Bruker Analytical X-ray Systems Inc., Madison, WI 53719-1173.
- (5) APEX2 (2007) version 2.4-0; Bruker Molecular Analysis Research Tool.

Appendix

Bruker AXS Inc., Madison, WI 53719-1173.

(6) Spek, A. L. (2008). PLATON, A Multipurpose Crystallographic Tool, Utrecht University, Utrecht, The Netherlands.

(7) Maris, T. (2004). UdMX, University of Montréal, Montréal, QC, Canada.

(8) XPREP (2005) Version 2005/2; X-ray data Preparation and Reciprocal space Exploration Program. Bruker AXS Inc., Madison, WI 53719-1173.